Engineering Geology and Geotechnical Investigation of Highwall Stability at the Proposed Terrace Opencast Coal Mine, Reddale Valley, Reefton.

A thesis submitted in partial fulfilment of the requirements
for the Degree of
Master of Science in Engineering Geology
at the
University of Canterbury
by

Joanna Lea

June 2006

Frontispiece: Looking north along the Reddale Valley, Reefton, 2005.

Abstract

This thesis presents an engineering geological and geotechnical investigation of the proposed Terrace Opencast Coalmine highwall in the Reddale Valley, Reefton. The proposed pit will target the 4-11m thick No. 4 Seam coal, which exists on the Valley floor beneath outwash gravels and Brunner Coal Measures (BCM) overburden dipping at 15-30˚ to the northwest. Rock coatings are providing friable sandstone units with protection from weathering in existing cut faces and may contribute to short term pit wall stability.

The BCM core was divided into four geotechnical units for rock material testing purposes: unit 1 siltstone, unit 2 carbonaceous mudstone, unit 3 interbedded sandstone and carbonaceous mudstone and unit 4 loose sandstone. The average results for units 1-3 gave classifications within the medium to high porosity (9-13%) and dry density (2250-2470kg/m^3) ranges, and medium to medium high slake-durability I_{d2} values (72-94% retained). Unit 4 (loose sandstone) recorded very low dry density (1694 kg/m^3) and slake-durability I_{d2} (9%) average values. Strength testing confirmed that the units can be classed as weak rocks, with average UCS values of 12.8-13.7MPa for units 1-3, and for all four units $I_{s(50)}$ from point load testing of 0.26-0.62MPa with low cohesion values (0-6.2MPa) from triaxial testing. Friction angles from triaxial tests gave high values of 32-45˚, while direct shear tests established 15˚ internal friction for bedding planes in carbonaceous mudstone and 37˚ for a high angle defect in interbedded sandstone/carbonaceous mudstone. The average Young's modulus values ranged from 0.82 to 10GPa, and Poisson's ratio between 0.39 and 0.50.

Eight scanline defect surveys established that the major discontinuities in existing cut faces consist of high angle tension joints, shallow dipping bedding, and faults related to regional uplift. The defect orientations from the scanlines located in the southwest were significantly different from those in the northeast, and may be due to the faults that cross the Valley. In general the majority of defects displayed low persistence (<3m), were clean and tight, and had low joint roughness coefficients (JRC<6). Joint wall compressive strengths gave an average of 32MPa, but were affected by case-hardening on weathered faces. The results from the 8 drill holes analysed show that 37% of core was within the excellent rock quality designation class (RQD = 90-100%), while 29% was in the very poor quality rock (RQD = 0-25%). A semi-confined aquifer in the outwash gravels that will drain into the proposed pit was found to have a transmissivity of 58m^2/day and hydraulic conductivity of 3.1 x 10^{-5} m/s.

Kinematic feasibility assessment determined an optimum highwall orientation of 65˚ dip to 120˚ (dip direction), which is within at least 20˚ of the coal seam strike. The likelihood of planar, wedge or toppling failure depends on whether the structural conditions are similar to those encountered in the southwest or northeast scanlines, as well as the persistence of the defects present. The occurrence of small scale (<1m offset) 'step-up' normal faults, and the three larger faults that cross the valley, all of which are related to regional uplift, will also affect which failure mode will be kinematically feasible. Other crucial slope stability considerations include groundwater inflow from the saturated overburden and bedding parallel failures on the footwall dip slope of the pit.

An investigation into case hardening on existing cut faces identified three interconnected rock coatings: iron films, lithobiontic (biological) and clay-dominated crusts. Jarosite was found at sites with abundant pyrite and the oxidation of iron may have been aided by microbial activity. A green algae inhabiting pore spaces approximately 1mm below the surface was noted beneath an iron film and it is suggested to be similar to that found in arid environments. Although lithobiontic and clay-dominated crusts did not provide the weathered surface with any additional strength, they were observed to form relatively quickly (from months to less than 5 years) and will aid short term stability by providing the batters with protection from weathering processes.

This project concluded that the overburden material in the proposed highwall can be expected to behave like weak rock and in some cases (such as the loose sandstone) can be expected to have soil characteristics. Highwall stability is more likely to be affected by substantial inflows of groundwater than highly persistent joint sets. Establishment of the highwalls in their final position in the early mining stages will enable development of rock coatings that are expected to aid short and long term stability.

Table of Contents

List of Figures

List of Tables

List of Appendices

Acknowledgements

Firstly I would like to thank Solid Energy for the opportunity to work on an industry related project and for the financial contribution that made it possible. Special thanks to Richard Mould, Rob Boyd, John Taylor and Tim Moore for providing information and contacts. Thanks also to Jim Foster for answering my questions from your wealth of knowledge on mining in Reefton and to Greg Almond for taking us underground. Many thanks to Adrian Field and Dave Stone for getting me involved in their part of the work being conducted on the Reddale Valley.

Thank you to CRL Energy for training in ArcGIS and an inside into the coal industry. Thank you to the New Zealand Federation of Graduate Women, the New Zealand Geological Society and AusIMM for much appreciated financial awards

A huge thank you to David Bell for organising and supervising the project, and to Joc Campbell for assistance with the structural aspects. Thank you to all the staff in the Department of Geological Sciences for their numerous roles, especially Joyce, Cathy and Vanessa for help with equipment; Kerry Swanson for instructions on microscope photography; Rob Spiers for producing thin sections how I wanted them, Stephen Brown for conducting XRD analysis, David Shelley for petrographic assistance, Steve Weaver for geochemical guidance and Kari Bassett for getting me started on the case hardening investigation.

This project also involved the School of Engineering and in particular I would like to thank Siale Faitotonu for his instructions on soil triaxial testing. From the Department of Biology I would like to thank Neil Andrews for all his help with the SEM and Laurie Greenfield for identifying the biological component of my samples. Thank you to Lynn Torgerson for hydrological assistance and to GNS for lending the triaxial cell, it was hugely appreciated!!

To the gals who stuck around to complete their masters: Carol, Francie, Olivia and Joyce and those who arrived from overseas: Amy and Tennille, thank you for all your encouragement and for always having time for a chat! Thank you to my family, especially my parents for investing in my education and my brother for being the best field assistant ever! and to my friends for making me take a break every now and then. Finally thank you to Mitch for always trying to make me smile.

Chapter 1

Introduction and Literature Review

1.1 Project Background

Terrace Mine is an underground coal mine owned and operated by Solid Energy New Zealand Ltd. It is situated near the southern limit of the Reefton Coalfield within the Brunner Coal Measures (BCM), which contains interbedded mudstones, sandstones and coal. Further underground mining in the area may encounter geotechnical difficulties, such as floor heave, as overburden pressures increase. The shallow 15 to 25˚ dip of the beds are also better suited for opencast mining. An opencast mine is therefore preferable to recover additional resources and the nearby Reddale Valley is being investigated as a possible site. No. 4 seam is known to be present beneath approximately 10m of overburden in the south end of the valley, and analysis of coal from drill core suggests it will be lower in sulphur content than that currently being mined and between 4 and 10m thick.

The opencast would include the construction of a substantial highwall on the down-dip side of the pit. Only limited geotechnical information is available for BCM within the Reefton Coalfield, and most is derived from the Terrace Underground Mine rather than within the Reddale Valley. The focus of this thesis is an engineering geological investigation of this proposed highwall to determine the most favourable design. This is achieved through surveying defects in existing cuts within the area and applying a kinematic feasibility analysis to establish optimum angle and orientation. Laboratory testing of drill core of overburden material investigates rock material strengths and characteristics. Groundwater conditions are also considered relevant when suggesting long and short term stability requirements.

The “Old” Terrace Opencast in the Reddale Valley, and Peerless Gully Opencast nearby, exhibit existing highwalls with exposed batters in friable BCM sandstone. These stand vertically to 10m+ without obvious deterioration. Case hardening, where a secondary cementation has occurred to form a protective “crust” making the surface resistant to erosion, can be seen on outcrop and cut faces. Open cast mining may not enable this shielding feature to develop, and therefore possibly encounter stability problems especially below the water table when substantial water inflow causes erosion, such as piping. The cement strengthening the exterior has been analysed in outcrop, hand specimen and by reflected light microscope, polarised microscope and

the scanning electron microscope (SEM). This information is combined with the geotechnical data (rock mass and rock material) to suggest further highwall stability criteria.

1.1 Project Aims and Objectives

The specific objectives of this study are to:

- Produce an engineering geological map and corresponding cross-sections of the Reddale Valley and the proposed opencast site.
- Determine rock material characteristics by means of relevant laboratory testing.
- Determine rock mass characteristics by performing scanline defect surveys along abandoned opencast cut faces and use the data gained to perform a kinematic feasibility analysis for failure potential.
- Analyse the near surface ground water conditions and how it will affect opencast mining.
- Determine properties enabling vertical stability of loose sandstone, in particular investigation of the "crusting" on weathered faces and the implications for short and long term batter performance.
- Suggest potential high wall design based on the geotechnical information gained from the objectives above.

1.2 Location and Setting

1.3.1 Location

Reefton Township is situated approximately 45km inland from the West Coast of the South Island of New Zealand. Reefton Coalfield extends approximately 2km north east of Reefton township within the Victoria Range foothills on the eastern side of the Grey-Inangahua depression. The outcrop zone is approximately 0.5km in width. The principal river in the area is the Inangahua River and together with tributaries, such as the Waitahu River and Burkes Creek, flow northwest through the coalfield. Solid Energy's Reefton office, Terrace mine entrance and screening plant are located at the north-eastern end of Bridge Street within Reefton Township.

The Reddale Valley is located on the northeast side of the glacial terrace which separates it from Reefton Township (figure 1.1). Terrace Mine is an underground mine beneath this terrace, which reaches a maximum vertical depth of approximately 200m. Access to Reddale Valley is via Gannons Road (off the main road heading towards Westport) and then the gravel Burkes Road, which continues to a radio tower up the valley. The creek runs parallel to Burkes Road

and is referred to as the Inglewood Creek on older maps and Burkes Creek on more modern maps as it is a tributary. Map C (map pocket) provides an aerial photograph of the site.

Figure 1.1 Location map of the study area.

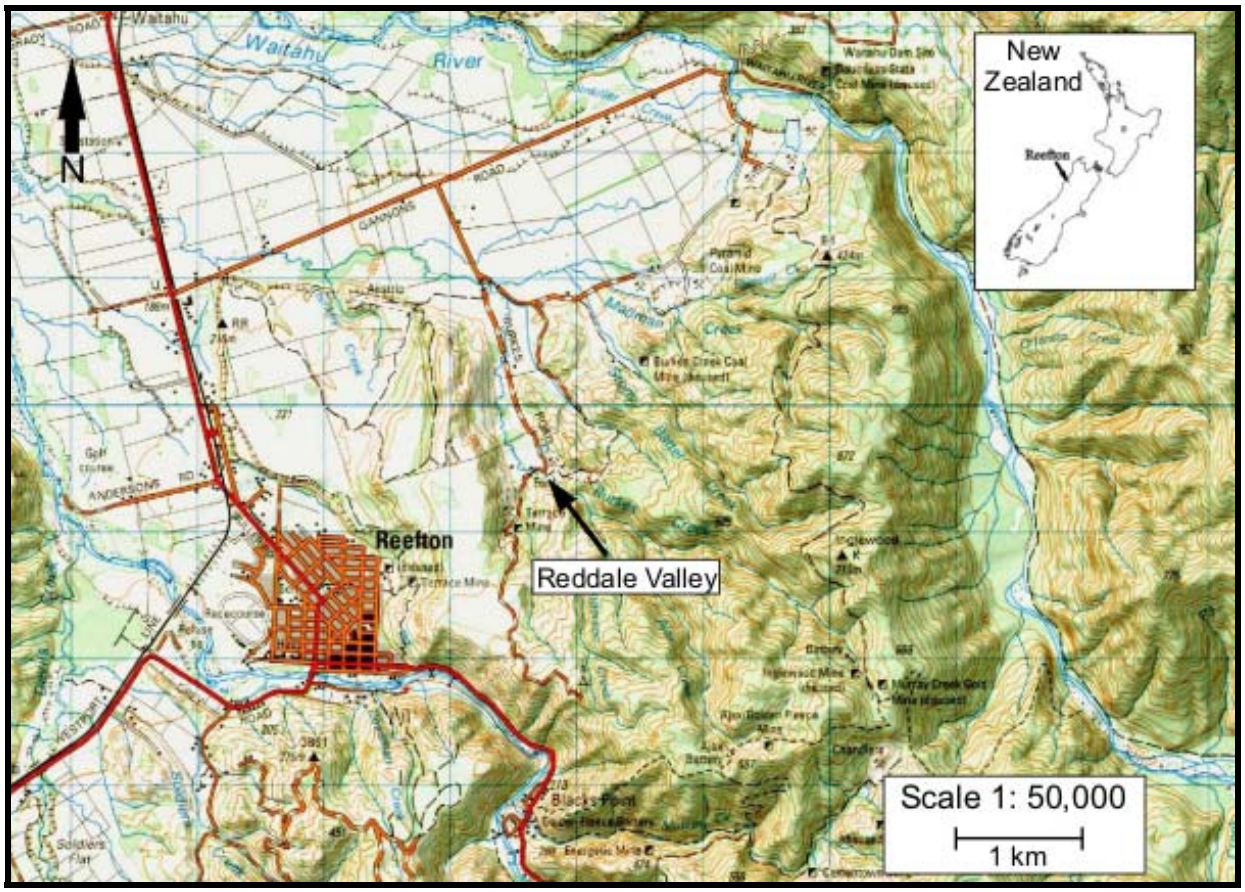

1.3.2 Proposed Opencast Site Description

The site for the proposed opencast is on the flat ground at the south-eastern end of the valley where the coal subcrop is known to traverse the valley floor beneath 10m+ of overburden. The land is currently being used for sheep and cattle farming by LandCorp and is Crown owned. Deer are also farmed further down the valley and on the terrace top and slopes. It is therefore mainly grass-covered terrain with occasional trees. Dead gorse and tussock covers most of valley slopes, and the upper reaches of the valley contains beech forest which is on DOC stewardship land (Stone *et al.*, 2005). A shed and cattle yards have been erected beside the road. A thicket of indigenous trees protected by a 'Queen Elizabeth the Second National Trust Open Space Covenant' exists approximately 250m back down the valley (Stone *et al.*, 2005). Old opencast mines are situated on the slopes of both sides of the valley. A pond has infilled the opencast pit on the north east side (see figure 1.2).

Figure 1.2 Photograph of the Reddale Valley showing the proposed opencast site.

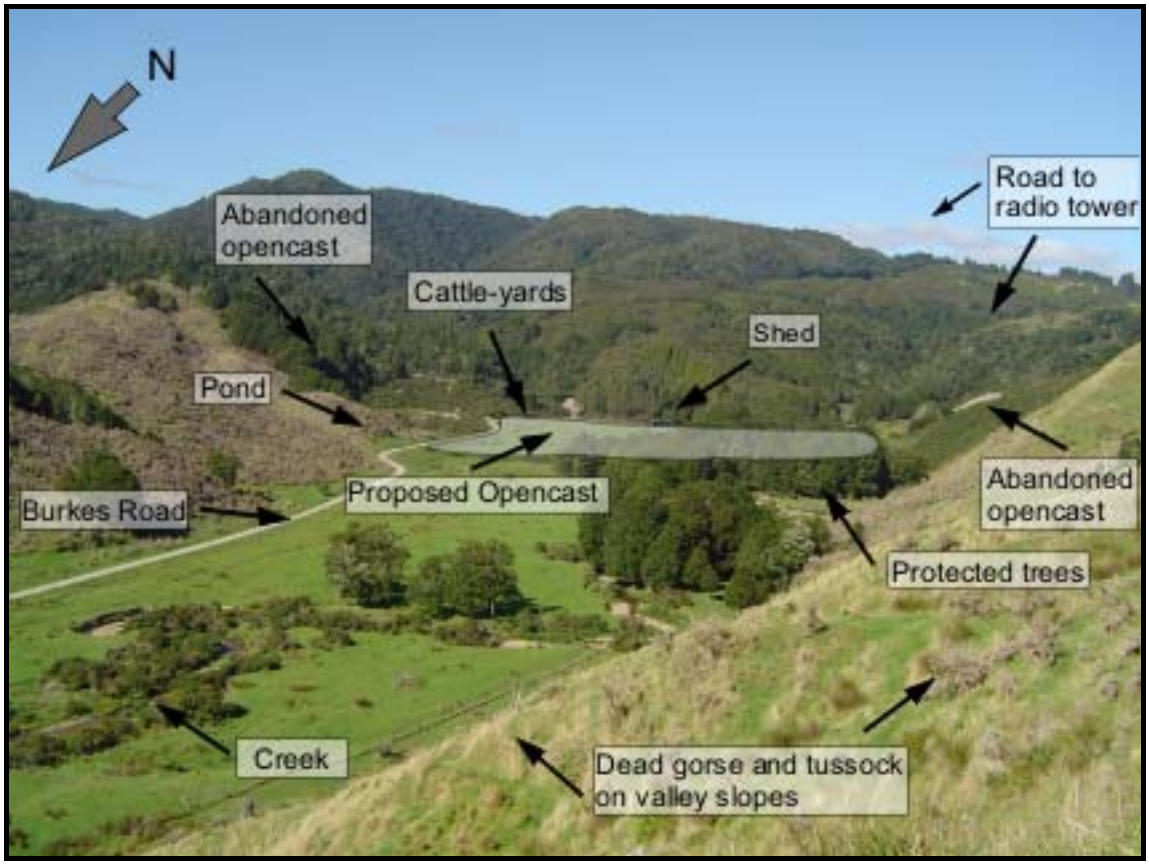

1.3.3 Climate

The West Coast has a temperate climate but experiences a greater amount of rain than the East Coast due to its proximity to the Southern Alps. The table below summarises NIWA's (National Institute of Water and Atmosphere; NIWA Science Website, 2006) records of rainfall in Reefton for the last 6 years, and shows that on average it experiences 1750mm of rain per year. Around 70mm of this may fall within a period of 24 hours. Annually Reefton encounters approximately 150 'wet days' and 180 days where at least 0.1mm of rain falls.

Table 1.1 Rainfall records for Reefton from NIWA.

Year	Total Rainfall mm	Max. 24-hrs Rainfall mm	Wet Days No. Of Days With 1mm Or More Of Rain	Rain Days No. Of Days With 0.1mm Or More
2000	1873.8	85.2	147	179
2001	1594.6	66.8	132	166
2002	1854	70.4	167	196
2003	1725.6	63.4	139	172
2004	2148.2	87	188	217
2005	1297.8	35.8	122	165

The West Coast is also more humid with temperatures in Reefton normally between 6 and 17˚C. The range of temperatures and average temperatures for Reefton available from NIWA are shown in table 1.2.

Table 1.2 Reefton temperature data from NIWA.

Year	Mean Air Temp Celsius	Mean Daily Max Air Temp Celsius	Mean Daily Min Air Temp Celsius	Lowest Daily Mean Temp Celsius	Highest Daily Mean Temp Celsius
2000	11.6	17	6.2	No data	No data
2001	11.6	17	6.1	No data	No data
2002	11.4	16.5	6.3	1	20.2
2003	11.2	16.6	5.8	0.6	20.5
2004	10.6	15.5	5.7	-0.1	21.7
2005	12.1	17.5	6.8	0.6	24.4

1.4 Geology

1.4.1 Regional Geology

1.4.1.1 Ordovician to Silurian

Basement rocks in the Reefton district belong to the Greenland Group (figure 1.3). Adam *et al.*, (1975) suggested a pre- upper Ordovician age for deposition based on K-Ar whole-rock ages of Greenland Group slates in Buller and Westland. They were deposited as quartz-rich turbidites (Cooper, 1989) that resulted from weathering of a passive continental margin (Roser *et al.* 1996). The Greenland Group sediments are part of the Buller Terrane, which is separated from the Takaka Terrane to the east by the Anatoki Thrust, although both terranes are west of the Alpine Fault. Large scale deformation throughout the Buller Terrane generally consists of north to north-north-east trending folds. In the Paparoa Range a swing of these folds towards the north-west has been observed, but is believed to be part of the same phase of folding (Cooper, 1989). The formation of cleavage and low grade regional metamorphism is also associated with this period of folding which occurred during the late Ordovician or early Silurian (Adams *et al.*, 1975). The metamorphism is responsible for the generation of metamorphic fluids that produced the gold and arsenic mineralization found in the Reefton Goldfield (Clark, 1996).

1.4.1.2 Devonian to Cretaceous

In the Devonian several hundreds of metres of limestone, mudstone and quartzite beds of the Reefton Group were deposited (Suggate, 1957). It is assumed that the Reefton Group sediments were deposited unconformably on top of the Greenland Group, although no observation of this have been recorded and all contacts found between them are faulted. During a compressional stage later in the Devonian, the Reefton Group rocks were folded and then down-faulted so that today they are next to the Greenland Group (figure 1.3), and form separate outliers in the Reefton District (Bradshaw, 1995). The granite and gneiss of the Paparoa and Victoria Ranges are part of the Karamea Batholith, which was a belt of magmatic activity near the Paleo-pacific

margin of Gondwana and were emplaced during the mid-late Devonian (Muir *et al.*, 1996). The Carboniferous to Cretaceous periods are unrepresented in the Reefton area.

1.4.1.3 Tertiary

The Hawke's Crag Breccia, which is composed of granite, greywacke and argillite fragments and was caused by fault movement, was deposited in the lower Cretaceous. Thin coal seams, mudstone and sandstone were also deposited in the lower Cretaceous along with minor basic intrusions and tuffaceous material (Topfer Formation) as tectonic movement decreased (Suggate, 1957).

Without tectonic activity occurring, subaerial erosion of older sediments and a lack of fresh sediment resulted in the reduction of the topography to a near peneplain during the Cretaceous. This period of weathering is indicated in the geological record by the highly leached nature of the rocks directly beneath the peneplain surface. The deposition of the Brunner Coal Measures on top of this surface began in the early Tertiary. A gradual marine transgression began in the early Eocene and resulted in interbedded freshwater and marine beds within the Brunner Coal Measures and the conformably overlying Kaiata Formation (figure 1.3). The development and reactivation of small local basins also influenced the sedimentation during this period (Nathan *et al.*, 1986). The basins were controlled by the 'Challenger Rift System' which caused 2 to 4km deep troughs and half grabens in western New Zealand between the middle Eocene and late Oligocene (Kamp, 1986). The rift system allowed New Zealand to split away from Australia and later became the Tasman Sea (Nathan *et al.*, 1986). The sea had completely covered the area by the middle of the Oligocene, as shown by the Landon Series Cobden Limestone and Pareora Series which consist of mainly fine calcareous sediments (Suggate, 1957; Nathan *et al.*, 1986).

The Grey-Inangahua Depression trends north-east, south-west and provided a new area for sediment accumulation during the upper Tertiary (Suggate, 1957). With the return of tectonic activity, freshwater clastic sediments were deposited in the upper Miocene (Southland and Taranaki Series). The Reefton area must have been near sea level at this time as further widespread marine deposits were laid down in the Pliocene and there is no evidence of erosion of older sediments (Nathan, 1986; Suggate, 1957).

1.4.1.4 Quaternary

The early Pleistocene brought a change from locally derived sediments deposited in narrow troughs to a massive influx of gravels (Upper Wanganui Series). This was due to the rapid rise of the Southern Alps caused by the development of the Australian-Pacific plate boundary in the late Cenozoic (Walcott, 1998), and the beginning of glaciation, both of which supplied sediment to adjacent basins. During the Pleistocene the supply of sediment was greater than the rate of subsidence, and therefore a broad piedmont alluvial gravel plain was created in the northern half of the West Coast (Nathan *et al.*, 1986). The gravels continued to dominate deposition until the Paparoa Range rose by high-angle over-thrusting along the Paparoa Tectonic Zone (Laird, 1968) and the Victoria Range rose as the continental crust continued to shorten. This cut off the supply of alpine gravels to the Reefton District. The Inangahua River was also forced to diverted part of its flow parallel to the ranges. The topography created by the rise of the ranges and river was altered by three periods of glaciation during the late Pleistocene. The glaciers left moraines and outwash gravels throughout the Reefton area, which were terraced by down-cutting rivers between glaciations, as shown in figure 1.3 (Suggate, 1957).

Figure 1.3 Regional scale geology map.

1.4.2 Stratigraphy of Reefton Coal Field

The best description of the stratigraphy within the Reefton Coal Field is given by Suggate (1957). The following account covers details of the stratigraphic units found in Reefton Coalfield, and specifically the Terrace Mine area from published accounts and the author's own field observations. Figure 1.5 provides a geological map adapted from Suggate (1957) and figure 1.4 summarises the following information in a stratigraphic column. Detailed geological and engineering geological descriptions of Brunner Coal Measures are given in Chapter 2.

Figure 1.4 Stratigraphic column for Reefton Coalfield adapted from Boyd (2002). Coal thickness derived from drill holes within the Reddale Valley.

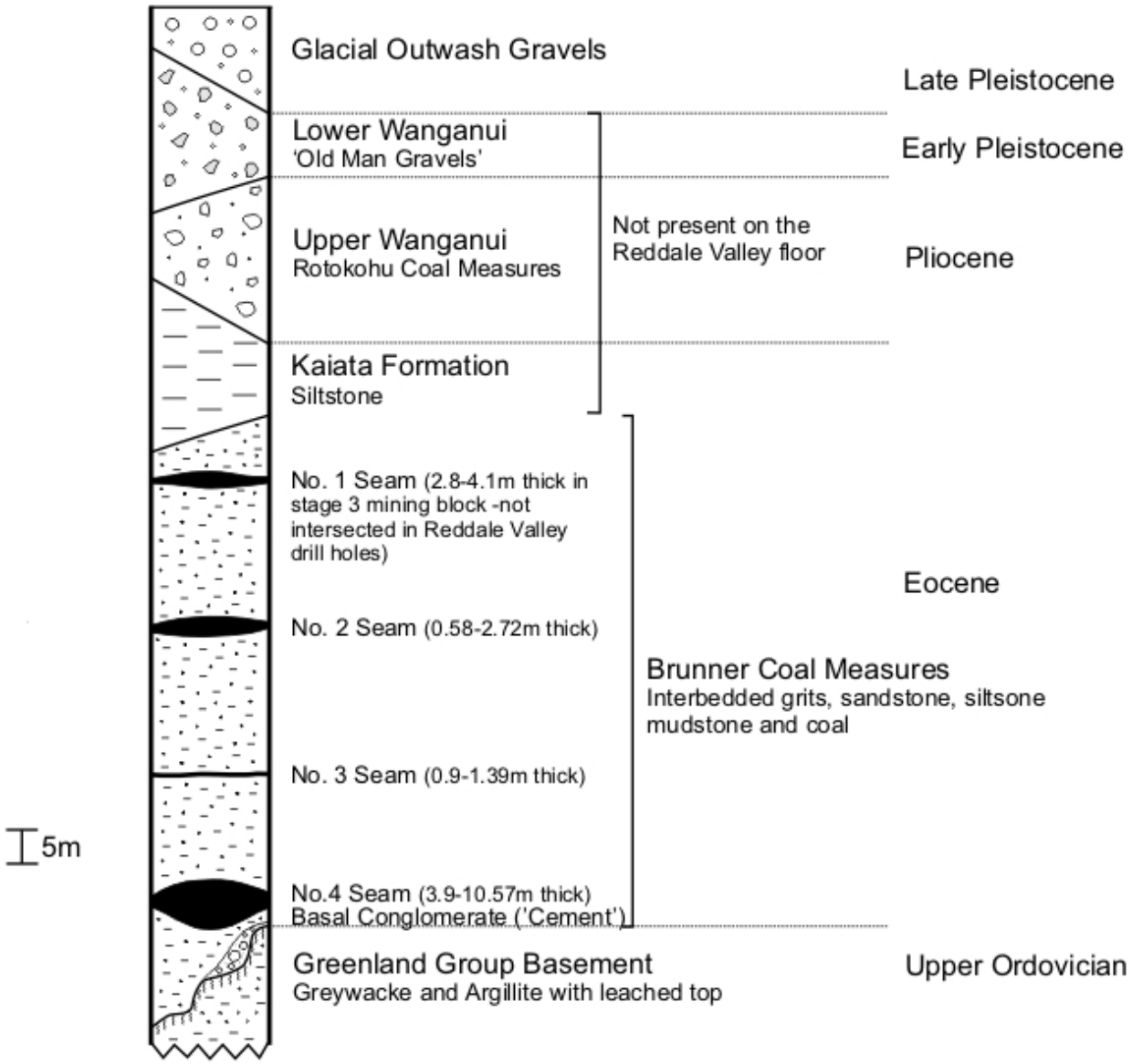

Figure 1.5 Geological Map.

1.4.2.1 Greenland Group (Upper Ordovician)

Suggate (1957) used the term 'Waiuta Group" to differentiate between structural regimes within the Greenland Group. Laird (1967) showed that within the Paporoa Tectonic Zone those classed as Waiuta Group had undergone the same amount of deformation as the rest of the Greenland Group and were most likely deposited at the same time. K-Ar whole rock ages given by Adams *et al.*, (1975) also showed no significant age difference and they are therefore refereed to as Greenland Group rocks throughout this report.

The Greenland Group forms the basement and is composed of extremely well indurated sandstone and mudstone. The sandstone, often referred to as greywacke, is normally medium grained and composed mainly of angular quartz and feldspar with some beds being highly micaceous. The high mica content suggests that it has been exposed to low grade metamorphism. It often displays a complex joint pattern and unless it is bedded with mudstone, establishing the dip direction is difficult. The mudstone or argillite is greenish grey in colour, has a sheen created by similarly orientated mica and often displays a fracture cleavage (Suggate, 1957).

The substantial period of weathering which occurred before deposition of the Brunner Coal Measures is indicated by the top of the Greenland Group being deeply leached (Fowke, 1998). The rocks have been softened and minerals "rotted" by infiltrating waters (Suggate, 1957). In the Reddale Valley drill core (figure 1.6) it often resembles a pale grey siltstone with a 'talc' or waxy feel, and may have a conglomerate texture induced by shearing (A. Field, Consultant Geologist, pers. comm., 2005)

Figure 1.6 Core photo of basement siltstone in Reddale Valley courtesy of Adrian Field.

1.4.2.2 Brunner Coal Measures (Eocene)

A thin basal conglomerate containing Greenland Group cobbles and quartz pebbles is often present in the Reefton Coalfield (Fowke, 1998). This is locally known as 'cement', and contains a significant amount of gold and associated minerals (Suggate, 1957). The majority of the Brunner Coal Measures (BCM) in the Reefton district consists of alternating and sometimes intermixed beds of grits, sandstone, siltstone, mudstone and coal. The absence of distinct and laterally continuous beds prevents correlation, but the coal measures are generally similar throughout the area (Suggate, 1957).

Henderson (1917) suggested the lower part of the coal measures were beach deposits with iron-rich blacksand creating the 'cement' below. Suggate (1957) however disputes this and proposes that they are fresh-water beds, as indicated by the preserved leached surface and the discovery of fresh-water mussels in several places. The upper part of the coal measures contain interbedded marine and non-marine, deposits as marine fossils have been located in the Reddale Valley below the upper coal seams (Suggate, 1957). The marine influence results in a higher sulphur content of the upper coal seams (Fowke, 1998). The thickness of the Brunner Coal Measures increases toward the northeast, and is approximately 120 metres in the Terrace area where they have not been subjected to erosion (Suggate, 1957).

1.4.2.3 Kaiata Formation (Eocene)

Beds belonging to the Kaiata Formation rest conformably on top of Brunner Coal Measures where the top has not been eroded. The boundary between the top of the coal measures and the bottom of the Kaiata Formation beds is difficult to define in places where the upper seams are not present, as the marine siltstones are very similar (Fowke, 1998). Throughout the Reefton Coalfield the Kaiata beds vary in lithology, and none can therefore be called typical. They include glauconitic and/or carbonaceous siltstone, conglomerate (in the north), muddy sandstones, marine fossils and some coal. In the Burkes Creek area however, calcareous and carbonaceous muddy siltstone with concretions, glauconite and some fossils has been recorded (Suggate, 1957). The Kaiata beds observed on the south east side of the Reddale Valley and in the neighbouring Peerless Gully by this author were highly weathered, cream/tan coloured siltstone containing iron and some glauconite. Originally more than 600m would have been present in the Terrace Mine area, but only basal remnants (less than 100m) remain today (Fowke, 1998).

1.4.2.4 Lower Wanganui Series/Rotokohu Coal Measures (Pliocene)

The erosion, which removed any sediment deposited during the Oligocene and Miocene, created a low-relief skyline on the eastern edge of the Grey-Inangahua Depression. It is from this surface that the Wanganui beds were stripped during the Pliocene. The succession of beds in the Reefton Coalfield is clearly illustrated in the cliffs beside the Waitahu River near Gannons Bridge (Figure 1.7), and shows that the Wanganui beds are derived from units lower in the sequence. The cliffs exhibit coarse, white quartz sand grading into leached Greenland group sandstone fragment conglomerate and lignitic wood in the basal beds. This is followed by conglomerate and sand derived from fresh Greenland Group sandstone and bright coal fragments (BCM-derived) in a granite sand matrix. This unit can be seen in the farm track cuttings on the north east end of the terrace in the Reddale Valley. A grey siltstone with lignite bands then passes into silty sandstone and fine granite fragment conglomerate (Suggate, 1957; Sykes, 1987).

Figure 1.7 Photograph showing the Lower Wanganui Series in the cliffs near the Gannons Bridge.

1.4.2.5 Upper Wanganui Series/Old Man Gravels (Early Pleistocene)

There is a sharp but conformable contact between the lower and upper Wanganui Series. The majority of the Old Man Gravels is conglomerate, with minor bands of sandstone, siltstone and lignite (Sykes, 1987). In the Reddale Valley beds of fine-grained mica-rich sandstone and a light brown mica-rich siltstone has been noted by this author on the northern end of the terrace. The pebbles, cobbles and small boulders in the conglomerate are mainly composed of leached and softened schist with minor granite and indurated sandstone, having an overall distinctive rusty brown colour. The amount of schist decreases upwards, while the coarseness increases. The schist probably originated from a source east of the Alpine Fault and was transported west before the rise of the ranges. The maximum thickness is estimated at 1500m (Suggate, 1957).

1.4.2.6 Glacial Gravels (Late Pleistocene)

Three stages of glaciation have resulted in the underlying units being unconformably overlain by glacial outwash gravels. In the initial 'Piedmont' glaciation during the late Pleistocene, ice extended over most of the Reefton District. In the 'First Valley' glaciation ice formed glaciated valleys as far as upper ends of the gorges of Ingangahua and Waitahu Rivers. The 'Second Valley' glaciation was much smaller than the first two (Suggate, 1957). During the interglacial and post-glacial periods river down-cutting created three corresponding levels of terraces (Sykes, 1987). The terrace that separates Reefton Township from the Reddale Valley was formed after the Piedmont Glaciation and is capped by the associated gravels. Reefton Township and Reddale Valley are located on Second Valley glacial gravels (figure 1.5) while the terrace created following the First Valley Glaciation can be seen in the area north of Reefton Township (Fowke, 1998). Figure 1.8 shows a cutting through these gravels created by the creek on the Reddale Valley floor. The size ranges from coarse pebble to cobble with occasional boulders and the orange colour seen lower down is surface river staining.

Figure 1.8 a) Photograph of Burkes Creek cutting, Reddale Valley. b) Close up of glacial gravels.

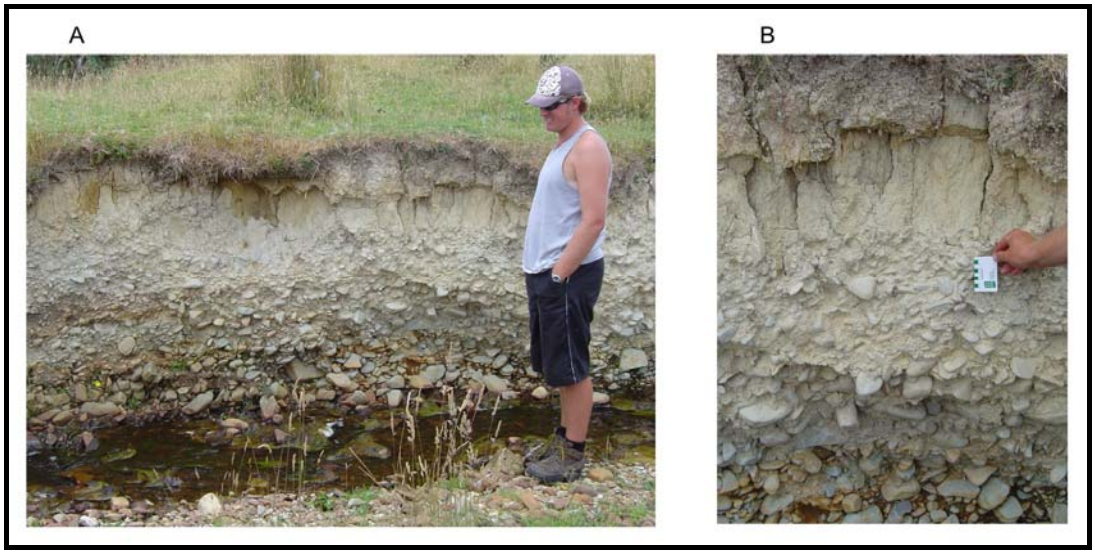

1.4.3 Active Faults

Reefton and the Reddale Valley are in reasonably close proximity to several active large scale faults as shown in figure 1.9. The Alpine Fault is only 40-50 km away to the east and geological evidence suggests it has produced earthquakes in the South Island of MM (Modified Mercalli Intensity scale) 8 or 9 in times before European settlement. The large ruptures along the fault have occurred at intervals of 100 to 300 years and as the most recent took place around 1720, a major earthquake should therefore be expected to occur some time in the next 15 to 20 years.

Due to the serious affect such an earthquake would have on the whole of the West Coast, the Alpine Fault is continuously monitored (Fowke, 1998).

The south end of White Creek Fault trace is approximately 12km southeast of Reefton Township, figure 1.9. Although the southern section has not been historically active, a magnitude 7.6 earthquake was recorded on an 8km section (40km northeast of Reefton) during the 1929 Murchison Earthquake (Fowke, 1998; Smith and Berryman, 1986). This displayed reverse (with a component of sinstral movement) and displaced man-made structures, including the West Coast Highway, as well as gravel outwash terraces created by the Buller River (Berryman, 1980). The displacement has been measured at 4.6m vertically and 2.4m horizontally, and the fault dips to the south east (Smith and Berryman, 1986).

The Inangahua Fault lies at the base of the Paparoa Range and is northwest of Reefton, parallel to the White Creek Fault as illustrated by figure 1.9. A magnitude 7.1 earthquake took place in 1968 and is the most recent severe earthquake experienced by New Zealand (Smith and Berryman, 1986). The rupture was almost purely reverse in nature, with a north-west dip and more than 4m of displacement occurring (Anderson at al, 1994).

The Lyell Fault is parallel to and between the Inangahua and White Creek Faults, figure 1.9. It is also a reverse fault and dips to the south east (Anderson at al, 1994). The Maimai Fault also bounds the Paparoa Range and has a similar trend as the other reverse faults. The Giles Creek Fault and Rotokohu Fault are also in the area surrounding Reefton, but exhibit normal faulting and a more easterly trend (Institute of Geological and Nuclear Sciences Limited Website, 2005). Recurrence intervals of 3000 to 10,000 years for surface faulting have been estimated for this region (Smith and Berryman, 1986).

The district is therefore currently active in seismic terms. Reefton falls within the Greymouth QMAP area (new national 1:250000 geological map series), which as a whole has experienced moderate to high levels of seismic activity in the last 150 years. It is has been predicted that the area may encounter a MM 7 event on average every 15 years, and a MM 8 event every 21 years. These would produce substantial ground shaking, several aftershocks, slope instability and potential surface rupture (Nathan *et al.*, 2002). The possibility of a severe earthquake occurring within the mine's life needs to be considered when designing the opencast and any other surface features, such as screening plants, settling ponds and ELFs (Engineered Landforms).

Figure 1.9 Map of active faults near Reefton, adapted from Greymouth QMAP.

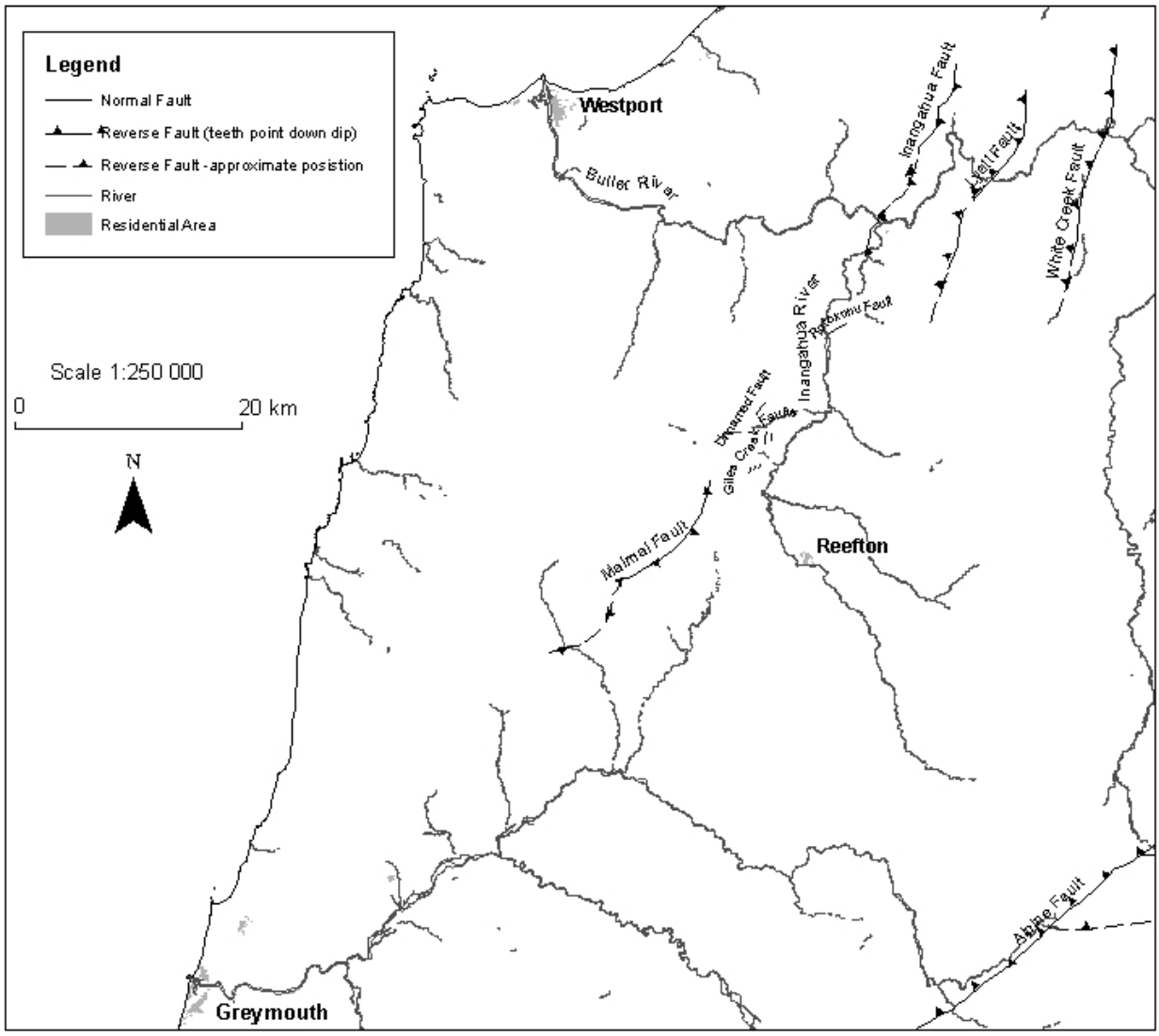

1.5 Reefton Coal Field

1.5.1 Coal

Although Terrace Mine coal is generally high in sulphur it is successfully blended with coal from other mines and is important to supplying South Island industrial customers. Six coal seams are recognised throughout Reefton Coalfield and are numbered 1 to 4 (from top to bottom), with splits in No. 1 and 2. No. 4 seam is the thickest, most laterally extensive, best quality coal, and is currently being extracted at Terrace Mine. Although the seams above may be encountered, No. 4 is the primary target for opencast mining as apart from No. 2 seam they are likely to be too high in sulphur and of insignificant thickness, being less than 2m (Stone *et al.*, 2005). This section therefore outlines details of No. 4 and No. 2 seam (where possible) only.

1.5.1.1 Coal Thickness

The No. 4 seam is known to vary in thickness in the Reddale Valley. From where it has been eroded by fluvial activity up-dip it can be less than 0.5m and thickens generally down-dip to approximately 12m (Stone *et al.*, 2005). The holes drilled by Solid Energy 2004/2005 (653-663) on the Reddale Valley floor show a variation of 3.9 to 10.57 m, with an average of 7 m thickness. The No. 4 seam varies in depth from approximately 10m in the south of the valley to 70 m further north and may increase up to around 140m. This is due to the 15 to 25˚ dip of the seam towards the northwest. The base of the No. 4 seam is generally within 2 to 3m of the basement, and there is no indication of splitting within the Reddale Valley area (Stone *et al.*, 2005).

No. 2 seam is consistently some 50m above No. 4 seam. It ranges from less then 0.5m to around 11m in thickness within the Reddale Valley. Very few drill holes intersect the seam, and therefore little is known of the resource. So far there has been no evidence of the splits that are known to occur in other parts of the Reefton Coalfield, but a number of partings have been observed (Stone *et al.*, 2005).

1.5.1.2 Coal Quality

No. 4 seam is classified as sub-bituminous B to A rank and is suited to domestic-type boilers due to being low in ash, non-swelling and with acceptable sulphur levels. Coals of this rank also produce a high burnout in combustion (Boyd, 2002). Analysis of coal drilled from the Reddale Valley indicates a block average ash content of 3.8%, with a range of composite ash content from 2.5 to 7.5% air dried bases (adb). Average sulphur content within the area has been obtained at approximately 1.18%, with a significant variance of 0.71 to 1.62% adb. However the average run-of-mine sulphur would decrease to 1.06% when pyrite-derived sulphur was removed from the coal by washing (Stone *et al.*, 2005). This is significantly lower than the current Terrace Mining Block 3 which ranges from 0.7 to 2.3% total sulphur (Boyd, 2002). A total moisture content of approximately 20% and inherent moisture of approximately 11% are assumed from the Stage 3 mining black at Terrace, as is a calorific value of approximately 25 Mj/kg (adb). Trace element analysis of Reddale Valley coal is currently being interpreted (Stone *et al.*, 2005).

1.5.1.3 Coal Resource

The data from the 2004/2005 drilling programme has been input into the modelling programme Vulcan and has indicated a resource of approximately 800,000 tonnes for seam No.4 (Stone *et al.*, 2005).

1.5.2 Depositional Environment of Brunner Coal Measures

The Brunner Coal Measures of the Reefton and Garvey Creek Coalfields were deposited in the Reefton Basin during the Eocene. Evidence for the existence of a basin is provided by scattered sequences but the exact shape is unknown and it is inferred to be roughly circular shape. The basin covered an area of approximately 80km^2 and minimal sediment accumulated in the surrounding land outside the basin. The substantial thickness of the BCM in the Reefton Basin is attributed to rapid local subsidence accompanied by some uplift of the basin margins (Nathan *et al.*, 1986). The thickness and splitting of the coal seams was also influenced by this tectonic subsidence (Titheridge, 1992).

In keeping with other thick basin sequences the BCM in the Reefton Basin is dominated by fluvial sand with a lesser amount of carbonaceous mudstone and coal. The presence of coarse, poorly rounded sand grains indicate granite and gneiss of the nearby Paparoa and Victoria Ranges as the source rocks. The weathering of these Pre-Tertiary rocks would have contributed enough quartz and possibly muscovite, and been close enough to create the sandstone units of the BCM. The source area must have been sufficiently exposed at this time to enable stripping of the deeply weathered mantle, but not great enough to provide large quantities of unweathered detritus. A network of streams would have transported the sediment into the basin (Nathan *et al.*, 1986).

The numerous and occasionally thick mudstone units indicate a meandering stream system on a relatively broad fluvial plain (Titheridge, 1992). Most BCM coal accumulated in peat swamps which were dominated by reed and small herbaceous vegetation with scarce trees (Nathan *et al.*, 1986). The substantial thicknesses of Reefton coals indicate a backswamp peat environment (Titheridge, 1992).

1.5.5 Structure

The major large-scale structure that affects the Reefton Coalfield is the Mawheraiti Syncline, which is approximately 10km wide and 80km long. The syncline forms part of the Grey-Inangahua Depression, and is asymmetrical with a steeply dipping north-western limb caused by

movement related to the Maimai Fault during the Pleistocene (Suggate, 1957). Reefton Coalfield, however, lies on the part of the south-eastern limb and the coal measures here dip at around 15-25˚ to the northwest. In the Terrace mine area they are the least tectonically disturbed of the coalfield (Fowke, 1998).

Small-scale faults in the Terrace area are generally first discovered in underground workings with no observable surface trace. Those mapped are all normal dip-slip faults with vertical displacements of less than 10m. Most trend towards the northeast (or north-north-east such as the Central Fault), and are downthrown on their northwest side. Fowke (1998) suggests the faults originate from local tension during uplift of the Victoria Range, especially as they trend sub-parallel to the strike of the coal seams.

The most significant fault in relation to the proposed opencast is the Burkes Creek Fault, which extends from the current Terrace mining panels across the Reddale Valley. The fault was encountered in the New Ferndale Opencast at the maximum down dip extent (now infilled with water), and has a down throw of approximately 6m to the northwest (Stone *et al.*, 2005). Parallel and with the same sense of movement the Morrisvale Fault to the north and Reddale Fault to the south are also believed to trend beneath the valley floor within close proximity to the proposed opencast. The Morrisvale Fault is known to change along its length into a steep monocline without interrupting the coal seam (Fowke, 1998).

Underground workings at Terrace Mine often experience small ‘step-up’ faults with approximately 0.5m of displacement down the dip of the coal seam. They may be monoclines, rolls or folds with axial shearing that do not fracture the seams (Boyd, 2002). The faults are considered to be related to the larger faults and also caused by uplift and should be expected in the Reddale Valley (Fowke, 1998).

The present drilling data is not able to provide enough detail for reliable fault modelling but faulting is not expected to cause significant problems in the proposed opencast (Stone *et al.*, 2005). Structure contours of the No. 4 seam produced in areas mined and explored in Reefton Coalfield show a uniform and regular seam structure (by New Zealand standards) with little faulting and local seem steepening (Fowke, 1998).

1.5.6 Coal Mining History

Coal mining in the Reefton district arose from the demand of the gold-mining industry for cheap local fuel. As the gold-mining companies often owned the coal mines they used haphazard uncomplicated mining methods to extract as much coal as was needed at the time. The many separate leases on old plans show that little attention was given to geological structure when establishing boundaries. This resulted in unsystematic mining practice, especially as several small mines opened and closed as market conditions altered between 1920 and 1940. World War Two brought a more stable economy and greater demand for coal, which resulted in the redevelopment of the coal mining industry (Suggate, 1957).

State Coal Mines (SCM which later became Coal Corporation and then Solid Energy Ltd) became involved in Reefton district in the 1940's to produce household coal, to stop extremely high wastage caused by private mines, and to ensure the continuation of production in the Reefton Coalfield as operations were unprofitable unless worked up-dip. While the original focus was on the Garvey Creek Coalfield, SCM acquired many of the existing private mines and licences over time in the Reefton Coalfield. The largest state-owned mine was the Burkes Creek Mine, which produced a total of 830 000 tonnes (Sykes, 1987). Underground mining methods were used until the coal was exhausted, then private companies undertook opencast mining of the shallow coal (Fowke, 1998). Opencast mining, which also began in the 1940's, was on a relatively small scale and lacked planning, targeting the easily-won coal only (Suggate, 1957).

Early mining consisted of bord and pillar mining methods, with the bords being driven as wide as the strata would permit. Most were abandoned before reaching the end of extractable coal and collapsed after the timbers rotted away (Suggate, 1957). Production in the Reefton Coalfield reached a peak around 1952 with an output of approximately 110,000 tonnes in that year, and then declined as 'easy to mine' reserves were exhausted and further exploration was not undertaken. Although hydromining became the dominant underground method around this time, it did not solve problems with pressure increases at depth and spontaneous combustion, and therefore failed to lift production (Fowke, 1998).

1.6 Terrace Mine

1.6.1 Terrace Underground Mine

Coal mining has taken place in the Terrace area (between Reefton Township and the Reddale Valley) for over 120 years. Solid Energy now possesses almost 153 hectares of permits and

licences within the area. The current underground mine uses standard bord and pillar methods, but the 20 by 20 metre pillars are split by 2 metre roadways to the rise and the coal is transported by water (Fowke, 1998). A significant number of rock bolts and mesh sheets are used to control rock spalls. Coal is left above and below the roads to prevent floor heave and roof collapse (G Almond, Mine Geologist Spring Creek, pers. comm., 2005). The coal is mined using a low-pressure monitor and is dewatered and screened at the surface, near the entrance portal which is currently on the edge of Reefton Township. It is then transported by truck to Solid Energy's rail load-out facility some 2km north of Reefton. Terrace Mine has now produced more than 800 000 tonnes of coal, and has been the only financially profitable mine owned by the state in the Reefton Coalfield (Fowke, 1998).

1.6.2 Reddale Valley

There are a number of existing abandoned mines in the Reddale Valley as shown in Map A (Engineering Geological Map –see map pocket). The Reddale Mine (No. 2 Seam) was purchased from the Halloran family by CoalCorp in 1996. It included the mining permit and mining licences, as well as several buildings which have since been removed (J. Foster, Reefton Surface Operations Manager, pers. comm., 2005). As part of the mining permit water rights were obtained for 20 years from 1993. This allows for the removal of up to 100 000 litres/day for coal washing, and the discharge of the same amount of settled effluent into Burkes Creek (Henley, 1995). The licences apply to underground mining only, and the mine has never been worked by Solid Energy.

"Old" Terrace Opencast mine today consists of a three bench pit with cut faces on the west and south sides, as shown in figure 1.10a. This opencast was operational from 1989 to 1993 and utilized coal remaining from the Empire Underground Mine (Fowke, 1998). It is currently being used to store very fine coal and is surrounded by filled ground (overburden stockpiles) that forms a dam around the excavation on the eastern side. Water from the slopes drain into the abandoned underground workings beneath the pit (Sleight, 2003). Terrace Opencast ('new' opencast) extends south from the old pit along the ridge line (figure 1.10b). It won left coal from the "Terrace Coal Party" underground and Halloran's Mine in the south, and was operational until 1998 (Fowke, 1998). Coal was excavated in the opencast from relatively shallow depths and overburden side cast forming a bank at the base of the cut (Sleight, 2003). The proposed Engineered Landform (ELF) for overburden would fill these existing opencasts and continue upwards towards the top of the terrace (Stone *et al.*, 2005).

Figure 1.10 a) Photograph of 'Old' Terrace Opencast and b) Photograph of the south end of the Terrace Opencast.

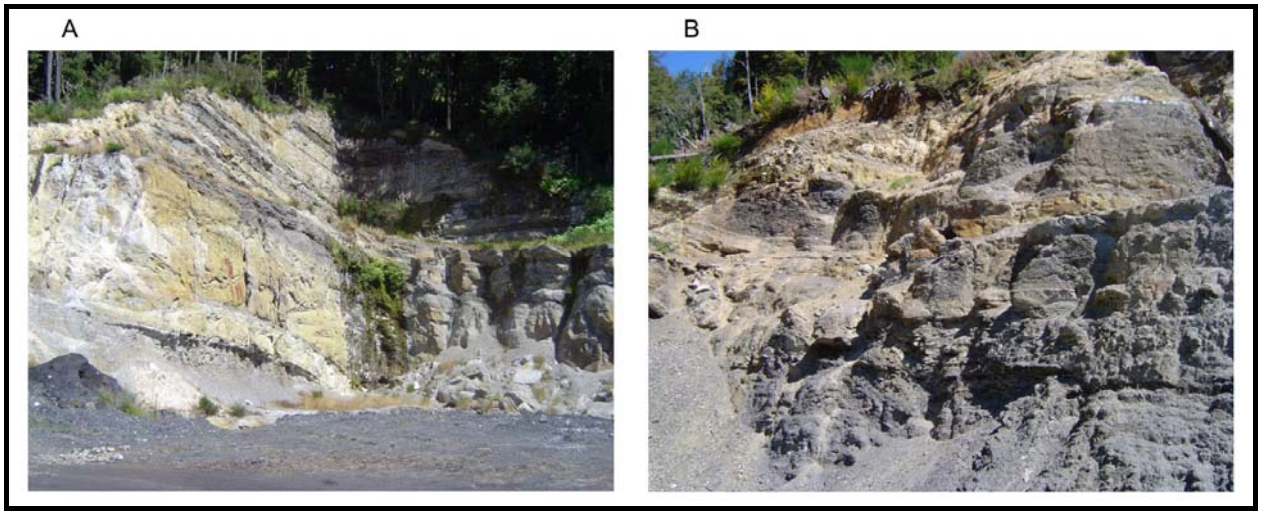

The New Ferndale Opencast on the opposite side of the valley (northeast) was originally owned by Mullken Mining Ltd, but ceased operations in the mid 1990's (J. Foster, Reefton Surface Operations Manager, pers. comm., 2005). The most prominent feature today is the pond which occupies the deepest part of the No. 4 seam workings, as shown in figure 1.11 (Fowke, 1998). The pond has a pH level around 3 and collects water from the surrounding waste piles (Hewlett, 2003). No. 2 seam was opencast along the ridge line to the north of the pond, which is also where the underground entrance was located. Ferndale Opencast follows the ridge line to the east and mined No. 4 seam (Sykes, 1987). The hills on this side of the valley contain many underground workings including the extensive Burkes Creek Mine. No underground mining has occurred under the Reddale Valley floor (Stone *et al.*, 2005).

Figure 1.11 Photograph of pond infilling the deepest part of the New Ferndale Opencast.

1.7 Previous Geotechnical and Geological Investigation

Several past thesis studies have analysed rock material parameters of units within the Brunner Coal Measures. None have focused on the Reefton Coalfield, although the study by Lucas (2002) in the Garvey Creek Coalfield is in close proximity, it is however in a more tectonically disturbed area. Harris (2002) did conduct rock material index tests on samples from Terrace Mine, but these were all within the coal bed rather than the overburden. Table 1.3 summarises the ranges found for rock material properties by four of the most recent projects.

Table 1.3 Summary of findings from recent geotechnical projects (ss = sandstone, zs = siltstone).

Author, year	Pehi, 2004	Lucus, 2002	Coote, 1991		Kennedy, 1988
Area	Cypress Nth Block	Island Block	Webb Block		Cedar Creek
Coalfield	Buller	Gravey Creek	Buller		Buller
Unit	Bioturbated ss	Four sandstones	Two sandstones	Fine ss/zs	Two sandstones
Porosity (n) -%	7.9	3.4 - 10.6	7.06 - 11.4	5.91	7.37 - 14.31
Void ratio (e)		0.03 - 0.12			0.08 - 0.17
Dry density -kg/m3	2411	2290 - 2560	2250 - 2380	2460	2220 - 2380
Saturated density -kg/m3	2489	2400 - 2590			2360 - 2450
Slake-Durability (Id2) -%	94	65 - 98.8	61.65 - 81.25	89.8	70.13 - 95.73
UCS -MPa	15.27	21.2 - 52.1	26.97 - 48.17	43.82	18.8 - 42.6
σci (intact/triaxial)-MPa	7.8	24.5 - 58.8			
Cohesion -MPa	2.1	5.7 - 14.3			
Friction angle -Degrees	33.2	37.7 - 47.1			
Young's Modulus (E) - GPa			8.6 - 18.8	10.9	12.20 - 15.70
Poisson's Ratio (v)			0.13 - 0.17	0.23	0.13 - 0.23
Point Load (Is)			1.33 -1.92	7.92	4.36 - 1.46
Unit		Mudstone	Mudstone		Mudstone
Porosity (n) -%		2	2.56		4.67
Void ratio (e)		0.02			0.05
Dry density -kg/m3		2570	2490		2440
Saturated density -kg/m3		2590			2480
Slake-Durability (Id2) -%		98.5	97.93		96.75
UCS -MPa		60.8	50.15		30.5 - 51.4
σci (intact/triaxial) -MPa		52.1			
Cohesion -MPa		15.8			
Friction angle -Degrees		34.8			
Young's Modulus (E) - GPa			13		21.1
Poisson's Ratio (v)			0.26		0.24
Point Load (Is)			15.27		6.37

The report prepared for Solid Energy by Fowke (1998) focuses on Terrace Underground Mine, but is a very thorough and comprehensive geological assessment. The geotechnical section includes the results from UCS tests of eight mudstone and two sandstone samples from a drill hole (615) on the Reefton side of the terrace. The mudstone produced a range of strengths from

4.2 to 7.2 MPa, and the sandstone produced 5.3 MPa and 57.7 MPa from a calcite cemented specimen. The report suggests the use of triaxial testing, as well as a wider range of geotechnical tests would be beneficial as part of future drilling programmes.

A study has recently been conducted by Solid Energy (Stone *et al.*, 2005) on the prospect of an opencast in the Reddale Valley. It covers environmental factors, geology, mine planning and procedure, coal processing, financial and non financial aspects. The geotechnical section includes hydrogeology, rock property data from this author and suggests potential pit slope designs. These will be tested by kinematic analysis of failures based on scanline data in this project to determine optimum high wall design.

Despite the large amount of literature on various types of 'case hardening agents' and weathering that increases the strength of the outer rock crust, there is little that directly relates to the situation found in the Reddale Valley and nearby Peerless Gully. Most research concentrates on arid climates and specifically desert varnishes. The most comprehensive study is by Dorn (1998) in which much of the past research completed has been assess and re-addressed by means of a mainly microscopic approach. He includes lithobiontic coatings, case hardening agents, dust films, iron films and silica glaze. In relation to iron films he notes that "The present knowledge is so poor that we need more well-controlled case studies, more research on specific types of iron films, and a better understanding of the interaction between mineralogy and environmental controls" (Dorn, 1998; page 144). A more detailed literature review, outlining aspects of case hardening relevant to the Reefton environment, is given in chapter 5.

1.8 Investigation Methodology

Several stages of investigation were necessary to determine the geotechnical issues facing a proposed opencast mine in the Reddale Valley. The approaches are briefly outlined in the following section.

1.8.1 Literature Review

The research began with a desk study of relevant background information pertaining to the study area, and included details of the location, geology of the region and specific geology of the Reefton Coalfield, the coal resource and coal mining background. Information was gained from published sources as well as internal Solid Energy reports, and included maps and aerial photos of the area. Suggate (1957) provided most of the geological background while past and current mining practise was largely taken from Fowke (1998).

1.8.2 Field Work

Initial field work involved checking lithological boundaries from existing geological maps with the aid of a handheld GPS. Scanline surveys where undertaken on both sides of the valley to enable prediction of defect patterns when excavating the valley floor. These were later accurately surveyed. Drill core was collected for laboratory testing and the water table measured in open bore holes. Different types of 'case hardening' were observed and six locations were selected for analysis and sampling.

1.8.3 Rock Material Parameters

Both physical and mechanical properties of the Brunner Coal Measures overburden was assessed by means of laboratory testing of drill core. The samples were divided into four lithological units and compared in terms of rock material behaviour. The physical tests chosen where porosity, density and slake-durability, which gave indications of strength and weathering properties. The mechanical tests included unconfined compressive strength, point load, triaxial, sonic velocity and shear box testing.

1.8.4 Rock Mass Properties

Eight discontinuity scanline surveys were completed with a total length on 221.93m. They were completed along walls with different orientations, which reduces sampling bias, and on both sides of the valley to include any large scale structural deformation. The properties recorded include defect type, defect orientation, spacing, hardness, strength, persistence, aperture, infilling and roughness. Drill core records were assessed to give an indication of rock quality and pump test data for the outwash gravels was analysed by graphical methods. From this the rock mass properties were determined to provide a prediction of what might be expected to occur in the highwall of an opencast on the valley floor.

1.8.5 Kinematic Feasibility Analysis of Potential Defects

Kinematic feasibility checks on proposed orientations for the highwall, were performed for planar, wedge and toppling type failures. Stereographic methods were applied to the defect data gained from the scanline surveys, in the Dips computer programme (Rocscience, 2004). An optimum orientation is suggested and any likely failures are discussed as well as other slope stability considerations.

1.8.6 Case Hardening Investigation

A description of the location of each type of case hardening was completed in the field and hand specimens carefully collected. A reflected light microscope and hand lens enabled detailed descriptions of the samples. Thin sections for analysis by polarised microscope were prepared, as well as polished thin sections for the scanning electron microscope (SEM). Stubs of the top and a cross section of the samples were also prepared, and coated with gold or carbon for use with a backscattered detector and energy dispersive spectrum (EDS). The surface was also scraped off and analysed by x-ray diffraction (XRD) for minerals present.

1.8.7 Production of Accompanying Maps

The data gained from the different aspects of this project was used to produce an engineering geological map of the Reddale Valley (Map A). The pit outline indicates the top edge of the opencast and filled land is defined as overburden dumps from abandoned opencast mines. Drill hole data and kinematic feasibility assessment was used to create cross sections through the site of the proposed pit (Map B). The faults are assumed to be near vertical from underground observations and their locations are approximated from where they have been intercepted underground. An aerial photograph shows the location of the proposed opencast and sample sites selected for the case hardening investigation (Map C). All three maps are found attached to the thesis in the map pocket at the back.

1.9 Thesis Format

Chapter 1 has provided a general background and outlined the objectives of the project. A literature review of the geological setting, coal field and mining history and previous work undertaken has been presented. On overview of the methods used to approach the geotechnical investigation was also included.

Chapter 2 presented the results from an extensive laboratory testing programme to characterise the rock material that will form the proposed highwall. After division into geotechnical units the core samples were tested to determine physical and mechanical parameters, which are summarised in table form in the chapter synthesis. The theory behind each rock strength test is discussed in the text and methods are presented in appendix 1.

Chapter 3 describes the rock mass properties determined by analysis of scanline defect surveys conducted on existing highwalls. The orientations of the defects suggest variations between the

data collected in the southwest compared to that in the northeast of the valley. The data is therefore assessed according to location were deemed necessary. This chapter also includes assessment of rock quality from defects recorded in drill core and analysis of pump test data to determine hydrological parameters of the overlying gravel aquifer.

Chapter 4 provides the kinematic requirements for different types of failures to occur, methods used and results for the southwest and northeast scanline data. A discussion of the findings and other slope stability considerations is included. Those factors deemed crucial to producing adequately stable pit walls are summarised at the end of the chapter.

Chapter 5 is a case study of possible rock coatings providing protection from weathering found in the area. The methods are explained and results from six sites discussed and categorised in terms of the components creating the outer 'crust'. A photographic study investigates formation rates and implications for opencast mining.

Chapter 6 summarises the previous chapters and outlines the conclusions made for the engineering geological aspects investigated. Suggestions are made as to further geotechnical research needed to advance towards establishment of the opencast mine. An engineering geological map, cross sections and an aerial photograph are attached to the thesis (map pocket).

Chapter 2

Rock Material Characterisation

2.1 Introduction

It is important to be able to predict rock behaviour when embarking on any engineering project, especially one that involves both material removal and continuing slope stability. Duncan (1969) defines 'rock material' as an aggregate of mineral particles and voids that may be isolated or interconnected, and air or water-filled. It is synonymous with the term 'intact rock' which specifically refers to rock containing no discontinuities (Johnson and DeGraff, 1988). It is essential to remember how highly variable rock is compared to synthetic engineered materials normally used in construction, such as concrete or steel (Hudson and Harrison, 1997).

The rock material strength is a fundamental quantitative geotechnical property. The units tested in this project can be considered 'weak' rock, which is a term conventionally applied to material with a saturated unconfined compressive strength of between 1 and 25 MPa (de Freitas, 1993). Intact rock strength by definition is the amount of applied stress at rock failure or rupture (Johnson and DeGraff, 1988). Strength is particularly affected by the nature of the bonds or cement between particles within a specimen. Precipitated minerals can join adjacent particles and occupy the voids between particles (de Freitas, 1993).

Water also substantially influences rock strength and is known to influence the molecular structure of mineral surfaces. Although all rocks appear to lose strength when exposed to moisture, rocks that are weak to begin with are often affected considerably more (de Freitas, 1993). Anisotropy, where a material varies in different directions, is also particularly important in terms of the strength of the Brunner Coal Measures (BCM) studied. Other factors which affect rock strength include amount of fracturing, degree of compaction and induration, mineralogy, grain size and interlock between grains (Bell *et al.*, 1997). The variability encountered in mechanical properties of weak rocks makes laboratory testing crucial to performance prediction.

In this chapter core samples of BCM overburden are laboratory tested in order to classify or characterise the material. Index tests are designed so that one rock can be compared with another (Franklin and Chandra, 1972). They are however intended to be sufficiently quick and

cheap so as to be used in practical classification systems (Broch and Franklin, 1972). Comparison and correlation between tests demonstrates reliability of test results.

The physical properties tests chosen were porosity, density and slake-durability index. Porosity and density directly affect strength and deformability, and are therefore crucial to predicting and evaluating mechanical properties. Slake-durability provides an indication of performance when subjected to short-term weathering. It is well known that the effects of weathering cause significant variations in engineering properties, and durability is therefore a very important quality to assess (Bell *et al.*, 1997). Mechanical properties were determined by uniaxial or unconfined compressive strength (UCS), point load, triaxial (rock and soil), sonic velocity and shear box testing. These provided essential strength estimates as well as the determination of an angle of internal friction and cohesion, which will be used to predict the behaviour of the overburden in the proposed highwall. Sonic velocity enables calculation of dynamic elastic moduli, while shear strength is estimated from shear box testing.

Each test is outlined and the results discussed in this chapter, while raw data and methods are given in appendix 1. Tables containing details of each sample and the location of all drill holes are also provided in appendix 1.10. Where possible ISRM standards (Brown, 1981) have been adhered to and appendix 1 also stipulates, and examines any alterations or non-standard procedures used. Systems previously used to classify BCM physical and mechanical properties have been used where possible, in particular those used by Kennedy (1988) and adapted by Lucas (2002), which was based on previously published rock mechanics data for the BCM. For tests not undertaken by those authors, well recognised classifications were used.

2.2 Geotechnical Units

The field description developed by Bell and Pettinga (1983) was used to describe each member of the Brunner Coal Measures (BCM) overburden tested (see appendix 1.1 for classification). A detailed lithological description is also given. The samples were divided into units according to their lithology as determined by examination of the drill core itself, field observations and drill core logs completed by Adrian Field (consultant geologist to Solid Energy). The units are kept relatively broad to ensure sufficient samples of each unit were tested, as the BCM varies significantly over short distances in terms of percentage of sand, mud, silt and carbon content. It is also enabled enough intact drill core of each lithology to be collected and tested to produce meaningful results.

2.2.1 Engineering Geology Description

Unit 1. Slightly weathered, moderately weak to moderately strong, light greenish grey or dark brownish grey, massive or finely layered, *siltstone* with carbonaceous fragments.

Unit 2. Unweathered, weak to very weak, dark greyish brown, massive or finely layered, carbonaceous *mudstone*.

Unit 3. Slightly weathered, moderately weak to very weak, light brownish or yellowish grey, fine layers (0.5-5mm) and coarse layers (80-100mm), *sandstone* interbedded with carbonaceous mudstone.

Unit 4. Unweathered, very weak, light brownish grey, massive, loose *sandstone*.

2.2.2 Lithological Description

2.2.2.1 Unit 1 Siltstone (ZS)

The siltstone samples in unit 1 display a varied amount of carbon content. These range from massive light grey with occasional carbonaceous fragments, such as that in figure 2.1b, to dark brown with coal bands in figure 2.1a. The dominant fraction in unit 1 however, is silt and does not include intergrades with fine sand. Some samples display partially developed (not well defined) bedding parallel to carbonaceous bands, but most are massive with randomly orientated carbonaceous or coal fragments. The samples are moderate to well indurated and well sorted. The siltstone is predominantly siliceous and has a significant micaceous component (approximately 5-10%) with occasional pyrite nodules which vary from approximately 4mm^2 to 20mm^2 in area.

Figure 2.1 a) Highly carbonaceous siltstone. b) Massive light grey siltstone.

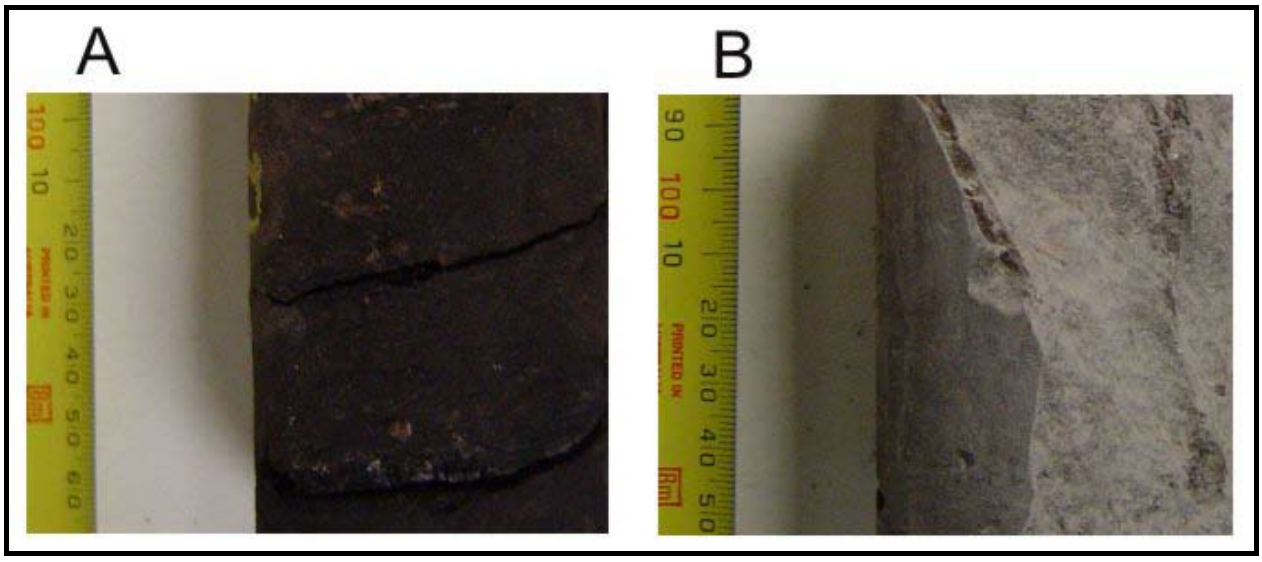

2.2.2.2 Unit 2 Carbonaceous mudstone (CM)

Samples belonging to unit 2 all display a dark chocolate brown colour due to their highly carbonaceous nature. They are poorly to moderately indurated when damp, and fissile when dry. Partially developed bedding at 10 to 20˚ to the horizontal, corresponds to carbonaceous concentration, and creates an inherent weakness along which the rock easily fails. The samples contain moderately to well sorted, coarse silt to clay with occasional sand size quartz and mica grains. Occasional lenticles of other lithologies, coal and pyrite nodules, some of which are surrounded in a yellow hallo, are also found. Figure 2.2 shows a typical massive carbonaceous mudstone sample.

Figure 2.2 Highly carbonaceous mudstone.

2.2.2.3 Unit 3 Sandstone interbedded with carbonaceous mudstone (SS/CM)

Unit 2 and unit 3 are the dominant lithologies in the sequence, but it is much easier to sample and test unit 3 as more of the core remains intact. The samples are either a yellowish or brownish grey, often with an orange or yellow surface staining probably originating from the abundant pyrite nodules. The grains are well sorted within beds, the medium to coarse sand forming larger beds (20-100mm width), while the silt to fine sand and carbonaceous mudstone is laminated (2-20mm width) and makes up the majority of the unit. This is illustrated by figure 2.3 where a coarser grained bed can be seen opposite the 60mm mark, towards the centre of the photo and the rest of the core is fine grain sand laminated with carbonaceous mudstone. Approximately 20% of unit 3 is composed of carbonaceous material. The bedding is orientated between 15 and 30˚ to the horizontal. The induration corresponds to the change in grain size, with the coarser beds being poorly indurated and the finer having more moderate induration. These quartz arenites are also mica-rich and may contain coal fragments.

Figure 2.3 Sandstone with carbonaceous mudstone laminations.

2.2.2.4 Unit 4 Loose sandstone (SS)

Figure 2.4 shows an example of unit 4 in the original drill core box. The core is mainly being held together by drilling mud, and once disturbed disintegrates easily. It has a characteristic grey colour and mostly massive structure with occasional widely spaced thin (less than 1mm) carbonaceous layers. It is moderately sorted with a combination of fine to coarse sand grains. It is made of predominately subangular quartz and mica with feldspars, which are in the process of breaking down to clays and provide the finer fraction.

Figure 2.4 Loose sandstone, mainly held together by drilling mud. Photo courtesy of Adrian Field.

2.3 Sampling Methodology and Considerations

The drill core samples where collected from holes completed for Solid Energy, between January and March 2005 by Diamond Drilling Ltd. Those within the vicinity of the proposed opencast area were selected for sampling, and the units above the No. 4 seam were targeted as they will

form the highwall of the pit. Sample selection was restricted to intact core of sufficient length for testing without discontinuities. This does result in a bias towards the strongest rock being sampled, and therefore the results should be considered as maximum values of intact rock strength. It is however, the only practical means of testing intact rock parameters and is widely accepted practice. The drill core sampled was HQ size, with an average diameter of 61mm, which lead to a minimum length of 160mm being necessary when following ISRM (1981) standards. This allowed for cutting and grinding of the ends to provide a length to diameter ratio of 2.0-3.0:1.0, depending on the test being performed.

The core boxes were being stored in a shipping container near Terrace Mine entrance in Reefton when this study commenced. Once selected each geotechnical sample was wrapped in plastic and sealed with tape to prevent any further moisture loss. The samples were placed in core boxes and transported by road back to Christchurch, where they were stored in a controlled environment in the Rock Mechanics Laboratory, University of Canterbury. Due to the natural moisture content being unknown, saturation of each sample before testing was attempted, as recommended by ISRM (1981). Water immersion however caused disaggregation of several samples. Those successfully tested for porosity and density, however showed that they were originally near saturation. This assumption was reached by weighing the samples before drying and after saturation, and discovering there was very little difference (less than 1 gram). The core was therefore tested as sampled and in-situ saturated moisture conditions were assumed.

As the core is ‘soft rock’ sample preparation to ISRM (1981) standards was difficult and time consuming. Frequently samples would break after cutting or grinding, often along bedding planes which were at a low angle to the end of the core. In some cases grinding to the required 0.02mm flatness without destroying the core was impossible. It was noted when a sample could not be ground but no substantial difference in results were observed. Chiu *et al.* (1983) note that while flat end preparation is critical for strong rocks, results from soft rocks such as mudstones, suggested that they are not influenced in the same way. The bedding and partially developed bedding associated with carbonaceous material prevented the samples from being tested as homogeneous soils. Unit 4 however was predominantly massive and loose enough to allow for recompaction in the soil triaxial apparatus. Apart from water content, slake durability and sonic velocity, no other physical or mechanical tests was attempted on unit 4 due to its weakness and a lack of undisturbed samples.

2.4 Physical Property Index Tests

2.4.1 Porosity-Density

The porosity of a sample of rock material is defined by Duncan (1969) as the ratio of the volume of voids to the total volume. It therefore depends on the shape of the grains within the sample, their size distribution, orientation and the amount of compaction and cementation that has occurred. When pores are present the strength decreases in the fabric of the rock material and the deformability or elastic modulus increases (Hawkes & Mellor, 1970). Correlations with mechanical properties such as unconfined compressive strength however usually involve significant scatter (Goodman, 1980). Most rocks show a correlation between porosity and dry density when they have similar grain densities. A low density rock is therefore normally highly porous (ISRM, 1981). Sedimentary rocks are known to have a highly variable percent porosity and clastic rocks can range from 3 to 30 percent (Fetter, 2001). Density is defined as the weight of the solid mineral matter per unit volume (Duncan, 1969). Table 2.1 provides a summary of the properties obtained from the ISRM (1981) porosity-density index test for each unit and the specific method, calculations and raw data collected are given in appendix 1.2. The standards were followed for the water saturation and caliper technique, which required more than three specimens in order to be representative.

Table 2.1 Summary of Porosity-Density Parameters.

Unit	**1 ZS**	**2 CM**	**3 SS/CM**
	Siltstone	Carbonaceous Mudstone	Interbedded Sandstone/Mudstone
Number of samples	7	7	11
Porosity (%) Average	**8.7**	**11.6**	**13.4**
Standard Deviation	2.7	2.4	1.7
Range	4.6 - 12.2	6.6 - 14.1	9.8 - 16.2
Void Ratio (e) Average	**0.1**	**0.13**	**0.15**
Standard Deviation	0.03	0.03	0.02
Range	0.04 - 0.14	0.07 - 0.16	0.11 - 0.19
Dry Density (kg/m^3) Average	**2470**	**2303**	**2250**
Standard Deviation	71.1	44.7	72.4
Range	2398 - 2492	2226 - 2357	2122 - 2391
Saturated Density (kg/m^3) Average	**2558**	**2419**	**2384**
Standard Deviation	80.6	42.9	60.8
Range	2500 - 2726	2340 - 2470	2273 - 2489

Table 2.2 Lucas (2002) classification for porosity and density.

Classification	Porosity (%)	Density (kg/m^3)
Very High	>30	>2500
High	10-30	2300-2500
Medium	5-10	2100-2300
Low	2.5-5	1900-2100
Very Low	<2.5	<1900

The results can be assessed using Lucas's rock classification table (table 2.2) as follows:

- Unit 1 Siltstone has a medium average porosity (8.7%), which is the lowest value for all the units tested. Similarly it has the lowest average void ratio (0.10) and a corresponding high average dry density (2470kg/m^3). The difference between average dry and saturated density values is also the lowest of the units (88 kg/m3). These values are a result of the fine grained and well compacted nature of the rock, which allows for little pore space between grains.
- Unit 2 Carbonaceous Mudstone has average values that are both high for porosity (11.6%) and dry density (2303kg/m^3). It has an average void ratio that is higher than the siltstone but lower than the sandstone (0.13). The difference between the average dry and saturated densities is also between the values for unit 1 and unit 3 (116 kg/m^3). As it is substantially less indurated than the siltstone it is not surprising that it has higher values, and as it is finer grained and has a more uniform particle size distribution it was expected to be less porous than the sandstone.
- Unit 3 Sandstone interbedded with mudstone has a high porosity (13.4%), which is close to the typical value (15%) of average sandstone (Goodman, 1980). A non uniform particle size distribution tends to produce a lower porosity because the finer grains can fill the spaces between the larger grains (Duncan, 1969). Given the mudstone component and range of grain sizes within this unit it is therefore not surprising that the porosity value is lower than the typical value. The results show a medium average dry density (2250kg/m^3), and the difference between the average dry and saturated densities is the largest of the units (134kg/m^3). Correspondingly the void ratio is the highest of the three units (0.15), which is expected due to the sand size grain size that would allow connection between voids.

The relationship between dry density and porosity for all the units is shown in figure 2.5, and the dry density does indeed decrease with increasing porosity for the BCM tested as was expected. There is a clear overlap between values for unit 2 and unit 3, which is not surprising considering the amount of mudstone within the sandstone. The scatter shown by unit 1 may be a result of the

variability of these samples within this unit and gives a correspondingly low R^2 value for all the data.

Figure 2.5 Scatter graph of dry density verses porosity.

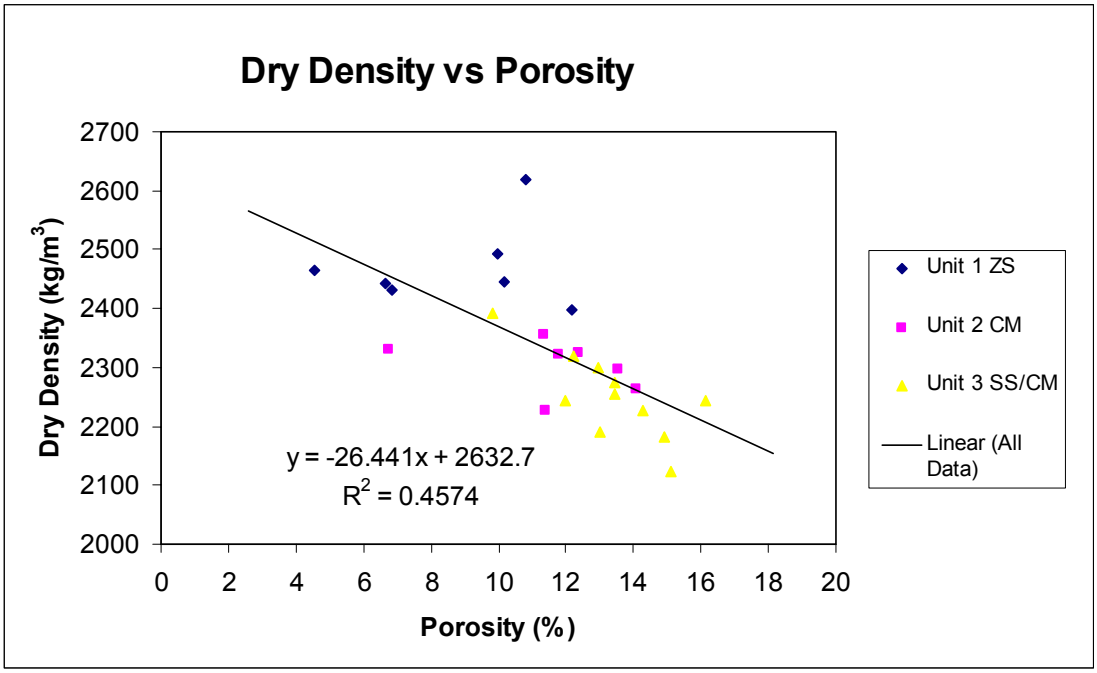

2.4.2 Slake-Durability Index

The slake-durability test is designed to determine the resistance to weakening and disintegration in a rock sample when subjected to cycles of drying and wetting. The intention is to simulate short term climatic weathering sequences rather than long term weathering deterioration by slow action such as chemical or biological processes. Neither is it intended to recreate extreme environment short-term processes, for example frost or salt crystallization (Franklin and Chandra, 1972). It has been noted that disintegration of coal measure rocks is promoted more by physical means than chemical weathering (Bell *et al.*, 1997). The test was originally devised to evaluate the weathering resistance of weak clay-bearing rocks such as mudstones and siltstones, especially because the degree of induration is not necessarily an indication of weatherability performance (Johnson and DeGraff, 1988).

The long-term stability of the planned opencast in the Reddale Valley, and the design and the degree of compaction of the ELF (Engineered Land Form) of excavated overburden, may be affected by the weatherability of the overburden material. There is also a potential for overhangs to develop as the alternating nature of the lithologies in the sequence may result in more resistant layers remaining while degradable layers disintegrate beneath them, causing rock-fall hazards

(Lucas, 2002). Slaking may also affect the selection of equipment and techniques for excavation of the overburden (Franklin and Chandra, 1972).

The mechanisms which control the durability of a rock depend on a number of factors. The permeability and porosity are crucial because they influence the entry and retention of pore fluids, and movement of water once introduced to the rock. The fluids may create surface energy changes, cause cement to go into solution, disrupt bonds (particularly by ion exchange), or generate significant pore-pressures. The ability of the rock to withstand these disruptive forces results in the amount of weakening, swelling or disintegration that will occur (Franklin and Chandra, 1972). The mineral composition and textural features (often depending on rock alteration associated with weathering or diagenetic processes) of the rock also influences the slake-durability index value (Dhakal *et al.*, 2002).

Samples of all four of the units were tested according to the ISRM (1981) suggested method for the determination of the slake-durability index, which was adapted from the method suggested by Franklin and Chandra (1972). The method, calculations and raw data are given in appendix 1.3. Tap water at 21 to 22˚C was used as the slaking fluid. The results provide the percentage of the initial mass retained after several cycles of rotation, wetting and drying (table 2.3). Four cycles were undertaken on units 1 to 3 as they had relatively high second-cycle indexes (I_{d2}), and a better idea of their material characteristics can be obtained from the additional slaking cycles. The standard weatherability classification however, uses I_{d2} as proposed by Johnson and DeGraff (1988), and is reproduced in table 2.4

Table 2.3 Summary of results for the slake-durability index.

Unit	1 ZS	2 CM	3 SS/CM	4 SS
	Siltstone	Carbonaceous Mudstone	Interbedded Sandstone/Mudstone	Loose Sandstone
No. of samples	20	40	40	20
Average I_{d1} (%)	**99.3**	**99.5**	**96.9**	**86.1**
S.D.	0.10	0.03	3.37	0.63
Range	99.27 - 99.41	99.48 - 99.52	91.87 - 98.70	85.63 - 86.52
Average I_{d2} (%)	**90.9**	**93.6**	**72.5**	**9.3**
S.D.	1.91	0.09	18.37	2.62
Range	89.50 - 92.20	93.651 - 93.73	45.90 - 88.04	7.29 - 11.15
Average I_{d3} (%)	**83.7**	**89.9**	**62.0**	**0.0**
S.D.	1.89	1.09	17.99	-
Range	82.38 - 85.05	89.10 - 91.43	39.16 - 83.10	-
Average I_{d4} (%)	**76.6**	**86.0**	**54.6**	**0.0**
S.D.	0.98	1.20	18.53	-
Range	75.92 - 77.32	85.00 - 87.60	32.67 - 77.53	-

S.D.: Standard Deviation

Table 2.4 Two-cycle Slake-Durability Classification (Johnson and DeGraff, 1988).

Classification	Slake-Durability (I_{d2} %)
Very High	98-100
High	95-98
Medium High	85-95
Medium	60-85
Low	30-60
Very Low	0-30

Figure 2.6 Graph of the number of slaking cycles performed and the reduction in percent of sample retained.

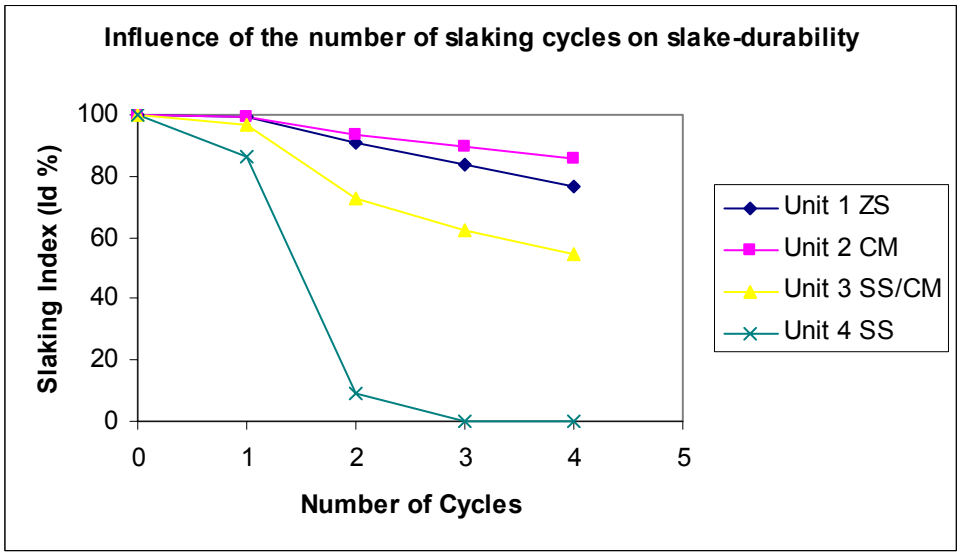

Figure 2.7 Scatter graphs of a) slake durability verse dry density and b) slake-durability verse porosity.

A.

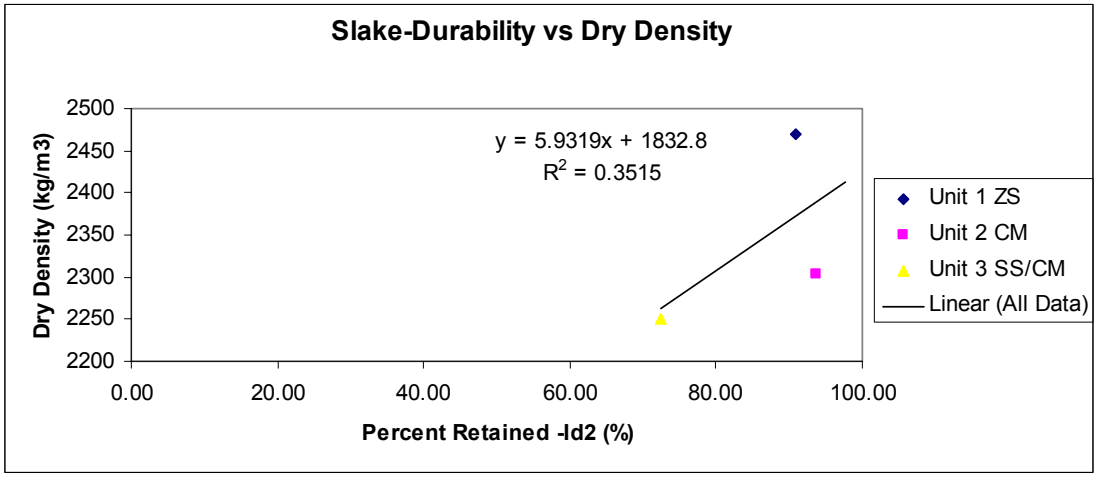

B.

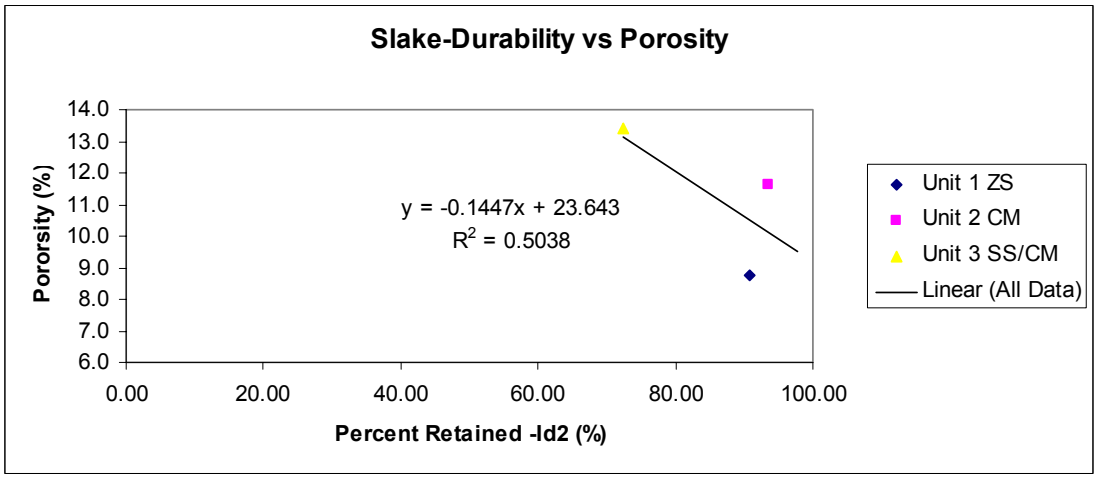

The graph in figure 2.6 shows the influence of the number of slaking cycles on the percentage remaining. For unit 1 siltstone, only 0.7% of the average weight is lost in the first cycle but the other cycles show a relatively regular drop with losses of 7 to 8% by weight per cycle. The I_{d2} average result of 90.9% retained for unit 1 suggests it has a medium-high classification and it is the second highest slake-durability index result. This is consistent with the I_{d4} average result of 76.6%, which also suggests that unit 1 is the second most durable and overall relatively resistant to disintegration when subjected to short-term weathering. The results correlate with the highest density and lowest porosity as shown in figure 2.7. The samples became rounded during the process but remained as ten lumps with only a few chips around 10mm in size retained in the basket (see figure 2.8). Following the cycles most of the lost sediment in the troughs was held in suspension by the slaking fluid, with less than 0.5 mm of silt covering the bottom.

The graph showing the effect of numerous cycles (figure 2.6) gives a similar pattern for unit 2 carbonaceous mudstone relative to unit 1, with the least loss occurring during the first cycle

(0.5%). The average percentage retained drops the most during the second cycle (6%) and then levels out to a 4% decrease for each following cycle. The average results categorise it as also having medium high durability with 93.6% retained for I_{d2}. It also has highest slake-durability index for I_{d4} (86%), and does not directly correlate with the porosity and density results (figure 2.7). Analysis of the material retained (figure 2.8), shows that the samples have disintegrated significantly into chips which range from 5 to 10mm, but do not pass through the 2mm mesh. Taylor and Spears (1970) observed that mudstones often degrade to a gravel-sized aggregate as a result of polygonal fracture patterns, joints and bedding. The occurrence of misleadingly high slake-durability index results for mudstones was also noted by Franklin and Chandra (1972). Despite the percent retained it is therefore proposed that unit 2 is not particularly durable and will slake when subjected to wetting and drying cycles, especially in a loosely compacted, exposed waste dump situation. The troughs contained chips of carbonaceous mudstone, which were less than 2mm in size, and silt held suspended in the water following each wetting cycle

Unit 3 sandstone interbedded with carbonaceous mudstone gave average values which indicated that substantial loss occurs during the second cycle (24%), and then levels out as shown in figure 2.6. With an average I_{d2} (72.5%), unit 3 is classified as having medium slake-durability. The slake-durability results correspond to the lowest density and highest porosity values of those measured (figure 2.7). The retained portions show significant rounding of the lumps and reduction in size, especially following the fourth cycle. The very small (5mm) lumps shown in figure 2.8 are composed of pyrite. The bottom of the troughs where covered with 1 to 2mm of sand and carbonaceous fragments following each cycle.

Unit 4 loose sandstone also showed a considerably large percent lost (77%) after the second cycle, while only 14% was lost in the first cycle (figure 2.6). Although not tested it is assumed that unit 4 would completely disintegrate if tested for 3rd and 4th cycles. Unit 4 is classed as very low durability based on the average I_{d2} of 9.3%. This is not surprising given that it has the largest grain size, and that it is the least indurated of the units tested. It can therefore be regarded as particularly susceptible to break-up during short-term weathering cycles. Figure 2.8 shows only those lumps containing an element of bedding and carbonaceous material remained intact, while the rest disintegrated into 3mm size balls.

Figure 2.8 Photos of samples before and following slaking cycles.

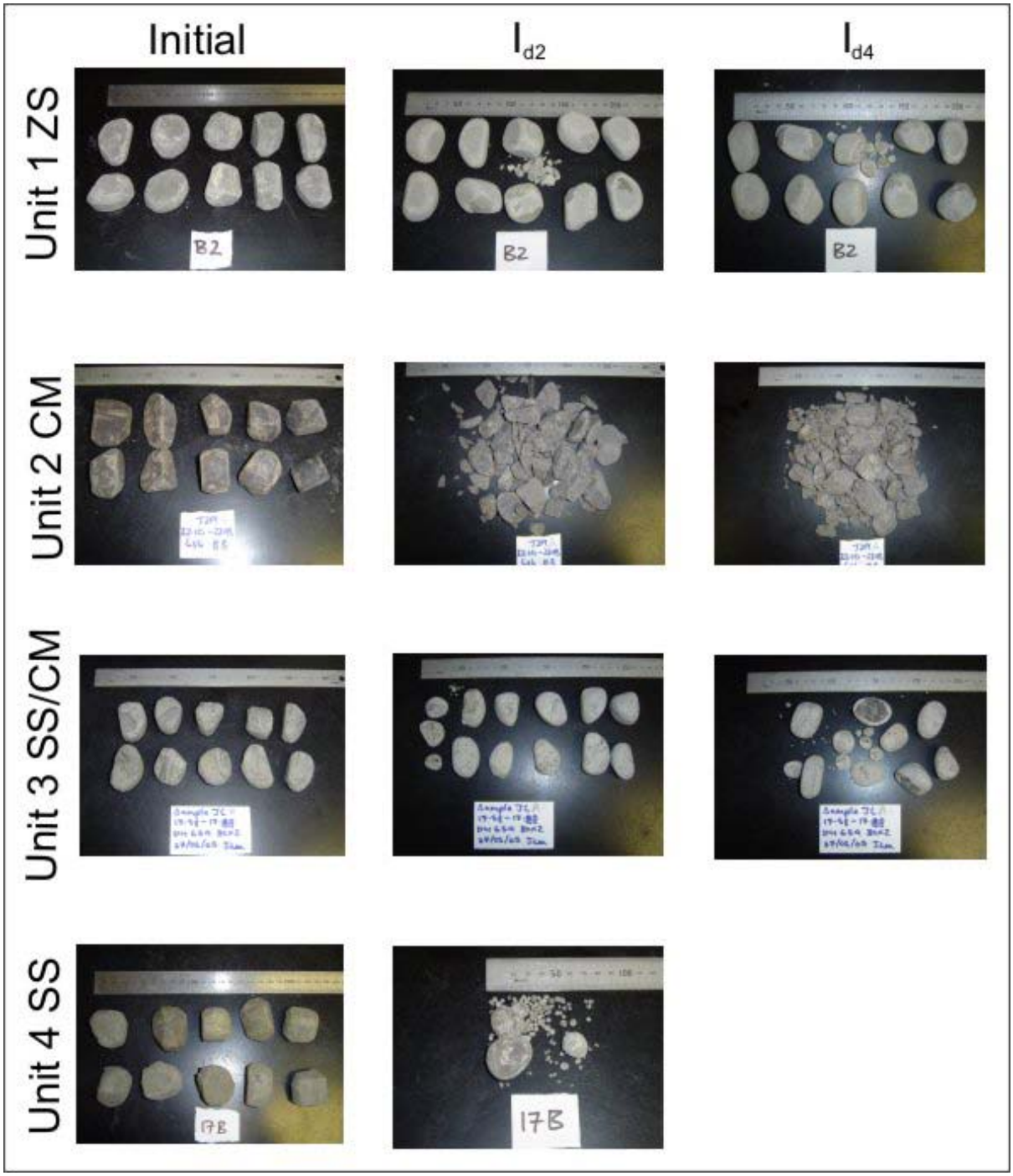

2.5 Mechanical Properties

2.5.1 Uniaxial Compression Strength (UCS) Test

This test is a measure of the maximum load an intact rock sample can withstand before failure in unconfined compression. The intact rock strength is often used to predict rock performance and is particularly applicable to rock behaviour when cut, crushed or blasted as is necessary in excavation for an opencast mine. It is the most frequently used strength test for rocks, but care needs to be taken to perform it properly to ensure consistent results (Goodman, 1980). Factors

such as length of the sample and smoothness of the ends may affect the results, and therefore need to be kept consistent and according to standard procedures. The ISRM suggested method (Brown, 1981) for determining the uniaxial compressive strength of rock materials was followed, and any variation from this is explained along with the method, calculations and raw results in appendix 1.4.

The angle between any defects and the loading direction also produces variations in the results obtained (Duncan, 1969). The entire drill core was from vertical holes and most of the samples tested were bedded to a varying degree, with dips of less than 30˚ (relative to horizontal). The main failures induced however, predominantly cut across the bedding, with only minor pieces or handling breaks occurring along the bedding. The modes of valid failure that occurred were:

- Shear (single oblique plane)
- Cataclasis (internal crumbling and collapse)
- Axial Cleavage (vertical splitting)
- Combinations (of the above modes)

as defined by Hawkes and Mellor (1970) in their paper which reviews in detail the processes and factors involved in laboratory testing of UCS. Examples of these failure modes are illustrated in figure 2.9, and only samples which failed by one of the above mechanisms were counted as having valid results. Non-valid failure modes included deformation without failure and pre-existing shears. The nature of the failure for each sample was recorded, and figure 2.10 provides a graph of the frequency of each type of failure. Shear failure was obviously the predominant mode of failure for these rocks with 58%, and the different lithologies did not favour one mode over another.

Figure 2.9 Photos of modes of failure resulting from UCS testing.

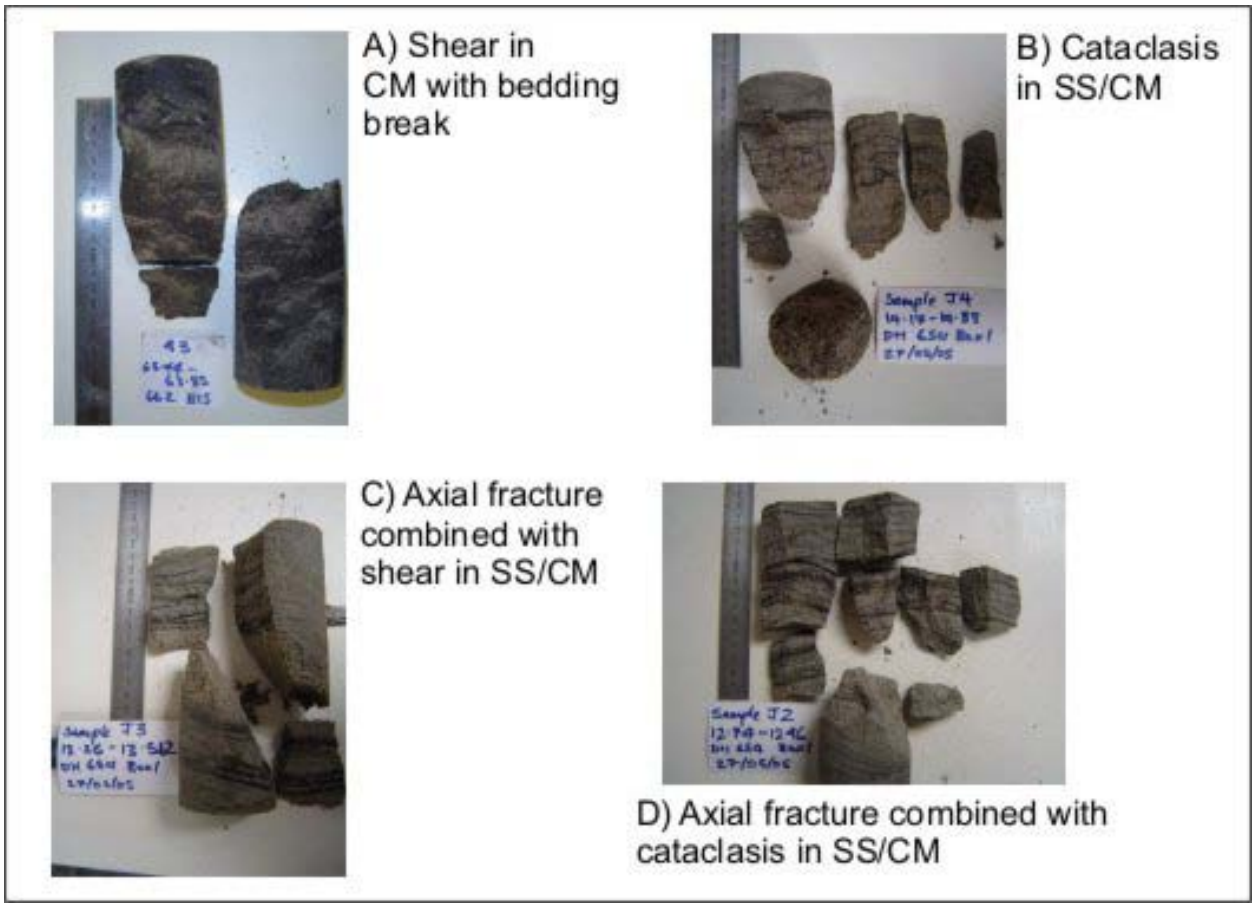

Figure 2.10 Graph of the frequency of the modes of failure.

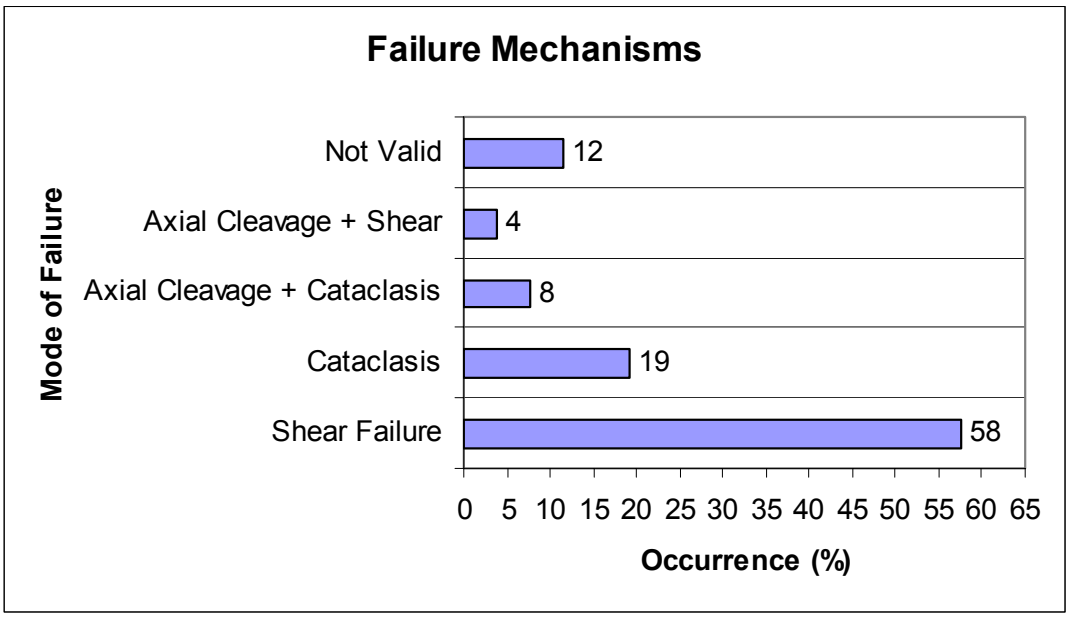

The average UCS results for each unit are given in table 2.5. Although UCS appears in many rock classification systems, table 2.6 reproduced from Lucas (2002) is used to analyse the results in this study.

Table 2.5 Summary of UCS results.

Unit	1 ZS	2 CM	3 SS/CM
	Siltstone	Carbonaceous Mudstone	Interbedded Sandstone/Mudstone
No. of Samples	6	3	14
Average UCS (MPa)	13.7	13.2	12.8
Standard Deviation	6.4	0.65	8.8
Range (MPa)	7.9 - 25.3	12.5 - 13.7	2.2 - 28.8

Table 2.6 Lucas (2002) classification for UCS values.

Classification	UCS (MPa)
Very High	>200
High	100 - 200
Medium	50 - 100
Low	25 - 50
Very Low	10 - 25
Extremely Low	<10

The nature and extent of the voids within the sample can affect the strength of the rock (Duncan, 1969). The raw and average results are therefore compared with porosity and dry density in figures 2.11 and 2.12. The degree of saturation is an important factor affecting strength, and as the samples were tested at full saturation the results can therefore be regarded as minimum values ('worst case scenario'). The depth of burial, and factors such as the increase of pressure and decrease of weathering associated with increasing depth, may also affect the compressive strength. Figure 2.14 shows each individual result plotted against the down hole depth of the sample.

Figure 2.11 Scatter plot of all data and average UCS verse porosity.

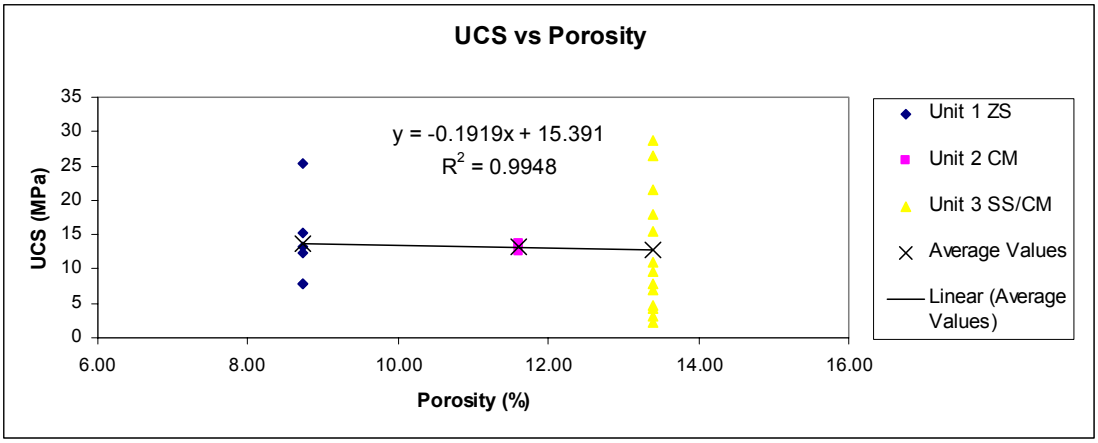

Figure 2.12 Scatter plot of average UCS verse dry density.

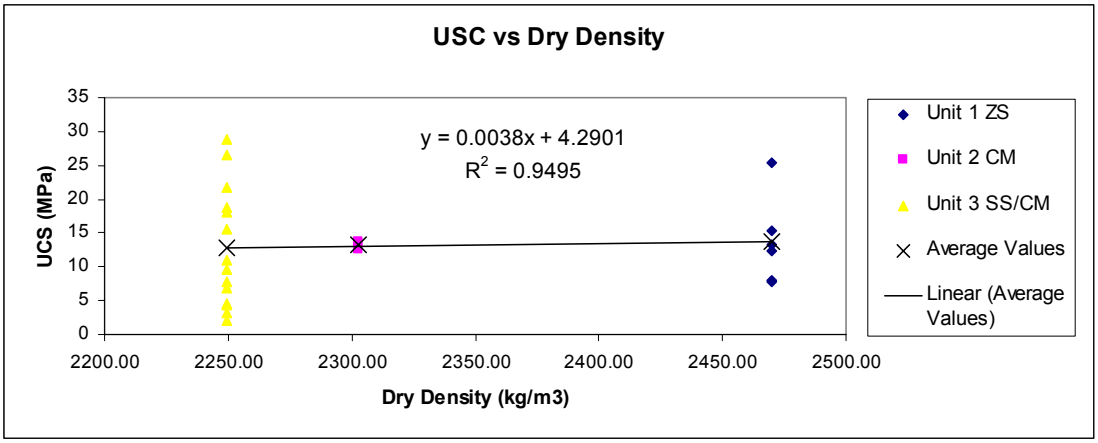

Figure 2.13 Graph of UCS verse depth of sample.

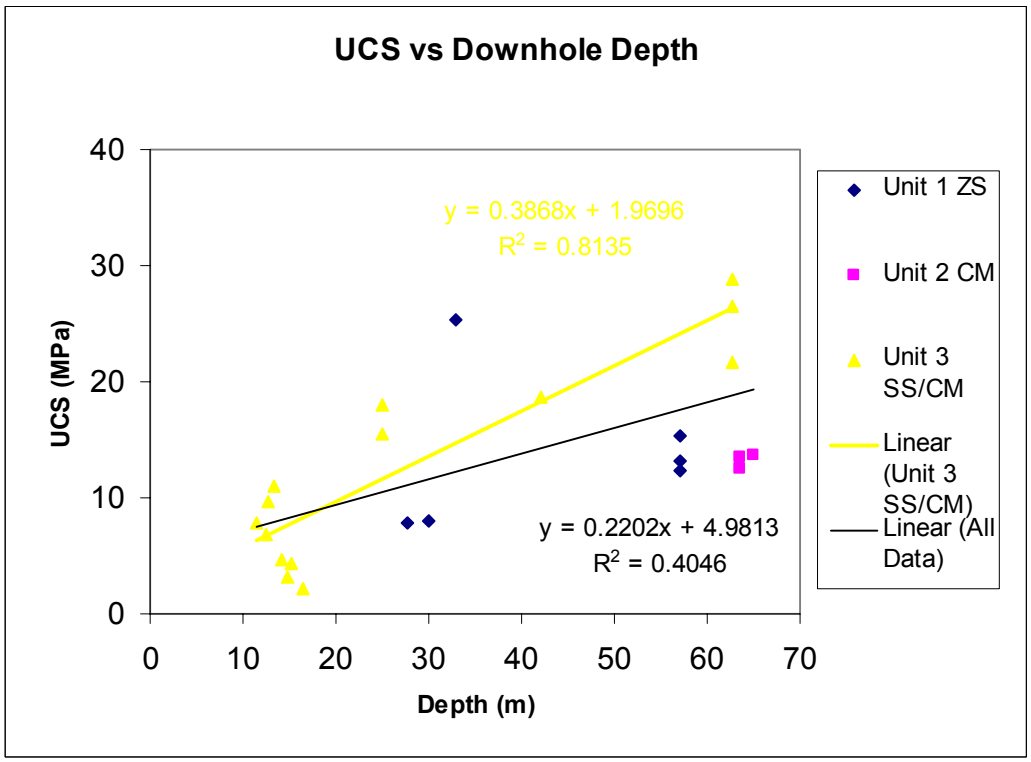

The average UCS results for the three units (12.8-13.6MPa) are very similar and can all be classified as having very low strength. Units 1 and 3 show a considerable range in values with significant overlap (7.9-25.3MPa and 2.2-28.8MPa respectively), which is illustrated in figures 2.11 and 2.12. All values recorded were beneath 30MPa and it is therefore valid to consider the units as weak rocks. Figures 2.11 and 2.12 show a very slight trend in average values whereby the highest UCS correlates with lowest porosity and highest density as expected. However, as the trend lines are virtually flat and the wide ranges indicate that the average values may not be representative of the individual units, no significant correlations can be drawn.

Figure 2.13 shows a clear increase in strength with increasing burial as expected; especially in unit 3 where a linear trend line can be drawn. All units still show considerable scatter, and one sample of unit 1 shows a relatively high strength (25MPa) at low depth. This causes the r^2 value to be low when a trendline is added for all of the data. The difficulty involved in producing a prepared specimen of carbonaceous mudstone resulted in very few samples surviving the processes to be tested successfully. The results for unit 2 are therefore inconclusive and no realistic correlation with depth can be drawn, although the trend certainly exists for the other units despite the low r^2 value (0.4) obtained.

2.5.2 Point Load Test

The point load test provides another indication of rock strength. The test measures the maximum load applied to a specimen by conical platens until failure occurs along tension cracks parallel to the loading direction (Goodman, 1980). The strength at failure is recorded as the point load index (I_s), which is corrected for the size of the sample to a standard 50mm diameter core ($I_{s(50)}$). Broch and Franklin (1972), who designed the original standard test that has since been adapted by the ISRM, listed several advantages of the point load test. These included that large numbers of tests can be performed for minimal cost, and core or irregular lumps can be tested without machining. Smaller samples of fragile material can be tested, and therefore the test is not biased to the same extent as UCS in favour of the more competent pieces. The ISRM method (Brown, 1981) was followed, and together with the calculation and raw data, is presented in appendix 1.5.

Mean values for $I_{s(50)}$ are calculated by excluding the two highest and lowest values when more than 10 valid tests are performed. This is due to average values for small populations being more representative when extreme values are discarded (Brown, 1981). The average values reported in table 2.7 have been calculated in this way, and those with less than 10 results have simply been averaged as they are. Broch and Franklin (1972) note that it is better to have a limited number of tests than none at all for cases were there are plenty of samples of one unit and few of another, as long as accuracy limitations are stipulated. The modes of failure illustrated in figure 2.14 show that only shears that pass through the whole length of the sample, parallel to the load direction, are counted as valid tests. Those axial tests which failed along bedding planes, are therefore also excluded from the results, while diametral tests are intended to fail on bedding planes.

Figure 2.14 The ISRM valid and invalid modes of failure (Brown, 1981).

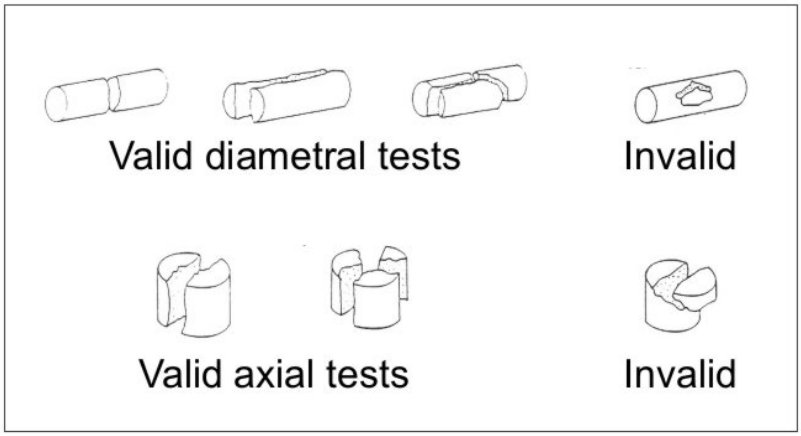

The Strength Anisotropy Index is calculated from the ratio of mean axial (perpendicular to bedding) to mean diametral (parallel to bedding) results, so that higher values indicate a greater degree of anisotropy (Brown, 1981). $I_{a(50)}$ results are also reported in table 2.7. Axial tests were also performed perpendicular to the top of the core and not at 90˚ to the bedding. This was to enable comparisons with the UCS results, as other studies have shown a close correlation between uniaxial and point load strength.

The ISRM method (Brown, 1981) suggests that UCS is between 20 and 25 times the point load strength, but acknowledge that this varies significantly with rock type, especially in anisotropic rocks. The study by Bieniawski (1975) that incorporated results from over 1000 tests found that UCS was 24 times the point load strength for a 54mm core, and this value is widely accepted. Those tests were performed on hard, strong rocks rather than the weak coal measure rocks being investigated here. Vallejo *et al.* (1989) tested rocks from surface coal mining sites in the Appalachian region and concluded that the UCS of saturated sandstones was 29 times the point load strength, while the UCS of saturated shale was 19.4 times the point load strength. However, Rusnak *et al.* (2000) analysed over 10,000 individual tests involving different coal measure rocks and proposed UCS values were 21 times the point load strength. The average results for each unit and each test are given in table 2.7, and the results can be classified according to scheme proposed by Bieniawski (1975), presented in table 2.8.

Table 2.7 Summary of point load results.

Unit	Unit 1 ZS	Unit 2 CM	Unit 3 SS/CM
	Siltstone	Carbonaceous Mudstone	Interbedded Sandstone/Mudstone
Number of valid tests	3	12	12
Axial -90° to bedding Average $I_{s(50)}$	**0.31**	**0.65**	**0.39**
Standard Deviation	0.14	0.13	0.11
Range	0.16 - 0.33	0.39 - 1.60	0.00 - 0.53
Number of tests	2	4	6
Diametral Average $I_{s(50)}$	**0.25**	**0.23**	**0.16**
Standard Deviation	0.28	0.17	0.08
Range	0.05 - 0.45	0.04 - 0.40	0.04 - 0.26
Strength Anisotropy Index $I_{a(50)}$	**1.23**	**2.82**	**2.43**
Number of valid tests	4	3	10
Axial -90° to core top Average $I_{s(50)}$	**0.62**	**0.79**	**0.26**
Standard Deviation	0.44	0.46	0.12
Range	0.18 - 1.24	0.26 - 1.06	0.06 - 0.56
UCS $24I_{s(50)}$	15	19	6
Multiplier required to gain av. UCS determined	22	17	49

N.B Ranges include highest and lowest values deleted when calculating mean but does not include invalid results

Table 2.8 Strength Classification for rock materials (Bieniawski, 1975).

Classification	Point Load Index – $I_{s(50)}$ (MPa)
Very High Strength	>8
High Strength	4 - 8
Medium Strength	2 - 4
Low Strength	1 - 2
Very Low Strength	<1

All of the units can be given a very low strength classification according to the average point load test results. Like the UCS results all the average point load strengths determined are similar (0.16-0.65MPa). Unit 1 siltstone is the strongest diametrically (0.25MPa), which corresponds with the lowest strength anisotropy index (1.23). As a value of 1 for $I_{a(50)}$ indicates a quasi-isotropic rock, this value suggests the siltstone has some partially developed bedding. The values for unit 2 carbonaceous mudstone indicate that it has the highest axial $I_{s(50)}$ perpendicular

to bedding (0.65 MPa), and the greatest amount of anisotropy (2.82). It also has the highest axial $I_{s(50)}$ perpendicular to the top of the core (0.79MPa). Unit 3 interbedded sandstone and mudstone has the lowest average diametral result (0.16 MPa) and the $I_{a(50)}$ indicates the obvious anisotropy (2.43).

Although Unit1 1 shows the best conversion to average UCS, no multiplier was found that would work for all three units. This is not surprising given the past studies mentioned above. When unit 1 was multiplied by 24 the point load value for axial tests (15 MPa) at 90˚ to top of core, it was close to the average value determined by UCS testing (13.6 MPa). However unit 2 produced a value (19 MPa), which is slightly higher than the 13.2 MPa measured and a multiplier of 17 would give a better conversion. A larger conversion factor than 24 is needed to translate point load to UCS for unit 3 (6 MPa calculated verse 12.8 MPa measured). The UCS values derived from $24I_{s(50)}$ are however, all within the range of UCS values measured (<30MPa) and as there were a limited number of tests performed in some cases (especially unit 1) this is still perhaps the most valid correlation from this data.

2.5.3 Hoek-Cell Triaxial Test for Rock

Triaxial testing is conducted by subjecting the rock sample to an axial load and a confining pressure simultaneously until failure occurs. It is intended to reproduce in-situ conditions and most rocks become stronger as confining pressures are increased (Goodman, 1980). The tests were conducted using a Hoek-type triaxial cell for HQ size core supplied by GNS (Geological and Nuclear Sciences) and performed in the rock mechanics laboratory at the University of Canterbury. The ISRM methods (Brown, 1981) were followed as recorded in appendix 1.6, along with the calculations used and raw data produced.

Low confining pressures were chosen due to the shallow depth of the samples and expected depth of the excavation (see appendix 1.6 for further explanation). Each lithology was subjected to the predetermined confining pressure at least three times to establish reproducibility. If only two similar samples were available of a unit then ‘in between’ confining pressures were used to check that they performed in the same way as those tested using three or more samples. For example 2 and 4MPa were used so that the results could be compared with a suite tested at 1, 3 and 5MPa.

Two mudstone samples underwent plastic deformation, and were excluded from the results, as they did not display a valid failure mode according to the procedure used. One sample displayed

axial cleavage, but all others failed along diagonal shears. This is expected, as vertical loading with lateral restraint is known to produce inclined planes (Duncan, 1969). The length of shear varied from half the length to the full length of the sample, and may be a result of conducting the tests with a fixed top platen. All of the main failures cut across bedding, but minor failures or handling breaks often occurred along bedding. Figure 2.15 shows two examples of the typical failures observed.

Figure 2.15 Modes of failure observed in triaxial testing.

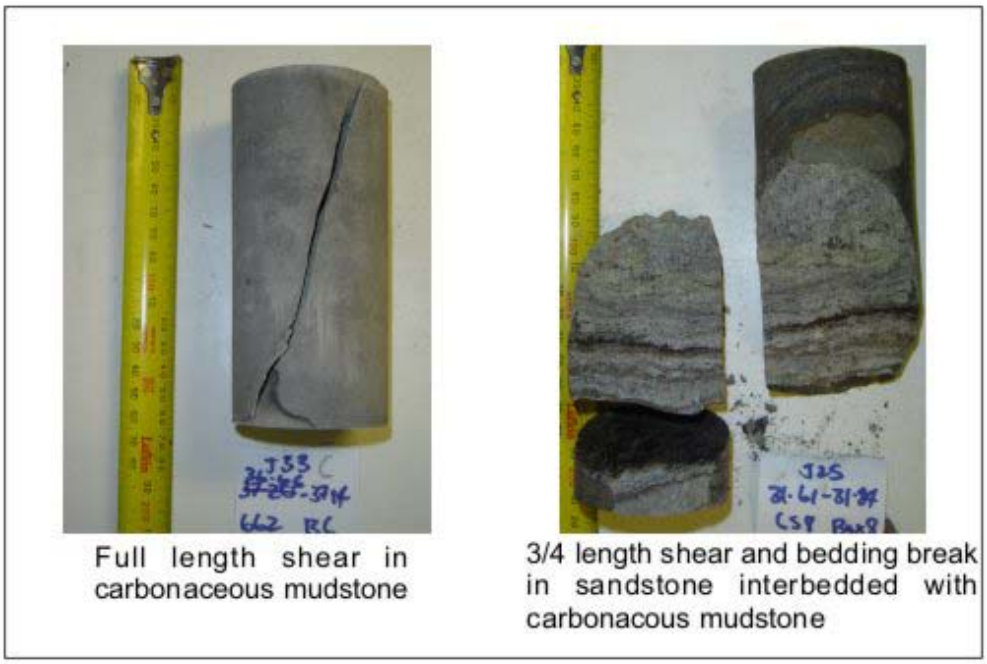

Using the Mohr-Coulomb Criterion in the RocData 3.0 programme (Rocscience Inc 2004), the maximum axial load or major principal stress (σ_1) was plotted against the confining pressure or minor principal stress (σ_3) for each unit (figures 2.16-2.18). The average UCS values for each unit were also added with zero confining pressure. A strength envelope was produced by a linear regression line of 'best fit' through the points and the gradient of this line (*m*) and intercept with the Y axis (*b*) was determined. The value *b* also gives an indication of intact uniaxial compressive strength. The angle of internal friction (ø) and cohesion (C) can then be calculated using *m* and *b* (see appendix 1.6 for equations). Alternatively Mohr circles could be drawn using σ_1 and σ_3, and fitting a Mohr envelope to get the cohesion from the intercept and the friction angle from the slope of the line. Table 2.9 gives a summary of the properties determined and the average values for strength at each of the confining pressures. Table 2.10 reproduces the classification scheme adapted by Lucas (2002) for friction angle and cohesion, and which has been used here to analyse the results.

Figure 2.16 Analysis of Unit 1 using RocData.

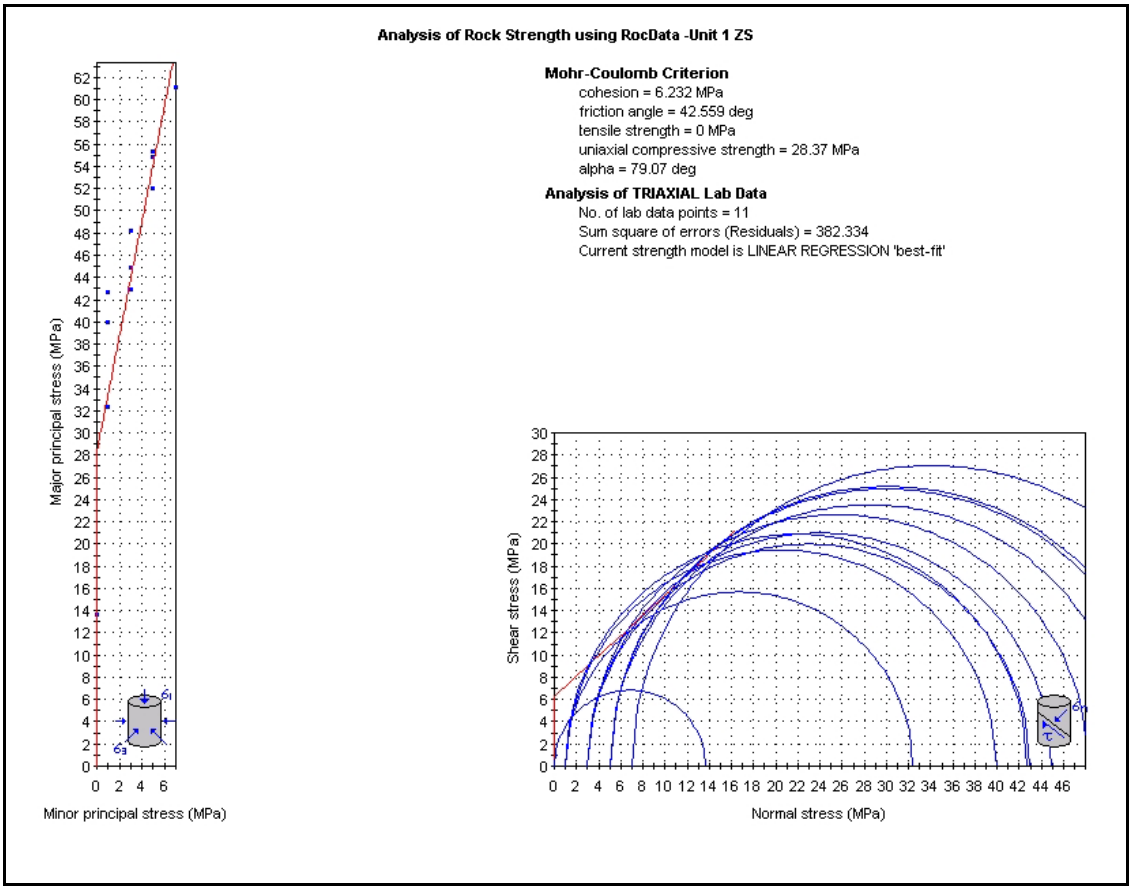

Figure 2.17 Analysis of Unit 2 using RocData.

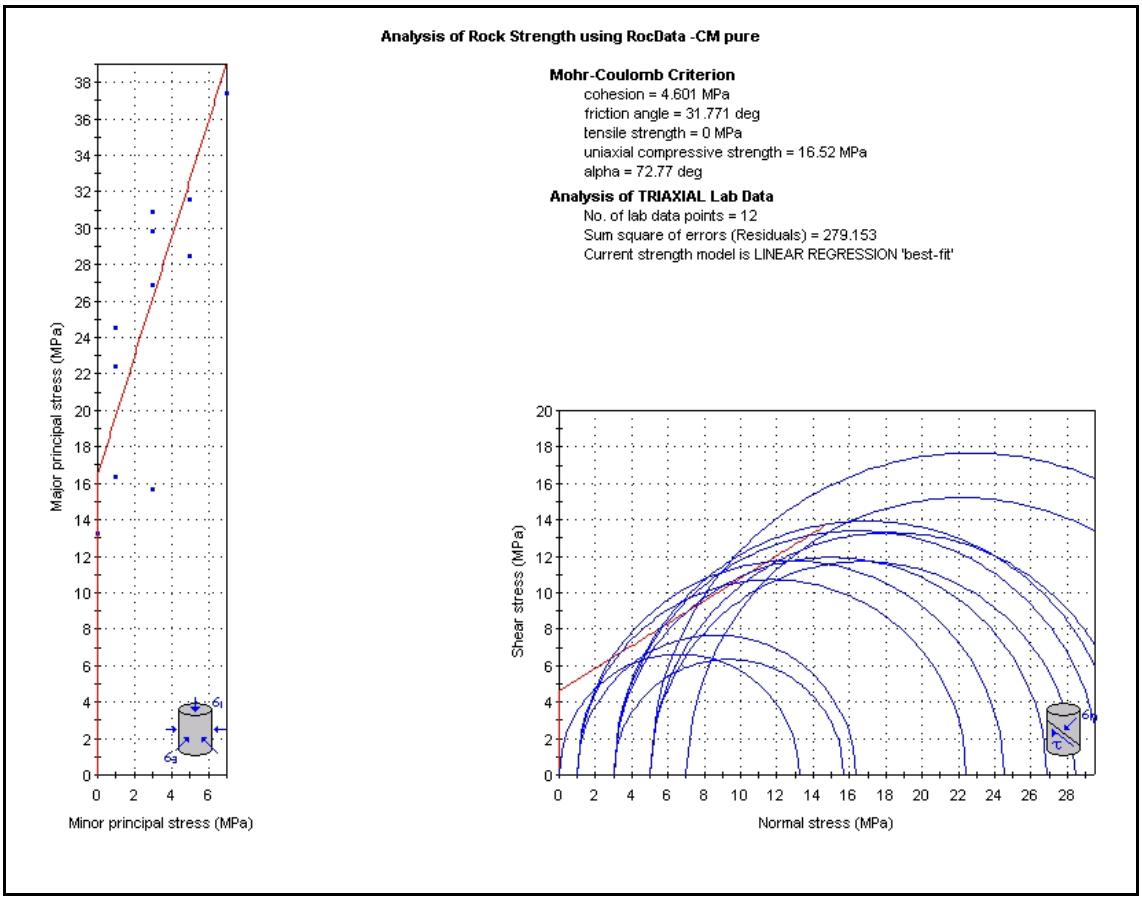

Figure 2.18 Analysis of Unit 3 using RocData.

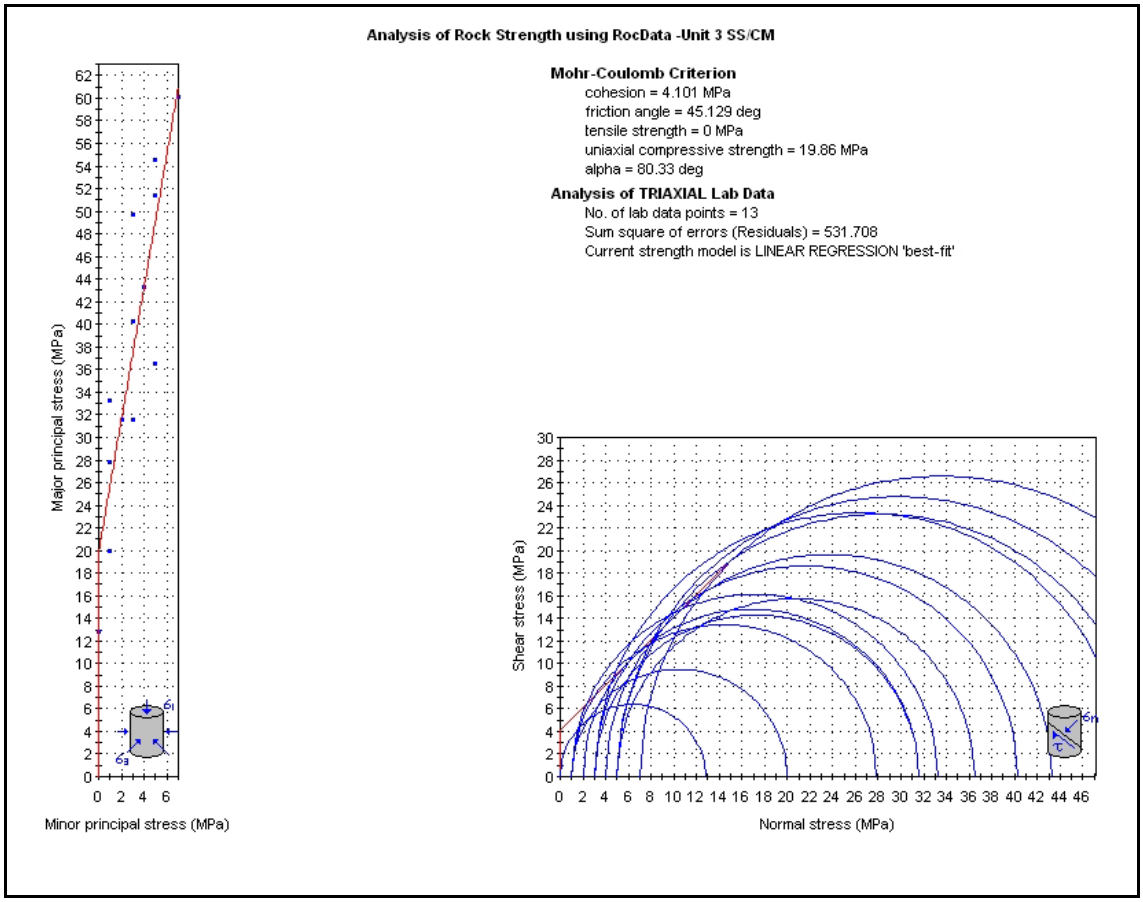

Table 2.9 Summary of triaxial results.

Unit	No. of tests	Average Strength (at each confining pressure)			Cohesion	Friction angle	σ_{ci}
		1 (MPa)	3 (MPa)	5 (MPa)	(MPa)	(Degrees)	(MPa)
Unit 1 ZS	10	38.3	45.4	54.1	6.2	42.6	28.4
Unit 2 CM	11	21.1	25.8	33.5	4.6	31.8	16.5
Unit 3 SS/CM	12	27.0	40.5	47.5	4.1	45.1	19.9

Table 2.10 Angle of friction and cohesion classification from Lucas (2002).

Classification	Angle of Friction (ø) -Degrees	Cohesion (C) -MPa
Very High	50 - 60	50 - 60
High	40 - 50	40 - 50
Medium	30 - 40	30 - 40
Low	20 - 30	20 - 30
Very Low	10 - 20	10 - 20
Extremely Low	<10	<10

Figure 2.19 Scatter graph of the average triaxial strengths at each confining pressure.

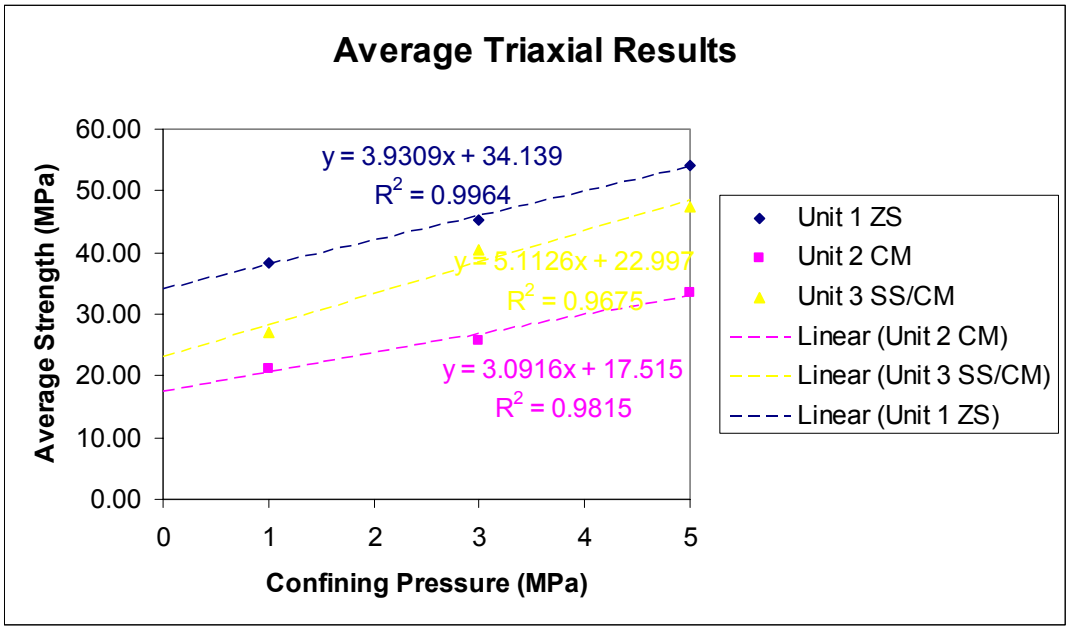

Figure 2.20 Cohesion verse average dry density.

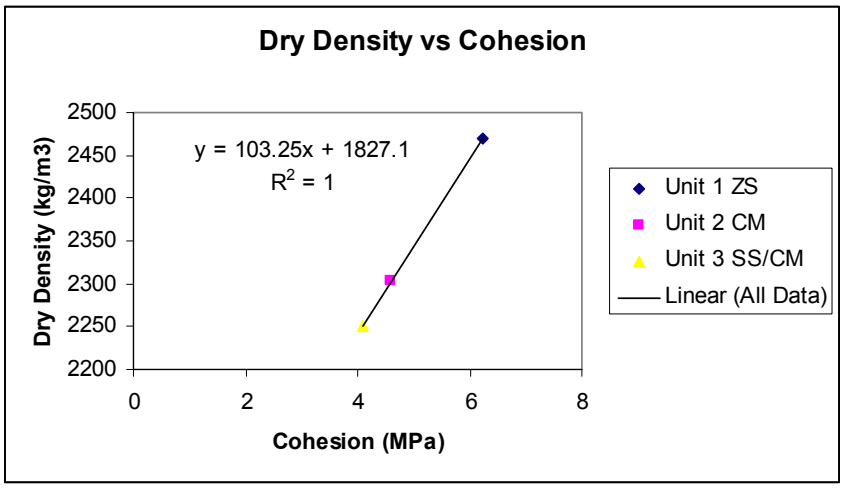

All three units show a clear linear trend in their average strength values (figure 2.19), with an obvious increase in strength with increasing confining pressure. The intercepts shown are generally within the range of UCS values determined by testing (<30MPa), although unit 1 siltstone is slightly higher than expected at 34MPa. Unit 3 carbonaceous mudstone has a series of strengths that are higher than unit 2 interbedded sandstone and mudstone. However the cohesion values derived are as expected from the previous tests completed.

Figure 2.20 illustrates the linear relationship between cohesion and dry density, and the inverse is true for cohesion verse porosity. The graph clearly shows that an increase in cohesion correlates with an increase in dry density. Like UCS the cohesion values are relatively close and

all fall within the extremely low classification (<10MPa), and further suggests that the overburden is composed of weak rocks.

The friction angles are surprisingly high given the cohesion values. Unit 1 and 2 are both within the high classification (43 and 45˚ respectively). Unit 3 is slightly lower at 32˚ and can be classed at medium according to table 2.10. No correlation was found between friction angle and cohesion or friction angle and intact uniaxial compressive strength (σ_{ci}). Nor did cohesion correlate with intact uniaxial compressive strength (graphs are given in appendix 1.6.), although unit 1 did display the highest of both parameters (6.2MPa and 28.4MPa respectively) suggesting it is the strongest unit. The intact uniaxial compressive strengths derived from graphs are all within the range determined by actual UCS tests.

Core from the same depth was able to be tested at three or four different confining pressures for unit 1. A correlation of increasing strength with increasing depth and therefore natural confining pressures, as shown in figure 2.21. It was not possible to get several samples from the same depth for the other two units as no intact core of a suitable length was available. The core used for groups of tests at different confining pressures were therefore more variable. For each group of tests the samples with the least down-hole depth were tested at the lowest confining pressure. Nevertheless scatter graphs for these units do not show a clear correlation with depth, and are given in appendix 1.6.

Figure 2.21 Example of depth effect.

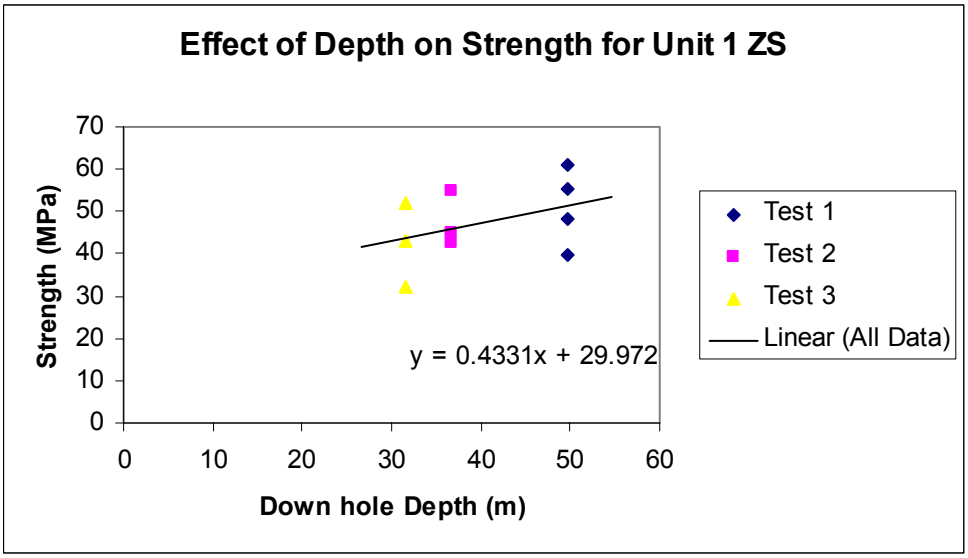

2.5.4 Soil Triaxial

The triaxial test is the most widely used shear strength test for soils and is suitable for all types of soil because the test can be performed in a number of ways (Craig, 1997). For unit 4 a drained test with increasing axial pressure was selected, so that results could be compared with the triaxial rock tests performed. The apparatus used for soil triaxial tests is not able to provide high confining pressures, and operates on a kPa scale rather than MPa used in rock tests. The two samples collected are from relatively shallow depths (12 and 20m), so fortunately low confining pressures were appropriate for the tests performed. The samples needed to be damp to be remoulded into the required specimen diameter to height ratio of 2:1. The water content was determined (given in appendix 1.7), and 'trial and error' used to establish the correct amount of water needed to remould the sample sufficiently. Water was added to bring the water content of each sample to 17%. Density was kept as consistent as possible throughout the tests by using the same remoulding technique for each sample (table 2.11).

All of the tests were performed under saturated conditions, which was ensured by applying a back pressure. The constant back pressure raises the pore pressure artificially, but prevents excess pore pressure occurring during the test. This means cell pressure and applied major principal stress can be considered effective stresses inside the sample (Bishop and Henkel, 1957). Mohr circle diagrams can therefore be directly plotted and RocData was utilised to create figure 2.22. Drained strength is reported in terms of effective angle of friction (ø') and effective cohesion (C'), and values for unit 4 are given in table 2.12. The cohesion is zero, which is expected for sand. The friction angle (36.7˚) can be classed as medium when compared to the rock classification used in section 2.5.3. The method used was adapted from the New Zealand Standard (NZS 4402 : 1986) and is discussed in appendix 1.7 with calculations and raw data.

Table 2.11 Summary of average parameters derived from the soil triaxial tests.

No. of tests	Av. Cell Pressure σ_3 (kPa)	Av. Back Pressure *u* (kPa)	Av. σ_1 (kPa)	Av. Max. Deviator σ_1-σ_3 (kPa)	Average Effective Stresses		Av. Dry Density (kg/m^3)	Av. Wet Density (kg/m^3)
					σ_3' (kPa)	σ_1' (kPa)		
3	100.0	100.0	115.1	15.1	0.0	15.1	1694.1	2020.3
3	200.0	100.0	442.1	242.1	100.0	342.1	1691.8	1993.2
3	300.0	100.0	910.3	610.3	200.0	810.3	1695.9	1983.9

Table 2.12 Parameters derived from graph.

No. of tests	Cohesion – C'(kPa)	Friction Angle –ø' (Degrees)	σ_{ci}' (kPa)
9	0	36.7	0

Figure 2.22 Analysis of unit 4 using RocData.

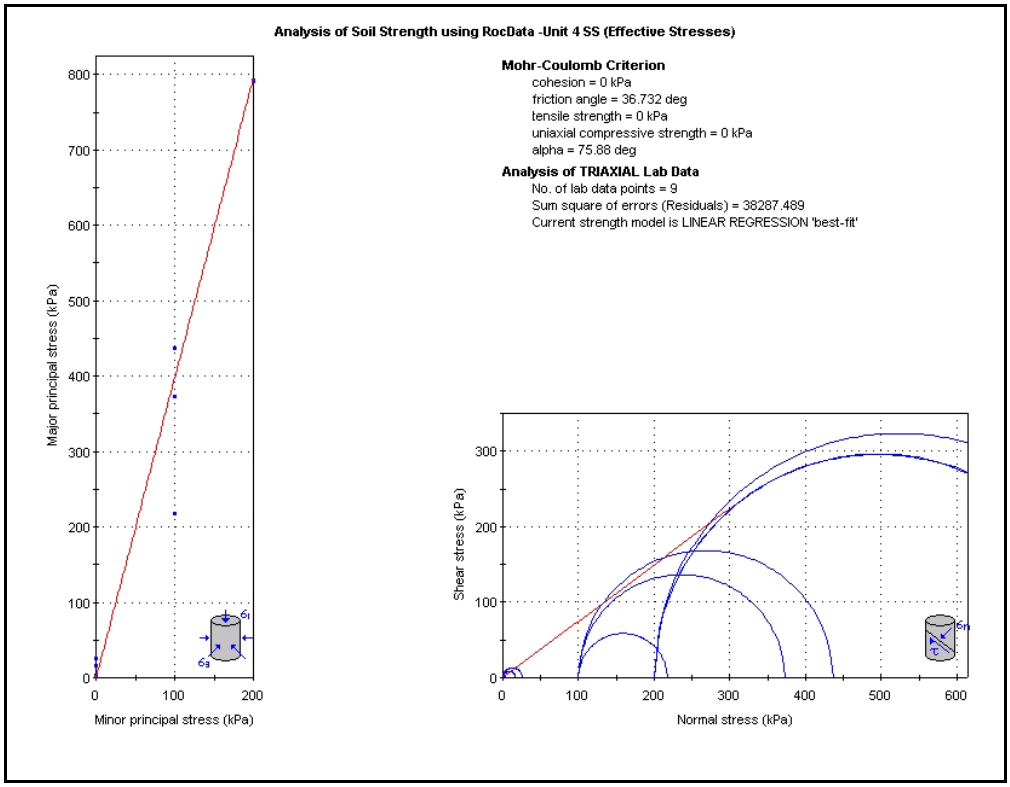

Drained triaxial tests also allow the change in volume to be measured and from this the axial and volumetric strains can be calculated (see appendix 1.7 for details). Characteristic graphs of these values indicate how loose or dense the sand is packed. The tests predominantly displayed typical graphs for loose samples of deviator stress verse axial strain, and an example is given in figure 2.23. This shape is formed because there is little interlocking of particles to be overcome and the deviator stress therefore increases gradually to a maximum value. This is compared to dense sands which have a prior peak that indicates the interlocking has been overcome, and the stress therefore reduces suddenly (Craig, 1997).

Figure 2.23 Example of typical loose sand graph.

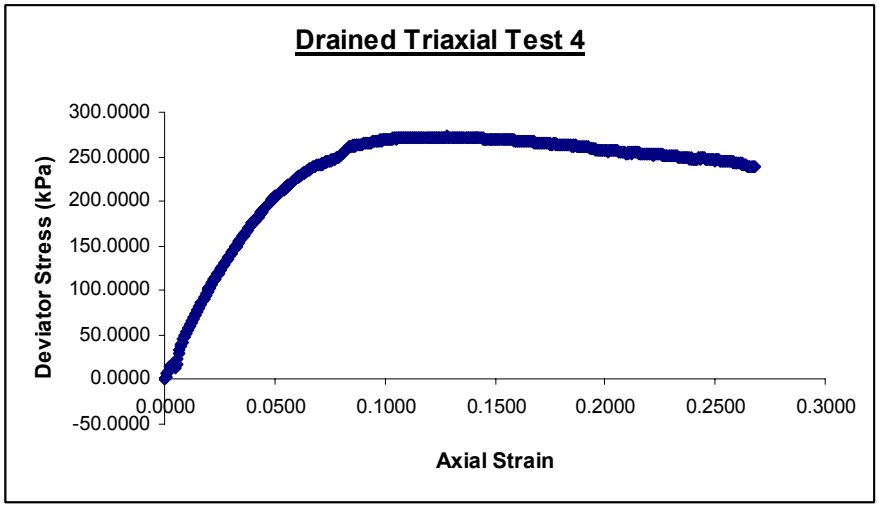

The tests showed mostly loose and some dense type plots for volumetric strain verse axial strain. Loose packed sample graphs show a decrease in volume, like the example given in figure 2.24. Dense graphs show an initial decrease in volume followed by a sharp increase as the degree of interlocking is reduced by shearing (figure 2.25). It is assumed that differences created by remoulding the samples cause some tests to be loosely recompacted while others were densely packed.

Figure 2.24 Example of a sample which showed a typical loose sand graph.

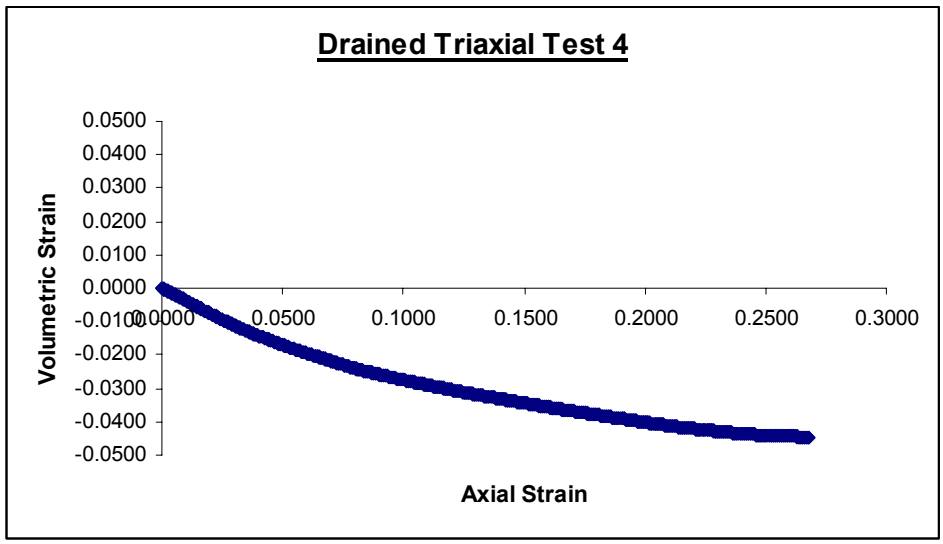

Figure 2.25 Example of a sample which showed a typical dense sand graph.

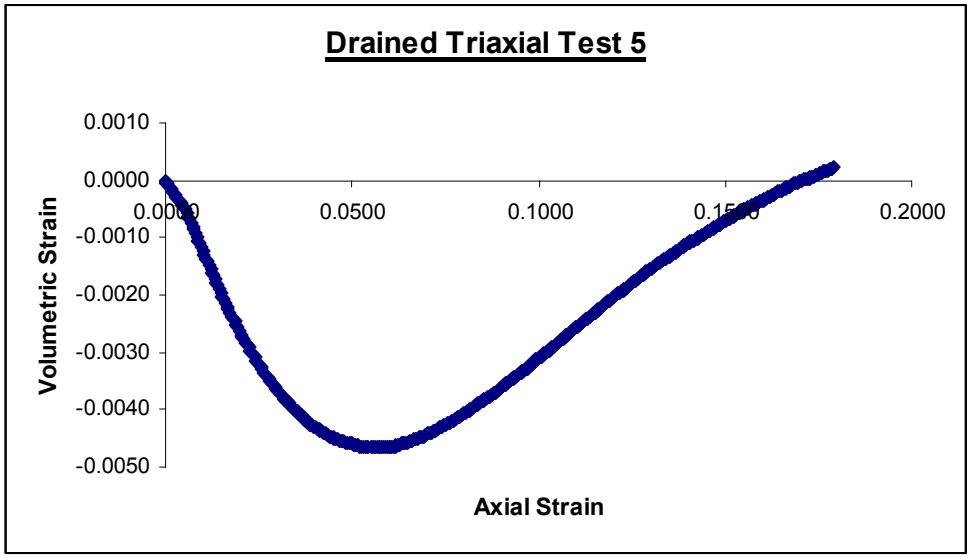

Most tests had obvious diagonal shear planes after failure. All tests had deformed into the characteristic 'barrel-shape' by the time the test was stopped. This is caused by non uniform strain conditions created by friction on the loading cap and base pedestal, which produces a 'dead zone' at the top and bottom. It has been shown that this has negligible effect on the measured strength of the sample (Craig, 1997).

2.5.5 Sonic Velocity

Determining static elastic moduli by means of strain gauges posed significant challenges when attaching them to damp weak rock. Dynamic elastic moduli, where the sample is subjected to the rapid application of stress without destroying the sample, was therefore a more favourable option. Sonic velocity equipment was used to measure the travel time taken by compression or p-waves and shear or s-waves to pass through the sample. The velocity of each wave can be calculated from this given the length of the sample. Young's modulus or the modulus of elasticity (E) is a proportionality constant that relates stress and strain. Poisson's ratio represents lateral or traverse strain which occurs with axial contraction and elongation. Both elastic moduli can be calculated from the p- and s- wave velocities if the density of the sample is known (Johnson and DeGraff, 1988). Appendix 1.8 discusses the method in accordance with the ISRM standard (Brown, 1981) in more detail, together with the calculations and raw data.

Table 2.13 provides a summary of the parameters derived from the sonic velocity testing. All tests were undertaken on horizontal core tops and therefore 15-25˚ to bedding, at in-situ moisture content. The values for Young's modulus can be classified according to the table produced by Kennedy (1988) and reproduced in table 2.14.

Table 2.13 Summary of parameters derived from sonic velocity tests.

Unit	No. of tests	P-wave velocity v_p (m/s)	S-wave velocity v_s (m/s)	Poisson's ratio *v*	Young's modulus E (GPa)
Unit 1 ZS Average	3	**2828.0**	**1166.0**	**0.40**	**10.0**
Standard Deviation		12.0	21.0	0.03	6.4
Range		2463.2 - 3412.7	918.7 - 1580.2	0.36 - 0.43	6.0 - 17.4
Unit 2 CM Average	5	**2108.1**	**796.5**	**0.39**	**4.5**
Standard Deviation		20.0	45.8	0.07	2.1
Range		986.5 - 2823.0	519.4 - 968.9	0.31 - 0.46	1.7 - 6.7
Unit 3 SS/CM Average	4	**2182.7**	**736.7**	**0.43**	**4.2**
Standard Deviation		21.4	42.1	0.04	2.6
Range		1376.0 - 2583.5	450.7 - 1009.4	0.38 - 0.47	1.3 - 6.7
Unit 4 SS Average	3	**25948.2**	**344.7**	**0.50**	**0.8**
Standard Deviation		0.1	24.7	0.00	0.1
Range		22037.5 - 30200.0	319.5 - 363.5	0.50 - 0.50	0.70 - 0.9

Table 2.14 Kennedy's (1988) classification for Young's modulus.

Classification	Young's Modulus (GPa)
Medium Strength	>20
Low Strength	10 - 20
Very Low Strength	5 - 10
Soft Rock	<5

Figure 2.26 Scatter graph of all dynamic moduli values measured..

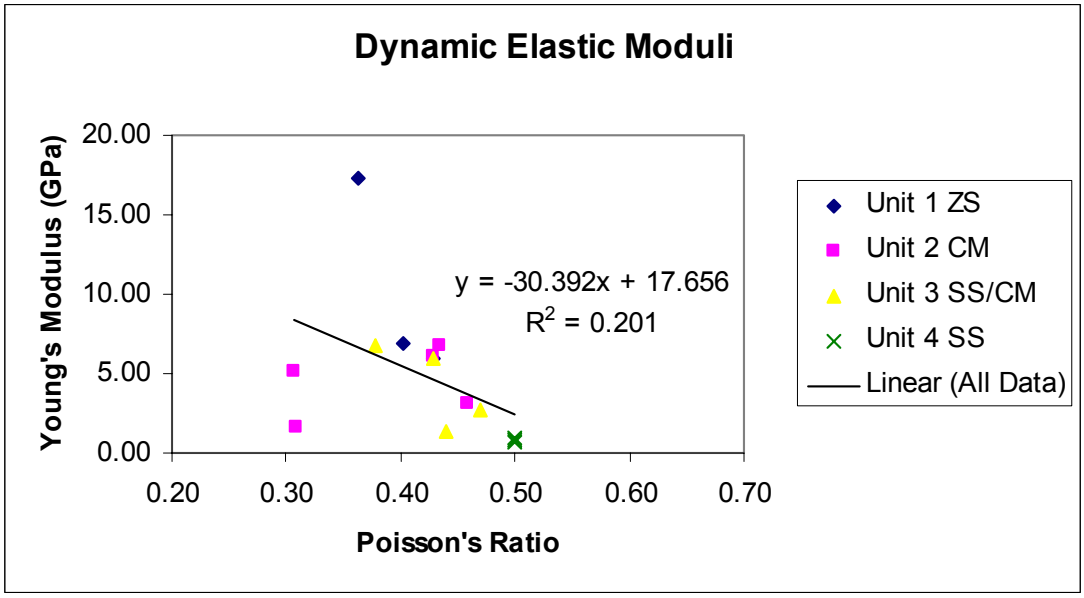

.

Figure 2.27 Scatter graph of point load verse Poisson's ratio.

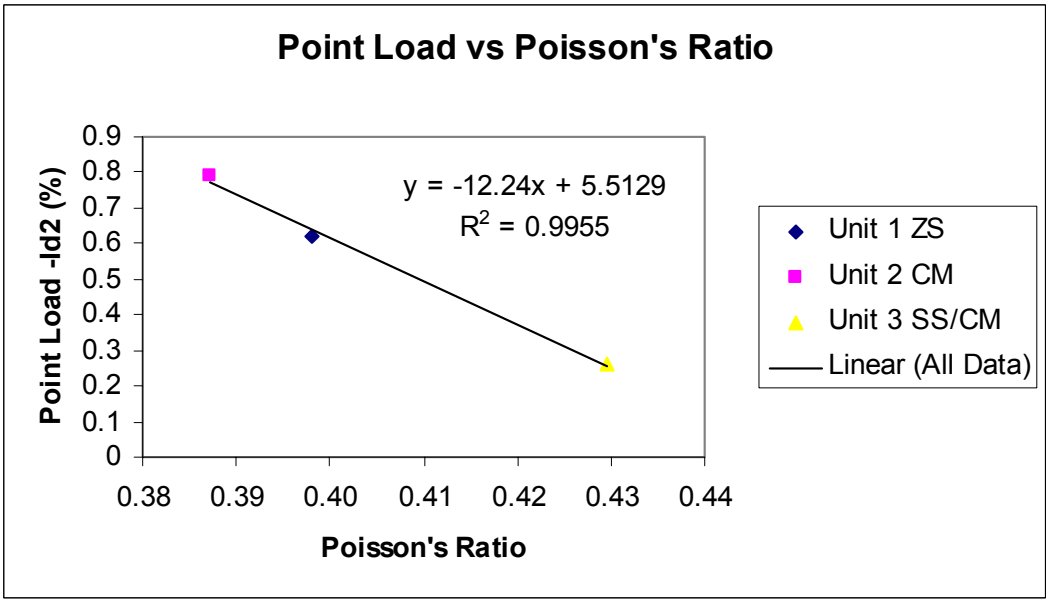

Figure 2.28 Scatter graph of dry density verse Young's modulus.

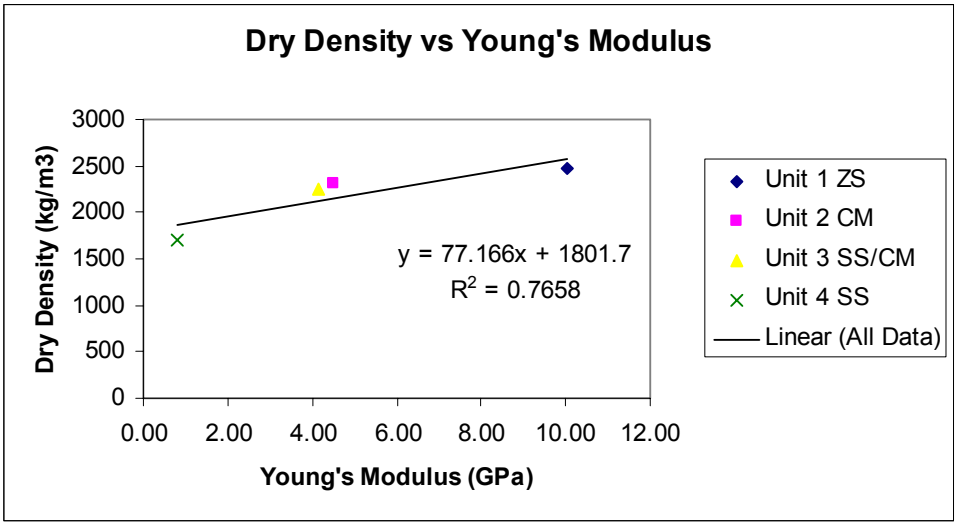

In general Young's modulus decreases with increasing Poisson's ratio (figure 2.26), however the low r^2 (0.2) suggests that there is significant scatter in the data giving this trend. Given that a value of 0.5 for Poisson's ratio indicates an ideal incompressible material (Johnson and DeGraff, 1988), the results for all the units are relatively high (0.39-0.50). The high values also suggest that these weak rocks may have properties more similar to soils than rocks, which generally have Poisson's ratios of around 0.25 (Goodman, 1980). As expected the most compressible unit is the carbonaceous mudstone (unit 2). Figure 2.27 shows the correlation between point load and Poisson's ratio, which suggests that Poisson's ratio increases with decreasing strength.

According to the classification in table 2.14 for Young's modulus, the average result for the siltstone (10.1GPa) implies a very low strength, while the other three units can all be classed as soft rock. This confirms that the siltstone is the strongest and most homogeneous unit, as also suggested by the other physical and mechanical tests completed. Unit 4 loose sandstone has a significantly lower average Young's modulus (0.82GPa) than all of the other units, which is due to the lack of cement and it having the coarsest grain size The average values for Young's modulus correlate well with the average dry densities determined for the units, as shown in figure 2.28. The trend suggests that elasticity increases with increasing density.

2.5.6 Direct Shear Test

A direct shear box was used to produce data on the characteristics of bedding planes in unit 2 and a high angle defect in unit 3, and to measure the peak shear strength under different normal stresses. Core samples were set in plaster with the shear held horizontal and remaining free between the two blocks. The ISRM standard method used is discussed in detail in appendix 1.9

along with calculations and raw data. The peak shear strength occurs before the asperities on the surface of the discontinuity are sheared by the differential horizontal movement of the top relative to the bottom block (Johnson and DeGraff, 1988).

Three carbonaceous mudstone samples were tested using broken but easily matched up bedding planes or bedding planes that were intact but had orientations that were obvious. One sandstone interbedded with carbonaceous mudstone sample displaying an intact high angle defect (approximately 60˚ to the top of the core) was also tested (figure 2.29). The tests on bedding planes showed lower average shear strength than the high angle defect. All tests showed the expected increase in both normal stress and shear stress with increasing normal force, as shown in table 2.15. Low normal load values were selected to simulate shallow (<100m) in-situ ground conditions. Only the first test at 2kN normal force is representative of intact conditions as the subsequent tests were performed on pre-sheared surfaces and therefore have fewer asperities to overcome. Figure 2.30 shows one of the mudstone bedding planes after the test has been completed. The smoothed top surface and crushed edge of the bottom can be clearly seen.

Figure 2.29 Sandstone interbedded with carbonaceous mudstone before testing showing a high angle defect, as indicated by the red arrows.

Figure 2.30 Carbonaceous mudstone sample showing a bedding plane after testing.

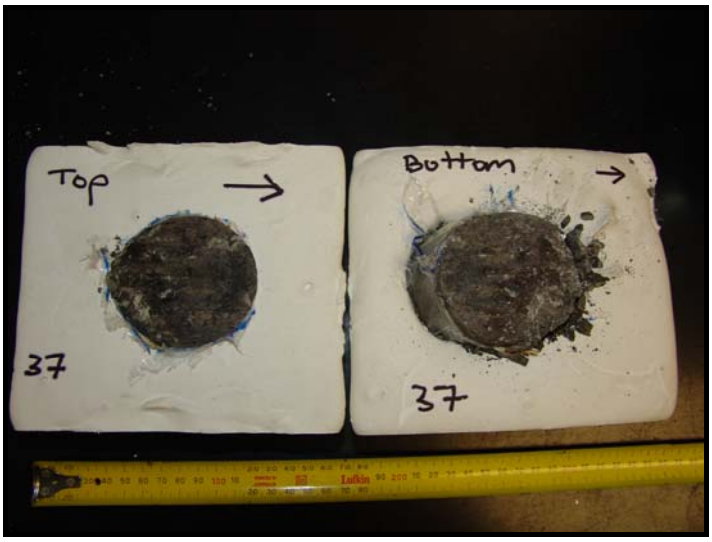

Graphs of shear stress verse shear displacement were plotted for all tests. Figure 2.31 is an example of one such graph and shows how the shear stress stepped up as the top block was displaced until reaching a peak and remaining at this value. The data was also plotted in RocData to determine values for cohesion and friction angle (Figures 2.32 and 2.33). The Levenberg-Marquardt 'best fit' model for non-linear regression gave a better trend line for the values derived for the high angle defect, the square sum of errors being only 0.028 compared to 0.122 for the linear regression model. Table 2.16 summarises the values obtained from the graphs. The bedding planes have a much lower angle of friction (14.6˚) than the high angle shear (36.7˚) but do have a very small element of cohesion (0.006 MPa). This is due to some of the test being conducted on unbroken bedding planes but should bedding shears occur in-situ, they will affectively have no cohesion.

Table 2.15 Summary of parameters derived from shear box tests.

Unit	**Unit 2 CM:**		**Bedding Planes**	
Normal Force (kN)	**Sample**	**2**	**5**	**7.5**
Normal Stress (MPa)				
	37	0.61	1.52	2.27
	11	0.65	1.01	No data
	49	0.65	1.63	2.44
	Average	0.63	1.39	2.36
Shear Stress (MPa)				
	37	0.06	0.30	0.61
	11	0.16	0.65	No data
	49	0.29	0.39	0.62
	Average	0.17	0.45	0.61
Unit	**Unit 3 SS/CM:**		**High angle defect**	
Normal Stress (MPa)	14	0.40	1.01	1.52
Shear Stress (MPa)	14	0.20	0.65	1.21

Figure 2.31 Graph of high angle defect.

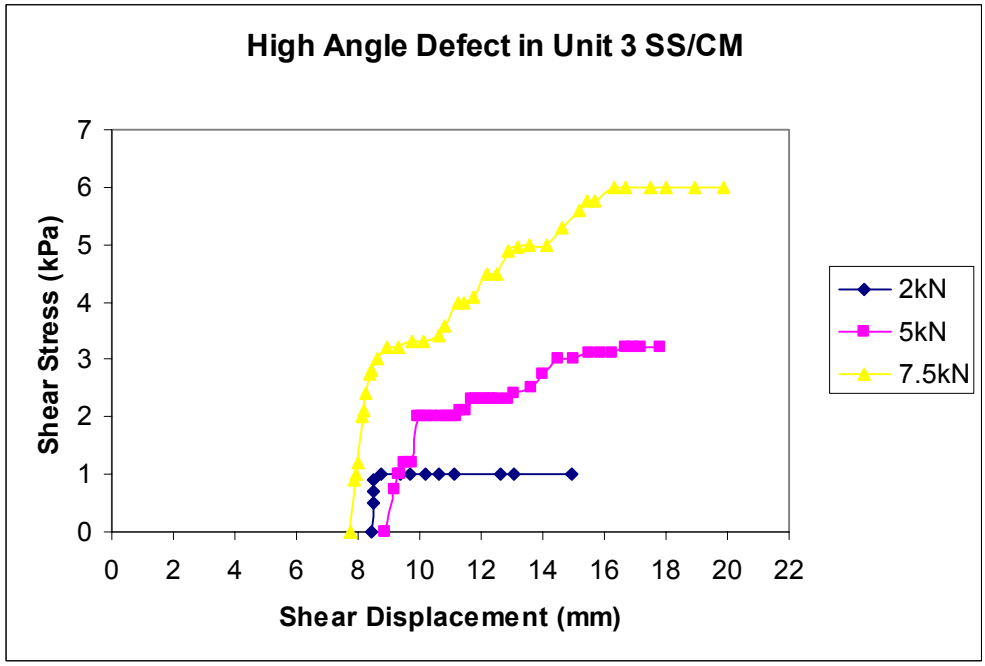

Table 2.16 Summary of parameters derived from data plotted using RocData.

Type of Shear and Unit	Cohesion (MPa)	Friction Angle (Degrees)
Bedding Planes in CM	0.006	14.6
High Angle Defect in SS/CM	0	36.7

Figure 2.32 Analysis of bedding planes using RocData.

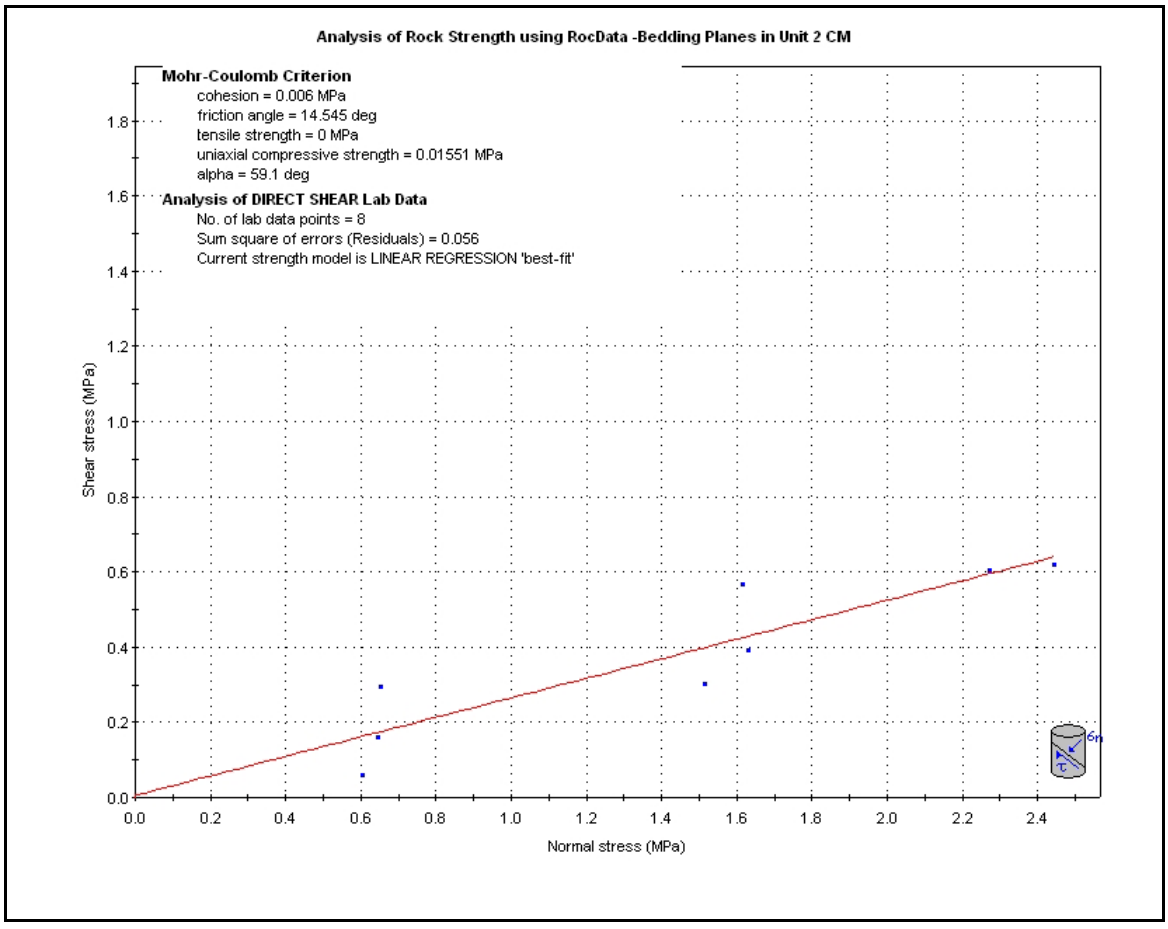

Figure 2.33 Analysis of high angle defect using RocData.

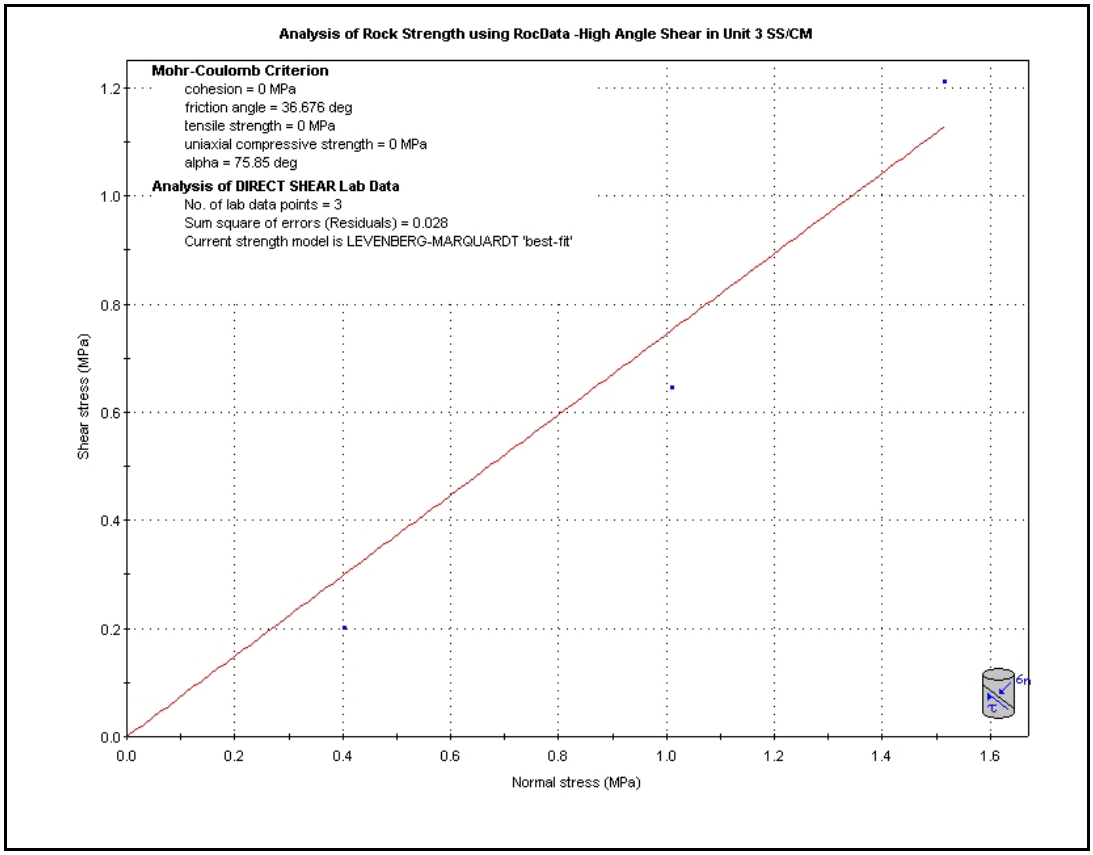

2.6 Synthesis

The BCM overburden at the proposed opencast site in the Reddale Valley has been divided into four units for geotechnical testing. Unit 1 includes all siltstones independent of the carbon content. Unit 2 comprises highly carbonaceous mudstone, while unit 3 includes silts to coarse sand arenites which are inter-bedded with the carbonaceous mudstone. Unit 4 is loose sandstone which is too friable to be tested by conventional rock strength tests. A number of physical and mechanical property laboratory tests where chosen to determine the rock material characteristics of these units. Table 2.18 gives a summary of the average parameters established for each unit.

A clear trend of increasing porosity with increasing grain size was established. This corresponded with an increase in average void ratio and decrease in both average dry density and average saturated density. The siltstone was found to be the most dense (average dry density of 2470kg/m^3) and the least porous (8.7%). Conversely the laminated sandstone was the least dense (average dry density of 2250kg/m^3) and the most porous (13.4%).

Units 1, 3 and 4 also became less durable and more susceptible to short term weathering with increasing gain size. Unit 2 (carbonaceous mudstone) had an unexpectedly high percentage of material retained after both two (96.6%) and four cycles (86%). Several authors have however,

noted the tendency for mudstones to give misleadingly high results, and it is therefore proposed that the mudstone is not as durable as the results suggest.

All of the units are classed as having very low strength (<30MPa) according to the results for uniaxial compressive strength and point load tests. Both tests provided results for the units that were very similar and few correlations with other parameters can therefore be concluded. A trend of increasing strength with increasing depth was noted in several cases. No consistent multiplier could be applied to the point load to convert the results to equivalent UCS values, although $24I_{s(50)}$ did give values within a sensible range (<19MPa). All the units have strength anisotropy index values of greater than 1 and, like most natural materials; all vary in character in different directions. The siltstone is the most 'massive' (21.2MPa) and the carbonaceous mudstone is the most anisotropic (2.8MPa).

All of the units produced low cohesion values from triaxial testing (0.0-6.2MPa) and a clear correlation between increasing cohesion and increasing dry density was observed. Surprisingly high friction angles were determined, especially for the interbedded sandstone and mudstone (45.3˚). Intact UCS values derived from these tests were within the range determined from actual tests (<28.4MPa). Friction angles were also determined from direct shear tests for bedding planes (14.6˚) and a high angle defect in laminated sandstone (36.7˚).

The dynamic elastic moduli calculated gave relatively high average Poisson's ratio values (0.39-0.50). Although considerable scatter was noted, Poisson's ratio generally increased with decreasing Young's modulus. The average Young's modulus values determined reinforced the weak nature of the units and showed an increase with increasing average dry density.

Most of the results were relatively similar to the past studies conducted on the Brunner Coal Measures. The mudstones had higher porosity values than previously determined (ranged from 2 to 4.67%). The high slake-durability index determined for the mudstone agreed with those found by other authors (96.75 to 98.5%). This study produced lower UCS, point load and intact UCS values for both mudstone and sandstone. It also determined lower Young's modulus and higher Poisson's ratio for similar units. It can therefore be concluded that the Reddale Valley rocks are weaker than other BCM previously strength tested.

Table 2.17 Summary of physical and mechanical parameters.

Unit	Unit 1 ZS Siltstone	Unit 2 CM Carbonaceous Mudstone	Unit 3 SS/CM Interbedded Sandstone/Mudstone	Unit 4 SS Loose Sandstone
Av. Porosity (n) %	8.7	11.6	13.4	n/a
Av. Dry Density (ρ_d) kg/m^3	2470.2	2302.9	2249.8	1693.9
Av. Saturated Density (ρ_{sat}) kg/m^3	2557.5	2419.0	2383.6	1999.1
Av. Void Ratio (e)	0.1	0.1	0.2	n/a
Slake-Durability (I_{d2}) %	90.9	93.6	72.5	9.3
Slake-Durability (I_{d4}) %	76.6	86.0	54.6	n/a
Av. Uniaxial Compressive Strength (UCS) MPa	13.7	13.2	12.8	n/a
Av. Point Load ($I_{s(50)}$) MPa	0.6	0.8	0.3	n/a
Strength Anisotropy Index ($I_{a(50)}$) MPa	1.2	2.8	2.4	n/a
Cohesion (C) MPa	6.2	4.6	4.0	0.0
Friction Angle (ø) Degrees	42.6	31.8	45.3	36.7
Intact UCS (σ_{ci}) MPa	28.4	16.5	19.6	15.9 (kPa)
Av. Young's Modulus (E) GPa	10.0	4.5	4.2	0.8
Av. Poisson's Ratio (v)	0.4	0.4	0.4	0.5
Av. P-wave Velocity (V_p) ms^{-1}	2828.0	2108.1	2182.7	25948.2

Chapter 3

Rock Mass Properties

3.1 Introduction

Eight scanline defect surveys were conducted to characterise the rock mass properties of the Brunner Coal Measures (BCM) in the Reddale Valley, following the ISRM Suggested Methods for the quantitative description of discontinuities in rock masses (Brown, 1981). To access exposed BCM the locations chosen were limited to existing opencast highwalls and cuts that are no longer in production. Five scanline surveys where carried out in the southwest end of the valley, while three were undertaken on the northeast side. The proposed opencast site is located between the two sets of surveys, and therefore the highwall is likely to encounter similar mechanical properties as those presently displayed. The surveyed locations of the scanlines are recorded in appendix 2.1 and plotted on map A (Engineering Geological Map –map pocket).

Rock mass is defined by Johnson and DeGraff (1988) as a mass of rock interrupted by discontinuities, with each constituent discrete block formed by the defects, having intact rock properties. The terms ‘discontinuity’ and ‘defect’ are used in this chapter synonymously to imply any mechanical break or structural feature in the rock mass (Brown, 1981; Hoek and Bray, 1977). The properties recorded included defect type, defect orientation (dip and dip direction), wall rock strength, persistence, aperture, infilling, roughness, waviness (if applicable), seepage and spacing. The table used to record the data was adapted from the discontinuity survey data sheets produced by the Geological Society Engineering Group Working Party (Anon, 1977), as shown in appendix 2.2, to include all of these properties.

Objective surveys of all discontinuities intersecting the fixed line, independent of persistence or whether they appeared to be important, were undertaken. The trend and plunge of each scanline was recorded along with any variations along that line. As the scanlines were at significantly different orientations it was deemed relevant to apply the Terzaghi correction to the data (Terzaghi, 1965). This bias correction enables the defects sets to be represented by true relative frequencies, because low dips and defects at an acute angle to the traverse will otherwise be under-sampled. The Dips (version 5.0) programme produced by RocScience Inc (1999-2004) was used to analyse all the scanline data, and this has a built-in Terzaghi correction function. Although the Terzaghi correction does not effectively deal with angles at a very acute angle to the scanlines, the trends for the scanlines shown in figure 3.1, covers a wide range of orientations so that collectively the most significant defect sets should be adequately identified.

Figure 3.1 Orientation of scanlines represented by points with a trend and plunge. The number in brackets beside scanlines 1-8 indicates the number of different orientations measured within that traverse.

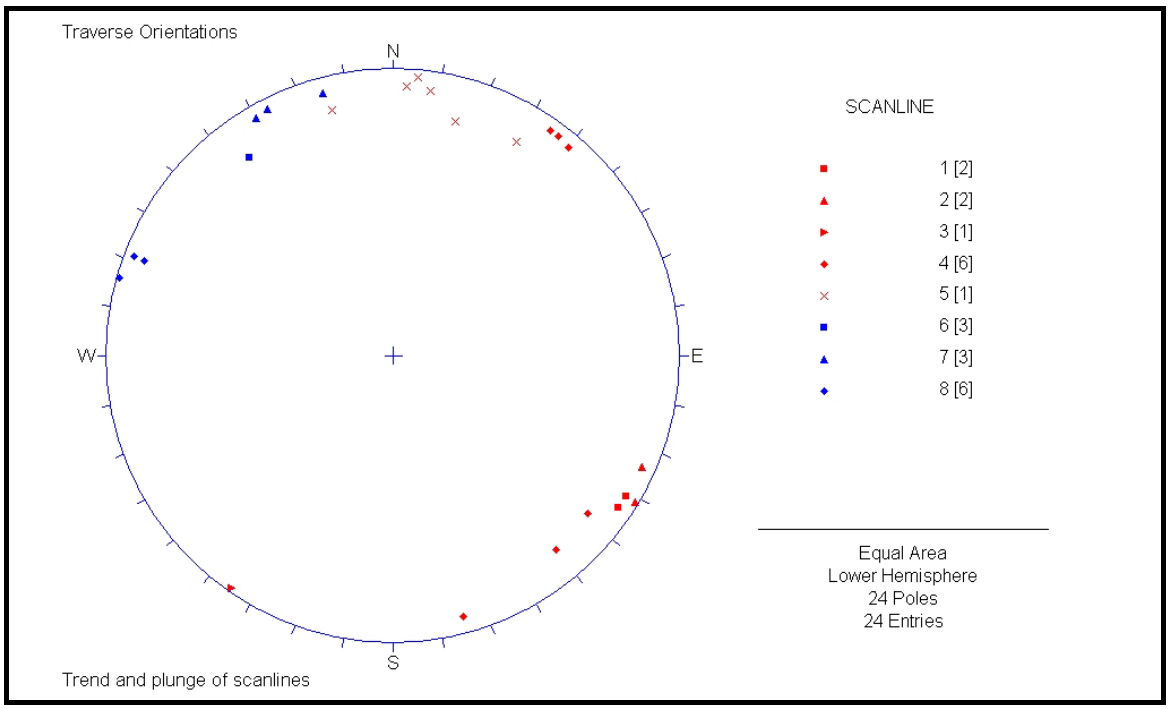

A total of 306 individual defects were measured along the eight scanlines, which had a combined length of 221.93m. All scanlines intersected sandstone laminated with carbonaceous mudstone and interbedded with thick (>1m) beds of carbonaceous mudstone. No siltstone was encountered and the loose sandstone appears in scanline 8 only. The physical properties of the defects recorded are described and discussed in this chapter. Drill-hole data was used to calculate defect spacing and an analysis of pump test data was performed to assess hydrological parameters of the overlying outwash gravels. The relevance and significance of the defects are analysed in chapter 4 along with an assessment of kinematic feasibility. All data collected from each scanline and drill core are presented in appendix 2.

3.2 Defect Types

Four distinctly different types of discontinuities were recorded where they intersected the scanlines. The predominant type was joints, which amounted to 86% of all the rock defects. As low dipping bedding was at an acute angle to the scanline only 8% of the defects recorded were beds that intersected the sub-horizontal line. Faults consisted of 6% and crush zones only 0.3%. Figure 3.2 displays the frequency of the defect types in a histogram and figure 3.3 shows some of the different types in an existing highwall.

Figure 3.2 Types of defects recorded in scanline surveys.

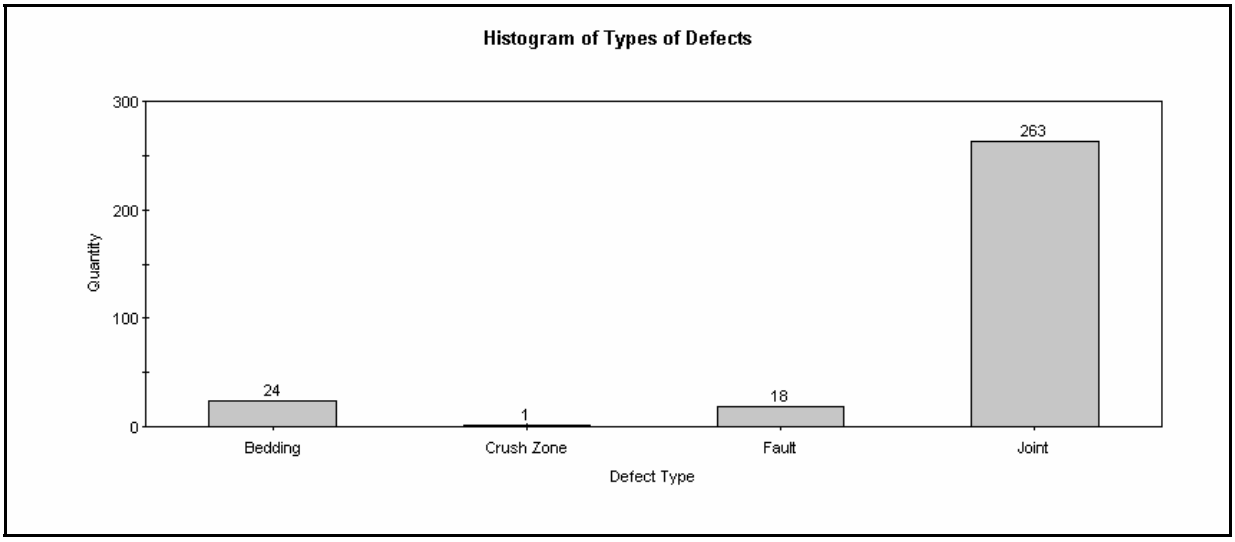

Figure 3.3 Photo of the north face of the 'Old' Terrace Opencast showing some of the defect types recorded.

The majority of the large scale (>2m) joints recorded exhibited tension characteristics as shown in figure 3.3. Care was taken not to mistake defects created by blasting with naturally occurring joints. Bedding can also be seen in figure 3.3 as a consistent plane of weakness and provides a potential plane of separation within the rock mass.

Figure 3.3 also illustrates the different character and strength displayed by the carbonaceous mudstone at the bottom of the photo, compared to the overhanging laminated sandstone above it. The mudstone displays complicated cleavage on exposed face and although this may be included as a defect, it is on such a small scale (< 1m) it has been excluded here. It should not however be

forgotten as it will influence rippability, and may cause small-scale stability problems. It can also be correlated with the behaviour displayed by the slake-durability test on the mudstone in chapter 2.

Most of the faults encountered in the scanlines were small (<1m displacement) normal faults such as that shown in figure 3.4. Their orientation suggests that they are exposed versions of the 'step-up' or in this case 'step-down' faults commonly seen underground. These have their down-thrown side down dip, and typically have 0.5m of displacement (Fowke, 1998). It has been suggested that they are related to surface subsidence caused by underground mining (Sleight, 2003), but there is no observable evidence of this at the outcrop or on the aerial photographs. Small circular subsidence features are present on top of the terrace, and so, graben-like structures would be expected in cross-section. These faults, and the larger faults recorded in the scanline and underground, are all sub-parallel to the strike of the coal seams, and they are therefore more likely be related to local tension during uplift of the area (Fowke, 1998). One crush zone was recorded and is described as disturbed, or crushed, rock where no obvious vertical displacement has taken place. This may be the result of shear movement out of the face and suggests that other stress regimes are also present (not orientated relative to local uplift).

Figure 3.4 'Step up' Faults intersected by scanline 5. An off set bed is indicated by the red dotted line. The round balls sticking out of the face are pyrite nodules which are numerous along this section. The dip of the fault is seen to refract and shallow across the more competent sandstone beds. This produces the characteristic secondary openings or 'pull apart' extensions along small scale conjugate wedges and makes the fault danger zone almost half a metre wide.

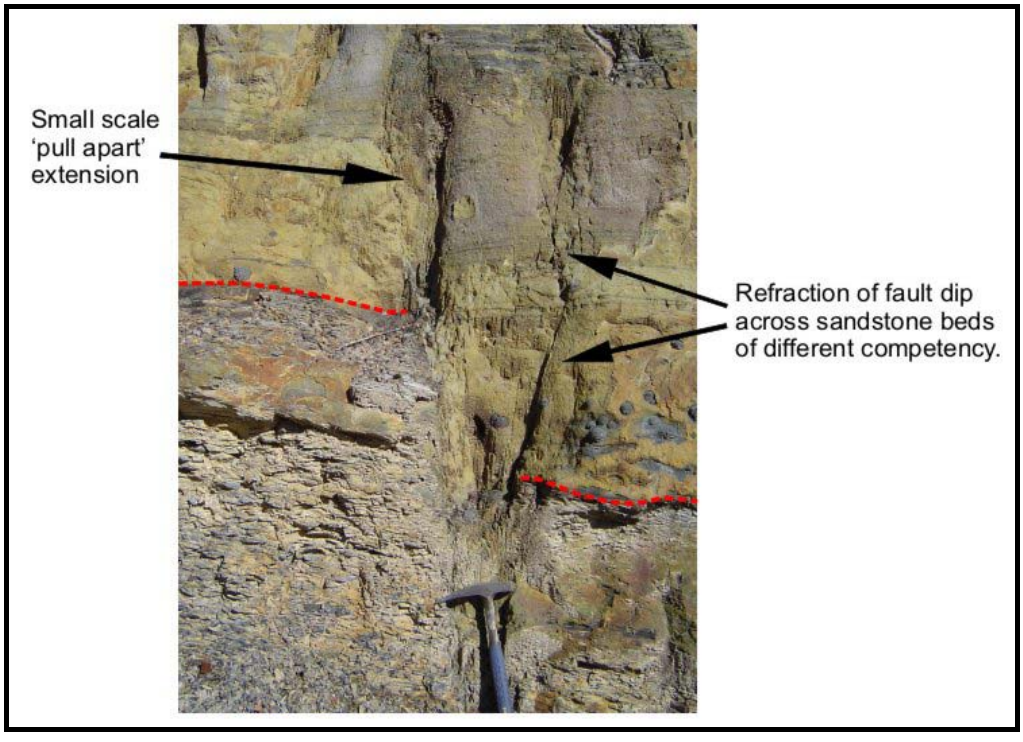

3.3 Defect Orientations

Differences in mean concentrations were observed between the defects recorded on the southwest side, and those on the northeast side, of the Reddale Valley when plotted in Dips. Equal area contour diagrams using dip and dip direction measurements where produced by the Fisher distribution method. This is similar to the Schmidt method, but is based on a distribution of influence which reflects an assumed probability of measurement error and produces smoothed density plots. The Dips *User's Guide* suggests that for most data sets clusters with a maximum concentration of greater than 6% can be classed as very significant, while 4-6% is marginally significant. This approach has been utilised here unless otherwise discussed. Each type of defect is dealt with and discussed separately in terms of mean orientation for the scanlines on both sides of the valley.

3.3.1 Bedding

The majority (79%) of the bedding was recorded in the southwest scanlines while the northeast only encountered 21% beds. This is due to under-sampling as all of the bedding is at an acute angle relative to the scanlines. The small amount of data resulted in the mean orientation for each side being best represented by a single point plotted in the centre of the maximum concentration. The dips for the south-west scanlines ranged from 2˚ to 38˚, with the maximum concentration occurring at 13˚ as shown in figure 3.5. The contour plot gave a relatively 'tight' concentration with only two outliers. The beds on the southwest side dip towards the northwest as previously documented by Suggate (1957), with the maximum concentration giving a dip direction of 323.

Figure 3.5 Dips contour plot of bedding data points (indicated by crosses) on the southwest side of the valley.

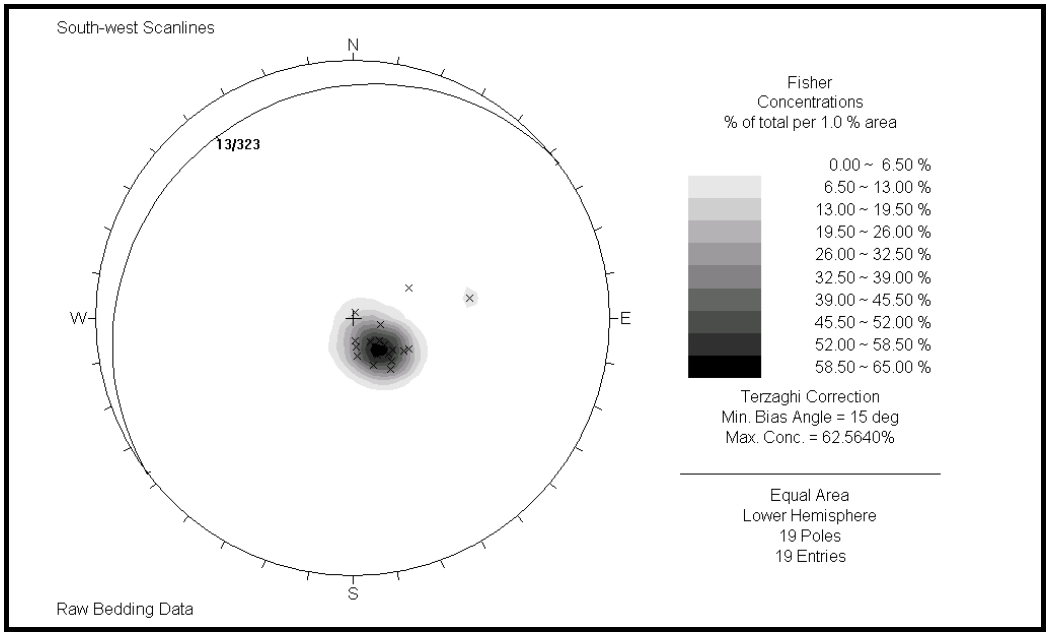

The maximum concentration for bedding in the northeast scanlines gives a dip direction almost due north at a bearing of 359, as shown in figure 3.6. The dip values ranged from 4˚ to 28˚ with the maximum concentration suggesting a mean dip angle of 9˚, which is slightly less than the southwest scanlines. While the Terzaghi correction adjusts the concentration percentage, the data is not necessarily a true sample of the bedding orientations present as it is such a small data set. Overall it can be assumed that although the dips will vary considerably the dip direction for bedding within the proposed opencast will generally be between 320 and 360.

Figure 3.6 Dips contour plot of bedding on the northeast side of the valley.

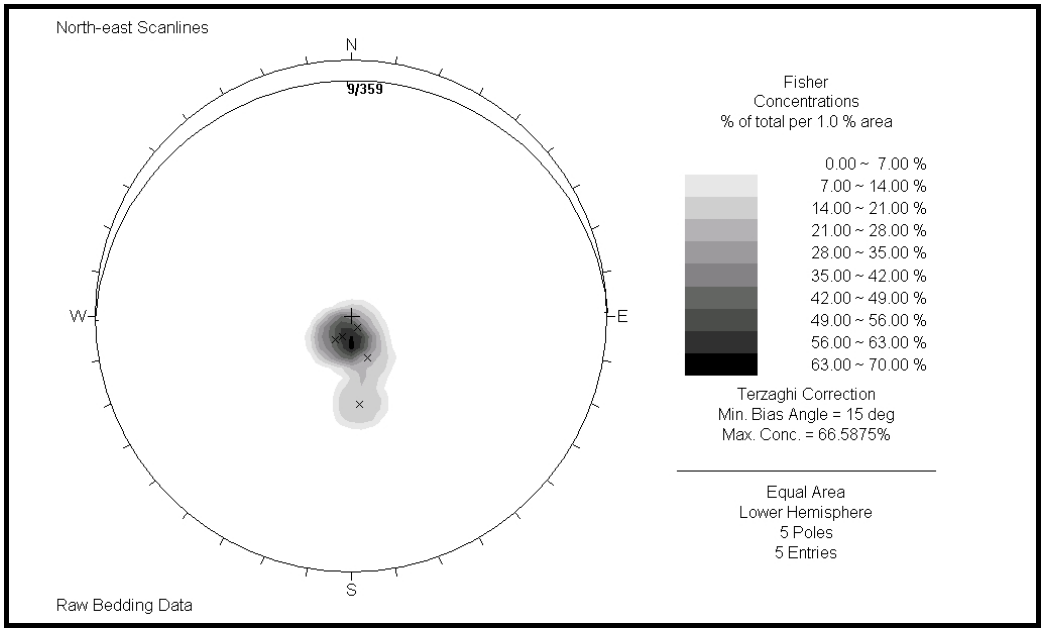

3.3.2 Faults and Crush Zone

All of the faults except one were recorded in the southwest scanlines. Most of these were the 'step-up' faults previously described, and have a mean concentration which dips at 84˚ towards 341 as shown in figure 3.7. The average orientation is calculated by Dips from a user-defined set window. Although there is a relatively wide spread, the poles are diametrically opposite and appear to be related. This is reinforced by that fact that their strikes are sub-parallel to that of bedding as previously suggested. One fault was however recorded at a significantly different orientation, and must be regarded as a separate set with a dip of 86˚ and a dip direction of 285. The single crush zone was also recorded in the southwest scanlines and gave a dip direction of 77˚ towards 184.

Figure 3.7 Contour plot of the faults intersecting the south-west scanlines.

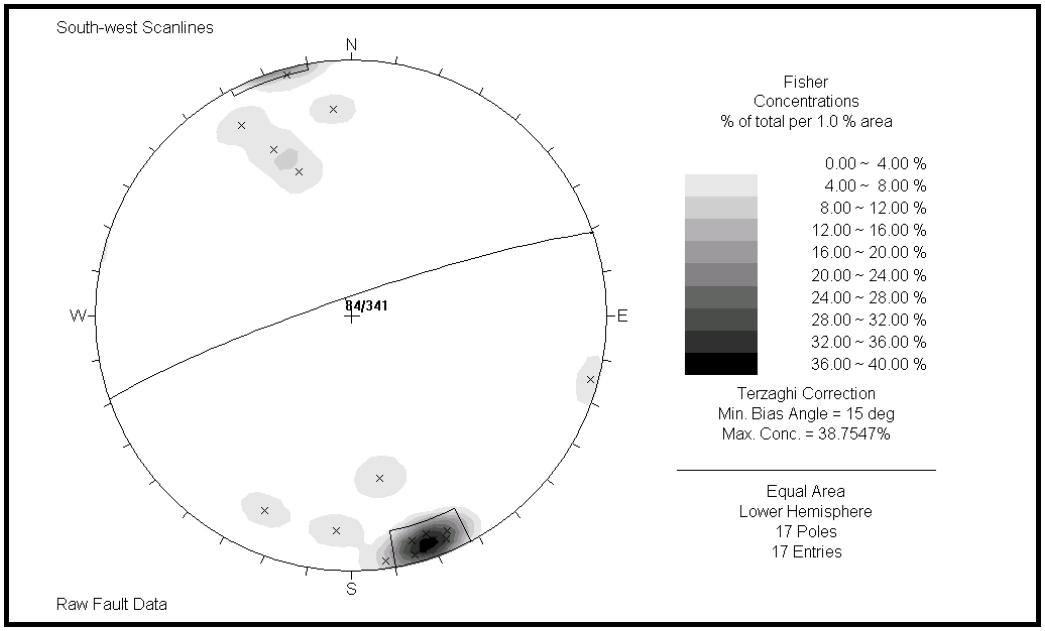

Although the single fault recorded in the northeast scanlines is dipping in the opposite direction to the main concentration, it appears to be related to those recorded in the southwest scanlines (diametrically opposite). The fault that dips at 77˚ towards 156 (figure 3.8) is most likely the surface expression of the Reddale Fault which has been observed underground and crosses the valley. It separates scanlines 6 and 7 as shown on map A (Engineering Geological Map –map pocket).

Figure 3.8 Contour plot of the Fault recorded in the northeast scanline.

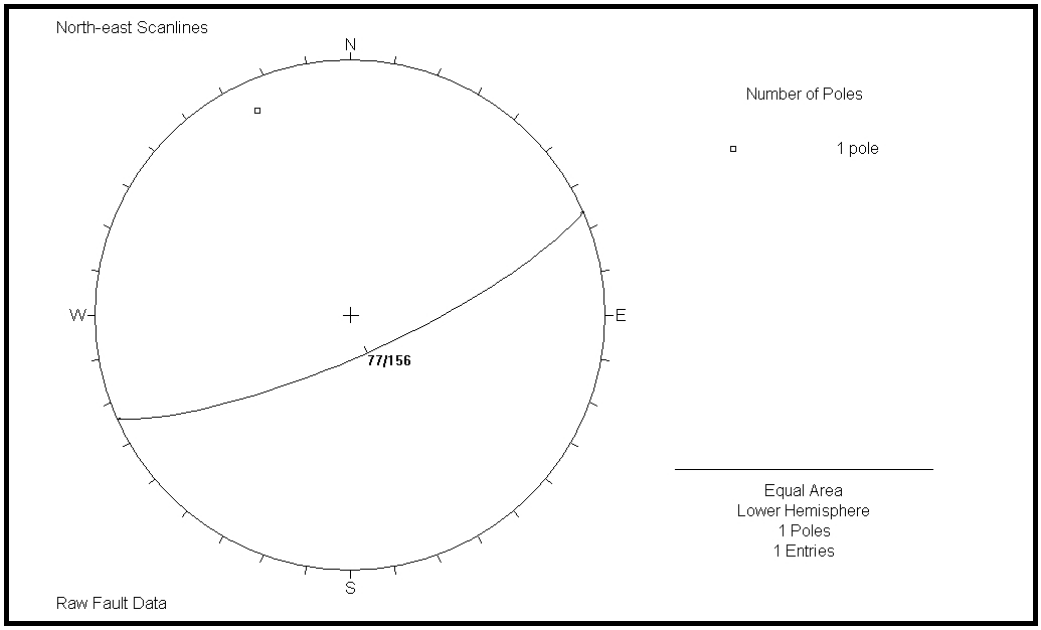

3.3.3 Joints

The joint maximum concentrations in the southwest and northeast scanlines were slightly different from each other. Table 3.1 shows a summary of the concentrations in each scanline. All Dips plots, from which these are derived, are presented in appendix 2.3. The major concentration of joints (JA1) in the southwest gave a mean set dip of 74˚ with a wide range of 13˚ to 90˚. The average dip direction is towards 078. A smaller concentration (JA2) of 4.5-6% is also present with a dip/dip direction of 72˚/156 but can only be considered marginally significant. A wide spread of steeply dipping joints in the south can be seen in figure 3.9 but has less than 3% concentrations.

Table 3.1 Summary of joint sets in each scanline (dip/dip direction).

Southwest Scanlines / **Joint Set Orientation**	**1**	**2**	**3**	**4**	**5**
JA1	65˚/071	75˚/079	80˚/083	74˚/083	72˚/075
JA2			70˚/156	69˚/155	
JA3	87˚/028	79˚/013		69˚/039	

Northeast Scanlines / **Joint Set Orientation**	**6**	**7**	**8**
JB1			81˚/177
JB2			79˚/201
JB3	68˚/219		79˚/230
JB4	64˚/244	88˚/241	

Figure 3.9 Contour plot of joints in the southwest scanlines.

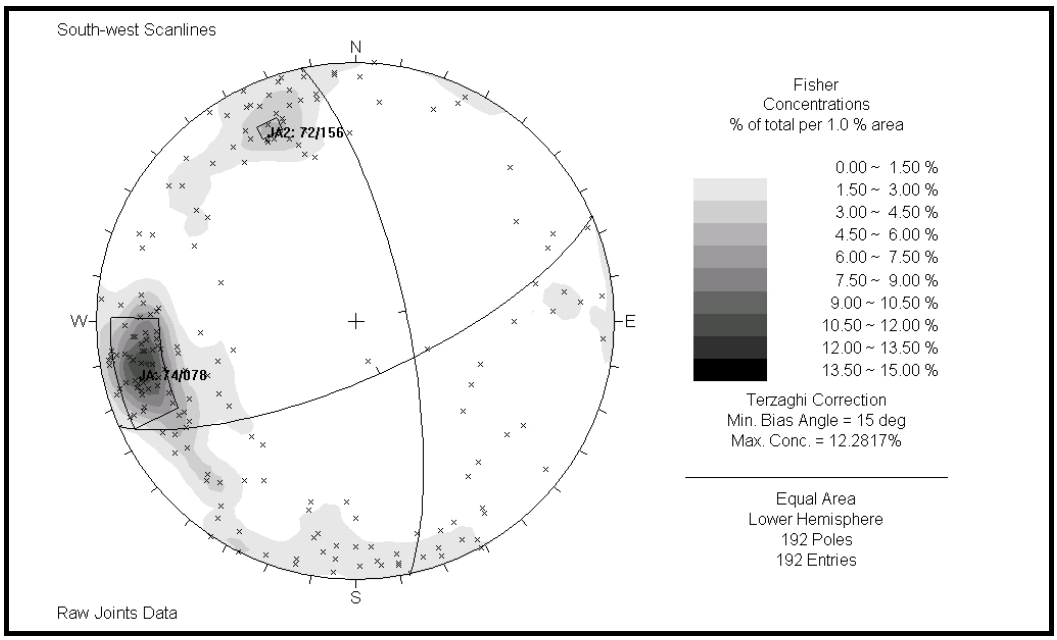

The northeast scanlines show four significant clusters which spread between north and east, as shown in figure 3.10. The main concentration has a maximum of 12-13.5% and dips towards the south (bearing of 177) at 82˚. The three smaller clusters have maximum concentrations of 7.5 to 9% and dip and dip directions which range between 74˚ and 88˚ towards 202 to 239. The joint sets are almost diametrically opposite, which suggests the two sides of the valley may be rotated and distorted relative to one another. This could be a result of the faults that cross the valley and intersect the scanlines on the northeast side, producing the scattered concentrations observed.

Figure 3.10 Contour plot of joints in the northeast scanlines.

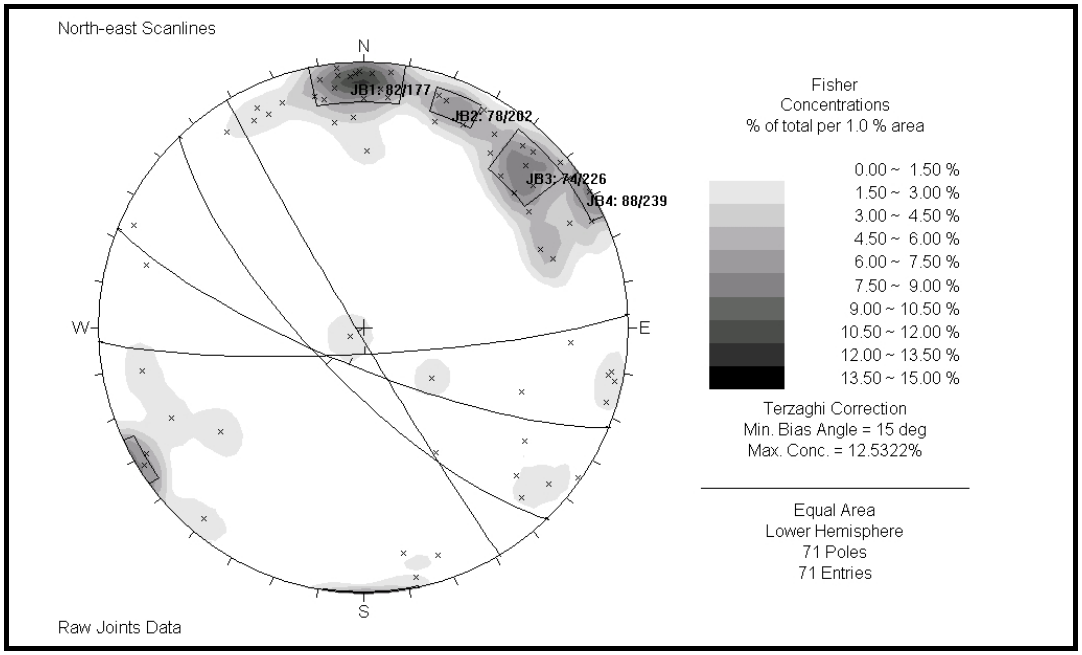

The clockwise swing in the strike of the southerly dipping set from the southwest scanlines (JA2), to the main set in the northeast scanlines (JB1), is similar to the rotation in bedding strike. This may reflect a pre-folding or pre-faulting relationship between these particular joint sets and bedding. The other sets do not show this behaviour and may be the result of a separate era of formation; however the wide scatter in the northeast scanlines makes it difficult to conclude any such relationships.

3.4 Defect Persistence

Persistence is defined by ISRM (Brown, 1981) as the discontinuity trace length as observed in an exposure. It gives an idea of the continuity of the defects in the rock mass and their relative importance to stability and strength. The exposure height varied from 5m or less on the ridge line to 10m+ visible in the highwalls. Defects with less than 2m continuity were measured with a tape measure and more persistent defects that could not be physically measured were estimated by sight by the author and field assistant. The type of termination displayed by the discontinuities at the top and bottom of the exposure was also recorded. The defects extended out of the exposure (x), terminated in the rock (r), or terminated against another discontinuity (d). The bias and errors caused by the angle of the discontinuity relative to the scanline, and the unknown length of those discontinuities which extend outside the exposure should not be ignored (Giani, 1992). The type of and amount of terminations for the different discontinuities are therefore discussed. Except when both ends of the trace length are observed to terminate in the rock mass, all persistence values should be regarded as minimum lengths (Johnson and DeGraff, 1998). The ISRM (Brown, 1981) classification scheme was used to analyse the persistence results, and is reproduced in table 3.2.

Table 3.2 Classification table for persistence (Brown, 1981).

Classification	**Persistence (m)**
Very low persistence	<1
Low persistence	1-3
Medium persistence	3-10
High persistence	10-20
Very high persistence	>20

Discontinuities reported in bedding were predominantly greater than 3m and could be traced across the length of exposure as previously shown in figure 3.3 (section 3.2). These therefore terminated outside of the exposure and can most likely be classified as having high to very high persistence, as several were observed to be greater than 20m. Several were measured as having around 2m length and terminated within the rock mass. They demonstrate the frequent

fluctuations in deposition within the Brunner Coal Measures. The rest of the beds which intersected the scanlines were less than 1.5m in length, as shown in figure 3.11. These laminations are often associated with carbonaceous concentrations and are within the larger beds of alternating lithologies.

Figure 3.11 Histogram of bedding persistence.

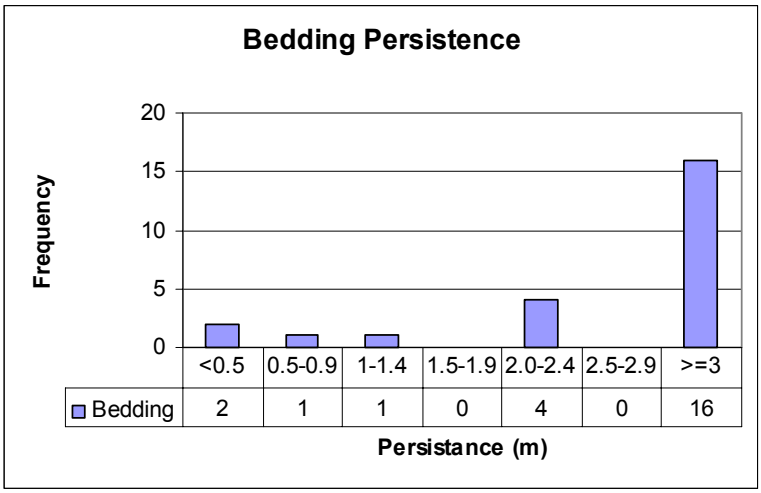

The faults showed a range of persistence from 1 to 6m in length, with an average of 2.2m for the normal 'step-up' faults recorded in scanline 5. The terminations are displayed in figure 3.12 and indicate that most of the faults died out in the rock at the top while the lower end terminated out of the exposure. This may be a result of the scanlines being situated near the top of the exposure (natural topographic surface) and little can be assumed about their depth beneath the ground if faulting post-dates the erosion surface. While these can be classified as having low persistence this may not be truly representative of the situation.

Figure 3.12 Column graph of fault terminations, where d represents defects which terminate against other defects, r is defects which terminated in rock and x is defects which extended out of the outcrop.

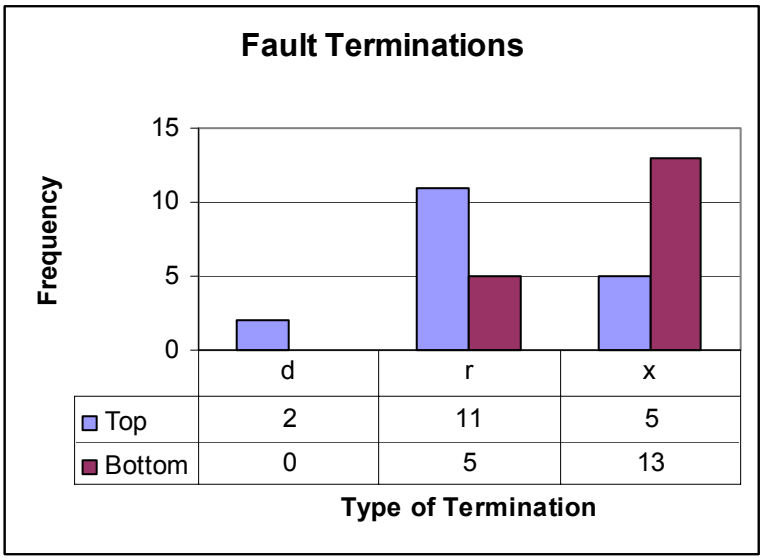

Joint persistence has been analysed according to the two locations of the scanlines. The southwest scanlines showed that a clear majority of joints had a persistence of 0.5-0.9m, as shown in figure 3.13. In fact 92% were less than 3m in length and they can therefore be considered as generally having low to very low persistence. The joints did however range from 0.2 up to 8m. The graph in figure 3.14 shows that the joints predominantly terminated against other defects at the top. The majority of joints terminate out of the bottom of the exposure, which is probably a result of the height of the scanline (approximately 1m) relative to the height of most of the exposures on this side of the valley (10m+). The termination index (T_r), as defined by ISRM (Brown, 1981) as the percentage of defects that terminate in rock compared to the total number of terminations, is 21% for the southwest scanlines.

Figure 3.13 Histogram of southwest scanlines joint persistence.

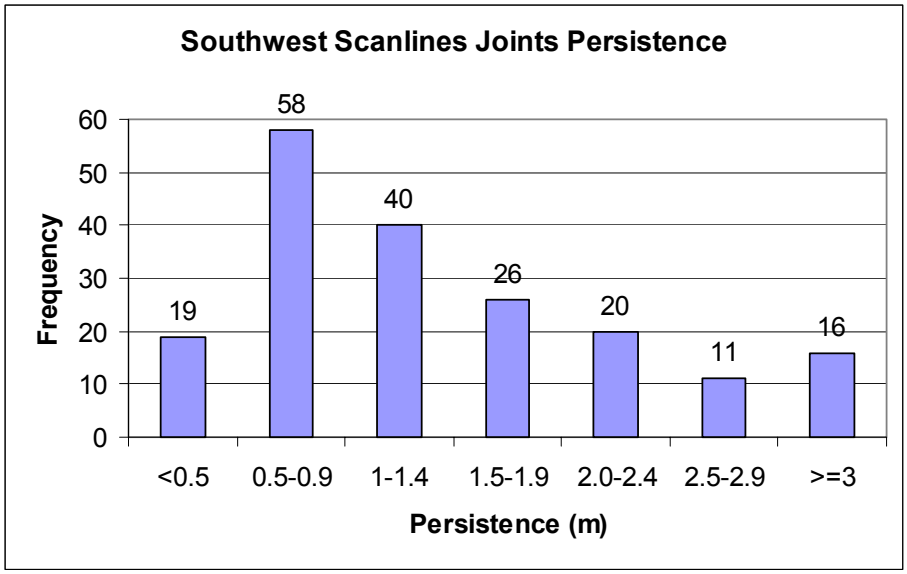

Figure 3.14 Column graph southwest scanlines joint termination, where d represents defects which terminate against other defects, r is defects which terminated in rock and x is defects which extended out of the outcrop.

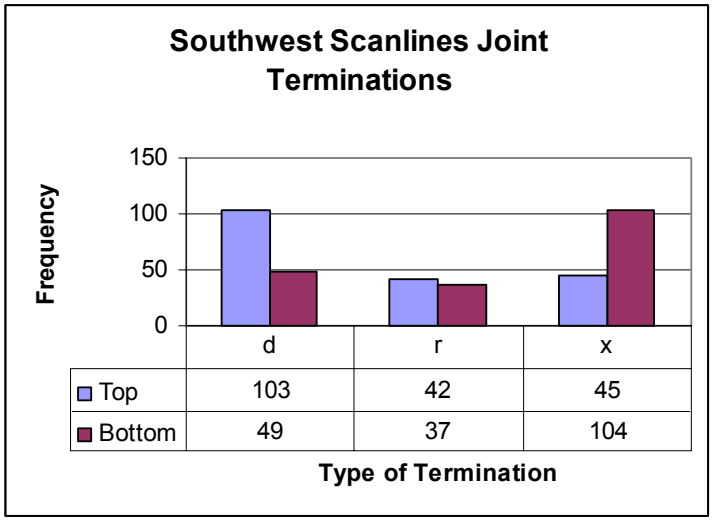

The major concentration of joints in the northeast scanlines gave a persistence of 1-1.4m as shown in figure 3.15. The persistence is more spread than the southwest scanlines and 20% have lengths which are greater than 3m. In general they can still be categorised as having low persistence and they range from 0.3 to 5m in length. The same trend of terminations, as discussed in the southeast is seen in the northeast (figure 3.16), with most terminations against other defects at the top and not visible at the bottom. The termination index (T_r) is only 10%, suggesting the defects are more continuous here than in the southwest.

Figure 3.15 Histogram of northeast scanlines joint persistence.

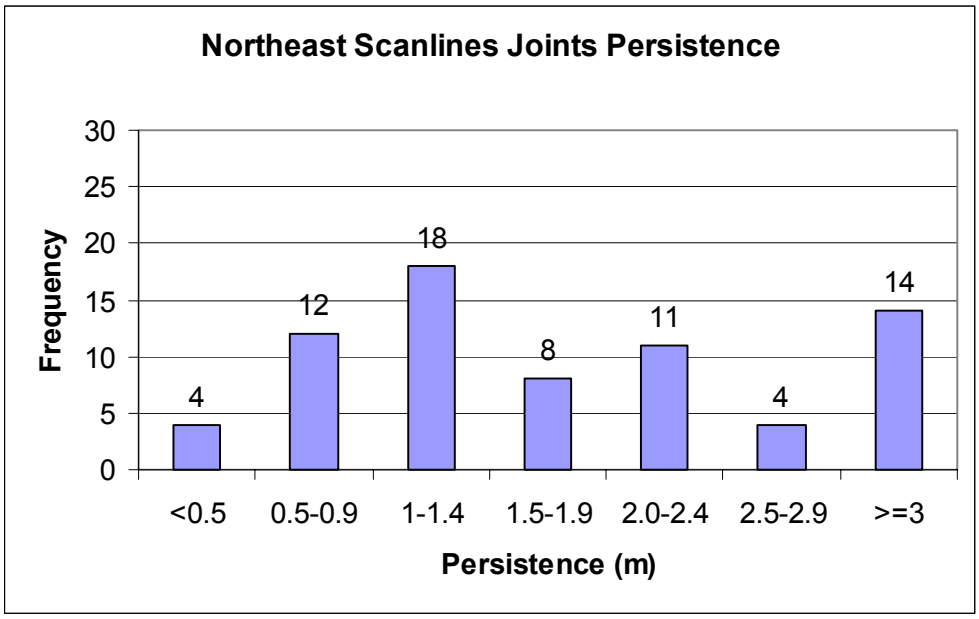

Figure 3.16 Column Graph of northeast scanlines joint terminations, where d represents defects which terminate against other defects, r is defects which terminated in rock and x is defects which extended out of the outcrop.

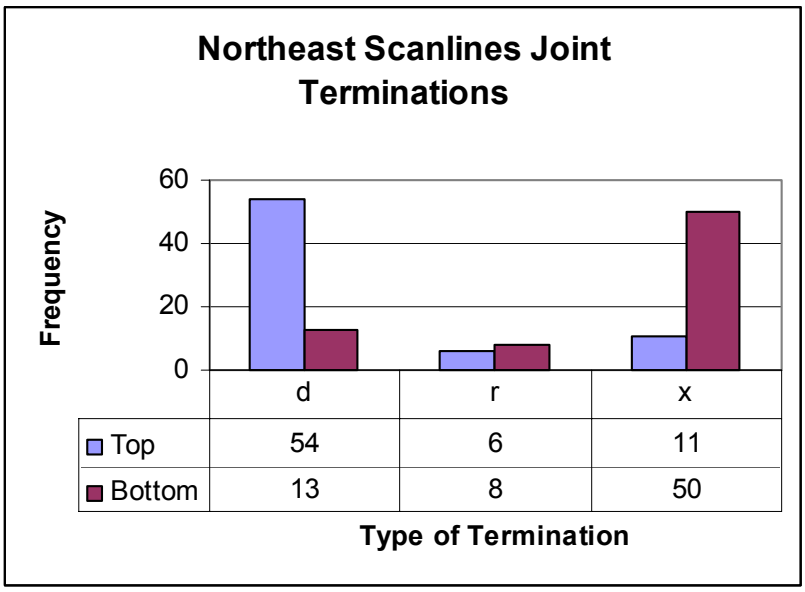

3.5 Defect Aperture and Infilling

The ISRM (Brown, 1981) specifies aperture as the perpendicular distance between adjacent rock walls of a discontinuity with the space between filled by air or water. Filling is defined as the material that separates the adjacent rock walls of a discontinuity, with a separate measurement for the width of filled discontinuities. These terms have been combined here with aperture referring to filled and open discontinuities, and the type of infilling incorporating those defects which are clean (without infilling) or filled by air. This approach was also adopted by Lucas (2002) and Pehi (2004).

The degree of separation between joint surfaces and the nature of the filling material may greatly influence the strength of the rock mass as a whole (Johnson and DeGraff, 1988). It is expected that the aperture will vary widely over the lateral extent of the defect. If this was observed in the exposure the maximum and minimum were recorded, but only the maximum values were used for analysis, to investigate the 'worst case' situation. Aperture measurements can be grouped by the descriptions stipulated by ISRM (Brown, 1981) and reproduced in table 3.3.

Table 3.3 ISRM Classification of Aperture (Brown, 1981).

Feature	Description	Aperture (mm)
"Closed"	Very Tight	<0.1
	Tight	0.1 - 0.25
	Partly Open	0.25 – 0.5
"Gapped"	Open	0.5 – 2.5
	Moderately Wide	2.5 - 10
	Wide	>10
"Open"	Very Wide	10-100
	Extremely Wide	100-1000
	Cavernous	>1000

Common infilling materials include clay, sand or other materials washed down into the rock mass from the ground surface. The zones may also be filled by alteration products of the rock material (Duncan, 1969). Filling material is normally weaker than the parent rock in which the defect occurs (Brown, 1981). Strength was estimated where possible by penetration or scraping with a knife blade. The infilling material was described by standard soil classification using visual examination and handling (Duncan, 1969), and was subsequently given the terms soft, firm, stiff or hard. Types of infilling recorded in the Reddale Valley were sand, clay, gouge or detritus (a mixture of material derived from surrounding units). Surface staining was also noted on joint faces and within apertures. The staining was predominantly orange (iron) or yellow (sulphur) in colour, derived from the pyrite within the units (discussed further in chapter 5).

Figure 3.17 shows the apertures recorded for bedding in all of the scanlines. These were mostly very tight which reflects the sharp cohesive contacts between lithologies and the shallow dip of bedding. The defects were therefore clean or showed surface staining. The four that displayed open or moderately wide apertures (0.5-3 mm) were either air or clay filled. The clay was recorded as being soft.

Figure 3.17 Histogram of bedding aperture.

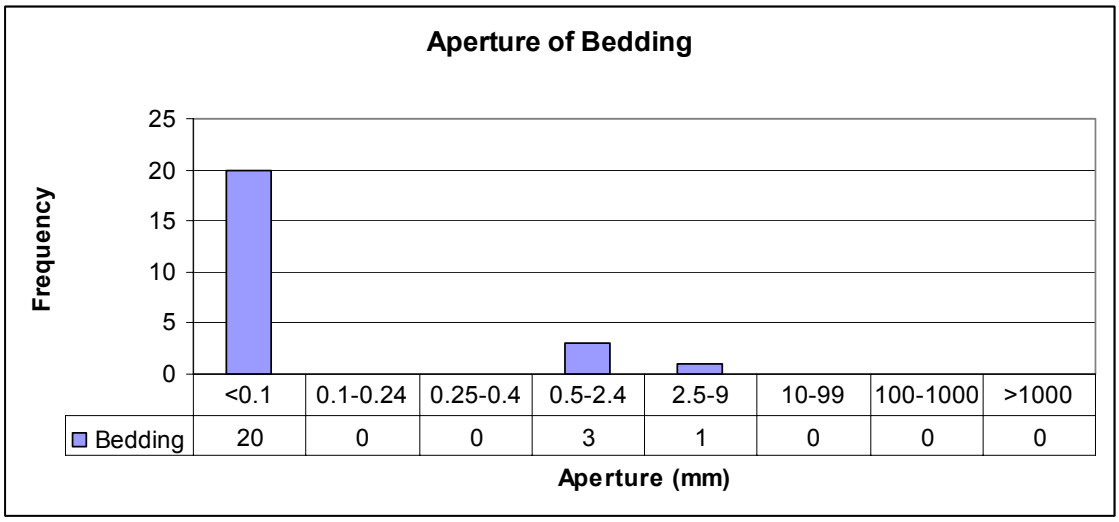

The majority of the apertures for the faults recorded fell between 0.5 and 100mm as shown in figure 3.18. They can be described as "gapped" features which are open to wide in nature. Figure 3.19 shows that 71% were infilled by gouge which is not surprising considering the 0.1-1m of observed displacement that has occurred along most of the faults. The gouge was soft in most locations and consisted of weakened mudstone, clay and clasts of sandstones from the surrounding units. Several were infilled with just clay, which appeared to have washed over the surface of the exposure and covered the gouge present beneath it.

Figure 3.18 Histogram of fault aperture.

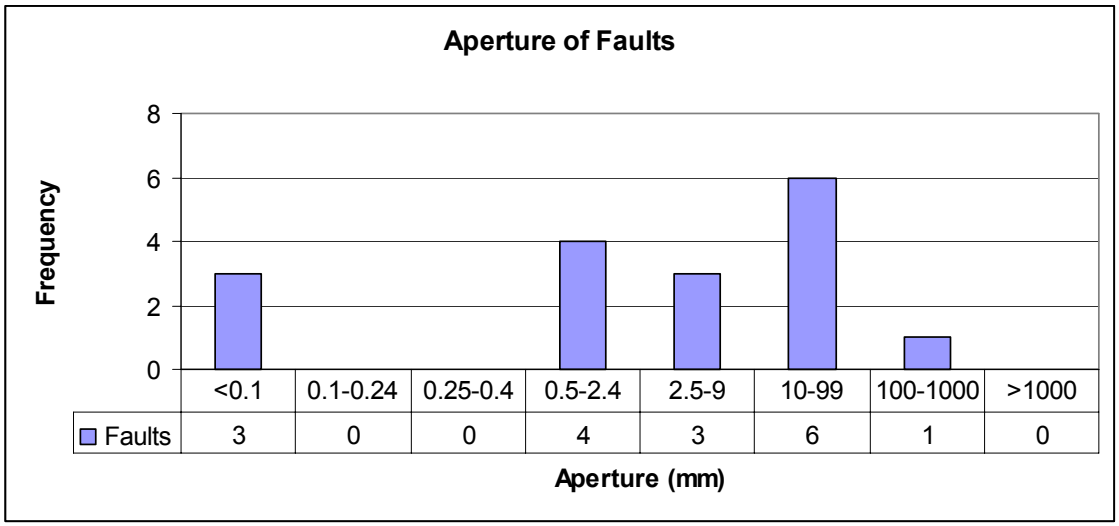

Figure 3.19 Pie chart of the types of infilling found in faults.

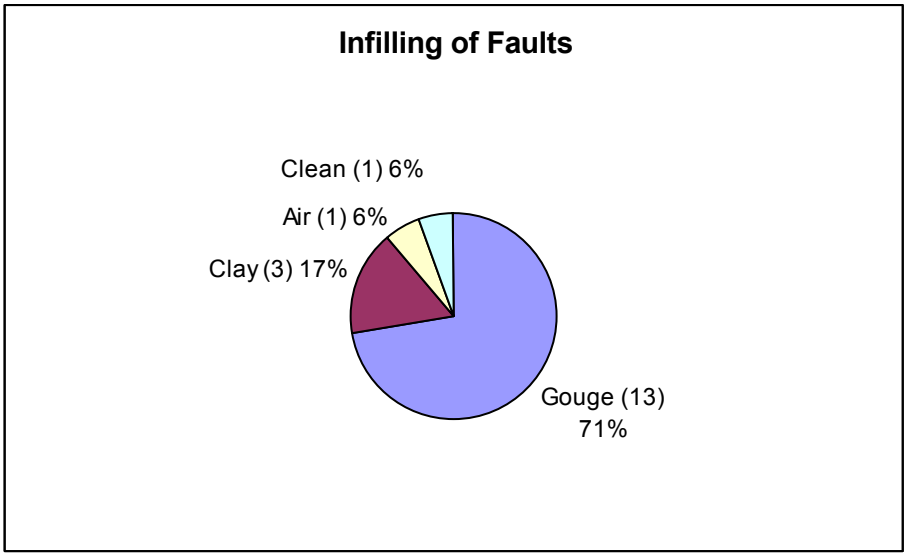

Figure 3.20 shows that 67% of the joints recorded in the southwest scanlines had a very tight aperture. The rest of the joints fell in the gapped features category (0.5-100mm). This corresponds to the majority (57%) of joints having no infilling (clean) as illustrated by figure 3.21. While 11% recorded surface staining only, many joints showed staining as well as another infilling. Where the surface coating was thick it was noted as being hard. Air (open unfilled defect) and clay infillings had similar frequencies and made up 29% combined. Sand infilling was recorded four times and detritus once, both of which were sourced from the surrounding rock. Strengths recorded ranged from very soft in the clay to stiff in sand.

Figure 3.20 Histogram of southwest scanlines joint aperture.

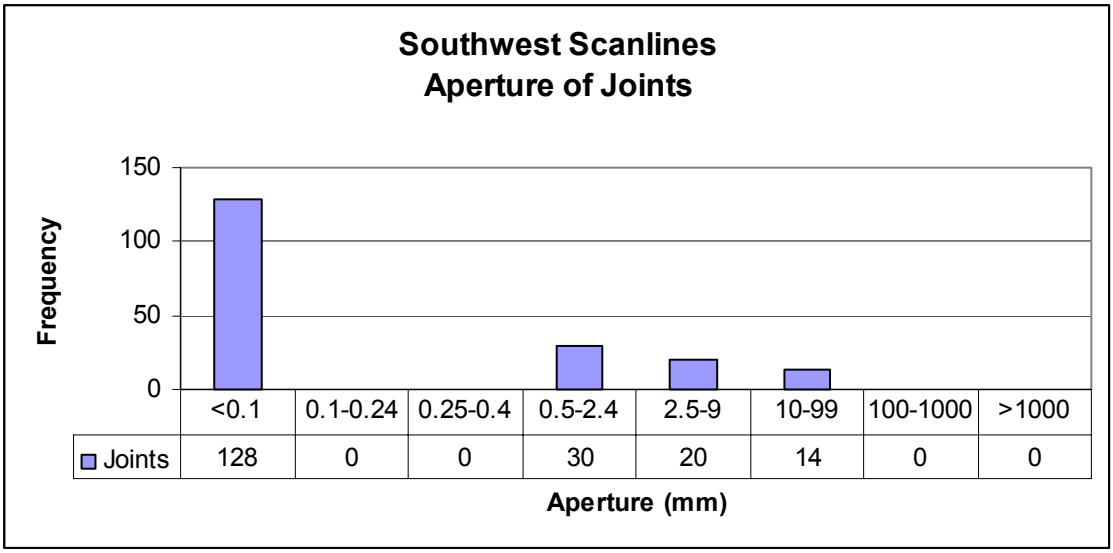

Figure 3.21 Column graph of the types of infilling found in southwest scanlines joints.

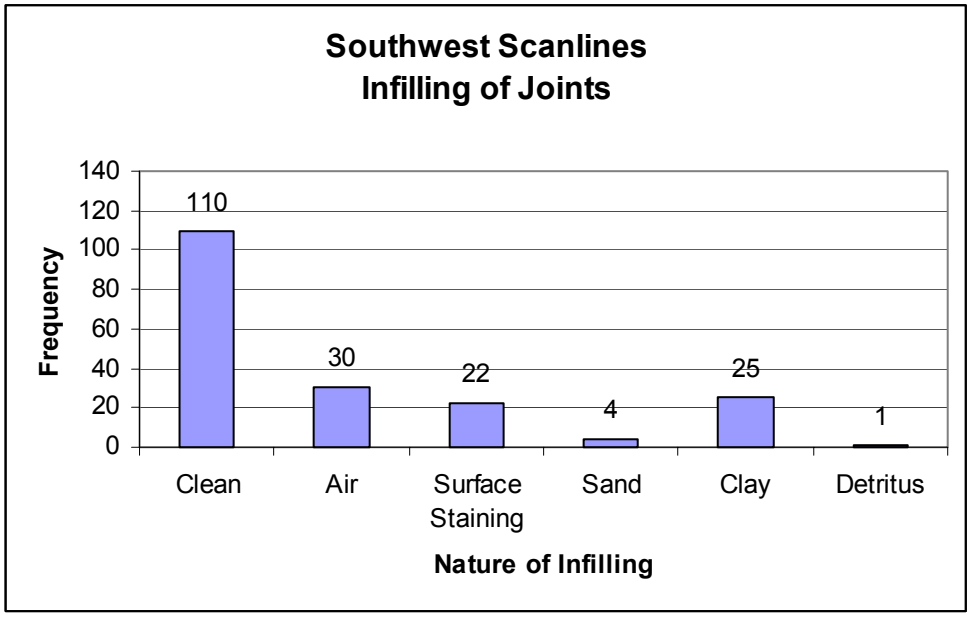

The northeast scanlines also display a high percentage (61%) of very tight joints as shown in figure 3.22. While a cluster of gapped features are present again, there are several open features with extremely wide or cavernous aperture. Figure 3.23 shows an example of a cavernous joint which should it daylight will cause a significant slab failure. The defect is most likely a product of tension joints related to the near vertical cut faces and such wide fissures are not expected to be present in the undisturbed rock mass beneath the valley floor.

Figure 3.22 Histogram of northeast scanlines joint aperture.

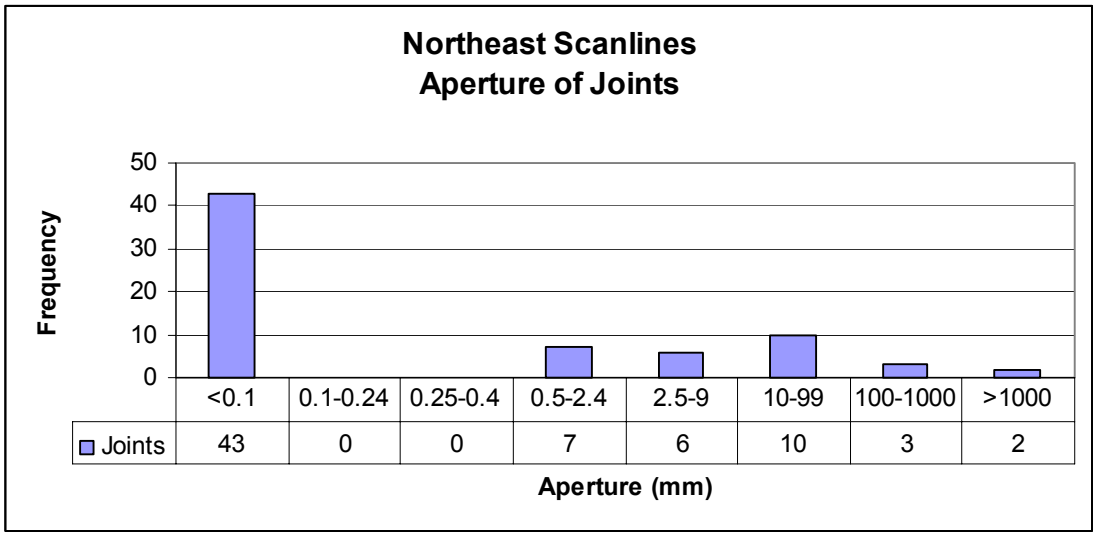

Figure 3.23 Photograph of cavernous joint in scanline 7.

Clean and surface stained joints make up 54% of the defects present which again correlates with the tight nature of most of the joints (figure 3.24). Surface staining is also present with other fillings and some of the larger aperture joints are partially infilled as well as open (air filled). Clay contributes to 23% of the filling material while 14% are just filled by air and 10% are infilled by detritus. The detritus and clay were recorded as having weak or soft strengths.

Figure 3.24 Column graph of the types of infilling found in northeast scanlines joints.

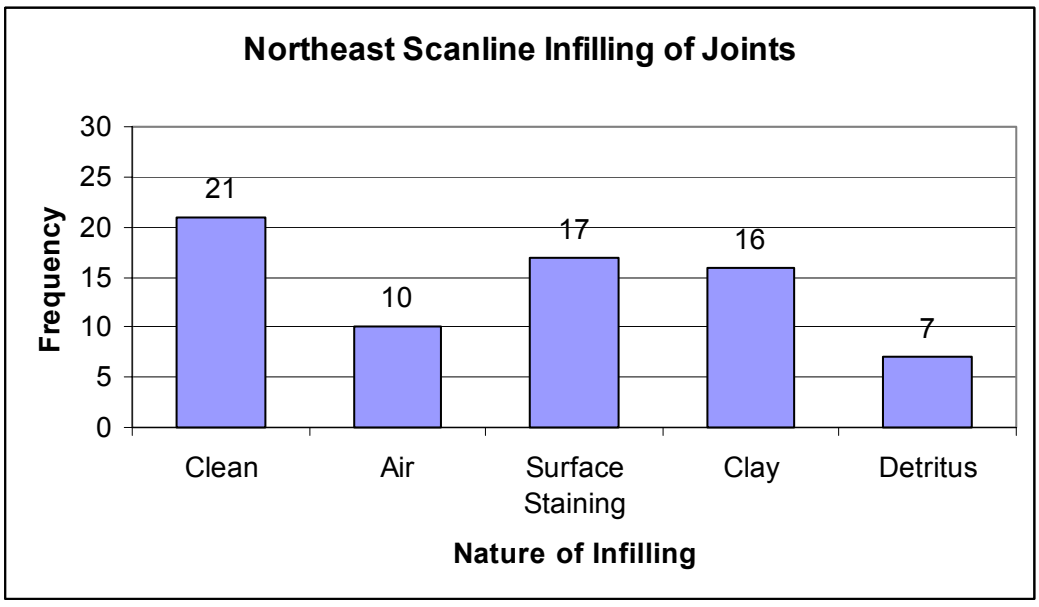

3.6 Defect Roughness and Waviness

Roughness is another way to characterise the defects present in the scanline surveys undertaken. Roughness according to ISRM (Brown, 1981) refers to the inherent surface unevenness and waviness relative to the mean plane of a discontinuity. Waviness is defined as large (metre) scale undulations and can cause dilation during shear displacement if interlocked and in contact.

Roughness is estimated in both a qualitative and quantitative manner. Descriptive terms of small (rough, smooth etc) and intermediate scales (planar, curved, stepped, irregular etc) were determined by touch and visual inspection. A metal profile contour gauge was also pressed against the defect surface and compared to the ten standard roughness profiles proposed by Barton and Choubey (1977). This gives a joint roughness coefficient (JRC) of between 0 and 20, with higher values indicating a greater degree of roughness as shown in figure 3.25. No JRC number was recorded if the defect displayed considerable variation along its length within the outcrop, and could not be represented by the standard profiles.

Figure 3.25 Roughness profiles and associated JRC values (Barton and Choubey, 1977).

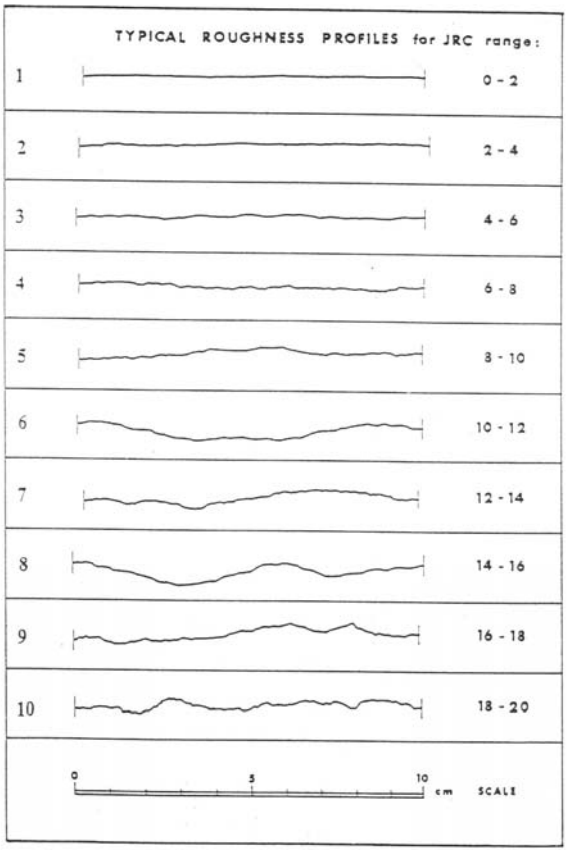

Waviness is more difficult to estimate and was only attempted on those defects which displayed an obvious reoccurring undulation. A measurement of wavelength and amplitude (both in metres) was approximated by sight. The parameters were measured according to their general

definition shown in figure 3.26 because most texts are vague about how to measure and use the terms, especially amplitude. It is however an influential characteristic in terms of slope stability because large scale waviness can prevent sliding when the asperities are too large to be sheared off (Giani, 1992).

Figure 3.26 Diagram of amplitude and wavelength definition.

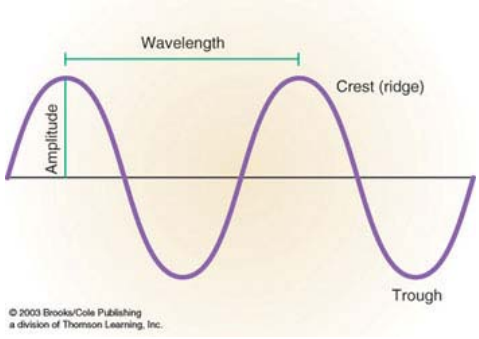

The bedding defects had generally low JRC values of predominantly less than 6 as shown in figure 3.27. Planar and smooth surfaces were observed on most beds. The JRC values that ranged from 6 to 9 were characterised by curved and rough surfaces, and a wavelength of 10m and amplitude of 0.25m was measured on one such defect. The defect with a high JRC (16) displayed a stepped defect plane. In most cases it was not possible to obtain JRC values for the faults recorded. The majority displayed a curved face that was smooth and several were planar and smooth.

Figure 3.27 Bar graph of bedding roughness.

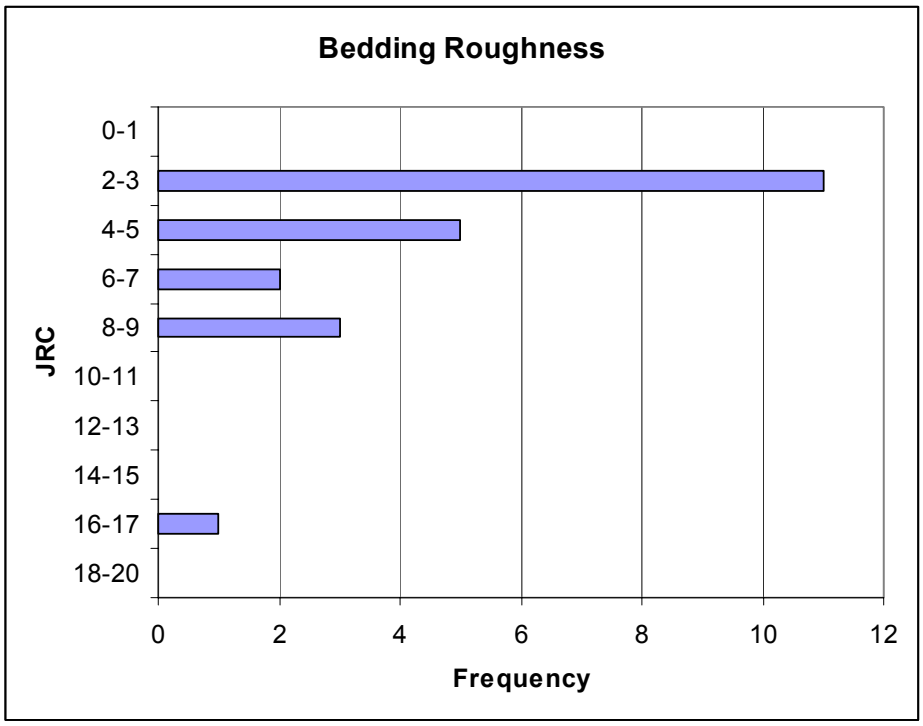

Figure 3.28 shows that joint roughness in the southwest scanlines exhibited mostly low JRC values with relatively smooth surfaces, although a variety of values were recorded. These were predominantly below a JRC of 10, and each grouping displays a similar frequency. The defects below a JRC of 6 were predominantly planar or curved and smooth. A wavelength of 1.5m and amplitude of 0.1 was measured at one locality. Those in the 6-7 JRC category had similar surface descriptions but with occasion irregular surfaces. The average wavelength was 2m and 0.12m amplitude, which was calculated from estimates on 5 separate joints. Those between 8 and 9 JRC were mostly planar and rough or curved and irregular. The roughness descriptions increase in severity for those above 10 JRC, which are increasing irregular and rough. Only waviness for two defects was recorded and gives an average of 0.75m wavelength and 0.075m amplitude.

Figure 3.28 Bar graph of southwest scanlines joint roughness.

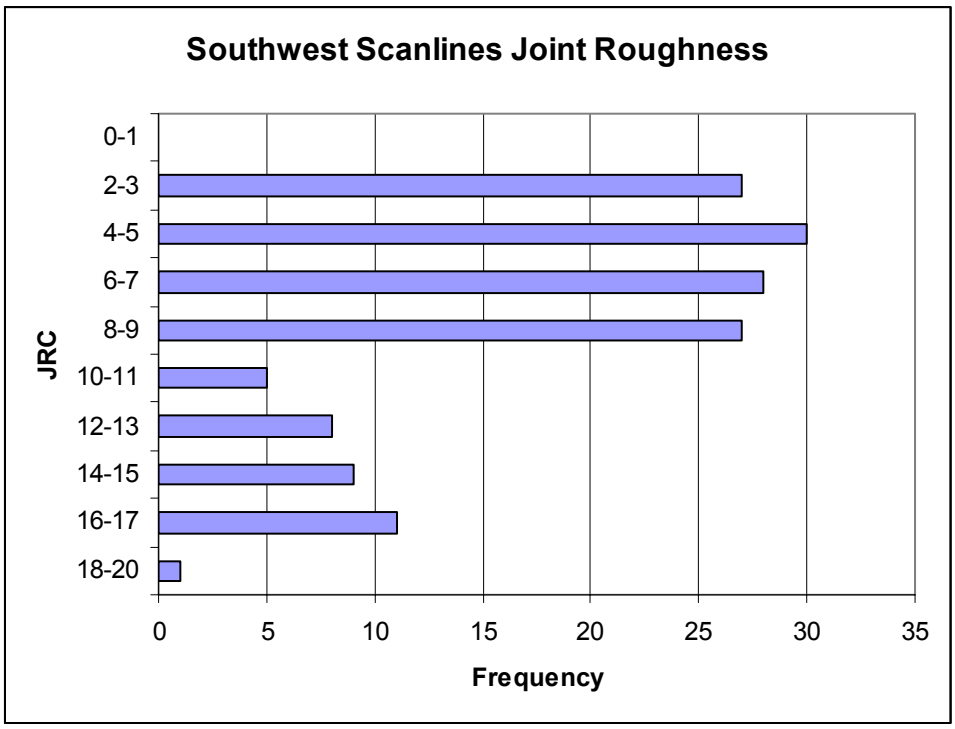

The northeast scanlines also have a spike of low JRC values, in particular 2-3 as shown in figure 3.29. There are however more joints with very high JRC values than the southwest scanlines. The same pattern of descriptions does apply with lower values having corresponding planar or curved and smooth surfaces. As the JRC values increase the faces get increasingly stepped and irregular. One joint in the 2-3 JRC bracket gave a wavelength of 1m and amplitude of 0.1m. Another in the 18-20 range gave a wavelength of 2m and amplitude of 0.15m.

Figure 3.29 Bar graph of northeast scanlines joint roughness.

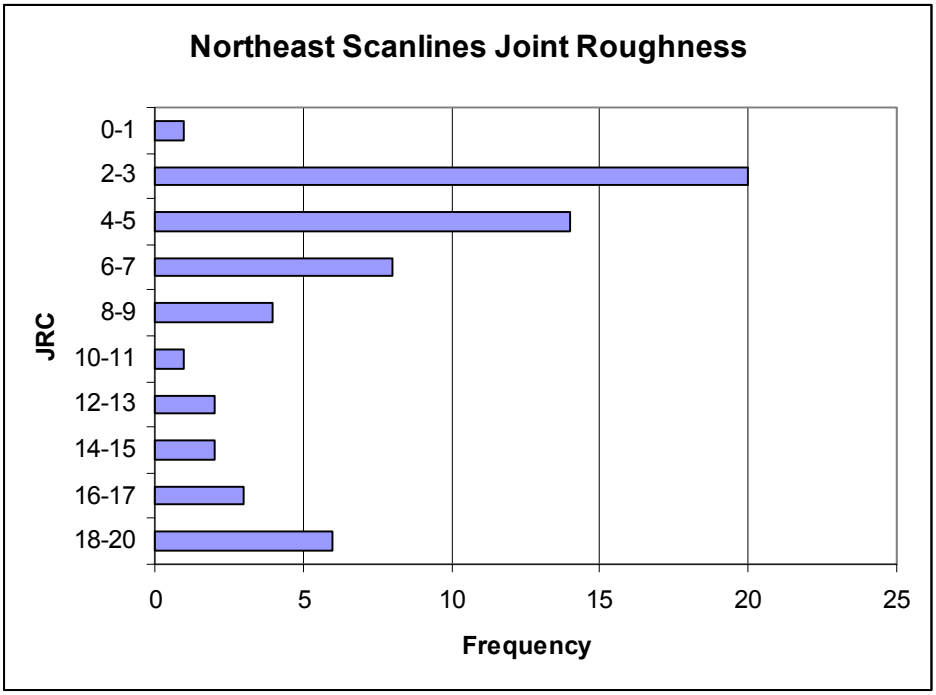

3.7 Wall Strength

Wall strength is also significant to shear strength and deformability if the defect walls are in contact. It is defined by ISRM (Brown, 1981) as the equivalent compressive strength of adjacent rock walls of a discontinuity. As defects allow weathering to penetrate the rock mass, wall strength is greatly affected by the degree and nature of alteration present. Wall strength is therefore generally lower than the overall strength of the rock mass (Giani, 1992). This was not the case for all the joints in the Reddale Valley where the sandstone laminated with carbonaceous mudstone, and containing significant pyrite, was highly discoloured (orange/yellow) on exposed surfaces by a coating which causes a 'case hardening' affect. This phenomenon is studied in detail and discussed in chapter 5. Those surfaces that were coated with clay did display weak characteristics. The results here reinforce this apparent strengthening when compared with the intact strength gained from unweathered drill-core, as discussed in chapter 2.

Several Schmidt hammer tests were untaken on joints surfaces in the scanlines on the southwest side of the valley. Ten or more readings were recorded for each test, and the average of the highest five was used to calculate the rebound number, as suggested by ISRM (Brown, 1981). Using an average density of 23kN/m^3 (as determined in chapter 2) this was then plotted on the graph shown in figure 3.30 to gain a joint compressive strength (JCS). All readings were taken

perpendicular to a near vertical surface and on dry or damp surfaces. The results are presented in table 3.4 (raw data in appendix 2.4) and show the average JCS to be 32 MPa.

Figure 3.30 Relationship between Schmidt Hammer hardness and compressive strength based on density and angle of hammer to surface (after Hoek and Bray, 1977).

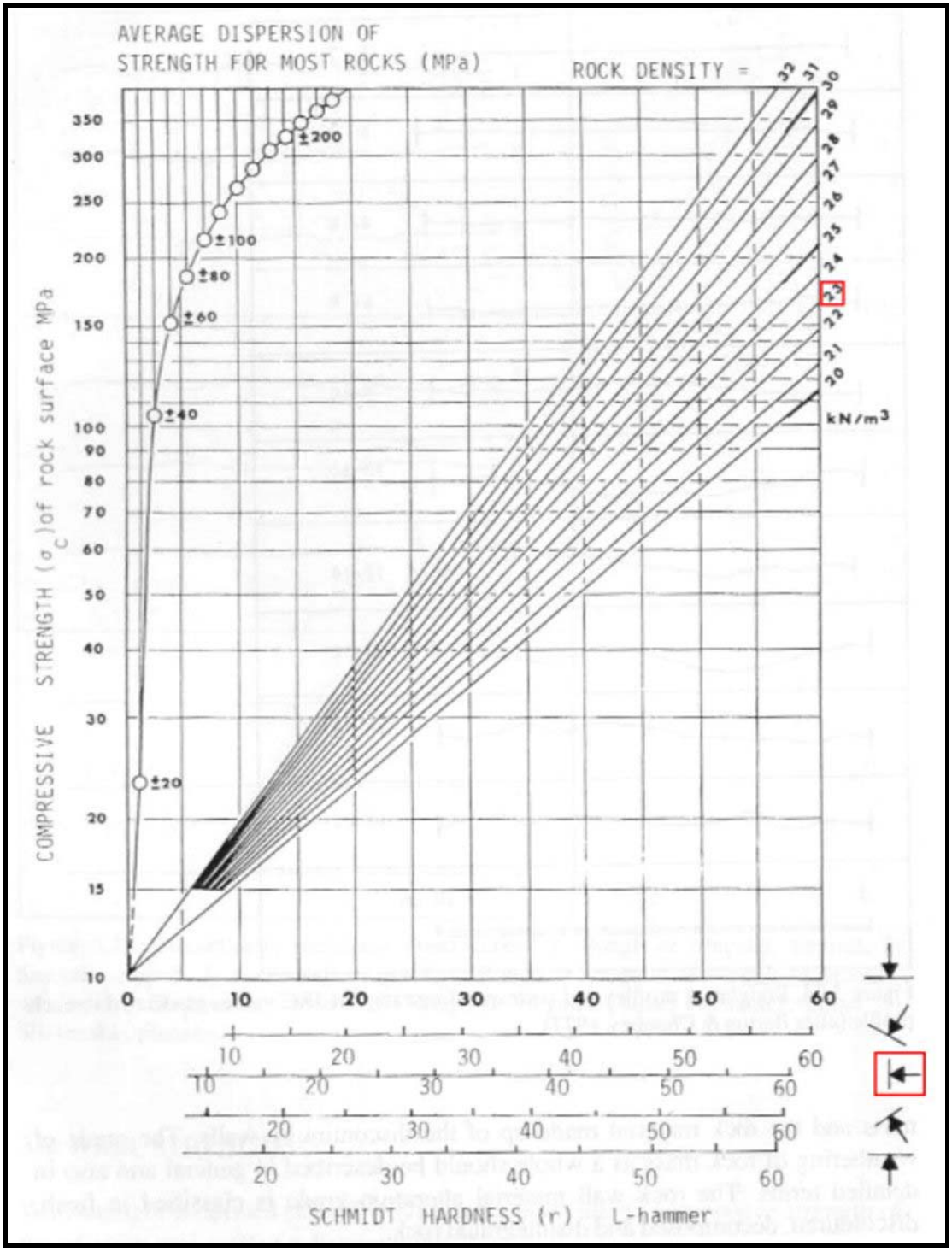

Table 3.4 Results from the Schmidt Hammer Tests.

Test	1	2	3	4	5	6	Average
Schmidt Hardness -r	28	25	27	28	23	25	26
JCS (MPa)	33	30	38	33	27	30	32

Manual index tests were also undertaken as a semi-quantitative approach to wall strength. They were recorded for each defect where possible and based on how the rock responded when scraped with a pocket knife and hit with a geological hammer. Table 3.5 displays the ISRM classification scheme and the associated approximate UCS used to asses the wall strength.

Table 3.5 Manual index test classification for rocks (Brown, 1981).

Grade	Description	Field Identification	Approx. range of UCS (MPa)
R0	Extremely weak rock	Indented by thumbnail	0.25 - 1.0
R1	Very weak rock	Crumbles under firm blows with point end of geological hammer, can be peeled by a pocket knife	1.0 - 5.0
R2	Weak rock	Can be peeled by a pocket knife with difficulty, shallow indentations made by firm blow with point of geological hammer	5.0 - 25
R3	Medium strong rock	Cannot be scraped or peeled with a pocket knife, specimen can be fractured with single firm blow of geological hammer	25 - 50
R4	Strong rock	Specimen requires more than one blow of geological hammer to fracture it	50 - 100
R5	Very strong rock	Specimen requires many blows of a geological hammer to fracture it	100 - 250
R6	Extremely strong rock	Specimen can only be chipped with geological hammer	>250

The wall strength of the bedding in all the scanlines was predominantly categorised as very weak rock, as shown in figure 3.31. As the bedding planes were at a low angle to the face of the exposure, little area was subjected to weathering and case hardening was not developed. The estimated UCS for all of the bedding strengths recorded was under 25MPa (R0-R2), which correlates with the intact strengths presented in chapter 2 (<30MPa). Wall strength for the faults was difficult to determine when neither of the walls were exposed. The limited observations recorded suggested a similar range to the bedding strengths, with a majority being very weak rock, which is probably due to the gouge within the fault zone.

Figure 3.31 Bar graph of bedding wall strength.

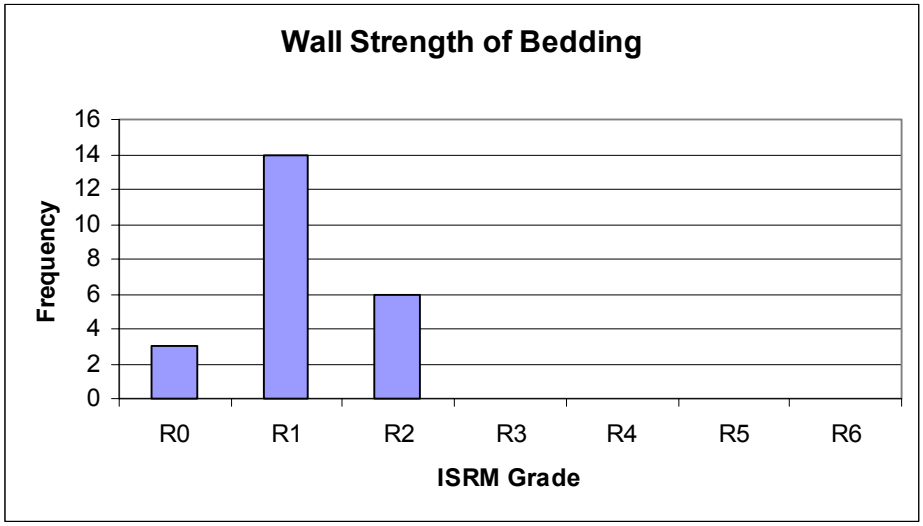

Although the scanlines in the southwest and northeast produced the same range of joint wall strengths, the concentrations were different and related to the unit and locations. The southwest scanlines, as shown in figure 3.32, displayed a larger proportion of medium strong rocks, which is directly related to the hardening crust covering the joint faces on the open highwalls and where the scanlines predominantly intersected laminated sandstone. The northeast scanlines were less exposed to weathering, and encountered more mudstone and loose sandstone, which is reflected by a spike of extremely weak wall rocks. Figure 3.33 is a graph of the values recorded for the northeast data.

Figure 3.32 Bar graph of southwest scanlines joint wall strength.

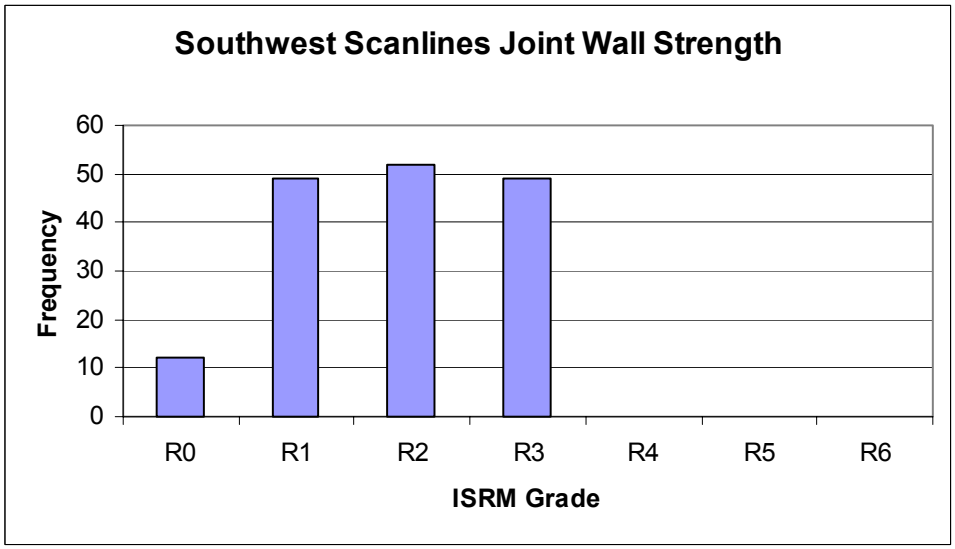

Figure 3.33 Bar graph of northeast scanlines joint wall strength.

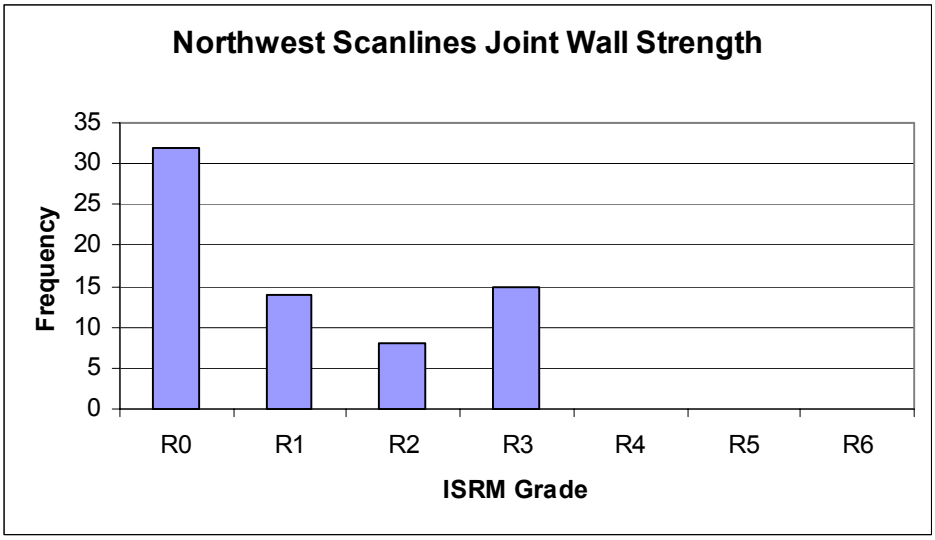

3.8 Seepage

ISRM (Brown, 1981) defines seepage as the water flow and free moisture visible in individual discontinuities, and it indicates the degree of 'secondary permeability' possible. It is a good indication of future stability problems and excavation difficulties, especially in areas with high rainfall such as the West Coast. For efficiency and due to the amalgamation of aperture and filled defects as explained in section 3.5, a simple classification was adopted to give an estimate of seepage condition in the scanlines. The defects were either termed dry (no moisture present), damp (some moisture present), seepage (evidence of some or past flow) or flow (water running over face of defect). No sites exhibited enough flow that a rate could be determined. They were assessed by visual inspection during the autumn months (April to June). The results however may not be representative of conditions once the valley floor is excavated below the water table and significant dewatering of the walls into the pit occurs.

As shown by figure 3.34, 91% of defects observed were dry which correlates with the predominantly 'tight' aperture discussed previously. Figure 3.35 shows an example of a defect in a northeast scanline where signs of past seepage, such as iron staining and transported clays, are visible. Seepage was recorded on 3% of defects within the scanlines. Both active flow and dampness also accounted for 3% each of the defects observed. In the cut walls above the water table seepage does not appear to pose a significant problem.

Figure 3.34 Pie graph of defect water flow for all of the scanlines.

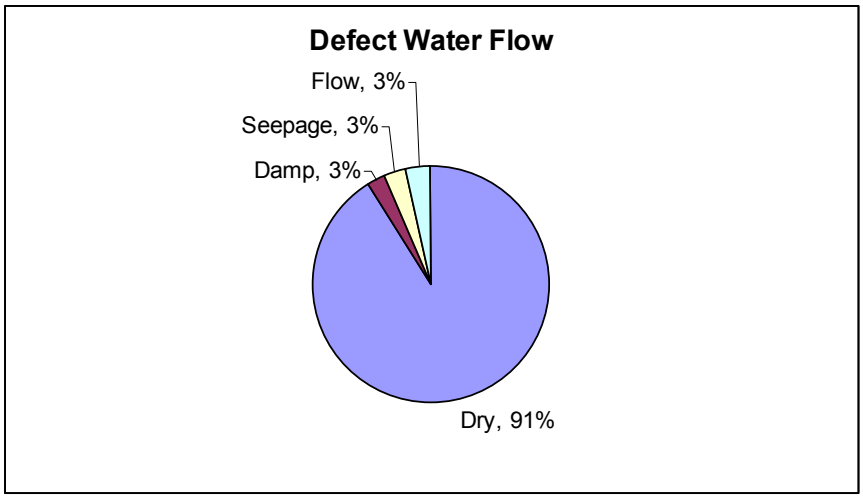

Figure 3.35 Photo of defect with orange staining showing signs of past water flow.

3.9 Defect Spacing and Rock Quality

Defect spacing is defined by ISRM (Brown, 1981) as the perpendicular distance between adjacent discontinuities. It controls the size of individual blocks of intact rock and influences rock mass permeability. Deere, (1968) suggested a method to determine the mean percentage of discontinuities in NX or larger core, which is known as the Rock Quality Designation (RQD). This is obtained by dividing the summed length of core pieces equal or greater then 0.1m by the core interval length. It is expressed mathematically by:

$$\text{RQD} = 100 \sum_{i=1}^{n} x_i/\text{L} \ \%$$

where x_i is the spacing values greater then 0.1m, n is the number of these intersections and L is the borehole or scanline length. It therefore provides a quantitative estimate of rock mass quality. Barton *et al.,* (1974) give a classification scheme for RQD which is used when calculating Tunnelling Quality Index (Q), and is used here to assess the results in terms of rock quality, as shown in table 3.6.

Table 3.6 Classification of rock quality based on RQD, after Barton et al., 1974 cited in Hoek et al., 1997.

Rock Quality	RQD (%)
Very Poor	0 - 25
Poor	25 - 50
Fair	50 - 75
Good	75 - 90
Excellent	90 - 100

Deere *et al.,* (1967) suggested that scanlines and borehole core were analogous when measuring discontinuity frequency as RQD can be calculated in both cases. While it is possible to calculate defect spacing from scanline data by analysis of average joint set spacing, there are several complications involved. Priest and Hudson (1981) state that the bias caused by linear sampling must be eliminated before the data can be used. Sen and Kazi (1984) also comment on the bias involved with using short scanline lengths. The drill hole data is therefore regarded as a more accurate representation of the defect spacing and rock quality. The drill holes will also give more meaningful results because they are situated on the valley floor compared to the scanlines, which are situated on the valley sides and not directly within the area of the proposed opencast.

The RQD for each interval of every drill core was calculated by Adrian Field (Consultant Geologist) when logging the core. He calculated the amount of intact core (m) greater than 0.1m and divided it by the length of the core run. For consistency only the core in BCM above the No. 4 seam that will make up the overburden, is analysed here. The drill core records of RQD are given in appendix 2.5 and drill hole locations are given in appendix 1.10. The number of RQD values within a given range were calculated as shown in table 3.7, and plotted as a histogram in figure 3.36.

Table 3.7 Frequency of values within a range of RQD (%).

	RQD (%) Frequency					
Drill Hole	**0-24**	**25-49**	**50-74**	**75-89**	**90-100**	**Total**
653	9	3	0	0	0	12
654	2	0	4	0	0	6
656	3	0	0	2	7	12
657	7	3	5	5	5	25
658	0	0	0	3	14	17
660	1	1	2	0	1	5
662	7	2	2	7	15	33
663	14	2	6	4	13	39
Total	43	11	19	21	55	149
Percent	29	7	13	14	37	

Figure 3.36 Histogram of rock quality using intervals determined by Barton et al., (1974) for Tunnelling Quality Index..

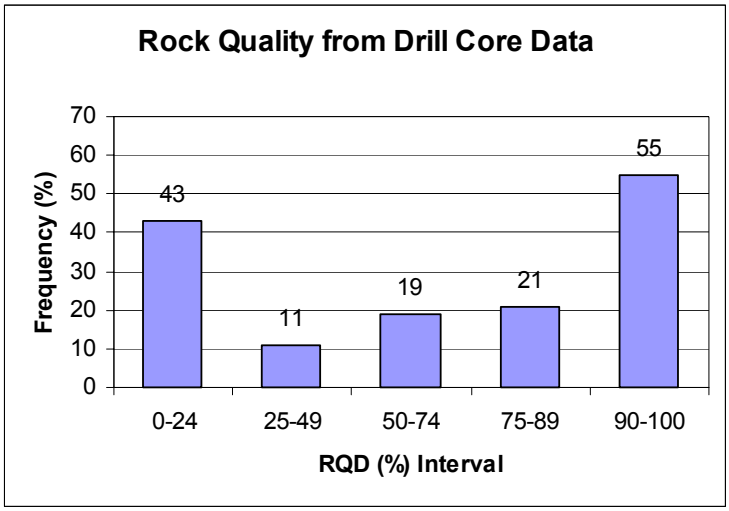

The results from the 8 drill holes show that 37% of core was within the excellent class (RQD = 90-100%), while 29% was at the other end of the scale, in the very poor quality rock (RQD = 0-25%). This suggests that while some of the rock mass may be reasonably sound other parts will be closely jointed and potentially unstable. The RQD values were also analysed according to the four units established in chapter 2 and are presented in table 3.8 and figure 3.37.

Table 3.8 Frequency of RQD (%) values for each unit.

Unit	1 ZS	2 CM	3 SS/CM	4 SS
	Siltstone	Carbonaceous	Interbedded	Loose
Interval		Mudstone	Sandstone/mudstone	Sandstone
0-24	0	20	17	7
25-49	0	5	4	1
50-74	1	6	5	3
75-89	7	9	3	2
90-100	13	20	12	9

Figure 3.37 Histogram showing the frequency of RQD for each unit as a percentage.

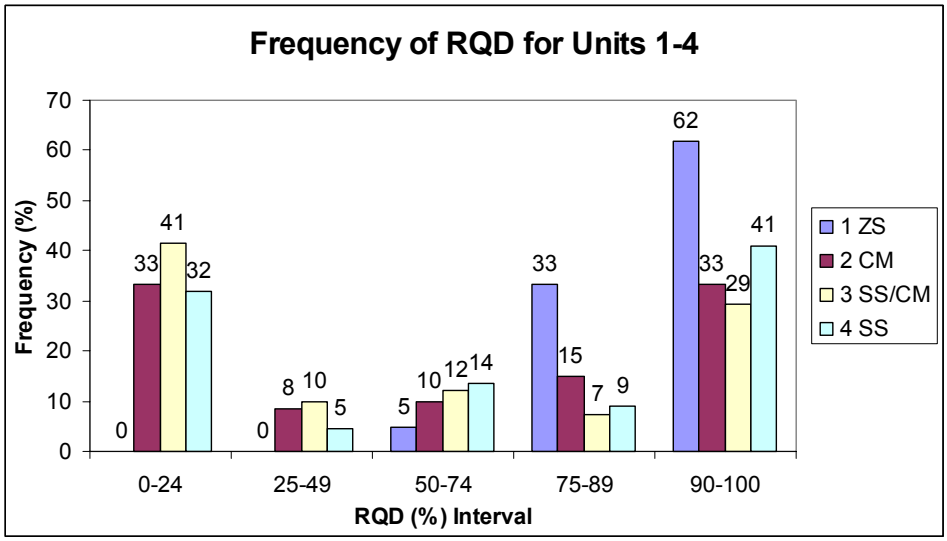

Figure 3.37 shows that the siltstone (unit 1) has the highest percentage of excellent (62%) and good quality rocks (33%), which is expected given the rock material properties (such as the highest density) determined in chapter 2. The siltstone does not have any RQD values below 50%. Surprisingly the loose sandstone (unit 4) has 41% of the RQD values within the 90-100% interval. This may be because well developed joints do not form in such uncemented material as it does not have enough tensile strength to fracture but instead is able to accommodate movement. This suggests that RQD calculations for material that is on the border between rocks and soils may not give meaningful indications of rock mass quality.

3.10 Near Surface Hydrogeology

The Reddale Valley experiences substantial rainfall throughout the year; the rock mass and overlying glacial outwash gravels on the valley floor are continuously saturated. The water table had been monitored throughout the last 12 months by measuring the depth of ground water in two bore holes. The results are presented in table 3.9 and show the water table is approximately at 1.5m below the ground. The depth to the water table increases slightly as distance away from the creek increases (on the southwest side of the valley). Very little seasonal change was observed, with the biggest difference of 0.25m occurring between May (winter) and December (summer) in DH 658. The hydrological conditions may cause a significant difficulty for excavation in terms of slope stability and erosion caused by inflow. When the base of the pit is below the water table, dewatering of the units within the walls will occur until a new equilibrium is reached. As significant amounts of water flowing into the pit are likely, this may cause progressive erosive channels in the highwall. The water may also fill and enlarge joints or fissures in the rock mass and affect stability. Unfortunately this analysis is restricted to the overlying gravels and does not provide hydrological parameters for the rock mass as a whole. However the aquifer identified is likely to be free draining into the pit and parameters derived will aid prediction of near surface inflows.

Table 3.9 Results from ground water monitoring.

	Depth to water table (m)	
Well	**656/7**	**658/2**
Date		
18/04/2005	1.9	1.24
20/04/2005	1.9	1.25
17/06/2005	1.7	1.25
11/12/2005	1.9	1.5
7/02/2006	1.86	1.48
Average:	1.85	1.34

Drill holes 656 and 658 completed by Solid Energy, together with two observation holes each, were used to perform pump tests to investigate ground water. They were drilled by rotary wash through the Quaternary gravels, and both were cased and screened. DH 656 was screened within the outwash gravels only (1-14m depth) and DH 658 was screen between 1 and 15m and encountered gravels for the first 10m, which was followed by BCM sandstone for the final 5m, with a band of carbonaceous siltstone between 11.8 and 13.4m. A clear flow was developed by air-lift compressing for several hours before testing. A summary of construction details are given in table 3.10. A constant rate pump test was undertaken for a period of 50 (DH 656) or 100 (DH 658) minutes. Drawdown and recovery measurements were recorded by Adrian Field, and raw data is presented in appendix 2.6.

Table 3.10 Summary of construction details.

	656			658		
Hole ID	**Pumped**	**656/2**	**656/7**	**Pumped**	**658/2**	**658/10**
Drilled Depth (m)	14.5	14.68	14.8	13.9	15	15
Screened Depth (mbgl)	12.00-14.00	1.00-14.68	1.00-14.80	8.90-10.90	1.00-15.00	1.00-15.00
Nominal Drilled Diameter (mm)	150	100	100	150	100	100
Nominal Cased Diameter (mm)	125	25	25	125	25	25
Casing Height (magl)	0.6	0.5	0.76	1	0	0
Pre-test Static Water Level (mbTOC)	2.45	2.25	2.56	2.39	1.43	1.21

Drawdown (Z) was plotted against time (t) for each hole and the results compared to the Theis Curve as shown in figure 3.38 and 3.39. The curves were significantly flatter than the type curve, suggesting the aquifer is unconfined or semi-confined, and data was therefore analysed by the Walton Graphical Method. This uses the modified type curves as shown in figure 3.40, devised by Walton (1960) and based on the Theis curve (r/B=0). Here u is a dimensionless constant, r is the distance from the pumping well, B is the leakage factor, and W(u, r/B) is the leaky well function. The data curve is matched to a type curve, giving a value for r/B, and a match point selected (Fetter, 2001). For simplicity W (u, r/B) =1 and 1/u = 1 is chosen here. Drawdown and time values for this point are read off from the data curve graph. Table 3.11 provides the values gained and transmissivity (T), storativity (S) and hydraulic conductivity (K) calculated from them. All equations used and assumptions are given in appendix 2.7.

Figure 3.38 Data curve for DH 656.

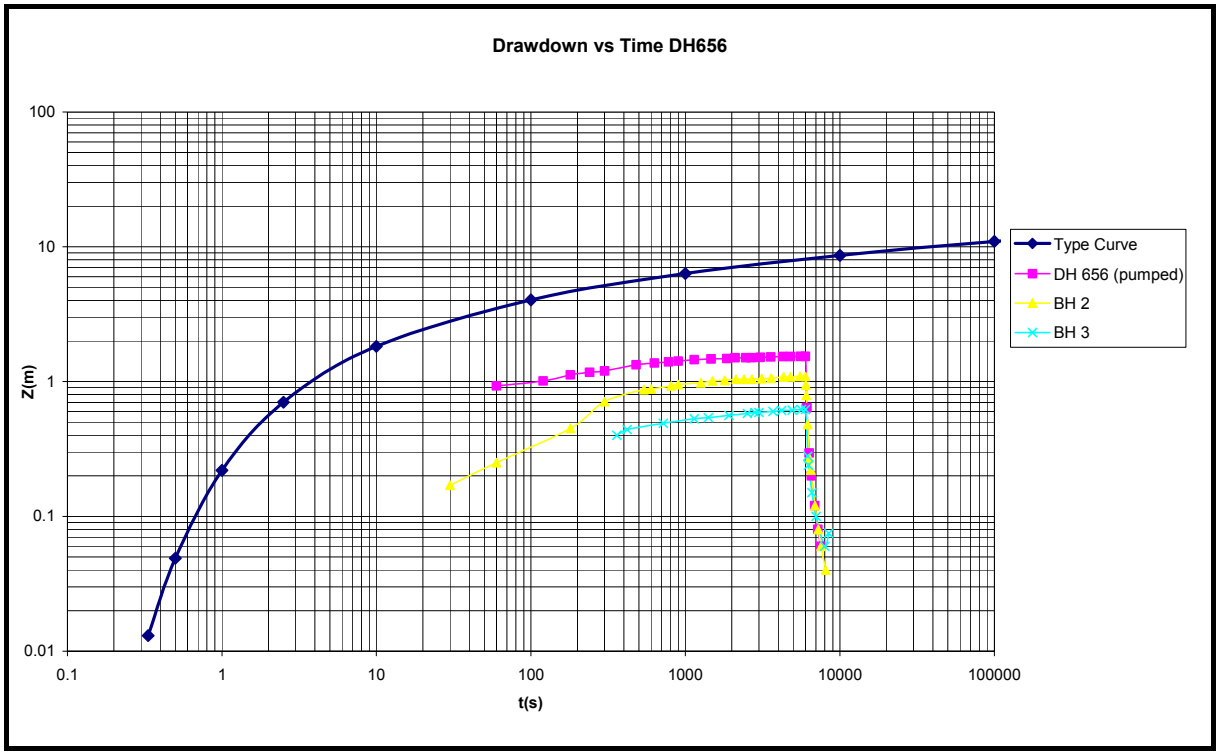

Figure 3.39 Data curve for DH 658.

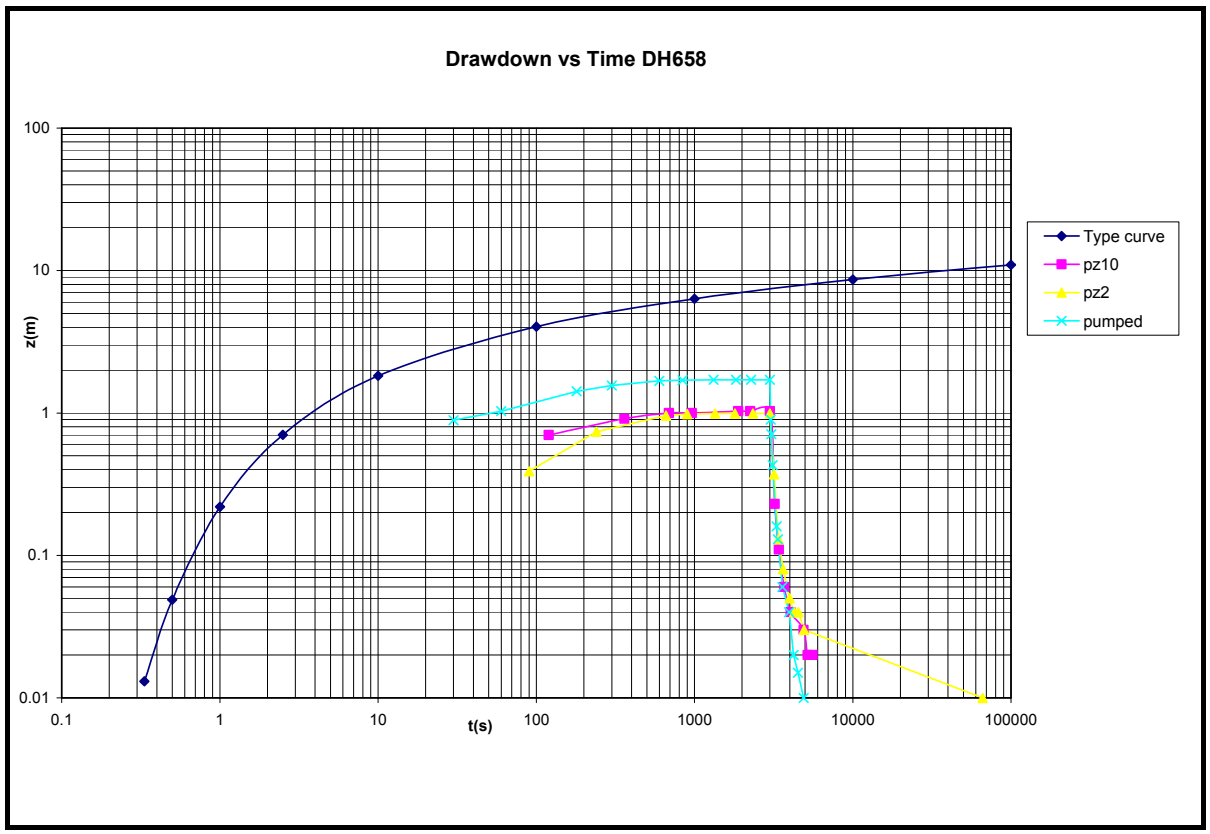

Figure 3.40 Walton (1960) Curves for semi-confined or unconfined aquifers.

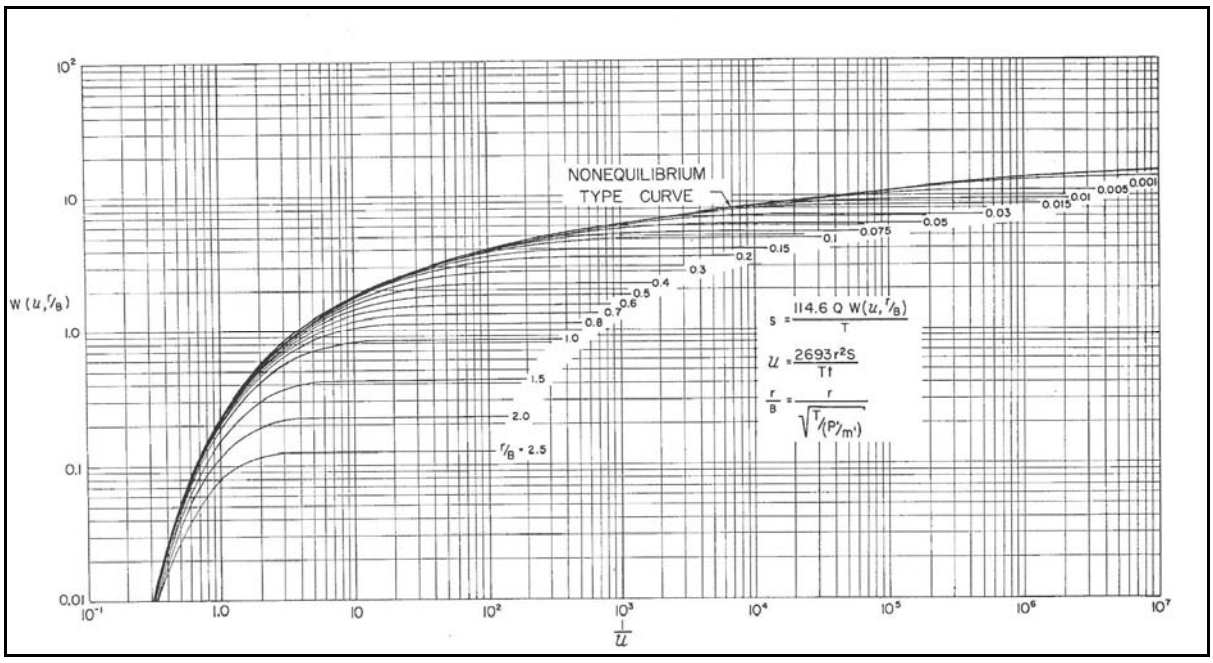

Table 3.11 Results from pump test using Walton Graphical Method..

	656			658		
Hole ID	Pumped	656/2	656/7	Pumped	658/2	658/10
Assumed aquifer thickness, b (m)	15	15	15	11	11	11
Distance from well, r (m)	0	2.88	7.25	0	2.44	10.06
r/B	0.1	0.1	0.2	0.1	0.4	0.15
Pumping rate, Q (m^3/s)	0.0024	0.0024	0.0024	0.00175	0.00175	0.00175
Drawdown, Z (m)	0.29	0.19	0.18	0.31	0.45	0.26
Time, t (s)	1.3	3.1	17	1.2	28	4.2
W (u, r/B)	1	1	1	1	1	1
1/u	1	1	1	1	1	1
Transmissivity, T (m^2/s)	0.00066	0.00101	0.00106	0.00045	0.00031	0.00054
(m^2/day)	56.90	86.85	91.67	38.81	26.74	46.28
Storativity		0.00150	0.00137		0.00582	0.00009
Hydraulic conductivity, K (m/s)		1.8×10^{-5}	1.2×10^{-5}		9.2×10^{-5}	1.3×10^{-5}

As the pumped well show curves of the same shape as the two observation wells they are all analysed together. The results give an average transmissivity of 58 m^2/day and an average hydraulic conductivity of 3.1×10^{-5}m/s. This agrees well with the values determined for the same data by Adrian Field (Stone *at al*., 2005). Using the Thiem-Dupuit Method, DH 656 transmissivity was calculated at 60 m^2/day and hydraulic conductivity at 4.6×10^{-5}m/s. DH 658 is noted to have unreliably high value for transmissivity (149 m^2/day).

The values for hydraulic conductivity are within the range expected for well-sorted sands and glacial outwash ($10^{-5} – 10^{-4}$m/s) as given by Fetter (2001). The transmissivity values, which are a measure of the amount of water that can be transmitted horizontally through a unit width by the full saturated thickness of the aquifer under a hydraulic gradient of 1 (Fetter, 2001), are relatively

moderate (Stone *et al.*, 2005). This is most likely due to the clay and silt present between the gravels as seen in chapter 1, figure 1.8. Although it can be established from the shape of the drawdown verse time graphs that the aquifer it is not confined, it is impossible to tell whether it is merely 'leaky' or unconfined. If longer tests are performed the curves may be observed to increase after a seemingly stable period. The BCM below the gravels also contain a significant proportion of clay which may form a low permeability barrier (Duncan, 1969). The shallow (<15m) aquifer is therefore probably a semi-confined in nature. The recharge is highly likely to come from the creek which runs the length of the valley and is at a similar level as the water table.

3.11 Synthesis

The qualitative and quantitative data obtained from scanline surveys and drill core were used to characterise the rock mass in the Reddale Valley. The main types of discontinuities are high angle tension joints, shallow dipping bedding, and faults related to regional uplift. A single crush zone was recorded and cleavage was observed in the mudstone beds; the latter may cause small scale (<1m) failures in the excavation walls.

Bedding orientation concentrations ranged from a dip/dip direction of 13˚/323 in the southwest to 09˚/359 in the northeast, but maximum concentrations showed a shallow north dip with a clockwise swing in strike. Faulting was predominantly by small (<1m throw) 'step-up' normal faults in the southwest, which were striking sub-parallel to bedding with average concentrations at 84˚/341. Although the major fault in the northeast appeared to dip in the opposite direction to the other faults, if it is a surface expression of the fault observed underground, then the northwest is known to be the down thrown side and they can therefore be regarded as related. The orientations of the joint sets were considerably different on each side of the valley. The southwest side displayed a major concentration around 74˚/078 and a marginally significant concentration at 72˚/156. The northeast side had a major concentration at 82/117 and a spread of significant clusters between 74-88˚ dip and 202-239 dip direction. The faults crossing the valley may have caused the joints to be tilted and rotated relative to one another, creating the differences observed.

The persistence for large scale bedding was high (>10m), while laminations within these beds had low persistence (<2m). Fault persistence suggests low classification but as most of the bottom ends terminated outside of the exposure this may not be an accurate description. The large majority of joints displayed low persistence, with most between 0.5 and 1.5m. This was

also affected by exposure as most joints intersected by the scanline terminated out of site beneath the exposure. They would be expected to continue until prevented by another joint, as the majority of joints terminated against another at their top end.

The bedding defects were mostly clean with very tight (<0.1mm) aperture. The majority of faults displayed 'gapped' (0.5-100mm) apertures that were infilled with gouge. The joints were mainly very tight with clean and/or surface staining. Some cavernous (>1000mm) joints were recorded in the northeast.

Low JRC (joint roughness coefficient) values (<6) were determined for bedding and they were mainly described as having planar and smooth surfaces. Although JRC values could not be obtained for the faults present, they were observed to have generally curved and smooth surfaces. The joints in all scan lines gave a majority of low JRC values although a complete range was recorded. Those with low JRC values were mostly planar or curved and smooth, and as JRC increased they became increasingly rough, irregular and stepped in nature. Overall the discontinuities can be regarded as being relatively smooth and may therefore have little shear strength. This correlated with the very low or zero cohesion determined by shear box testing in chapter 2. Wavelength estimations varied from 10 to 0.75m with most around 2m. Amplitude varied from 0.0075-0.25m with the average approximately 0.1m. For most joints it was not possible to estimate a value as they were generally planar, slightly curved or irregular. The larger values of waviness and amplitude were determined from bedding only. As these values was only approximated by visual inspection when possible these results can not be regarded as reliable for characterising the whole of the rock mass.

Schmidt Hammer tests produced an average JCS (joint compressive strength) of 32MPa. This value is higher than expected and is most likely due to the 'case hardening' developed on the joint faces. Manual index tests reported bedding wall strength to be extremely weak to weak rock (<25MPa). The majority of faults were characterised as having very weak wall rock strength. The southwest joints displayed a higher number of medium strong wall strengths, which is probably related to the case hardening in this area. The northeast joints were mostly extremely weak as expected by the weaker lithologies the scanlines intersect.

A range of RQD values were calculated from drill hole data with concentrations occurring in the excellent (90-100%) and very poor (0-25%) quality categories. When RQD was correlated with lithology the siltstone was found to have the highest percentage (62%) of excellent quality rocks.

The carbonaceous mudstone, and interbedded sandstone and carbonaceous mudstone, had relatively high percentages of very poor quality rocks (33 and 41% respectively).

Water was assessed as seepage in the scanline defects and from pump tests bore holes. 91% of the defects were recorded as being dry but this is not considered representative of the saturated rock situated beneath the valley floor. By using the Walton Graphical method moderate transmissivity ($58m^2$/day) and hydraulic conductivity (3.1×10^{-3}cm/s) values were established for the glacial outwash gravels overlying the BCM. The shallow (<15m depth) aquifer is most likely to be semi-confined, and will drain into the pit once the excavation is below the water table.

Chapter 4

Kinematic Feasibility Analysis

4.1 Introduction

This chapter builds on the rock material and mass characteristics previously determined, to conduct a slope stability analysis using stereographic methods. This utilises a kinematic feasibility approach, whereby blocks created by defects are assessed on the basis of their physical potential (angular relationships) to move, rather then analysing the forces that may cause them to move (Priest, 1993). The analysis considers the angular relationships present, but it should be remembered that volume of the features is not assessed by this method (Norrish and Wyllie, 1996). When there is no 'freedom' for a block to move, normally due to the presence of intact rock, a cut slope may remain stable even if it is steep and contains defects with low strength. The orientation of the discontinuities relative to one another and the excavation is therefore of primary importance (Goodman, 1980).

Chapters 2 and 3 showed that the rock mass can be considered heterogeneous and anisotropic. Properties such as rock strength and density/porosity vary between units and the continuity of beds fluctuate significantly from one place to another (within approximately $50m^2$ area). It was not considered appropriate to assign structural domains (areas of similar lithological and structural characteristics) to the completed scanlines, apart from the clear distinction between characteristics on either side of the valley, as they are positioned some distance from the proposed opencast location. The rock mass in the valley floor may have similar structural characteristics to the southwest or northeast sides, or a composite of both sets of data. Each side of the valley is analysed separately as it is not known which sets will dominate in the proposed site and the scanlines were not long enough to warrant individual analysis. Several proposed orientations of the future highwall are utilised for the kinematic feasibility, rather than the orientation of the existing cuts, for the same reason.

Initially the scanline data presented in chapter 3 was filtered on persistence. The process however showed the majority of small defects (<1m) occurred within the clusters which incorporated more persistent discontinuities. The small defects were responsible for most of the spread, but the widespread scatter did not affect the concentrations as they were not significantly concentrated on their own. This is illustrated in figure 4.1 and 4.2, which shows the persistence of the defects in Dips plots for both sets of scanlines. Many of the persistence

measurements were also less than the complete length of the defect, given that many terminated outside the exposure, as discussed in chapter 2. The kinematic feasibility undertaken therefore used all the data collected from the objective scanline surveys.

Figure 4.1 Persistence plot for the southwest scanlines.

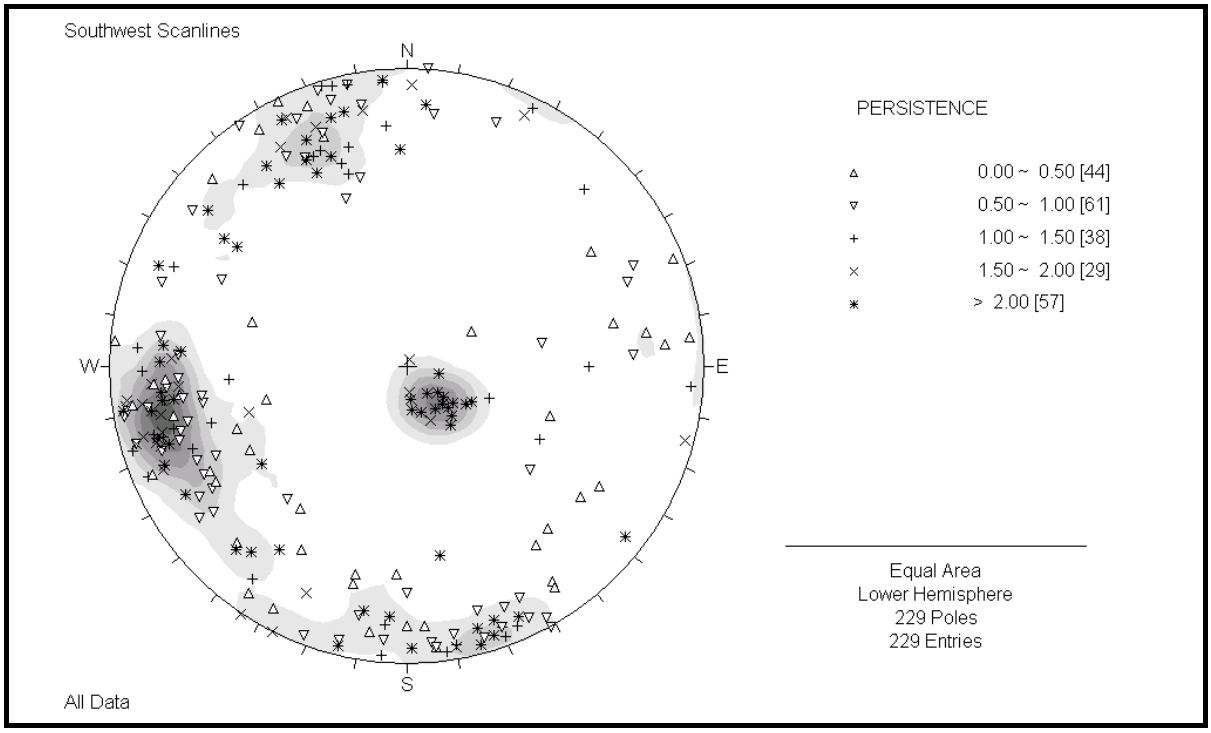

Figure 4.2 Persistence plot for the northeast scanlines.

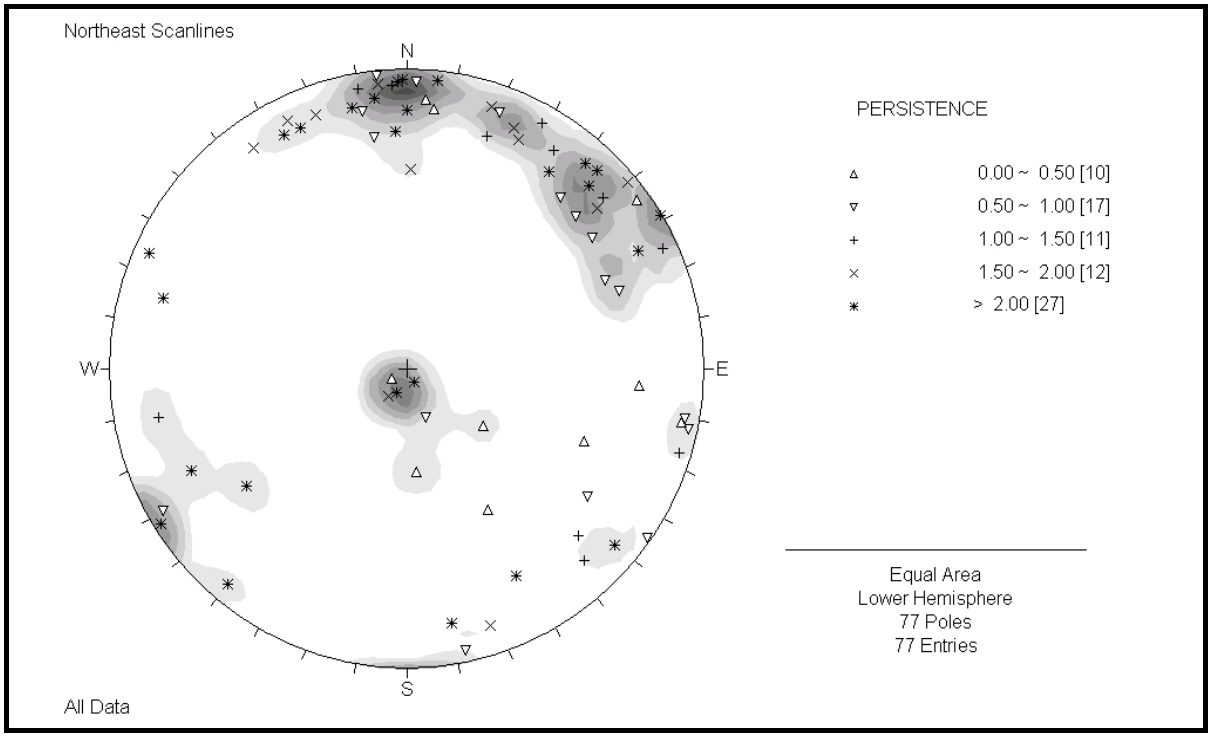

This chapter outlines the theory and selected methods used to analyse slope failure. Kinematic feasibility tests are then carried out in Dips for each failure type on the two sets of defect data, using proposed highwall orientations. All Dips plots used for analysis are presented in appendix 3 if not incorporated with the text. An optimum highwall orientation, based on the kinematic checks performed and given the geological consideration so far investigated, is suggested and other slope stability considerations discussed.

4.2 Types of Failures and Analysis Methods

4.2.1 Types of Failure

There are four categories of rock slope failure; planar, wedge, toppling or circular. These are governed by the type and degree of structural control, and recognition of the failure mode present is crucial as to which analytical method is used (Norrish and Wyllie, 1996). The theory and methods used in this study to assess planar, wedge and toppling failures are outlined below. Circular failures occur when the rock mass is highly fractured or composed of rocks with low intact strength. In circular failures it is not possible to identify individual discontinuity sets, as shown in figure 4.3 (Giani, 1992). The discontinuities do not form distinct patterns and the controlling structures are not orientated relative to the slope. One such example is when the bedding planes dip into the slope (Norrish and Wyllie, 1996). Given that this is the case in the proposed opencast, relatively low intact strength of the Brunner Coal Measures overburden and the fairly widespread defect poles, it is important not to discard circular failures, although analysis by stereographical methods cannot be performed. The loose sandstone unit may be susceptible to such failures, should it behave as a soil, but the other three units are probably too well bedded to allow circular failure to occur.

Figure 4.3 Three dimensional diagram and stereographical representation of circular failure (Giani, 1992). The dots represent poles to randomly orientated defects.

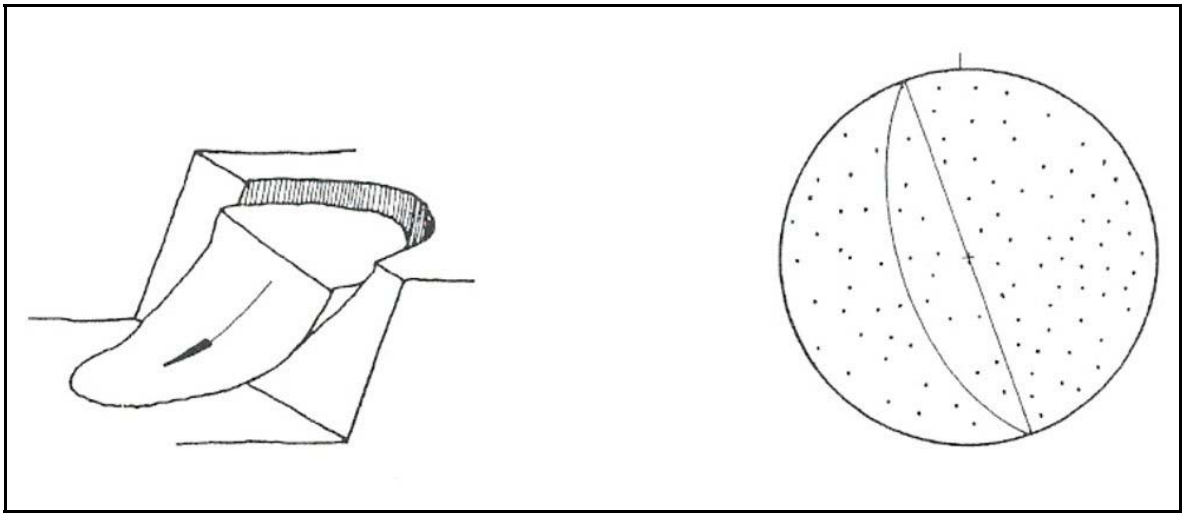

4.2.2 Planar Failure

A planar failure is possible when a single discontinuity dips out of the slope face and daylights on that face. This enables sliding to occur on a single discrete surface that approximates a plane (Norrish and Wyllie, 1996). The lateral extent of the failure may be defined by other discontinuities, which do not contribute to the stability of the failure mass but act as 'release surfaces' (Norris and Wyllie, 1996), as shown in figure 4.4a. Usually a slice of unit thickness, perpendicular to the slope face is used to analyse planar failures, as shown in figure 4.5b (Hoek and Bray, 1977).

Figure 4.4 Planar failure a) Release surfaces b) Slice of unit thickness (Hoek and Bray, 1977).

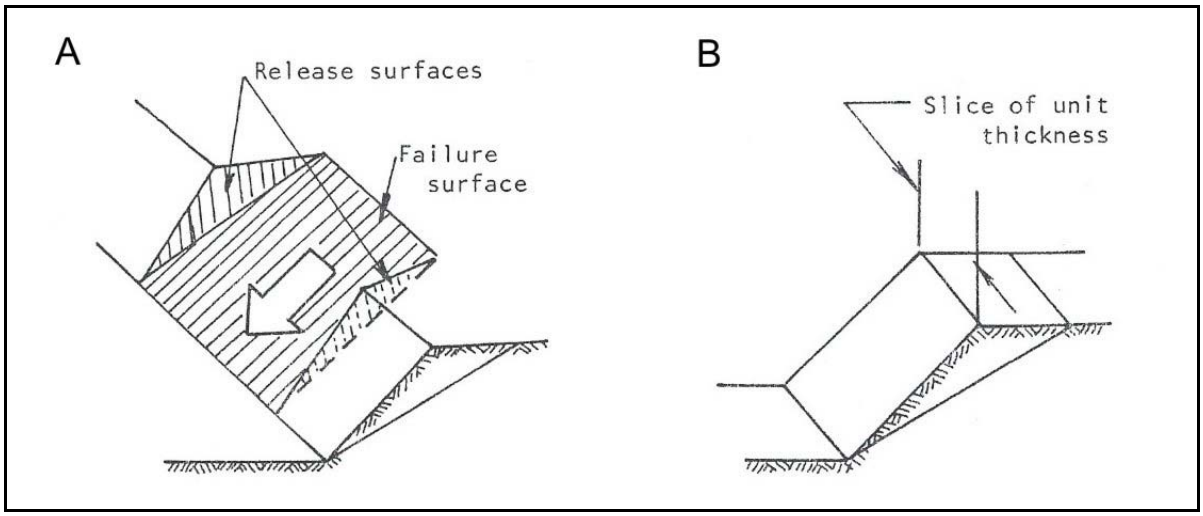

The geometrical conditions that allow sliding along a single planar failure are as follows (Norrish and Wyllie, 1996):

- The dip direction of the planar discontinuity must be within ±20˚ of the dip direction of the slope face.
- The dip of the planar discontinuity must be less than the dip of the slope face and will therefore 'daylight' in the face.
- The dip of the planar discontinuity must be greater than the angle of friction of the surface.
- The lateral extent of the potential failure mass must be defined by lateral release surfaces, which provide negligible resistance to sliding or by a convex slope shape.

Analysis of planar failure is possible in the Dips program by using a variation of the method shown in figure 4.5. The data are presented as poles rather than planes, and this combines frictional and kinematic possibilities of planar sliding. A 'daylight envelope' around any poles of defects that lie inside the pole of the slope face is added to the plot. A pole friction

cone, in which is the angle of internal friction is measured from the centre of the stereonet (rather than the outside) is added (Rocscience Inc, Dips User's Guide, 2004). A cone representing kinematic bounds of ±20˚ of the pit slope restricts the 'danger zone' created where the daylight envelope and the friction cone overlap, as suggested by Wyllie and Mah (2004). Poles within this area fulfil the geometrical conditions above and sliding can therefore occur.

Figure 4.5 Kinematic requirements for planar failure (Norrish and Wyllie, 1996).

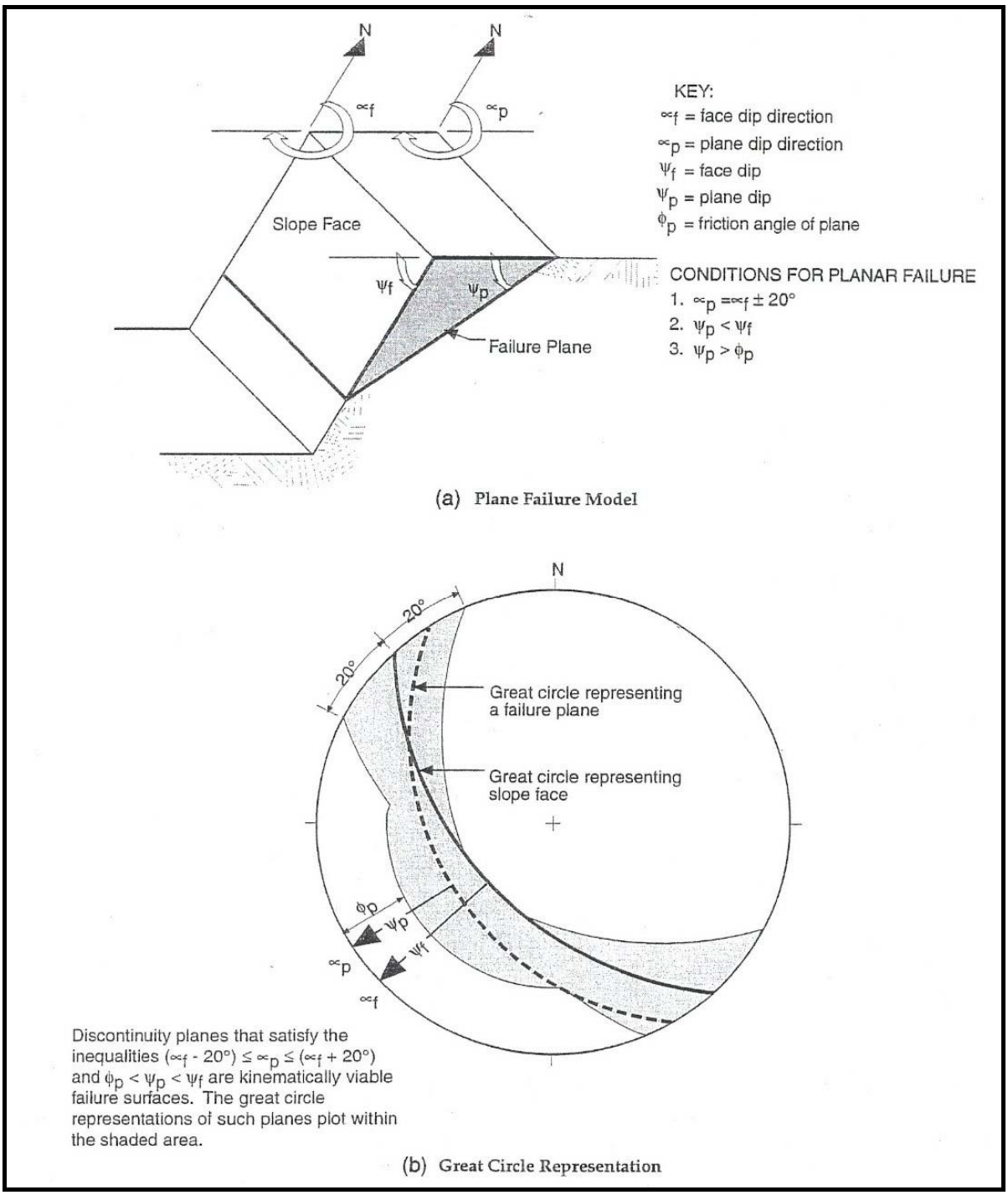

4.2.3 Wedge Failure

When two discontinuities intersect and dip out of the slope at an oblique angle to the face, they create a wedge-shaped failure (see figure 4.6a). The structural requirements necessary for wedge failure to occur are as follows (Norrish and Wyllie, 1996):

- The trend of the line of intersection must be approximately the same as the dip direction of the slope face.
- The plunge of the line of intersection must be less than dip of the slope face and the line of intersection can therefore daylight on the face.
- The plunge of the line of intersection must be greater than the angle of friction for the surface. If the angle of friction for each plane is significantly different from one another, an average friction angle is applicable.
- The line of intersection must lie between the dip vectors of the bounding planes.

Markland's test has been developed to analyse whether it is possible for wedge failures to occur along the line of intersection with a given slope orientation (Hoek and Bray, 1977). Figure 4.6 illustrates the structural requirements stipulated above as they appear on a stereonet. This test is easily applied to data in the Dips programme. A plane for each set of defects is displayed on the plot and similarly a great circle represents the slope face. A friction cone is added and care must be taken to ensure it is measured from the perimeter of the stereonet rather than the centre (Rocscience Inc, Dips User's Guide, 2004). The slope is potentially unstable when points of intersection (where defect planes cross) fall within the zone bounded by the slope face and the angle of friction (Hoek and Bray, 1977).

Figure 4.6 Kinematic requirements for wedge failure (Norrish and Wyllie, 1996).

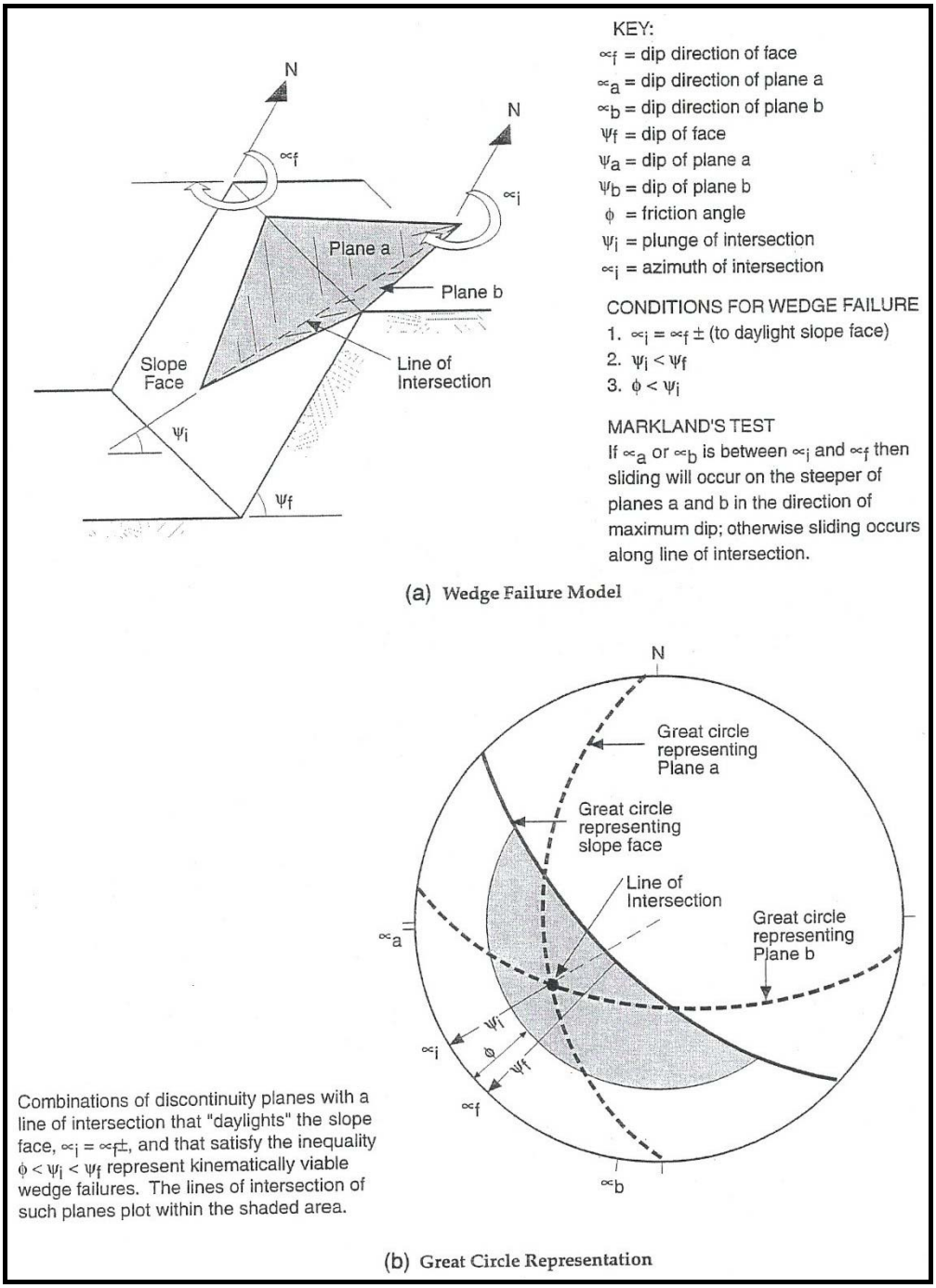

4.2.4 Toppling Failure

Toppling failures occur when discontinuities strike approximately parallel to the face and dip steeply into the slope, creating slabs or columns. Three types of toppling failures, which are often encountered in the field and described by Goodman and Bray (1976), are discussed in Hoek and Bray (1977). Flexural toppling involves well developed steeply dipping discontinuities in continuous columns that break in flexure as they topple forward (figure 4.7a). Widely spaced orthogonal joints within the columns produces block toppling, as shown in figure 4.7b. Block-flexure toppling occurs when pseudo-continuous flexure of long

columns, which are divided by numerous cross joints, causes accumulated movement to take place (figure 4.7c).

Figure 4.7 Types of toppling failure a) flexure toppling b) block toppling c) block-flexure toppling (Hoek and Bray, 1977).

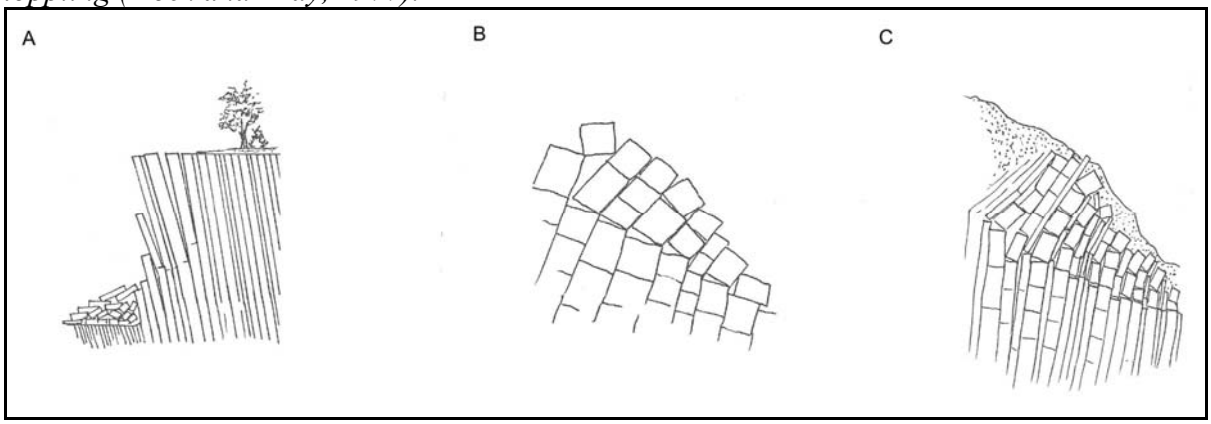

For analysis of toppling failures, a stepped failure base is assumed to develop along cross fractures between columns (figure 4.8). The structural conditions necessary for toppling failure to occur are as follows (Norrish and Wyllie, 1996):

- The strike of the slabs must be approximately parallel to the slope face. The deviation in orientations used varies between 15 and 30˚ depending on the author.
- The dip of the layers must be into the slope face.
- The normal to the toppling plane must have a plunge less than the inclination of the slope face, minus the friction angle for interlayer slip to occur.
- The lateral extent of the toppling failure is limited by zero-strength lateral release surfaces or a convex slope shape.

Figure 4.8 Kinematic requirements for toppling failure (Norrish and Wyllie, 1996).

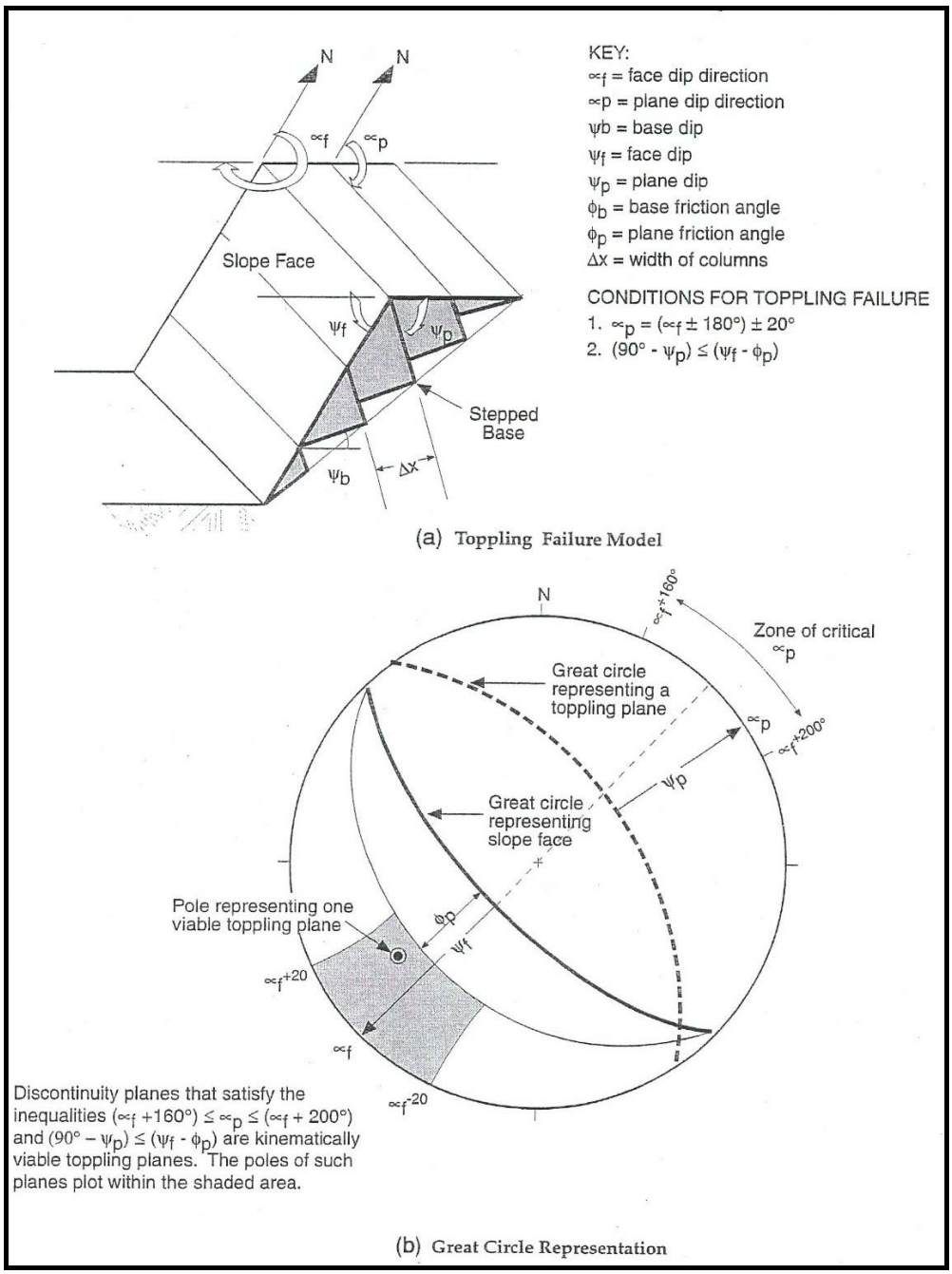

The stereographic method displayed in figure 4.8 can also be conducted in Dips and is based on the suggestions made by Goodman (1980). A plane representing the 'slip limit' is added to the plot by subtracting the friction angle from the slope angle and having the same dip direction as the slope. Kinematic bounds are also added as a cone to create limits of ±30˚ off parallel for the orientation of the slabs with respect to the dip direction of the slope. This was suggested by Goodman (1980) as a better limit than the 15˚, which was found to be too small. Poles that are therefore within the region between slip limit and kinematic bounds, as shown in figure 4.9, have the potential for toppling failure.

Figure 4.9 Method to test for kinematic feasibility of toppling failure, adapted from Goodman, 1980. a) (90 – δ) + $ø_j$ < α where δ is the sip of the layer, $ø_j$ is angle of friction of the layers and α is the dip of slope b) Stereographic representation where N must plot in the shaded zone to fail.

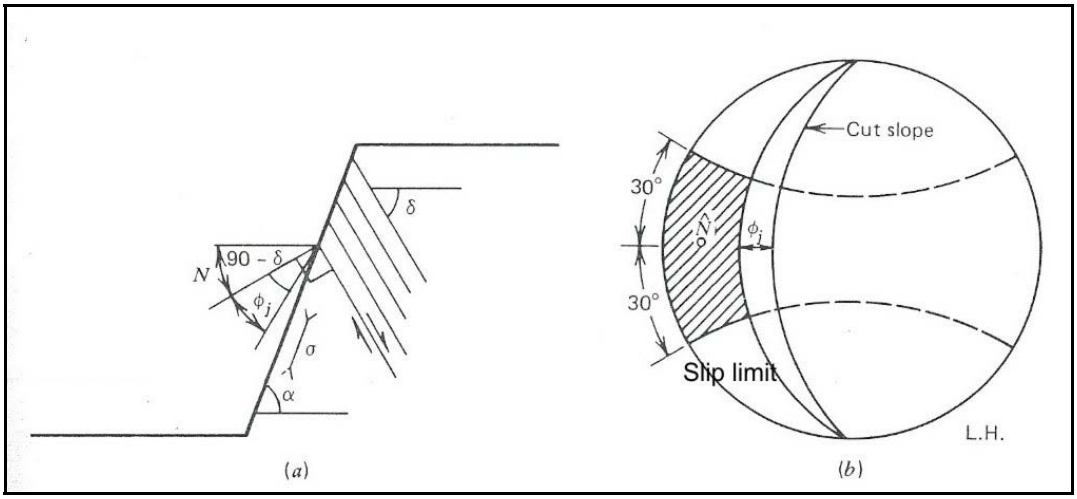

4.3 Kinematic Feasibility Study

4.3.1 Approach Adopted

The data for all of the different types of defects were analysed as a single data set for each side of the valley. The average orientation of each concentration established and defined in chapter 3 was used, despite the slightly different concentration percentages in the combined plots. Variability cones were added to the set windows to show one (68%) and two (95%) standard deviations of orientation uncertainty, centred on the calculated means (Rocscience Inc, Dips User's Guide, 2004).

A friction angle of 37˚ was used, as determined from shear box testing in chapter 2 of a high angle defect in laminated sandstone. It falls within the range of friction angles derived for each individual unit (32-45˚) from triaxial testing. This was concluded to be a better estimate of friction angle than the effective peak friction angle (Φ_{peak}) determined from the Barton (1973) Equation, which takes JRC and JCS into account because it does not allow for large scale roughness (wavelength and amplitude) and assumptions regarding basic friction angle and normal load have to be made. As the joints are predominantly steep the friction angle used did not greatly affect the kinematic feasibility results and an angle of 37˚ is considered a conservative assumption for all defect surfaces.

The slope of the proposed pit walls will be 76˚ (1:4) or 60˚ (industry standard) which is based on past mining operations on the West Coast and will depend on blasting techniques and kinematic analysis of the final pit limits (Richard Mould, Engineering Geologist, Solid

Energy, pers com, 2006). The highwall will slope towards the southeast, and orientations of 130, 150 and 170 dip direction are analysed here. Examples of the kinematic feasibility tests are included in the text for significant pit slope orientations. All Dips plots not presented in this section are provided in appendix 3. A discussion of the importance and implications of the results from the kinematic feasibility checks is presented in section 4.4 (Slope Stability Considerations).

4.3.2 Southwest Scanlines

4.3.2.1 Planar Failure Test

The first kinematic test performed was for planar sliding. The pit walls with a slope of 60˚ did not indicate any significant potential for planar failure irrespective of the orientation, although the edge of the minor joint set (JA2: 74˚/077) was just within the danger zones for pit slopes with a dip direction of 150 and 170. Figure 4.10 shows a pit slope orientated at 60˚/170 as an example, all other plots are given in appendix 3.1. When the angle was altered to 76˚ the sliding zone was substantially larger, and a dip directions of 150 and 170 included most of the minor concentration (JA2). Figure 4.11 shows an example of a slope at 76˚/150. These results suggest that a 76˚ slope angle is more likely to produce planar failures along the steep joints present, than a 60˚ slope.

Figure 4.10 Kinematic check for planar failures with a pit slope orientated at 60˚/170.

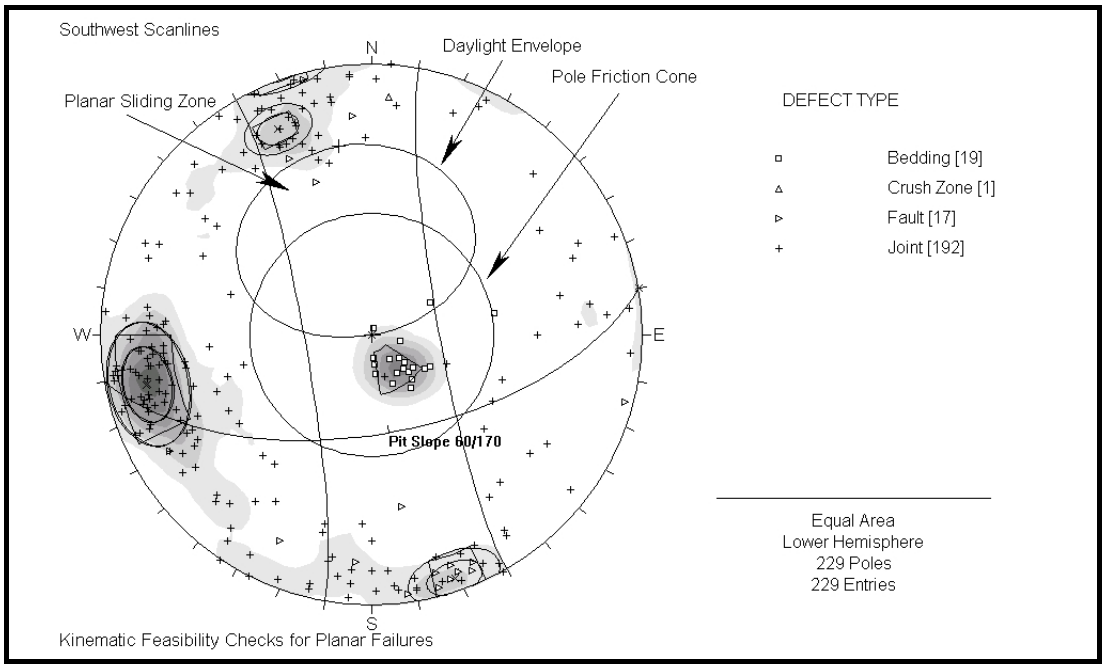

Figure 4.11 Kinematic check for planar failure with a pit slope orientated at 76˚/150.

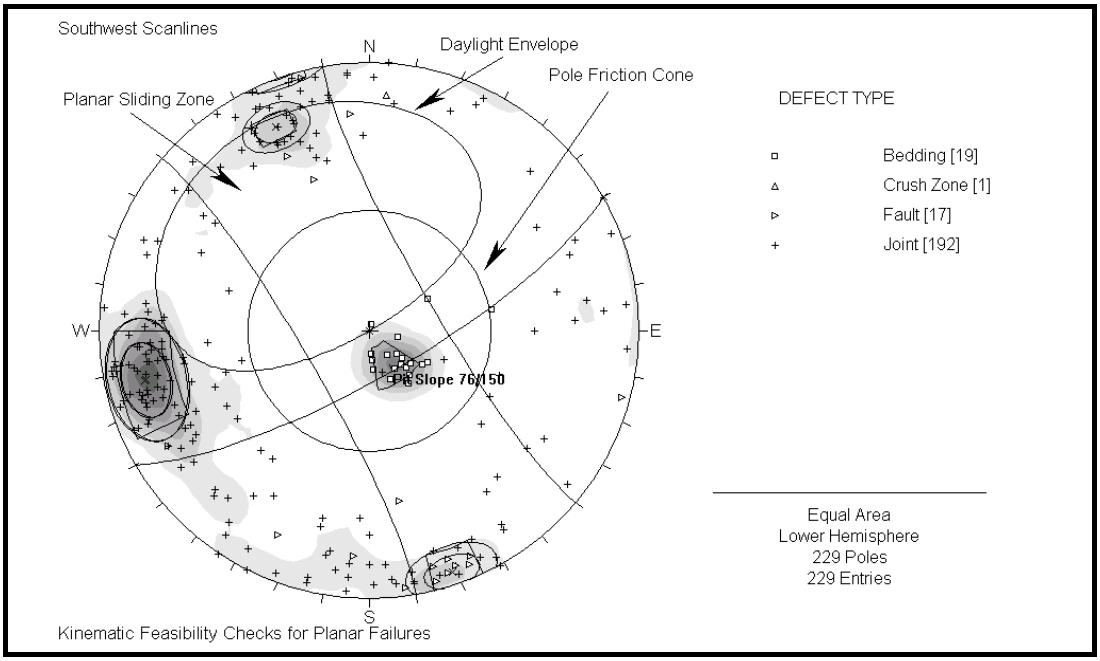

4.3.2.2 Wedge Failure Test

Wedge failures do not pose a potential problem for any of the highwall orientations with a 60˚ slope according to the kinematic feasibility checks performed. Although the plane for the major joint set (JA1: 74˚/078) crosses through the centre of all of the 'danger' zones, it does not intersect any of the other defects within this area. An example of a pit slope at 60˚/150 is given in figure 4.12 and all other plots are presented in appendix 3.2. Conversely all three orientations at 76˚ display intersections of the joint sets JA1 and JA2 within the wedge sliding zone, as shown by a black dot in figure 4.13. Wedge failures may therefore cause significant problems should the batters be constructed at these orientations.

Figure 4.12 Kinematic check for wedge failure with a pit slope orientated at 60˚/150.

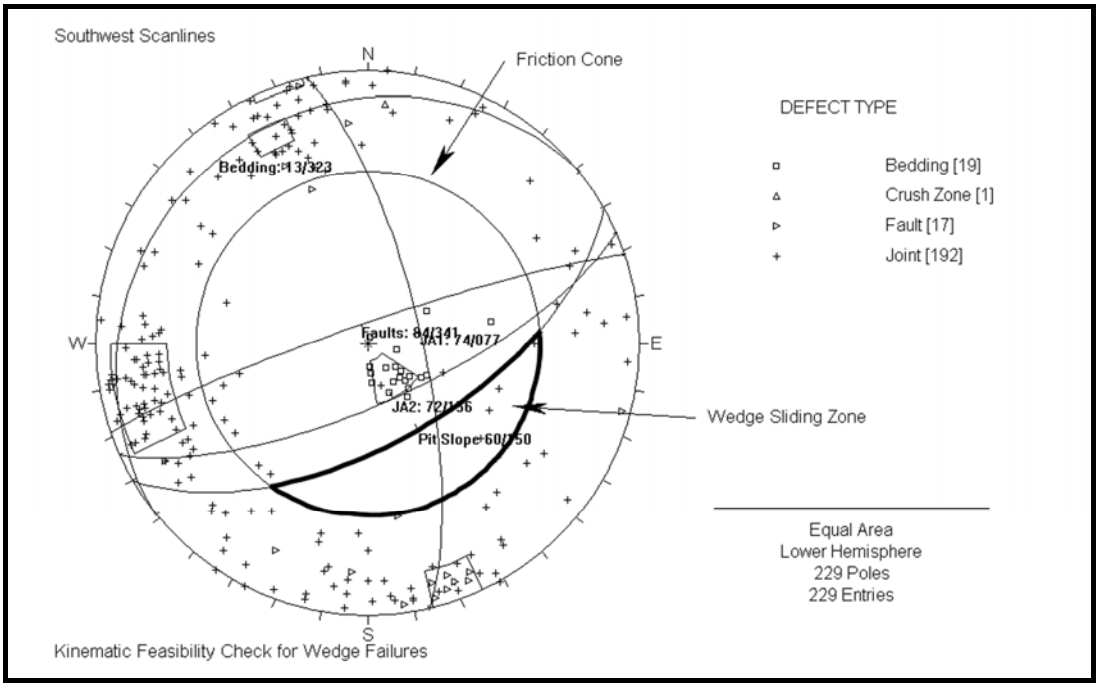

Figure 4.13 Kinematic check for wedge failure with a pit slope orientated at 76˚/130, intersecting defects with failure potential are shown by a black dot.

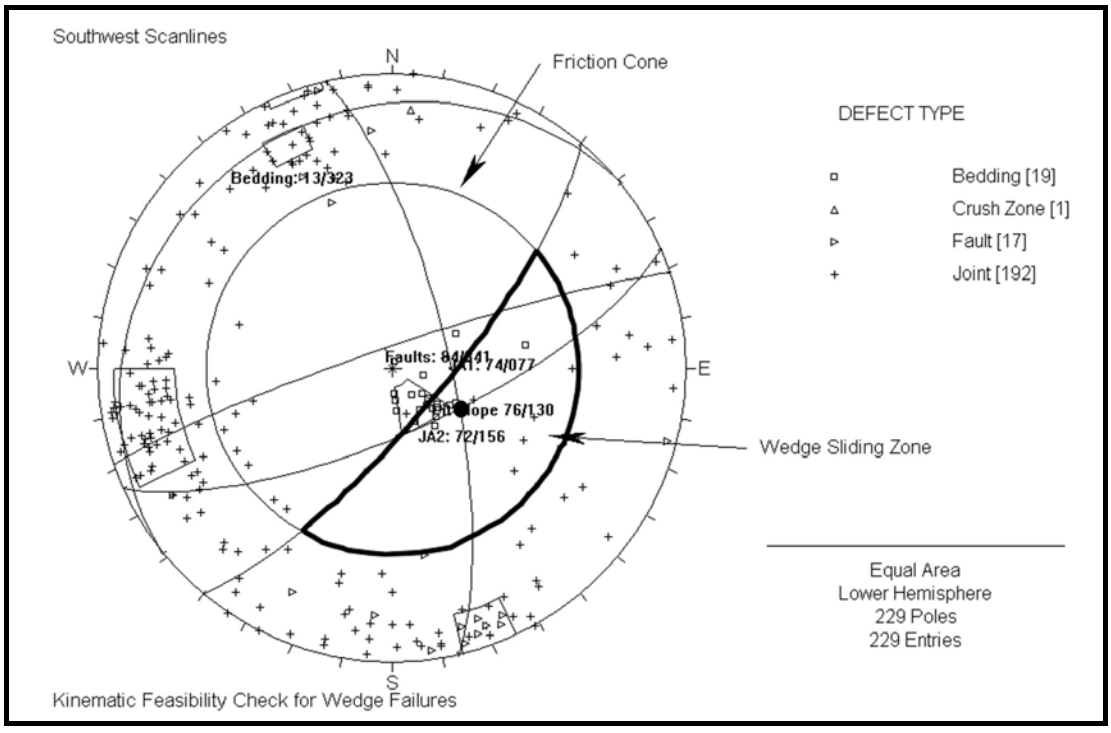

4.3.2.3 Toppling Failure Test

The third kinematic test applied to the data for the southwest scanlines was for toppling failure. All of the orientation combinations displayed the potential for toppling to occur on the faults present. Those with a dip direction of 130 only incorporated approximately 50% of the fault concentration, as shown in figure 4.14. Dip directions of 150 and 170 included the whole concentration of faults and therefore have a higher potential for toppling failure. In this

case the dip of the highwall does not affect the results, and figure 4.15 shows an example of a pit slope at 60˚/170. All other plots are presented in appendix 3.3.

Figure 4.14 Kinematic check for toppling failure with a pit slope orientated at 76˚/130.

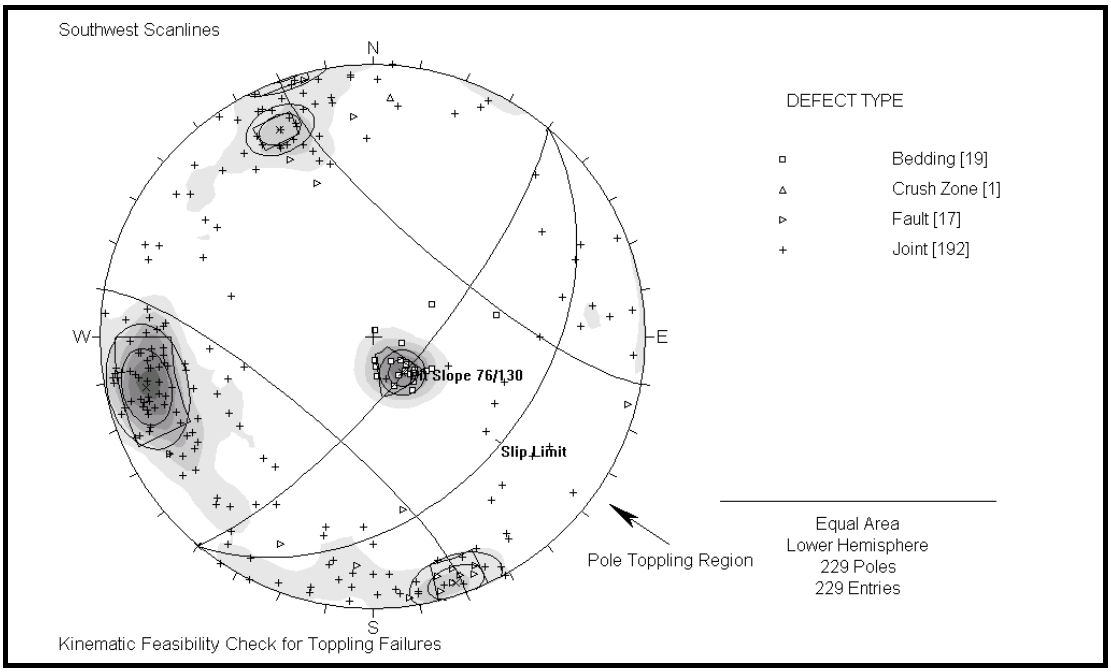

Figure 4.15 Kinematic check for toppling failure with a pit slope orientated at 60˚/170.

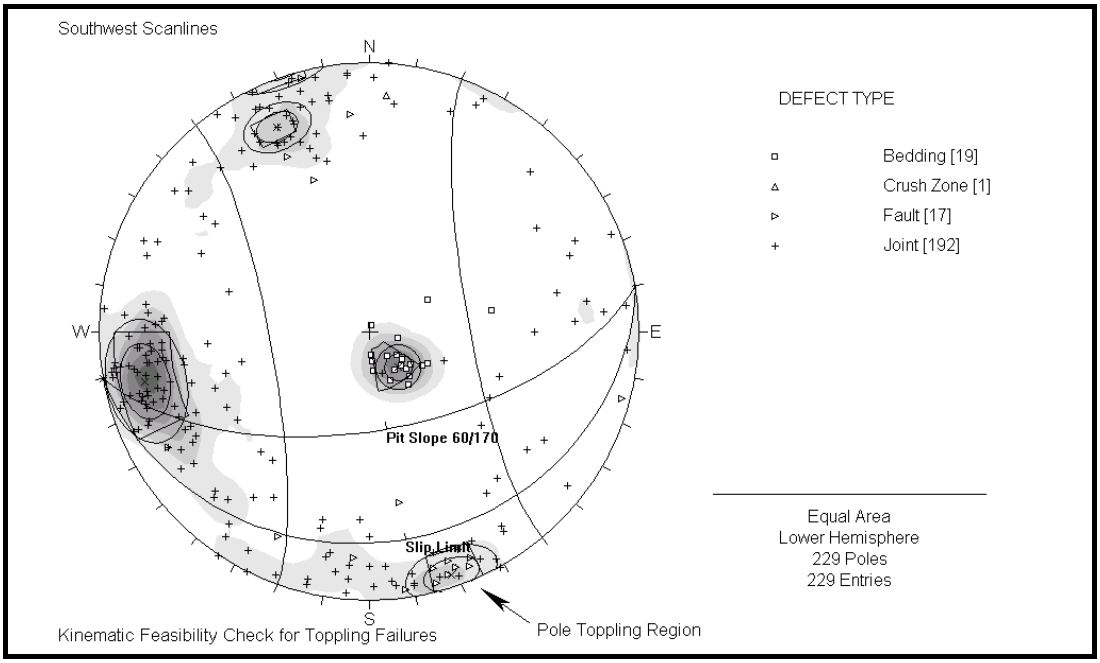

4.3.3 Northeast Scanlines

4.3.3.1 Planar Failure Test

Kinematic feasibility tests on the data from the northeast scanlines showed no significant potential for planar failure on pit slopes with a slope 60˚ at any of the orientations and an example of 60˚/130 is given in figure 4.16. Pit slopes of 76˚/130 and 76˚/150 do not have any

significant defect clusters within the 'danger zone'. Figure 4.17 shows that with a pit slope of 76˚/150 the major joint set (JB1: 82˚/177) and fault are only marginally within the danger zone. At 76˚/170 a greater amount of the major joint set is within the sliding zone (figure 4.18) and planar failure is kinematically feasible for the northeast data if this orientation is used.

Figure 4.16 Kinematic check for planar failures with a pit slope orientated at 60˚/130.

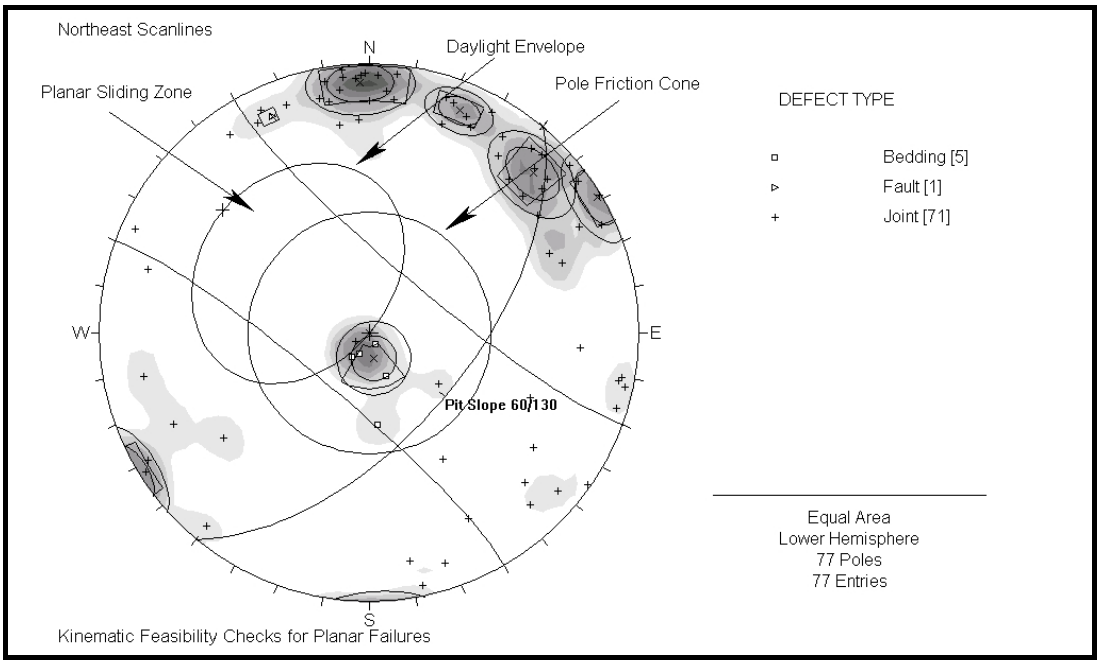

Figure 4.17 Kinematic check for planar failure with a pit slope orientated at 76˚/150.

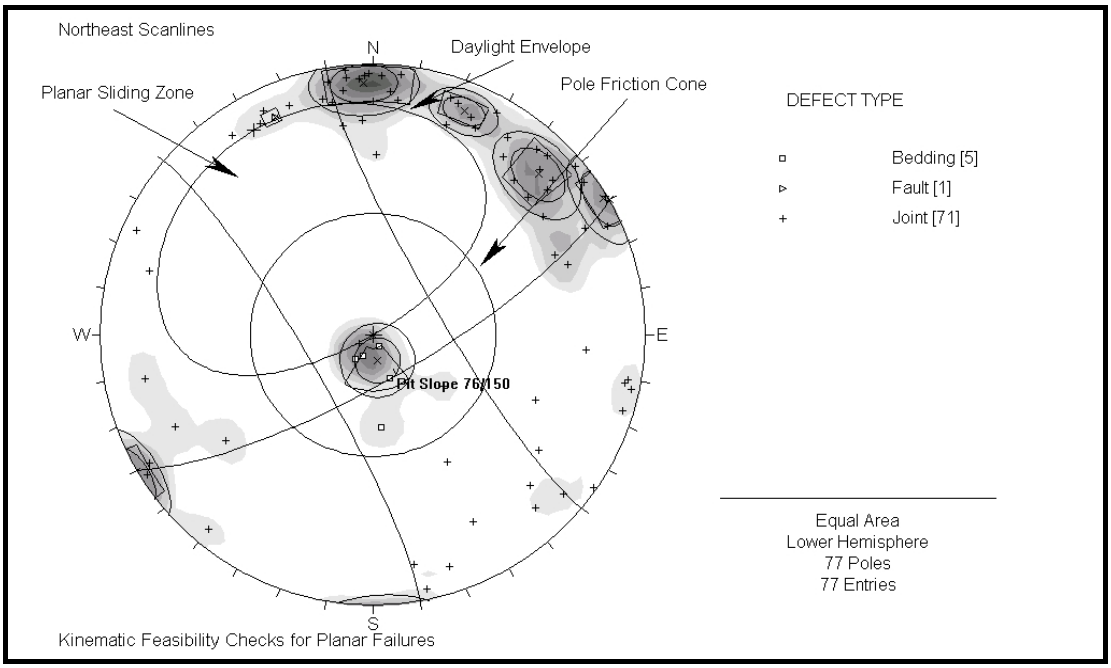

Figure 4.18 Kinematic check for planar failure with a pit slope orientated at 76˚/170.

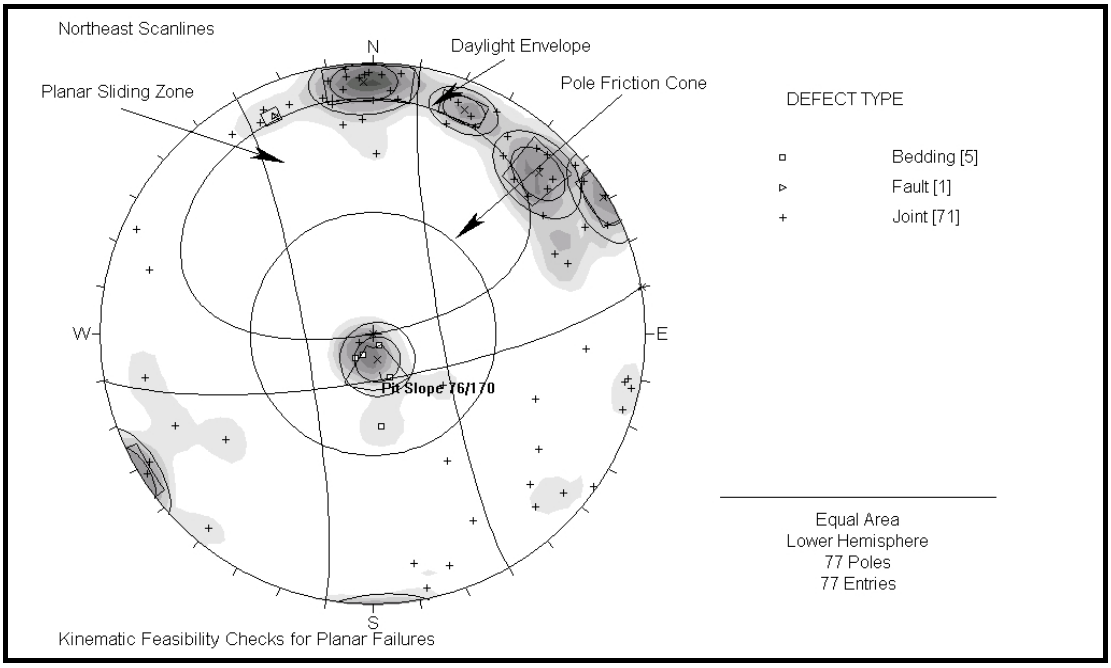

4.3.3.2 Wedge Failure Test

All of the proposed highwall orientations displayed potential wedge failures for defects found in the northeast scanlines. With a 60˚ dip the intersection between joint sets JB3 (74˚/226) and JB4 (88˚/239) occurred within the sliding zone at each of the orientations. An example of the pit slope at 60˚/150 is shown in figure 4.19 and all other plots are given in appendix 3.5. At orientations of 76˚/130 and 76˚/150 this same intersection occurred, as well as an intersection between JB2 (78˚/202) and JB4 and a third between JB1 (82˚/177) and the fault. An example of these intersections is given in figure 4.20. With a pit slope constructed at 76˚/170 the three intersections are JB3 with JB4, JB2 with JB4, and JB3 with the fault (figure 4.21). The fault also gives intersections on the margin of the 'danger zone' with JB3 and JB4 for all dips slopes of 76˚, and with JB2 as well for 76˚/150. With multiple intersections within the danger zones and on the margin, there is a high potential for wedge failure with a batter angle of 76˚, and a lesser possibility at 60˚ which has one central intersection only.

Figure 4.19 Kinematic check for wedge failure with a pit slope orientated at 60˚/150, intersecting defects with failure potential are shown by a black dot.

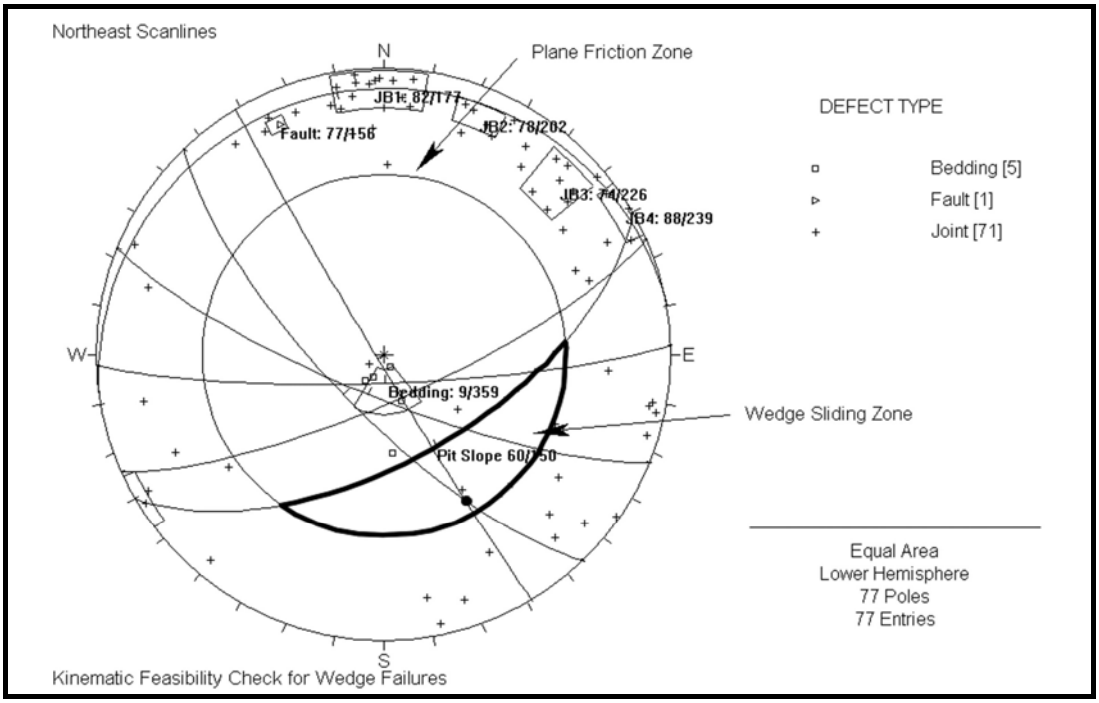

Figure 4.20 Kinematic check for wedge failure with a pit slope orientated at 76˚/130, intersecting defects with failure potential are shown by a black dot.

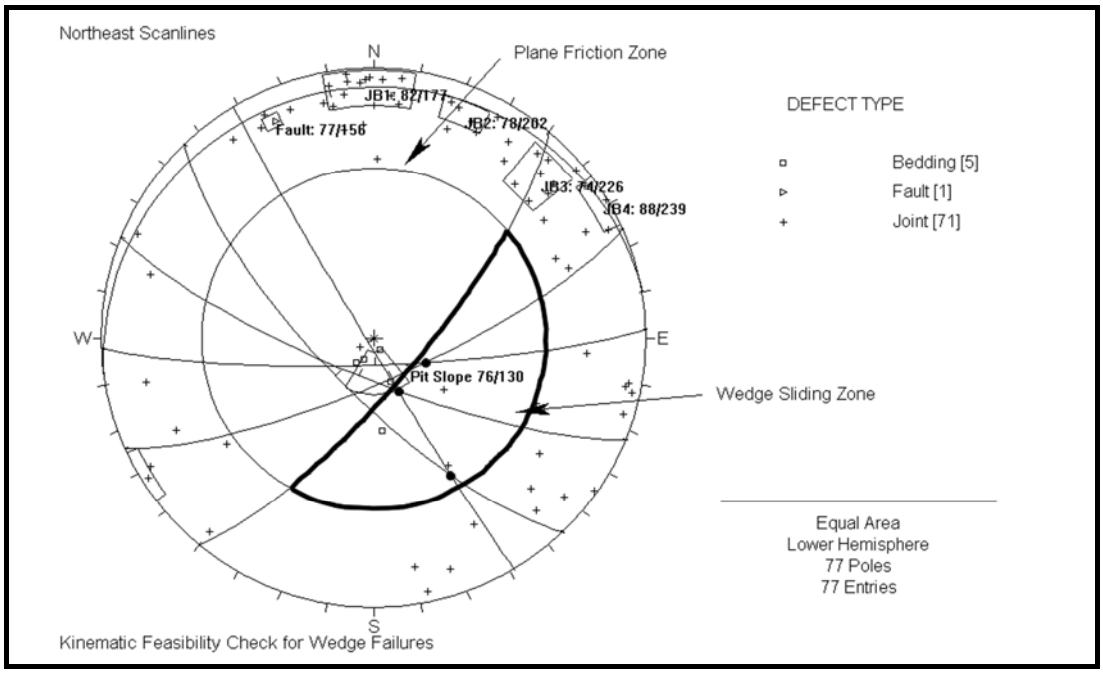

Figure 4.21 Kinematic check for wedge failure with a pit slope orientated at 76˚/170, intersecting defects with failure potential are shown by a black dot.

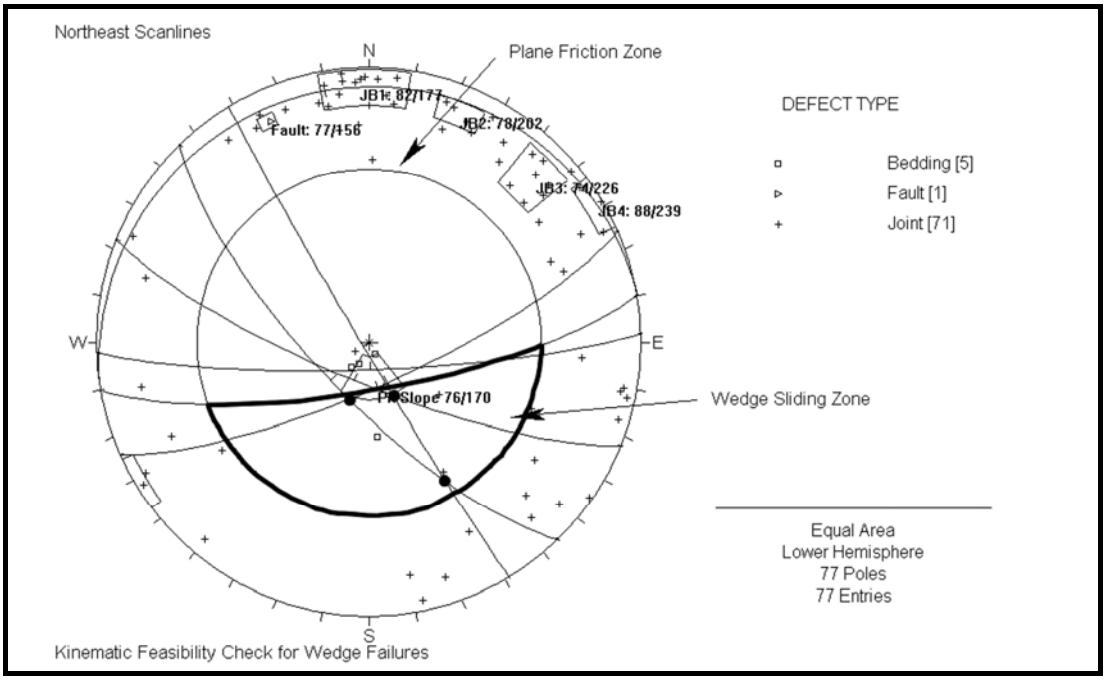

4.3.3.3 Toppling Failure Test

Kinematic tests for toppling failures showed no potential at an orientation of 130 dip direction for either slope angles, and 60˚/130 is shown in figure 4.22. For all other combinations of dip and dip direction the edge (2 standard deviations from the mean) of the major joint set (JB1) is either partly or fully within the toppling region. An example of this is shown in figure 4.23, and all other Dips plots are presented in appendix 3.6. There is therefore a small chance of toppling occurring at 150 or 170 highwall orientations, irrespective of the cut batter angle.

Figure 4.22 Kinematic check for toppling failure with a pit slope orientated at 60˚/130.

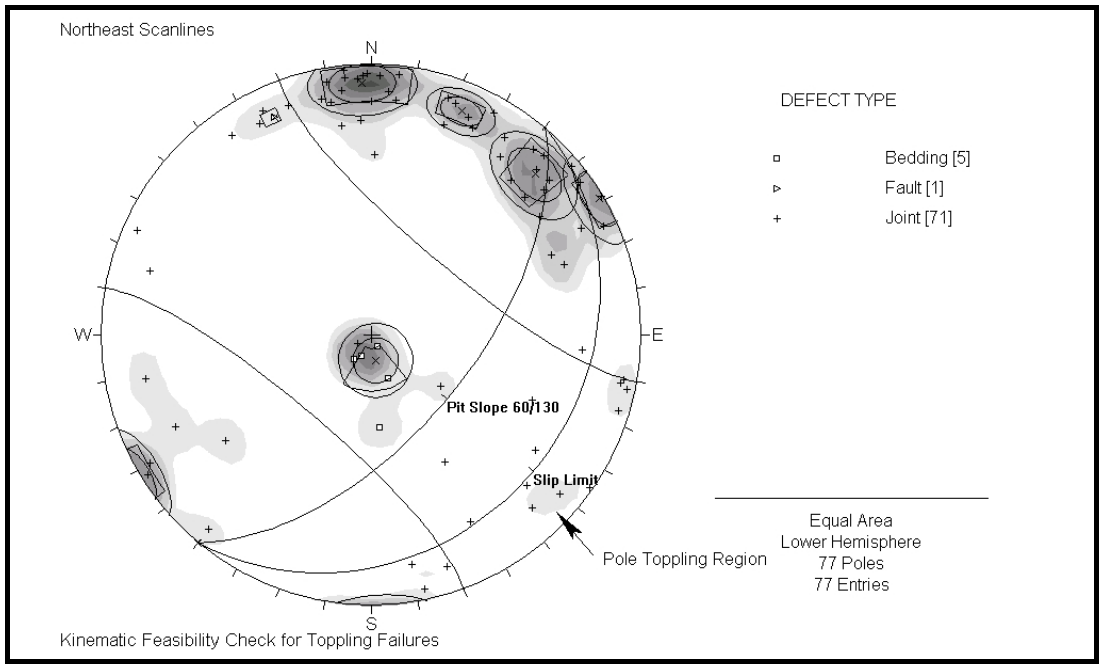

Figure 4.23 Kinematic check for toppling failure with a pit slope orientated at 76˚/170.

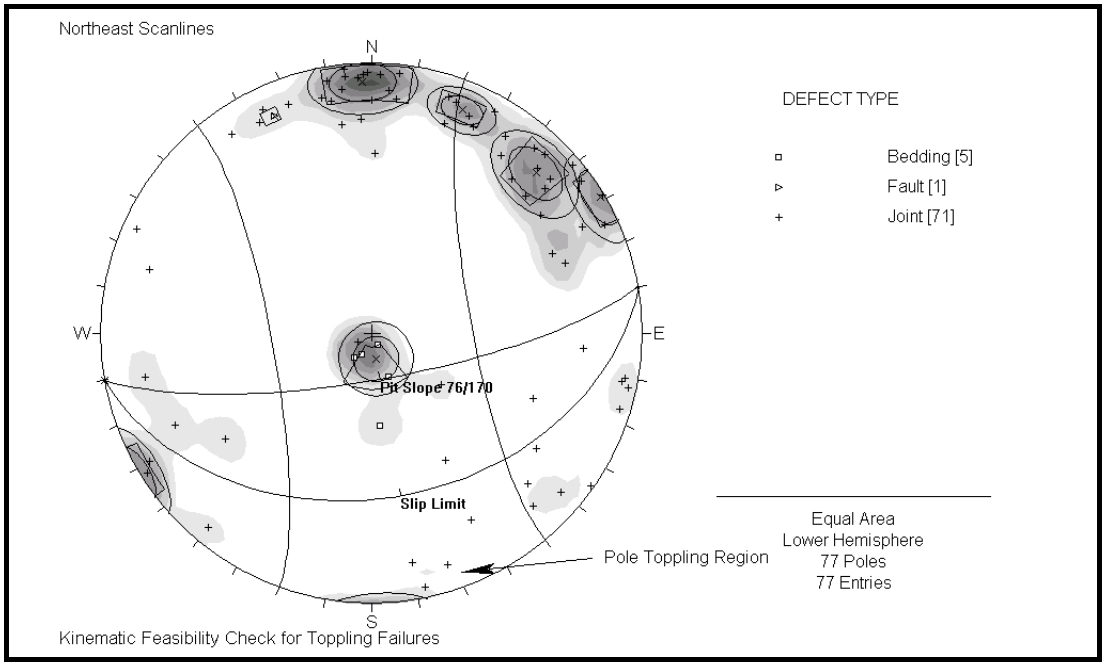

4.3.4 Optimum Highwall Orientation

The kinematic feasibility tests, discussed above, suggest that a pit slope angle of 76˚ is too steep, while 60˚ may be overly conservative. A pit slope angle of 65˚ is therefore proposed. The dip directions that are closer to the east provide more stable pit slopes and an optimum orientation of 120 is therefore suggested. The final orientation used will depend on a number of factors, particularly the strike of bedding that was determined in chapter 3 to have dip directions between 320 and 360. An orientation of 120 therefore means mining will occur at an oblique angle (20˚ minimum) to strike. While this may not be idea it is used here as the best orientation relative to defect orientations, which is the primary concern of this investigation. A pit slope of 65˚/120 was checked for kinematically feasible failures for both sets of data. There were no significant potential for planar failures at this orientation for the southwest or northeast scanlines, as shown by figures 4.24 and 4.25. Apart from small clusters which are contoured as less than 3% and should therefore be regarded with suspicion, there is also very little potential for toppling failure at 65˚/120. Figures 4.26 and 4.27 show the optimum pit slope orientation applied to the southwest and northeast scanlines respectively.

Figure 4.24 Kinematic check for planar failure with a pit slope orientated at 65˚/120 using the southwest data.

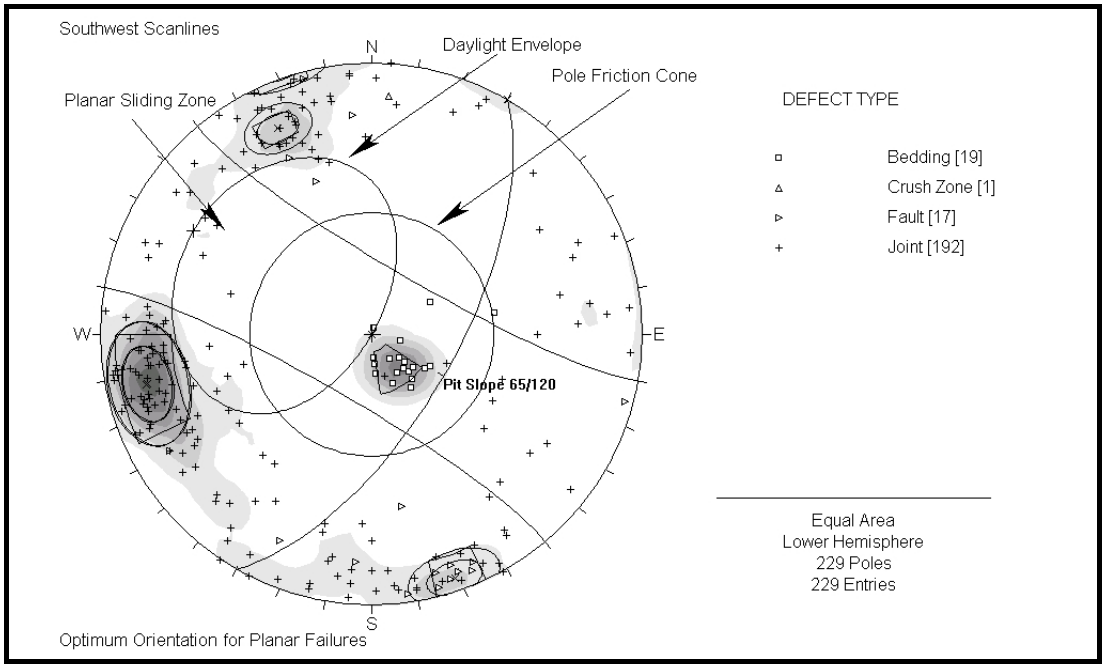

Figure 4.25 Kinematic check for planar failure with a pit slope orientated at 65˚/120 using the northeast data.

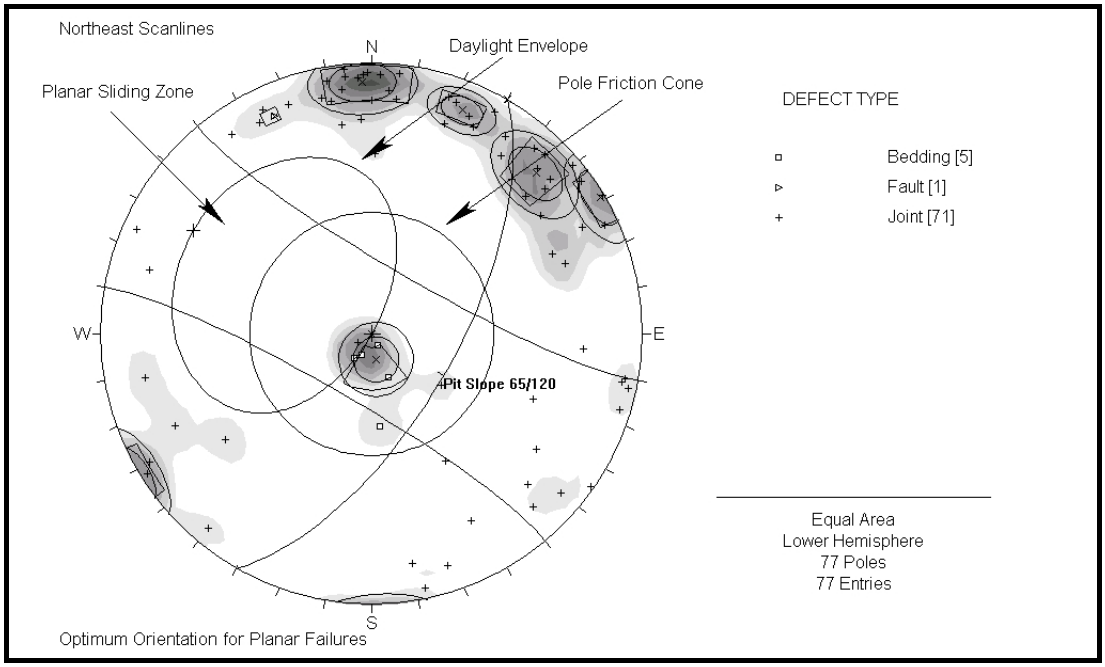

Figure 4.26 Kinematic check for toppling failure with a pit slope orientated at 65˚/120 using the southwest data.

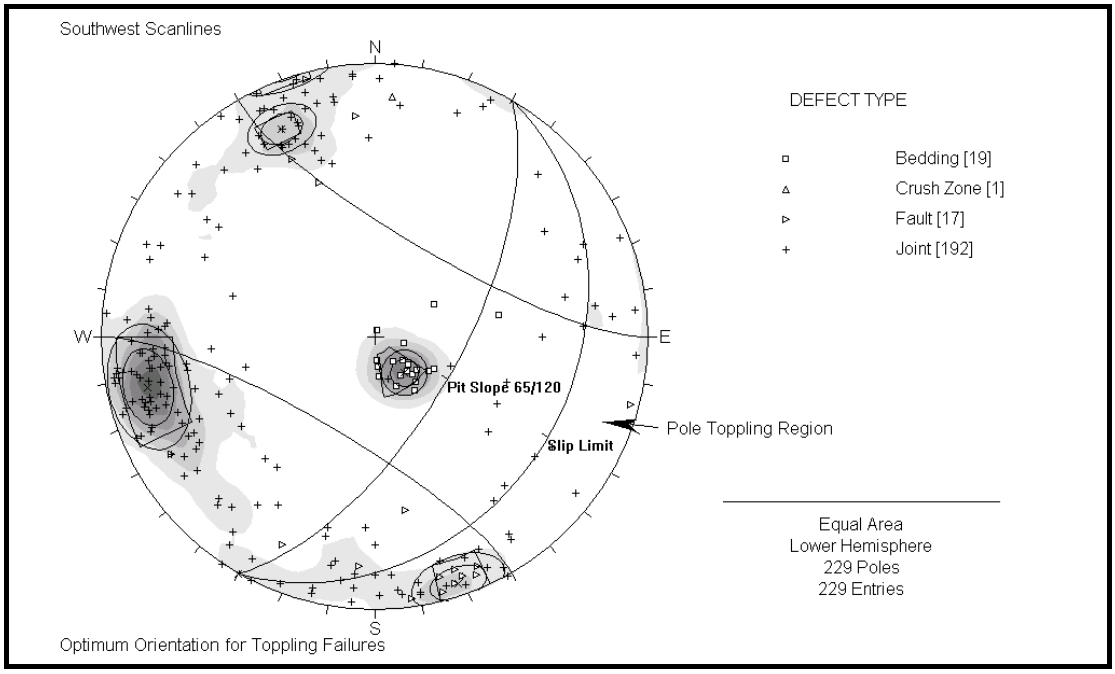

Figure 4.27 Kinematic check for toppling failure with a pit slope orientated at 65˚/120 using the northeast data.

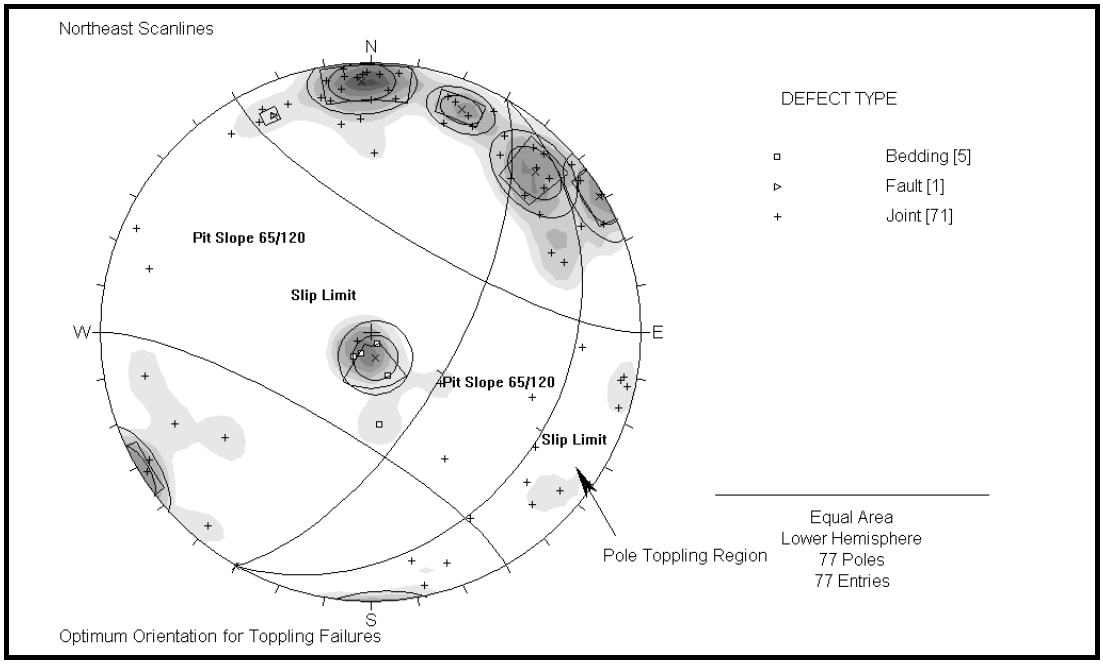

Wedge failures are the most likely mode of failure to affect pit slope stability. With an orientation of 65˚/120 there are no kinematically feasible wedge failures in the southwest scanlines as shown in figure 4.28. There is however, a marginal intersection of JA1 and JA2 and the limits of the concentrations would fall within the 'danger zone' for any combination of changes in dip or dip direction. An intersection between JB3 and JB4 is still present within the sliding zone of the northeast scanlines with a pit slope of 65˚/120, as shown in figure 4.29.

It is important to recognise that these joint concentrations may not truly represent separate sets in the northeast, but could be the same set distorted by the large scale faulting in the area. Although individually the three scanlines show at least 3 of the 4 joints sets (see appendix 3.7), suggesting that they are separate sets, with less than 30 poles each, there is not enough data to be confident. Whether wedge failures will cause significant problems, should conditions like those in the northeast be encountered in the valley floor, will largely depend on the number of different joint sets present, their angular relationship to one another and their persistence. It will also depend on how the rock mass has responded to the fault movement, and it may have caused corresponding joints that will form wedge failures at unanticipated orientations.

Figure 4.28 Kinematic check for wedge failure with a pit slope orientated at 65˚/120 using the southwest data.

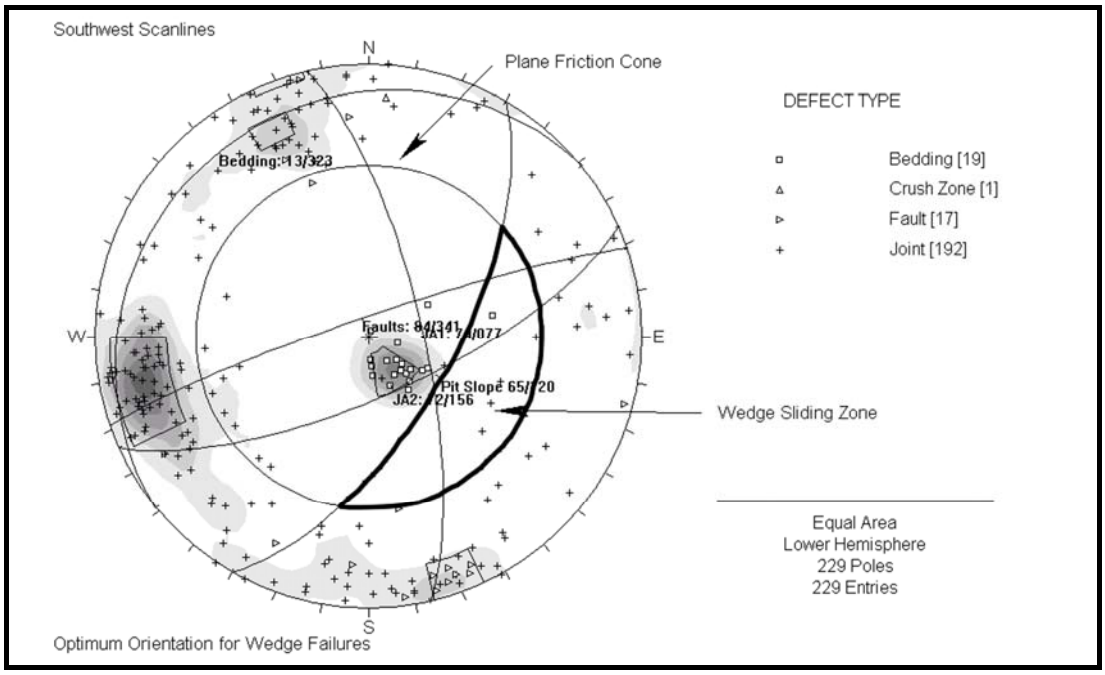

Figure 4.29 Kinematic check for wedge failure with a pit slope orientated at 65˚/120 using the northeast data.

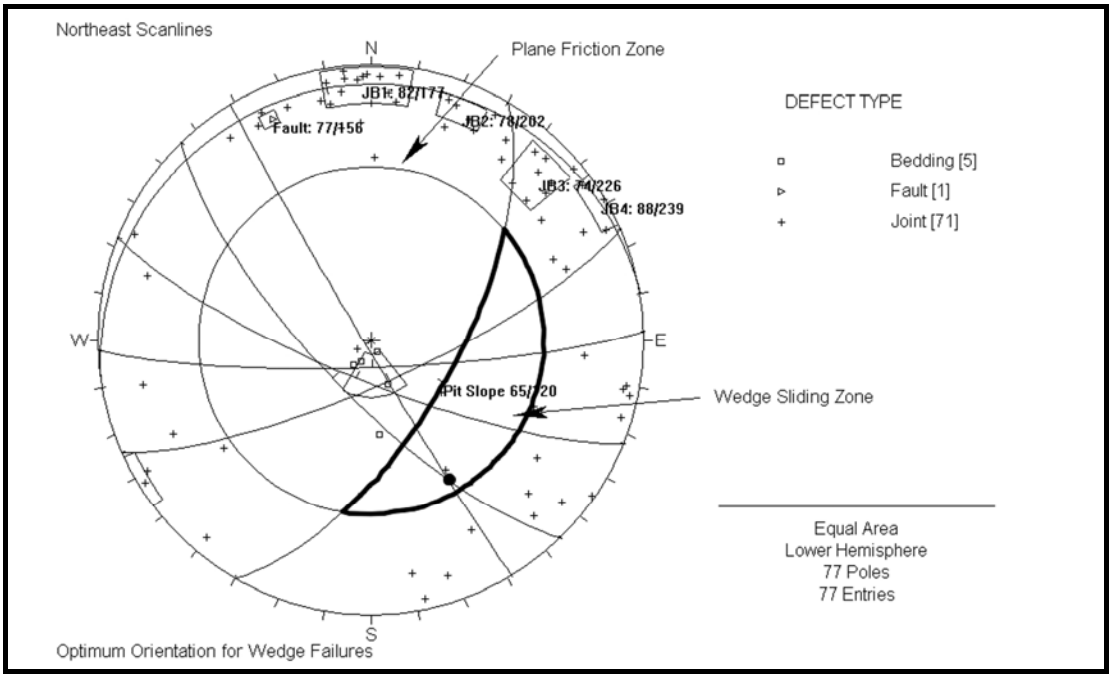

Using the Swedge programme (Rocscience, 2004) the intersection of the two joints in the northeast was analysed in case the joint clusters are representative and may cause wedge failures in the highwall. A deterministic analysis (rather than probabilistic) was performed to gain a factor of safety for certain conditions. A 15m bench height and 8.5m berm width was used in each test (as proposed by Stone *et al*., 2005) with the pit slope orientated at 65˚/120. A rock unit weight of 2.3 tonne/m^3, was used based on average unit density derived in chapter 2. JB3 (74˚/226) and JB4 (88˚/239) were assumed to have zero cohesion and a friction angle of 37˚ based on the shear box testing also discussed in chapter 2. The line of intersection for the two joints had a plunge of 42˚ and a trend of 151. Three tests were performed and the results are summarised in table 4.1. Full analysis information is given in appendix 3.8.

Table 4.1 Summary of results from Swedge tests for a pit slope orientation of 65˚/120.

Test	**1**	**2**	**3**
Water pressure	No	Yes	Yes
Tension crack	No	No	Yes
Wedge volume (m^3)	37.53	37.53	29.56
Wedge weight (tonnes)	86.31	86.31	67.98
Normal force -joint 1 (tonnes)	198.13	46.14	57.5
Normal force -joint 2 (tonnes)	184.36	23.68	38.71
Driving force (tonnes)	57.37	57.37	50.49
Resisting force (tonnes)	288.23	52.62	72.5
Intersection length (m)	22.57	22.57	13.89
Maximum persistence of joints (m)	23	23	18
Factor of safety (F.S.)	5.02	0.92	1.44

Test 1 was performed with no water pressure or tension cracks and gave a very stable factor of safety of 5.0. By introducing 1 tonne/m^3 of water pressure to fill the fissures (test 2) the factor of safety dropped considerably to 0.92, which is considered to be unstable (F.S.<1). Although the dimensions of the wedge remain the same as test 1, the resisting force is reduced by the presence of water to such an extent that it is less than the driving force, making sliding possible. The third test incorporated a tension crack as well as water pressure in the slope. Based on field observations, the tension crack used was vertical, extended parallel to the slope face and was 2m from the slope crest. By introducing a tension crack the dimensions of the wedge (weight, volume, intersection length etc) were reduced. Correspondingly the driving force is also reduced and therefore gave a stable factor of safety of 1.44.

4.4 Slope Stability Considerations

4.4.1 Kinematic Synthesis

Table 4.2 provides a summary of the results determined by kinematic feasibility tests of the data from the scanlines undertaken in the southwest and northeast of the Reddale Valley. An indication of the possibility of failure according to the authors interpretation of the results is given, as well as the defect sets involved. The classification system established was based on the amount of defects within the danger zone. Those that did not display any of the contoured defect sets identified as significant within the danger zone are deemed to be not feasible (N.F) failures. If under a quarter of the contoured cluster was within the danger zone, then there was little possibility (L.P) of failure occurring. Failures are classed as possible (P) if between 25 and 50% of the contoured group is within the danger zone. If over half the contoured set is within the danger zone, there is considered a high possibility (H.P) of failure occurring. All groupings assume the contoured data is representative of the maximum variations of the sets. The criterion does not take into account persistence or volume of potential failures. Based on the persistence plots presented in figures 4.1 and 4.2, 75% of all defects in the southwest and 65% of defects in the northeast were less than 2m in persistence. Should failures occur they are therefore unlikely to cause very large volume slides.

Table 4.2 Summary of kinematic feasibility test results.

Orientation	60˚/130	60˚/150	60˚/170	76˚/130	76˚/150	76˚/170	65˚/120
Southwest							
Planar Defect Sets	**N.F**	**L.P** JA2	**L.P** JA2	**L.P** JA2	**H.P** JA2	**H.P** JA2	**N.F**
Wedge Defect Sets	**N.F**	**N.F**	**N.F**	**P** JA1 & JA2	**P** JA1 & JA2	**P** JA1 & JA2	**N.F**
Toppling Defect Sets	**P** Faults	**H.P** Faults	**H.P** Faults	**P** Faults	**H.P** Faults	**H.P** Faults	**N.F**
Northeast							
Planar Defect Sets	**N.F**	**N.F**	**L.P** JB1	**N.F**	**L.P** JB1 Fault	**P** JB1 Fault	**N.F**
Wedge Defect Sets	**P** JB3 & JB4	**P** JB3 & JB4	**P** JB3 & JB4	**H.P** JB3 &JB4 JB2 &JB4 JB1 & Fault	**H.P** JB3 &JB4 JB2 &JB4 JB1 & Fault	**H.P** JB3 &JB4 JB2 &JB4 JB3 & Fault	**P** JB3 & JB4
Toppling Defect Sets	**N.F**	**L.P** JB1	**L.P** JB1	**N.F**	**L.P** JB1	**L.P** JB1	**L.P** JB1

Key:
N.F = Not Feasible
L.P = Little Possibility
P = Possible
H.P = High Possibility

4.4.2 Southwest Scanlines

In the southwest scanlines there was a high possibility of planar failures occurring with pit slopes orientated at 76˚/150 and 76˚/170. The persistence plots shown in figure 4.1 of the introduction show that at least 3 defects that have greater than 2m persistence will fall within this danger zone, which suggests that should failures occur, they may involve reasonably sized blocks. All pit slopes at 76˚ suggested wedge failures were possible by the intersection of the major (JA1) and minor (JA2) joint sets. With an optimum orientation of 65˚/120 there is still a marginal intersection of JA1 and JA2, and by altering the dip or dip direction for either joints so that it still lies within the concentration, the intersection is easily moved within the danger zone. It was indicated in chapter 3 that the concentration of JA2 is only marginally significant at 4.5-6% and therefore the likely hood of both planar failures and wedge failures occurring is questionable.

All pit slope orientations in the southwest showed that toppling failure was kinematically feasible along the steeply dipping faults. As these have been noted both underground and in the scanlines, it is highly likely that they would be encountered in the valley floor. Figure 4.1 showed that 5 of the faults within the cluster had a persistence of greater than 2m. In order to avoid any toppling failures an optimum dip direction for the pit slope of 120 is needed.

4.4.3 Northeast Scanlines

In the northeast scanlines the 'little possibility' class for planar failures with a pit slope of 60˚/170 given by the classification system, is probably misleading as only one data point plots within the danger zone. Planar failure at any of the orientations with a pit slope of 60˚ is therefore highly unlikely. Although planar failures are possible at 76˚/150 and 76˚/170, only one joint with persistence greater than 2m falls within the danger area. The Reddale Fault has been recorded and mapped underground, and although it is only represented by one data point in the northeast scanlines on the very edge of the 'danger zone', a certain degree of variation can be expected in the dip and dip direction. It is parallel to the Burkes Creek and Morrisvale Faults, and as all three cross the proposed pit site, they are particularly important structural controls on pit stability.

The orientation of the faults will also affect whether wedge failures will occur as there are several marginal intercepts (within and on the outside of the danger zone) between the fault and the joint sets in the northeast data. Wedge failures are therefore highly likely to occur when the fault intersects joints, based on data from the northeast side of the valley. Wedge failures caused by the intersection of one joint set with another is dependent on whether the data is truly showing separate sets or a single widely scattered set, which has been distorted by fault movement, as discussed in section 4.3.4. This also affects the possible wedge failure incurred in a pit slope with the optimum orientation (65˚/120). It should also be remembered that the wedge analysis is only based on the average orientation of the concentration, and as the plots show there is considerable scatter in most sets, so that in reality there is a range of possible orientations.

The set which may produce toppling failure in the northeast is JB1, but only the very edge of the diametrically opposite concentration falls within the danger zone. There are no joints recorded that dip in this direction, but as the centre of the cluster is near 90˚, which includes several defects with greater than 2m persistence (figure 4.2), the contoured area extends across the other side of the stereonet. With such steep dips it is possible for a change in dip direction to happen but in general there is a low possibility of toppling failures occurring with any of the pit slope orientations.

4.4.4 Bedding in Dip Slope (Footwall)

As bedding dips into the highwall it is not expected to cause any problems except to provide releasing surfaces for cleavage in the mudstone, which may cause overhangs to develop.

Again with batter angles of 76˚ or less it would be unlikely to cause any large scale instability. In the dip slope, however there is a chance that bedding parallel failures will result from the low shear strength, especially given that that the direct shear test reported in chapter 2 gave a friction angle of approximately 15˚ for the carbonaceous mudstone bedding planes. When this situation is combined with the expected fault in the pit floor, which is downthrown to the northwest, it may cause the slope to 'release' along bedding. This is illustrated in figure 4.30 which was produced by Solid Energy. If the faulting has caused local steepening of bedding in the foot wall, combined with low cohesion and internal friction angles, slab sliding is geotechnically feasible according to these preliminary investigations.

Figure 4.30 Cross-section of proposed pit showing potential for bedding plane failures, released by the fault in the pit floor (Stone et al., 2005).

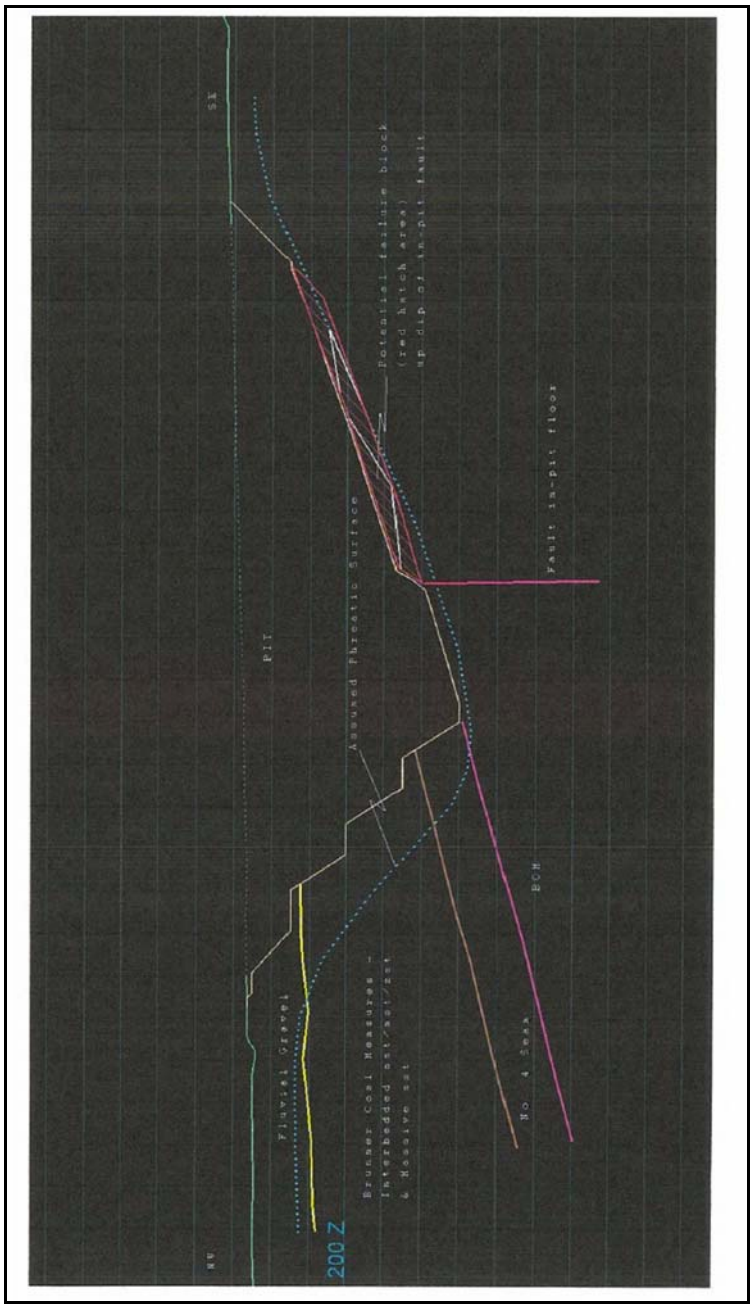

4.4.5 Groundwater Influence

Figure 4.30 also shows a high phreatic surface produced by mining beneath the water table. The pond shown in figure 1.11 chapter 1, gives an indication of amount of water that will fill an open pit in valley floor. This pond is likely to be storing water that has drained from underground workings, but the sides of the proposed opencast may also encounter abandoned and flooded underground workings. If substantial quantities of water are discharged into the excavation, the pit slopes will be subjected to erosion, which may cause progressive channelling of flow paths and enlargement of tension cracks and joint aperture. Measures may need to be implemented to prevent or control the inflow paths, such as cut-off drains above the lateral batters and highwall.

The most crucial effect of significant amounts of ground water present in a rock mass is the reduction in slope stability caused by water pressure within discontinuities (Hoek and Bray, 1977). The presence of substantial pore-water pressure as shown in sections 4.3.4 can greatly reduce the factor of safety. It may also alter the kinematic possibility of failure; for example in the case of planar failure, water pressure may result in slip despite the dip of the failure plane being less than the frictional strength of the plane (Norrish and Wyllie, 1996). Water can therefore be considered the most important factor affecting the development of an opencast mine in this area. It will be crucial to de-pressurise the pit slope and a combination of measures which may include horizontal drainage holes, pumped vertical dewatering holes, perimeter drains and in-pit sumps, have been proposed (Stone *et al.*, 2005). The investigations presented in this study have confirmed the importance of this requirement.

4.4.6 Existing Highwall Observations

4.4.6.1 Wedge Failures

Large scale (5m+) and persistent joints that intercept to form wedge failures were observed in scanline 3, which is shown in figure 4.31. The highwall in figure 4.31a is around 15m high and would give an individual wedge volume of approximately 30-50m^3. A fan of rubble containing blocks approximately 1.5m^2 can be seen at the bottom of each intersection, on the bench beneath the face. The bench and highwall further to the northeast has not remained stable and the red line shown in figure 4.31b shows the approximate location of the end of the bench when it was in place. Although the existing highwalls are near vertical, and therefore steeper than the proposed pit slopes, wedge failures are likely to cause instability based on these observations combined with the kinematic feasibility results.

Figure 4.31 a) Photograph of wedge failures in current highwall of 'Old' Terrace Opencast. Fluorescent crosses mark the location of scanline 3. b) Photo along the bench shown in a) with a red line indicating the approximate position of the northeast continuation of the bench before failure.

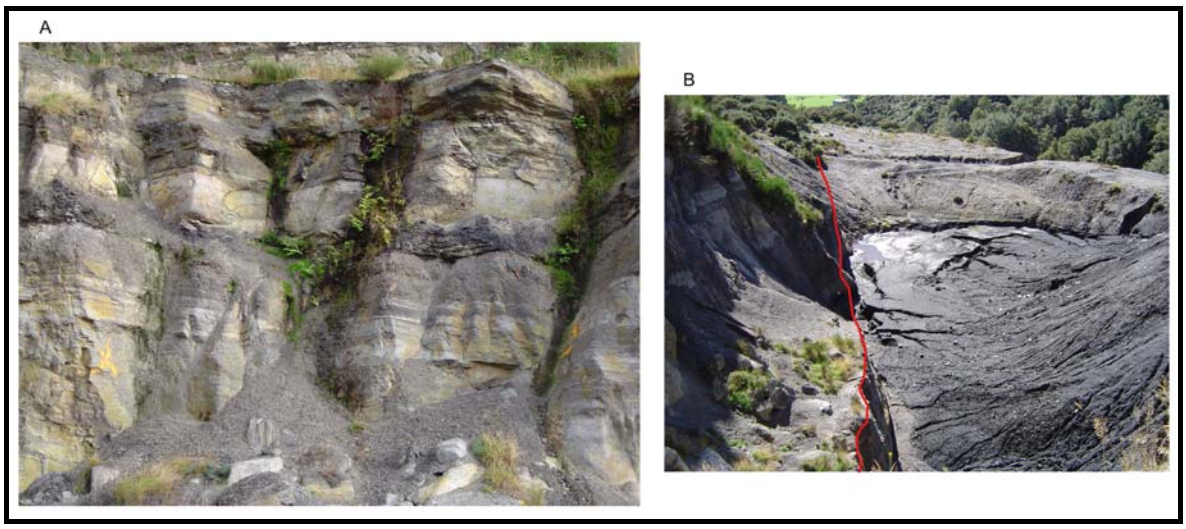

4.4.6.2 Tension Cracks

The occurrence of substantial tension cracks has also been noted in the present highwalls. Tension cracks are known to be generated by small shear movements within the rock mass, which cumulate to cause separation within the rock mass to form vertical joints behind the slope crest (Barton, 1971). There is some debate surrounding whether they are an indicator of instability. Slopes in which they occur may remain stable for tens of years, and in certain situations could improve drainage by opening up the rock structure and interlocking individual blocks within the rock mass (Hoek and Bray, 1977). However in general they are assumed to be a sign of potential instability, and Hoek and Bray (1977) suggest detailed investigation should be undertaken into any slope in which they occur. Figure 4.32 shows an example of a tension crack found on an existing highwall in the 'Old' Terrace Opencast, which may potentially cause toppling failure.

Figure 4.32 Photographs of a tension crack in an existing highwall a) Close up of tension crack on berm b) Tension crack can be seen daylighting in the left hand side of the photo.

4.5 Synthesis

The analysis of kinematic feasibility for planar, wedge and toppling failures combined with other slope stability considerations, suggest that the following factors will control highwall stability in the Reddale Valley:

- The most important influence on slope stability will be the flow rate and pressure created by water within the rock mass. With the aid of further hydrological investigation an adequate drainage scheme will need to be designed.
- As the majority of joints recorded in the scanlines have low persistence (less than 3m) as discussed in chapter 3, stability issues relating to joint set orientation are unlikely to cause significantly large failures.
- If structural conditions such as those seen in the southwest are encountered in the valley floor, kinematic feasibility will depend on the significance of JA2 (76˚/156). Should it prove significant pit slopes of 76˚ may encounter planar and wedge failures. All suggested orientations give a relatively high possibility for toppling failures along high angle normal faults which are expected to occur in the highwall.
- If structural conditions such as those seen in the northeast are encountered in the valley floor, kinematic feasibility will depend on whether the joints observed are separate sets or a widely scattered single set that has been distorted after

formation. The Reddale, Burkes Creek and Morrisvale Faults that cross the valley are likely to cause planar and wedge failures in the highwall. Toppling failures are unlikely to occur based on the collected data.

- An optimum orientation for the pit slope of 65˚/120 is suggested to avoid most kinematically feasible failures. Should wedge failures between JB3 (74˚/226) and JB4 (88˚/239) occur, analysis using Swedge has suggested the wedge will be stable when dry, marginally stable with a tension crack and water pressure present and unstable when the fissures are filled with water
- Failures may occur along bedding in the dip slope, especially given the low friction angle of the carbonaceous mudstone bedding planes determined in chapter 2 (15˚). The fault which intersects the pit may provide a releasing surface and local steepening of bedding making slab sliding likely to occur.
- Large (5m+) wedge failures and tension cracks have been observed in existing highwalls and although the proposed pit walls are less steep, they may occur in the proposed excavation.

The kinematic checks do not assess failure by circular slip, which is a possible failure mode in the loose sandstone unit but nor likely as confined by other lithologies. The cleavage associated with exposure of the mudstone has also not been assessed here and may influence small scale slope stability. While the more easterly dip directions give better kinematic results the eventual highwall orientation will also be controlled by the strike of bedding and possibly the requirement to mine around the block of trees protected by the QEII trust. Map A (map pocket) provides a basic highwall outline based on the optimum orientation (120 dip direction) determined by kinematic feasibility assessment. This chapter has shown that kinematic feasibility tests produce a useful initial assessment but as suggested by Hudson and Harrison (1997) are only the first approach in a long line of design and analysis tools used to ensure optimum recovery with acceptable slope stability conditions.

Chapter 5

Case-hardening Investigation

5.1 Introduction

Case-hardening and associated weathering coatings are diverse subjects, with a considerable amount of documentation in the literature. They incorporate many disciplines including geomorphology, geochemistry, geomicrobiology, ecology and geography. While this chapter attempts to incorporate as many approaches as possible, it focuses on situations and studies which are applicable to that observed in the existing highwalls in the Terrace Mine area and how the development of rock coatings will affect short and long term pit slope stability. It is intended as a study of case-hardening of sandstones in a temperate environment, about which there is a lack of knowledge, especially in relation to iron films and the interaction between mineralogy and environmental controls, as noted by Dorn (1998). He points out that although the majority of universities are within temperate zones, there has been a larger amount of research conducted on Antarctic iron films.

The weathering of weak sedimentary rocks is crucial to geological engineering projects such as the proposed opencast, as the mechanical properties are influenced more by the extent and type of weathering than fracture density (Chigira and Oyama, 1999). This has been indicated by the data presented in chapters 3 and 4, which suggests that the joints are likely to have low persistence and do not pose significant problems with large scale failures at the proposed orientations. Rapid weathering of sedimentary sequences can cause instability and environmental problems (Chigira and Oyama, 1999). Case hardening protects the rock beneath from such weathering and when conditions allow this protective crust to develop, it may aid stability as observed in the existing cut faces.

Weathering is defined by Ollier (1969, page 1) as “the breakdown and alteration of materials near the earth’s surface to products that are more in equilibrium with newly imposed physico-chemical conditions”. Although weathering is commonly associated with disintegration and decomposition of rocks, it can however assume a protective role (Robinson and Williams, 1986). Dorn (2004) defines case-hardening as rocks with an outer shell that is more resistant to erosion than the interior material. The origin, nature and geomorphic importance are the focus of debate within the literature (Viles and Goudie, 2004). Fundamentally the interior and exterior are the same rock type only altered by weathering or the addition of external agents (Dorn, 1998). Various rock coatings therefore often cause case-hardening of the exterior, especially in clastic

rocks, while core-softening of the interior is more common in crystalline rocks (Conca, 1985). The 'growth' of a thin (mm to cm scale) hardened layer on the surface of the rock may be created by cementation of externally sourced material, and/or the accretion of material from within the rock itself. Clays and micro-organisms are often involved, although whether they aid in strengthening the rock surface is controversial (Viles and Goudie, 2004).

Differential weathering of sandstones often results in karst-like features, as seen in the East Kimberley Region, Australia (Young, 1987) and caverns or tafoni, as seen in the Valley of Fire, Nevada (Turkington and Phillips, 2004),as shown in figure 5.1. Salt crystallization is one of the contributing factors in the mechanical breakdown or chemical weathering that creates these landforms (Turkington, 1998). They are often associated with arid and salt-rich environments such as deserts (Turkington and Phillips, 2004). Case-hardening on sandstones in the Valley of Fire has been studied extensively, and is believed to be produced by fine-grained cement from within the host rock and wind deposited kaolinite (Conca and Rossman, 1982). The Dry Valleys of Antarctica also display case-hardening on sandstones, with crystallization of silica increasing the hardness of the exterior (Conca, 1985; Weed and Ackert, 1986). Examples of various types of case-hardening are however found in all terrestrial environments. The wet tropics frequently display iron-rich coatings on bedrock in river beds that is only reached by wet-season floods (Dorn, 2004). Temperate environments tend to exhibit localised case-hardening from rock coatings composed of a variety of components. Robinson and Williams (1986) suggest that although sandstones in England and Northern France are discoloured by iron and carbon compounds, it is the secondary deposition of silica on quartz grains and in pore spaces which dominates the crust.

Figure 5.1 Several outcrops displaying cavernous weathering in the Valley of Fire State Park (Turkington and Phillips, 2004).

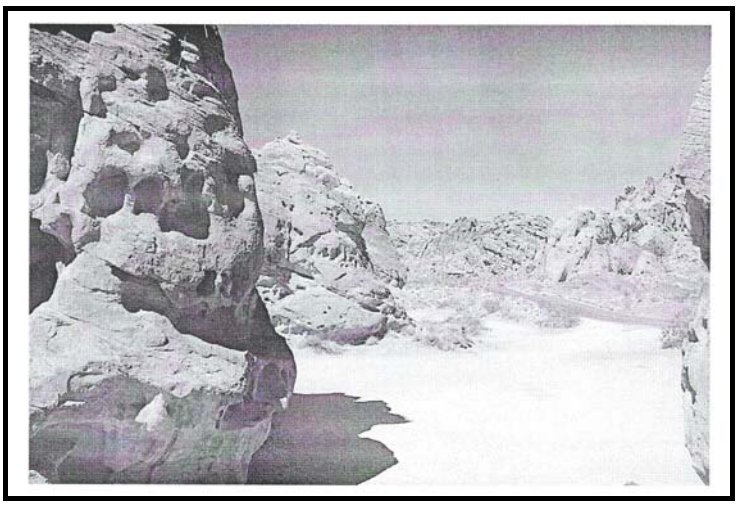

This chapter firstly provides general background on aspects of the rock coatings which are likely to be present in the Reefton area. The methods used to investigate case-hardening were outcrop, hand specimen and thin section description; SEM (Scanning Electron Microscope) combined with EDS (Energy Dispersive Spectrum); XRD (X-ray Diffraction) analysis, pH and EC (Electrical Conductivity) determination. Appendix 4.1 gives details of the methods and appendix 4.2 presents the co-ordinates of each site, which are also plotted on map C (Aerial Photograph –map pocket). The components of the coatings identified from the six sites selected from the Reddale Valley and nearby Peerless Gully are presented. Each crust was strength tested to give Schmidt Hammer readings as well as a qualitative description of the difficulty to scrape and penetrate by a knife blade, in order to determine whether the outer layer is stronger ('hardened') than the host rock. The discussion compares the finding with other studies and categorises each crust. The rate of formation and implications for opencast mining are also considered in terms of how the rock coatings will affect short and long term stability.

5.2 Types of Rock Coatings

5.2.1 Lithobiontic Coatings

The term 'lithobiontic' is defined by Golubic *et al.* (1981) to describe organisms that grow on and within rock substrates. They are also often referred to as biofilms but this term can be applied to a variety of situations (Dorn, 1998). The micoorganisms can be classified by the ecological niche they occupy. As shown in figure 5.2, epiliths are organisms attached to the external surface of the rock while endoliths penetrate the rock mass. When the rock contains transparent minerals such as quartz, light is able to reach the organisms for photosynthesis and they are protected from fluctuations in moisture and temperature (Dorn, 1998). If the endoliths inhabit fissures they are known as chasmoendoliths, if they live within pore spaces they are called cryptoendoliths and if they actively bore into the rock they are termed euendoliths (Golubic at al, 1981). Some organisms can occupy different locations at the same time (Dorn, 1998).

Figure 5.2 Microbial ecological niches (Golubic et al., 1981).

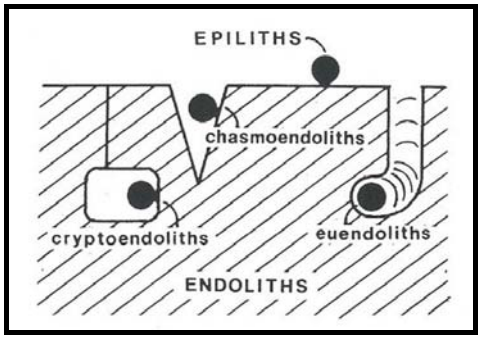

There are many different types of organisms that form lithobiontic coatings, and often there is more than one present at any time (Dorn, 1998). Only the main groups are outlined here. Most are protists, which are differentiated from plants and animals as typically unicellular, with simple internal structure. The first type of organism is bacteria and they are procaryotic or lower protist (figure 5.3a), which means there is little differentiation between cells and they do not have a true nucleus (Mitchell, 1974). Bacteria are associated with the dissolution as well as formation of minerals. Both processes provide them with energy and aid respiration in situations where oxygen is limited or absent (Ehrlich, 1996). It has been suggested that organic acids at the bacteria-mineral interface are able to mobilize silica and aluminium, and cause etching of the mineral surface (Hiebert and Bennett, 1992). There is significant evidence also to suggest that bacteria are involved in the accretion of inorganic minerals such as the manganese hydroxide found in rock varnish (Dorn, 1998). Fyfe and Beveridge (1985) showed that bacteria can interact with metallic ions (copper, zinc, iron, uranium) in solution and bind a significant amount to their walls. This may provide a site for nucleation and growth of new minerals.

Cynobacteria, commonly known as blue-green algae, are also procaryotic but unlike bacteria create oxygen during photosynthesis (Singleton and Sainsbury, 1978). Cynobacteria are common on rock and soil surfaces and often aid weathering. They also form new minerals deposits, the most well known being the stromatolites of calcium carbonate precipitated by Archaean cynobacteria (Dorn, 1998). They often occur in deserts where no other organic material is present, and grow well under bright sunlight in areas with abundant inorganic nutrients (Mitchell, 1974).

Fungi are eucaryotic or higher protist (figure 5.3b), a group which have a discrete nucleus similar to animals and plants, undergo mitosis and have many chromosomes. Fungi in particular are nonphotosynthetic and grow by elongation of thread-like hyphae (Mitchell, 1974). They often coat rock surfaces and many studies have been conducted on their behaviour on stone monuments, which they frequently discolour (Dorn, 1998). Microcolonial fungi have been observed to contain a higher concentration of manganese than the surrounding substrate in Australian deserts, which suggests they may also play a role in formation of desert rock varnish (Staley *et al.*, 1983). Fungi occur in many different settings and Dorn (1998) notes that he has observed fungi, generally in filamentous form, in the majority of all samples investigated under the SEM.

Algae are photosynthetic eucaryotes and may be unicellular or multicellular (Mitchell, 1998). They often dominate rock surfaces in damp situations and can occupy several ecological niches. When present as chasmolithic algae, they can aid weathering by expansion and contraction causing flaking. They often occupy pore spaces within the upper few millimetres of the weathering rind in sandstones (Dorn, 1998).

Figure 5.3 Typical protest cells a) procaryotic b) eucaryotic cells.

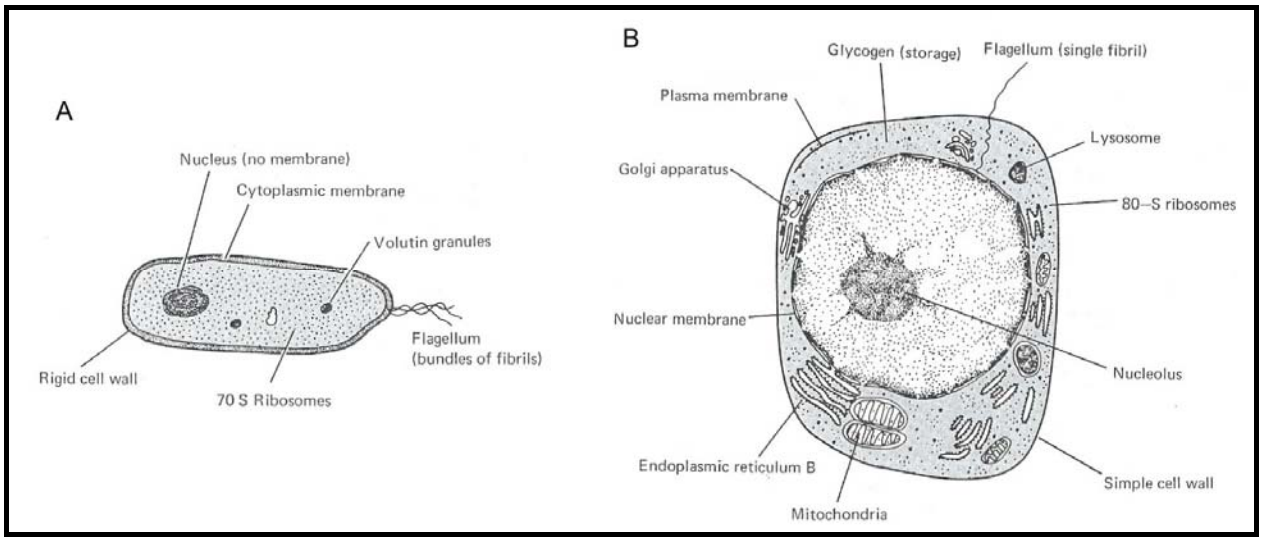

Lichens are composite organisms that consist of a fungus living in close physical association with an alga (Singleton and Sainsbury, 1978). They are very hardy organisms that can survive in extreme conditions. Lichens often erode rock surfaces creating distinctive weathering patterns, but they may also protect them from further erosion when the surface is stabilized in wetter climates (Dorn, 1998). Higher organisms, such as mosses and plants, can also form lithobiontic coatings. Mosses are both epiliths and euendoliths because they penetrate into pore spaces as they colonize a rock surface (Dorn, 1998).

The distribution of lithobionts is controlled by many factors, which includes moisture, position, rock type and time. As they grow faster than most other rock coatings, they often dominate the available space. Other rock coatings are possibly restricted to places where biological weathering is less effective (Dorn, 1998).

5.2.2 Iron Films

Iron films are rock coatings with iron as the major element, and a distinctive reddish colouring being produced by iron oxides. It should not be confused with rock or desert varnish, which is generally a much darker coating and is characterised by clay minerals, cemented predominantly by oxides and hydroxides of manganese (Dorn, 1998).

Dorn (1998) divides iron films into three types based on their chemistry and mineralogy. The form of iron depends on the pH, solubility and amount of oxygen present, as well as the abundance of other dissolved minerals. Type I have iron as the only major element and are found in a wide variety of environments. Type II contains aluminium and silicon as major elements, but together still make up less of the coating than iron. They have only been observed in subaerial exposures and often interfinger with other rock coatings or other iron film types. In type III iron films, aluminium and silicon combined are more abundant than iron, and they are therefore mostly made up of clays.

Iron films may originate from a variety of sources. In some environments there may be enough iron in aquatic, soil and eolian transportation pathways to create iron films (Dorn, 1998). In Antarctica, the K-Fe mineral jarosite is the main component of the iron films in the Sør Rondane Mountains. Sulfuric acid in the soil mobilizes the iron and potassium and it moves up through fractures in the rock to be deposited on the surface by evaporation (Hayashi and Miura, 1989). It is also likely that biotic agencies are influential in producing iron films, especially as bacteria are able to oxidise iron in acidic conditions (Dorn, 1998). They may behave as microbial catalysis in mineral dissolution, especially in the oxidation of pyrite to ferric sulfates such as jarosite (Ehrlich, 1996). Singer and Stumm (1970) noted that microoganisms, when compared to other possible catalysis in acid mine drainage from coal mines, appear to exhibit the greatest effect in accelerating the oxygenation of Fe^{2+}. Photoreduction may also influence iron film genesis in areas with acid mine drainage, as the amount of dissolved Fe(II) was noted to increase with increasing light intensity (McKnight *et al.*, 1988).

Iron films often incorporate components of other rock coatings. Friedmann (1982) suggests that the endolithic microoganisms found in sandstone within the Antarctica Dry Valleys may contribute to the mobilization of iron. In temperate environments a connection between iron and silica glaze has been noted. Robinson and Williams (1986) found that surface crusting of sandstones in Southern France and Northern England was dominated by secondary silica, despite

the iron discolouring. Dorn and Meek (1995) observed the formation of silica glaze as well as iron skins on 20-40 year old steel and iron slag piles. They also noted that bacterial activity observed on the surface probably caused iron to be deposited, while the manganese present remained in solution. There are cases where the formation of iron films has only taken a number of years (Dorn and Meek, 1995). Conversely accretion rates may be in the order of microns per thousand years, and this depends largely on the local environment in which it is forming (Dorn, 1998).

5.2.3 Silica Glaze

Although silica is relatively resistant to chemical weathering, terrestrial weathering does release some silica from rocks and it is re-deposited in soil, water or the atmosphere (Dorn, 1998). Silicates are broken down by the action of water, which oxidises the ferrous ions present and cause hydration of unstable lattice fragments that become aqueous or form a poorly organised layer attached to the surface. The hydroxyl groups within the hydrated fragments of this layer are very sensitive to changes in the outer solution, and their stability largely depends on the pH of the weathering solution (Ollier, 1969). Silica glaze has a lustrous appearance and is characterised by amorphous silica, often in conjunction with alumina and detrital clasts (Curtis *et al.*, 1985).

Dorn (1998) recognises six types of silica glazes, which are classified according to quantitative chemical analyses of silica and other components present. Type I is named homogeneous amorphous silica glaze and only contains traces of other minerals, giving is a translucent or white colour. Type II is a detrital-rich silica glaze, where amorphous silica cements fragments of rock material and fills pore spaces on the rock surface. Type III silica glazes have relatively high concentrations of iron and aluminium, but silicon remains the dominant component. Type IV are characterised by silica glazes with aluminium concentrations greater than 10%. Type V has iron as the second major component other than silica. They are differentiated from type III iron films by having lower concentrations of aluminium and clay minerals. Type VI is known as alumina glaze and contains aluminium oxides, which make up more than 50% of the coating.

Silica glazes are considered as external accretions, although the source material may only be a few microns away (Paraguassu, 1972). A distinct morphological boundary exists between the silica glaze and host rock, and as no loss of mass from beneath the weathering rind has been observed, external accretion is assumed (Dorn, 1998). Curtiss *et al.* (1985) suggest that the

source material is dissolved and deposited as a rock coating, which incorporates dust particles blown from local surface soil. Paraguassu (1972) has shown by experimental silicification of sandstone that silica is easily mobilized by the percolating water. Watchman (1992) studied several Australian examples and concluded that the silica was derived from the rocks above seepage areas by natural chemical weathering of siliceous minerals and amorphous silica cement. Soluble aluminium and silica may be critical components that control the formation of metastable and new stable minerals (secondary clays) when water interacts with rocks and soils (Browne and Driscoll, 1992). Watchman (1992) noted the presence of mircoorganisms in rock skins and suggested that some may have been trapped in the silica when it was deposited by seepage water. Silicates are known to dissolve faster in microbially active organic rich waters, and bacteria may aid mobilization of silica and aluminium from mineral surfaces (Hiebert and Bennett, 1992). Iron may also enhance the ability of bacterial to bind silica (Urrutia and Beveridge, 1994). Once established the silica glaze will reduce the amount of water able to infiltrate the sandstone and may slow the formation of the crust itself (Robinson and Williams, 1986).

Silica glazes have been observed in a variety of environmental settings. They have been particularly noted in Antarctica, where they form subaerially under arid conditions and develop slowly over time (Weed and Ackert, 1986). Figure 5.4 shows a model for the staining and encrusting of the Antarctic sandstone. Using the SEM, Robinson and Williams (1986) observed nodular and filamentous growths of secondary silica between sand grains in temperate sandstones. Caverns in greenschist on the coastal slope of South Devon also display case-hardening, but it occurs within the rock mass. It is suggested that alumino- and iron silicate materials are released by chemical weathering and transported along joints, where some of it is reprecipitated (Mottershead and Pye, 1994). Opaline silica coatings are deposited in a range of settings throughout Australia, and are often associated with Aboriginal rock art (Watchman, 1992).

Figure 5.4 The process which stains and encrust Antarctic sandstones proposed by Weed and Ackert (1986).

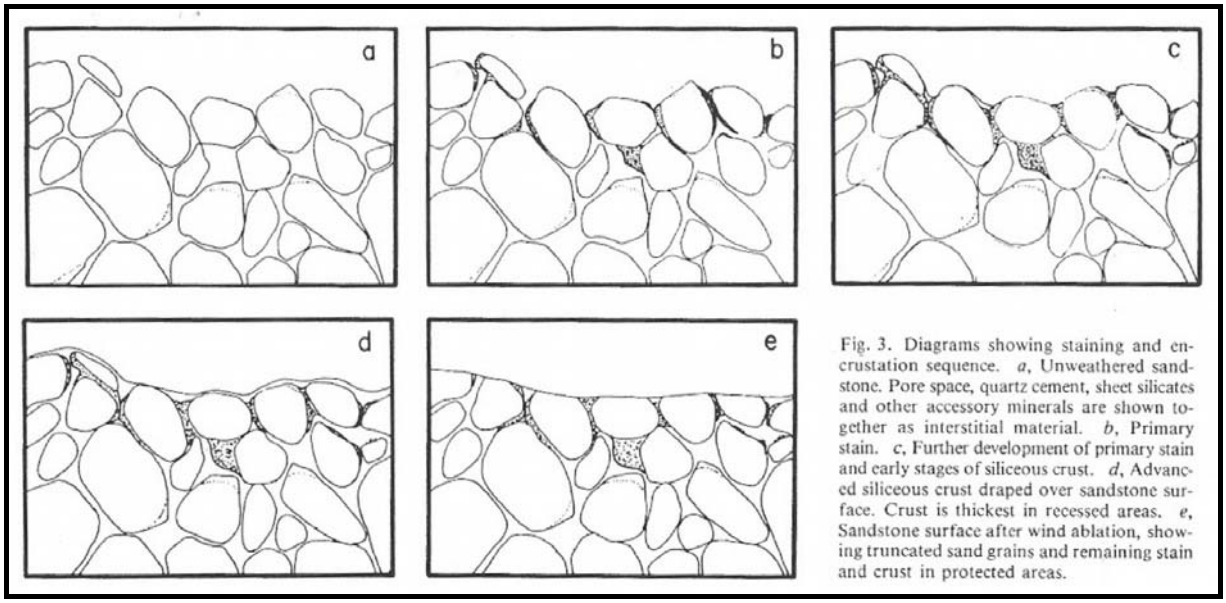

5.2.4 Other Rock Coatings

There are several other types of common rock coatings that may cause case-hardening but are not expected to form within the study area. Efflorescent salt crusts are often found in drylands and result from evaporation of saline water, or by recycling of airborne minerals by rainfall and evaporation (Smoot and Castens-Seidell, 1994). Due to their soluble nature, salt crusts on the surface of sediments usually only form temporary coatings (Goodall *et al.*, 2000). The term duricrust refers to metre thick concentrations of subsurface salts (Dorn, 1998). The constituents may involve iron (ferricrete), silica (silcrete), calcite (calcrete), gypsum or halite (Selby, 1993). Carbonate crusts on subaerial exposures are commonly found integrated with other rock coatings such as desert varnish and lithobiontics (especially in forming dolomite). They also case-harden limestone in tropical regions (Dorn, 1998).

Dust films are composed of clay- and silt-sized particles that form a light powder on rough surfaces and in rock fractures (Dorn, 1998). Metals with high atomic numbers, or heavy metals, such as copper, also form hardened rock coatings. They are frequently seen on rocks downstream from mine tailings. Manganese is a common constituent and may form a skin, which has manganese as the dominant mineral but lack the clays which bind desert varnish (Dorn, 1998). Desert or rock varnish is known to be an accretion on the surface which does not originate from the underlying rock. Dorn (1998) suggests that rock varnish is formed by the weathering of both bacterial casts and clay minerals.

5.3 Site Investigation

Although six sites were originally selected, some sites showed considerable similarities on inspection and are reported here together. The findings from thin section, XRD and EDS are used together to provide a complete understanding of the components of the crust and material directly beneath it. Raw data for the Schmidt Hammer is provided in appendix 4.3. The XRD scans and bulk EDS scans are provided in appendices 4.4 and 4.5. An example of the EDS line scans completed for each site is also given in appendix 4.6.

5.3.1 Sites 1 and 2

5.3.1.1 Outcrop and Hand Specimen Description

The first site was located on the top wall of the 'Old' Terrace Opencast and consisted of a predominantly yellow and orange crust on the fine grained sandstone interbedded with carbonaceous mudstone (unit 3). As figure 5.5 shows it had a patchy appearance, with the bedding being seen through the crust in thinner areas. The surface was dry and relatively smooth, and the crust is approximately 5mm thick.

Figure 5.5 Outcrop at site 1. a) Close up of the face where samples were collected. b) Photograph showing the surrounding units. The bottom scale on the tape measure is in cm.

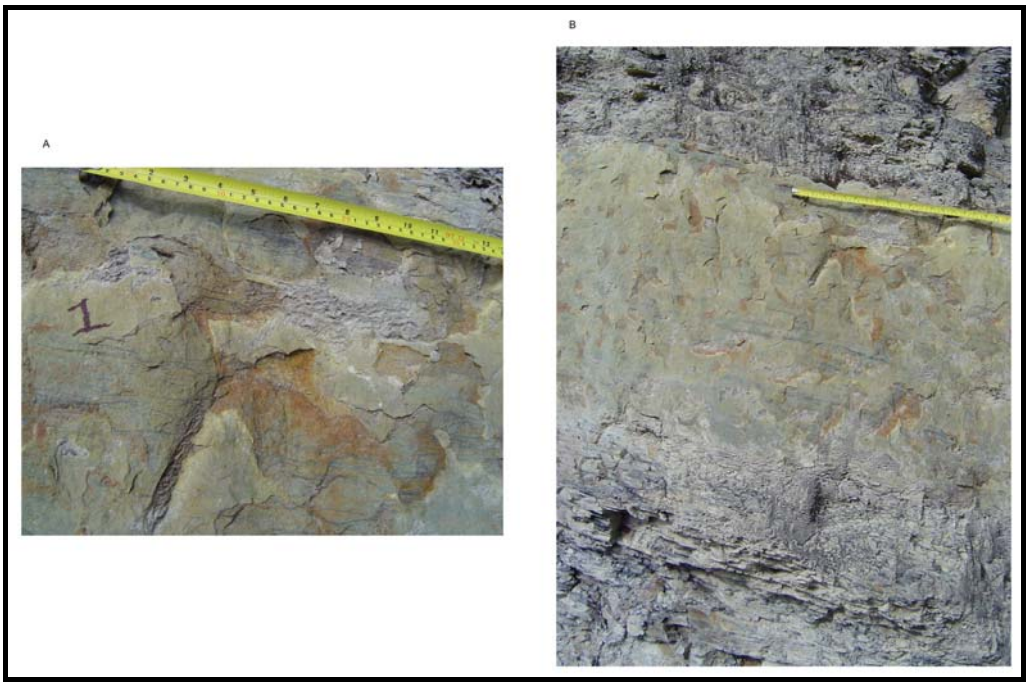

Site 2 was also in the 'Old' Terrace Opencast, on the middle highwall beneath site 1. The crust here was thicker (approximately 10mm thick) than site 1 and displayed a relatively consistent (especially on east facing joints), opaque, yellow/white coating with orange weathering beneath as seen in figure 5.6. The host material was also laminated sandstone and most surfaces were

generally smooth. Although dry when investigated, concentrations of soft 'knobbly' clays appear to have been deposited by seepage at some stage. This can be seen to the left of the end of the tape measure in figure 5.6a, where water previously followed the intersection between joint surfaces.

Figure 5.6 Outcrop at site 2. a) Close up of the face where samples were collected. Accumulated clays can be seen in the top left corner. b) Photograph showing the surrounding units. Hammer at the bottom of cut face provides scale.

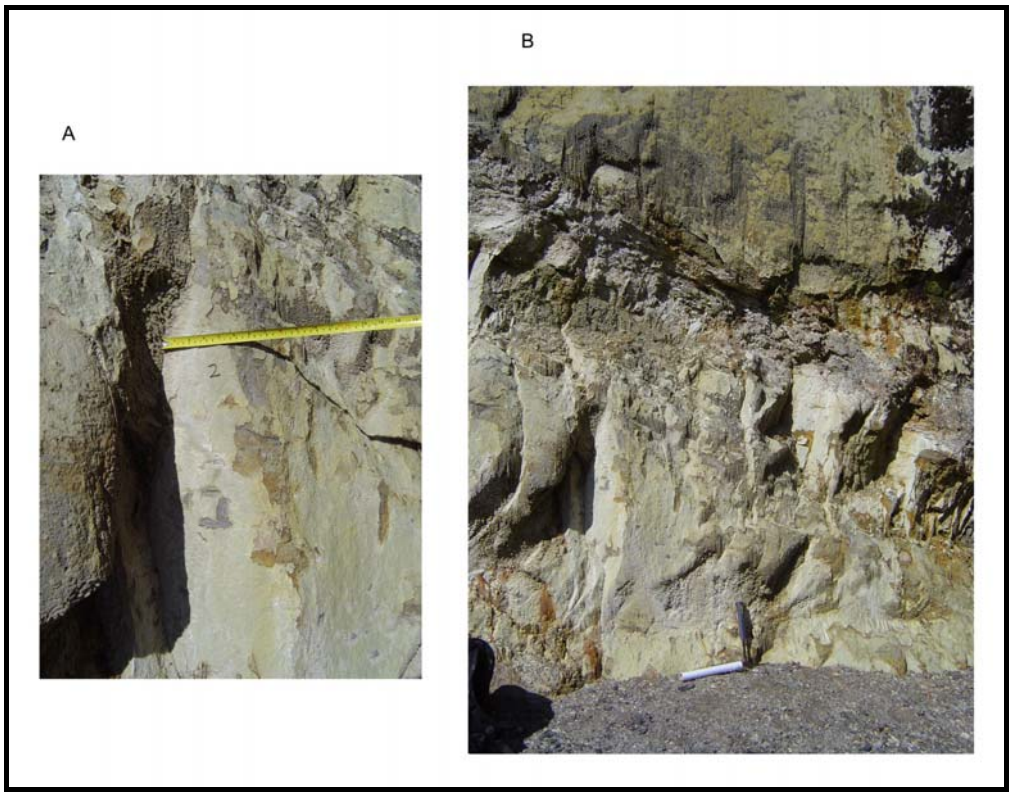

At both sites the crust could not be scraped with a knife blade and was difficult to indent with the tip of the knife. Visual inspection certainly suggested that the coating was case-hardening the underlying sandstone with carbonaceous laminations, although not the nearby units that were composed of carbonaceous mudstone only. This was reinforced by the average of the top five rebound numbers giving 29 and 26 at sites 1 and 2 respectively. The rebound number for areas where the crust had been removed in sampling gave significantly lower values of 22 and 21.

Hand specimens of site 1 show a series of layers on the outside, as seen in figure 5.7. A light yellow crust of approximated 0.3mm thickness forms an impermeable layer across the surface, and has a distinct boundary with the sediment below. The grains beneath this are bound by an orange and cream cement which stops relatively abruptly at approximately 4mm below the

surface. This colour variation has also been captured by placing the thin section of site 1 on a black background under the reflected light, as shown in figure 5.8.

Figure 5.7 Hand specimens for site 1 as seen through the reflected light microscope at a) 10x magnification and b) 25x magnification.

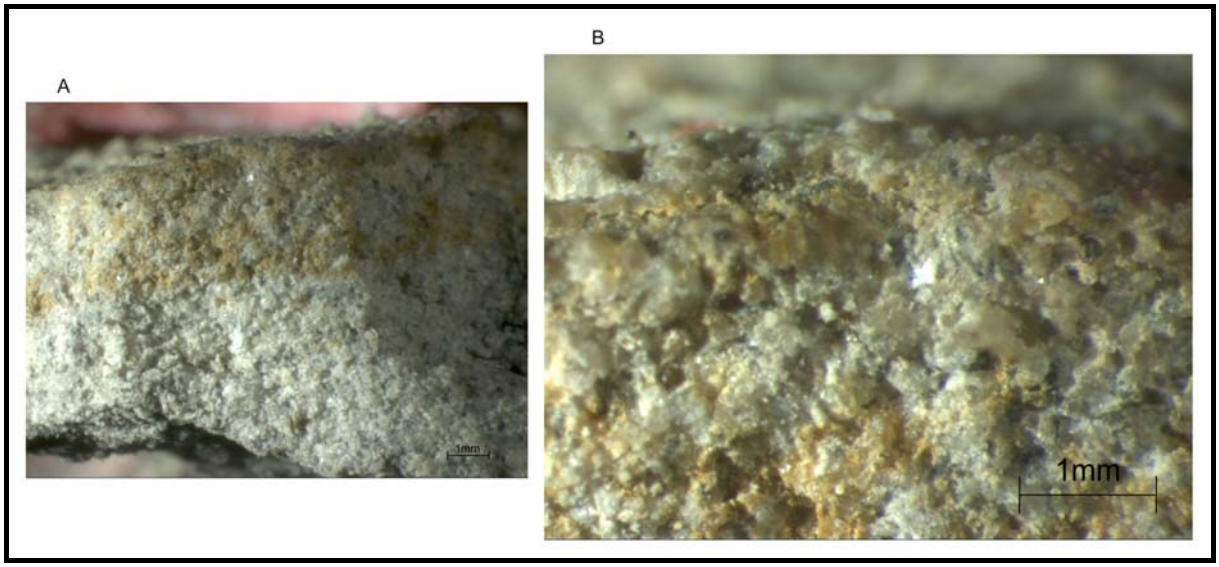

Figure 5.8 Thin section for site 1 under the reflected light with a black background at 16x magnification.

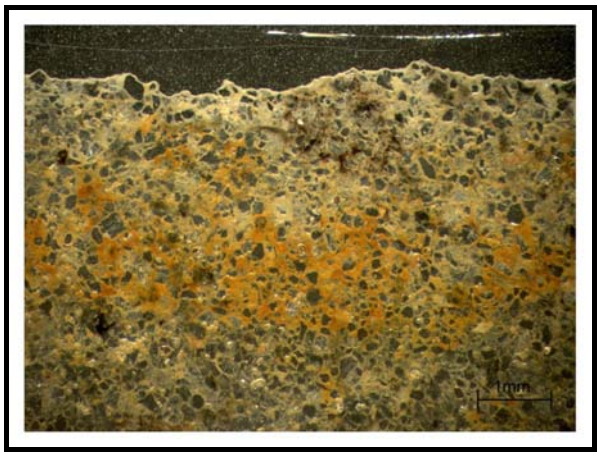

Figure 5.9 gives photographs of a sample from site 2 taken through the reflected light microscope. A similar opaque discrete crust to site 1 is seen here. Beneath the crust the space between the quartz grains is occupied by a creamy substance that gradually disappears at approximately 0.5mm beneath the surface. Of particular interest is the green layer, roughly 0.3mm thick beneath the creamy layer. It is clearly seen in figure 5.9b above the generally grey host rock, and is likely to be cryptoendolithic cynobacteria.

Figure 5.9 Hand specimens for site 2 as seen through the reflected light microscope at a) 10x magnification and b) 25x magnification. Note the distinctive layer of green algae approximately 1mm from the surface.

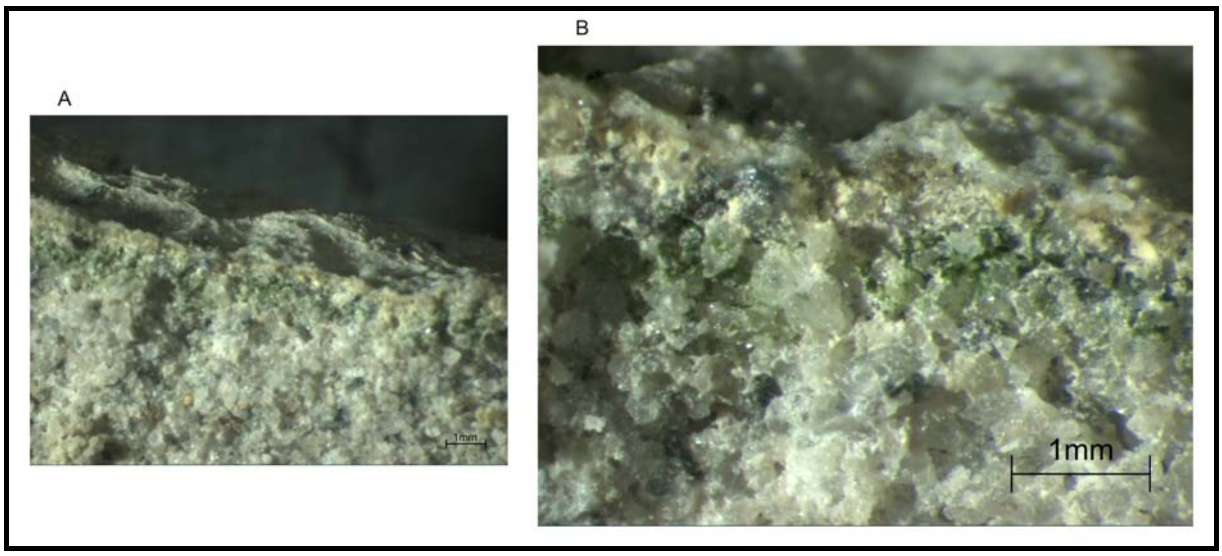

5.3.1.2 Microscope Study and Chemical Analysis

The thin section of site 1, when viewed by a polarising microscope, showed a continuous red/brown coating on the surface and between clasts (figure 5.10b). The thin section contains fine grained quartz, feldspar (microcline), muscovite and biotite, which are all primary minerals within the BCM. When viewed at a high magnification the cement appeared to be made up of a large amount of tiny grains (figure 5.10a). These did not appear to have any colour of their own, and may therefore represent clays stained and bound by the brown/red material which is impossible to determine optically. A brownish colour may be produced by the optical effects caused by the overlap of the many extremely small kaolinite flakes, and from minute inclusions within them (Scholle, 1979), or it may be iron staining derived from the abundant pyrite in the sediment. This stain also appeared to be infiltrating the muscovite, turning it yellow. The biotite present was highly degraded and it was likely to be adding to the red/brown cement and cause the orange substance noted in hand specimen.

Figure 5.10 Thin section for site 1. a) Plane polarised light at 40x (scale bar =0.05mm) magnification showing tiny clay minerals in the thinned edge of the red/brown cement. b) Cross polarised light at 20x magnification.

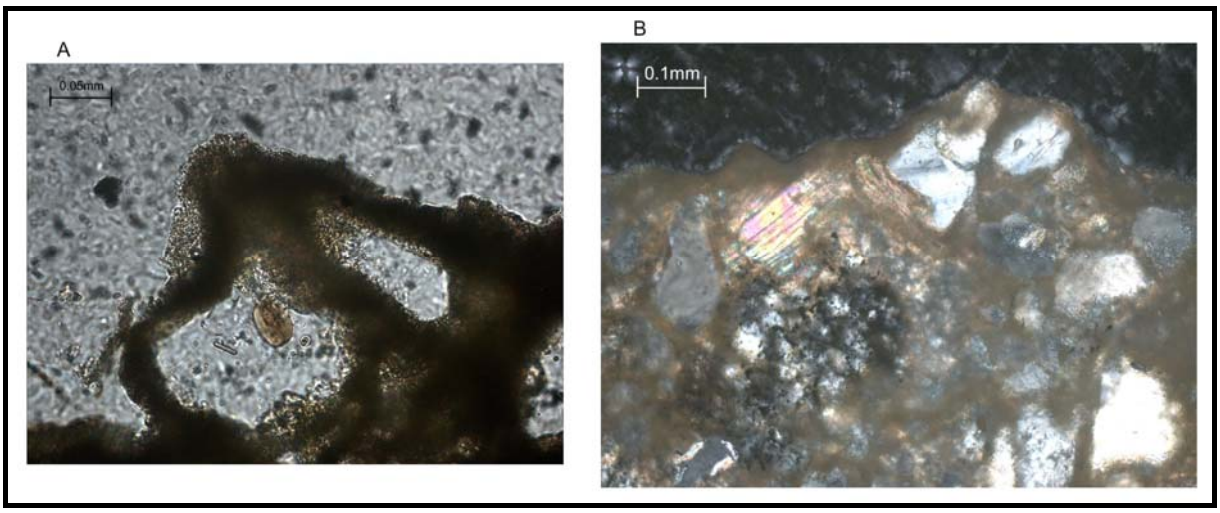

The thin section for site 2 showed a similar red/brown stain on the outer edge, although here grains of different sizes to the host rock were included in the cement (figure 5.11a), suggesting the crust may have trapped grains transported from elsewhere. The same primary minerals as site 1 were identified, as well as a significant amount of sericite which is fine grained muscovite, probably altered from the feldspars, and is shown in figure 5.11b. Some of the sericite may be the clay mineral illite. The occasional detrital zircon or other heavy metal was also noted as primary minerals.

Figure 5.11 Thin section for site 2. a) Plane polarised light at 2.5x (scale bar=0.5mm) magnification showing the different grain sizes within the upper crust compared to the rest of the rock. b) Cross polarised light at 20x magnification, with sericite in the bottom centre of the photograph..

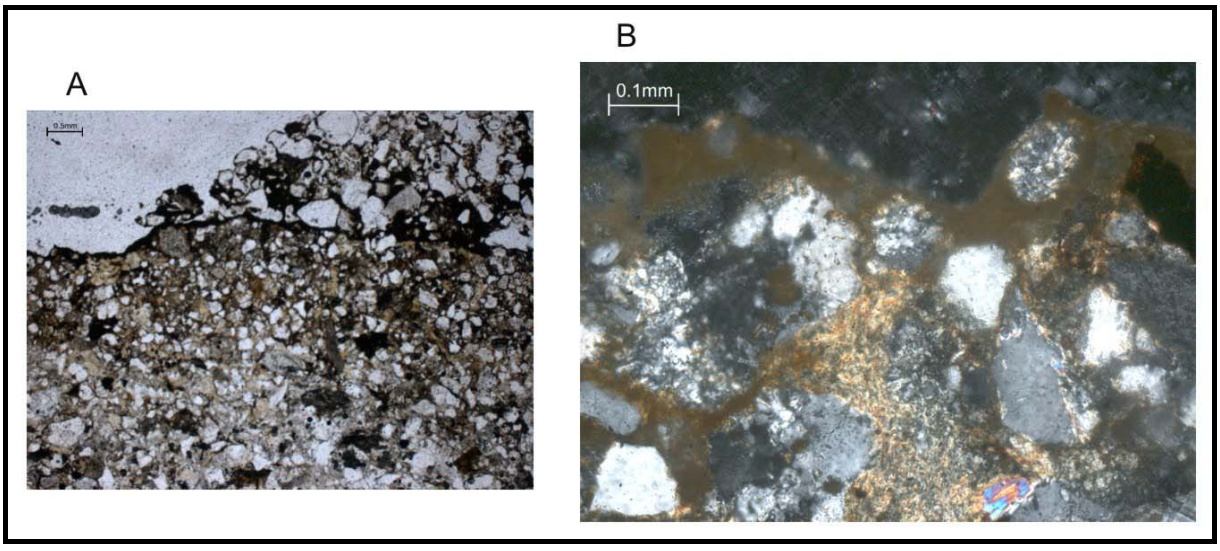

The XRD, bulk EDS and minerals identified in thin section correlated well for site 1. XRD results suggest that quartz makes up approximately 80% of the crust at site 1, with jarosite (an

iron sulphate) being the second most abundant at 15%. Clay minerals amount to approximately 5%, and traces of feldspar (microcline) were also found. The clay minerals are assumed to be from the kaolinite group based on the composition of the rock and XRD analysis on other samples from within the area. The EDS bulk scan showed the major elements present to be silica, aluminium, iron and oxygen, with minor amounts of potassium, all of which were expected from the minerals recognized. Also present was sulphur, probably originally from the pyrite and now within the jarosite. Titanium was also identified and may be from the degraded biotite plus there is likely to be primary ilmenite present. Line scans showed a relatively consistent decrease in iron away from the rock surface. Sulphur also showed a definite spike on the crust edge. This reinforced the presence and importance of jarosite in forming the outer crust at this site.

Site 2 crust contained the same minerals in XRD with approximately 85% of quartz and 5% each of jarosite, clay minerals and microcline. The EDS also showed the same elements present with the addition of chlorine. Chlorine also showed up in EDS at sites 4, 5 and 6 and was likely to be derived from a secondary mineral, possibly a salt deposited from the atmosphere or ground water. Although the high acidity would support this the temperate environment makes it unlikely. Slurry created from the crusts at sites 1 and 2 (see appendix 4.1 for method) had pH values of 2.76 and 2.72 respectively, and correspondingly high EC values of 15.4 and 16.27mS. Line scans for site 2 produced a band of sulphur and iron (k alpha) concentration on the crust edge, followed by a significant drop in these elements.

The SEM showed some interesting features of the rock coating at site 1 not seen with other methods. Figure 5.12a shows a general view looking directly down on the surface. Figure 5.12b is an extreme close up (3000x) of the surface, and shows the many tiny clay particles present along with some much bigger platy minerals. There was also a surprising amount of biological activity on the surface, given the acidity recorded. Figure 5.12c shows a mycelium or mass of individual hypha. While the straight thin hyphae at the top of figure 5.12d have probably grown subsequent to sample collection, the mesh-like hyphae beneath are much older and appear to be helping cement the surface of the rock.

Figure 5.12 SEM images of site 1. a) View of surface. b) Many tiny clay particles coating the surface as well as larger platy minerals. c) Mycelium or mass of individual hypha. b) Mesh-like old fungal hyphae.

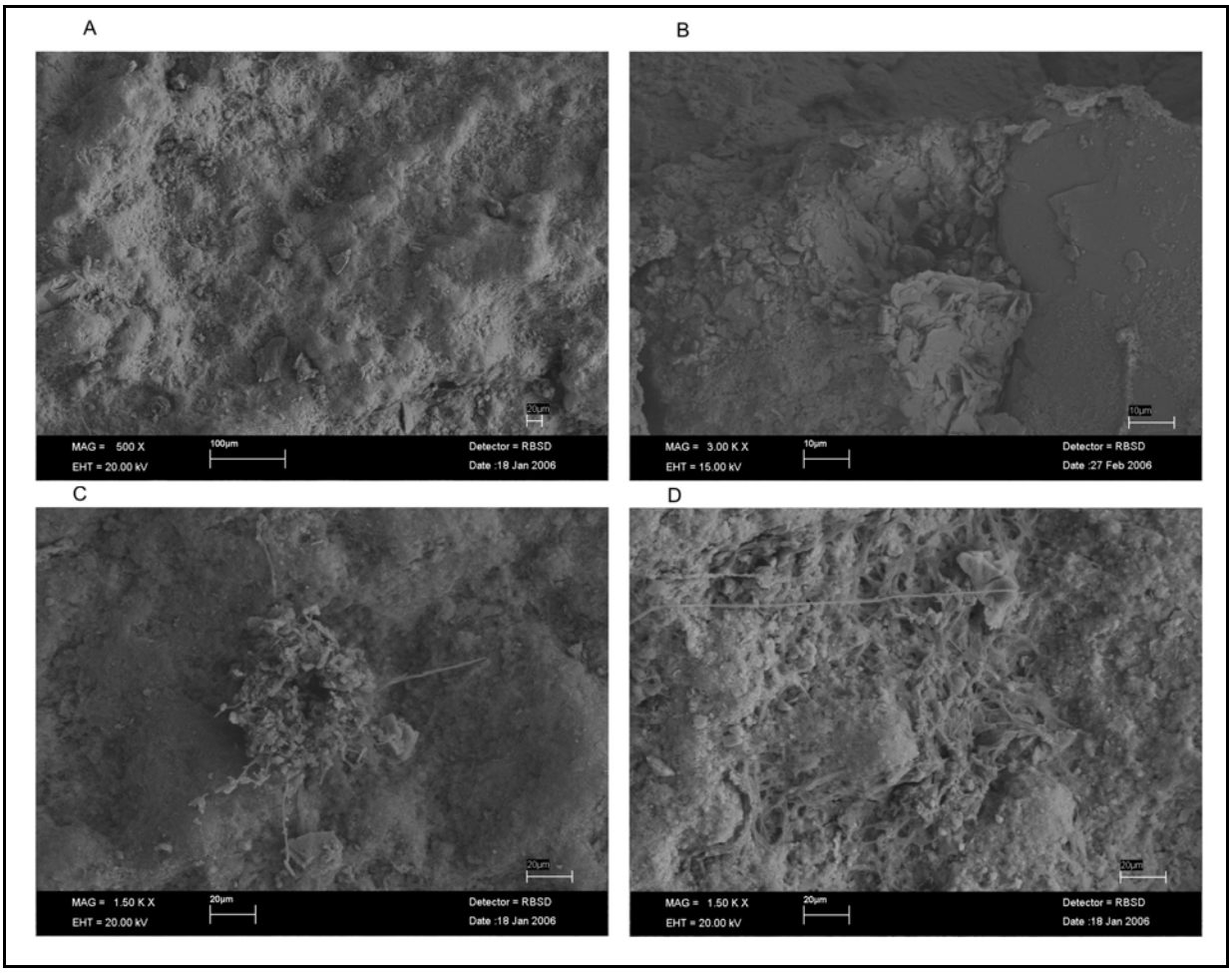

Similarly biological matter was observed in site 2 SEM photographs. Figure 5.13a shows fungal hyphae encrusted with tiny particles of the surrounding sediment. A filamental hypha can be seen in the upper left side of figure5.13b. The extremely thin hyphae seen in both photos have grown since the rock was sampled.

Figure 5.13 SEM images of site 2. a) Encrusted fungal hyphae. b) Filamental fungal hyphae.

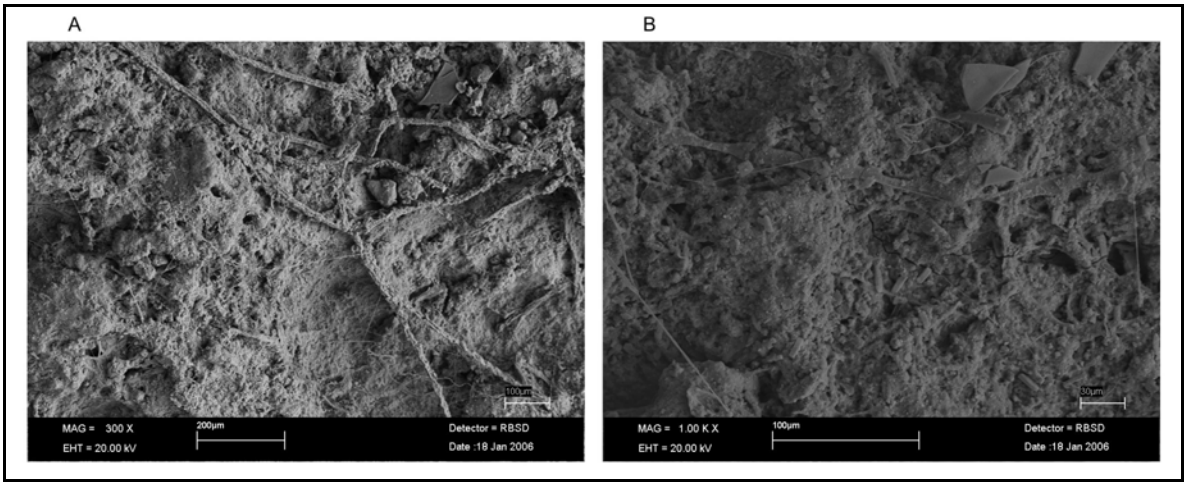

5.3.1.3 Summary of Results

The results presented for crusts at sites 1 and 2 can be summarised as follows:

- A yellow/orange surface crust approximately 0.3mm thick is present, and is underlain by a host rock with an orange or cream cement and/or blue-green algae filling pore spaces to approximately 0.5mm depth.
- The rock coating had higher rebound numbers than fresh rock, and the sandstone can therefore be considered 'case-hardened'.
- A red/brown stain, which is too fine to identify in thin section but is likely to be caused by iron minerals and the breakdown of biotite, appeared to cement tiny clay particles on crystal boundaries.
- Primary minerals identified in the crust were quartz, microcline and muscovite and minerals likely to be secondary were jarosite (containing iron and sulphur derived from pyrite) and clay minerals (kaolinite group).
- The crusts were highly acidic with pH values of around 2.7.
- SEM confirmed the presence of clay minerals on the surface and showed an unexpected amount of microbial activity.

5.3.2 Site 3

5.3.2.1 Outcrop and Hand Specimen Description

Site 3 was located along the ridge line cut within scanline 5. The colour of the crust was a distinctive orange/red, with the underlying laminated sandstone also displaying a more orange tint, as seen in figure 5.14. The thickness of the crust was relatively consistent on the north facing surface, although the colours gave it a patchy appearance. The sandstone did not contain as many laminations of carbonaceous mudstone as in sites 1 and 2. There were however, numerous pyrite nodules within the unit, and a layer made almost entirely of pyrite can be seen on the left hand side of figure 5.14b, beneath the sample site.

Figure 5.14 Outcrop at site 3 a) Close up of the face where samples were collected from. b) Photograph showing the surrounding units.

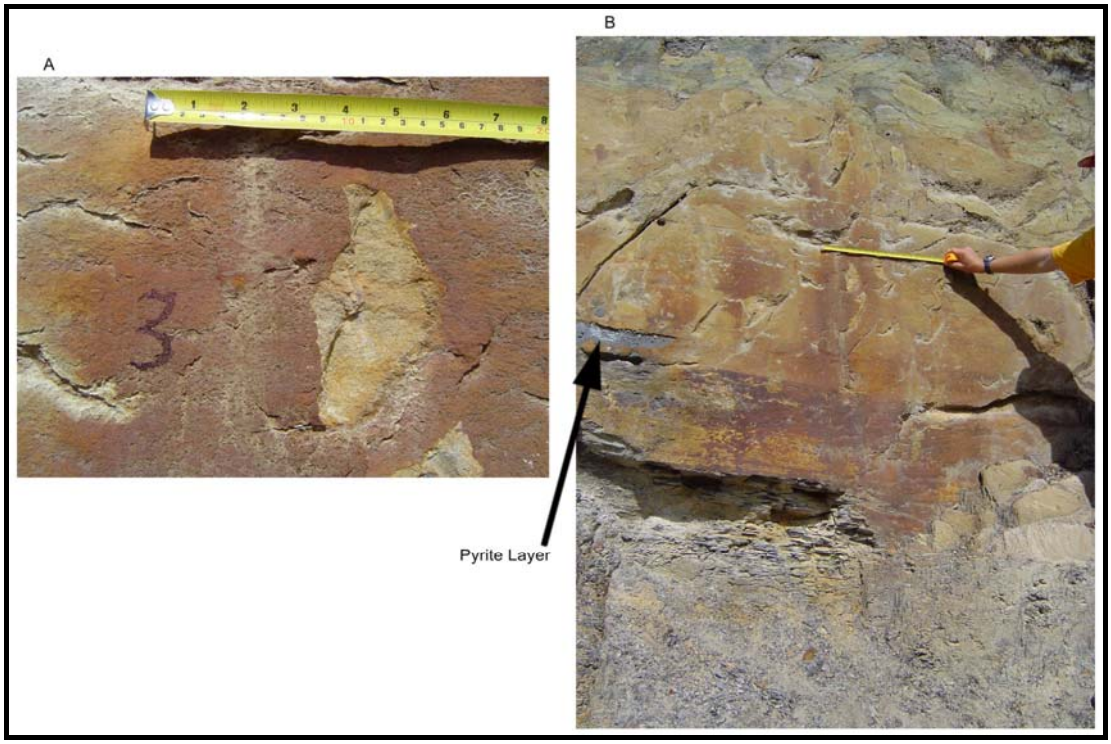

The coating was certainly hardened, as scraping with a knife blade had no impact and the tip of the knife would only penetrate the surface with extreme difficulty. Correspondingly a rebound number for the Schmidt hammer on this surface was determined as 28. However the rebound number calculated from measurements on fresh rock showed a slight decrease at 27, which is not statistically significant.

The hand specimens for site 3 when viewed under the reflected light microscope showed a dark brown/orange crust that is very thin (approximately 0.1mm). It coated individual grains on the surface, and has a discrete boundary with the underlying rock. This is shown in figure 5.15a, which is at 10x magnification. As with site 1 an orange material can be seen between grains beneath the surface, but at site 3 this extends deeper into the host rock. The thin section under reflected light on a white background also shows a thin red coating on the outside and orange patches within the rock (figure 5.15b).

Figure 5.15 a) Hand specimens for site 3 as seen through the reflected light microscope at 10x magnification. b) Thin section of site 3 viewed under the reflected light microscope on a white background at 10x magnification.

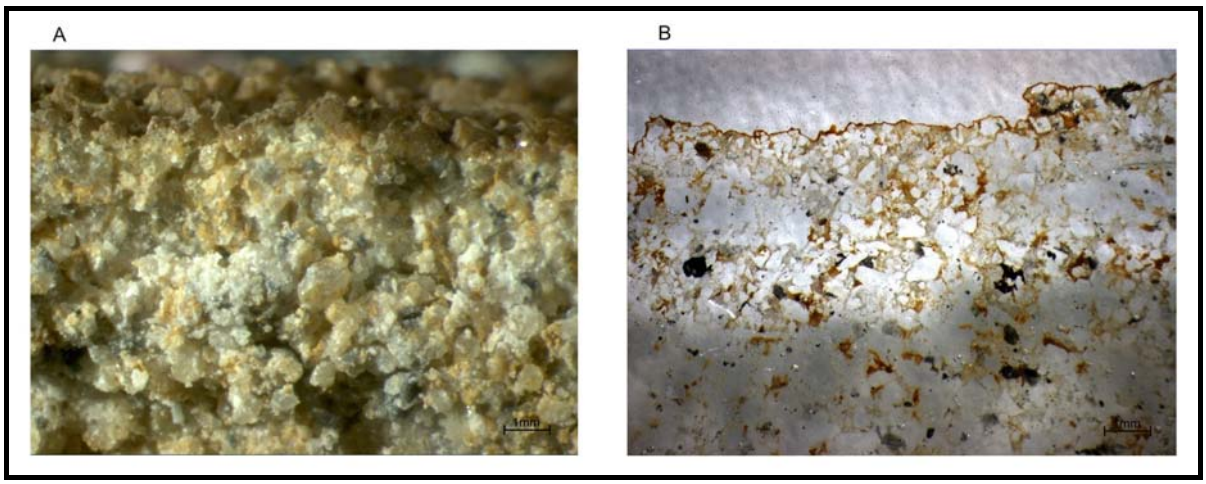

5.3.2.2 Microscope Study and Chemical Analysis

The thin section for site 3 showed the distinct red outer crust that formed a thin layer across the surface of the rock, as shown in figure 5.16. Again the material is too fine to see in thin section. This rock shows indications of complicated diagenetic processes, which have aided the coherence of the sample. Primary quartz and mica where observed to have undergone mutual dissolution along grain boundaries. The micas are often buckled and growth of new minerals as well as degraded muscovite (sericite) could be seen in spaces between grains. Pressure shadows were noted on two quartz grains within the sample indicating significant compression.

Figure 5.16 Thin section for site 3 at 20x magnification under cross polarised light. Note the obvious outer red coating.

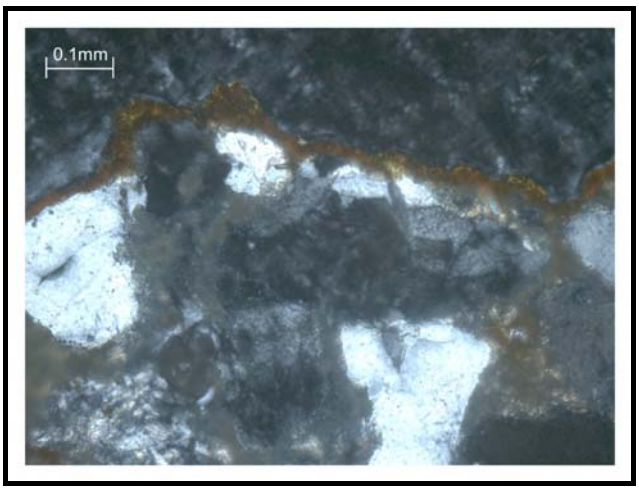

The XRD results for site 3 indicated that the crust is made up of approximately 75% quartz and 20% microcline. It also consists of approximately 5% clay minerals and had traces of muscovite. These results may be misleading, as the thin crust is difficult to separate from grains which are likely to be incorporated in analysis. EDS suggests mainly silica, aluminium, iron and oxygen,

with minor amounts of sulphur and potassium. Line scans consistently showed a spike of sulphur on the very outside of the sample. Like sites 1 and 2, the slurry created from the crust is very acidic with a pH of 2.82, although slightly less electrically conductive at 1.23 mS.

Microbial activity was also noted on the surface of samples from site 3 when viewed under the SEM. Although there is a chance the fractures seen in figure 5.17a are caused by the drying during preparation, this rock would have experienced heating and drying insitu. The cracks would allow chasmoendoliths to infiltrate the rock, and an encrusted epilith is also seen in figure 5.17a. Figure 5.17b shows clay minerals beneath the surface, in this case probably kaolinite based on their structure of stacked plates.

Figure 5.17 SEM images for site 3. a) Cracked surface and encrusted epilith. b) Stacks of kaolinite clay.

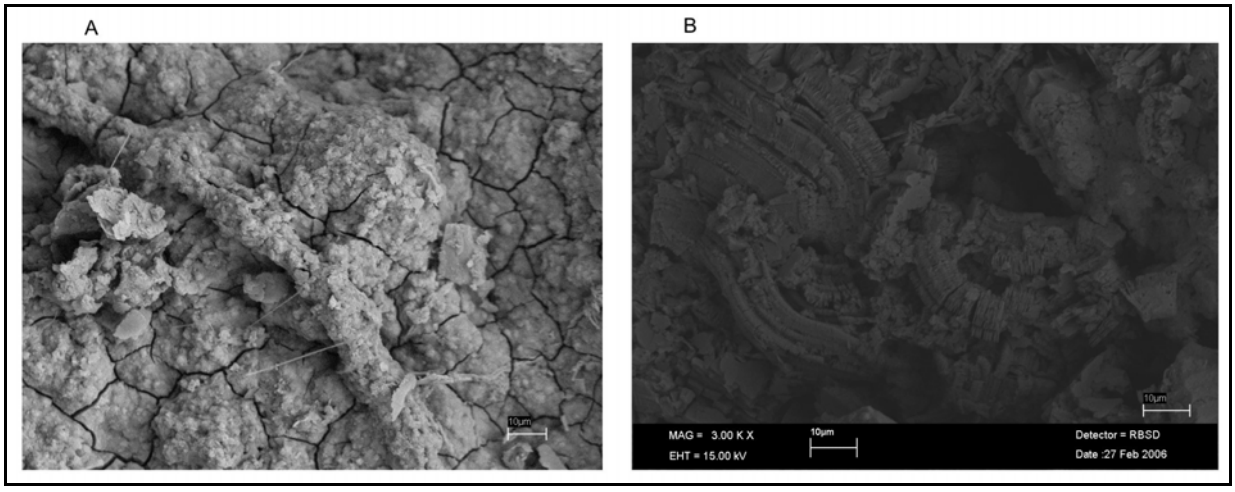

5.3.2.3 Summary of Results

The results presented for the crust at site 3 can be summarised as follows:

- A very thin (0.1mm) orange/red coating on the outside of the grains, which did not show any significant difference in hardness, was observed.
- The microstructure of the rock may be providing internal strength by grain interlock.
- Difficulties in separating the crust from the grains it binds may have led to a disproportional amount of quartz identified in XRD. The colour and iron present in the EDS, suggests an iron coating (probably containing jarosite from the spike in sulphur in the EDS), perhaps combined with clay particles.
- Microbial activity was seen on the surface and may also inhabit tiny fissures in the acidic crust.

5.3.3 Site 4

5.3.3.1 Outcrop and Hand Specimen Description

Site 4 was chosen further towards the south along the same ridge line as site 3. It had a very different appearance compared to previously discussed sites, although the material beneath the crust was essentially the same as the medium to fine sandstone at site 3. The crust was light brown in colour, with occasional sand size grains collecting in it that may have fallen from the uncoated unit above as seen at the top of figure 5.18b.

Figure 5.18 Outcrop at site 4. a) Close up of the face where samples were collected from. b) Photograph showing the surrounding units.

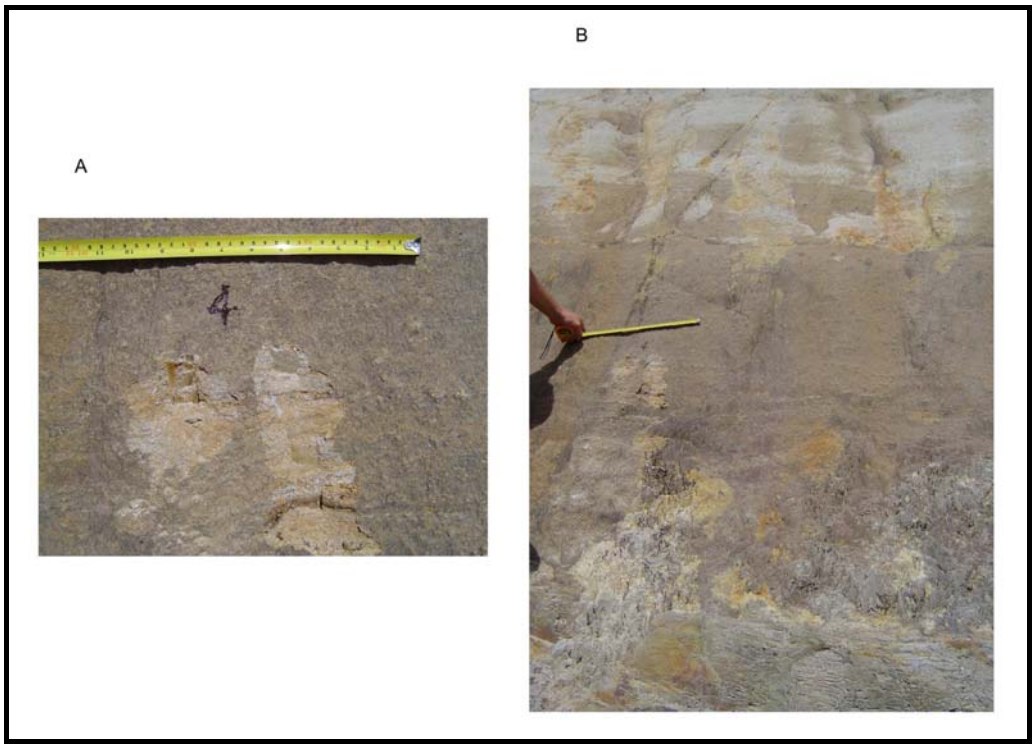

The coating was thin (approximately 0.1mm) and more friable than those previously observed. It was easily scraped off and penetrated by a knife blade. The rebound numbers generated from the Schmidt hammer also gave much lower values than previous crusts with an average of 13 and fresh surfaces giving an average of 14. This suggests the crust was not providing any case-hardening to the host rock, but was merely a weathered exterior.

Hand specimens for site 4 show a very thin (<0.1mm) indistinct coating of light brown colour on the surface, as shown in figure 5.19a. There are also patches of a black substance that resembles organic material. This shows up well in the thin sections when viewed in reflected light on a white background, as shown in figure 5.19b. The host rock was very similar to site 3 with orange traces between grains.

Figure 5.19 a) Hand specimen for site 4 as seen through the reflected light microscope at 10x magnification. b) Thin section of site 4 viewed under the reflected light microscope on a white background at 25x magnification.

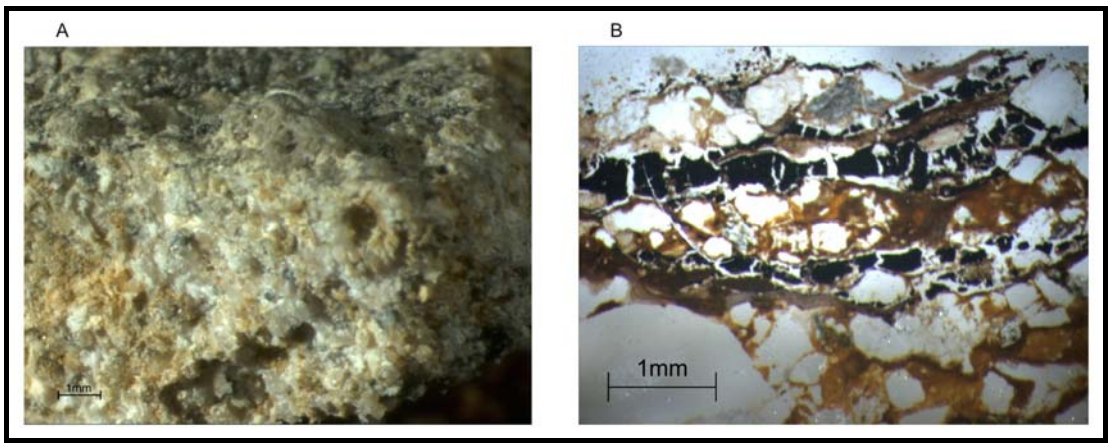

5.3.3.2 Microscope Study and Chemical Analysis

The thin sections for site 4 exhibited the same minerals as previously cited, as well as chlorite (an alteration product of biotite) and rock fragments, some of which appear to be slate, probably from the Greenland Group. The outer edge is cemented by a degraded biotite rich layer as shown in figure 5.20b. The curved/flowing pattern displays relicts of the bent mica cleavage, which has been spread out along the grain boundaries. This crust also displays occasional large crystals that may be foreign objects incorporated in the coating (figure 5.20a). Within the rock mass the alteration product from biotite occurs in isolated areas in this sample rather than a layer of continuous cement as seen at sites 1 and 2.

Figure 5.20 Thin section for site 4. a) Plane polarised light at 2.5x magnification (scale bar = 0.5mm). b) Cross polarised light at 20x magnification.

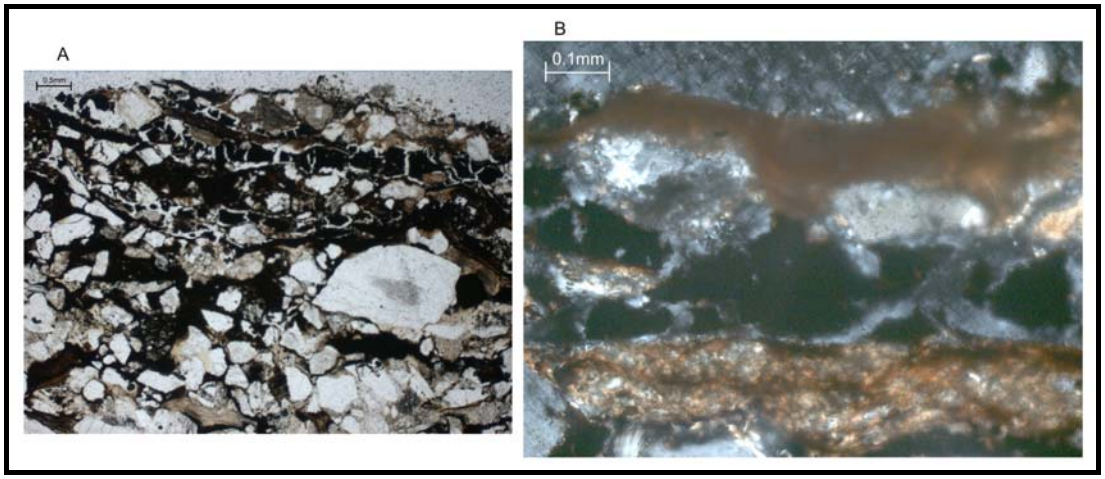

The XRD results suggested that the crust was composed of approximately 90% quartz and 10% clay minerals. There were also traces of jarosite, microcline and muscovite. The bulk EDS gave corresponding results, with significant amounts of silica, aluminium and oxygen and minor iron,

sulphur, potassium and titanium. Magnesium was also present and can be assumed to be produced from the alteration of mafic minerals, possibly to iddingsite, which is a mixture of smectite, chlorite, goethite or hematite and may look similar to biotite in thin section (Shelley, 1974). Line scans did not show any patterns other than a general increase in aluminium with depth. A pH of 3.47 was recorded for the crust, and an EC much lower than the previous sites of 0.306mS.

Examination of the samples for site 4 suggested the microbial activity was purely on the surface (epiliths). Individual cells showed a green tinge and may be cynobacteria or algae. Under the SEM encrusted hyphae and large platy crystals were also seen. Figure 5.21 shows a diatom at 1000x magnification, which is an alga with a siliceous cell wall and is covered in surrounding material.

Figure 5.21 SEM image of diatom surrounded in particles in a sample from site 4.

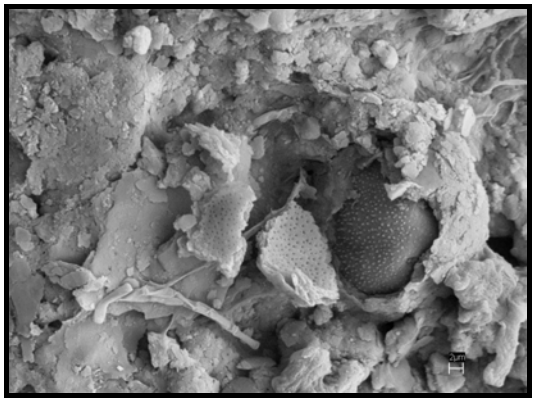

5.3.3.3 Summary of Results

The results presented for the crust at site 4 can be summarised as follows:

- A light brown crust that incorporates detrital grains and organics was extremely friable, and did not provide the exterior of the rock with any additional strength.
- The crust was cemented by degraded biotite and composed of approximately 10% clay minerals, most probably kaolinite.
- Microbial activity was restricted to the surface and the crust was slightly less acidic than the first three crusts (pH 3.5).

5.3.4 Sites 5 and 6

5.3.4.1 Outcrop and Hand Specimen Description

Sites 5 and 6 are both within the neighbouring Peerless Gully, along the bottom of highwalls composed largely of the loose, predominantly coarse grained sandstone, recorded as unit 4 in the

Reddale Valley core samples. This opencast coal mine is also currently out of production and a photograph of the whole cut is given in figure 5.22.

Figure 5.22 Photograph of Peerless Gulley opencast mine.

Site 5 displayed a light brown film covering the host rock, with no distinct change from inside to outside. There were also dark patches on the surface, with a distinctly organic look, as seen in the left of figure 5.23b. There were signs of water having run down the surface in the past. The crust and sandstone beneath were very friable and very difficult to collect as hand specimens.

Figure 5.23 Outcrop at site 5. a) Close up of the face where samples were collected from. b) Photograph showing the surrounding units. Intervals on scale bar in centimetres.

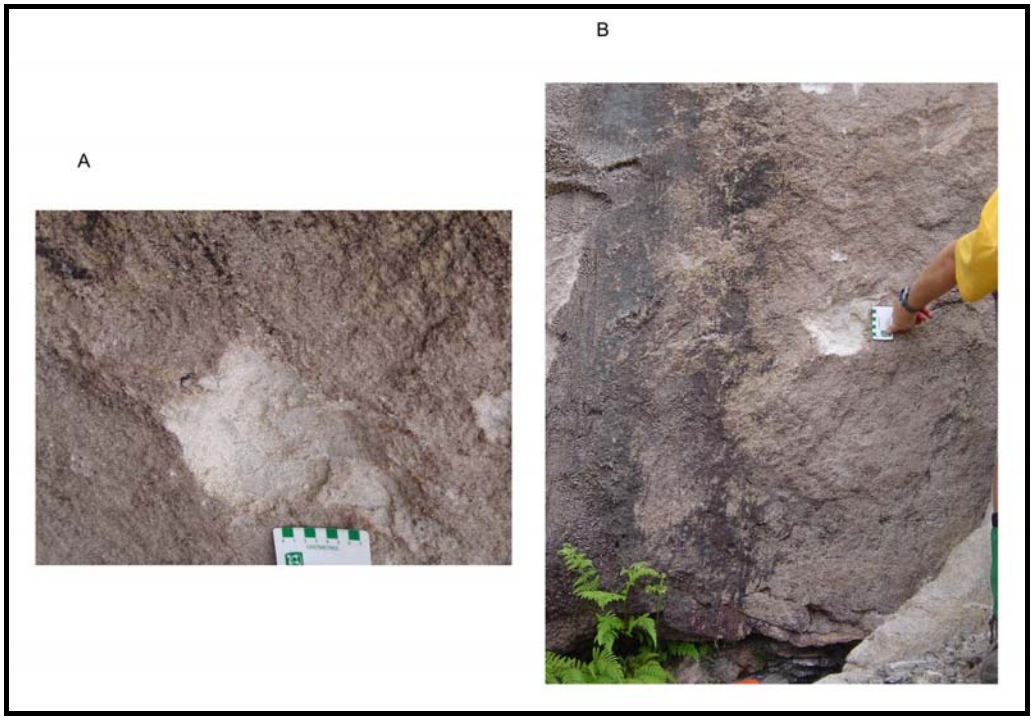

Site 6 exhibited a relatively thick (approximately 2mm) coating of purple/brown colour and obviously organic rich with plant life on the surface, as shown in figure 5.24. Biological bore holes of approximately 5mm diameter where also noted. Although the crust was only slightly

damp there may have been more water running over the face previously, as indicated by the clay formation on top of the organic mat.

Figure 5.24 Outcrop at site 6. a) Close up of the face where samples were collected from. b) Photograph showing the surrounding units. Intervals on scale bar in centimetres.

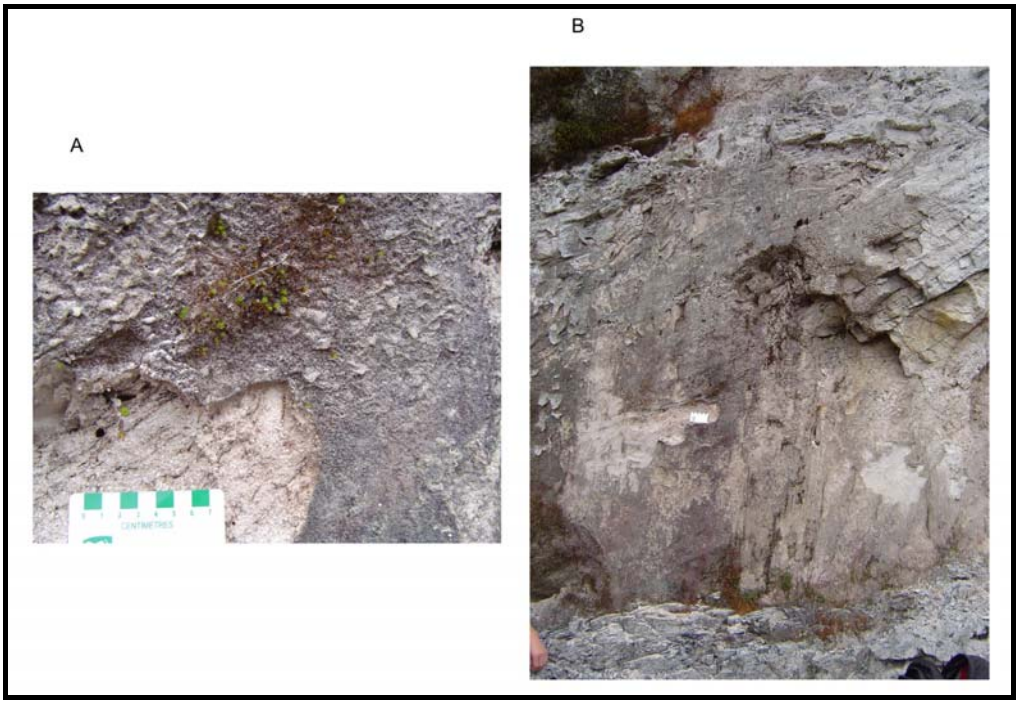

The coating at site 5 was hard to scrape off, as it was sufficiently thin that the blade was scraping directly on the grain surfaces. The rebound number was relatively high (22) on the surface and the fresh surface was slightly higher at an average of 24. At site 6 the crust was not well attached to the sandstone, but rather a living entity, parts off which were peeling off. It had a soft spongy feel that was easily scrapped and penetrated with a knife blade. It therefore had a lower average rebound number of 12 on the surface, and again the fresh sample was slightly higher at 14. Based on this data, neither of the coatings were therefore providing any case-hardening.

The crust on the hand specimens collected from site 5 was difficult to photograph under reflected light, as there did not appear to be a mineralogical change but rather a thin coating on the outside of the quartz grains that is slightly darker in colour. The coating can be seen in figure 5.25 as a dark brown surface coating with patches of cream coloured clays.

Figure 5.25 Hand specimen from site 5 under the reflected light microscope at 10x magnification. A slight variation in colour can be seen on the top surface (darker brown coating).

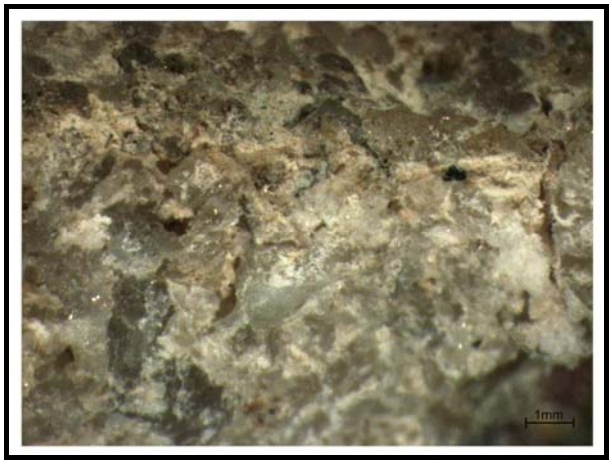

The organic mat noted in outcrop at site 6 was reinforced by viewing through a reflected light microscope. Figure 5.26a shows a magnified cross-section through the sample. The brown and green coating was the thickest observed of all the units, at approximately 1mm and appears to be composed of clay minerals and organic material. Figure 5.26b illustrates one of the plants growing on the surface, at 10x magnification. The host material is composed of medium grained primary quartz and mica crystals with some carbonaceous laminations. There are numerous unfilled pore spaces within this uncemented sandstone.

Figure 5.26 Hand specimens from site 6 viewed under the reflected light microscope. a) Cross section through sample at 10x magnification. b) Plant on the surface of the rock at 10x magnification.

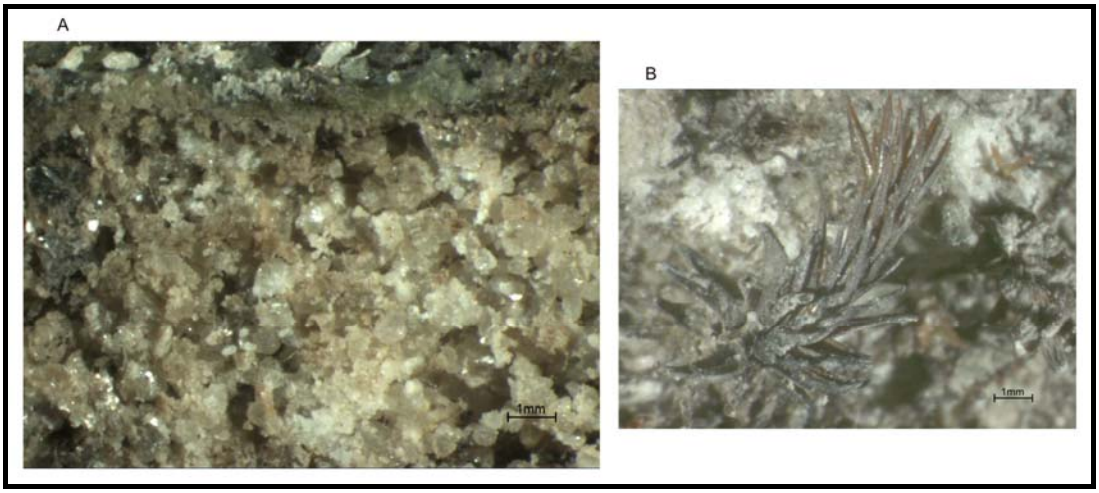

5.3.4.2 Microscope Study and Chemical Analysis

Although the thin section for site 5 did not show the outer coating it did illustrate that the relatively coarse grained loose sandstone was slightly different than the other sites, as shown in figure 5.27a. The grains are well interlocked and there is a large amount of shattered material that may help hold the unit together. In this sample the main primary minerals were quartz, microcline and muscovite with no biotite or red/brown stain present. There were fine grained

crystals present along grain boundaries but it is difficult to determine weither they were part of the original texture or alteration products.

Similarly the thin section preparation of site 6 did not retain the largely organic surface coating. Biotite was however, present at this location as well as significant amounts of muscovite, which was often bent as shown in figure 5.27b. A conclusion could not be drawn from thin sections as to weither the opaque/black material present in all thin sections except site 3 and often with stained red edges, represented organic material or perhaps a concentration of iron oxide. The lack of texture and depth of penetration suggests that they are not biological remains. One likely mineral however is ilmenite which is opaque in thin section and corresponds with the titanium noted in the EDS scans in all sites except site 3.

Figure 5.27 Thin sections under cross polarised light at 2.5x (scale bar = 0.5mm) magnification. a) Site 5 showing interlock of grains despite lack of coating. b) Site 6 with multiple bent micas.

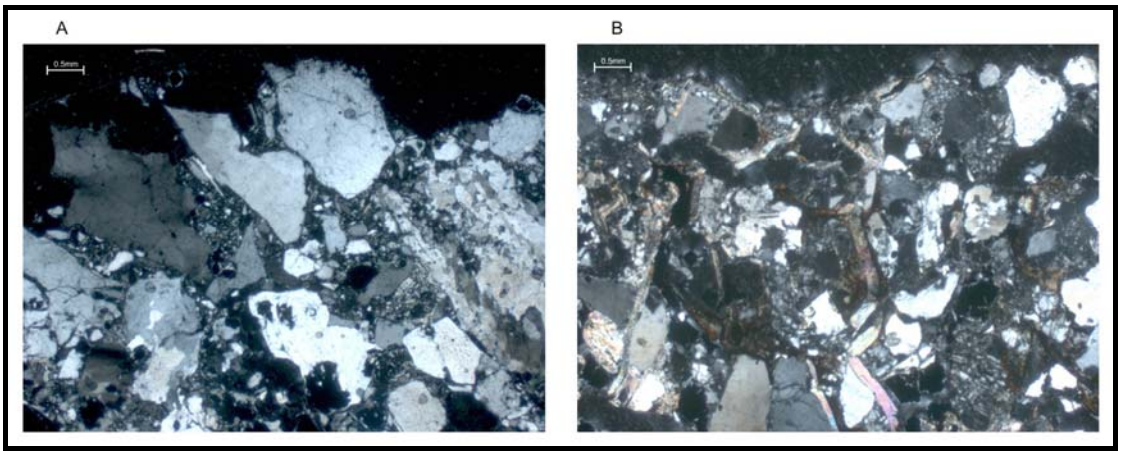

The XRD results for crystalline material indicated that the crust found at site 5 was composed of mostly quartz (approximately 95%) with a minor amount of muscovite (5%). Traces of clay minerals were also present. The major elements in bulk EDS where silica and oxygen, with minor amounts of aluminium, potassium, titanium, chlorine and magnesium. Manganese was also present in minor amounts and like magnesium is assumed to be a secondary mineral from the break down of mafic minerals, probably biotite.

Site 6 showed significantly more clay minerals in the coating with approximately 10% measured by XRD as well as 80% quartz. Microcline and muscovite each recorded approximately 5%. Correspondingly the major elements recorded in EDS were silica, aluminium and oxygen. The minor elements were potassium, titanium, chlorine, magnesium, sodium and phosphorous, which is probably derived from detrital heavy minerals. In this instance the salt halite (sodium chloride) may be present. Line scans for both site 5 and 6 did not show any patterns other than a

very high amount of silica throughout the sample. Both sites were acidic with pH values of 3.68 and 3.38 respectively but with low EC values of 0.584 and 0.75 mS.

The SEM images showed a much larger biological presence on the surface of site 5 and 6. Figure 5.28a is a close up (1000x magnification) of a platy mineral which was most likely mica. Figure 5.28b shows a fungal spore on a sample from site 5. Diatoms have also been noted at site 5 and 6. The growth at site 6 was endolithic and the quartz grains may filter the light, enabling photosynthesis of the higher organisms. Moss was abundant with the microbial material and was holding the outside of the rock together, although no algae were present. Figure 5.29a shows plant life on the surface of site 6 and figure 5.29b is a close of another moss showing the texture of the material. Figure 5.29c is an example of the many rhizoids or root structures, which anchors the moss to the substrate and are encrusted in platelets that stick to their outsides. Figure 5.29d illustrates quartz grains on the surface of site 6 under the SEM at high magnification.

Figure 5.28 SEM images of site 5. a) Platy mineral probably muscovite. b) Fungal spore.

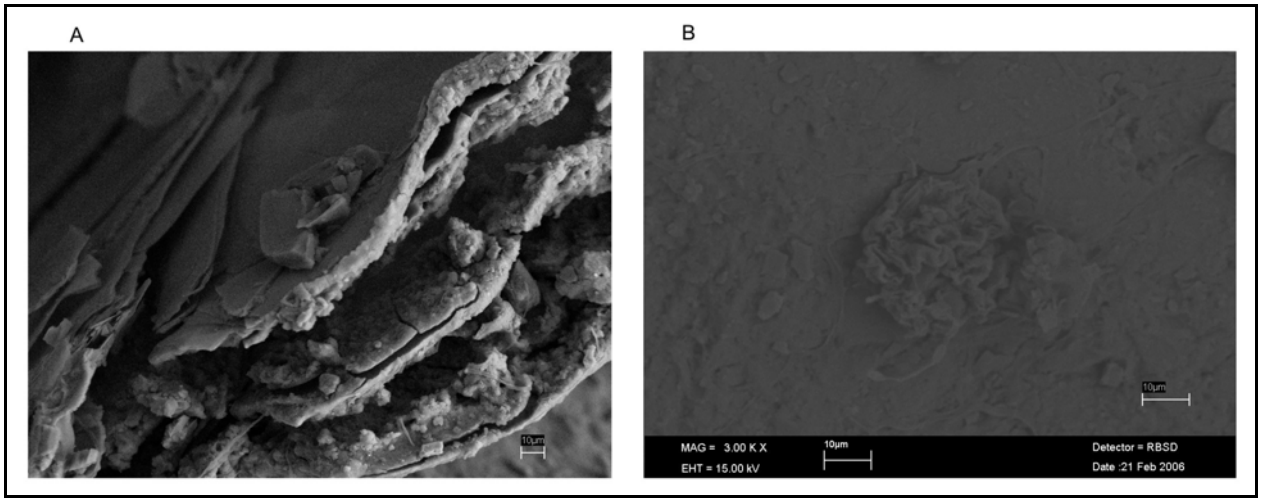

Figure 5.29 SEM images of site 6. a) Plant on surface of rock. b) Texture of moss. c) Rhizoids or moss root structure. d) Quartz grains.

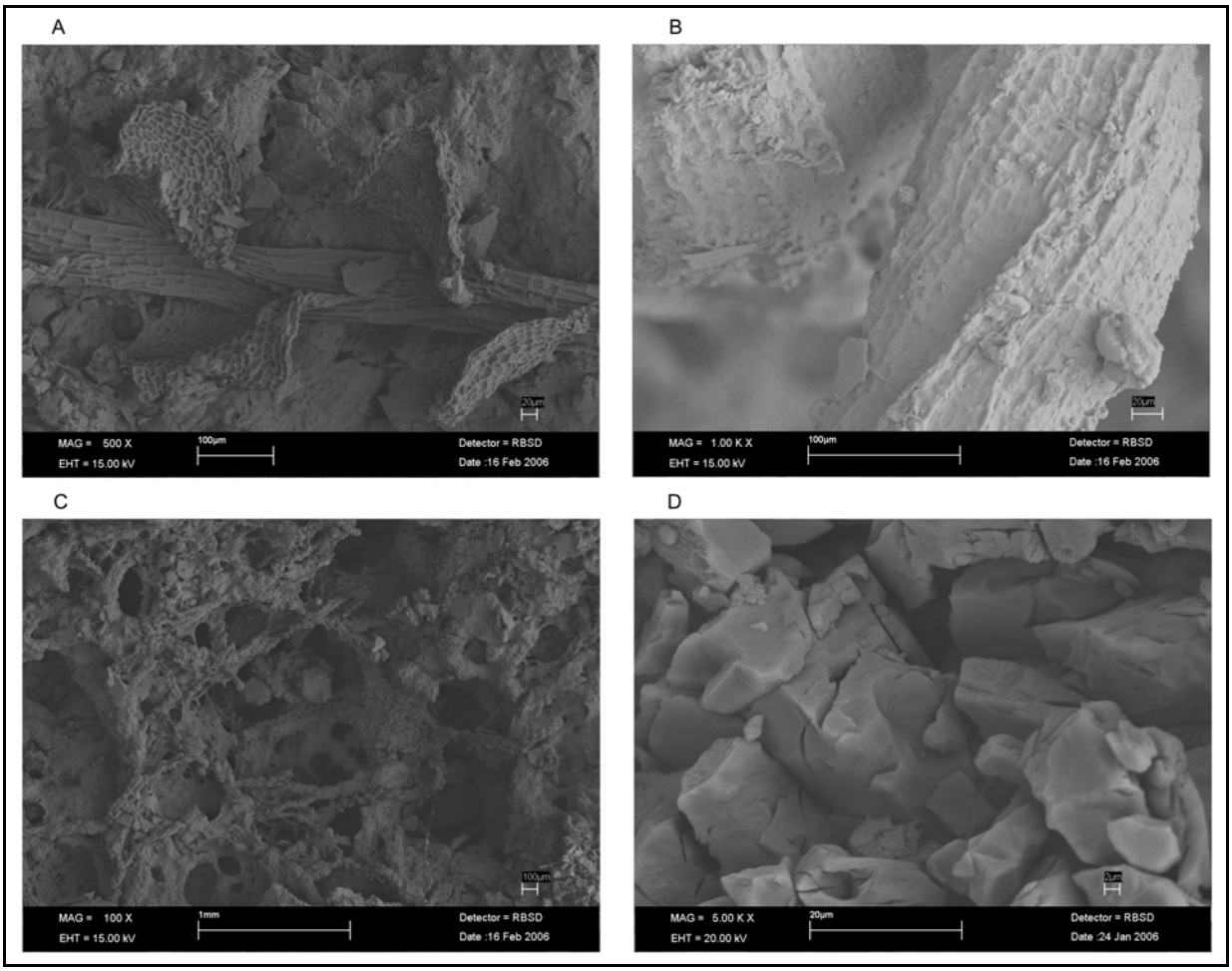

5.3.4.3 Summary of Results

The results presented for crusts at sites 5 and 6 can be summarised as follows:

- A light brown to purple coating with biological activity visible in hand specimens was observed, and did not provide any 'case-hardening' of the underlying rock.
- Although thin sections did not retain the organic crust they did show considerable grain interlock.
- The crusts are dominated by primary quartz, but clay minerals are also a significant component with approximately 10% recorded at site 6.
- The coatings were also acidic, with pH values of 3.4-3.7 determined.
- Micro-organisms, as well as high organisms such as mosses, dominated the rock coatings at these sites.

5.4 Discussion and Interpretation

5.4.1 Comparison with Previous Studies

A layer of cryptoendoliths that inhabit the pore space between grains beneath the surface of sandstones have previously been noted in desert environments. Figure 5.30 shows a Nubian sandstone with a layer of cryptoendoliths 1-2 mm below the rock surface. Considerable research has been conducted in the Dry Valley region (Ross Desert) of Antarctica, where the microbial community is protected from the hostile environment by living within the rock. A series of distinctive coloured layers have been recognised. Beneath the crust there is a black zone followed by a white zone which is formed by filamentous fungi and chlorophycean algae that together form a lichen association. This is followed by a green zone, like that noted at site 2 that is formed from algae and cyanobacteria, and which may be absent in places. Occasionally a blue-green zone is also found beneath this (Nienow and Friedmann, 1993). A thin green line, approximately 1mm beneath the rock surface, containing cryptoendolithic growth has also been noted on case hardened sandstones in Jordan (Viles and Gouldie, 2004). A cold temperate zone sandstone in Arizona has also been found to have a green band, which extends from 0.5 to 1.5mm beneath the surface and contains cryptoendolthic algae (Bell and Sommerfeld, 1987). It is therefore proposed that a similar green layer is present beneath the rock surface in some parts of the Reddale Valley, although further microbiological investigation is needed to ascertain the type of organisms.

Figure 5.30 Green band within Nubian sandstone (Golubic at al, 1981).

The interlock of the grains, especially in the coarser grained loose sandstone, may play a part in their apparent stability in existing highwalls (figure 5.31). Uncemented sands may have a 'jigsaw' interlock microfabric which produces cohesion within the sediment, imparting a certain amount of strength. While cementation produces true cohesion, a clay matrix will certainly increase cohesive resistance (Barton *et al.*, 1993). Robinson and Williams (1986) attribute the limited strength possessed by the Ardingly Sandstone to partial interlocking of grains. Young

(1987) also noted that the degree of interlocking in friable Australian sandstones, observed in thin section and SEM, indicated high angles of internal friction. It is therefore proposed that the apparent strength observed is at least partially due to grain interlock, especially at sites 3 and 5.

Figure 5.31 Diagrams illustrating the sources of cohesion in natural sands. Void spaces are shown hatched, cementing by stipple and clay matrix by fine lines (Barton et al., 1993).

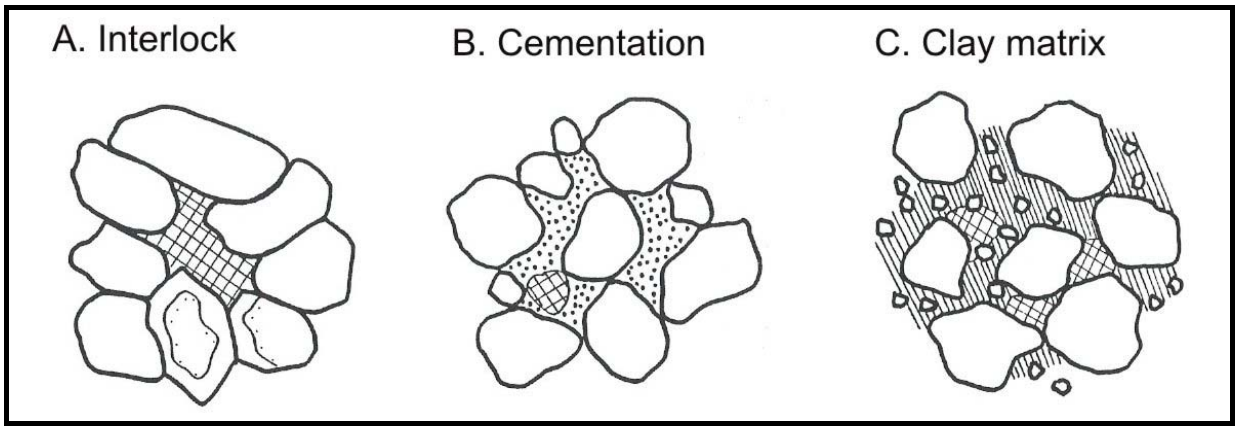

The presence of pyrite plays an important role in the case-hardening of some sandstones. Chigira and Oyama (1999) propose that the sandstone is strengthened in the oxidized zone by the cementation of iron oxide or hydroxide from pyrite. Jarosite has also previously been noted as a product of acid mine drainage from coalfields (Bell at al, 2002), as well as in iron films in Antarctica (see section 5.1.2). Herbert (1995) suggests that jarosite can form at the capillary fringe when very acidic and high sulphate conditions develop within micropores, despite not being thermodynamically stable in such conditions. It is therefore not surprising to find the mineral jarosite present in the Reddale Valley, especially given the amount of biological activity that may act as a catalyst.

The role of silica in the case-hardening of the BCM sandstones has not been completely assessed. No nodular or filamentous growths, like those noted by Robinson and Williams (1986), were observed under the SEM in this study. The large amount of quartz reported in XRD may result from grains beneath the surfaces being incorporated in the scraped sample, which will often mask minerals of smaller quantities and it can therefore be considered a primary minerals. Perhaps salts are playing a more active role, the evidence being the chlorine noted in EDS, but salt crusts are commonly unstable and form in arid environments (see section 5.2.4). Clays may also contribute significantly to the case-hardening, even if not accreted by wind like those in desert varnish but derived from the alteration of minerals from within the rock. All sites show signs of past water seepage, and this will have substantially aided the formation of all types of crusts.

5.4.2 Results from this study

5.4.2.1 Summary of Case–hardening Mechanisms

Table 5.1 provides a summary of the 'case-hardening' mechanisms identified in this study. Maximum XRD percentages are given for each site or site grouping. A general trend can be observed in that those sites with larger iron-derived minerals had less quartz, clay minerals and biological activity. It is obvious from the table that no single factor is responsible for the outer crusts observed at any of the sites, but rather a mixture of components. As discussed above the amount and influence of quartz is likely to be exaggerated by the XRD results and while it is certainly a contributing component, no sites are considered to display silica glaze.

Table 5.1 Summary of Case-hardening Mechanisms.

Site	Quartz	Iron	Clay Minerals	Cement	Biological Activity	Grain Interlock
1 & 2	• 85 %	• 15% Jarosite	• %5	• Degraded Biotite (red/brown stain) • Sericite	• Microbial Epiliths • Microbial Cyrptoendoliths	
3	• 75 %	• Iron spike in EDS	• %5 • Kaolinite in SEM	• Degraded Biotite • Sericite	• Microbial Epiliths • Microbial Chasmoendoliths	• Complicated Diagenetic Processes
4	• 90 %	• Trace Jarosite	• 10%	• Degraded biotite on surface • Isolated areas of degraded biotite	• Microbial Epiliths	
5 & 6	• 95 %		• 10%		• Microbial Epiliths • Microbial Endoliths • Higher Organisms (mosses)	• Shattered Material • Range of Grain Sizes

5.4.2.2 Iron Rich Coatings

The data collected indicates that the coatings observed at sites 1-3 are predominantly influenced by the significant amount of pyrite in the host rock, which has produced the jarosite identified by the oxidation of iron. The XRD data suggests a types III iron film where silica and aluminium combined are still more abundant than iron (Dorn, 1998). While the crusts contain significant amounts of silica as well as iron, the iron is most likely derived from internally sourced pyrite rather than an external accretion and is therefore not considered to be a type V silica glaze. The

oxidation of the iron to form the crust may be aided by the microbial activity present, especially given the highly acidic nature of the coatings. The degradation of iron-rich biotite aids cementation and contributes to the red/brown stains seen in thin section, which binds tiny clay particles. Schmidt Hammer and blade penetration tests indicate that the iron films are strengthening the exterior of the rock, and it is safe to conclude that case-hardening is occurring

5.4.2.3 Lithobiontic Coatings

Microbial activity in a variety of ecological niches was observed at all six locations. The green algae, approximately 0.5mm below the surface, observed at site 2 is suggested to be similar to that found in Antarctica and other arid environments. The literature study has shown that cyanobacteria will flourish in the presence of inorganic nutrients and high acidity. At site 6 biological activity was the dominant factor in creating the outer crust, and involved both micro-organisms and plant life. Endoliths thrive in an environment which provides light and, at the same time, protection by quartz and clay particles. Higher organisms such as mosses are also found on the surface, and outcrop evidence suggests that they are also actively boring into the rock (euendoliths). The moss roots (rhizoids) form a mesh within the substrate and are encrusted by clay particles. Lithobiontic coatings observed in the Peerless Gully are not case-hardening the rock, but provide relatively fast forming, temporary protection from weathering processes.

5.4.2.4 Clay Minerals, Cement and Grain Interlock

Clay minerals and grain interlock contribute to crusts which can be considered iron films or lithobiontic coatings. Clays are unlikely to be deposited by wind blown dust in the Reddale Valley, unlike desert varnish formation and outcrops have shown accumulations relating to water seepage, possibly from soil above the face. The crust at site 4 is dominated by clay minerals which have cemented detrital grains into the thin friable coatings. Thin sections indicate that the feldspars and micas are in the process of breaking down within the rock, and sericite/illite was abundant at most sites. The presence of clays and a variety of quartz and microcline grain sizes, which are predominantly subangular, gives the rock a certain natural degree of cohesion, as discussed in section 5.4.1. Sites 3 and 5 showed signs of compression and subsequent grain interlock, which also aided cohesion. Cementation, as observed as a red/brown stain surrounding clay particles in sites 1-3, provides the strongest bonds between grains and these sites correspondingly had higher rebound numbers than those bound by other means.

5.5 Rate of Formation and Relevance to Opencast Mining

A photographic study of areas where the lithobiontic coating had been chipped off by the author was also conducted at the same locality as sites 5 and 6 (Peerless Gully). This was undertaken to assess formation rates for the crust. Although little change, other than a slight accumulation of clays by seepage, was seen at most sites over an eight month period, one site displayed a definite discolouration from clay minerals and is shown in figure 5.32. It can therefore be assumed that the coating here is relatively fast forming, and may take as little time as a year to accumulate or grow. The opencast was lasted operational in 2000 (J. Foster, Reefton Surface Operations Manager, pers. comm., 2006), so the maximum time for the crust observed to form is 6 years.

Figure 5.32 Photographs of area with crust scrapped off over time.

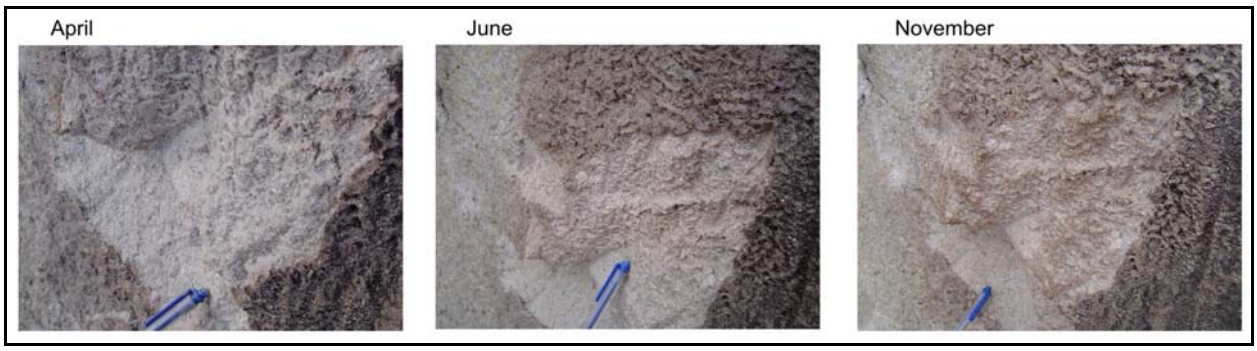

In the Reddale Valley photographs were taken of the first four sites in December 2005 and February 2006. No significant change was observed at sites 1-3, but as shown in figure 5.33 the thin friable crust at site 4 had partially developed over the three month period. Mining operations ceased at site 1 and 2 in 1993, and it can therefore be assumed the iron films identified have taken at most 13 years to form. At sites 3 and 4 mining was last operational in 1998, which suggests the iron film at site 3 has formed in less than 8 years.

Figure 5.33 Outcrop at site 4 in a) December 2005 and b) February 2006 showing the redevelopment of a clay dominated crust. Intervals on top scale of tape measure and on card in centimetres.

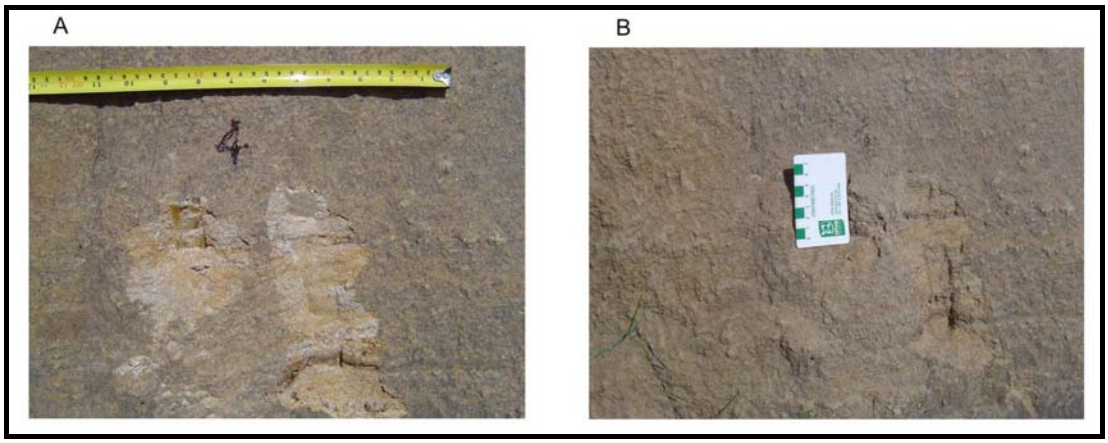

It can be concluded that clay-dominated crusts are likely to form after a number of months. Lithobiontic crust may take around 5 years to completely develop on a cut face, and jarosite-dominated iron films will form on a 10+ years scale. In places it was observed that the biological growth became too heavy to remain attached to the surface, and that the coating broke off from the face. It is expected that in the presence of such a large amount of biological activity on the face as a whole, that the area will be quickly inhabited by replacement organisms until the coating again becomes to heavy support itself. Despite this cycle of regeneration and collapse, and the fact that lithobiontic coatings and clay crusts disintegrate easily when disturbed and are no 'stronger' than the host rock, both coatings aid stability. The crusts provide protection from further weathering, and increase cohesion of the otherwise friable material. It would therefore be advantageous to excavate substantial highwalls to their final position initially so that the coatings have the maximum time to develop. Fast-forming clay-dominated crust will aid short (less than 6 month) stability, as long as water flow down the batter face is not substantial enough to prevent development. A small amount of seepage is likely to help transport clay minerals across the face. The gradual oxidation of pyrite to iron minerals will assist long term stability over periods greater than 6 months, and may take somewhere in the order of 10 years to form completely.

5.6 Synthesis

This chapter has provided a literature study of lithobiontic coatings, iron films, silica glaze and other rock coatings which can cause case-hardening of otherwise friable rocks. Six sites were investigated using outcrop and hand specimen description along with microscope and chemical analysis methods. The results have shown that the rock coatings on the existing highwalls in the Reddale Valley and Peerless Gully can be categorised as iron films from pyrite breakdown, lithobiontic coatings or clay-dominated surface coatings. However, a combination of factors are involved and includes cementation and grain interlock. All crusts reported high acidity (pH 2.72-3.68) but despite this biological activity, in a number of ecological niches, made up a significant part of the crusts observed. A green algae inhabiting pore spaces approximately 1mm below the surface was noted beneath an iron film and it is suggested to be similar to that found in arid environments, such as Antarctica. The iron films are the only coatings that provided a strengthened exterior, but as they have the longest rate or formation (10+ years), they are less likely to provide short term stability for pit walls than the faster forming (less than 6 months) clay-dominated crusts.

Chapter 6

Summary and Conclusions

6.1 Project Outline

This study provides an engineering geological and geotechnical investigation of the proposed Terrace Opencast Coalmine highwall in the Reddale Valley, Reefton. The high quality No.4 coal seam exists in the valley floor beneath outwash gravels and bedded Brunner Coal Measures (BCM) overburden, the latter dipping at 15-30˚ towards the northwest. Knowledge of the rock material parameters and rock mass characteristics is essential for predicting overburden behaviour in the excavation walls. To this end, laboratory rock strength testing was completed on core samples, and scanlines defect surveys were performed on existing highwalls in the area. The data from the defect surveys was also used to perform kinematic feasibility checks to assess slope stability relative to proposed pit slope orientations. An investigation into the case hardening observed on cut faces utilised a variety of methods to characterise several types of rock coatings and assess the affect of crust development on short term pit slope stability.

6.2 Rock Material Characterisation

6.2.1 Geotechnical Units

The core samples were divided into four broad lithological units so that a representative amount of tests could be performed. All units were predominantly quartoze, with weathered feldspar and abundant muscovite flakes. Pyrite nodules were common throughout the core samples. Unit 1 consisted of a predominantly massive siltstone with varied carbon content. Unit 2 contained carbonaceous mudstone, and Unit 3 was defined as interbedded sandstone and carbonaceous mudstone, with a variety of bedding grades -laminated mudstone and fine sand (mm scale) and bedding (cm scale) in medium to coarse sand. Unit 4 was a loose sandstone that could not withstand rock strength testing preparation, and tests were therefore conducted using soil equipment.

6.2.2 Physical Property Tests

Physical property testing showed that porosity increased, density decreased and slake durability index values decreased with increasing grain size. The mudstone gave a misleadingly high slake durability result, which occurred due to the highly disintegrated samples being in larger fragments than the mesh of the basket. The average results for units 1-3 gave classifications within the medium to high porosity (9-13%) and dry density (2250-2470kg/m^3) ranges, and

medium to medium high slake-durability I_{d2} values (72-94% retained). Unit 4 (loose sandstone) recorded very low dry density (1694 kg/m^3) and slake-durability I_{d2} (9%) average values.

6.2.3 Mechanical Property Tests

Mechanical property tests confirmed that the BCM overburden can be classified as weak rocks (<30MPa). The UCS result gave overlapping ranges (between 2.2 and 28.8MPa) for Units 1-3, with very similar average values (12.8-13.7MPa) that made correlations with other parameters inconclusive. A trend of increasing strength with increasing depth was noted from several UCS and triaxial tests. The point load tests also gave similar average $I_{s(50)}$ results for all units (0.26-0.62MPa). When converted to UCS by a factor 24, the results were all within the range determined by testing (6-19MPa) although the conversions did not match the average results for units 2 and 3, which required multipliers of 17 and 49 respectively. Intact UCS values derived from triaxial tests by the Mohr-Coulomb relationship were also within the range determined from actual tests (<28.4MPa). The strength anisotropic index confirmed the presence of bedding, especially in the carbonaceous mudstone (2.8MPa) where it only appeared to be partially developed.

Units 1-3 confirmed that average strength increased with increasing confining pressure when subjected to triaxial testing. A linear trend between increasing cohesion and dry density was also established. The cohesion values for all units were within the low category (0.0-6.2MPa), although high friction angles (32-45˚) were also determined from triaxial tests. Realistic friction angles were determined from direct shear tests of bedding planes (average 14.6˚) and a high angle defect in laminated sandstone (36.7˚).

Dynamic elastic moduli were determined from sonic velocity equipment and a general decrease in Young's modulus with increasing Poisson's ratio was noted, as well as a trend suggesting that elasticity increased with increasing density. The average Young's modulus values determined reinforced the weak nature of the units (0.82-10GPa). The values for Poisson's ratio for the four units were high (0.39-0.50) and suggest that these weak rocks have properties more similar to soils than rocks.

6.3 Rock Mass Characterisation

6.3.1 Scanline Surveys

Eight scanline defect surveys were undertaken along existing cut faces in the southwest and northeast of the Reddale Valley. Significantly different sets of defects were observed on each

side of the valley, and as the proposed opencast is situated between the two it is difficult to predict whether one or a mixture of both structural conditions will control the structure in the pit. Analysis was therefore performed on the data from the southwest and northeast scanlines separately.

6.3.2 Defect Properties

The major types of discontinuities encountered in scanline surveys on both sides of the Reddale Valley are high angle tension joints, shallow dipping bedding, and faults related to regional uplift. The average orientations are presented in table 6.1, and a clockwise rotation from the southwest to the northeast data was observed in bedding and from the minor joint set in the southwest (JA2) to the major northeast joint set (JB1). The other joint sets do not appear to be related, but the results are inconclusive due to the spread of similarly orientated sets in the northeast that may be a result of the faults that cross the valley. A single crush zone was also recorded and cleavage was noted in the mudstone beds but as it was on such a small scale (<1m) was not assessed.

Table 6.1 Average defect orientations determined by stereographic analysis of scanlines data.

Defect Type	Southwest Scanlines	Northeast Scanlines
Bedding	13/323	9/359
Faults	84/341	77/156
Joints	JA1: 74/078 JA2: 72/156	JB1: 82/177 JB2: 78/202 JB3: 74/226 JB4: 88/239

The majority of all the types of defects exhibited low persistence (less than 3m), although as the type of terminations suggest, this may be affected by the size of the exposure. The bedding defects were generally clean, with very tight (<0.1mm) aperture. The majority of faults displayed ‘gapped’ (0.5-100mm) apertures that were infilled with gouge. Most joints displayed very tight aperture with clean and/or surface stained walls.

Although the full range of JRC (joint roughness coefficient) values were recorded, most defects gave low numbers (JRC<6) and had planar or curved and smooth surfaces. This suggests that the discontinuities have little asperity shear strength and reinforces the very low (0.006MPa) or zero cohesion determined by shear box testing. Wavelength and amplitude data was only approximated by visual inspection on selected defects, and the results cannot be regarded as reliable for characterising the whole of the rock mass.

Schmidt Hammer tests produced an average JCS (joint compressive strength) of 32MPa. This value is higher than expected and is most likely due to the 'case hardening' developed on the joint faces, especially on the southwest joints that displayed a higher number of medium strong wall strengths in manual index tests. The majority of defects (91%) in the scanlines were recorded as being dry, but this is not considered representative of the saturated rock situated beneath the valley floor.

6.3.3 Rock Quality Designation (RQD)

The results from the 8 drill holes analysed show that 37% of core was within the excellent class (RQD = 90-100%), while 29% was at the other end of the scale, in the very poor quality rock (RQD = 0-25%). When RQD was correlated with lithology the siltstone was found to have the highest percentage (62%) of excellent quality rocks, as expected. The carbonaceous mudstone, and interbedded sandstone and carbonaceous mudstone, had relatively high percentages of very poor quality rocks (33 and 41% respectively). Surprisingly the loose sandstone (unit 4) has 41% of the RQD values within the 90-100% interval, which may be because the uncemented nature enables the unit to accommodate movement without fracturing.

6.3.4 Near Surface Hydrogeology

The pump test data analysed is only relevant to the overlying outwash gravels rather than the whole BCM rock mass, as the wells were only screened over the top 15m in the gravels. However the aquifer identified will drain into the pit and parameters determined will aid near surface inflow prediction. The Walton Graphical method was used and a moderate transmissivity (58m^2/day) and hydraulic conductivity of 3.1 x 10^{-5}m/s was established. The shallow aquifer is most likely to be semi-confined and recharged by the nearby creek.

6.4 Kinematic Feasibility Assessment

6.4.1 Procedure

A series of kinematic feasibility checks, using stereographic methods in the Dips program, were carried out to assess the possibility of planar, wedge and toppling failures on data from the southwest and northeast sides of the valley. Proposed pit slopes of 60˚ and 76˚, with dip directions of 130, 150 and 170 were used. An optimum orientation of 65˚/120 was suggested from the results presented. A discussion of other important slope stability considerations was included.

6.4.2 Southwest Scanlines

Planar and wedge failures are possible for pit slopes of 76˚ based on the southwest data. The likelihood of failure occurring is largely dependent on the importance of the minor joint set (JA2: 76˚/156), which is only marginally significant with a maximum concentration of 4.5-6%. All pit slope orientations in the southwest showed that toppling failures were kinematically feasible along steeply dipping normal faults (84˚/341). As these have been noted underground as 'step-up' faults with approximately half a metre of displacement and several were recorded in the scanlines, it is highly likely that they would be encountered in the valley floor.

6.4.3 Northeast Scanlines

The possibility of all types of failures in the northeast data is reliant on whether the four joint concentrations are separate sets or a single widely scattered set that has been distorted by post-creation deformation. The optimum orientation for the pit slope (65˚/120) may encounter wedge failures between JB3 (74˚/226) and JB4 (88/239) if they are indeed individual sets. Analysis using Swedge has suggested the wedge will be stable when dry, marginally stable with a tension crack and water pressure present and unstable when the fissures are filled with water

The second controlling factor is the variation in orientation of the Reddale, Burkes Creek and Morrisvale Faults that cross the valley and will intersect the proposed opencast site. They will particularly affect the possibility of wedge failures, as the single orientation recorded (77˚/156) creates several intersection with the joint sets within and on the margin of the danger zone. The data suggests that there is only a low possibility of the occurrence of toppling failures in the northeast situation.

6.4.4 Other Slope Stability Considerations

The low persistence of the majority of the defects recorded suggests that only relatively small (~1m^2) failures are likely, therefore other considerations are equally important. The most crucial impact on slope stability will be ground water flowing into the pit, which may cause erosion of the pit walls and increase pressure in discontinuities. Bedding parallel failures may occur in the dip slope, especially as an average bedding plane friction angle of 15˚ was determined for carbonaceous mudstone by shear box testing. The fault crossing the pit may provide a releasing surface and cause bedding to steepen locally, making slab sliding more likely. The proposed opencast may encountered large scale (5m+) wedge failures and tension joints based on observation in existing near vertical highwalls.

6.5 Case Hardening Investigation

6.5.1 Study Objectives

An investigation of the outer weathered 'crust' (mm scale) developed on cut faces in the Reddale Valley and Peerless Gully was performed to determine the components forming the coatings and the influence it had on slope stability. A variety of methods were used and included outcrop and hand specimen description, thin sections viewed through a polarised microscope, SEM (Scanning Electron Microscope) combined with EDS (Energy Dispersive Spectrum) analysis, XRD (X-ray diffraction), pH and EC (Electrical Conductivity). Six sites were investigated and they can be divided into three general categories (iron films, lithobiontic and clay dominated coatings) although several common aspects were noted.

6.5.2 Common Aspects

There are several common aspects that were identified at all sites investigated, and they are generally derived from components originating from the host rock rather than external accretions. All crusts contained a substantial amount of quartz, with significant amounts of clay minerals (kaolinite group), and in all but site 5 microcline. Muscovite was a common mineral within and on the surface of the rocks. The thin sections showed degraded mafic minerals, especially biotite and it is proposed that this is contributing to the red/brown cement surrounding clay minerals, which is too fine to see optically, as well as iron derived from pyrite within the host rock. Sericite or illite have also filled the space between grains and may be aiding strength by increasing the clay content. Grain interlock is indicated by thin section analysis to be providing otherwise friable sandstones with a certain degree of cohesion. Despite the pH tests showing that all crusts were highly acidic (pH 2.72-3.68) biological activity, in a number of ecological niches, made up a significant part of the crusts observed.

6.5.3 Coating Types

The following coatings were identified:

- Iron Films: At sites 1-3 significant amounts of jarosite (iron sulphate) were identified by XRD and/or an iron spike in the EDS. Schmidt hammer tests on the weathered crust (average rebound number of 25), when compared to fresh surfaces (average rebound number of 22), showed that the iron films are hardening the surface. The oxidation of iron may be aided by microbial activity within and on the surface of the crust.
- Lithobiontic Coatings: Biological activity was observed at all sites and microbial and plant structures dominated the coatings at sites 5 and 6 in the Peerless Gully. Clays and

quartz were determined to be important factors as they aided growth by providing light, and at the same time as protection from the elements, for organisms living within the substrate (endoliths). The coatings are not providing any additional strength to the rock surface but offer relatively fast forming, temporary protection from weathering processes.

- Clay-dominated Crusts: Clay minerals and grain interlock contribute to crusts which can also be considered iron films or lithobiontic coatings. The crust at site 4 is dominated by clay minerals which have cemented detrital grains into the thin friable coatings. Sericite or illite forming from the degradation of feldspar and mica, filled the space between grains at the majority of sites and may be aiding strength by increasing the clay content. Grain interlock is indicated by thin section analysis to be providing the otherwise friable sandstones with a certain degree of cohesion.

6.5.4 Relevance to Opencast Mining

Photographic studies have shown that that clay dominated crusts are likely to form after number of months, lithiobiontic crust may take around 5 years to completely develop on a cut face and iron films can form on a 10+ years scale. Despite the fact that lithobiontic coatings and clay-dominated crusts disintegrate easily when disturbed and are no 'stronger' than the host rock, both coatings aid stability. The crusts provide protection from further weathering and increase cohesion of the otherwise friable material. It would therefore be advantageous to excavate substantial highwalls to their final position initially so that the coatings have the maximum time to develop. The gradual oxidation of pyrite to iron minerals will assist long term stability (greater than 6 months).

6.6 Key Conclusions

The key conclusions drawn from this study regarding highwall stability can be summarised as:

- The region is expected to encounter a severe (MM 7-8) earthquake during the proposed mine's life based on recent seismic activity.
- The overburden material in the proposed highwall can be expected to behave like weak rock, and some units (such as the loose sandstone) will have soil characteristics. The strength testing performed is biased towards intact core samples, and the results must therefore be considered maximum values. The results from UCS, point load and Young's moduli from this study were also generally lower than values determined for BCM in other areas and it is suggested that the overburden may be weaker in the Reddale Valley.

- Highwall stability is more likely to be affected by a substantial inflow of groundwater than highly persistent joint sets. The successful dewatering of the saturated units, while enabling mining to progress (probably by pumping water out of the pit) will be crucial to the development of the proposed mine.
- Establishment of the highwalls in their final position in the early mining stages will enable development of rock coatings that are expected to aid short and long term stability.

6.7 Recommendations for Further Research

Further geotechnical investigation is recommended in the next stage of assessment for the proposed opencast. Additional drilling may be required within the area to assist continued investigations which should include:

- Investigation into physical ground water characteristics of BCM which will make up the highwall including further borehole pump tests -screened to greater depths, installation of peizometers and modelling of the phreatic surface for the proposed pit. Development of a successful method to test permeability and investigation into whether the sandstone units will act as aquifers, together with a study on how they will be affected by internal erosion when the water is discharged into the pit.
- Additional rock strength testing including tensile ('Brazilian') tests and further direct shear tests.
- Slope stability modelling and three-dimensional analysis including volume estimates of potential failures.
- Investigation of bedding parallel failures on dip slope and potential redesign of low wall.
- Detailed evaluation of the Reddale, Burkes Creek and Morrisvale Faults, possibly including geophysical methods to investigate behaviour in the valley floor, and reassessment of underground observations.
- Extension of initial case hardening investigation presented here to identify clay minerals and microbial species forming rock coating.

References

Adams, C.J.D., Harper, C.T., and Laird, M.G., 1975. K-Ar ages of low grade metasediments of the Greenland and Waiuta groups in Westland and Buller, New Zealand: New Zealand Journal of Geology and Geophysics, v. 18, p. 39-48.

Anon, 1972. Instruction Manual: Terrametrics Triaxial Confinement Chamber: Colorado, p. 5.

Anon., 1977. *The description of rock masses for engineering purposes*. Report by the Geological Society Working Party: Quarterly Journal of Engineering Geology, v. 10, p. 355-388.

Aydin, A., and Basu, A., 2005. The Schmidt hammer in rock material characterization: Engineering Geology, v. 81, p. 1-14.

Barnes, G.E., 2000. Soil Mechanics: Principles and Practise: London, MacMillan Press Ltd, 493 p.

Barton, M.E., Mockett, L.D., and Palmer, S.N., 1993. An engineering geological classification of the soil/rock borderline materials between sands and sandstones, *in* Cripps, J.C., Coulthard, J.M., Culshaw, M.G., Forster, A., Hencher, S.R., and Moon, C.F., eds., The engineering geology of weak rock: Engineering Geology Special Publication, vol.8, p. 125-138.

Barton, N., and Choubey, V., 1977. The shear strength of rock joints in theory and practice: Rock Mechanics, v. 10, p. 1-54.

Barton, N., Lien, R., and Lunde, J., 1974. Engineering classification of rock masses for design of tunnel support: Rock Mechanics, v. 6, p. 189-236.

Barton, N.R., 1971. A model study of the behaviour of excavated slopes [Unpublished Ph.D. thesis]: London, University of London.

Barton, N.R., 1973. Review of a new shear strength criterion for rock joints: Engineering Geology, v. 7, p. 287-322.

Bell, D.H, and Pettinga, J.R., 1983: Rock Material Description System, University of Canterbury, Christchurch, New Zealand.

Bell, F.G., Entwisle, D.C., and Culshaw, M.G., 1997. A geotechnical survey of some British Coal Measures mudstones, with particular emphasis on durability: Engineering Geology, v. 46, p. 115-129.

Bell, F.G., Halbich, T.F.J., and Bullock, S.E.T., 2002. The effects of acid mine drainage from an old mine in the Witbank Coalfield, South Africa: Quarterly Journal of Engineering Geology and Hydrogeology, v. 35, p. 265-278.

Bell, R.A., and Sommerfeld, M.R., 1987. Algal biomass and primary production within a temperate zone sandstone: American Journal of Botany, v. 74, p. 294-297.

Beveridge, T.J., and Fyfe, W.S., 1985. Metal fixation by bacterial cell walls, *in* Macqueen, R.W., and Coope, J.A., eds., Role of organisms and organic matter in ore deposition, Volume 22: Canadian Journal of Earth Sciences, p. 1893-1898.

Bieniawski, Z.T., 1975. The point-load test in geotechnical practice: Engineering Geology, v. 9, p. 1-11.

Bishop, A.W., and Henkel, D.J., 1957. The Measurement of Soil Properties in the Triaxial Test: London, Edward Arnold Ltd, p. 122-131.

Boyd, R., 2002. Terrace Underground Mine Stage 3 Development, Internal report prepared for Solid Energy, 35 p.

Bradshaw, M.A., 1995. Stratigraphy and structure of the Lower Devonian rocks of the Waitahu and Orlando outliers, near Reefton, New Zealand, and their relationship to the Inangahua Outlier: New Zealand Journal of Geology and Geophysics, v. 38, p. 81-92.

Broch, E., and Franklin, J.A., 1972. The point-load strength test: International Journal of Rock Mechanics and Mining Sciences, v. 9, p. 669-693.

Brown, E.T. (Editor), 1981. Rock Characterisation, Testing and Monitoring, ISRM Suggested Methods: England, Pergamon Press, 211 p.

Browne, B.A., and Driscoll, C.T., 1992. Soluble aluminium silicates; stoichiometry, stability, and implications for environmental geochemistry: Science, v. 256, p. 1667-1670.

Chigira, M., and Oyama, T., 1999. Mechanism and effect of chemical weathering of sedimentary rocks: Engineering Geology, v. 55, p. 3-14.

Chiu, H.K., Johnston, I.W., and Donald, I.B., 1983. Appropriate techniques for triaxial testing of saturated soft rock: International Journal of Rock Mechanics and Mining Sciences & Geomechanics Abstracts, v. 20, p. 107-120.

Conca, J., 1985. Field and laboratory studies of geologic case hardening: Antarctic Journal of the United States, v. 19, p. 18-20.

Conca, J.L., and Rossman, G.R., 1982. Case hardening of sandstone: Geology, v. 10, p. 520-523.

Cooper, R.A., 1989. Early Palaeozoic Terranes of New Zealand: Journal of the Royal Society of New Zealand, v. 19, p. 73-112.

Curtiss, B., Adams, J.B., and Ghiorso, M.S., 1985. Origin, development and chemistry of silica-alumina rock coatings from the semi-arid regions of the island of Hawaii: Geochemica et Cosmochimica Acta, v. 49, p. 49-56.

de Freitas, M.H., 1993. Introduction to Session 1.2; Weak arenaceous materials, *in* Cripps, J.C., Coulthard, J.M., Culshaw, M.G., Forster, A., Hencher, S.R., and Moon, C.F., eds., The engineering geology of weak rock: Engineering Geology Special Publication, vol.8, p. 115-123.

Deere, D.U., 1968. Geological consideration, *in* Stagg, K.G., and Zienkiewicz, O.C., eds., Rock mechanics in engineering practice: London, Wiley, p. 1-20.

Deere, D.U., Hendron, A.J., and Patton, F.D., 1967. Design of surface and near surface construction in rock, *in* Fairhurst, C., ed., Failure and Breakage of Rock: New York, AIME, p. 237-302.

Dhakal, G., Yoneda, T., Kato, M., and Kaneko, K., 2002. Slake durability and mineralogical properties of some pyroclastic and sedimentary rocks: Engineering Geology, v. 65, p. 31-45.

Dorn, R.I., 1998. Rock Coatings: Amsterdam, Elsevier, 429 p.

—, 2004. Case hardening, *in* Goudie, A.S., ed., Encyclopaedia of Geomorphology: London, Routledge, p. 118-119.

Dorn, R.I., and Meek, N., 1995. Rapid formation of rock varnish and other rock coatings on slag deposits near Fontana, California: Earth Surface Processes and Landforms, v. 20, p. 547-560.

Duncan, N., 1969. Engineering Geology and Rock Mechanics: London, Leonard Hill, 267 p.

Ehrlich, H.L., 1996. How microbes influence mineral growth and dissolution: Chemical Geology, v. 132, p. 5-9.

Fetter, C.W., 2001. Applied Hydrogeology: New Jersey, Prentice-Hall, 598 p.

Finnemore, M., 2000. Unpublished Manual for Seismic Analyser: Model 1007H: Christchurch, University of Canterbury, 12 p.

Fowke, N.C., 1998. Geological Assessment of No. 4 Seam in and around Terrace Mine, Reefton Coalfield, Report prepared for Solid Energy Ltd, 116 p.

Franklin, J.A., and Chandra, R., 1972. The Slake-durability Test: International Journal of Rock Mechanics and Mining Sciences, v. 9, p. 325-341.

Friedmann, E.I., 1982. Endolithic microorganisms in the Antarctic cold desert: Science, v. 215, p. 1045-1052.

Giani, G.P., 1992. Rock Slope Stability Analysis: Rotterdam, A.A. Balkema, 361 p.

Institute of Geological and Nuclear Sciences Limited, 2005. New Zealand Active Faults Database: http://data.gns.cri.nz/af/

Golubic, S., Friedmann, E.I., and Schneider, J., 1981. The lithobiontic ecological niche, with special reference to microorganisms: Journal of Sedimentary Petrology, v. 51, p. 475-478.

Goodall, T.M., North, C.P., and Glennie, K.W., 2000. Surface and subsurface sedimentary structures produced by salt crusts: Sedimentology, v. 47, p. 99-118.

Goodman, R.E., 1976. Methods of geological engineering in discontinuous rocks: St Paul, Minnesota, West Publishing Co., 472 p.

—, 1980. Introduction to Rock Mechanics: New York, John Wiley & Sons, 478 p.

Graig, R.F., 1997. Soil Mechanics: London, E & FN Spon, 485 p.

Grasso, P., Xu, S., and Mahtab, A., 1992. Problems and promises of index testing of rocks, *in* Tillerson, J.R., and Wawersik, W.R., eds., Rock mechanics; Proceedings of the 33rd U.S. symposium on Rock Mechanics, vol.33, p. 879-888.

Hack, R., and Huisman, M., 2002. Estimating the intact rock strength of a rock mass by simple means, *in* van Rooy, J.L., and Jermy, C.A., eds., Engineering Geology for Developing Countries -Proceeding of the 9th Congress of the International Association for Engineering Geology and the Environment: Durban, South Africa, p. 1971-1977.

Hantush, M.S., and Jacob, C.E., 1955. Non-steady radial flow in an infinite leaky aquifer: Am. Geophys. Union Trans., v. 36, p. 95-100.

Hawkes, I., and Mellor, M., 1970. Uniaxial testing in rock mechanics laboratories: Engineering Geology, v. 4, p. 177-285.

Hayashi, M., and Miura, K., 1989. Glacial landforms and weathering processes in the Balchenfjella region, eastern part of the Sor Rondane Mountains, East Antarctica, *in* Yoshida, Y., Hiroi, Y., Kaminuma, K., Segawa, J., Torii, T., Shibuya, K., and Shiraishi, K., eds., Papers presented at the Ninth symposium on Antarctic geosciences [modified]: Proceedings of the NIPR Symposium on Antarctic Geosciences, vol.3, p. 65-80.

Henley, S.N., 1995. Reddale Coal Prospect, Reefton Coalfield, Internal CoalCorp Report, 7 p.

Herbert, R.B., Jr., 1995. Precipitation of Fe oxyhydroxides and jarosite from acidic groundwater: GFF, v. 117, p. 81-85.

Hewlett, L., 2003. Environmental Geology of Gold and Coal Mines, Reefton, New Zealand. [Unpublished B.Sc. (Hons) in Geology thesis]: Dunedin, University of Otago.

Hiebert, F.K., and Bennett, P.C., 1992. Microbial control of silicate weathering in organic-rich ground water: Science, v. 258, p. 278-281.

Hoek, E., and Bray, J., 1977. Rock Slope Engineering: London, The Institution of Mining and Metallurgy, 402 p.

Hoek, E., and Kaiser, P.K., 1997. Support of Underground Excavations in Hard Rock, Balkema, p. 27-47.

Hudson, J.A., 1989. Rock Mechanics Principles in Engineering Practice: London, Butterworths, 72 p.

Hudson, J.A., and Harrison, J.P., 1997. Engineering Rock Mechanics: An Introduction to the Principles: Oxford, Pergamon, 444 p.

Ian Wark Research Institute, 2002. Environmental Geochemistry International (IWRI and EGi), ARD Test Handbook: AMIRA P387A Project; Prediction and Kinetic Control of Acid Mine Drainage. AMIRA International, Melbourne, Australia, p. E-1.

Johnson, R.B., and DeGraff, J.V., 1988. Principles of Engineering Geology: New York, John Wiley & Sons, 497 p.

Kamp, P.J.J., 1986. The mid-Cenozoic Challenger rift system of western New Zealand and its implications for the age of Alpine Fault inception: Geological Society of America Bulletin, v. 97, p. 255-281.

Kennedy, J.F., 1988. Engineering Geological Characterisation of the Brunner Coal Measures, Cedar Creek Area, Buller Coalfield [Unpublished M. Sc. in Engineering Geology thesis]: Christchurch, University of Canterbury.

Laird, M.G., 1968. The Paparoa tectonic zone: New Zealand Journal of Geology and Geophysics, v. 11, p. 435-454.

Lucas, T., 2002. Engineering Geology Assessment of the Brunner Coal Measures, Island Block Opencast Coalmine, Reefton. [Unpublished M.Sc. in Engineering Geology thesis]: Christchurch, University of Canterbury.

McKnight, D.M., Kimball, B.A., and Bencala, K.E., 1988. Iron photoreduction and oxidation in an acidic mountain stream: Science, v. 240, p. 637-640.

Mitchell, R., 1974. Introduction to Environmental Microbiology: New Jersey, Prentice-Hall, 355 p.

Muir, R.J., Weaver, S.D., Bradshaw, J.D., Eby, G.N., Evans, J.A., and Ireland, T.R., 1996. Geochemistry of the Karamea Batholith, New Zealand and comparisons with the Lachlan fold belt granites of SE Australia: Lithos, v. 39, p. 1-20.

Nienow, J.A., and Friedmann, E.I., 1993. Terrestrial Lithophytic (Rock) Communities, *in* Friedmann, E.I., ed., Antarctic Microbiology: New York, Wiley-Liss, p. 343-412.

NIWA Science, 2006. Climate Stuff for Students: http//:www.niwascience.co.nz/edu/students/faq/climate

Norrish, N.I., and Wyllie, D.C., 1996. Rock Slope Stability Analysis, *in* Turner, A.K., and Schuster, R.L., eds., Landslides, Investigation and Mitigation: Washington, D.C., Transport Research Board, National Research Council, Special Report 247, p. 391-425.

Ollier, C., 1969. Weathering: Edinburgh, Oliver & Boyd, 304 p.

Paraguassu, A.B., 1972. Experimental Silicification of Sandstone: Geological Society of America Bulletin, v. 83, p. 2853-2857.

Pehi, T.N.R., 2004. Engineering Geology and Geotechnical Investigation of Highwall Stability of the Proposed Cypress Opencast Mine, Mt William Fault Zone, Cypress North Block, Upper Waimangaroa. [Unpublished M.Sc. in Engineering Geology thesis]: Christchurch, University of Canterbury.

Priest, S.D., 1993. Discontinuity Analysis for Rock Engineering: London, Chapman & Hall, 473 p.

Priest, S.D., and Hudson, J.A., 1981. Estimation of Discontinuity Spacing and Trace Length Using Scanline Surveys: International Journal of Rock Mechanics, Mining Sciences and Geomechanics Abstracts, v. 18, p. 183-197.

Robinson, D.A., and Williams, R.B.G., 1986. Surface crusting of sandstones in Southern England and Northern France, *in* Gardiner, V., ed., International Geomorphology, Volume 2: New York, Wiley, p. 623-635.

Rocscience Inc., 1999-2004. Dips User's Guide -Plotting, Analysis and Presentation of Structural Data Using Spherical Projection Techniques: Toronto, 84 p.

Rusnak, J.A., and Mark, C., 2000. Using the point load test to determine the uniaxial compressive strength of coal measure rock, *in* Peng, S.S., and Mark, C., eds., Proceedings of the 19th international conference on Ground control in mining, Volume 19, p. 362-371.

Scholle, P.A., 1979. A Color Illustrated Guide to Constituents, Textures, Cements, and Porosities of Sandstones and Associated Rocks: Oklahoma, The American Association of Petroleum Geologists, 201 p.

Selby, M.J., 1993. Hillslope Materials and Processes: Oxford, Oxford University Press, p 175-185.

Sen, Z., and Kazi, A., 1984. Discontinuity Spacing and RQD Estimates from Finite Length Scanlines: International Journal of Rock Mechanics, Mining Sciences and Geomechanics Abstacts, v. 21, p. 203-212.

Shelley, D., 1974. Optical Mineralogy: Christchurch, Canterbury University Press, 321 p.

Singer, P.C., and Stumm, W., 1970. Acid Mine Drainage: The Rate-Determining Step: Science, v. 167, p. 1121-1123.

Singleton, P., and Sainsbury, D., 1978. Dictionary of Microbiology: London, Wiley-Interscience, 481 p.

Sleight, A., 2003. Terrace Opencast Mine, Reefton, Stability Risk Assessment: Christchurch, Report prepared for Solid Energy Ltd by Tonkin & Taylor, p. 25.

Smoot, J.P., and Castens-Seidell, B., 1994. Sedimentary features produced by efflorescent salt crust, Saline Valley and Death Valley, California, *in* Renaut, R.W., and Last, W.M., eds., Sedimentology ands Geochemistry of Modern and Ancient Saline Lake, Volume Special publication No. 50: Tulsa, SEPM (Society for Sedimentary Geology), p. 73-90.

Staley, J.T., Palmer, F., and Adams, J.B., 1982. Microcolonial fungi; common inhabitants on desert rocks?: Science, v. 215, p. 1093-1095.

Stone, D., Harvey, I., and Bell, S., 2005. Reddale Opencast Project L3 Secondary Assessment Final Report, Unpublished Internal Solid Energy Report, 52 p.

Suggate, R.P., 1957. The Geology of the Reefton Subdivision: Wellington, New Zealand Geological Survey, 146 p.

Sykes, R., and Anonymous, 1986. Reefton Coalfield, recommendations for exploration, Geological Society of New Zealand, 16th annual conference; programme and abstracts: Geological Society of New Zealand Miscellaneous Publication, vol.35A, 102 p.

Taylor, R.K., and Spears, D.A., 1970. The breakdown of British Coal Measure rocks: International Journal of Rock Mechanics and Mining Sciences, v. 7, p. 481-501.

Terzaghi, R.D., 1965. Sources of Error in Joint Surveys: Geotechnique, v. 15, p. 287-304.

Titheridge, D.G., 1992. The depositional setting of the Brunner Coal Measures, Buller Coalfield., Resource Information Report, 40 p.

Turkington, A.V., 1998. Cavernous weathering in sandstone: lessons to be learned from natural exposure: Quarterly Journal of Engineering Geology, v. 31, p. 375-383.

Turkington, A.V., and Phillips, J.D., 2004. Cavernous weathering, dynamic instability and self-organization: Earth Surface Processes and Landforms, v. 29, p. 665-675.

Urrutia, M.M., and Beveridge, T.J., 1994. Formation of fine-grained metal and silicate precipitates on a bacterial surface (Bacillus subtilis): Chemical Geology, v. 116, p. 261-280.

Vallejo, L.E., Welsh, R.A., Jr., and Robinson, M.K., 1989. Correlation between unconfined compressive and point load strengths for Appalachian rocks, *in* Khair, A.W., ed., Rock mechanics as a guide for efficient utilization of natural resources; proceedings of the 30th U. S. symposium on rock mechanics, p. 461-468.

Viles, H.A., and Goudie, A.S., 2004. Biofilms and case hardening on sandstones from Al-quwayra, Jordon: Earth Surface Processes and Landforms, v. 29, p. 1473-1485.

Walcott, R.I., 1998. Modes of oblique compression; late Cenozoic tectonics of the South Island of New Zealand: Reviews of Geophysics, v. 36, p. 1-26.

Walton, W.C., 1960. Leaky Artesian Aquifer Conditions in Illinois, Report of investigation 39: Urbana, State Water Survey Division, 27 p.

Watchman, A., 1992. Composition, formation and age of some Australian silica skins: Australian Aboriginal Studies, p. 61-66.

Weed, R., and Ackert, R.P., Jr., 1986. Chemical weathering of Beacon Supergroup sandstones and implications for Antarctic glacial chronology, *in* Burckle, L.H., Denton, G.H., Vrba, E.S., and Partridge, T.C., eds., Third meeting in the paleoclimate and evolution series, Volume 82: South African Journal of Science, p. 513-516.

Wyllie, D.C., and Mah, C.W., 2004. Rock Slope Engineering: New York, Spon Press, 431 p.

Young, R.W., 1987. Sandstone landforms of the tropical East Kimberley region, Northwestern Australia: Journal of Geology, v. 95, p. 205-218

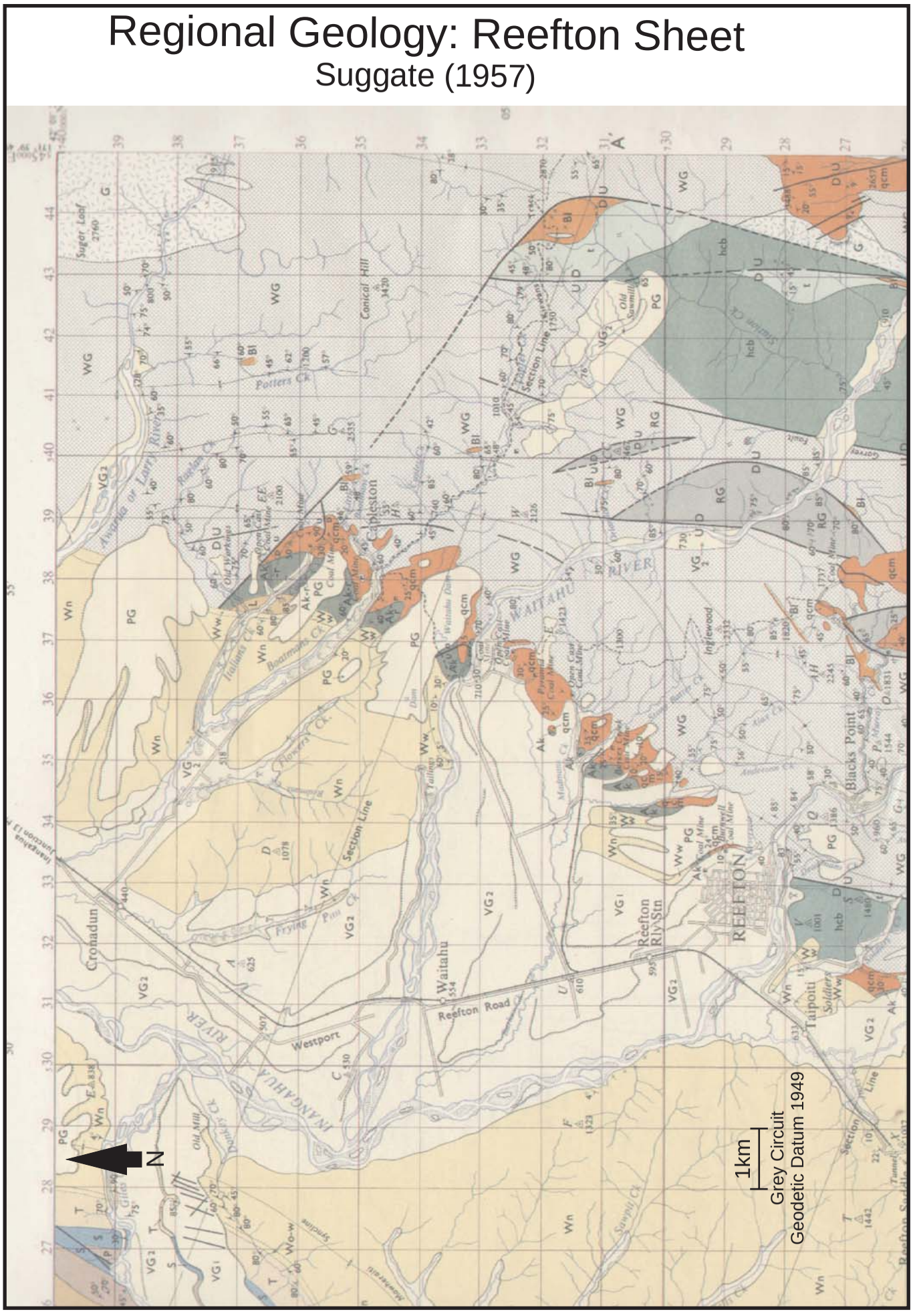
Regional Geology: Reefton Sheet
Suggate (1957)
REEFTON
Reefton Road
Reefton Rly Stn
Cronadun
Waitahu
Westport
Blacks Point
Taipoti
Capleston
Conical Hill
Sugar Loaf
Potters Ck
Section Line
WAITAHU RIVER
INANGAHUA RIVER
Flowers Ck
Pine Ck
Old Mill
Old Workings
Open Cast Coal Mine
Coal Mine
Tailings Dam
Tunnel
Grey Circuit
Geodetic Datum 1949
1km
N

Regional Map Key: Suggate (1957)

Sedimentary Rocks

VG2	Second Valley Glaciation Deposits Outwash and moraine gravel and sand	Late Pleistocene
VG1	First Valley Glaciation Deposits Outwash and moraine gravel and sand	
PG	Piedmont Glaciation Deposits Outwash and moraine gravel and sand	

~Unconformity~

Wn	Upper Wanganui Series 'Old Man Gravels'	Pliocene
Ww	Lower Wanganui Series Rotokohu Coal Measures	
T	Taranaki Series Freshwater conglomerate, sandstone, mudstone and coal	Miocene
S	Southland Series Freshwater conglomerate, sandstone, siltstone and lignite	
P	Pareora Series Marine sandstone and siltstone	Oligiocene
L	Landon Series Marine mudstone and limestone	
A	Arnold Series Kaiata Formation	Eocene
qcm	Quartoze Coal Measures Brunner Coal Measures	

~Unconformity~

t	Topfer Formation Freshwater sandstone, mudstone,and coal, tuff and igneous conglomerate	Lower Cretaceous
hcb	Hawks Crag Breccia	

~Unconformity~

RG	Reefton Group Indurated sandstone and mudstone, quarztite and limestone	Devonian

~Unconformity~

WG	Waiuta Group Greenland Group	Upper Ordovician

Igneous Rocks

G	Karamea Batholith Granite and gneiss (Devonian)

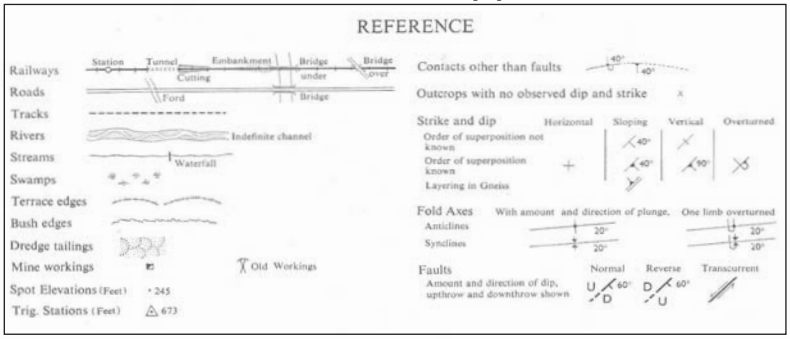

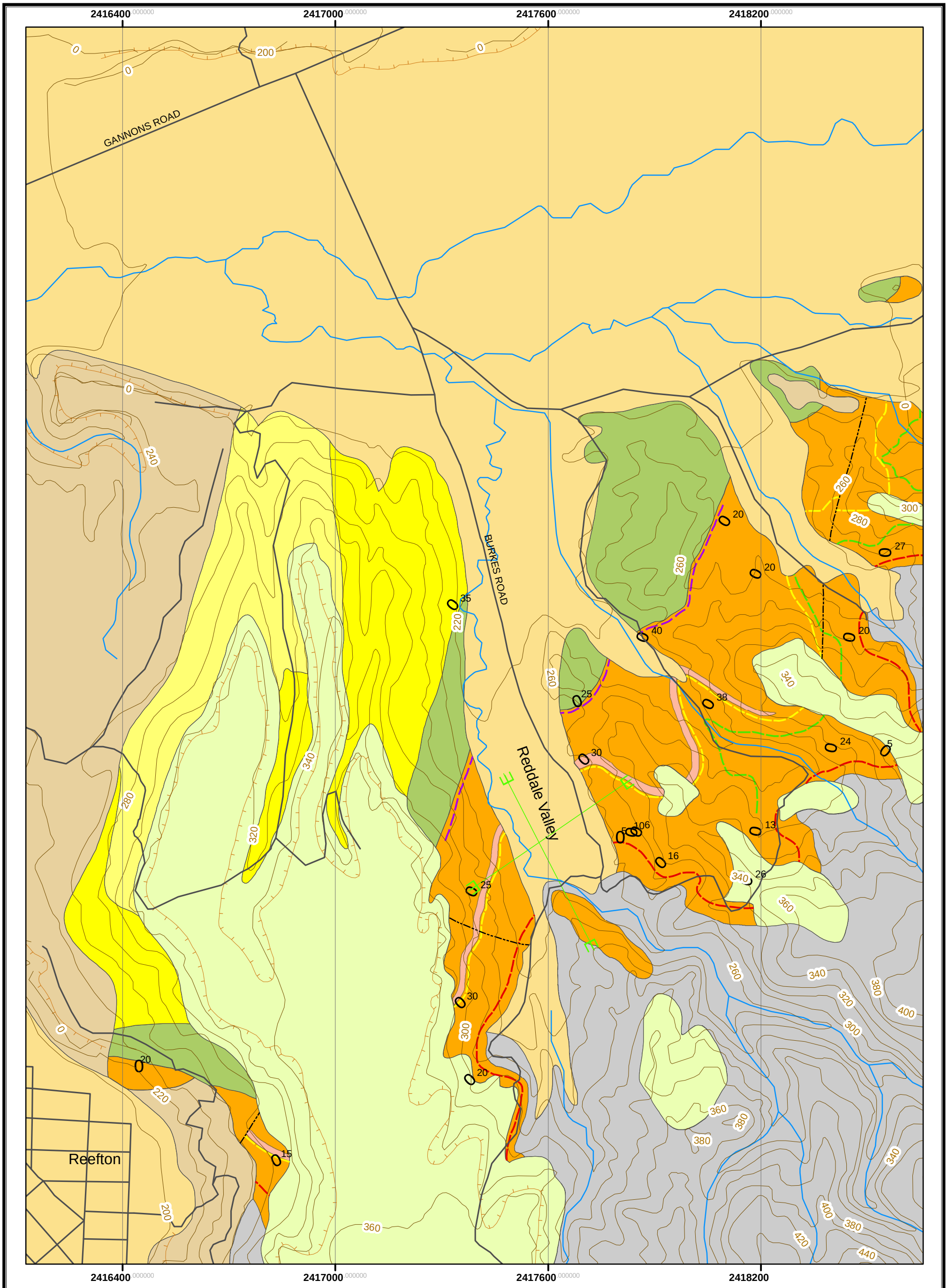
2416400.000000
2417000.000000
2417600.000000
2418200.000000
GANNONS ROAD
BURKES ROAD
Reddale Valley
Reefton

Appendix 1: Rock Material Characterisation

Table of Contents

Appendix 1.1 Rock Material Description Sheet

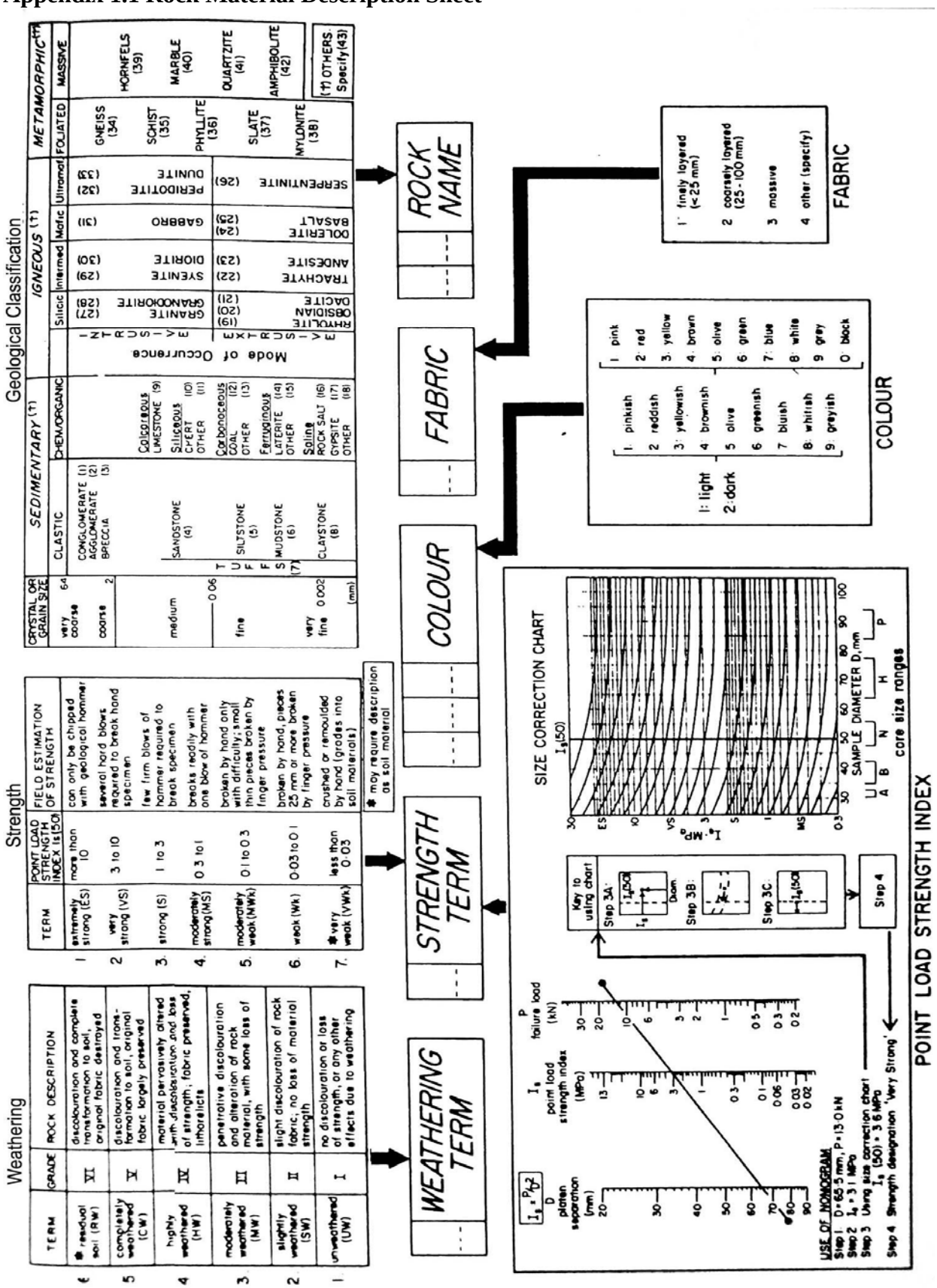

Bell and Pettinga's Rock Classification System (1983).

Appendix 1.2 Porosity and Density Determination

Method

The suggested method for porosity/density determination using saturation and caliper techniques as stipulated by the ISRM (Brown, 1981) was followed. This required more than three representative cylindrical samples, and so collected drill core was tested. The dimensions (diameter and length) were measured three times using a caliper and then averaged. The samples were water saturated using a vacuum for at least an hour or until no more mass was gained. The surface was patted dry and the saturated sample was weighed. They were then oven dried at a 100 degrees celcius temperature (top temperature of the oven but 5 degrees less then recommended) until a constant mass was gained. After cooling in a desiccator a final mass reading was recorded.

Calculations

The calculation used to manipulate the raw data were those suggested by ISRM (1981) together with standard area and volume equations and are given below.

Cross-Sectional Area [m^2] = ((Average Diameter [mm] / 1000) / 2)^2 x Pi

Volume [m^3] = Cross-Sectional Area [m^2] x (Average Length [mm] / 1000)

Wet Density [kg/m^3] = Wet Mass [kg] / Volume [m^3]

Dry Density [kg/m^3] = Dry Mass [kg] / Volume [m^3]

Pore Volume [m^3] = (Wet Mass [kg] – Dry Mass [kg]) / Water Density [mm^3]

where Water Density [mm^3] = 1000

Porosity [%] = (Pore Volume [m^3] / Volume [m^3]) x 100

Void Ratio = Porosity [%] / (100 – Porosity [%])

Raw Data

Test No.	Sample	Litho	Average Diameter	Cross-sectional	Average Length	Volume	Initial Weight	Wet Mass	Wet Density	Dry Mass	Dry Density	Pore Volume	Porosity	Void Ratio
			(mm)	Area (m^2)	(mm)	V (m^3)	(kg)	m_{sat} (kg)	ρ_{sat} (kg/m^3)	m_s (kg)	ρ_d (kg/m3)	V_v (m3)	n (%)	e
1	17	CS	60.63	0.00289	30.31	0.00018	0.4239	0.4236	2390.50	0.3998	2256.19	0.0000238	13.43	0.15515
2	7	CS	60.42	0.00287	156.00	0.00045	1.0473	1.0430	2332.15	0.9764	2183.23	0.0000666	14.89	0.17497
3	9	CS	60.47	0.00287	154.50	0.00044	1.0775	1.0771	2427.76	1.0197	2298.38	0.0000574	12.94	0.14860
4	4	CS	60.87	0.00291	148.50	0.00043	1.0237	1.0234	2368.48	0.9618	2225.92	0.0000616	14.26	0.16627
5	1	CS	60.75	0.00290	30.38	0.00009	0.2020	0.2017	2319.54	0.1904	2189.60	0.0000113	12.99	0.14936
6	2	CS	60.89	0.00291	30.44	0.00006	0.1385	0.1380	2364.69	0.1310	2244.75	0.0000070	11.99	0.13630
7	27	CS	59.79	0.00281	29.90	0.00011	0.2606	0.2561	2273.16	0.2391	2122.26	0.0000170	15.09	0.17771
8	25	CS	60.78	0.00290	30.39	0.00009	0.2143	0.2170	2408.21	0.2049	2273.93	0.0000121	13.43	0.15511
9	58	CS	60.67	0.00289	30.33	0.00014	0.3273	0.3375	2488.78	0.3242	2390.71	0.0000133	9.81	0.10874
10	31	CS	60.75	0.00290	30.38	0.00018	0.4201	0.4311	2440.45	0.4095	2318.17	0.0000216	12.23	0.13931
11	65	CS	60.84	0.00291	30.42	0.00016	0.3517	0.3769	2406.08	0.3516	2244.57	0.0000253	16.15	0.19262
								Average:	2383.62		2249.79	0.0000288	13.38	0.15492
								Standard Deviation:	60.78		72.43	0.0000220	1.73	0.02295
12	42	CM	60.60	0.00288	30.30	0.00006	0.1335	0.1336	2339.67	0.1271	2225.84	0.0000065	11.38	0.12845
13	43A	CM	60.71	0.00289	30.36	0.00014	0.3485	0.3522	2440.86	0.3352	2323.04	0.0000170	11.78	0.13355
14	44	CM	60.27	0.00285	30.14	0.00004	0.1034	0.1048	2447.85	0.0995	2324.06	0.0000053	12.38	0.14128
15	36	CM	61.22	0.00294	30.61	0.00012	0.3026	0.2981	2397.52	0.2897	2329.96	0.0000084	6.76	0.07245
16	67	CM	60.10	0.00284	30.05	0.00013	0.3210	0.3272	2470.13	0.3122	2356.89	0.0000150	11.32	0.12770
17	28	CM	60.66	0.00289	30.33	0.00007	0.1571	0.1604	2405.04	0.1510	2264.09	0.0000094	14.09	0.16407
18	60	CM	60.54	0.00288	30.27	0.00019	0.3698	0.4554	2431.77	0.4300	2296.14	0.0000254	13.56	0.15692
								Average:	2418.98		2302.86	0.0000124	11.61	0.13206
								Standard Deviation:	42.89		44.70	0.0000072	2.39	0.02976
19	16	CZ	57.08	0.00256	28.54	0.00020	0.5419	0.5406	2725.67	0.5192	2617.78	0.0000214	10.79	0.12095
20	63	ZS	60.62	0.00289	30.31	0.00014	0.3534	0.3552	2500.40	0.3455	2432.12	0.0000097	6.83	0.07329
21	33	zs/cz	60.68	0.00289	30.34	0.00014	0.3483	0.3461	2510.16	0.3398	2464.47	0.0000063	4.57	0.04788
22	B	SZ	60.68	0.00289	30.34	0.00018	0.4600	0.4593	2508.27	0.4471	2441.65	0.0000122	6.66	0.07138
23	GB	ZS	61.18	0.00294	30.59	0.00038	0.9772	0.9781	2547.10	0.9390	2445.28	0.0000391	10.18	0.11336
24	G	ZS	60.93	0.00292	30.47	0.00007	0.1878	0.1896	2591.70	0.1823	2491.92	0.0000073	9.98	0.11085
25	16	CZ	60.38	0.00286	30.19	0.00018	0.4350	0.4435	2519.46	0.4221	2397.89	0.0000214	12.16	0.13840
								Average:	2557.54		2470.16	0.0000168	8.74	0.09659
								Standard Deviation:	80.55		71.18	0.0000116	2.73	0.03260

Appendix 1.3 Slake-Durability Index Test

Method

The suggested method for determination of the slake-durability index outlined in ISRM (1981) was undertaken. Using core that had been broken by triaxial strength testing, the samples were cut in the rock mechanics lab until roughly spherical and weighing between 40 and 60 grams. Ten such samples were needed per basket and gave a total sample mass between 450 and 550 grams. The samples within the clean drums were then dried at 100˚C (top temperature of the oven but 5 degrees less than recommended) until a constant mass was achieved. The initial mass (mass A) of the drum and the sample is then recorded and then cooled. The drums are placed in the troughs and coupled to the motor. The trough is filled until reaching 20 mm below the drum axis (as marked on the trough), with tap water at room temperature (around 20˚C). The motor is then turned on so that the drums rotate for 200 revolutions for a period of 10 minutes. The drums are then removed from the troughs and placed in the oven until a constant mass is again gained. Mass B (cycle 1) is then recorded for the drum and remaining sample, following cooling. This process is repeated and mass C, E and F gained from the weight of the drum and remaining sample after each cycle. Once the required number of cycles are completed the drum is brushed clean and weighed as mass D.

Calculations

The slake-durability index (I_d) is established by calculating the percentage ratio of final to initial dry sample masses as follows:

I_{dx} [%] = (Y – D)/ (A - D) x 100

where x = the number of cycles and Y = mass for that cycle ie cycle 1, mass B etc

Raw Data

Slake-Durability Index Results

Sample	Test	Unit	Basket	Mass A	Mass B	I_{d1}	Mass C	Mass D	I_{d2}	Mass E	I_{d3}	Mass F	I_{d4}
				Initial	Cycle 1		Cycle 2	Basket only		Cycle 3		Cycle 4	
				(g)	(g)	(%)	(g)	(g)	(%)	(g)	(%)	(g)	(%)
43A	1	cm	L 3-4	2800.9	2786.4	99.48	2766.2	2253.7	93.66	2754	91.43	2733	87.59
43B	1	cm	L 1-2	2700.7	2688.6	99.55	2667.3	2172	93.68	2647.6	89.96	2627.4	86.14
29A	3	cm	R 1-2	2749	2735	99.491	2712.2	2182.2	93.507	2687.2	89.097	2664.7	85.13
29B	3	cm	R 3-4	2789.2	2775.7	99.516	2755.6	2253.7	93.725	2731	89.132	2708.9	85
					Average:	99.51			93.64		89.90		85.96
2	1	ss/cm	R 1-2	2733.2	2510.8	91.86	2435.3	2182.6	45.90	2398.2	39.16	2362.5	32.67
9	1	ss/cm	R 3-4	2786	2742.2	98.43	2663.1	2254.2	76.89	2581.2	61.49	2524.3	50.79
6A	3	ss/cm	L 1-2	2702.7	2666.2	98.649	2639.2	2171.7	88.041	2612.7	83.051	2583.4	77.53
6B	3	ss/cm	L 3-4	2794.9	2758.5	98.698	2681.8	2253.4	79.114	2601.9	64.358	2564.7	57.49
					Average:	96.91			72.49		62.01		54.62
B1	2	zs	R 1-2	2708.4	2692.4	99.41	2667.4	2182.5	92.20	2629.8	85.05	2589.1	77.32
B2	2	zs	R 3-4	2762.3	2742.1	99.27	2708.9	2253.9	89.50	2672.7	82.38	2639.9	75.92
					Average:	99.34			90.85		83.72		76.62
17A	2	ss	L 1-2	2611.3	2236.1	85.63	2204.5	2171.8	7.44				
17B	2	ss	L 3-4	2692.2	2329.4	86.52	2302.4	2253.5	11.15				
					Average:	86.08			9.29				

Appendix 1.4 Uniaxial Compressive Strength (UCS)

Method

The ISRM suggested method for determination of the uniaxial compressive strength of rock materials as published in Brown (1981) was followed for sample preparation and testing. The HQ (61mm diameter) core was cut to as close to 152.5mm as possible to comply with the length to diameter ratio of 2.5:1 suggested. However the grinding process to produce flat and parallel ends caused several samples to lose some length when they broke along bedding planes. Hawkes and Mellor (1970) reviewed the effect of varying the specimen length and they concluded that minimum acceptable L:D ratio was 2.0:1. The minimum length tested by this author was 140 mm (2.3:1) which is well above this. The diameter of each sample was measured at the top, middle and bottom of the sample and averaged. The diameter and length were both measured using a digital calliper to 0.01mm. All samples were tested as collected and saturation was assumed as natural moisture content. The tests were undertaken in the rock mechanics laboratory, owned by the Department of Geological Sciences and situated in the Department of Civil Engineering, using a Controls 50-C36H2 compression testing machine with a digital microprocessor providing readout. The upper steel compression platen is spherically seated. Once placed in the loading frame with HQ steel platens beneath and above the sample, the specimens were loaded at a constant average rate of 0.5 to 1.0 MPa per second so that failure would occur within 5 to 10 minutes. The maximum load was recorded in kilonewtons (kN) and the UCS (MPa) value calculated. ISRM suggests at least 5 samples for testing, unfortunately only 3 samples of carbonaceous mudstone survived the preparation process and failed with valid results. The composition of the other two units enabled more intact samples to be collected and therefore more than the required number could be tested.

Calculations

Cross-Sectional Area [mm^2] = ((Average Diameter / 2)^2 x Pi

UCS [MPa] = (Maximum Load [kN] x 1000) / Cross-Sectional Area [mm^2]

Raw Data

Uniaxial Compressive Strength Results

Sample	Box	Depth	Unit	Litho	Av Diameter	Length	X-sectional Area	Weight	Failure Load	USC	Failure type
		(m)			(mm)	(mm)	(mm^2)	(g)	(kN)	(Mpa)	
1	654	12.48-12.74	3	CS/CM	60.46	159	2871		19.8	6.9	Shear Failure
2	654	12.74-12.96	3	CS/CM	60.76	160	2900	1091.3	27.9	9.6	Axial/Cataclasis
3	654	13.26-13.52	3	CS/CM	60.95	159.05	2918	1110.0	32.3	11.1	Axial/Shear
4	654	14.17-14.58	3	CS/CM	60.87	148.5	2910	1023.7	13.6	4.7	Cataclasis
30A	656	25.1-25.5	3	CS	60.83	155.14	2906	1061.9	52.4	18.0	Cataclasis
30B	656	25.1-25.6	3	CS	60.71	145.12	2895	984.4	45.0	15.5	Shear Failure
52A	663	62.8-63.34	3	SS/CM	60.29	146.52	2855	1020.8	61.8	21.6	Shear Failure
52B	663	62.8-63.34	3	SS/CM	60.59	145.92	2883	1038.6	76.3	26.5	Shear Failure
52C	663	62.8-63.34	3	SS/CM	60.62	148.91	2886	1063.5	83.1	28.8	Shear Failure
35	662	41.99-42.19	3	CS	60.84	148.01	2907	1120.7	54.2	18.6	Shear Failure
16	658	11.49-11.80	1	CS	60.59	152.92	2884	1079.8	22.7	7.9	Shear Failure
17	658	14.7-14.37	3	CS	60.97	156.08	2920	1064.4	9.3	3.2	Cataclasis
18	658	16.55-16.8	3	CS	61.31	144.35	2952	1009.1	6.4	2.2	Cataclasis
27	656	15.30-15.37	3	CS	60.33	146.04	2859	975.7	12.3	4.3	Cataclasis
48A	663	43.94-44.25	3	SS/CM	58.83	140.17	2718	892.6	1.9	0.7	Not Valid
48B	663	43.94-44.25	3	SS/CM	58.83	141.77	2718	909.0	2.2	0.8	Not Valid
									Average:	12.8	

62	657	29.9-30.11	1	CZ	60.55	150.77	2880	961.3	22.9	8.0	Shear Failure
63	657	33.01-33.25	1	ZS	60.58	140.42	2882	1014.9	73.0	25.3	Axial/Cataclasis
61	657	27.78-27.97	1	CZ	60.24	147.88	2850	1032.6	22.4	7.9	Shear Failure
41A	662	57.03-57.55	1	CZ/CM	61.36	150.05	2957	1078.4	45.2	15.3	Shear Failure
41B	662	57.03-57.55	1	CZ/CM	61.05	154.47	2927	1089.1	36.2	12.4	Shear Failure
41C	662	57.03-57.55	1	CZ/CM	60.87	152.82	2910	1050.8	38.5	13.2	Shear Failure
									Average:	13.7	

47	663	42.99-43.19	2	CM	59.71	152.58	2800	1054.1	1.4	0.5	Prexisting shear
44	662	64.98-65.19	2	CM	60.7	154.8	2894	1086.0	39.5	13.6	Shear Failure
43A	662	63.44-63.85	2	CM	60.75	143.89	2899	1010.3	36.2	12.5	Shear Failure
43B	662	63.44-63.85	2	CM	60.63	149.85	2887	1054.3	39.2	13.6	Shear Failure
									Average:	13.2	

Appendix 1.5 Point Load Test

Method

The suggested method for determining point load strength by ISRM (Brown, 1981) was followed for sample preparation, testing procedures and calculations. The Point Load Tester (model 6500) produced by Geotechnical Systems Australia Ltd in the rock mechanics laboratory, University of Canterbury was used to perform the test. This incorporates a loading system with spherically-truncated, conical platens, a load measuring system which records and holds the peak failure load as well as a distance measuring system in the form of an attached steel rule as recommended. Diametral and axial tests were performed on core samples according to the specifications for anisotropic rocks as outlined below:

A) Diametral tests – Specimens required a total length to diameter ratio of greater than 1.0 to be suitable for diametral testing. Although it is suggested to perform 10 or more tests per unit this was not possible with the diametral tests as core that remained intact following UCS or triaxial tests was mainly utilized for point load. It was therefore unusual that the samples were long enough to meet the above requirement. The sample is inserted in the testing machine on its side so that the platens are closed to make contact along the diameter. The distance between the platens is measured as D. Care is to be taken to make sure that the distance between the contact points and the ends is at least 0.5 times the core diameter. Also the core must be lined up so that a single weakness plane (bedding in this case) is subjected to the applied load. The load is increased at a steady pace until failure occurs within 10-60 seconds, recording the peak load as P.

B) Axial tests – Core specimens with a length to diameter ratio of 0.3-1.0 can be considered for axial testing. In most cases plenty of remaining core filled this criteria and more than 10 samples could be tested but for units that were less numerous fewer remained intact for testing. Often those pieces that are long enough for diametral testing, once broken can then be re-used for axial tests if they remain intact, otherwise saw cutting was used to prepare the samples. The samples were tested perpendicular to bedding (maximum strength) by cutting along bedding planes or using natural breaks and perpendicular to the horizontal (between 15 to 30 degrees to bedding) to be comparable with the UCS tests performed. The samples were placed between the platens so that the core end faces were perpendicular to the load direction (core axis therefore on an angle for those at 90 degrees to bedding). D is then recorded as the distance between the platens and W as the

specimen width perpendicular to the loading direction. The load is steadily increased for 10-60 seconds until failure occurs and P is recorded as the peak strength.

Calculations

Uncorrected Point Load Strength Index: $I_s = P / D_e^2$

where P is the peak load (kN) and D_e is the 'equivalent core diameter' as calculated by:

$D_e^2 = D^2$ for diametral tests (distance between platens in mm)

$= 4A / Pi$ for axial tests and A = WD (minimum cross sectional area of a plane through the platen contact points).

Size Correction Factor: $F = (D_e / 50)^{0.45}$

Size-corrected (for D = 50mm) Point Load Strength Index: $I_{s(50)} = F \times I_s$

Raw Data

DIAMETRAL POINT LOAD TESTING

Sample ID	Sample	Litho.	Description of Failure	P (kN)	D (mm)	D_e^2	D_e	I_s	F	$I_{s(50)}$ (MPa)
1	9C	SS/CM	central single shear	0.59	59.00	3481	59.0	0.17	1.077	0.18
2	7	SS/CM	central single shear	0.12	57.00	3249	57.0	0.04	1.061	0.04
3	27	SS/CM	bedding plane	0.43	59.00	3481	59.0	0.12	1.077	0.13
4	8	SS/CM	bedding plane	0.75	59.00	3481	59.0	0.22	1.077	0.23
5	65	SS/CM	single vertical shear	0.87	60.00	3600	60.0	0.24	1.086	0.26
6	31	SS/CM	bedding plane	0.39	58.50	3422	58.5	0.11	1.073	0.12
									Rejecting lowest and highest results, the **mean $I_{s(50)}$ =**	0.16
1	28	CM	bedding plane	1.14	59.00	3481	59.0	0.33	1.077	0.35
2	42	CM	bedding plane	0.14	60.58	3670	60.6	0.04	1.090	0.04
3	59	CM	bedding plane	0.45	59.00	3481	59.0	0.13	1.077	0.14
4	66	CM	bedding plane	1.28	59.00	3481	59.0	0.37	1.077	0.40
									Rejecting lowest and highest results, the **mean $I_{s(50)}$ =**	0.23
1	G	ZS	bedding plane	0.16	59.50	3540	59.5	0.05	1.081	0.05
2	G	ZS	bedding plane	1.46	59.00	3481	59.0	0.42	1.077	0.45
									Rejecting lowest and highest results, the **mean $I_{s(50)}$ =**	0.25

AXIAL POINT LOAD TESTING

	90 to bedding											
Sample ID	**Sample**	**Litho.**	**Description of Failure**	**P (kN)**	**D (mm)**	**W (mm)**	**A = WD(mm^2)**	**D_e^2**	**D_e**	**I_s**	**F**	**$I_{s(50)}$ (MPa)**
1	9A	SS/CM	central vertial shear	0.89	37.50	60.63	2274	2895	53.8	0.31	1.034	0.32
2	9B	SS/CM	central vertial shear	0.63	28.50	60.90	1736	2210	47.0	0.29	0.973	0.28

3	17	SS/CM	central vertial shear	0.51	29.00	60.13	1744	2220	47.1	0.23	0.974	0.22
4	18	SS/CM	central vertial shear	0.00	20.50	62.00	1271	1618	40.2	0.00	0.907	0.00
5	27	SS/CM	central vertial shear	0.22	22.00	61.00	1342	1709	41.3	0.13	0.918	0.12
6	5	SS/CM	central vertial shear	0.73	23.00	61.00	1403	1786	42.3	0.41	0.927	0.38
7	8A	SS/CM	central vertial shear	0.85	19.00	60.68	1153	1468	38.3	0.58	0.887	0.51
8	8B	SS/CM	central vertial shear	1.44	39.00	60.90	2375	3024	55.0	0.48	1.044	0.50
9	65A	SS/CM	central vertial shear	1.14	30.00	61.50	1845	2349	48.5	0.49	0.986	0.48
10	3	SS/CM	central vertial shear	0.95	20.00	64.00	1280	1630	40.4	0.58	0.908	0.53
11	25	SS/CM	central vertial shear	0.81	20.00	62.60	1252	1594	39.9	0.51	0.904	0.46
12	65	SS/CM	bedding plane	0.26	33.00	60.84	2008	2556	50.6	0.10	1.005	0.10
13	65B	SS/CM	central vertial shear	0.96	22.00	61.20	1346	1714	41.4	0.56	0.919	0.51
											Rejecting lowest and highest results, the **mean $I_{s(50)}$ =**	0.39
	90 to bedding											
1	62	ZS	4 vertical pieces	0.43	14.00	60.97	854	1087	33.0	0.40	0.829	0.33
2	G	ZS	3 vertical shears	0.93	25.50	63.00	1607	2045	45.2	0.45	0.956	0.43
3	G	ZS	central vertial shear	0.41	32.50	63.00	2048	2607	51.1	0.16	1.009	0.16
											Rejecting lowest and highest results, the **mean $I_{s(50)}$ =**	0.31
	90 to bedding											
1	A4	CM	irregular vertical shear	1.12	39.00	61.00	2379	3029	55.0	0.37	1.044	0.39
2	22	CM	Bedding planes	0.35	18.00	63.00	1134	1444	38.0	0.24	0.884	0.21
3	22	CM	Bedding planes	0.24	16.00	63.00	1008	1283	35.8	0.19	0.861	0.16
4	28	CM	central vertical shear	1.30	26.50	63.00	1670	2126	46.1	0.61	0.964	0.59
5	28	CM	central vertical shear	3.37	25.00	62.80	1570	1999	44.7	1.69	0.951	1.60
6	42	CM	central vertical shear	1.30	39.00	62.40	2434	3099	55.7	0.42	1.049	0.44
7	42	CM	central vertical shear	2.56	52.00	61.60	3203	4078	63.9	0.63	1.116	0.70
8	50	CM	central vertical shear	2.01	23.00	72.00	1656	2108	45.9	0.95	0.962	0.92
9	50	CM	bedding plane	1.67	39.00	64.00	2496	3178	56.4	0.53	1.055	0.55
10	59	CM	irregular vertical shear	0.91	18.00	61.00	1098	1398	37.4	0.65	0.877	0.57
11	59	CM	central vertical shear	0.75	16.00	61.24	980	1248	35.3	0.60	0.855	0.51
12	59	CM	vertical shear	1.40	31.00	60.17	1865	2375	48.7	0.59	0.989	0.58
13	66	CM	bedding plane	3.64	51.00	60.66	3094	3939	62.8	0.92	1.108	1.02
14	66	CM	central vertical shear	2.22	38.00	62.00	2356	3000	54.8	0.74	1.042	0.77
15	66	CM	vertical shear	3.54	35.00	60.50	2118	2696	51.9	1.31	1.017	1.34
16	22	CM	bedding plane	0.55	28.00	64.30	1800	2292	47.9	0.24	0.981	0.24

17	60	CM	single vertical shear	1.18	24.00	61.50	1476	1879	43.4	0.63	0.938	0.59
Rejecting lowest and highest results, the **mean $I_{s(50)}$ =**												0.65
	90˚ to top of core											
1	1	SS/CM	central vertial shear	0.28	28.00	60.75	1701	2166	46.5	0.13	0.968	0.13
2	2	SS/CM	irregular vertical shear	0.37	18.00	60.89	1096	1395	37.4	0.27	0.877	0.23
3	27	SS/CM	3 vertical shears	0.18	38.00	59.79	2272	2893	53.8	0.06	1.033	0.06
4	25	SS/CM	central vertical shear	0.87	30.00	60.78	1823	2322	48.2	0.37	0.983	0.37
5	58	SS/CM	central vertical shear	1.16	45.50	60.67	2760	3515	59.3	0.33	1.080	0.36
6	7	SS/CM	central vertical shear	0.22	33.50	60.50	2027	2581	50.8	0.09	1.007	0.09
7	7	SS/CM	central vertical shear	0.20	21.50	60.80	1307	1664	40.8	0.12	0.913	0.11
8	24B	SS/CM	central vertical shear	0.95	28.00	61.04	1709	2176	46.6	0.44	0.969	0.42
9	25	SS/CM	central vertical shear	0.69	22.00	60.85	1339	1704	41.3	0.40	0.917	0.37
10	25	SS/CM	central vertical shear	1.71	42.00	60.84	2555	3253	57.0	0.53	1.061	0.56
Rejecting lowest and highest results, the **mean $I_{s(50)}$ =**												0.26
	90˚ to top of core											
1	58	ZS	bedding plane	2.46	49.00	60.65	2972	3784	61.5	0.65	1.098	0.71
2	41	ZS	bent vertical shear	0.65	51.50	60.70	3126	3980	63.1	0.16	1.110	0.18
3	62	ZS	central vertical shear	1.26	27.00	60.20	1625	2070	45.5	0.61	0.958	0.58
4	G	ZS	central vertical shear	2.64	27.00	59.25	1600	2037	45.1	1.30	0.955	1.24
5	G	ZS	central vertical shear	1.36	37.50	60.37	2264	2882	53.7	0.47	1.033	0.49
6	G	ZS	bedding plane	1.24	42.00	60.78	2553	3250	57.0	0.38	1.061	0.40
Rejecting lowest and highest results, the **mean $I_{s(50)}$ =**												0.62
	90˚ to top of core											
1	50	CM	irregular vertical shear	1.59	17.00	60.55	1029	1311	36.2	1.21	0.865	1.05
2	59	CM	vertical shear	0.45	21.00	59.95	1259	1603	40.0	0.28	0.905	0.25
3	60	CM	bedding plane	2.05	47.00	59.40	2792	3555	59.6	0.58	1.082	0.62
4	66	CM	central vertical shear	1.89	21.00	60.75	1276	1624	40.3	1.16	0.908	1.06
5	51	CM	bedding plane	1.00	18.50	60.61	1121	1428	37.8	0.70	0.882	0.62
Rejecting lowest and highest results, the **mean $I_{s(50)}$ =**												0.79

: Discarded extreme low value
: Discarded extreme high value
: Invalid failure mode

Appendix 1.6 Rock Tiaxial Compression Test

Method

The ISRM suggested method Brown (1981) for determining the strength of rock materials in triaxial compression was followed with some minor alterations suggested by the cell manufacturer. Test samples consisted of HQ (61mm) core providing right circular cylinders with a length to diameter ratio of 2.0-3.0:1. As 2.25:1 suits the cell dimensions the best a length of 137.25 mm was aimed for. The ends of the core were cut and ground (where possible) to 0.02 mm flatness and samples were tested as collected (saturation assumed). They were therefore tested at 15 to 25˚ to bedding.

A triaxial Hoek cell was used where axial stress (σ_1) is applied by the loading frame and confining pressure (σ_3) is applied perpendicular to this axial stress by a hydraulic pump (with attached pressure gauge). A rubber membrane inside the cell prevents the hydraulic oil from connecting with the sample but is flexible enough to provide confining pressure. ISRM suggests the use of spherical platens above and below the sample but the instruction manual provided by Terrametrics (1972) recommends the use of a spherical seat on the top only. This reduces instability, insures correct alignment of the sample axis and, with the support of a locked collar on the bottom platen, allows for easier positioning of the cell within the load frame. Draining platens to reduce pore pressure were used above and below the specimen. The Controls 50-C36H2 compression testing machine in the rock mechanics laboratory was again used to provide an axial load.

Once the cell is assembled and the rock specimen was placed inside it with supporting top and bottom platens, it was placed in the centre of the loading frame and connected to the hydraulic pump. Small amounts of axial load were alternatively applied with increments of confining pressure until the required confining pressure was reached. The support collar was then released and the axial load increased continuously at a constant stress rate so that failure occurred within 5 to 15 minutes. As the samples were soft rock the specimens tended to ‘barrel out’(increase diameter) during testing, which increased the confining pressure. The excess pressure was bled off to maintain the confining pressure within 2% of the pre-determined value. The maximum axial load and confining pressure were recorded when the sample failed.

Calculations

Cross-Sectional Area [mm^2] = ((Average Diameter / 2)^2 x Pi

Low confining pressures (1,3,5 MPa) were choosen using the equation:

$\sigma = \rho gh$

where average density (ρ) is 2300 Kgm^3,gravity is 9.8 ms^2 and a maximum depth (h) of 200m.

Triaxial Compressive Strength (MPa) = (Maximum Load [kN] x 1000) / Cross-Sectional Area [mm^2]

Cohesion (C) = b (1 – sin ø) / (2 cos ø)

where b is the y intercept of strength envelope and

Internal friction angle (ø) = arc sin (m – 1) / (m+1)

where m is the gradient of the strength envelope.

Raw Data

Triaxial Test Results

Sample	Litho	Av. Diameter	X-sectional area	Length	Weight	Confining Press.	Failure	Strength	Failure type
		(mm)	(mm)	(mm)	(g)	(MPa)	(kN)	(Mpa)	
23	SS/CM	61.03	2925.34	136.8	972.8	1	97.3	33.26	Shear (Full + broken)
24A	SS/CM	61.12	2933.98	130.31	940.9	3	118.1	40.25	Shear (Full + damp)
24B	SS/CM	61.15	2936.86	133.28	939.5	5	151	51.42	Shear (1/2 + damp)
21A	SS/CM	61.49	2969.61	119	786.3	1	59.3	19.97	Shear (Full/compression + damp)
21B	SS/CM	60.99	2921.51	122	810.9	3	92.2	31.56	Shear (1/2/compression + damp)
19	SS/CM	61.1	2932.06	133.38	891.7	5	107	36.49	Shear (1/2 + Wet)
5	SS/CM	60.7	2893.79	141.16	947.8	1	80.6	27.85	Shear (1/2)
6A	SS/CM	61.06	2928.22	134.26	959.1	3	145.5	49.69	Shear (Full/curved + damp)
6B	SS/CM	61.01	2923.42	127.15	891.6	5	159.4	54.53	Shear (Full + damp)
25	SS/CM	60.88	2910.98	142.5	1054.8	7	175.1	60.15	Shear (Central + bddg)
32A	SS/CM	58.21	2661.25	134.64	850.9	2	84.1	31.60	Shear (Full + wet)
32B	SS/CM	59.82	2810.49	139.95	937.9	4	121.7	43.30	Shear (Full/curved + wet)
38A	ZS	60.94	2916.72	128.8	945.2	3	140.7	48.24	Axial cleavage
38B	ZS	60.55	2879.51	120.65	884.5	5	159.3	55.32	Shear (+small conjugate)
38C	ZS	60.89	2911.94	140.6	1032.5	7	177.9	61.09	Shear (Full)
38D	ZS	60.74	2897.61	135.24	992.1	1	115.7	39.93	Shear (Full)
33A	ZS	60.88	2910.98	137.05	1001.9	1	124.4	42.73	Shear (Full + Jagged-Cataclasis?)
33B	ZS	60.87	2910.02	138.09	1007.9	3	130.8	44.95	Shear (Full)
33C	ZS	60.82	2905.24	138.09	1015.6	5	159.4	54.87	Shear (Full + moist)
B1	ZS	60.91	2913.85	136.46	993.7	1	94.3	32.36	Shear (Full)
B2	ZS	60.76	2899.52	137.81	1008.5	3	124.6	42.97	Shear (Full)
B3	ZS	60.86	2909.07	133.13	970.8	5	151.3	52.01	Shear (Full)

Sample	Litho	Av. Diameter	X-sectional area	Length	Weight	Confining Press.	Failure	Strength	Failure type
		(mm)	(mm)	(mm)	(g)	(MPa)	(kN)	(Mpa)	
51A	CM	60.43	2868.11	128.87	932.8	3	88.5	30.86	Parrallel Shears
51B	CM	60.45	2870.00	120.92	876.3	5	90.7	31.60	Shear (Almost Full)
36A	CM	61.04	2926.30	125.04	892.1	1	47.8	16.33	Shear (Full + damp)
36B	CM	61.05	2927.26	133.44	921	3	45.9	15.68	Shear (1/2 + damp)
67	CM	60.64	2888.07	139.19	985.3	2	122.5	42.42	Compression -Not valid
56	CM	58.78	2713.62	131.97	859.3	4	63.2	23.29	Compression -Not valid
60	CM	60.37	2862.41	133.46	915.7	5	81.4	28.44	Shear (Full/curved)
A1	CM	60.9	2912.89	122.4	876.4	1	71.4	24.51	Shear (Full + damp)
A2	CM	61	2922.47	126.61	914.3	3	87.1	29.80	Shear (Full + damp)
A3	CM	61.02	2924.38	130.34	934.9	5	118	40.35	Shear (Full + damp)
A4	CM	60.98	2920.55	141.93	1018.8	7	109.3	37.42	Shear (1/2 + damp)
29A	CM	60.73	2896.65	122.58	870.7	3	77.9	26.89	Shear(Full + damp)
29B	CM	60.77	2900.47	131.3	937.3	1	65.1	22.44	Shear(3/4 +damp)

: discarded

Scatter graphs showing little correlation between parameters.

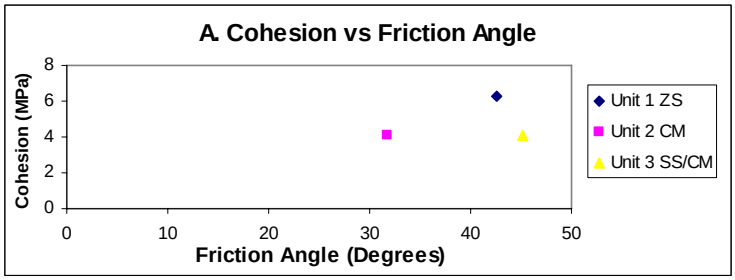

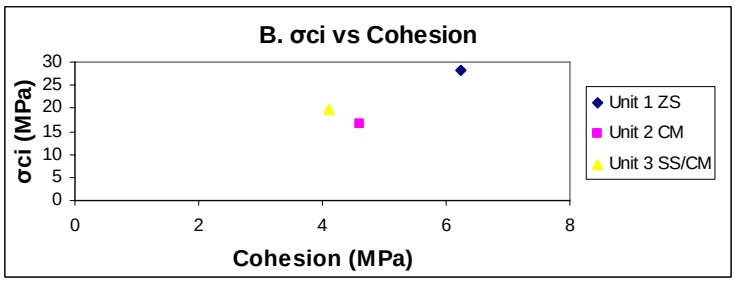

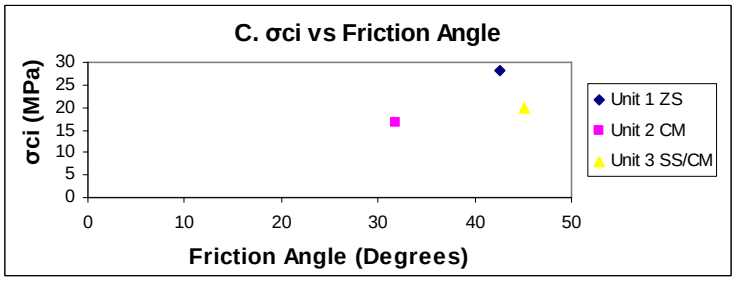

Samples showing no correlation between strength and down hole depth.

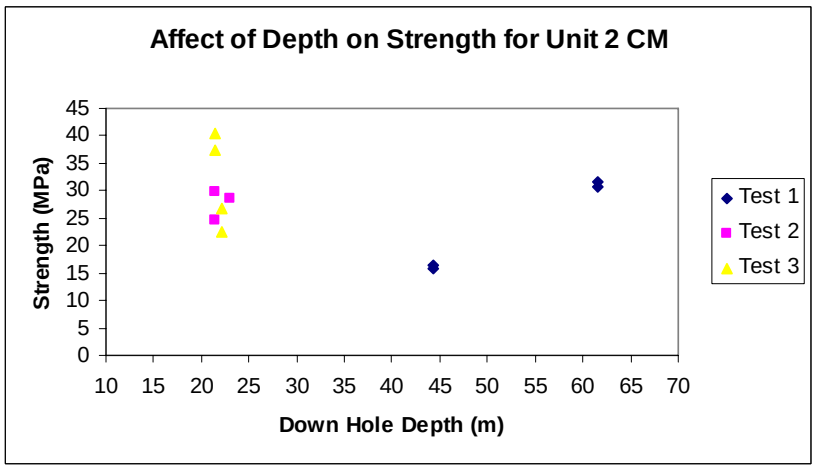

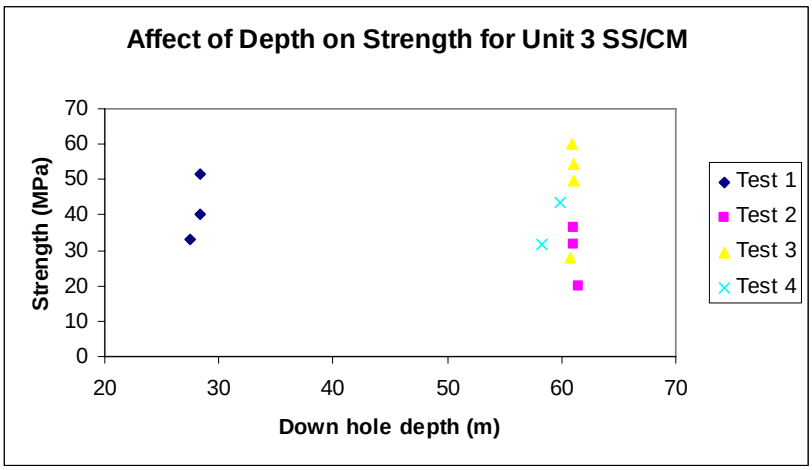

Appendix 1.7 Soil Triaxial Compression Test

The New Zealand Standard (NZS 4402 : 1986) for the determination of the compressive strength of specimens tested in undrained triaxial compression (Soil strength test 6.2) was followed for sample preparation and method. Although there is no New Zealand standard for drained conditions, Bishop and Henkel (1957) state that sample preparation and initial consolidation is performed in exactly the same way as a drained test and the above standard was therefore adapted to ensure no excess pore pressures develop by allowing full drainage.

Method

A remoulded, saturated drained test, with each sample having approximately the same density, was determined appropriate for unit 4. A Tritech ID, 10 kN Compression Test Machine produced by Wykeham Farrace Engineering Ltd was used in the Geomechanics Laboratory in the Civil Engineering Department. The water content of the sample was measured and an appropriate amount of water added to ensure all tests were compacted to the same density (approximately 2000kg/m^3). A rubber membrane was stretched over a metal case and sealed with two rubber rings to the pedestal of the triaxial cell base and a porous stone inserted. The number of layers and amount of tamping was determined by trial and error, in the aim of producing a sample that had consistent compaction along its length. The final method involved five scoops of damp sample being placed in the membrane and tamped 100 times (at the same intensity) between each layer. A porous stone was placed on top and the membrane was attached to the top cap by another two rubber rings.

Once attached, the vacuum was applied and the casing was removed. The sample diameter and length was then measured using digital callipers. The cell was placed carefully over the sample and screwed onto the loading machine. The cell was then filled with water (de-aired water is used throughout the test) and a small amount of cell pressure applied so that the vacuum could be turned off. Some back pressure was then applied and saturation confirmed by checking for air bubbles in a pipe held vertical attached to the vacuum outlet. Volume change is measured by a volume transducer connected to the back pressure outlet and recorded by a digital dial. Displacement was measured by how far the loading ram moved toward the base of the cell by a digital dial gauge.

When the required back pressure had been applied and volume change and displacement become stable the test was started. The computer linked to the triaxial cell and loading machine recorded

these measurements along with axial load, back pressure and cell pressure. Axial load is measured by an immersed load-cell within the triaxial cell. Cell and back pressures are measured by electronic pressure transducers. The values were graphed instantly so that failure or peak strength could be observed and happened within approximately 5 to 10 minutes. The load was then released and the cell drained and dismantled. The sample was carefully removed from the membrane, weighed, dried and re-weighed so that saturated and dry density could be calculated.

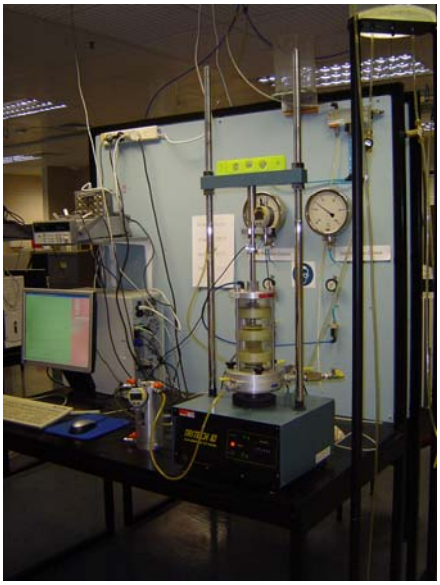

Calculations

These equations can be found in most soil mechanic text books, in particular Barnes (2000) and Craig (1997).

Wet Density [g/cm^3] = Wet Mass [g] / Volume [cm^3]

Dry Density [g/cm^3] = Dry Mass [g] / Volume [cm^3]

Cross-Sectional Area [mm^2]: A_0 = ((Average Diameter [mm] / 2)^2 x Pi

Volume [mm^3]: V_0 = A_0 x (Average Height [mm])

Cell Pressure [kPa] = σ_3

Back Pressure [kPa] = u

Deviator Stress = $\sigma_1 - \sigma_3$

Effective Stress: $\sigma' = \sigma - u$

Axial Strain: ε_1 = Displacement [mm] / Height [mm]

Volumetric Strain: ε_v = (Volume Change [ml] – First Volume Change Reading) / V_0

'Corrected'Area [mm^2] = A_0 ((1 - ε_v) / (1 - ε_v))

Calculated from readings at 1/3 the maximum deviator stress:
Young's Modulus: E = Deviator stress [kPa] / ε_1

Poisson's Ratio: $\upsilon = 0.5 (1 – (\varepsilon_v / \varepsilon_1))$

Friction Angle: ø [Degrees] = arc tan (gradient of Mohr failure envelope) x 180 / Pi

Raw Data (Test Summaries)

Test No.	Sample	Dry Density (gm/cm^3)	Wet Density (gm/cm^3)	Cell Pressure σ_3 (kPa)	Back Pressure (kPa)	σ_1 (kPa)	Max Deviator σ_1-σ_3	Effective Stresses σ_3' (kPa)	σ_1' (kPa)
1	10	1.68	2.03	100.00	100.00	125.52	25.52	0.00	25.52
2	10	1.64	1.94	100.00	100.00	116.59	16.59	0.00	16.59
7	20	1.76	2.09	100.00	100.00	103.19	3.19	0.00	3.19
4	10	1.61	1.89	200.00	100.00	472.62	272.62	100.00	372.62
5	10	1.72	2.01	200.00	100.00	536.35	336.35	100.00	436.35
8	20	1.74	2.08	200.00	100.00	317.31	117.31	100.00	217.31
6	10	1.69	1.95	300.00	100.00	890.96	590.96	200.00	790.96
3	10	1.68	1.95	300.00	100.00	947.12	647.12	200.00	847.12
9	20	1.71	2.04	300.00	100.00	892.87	592.87	200.00	792.87

Sample	**10**	**20**
Average Water Content (%)	12.0	8.4

Appendix 1.8 Sonic Velocity

Method

The first method (high frequency ultra sonic pulse technique) of the ISRM suggested methods for determining sound velocity (Brown, 1981) was followed to determine the dynamic elastic modulii of the units tests by measuring the travel times of p- and s-waves. A Model 1007H Seismic Analyser connected to a Trio 40 MHz Oscilloscope (CS-1040) was used in the Rock Mechanics Laboratory of the Civil Engineering Department. The settings are illustrated in figures a and b.

Figure A Set up for Seismic Analyser (Finnemore, 2000)

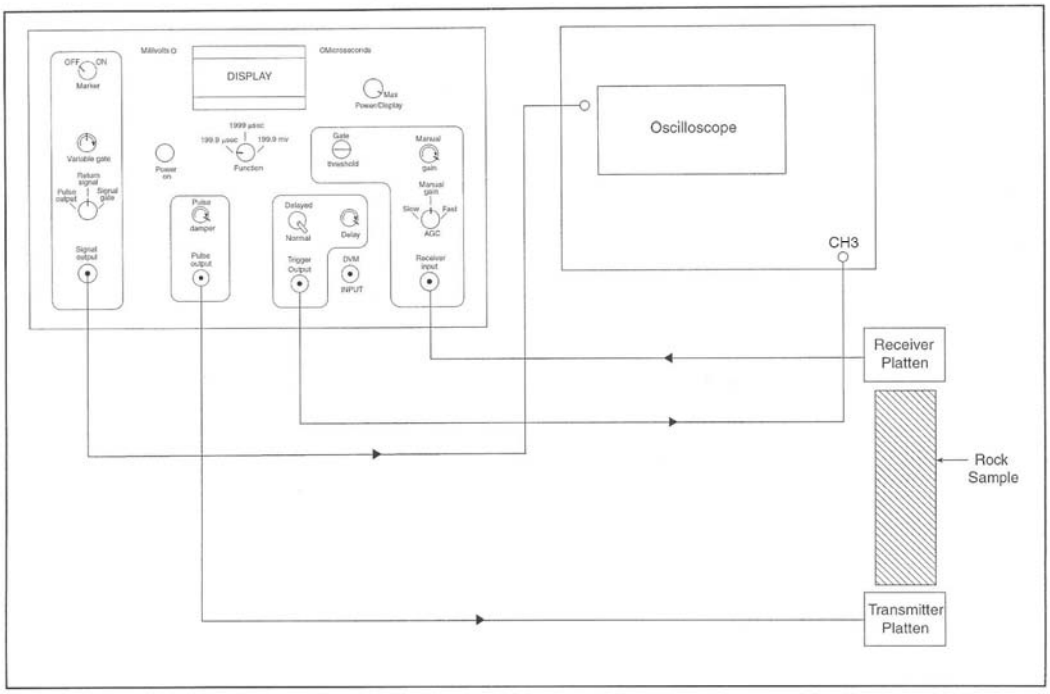

Figure B Set up for Oscilloscope when using Seismic Analyser (Finnemore, 2000)

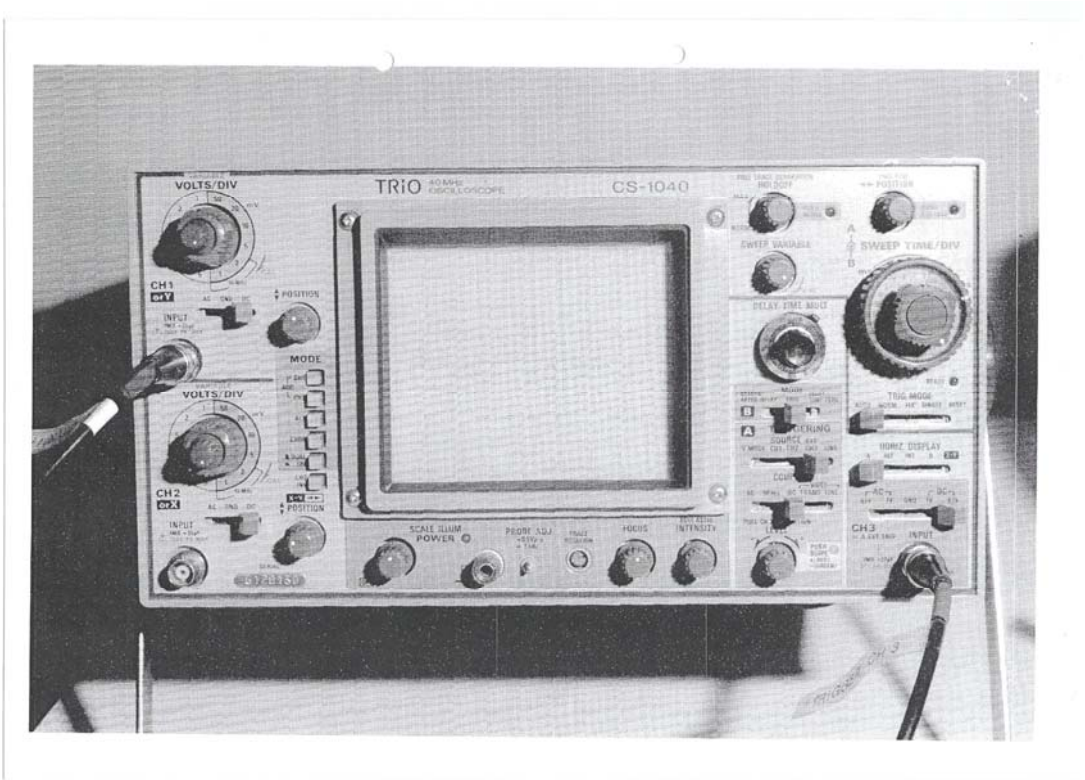

Off cuts of core and samples prepared for point load testing were mainly used as they produced stronger waves than the longer core samples. Samples less then 30 mm long were not used as errors are introduced when approaching the wavelength of the core itself. Care was taken not to

cause any mechanical damage when preparing the sample and tests were conducted under in-situ moisture content (saturation assumed).

The seismic analyser was calibrated regularly using an aluminium rod within known travel times. Both ends of the core and the transmitter and receiver platens were coated with a thin film of Vaseline to aid coupling. When this was not enough to produce an obvious wave the core with the platens on each end were placed in the loading frame and less than 2 kN of compression was applied. The travel time for the compression or p-waves is displayed on the seismic analyser (in μs) and can be checked by reading off the first arrival which gives a positive going peak on the oscilloscope. The platens were then swapped with those for the shear or s-waves and the procedure repeated. It is necessary to subtract the delay time of the platens from the values recorded to give the true travel time.

Calculations

From ISRM (Brown, 1981):
P-wave velocity: V_p [m/s] = Sample length [mm] / P-wave travel time [s]
S-wave velocity: V_s [m/s] = Sample length [mm] / S-wave travel time [s]

From Finnemore (2000) and Johnson and DeGraff (1988):

Poisson's Ratio: $\nu = 1 - (V_p^2 / 2(V_p^2 - V_s^2))$

Young's Modulus: $E\ [GPa] = \rho V_s^2 (3V_p^2 - 4V_s^2) / (V_p^2 - V_s^2)$

Raw Data (Shaded squares = discarded values)

Sample	Unit	Diam (mm)	Mass (g)	Volume (m^3)	Density (kg/m^3)	P-wave travel time (μs)	S-wave travel time (μs)	Length (mm)	P-wave velocity V_p (m/s)	S-wave velocity V_s (m/s)	Poisson's ratio *v*	Young's modulus E (GPa)
67	CM	60.21	321.60	0.00013	2423.83	28.00	58.00	46.60	2647.73	932.00	0.43	6.02
F	CM	60.98	1142.70	0.00046	2492.75	66.00	170.00	156.96	2823.02	968.89	0.43	6.71
56	CM	57.90	381.40	0.00016	2383.66	72.00	125.00	60.77	986.53	519.40	0.31	1.68
28	CM	60.50	402.80	0.00017	2432.15	44.20	72.00	57.61	1704.44	900.16	0.31	5.15
51	CM	60.61	141.80	0.00006	2503.67	16.00	43.50	19.63	3505.36	552.96	0.49	2.28
50	CM	60.55	127.30	0.00005	2367.91	17.60	31.60	18.67	2593.06	791.10	0.45	4.29
59	CM	59.95	154.50	0.00005	3090.59	19.70	39.40	17.71	1904.30	564.01	0.45	2.85
60	CM	59.40	327.00	0.00014	2408.18	31.00	82.00	49.00	2378.64	662.16	0.46	3.08
66	CM	60.72	157.50	0.00007	2414.16	18.00	37.30	22.53	2964.47	768.94	0.46	4.18
										Average:	0.39	4.53
62	ZS	60.20	187.90	0.00008	2214.53	26.00	75.00	29.81	1910.90	444.93	0.47	1.29
16	ZS	60.50	436.30	0.00018	2465.79	34.00	75.00	61.55	2608.05	918.66	0.43	5.95
G	ZS	60.66	1071.20	0.00042	2549.60	53.00	100.00	145.38	3412.68	1580.22	0.36	17.36
58	ZS	60.65	354.30	0.00015	2440.53	30.80	58.30	50.25	2463.24	999.01	0.40	6.83
41	ZS	60.70	154.70	0.00007	2328.37	23.00	54.00	22.96	1822.22	499.13	0.46	1.69
										Average:	0.40	10.05
30	SS/CM	60.70	378.20	0.00017	2283.26	52.00	135.00	57.24	1375.96	450.71	0.44	1.34
52	SS/CM	60.19	374.00	0.00015	2469.78	31.00	95.00	53.22	2583.50	611.72	0.47	2.72
D	SS/CM	60.92	1015.40	0.00042	2396.53	74.00	152.00	145.36	2285.53	1009.44	0.38	6.73
24B	SS/CM	61.04	207.40	0.00009	2400.90	24.00	51.00	29.52	2170.59	686.51	0.44	3.27
25	SS/CM	60.85	167.80	0.00007	2367.69	22.00	55.00	24.37	2100.86	518.51	0.47	1.87
26	SS/CM	60.84	342.20	0.00013	2690.50	28.00	58.00	43.75	2485.80	875.00	0.43	5.89
										Average:	0.43	4.17
7	SS	60.73	236.70	0.00010	2317.50	12.00	105.00	35.26	22037.50	363.51	0.50	0.92
7	SS	60.22	150.20	0.00007	2273.06	34.00	85.00	23.20	983.05	301.30	0.45	0.60
19	SS	61.20	299.70	0.00013	2249.03	11.90	150.00	45.30	30200.00	319.01	0.50	0.69
21B	SS	60.8	242.6	0.00010	2330.80	11.8	110	35.85	25607.14	351.47	0.50	0.86
										Average:	0.50	0.82

Appendix 1.9 Direct Shear Test

Method

The ISRM suggested method for laboratory determination of direct shear strength as published by Brown (1981) was applied to three bedding shears in unit 2 and one high angle shear in unit 3. The test measures peak direct shear strength as a function of stress normal to the sheared plane. Although five tests of the same specimen are preferred by ISRM, only two or three were carried out as the successive tests gradually wear the surface smooth and it therefore not a true test of shear strength after several tests.

The core sample was held together by wrapping it in plastic wrap which also prevented it from drying out. The bottom carrier was filled with wet plaster and the core suspended in it by means of a metal rack. This was done in such a way that the shear plane was horizontal. This was left to set and then wet plaster was poured into the other half and the set half placed upside down on top so that the both ends of the core were encapsulated. A zone of at least 5mm either side of the shear plane was left from plaster.

As the carrier was coated with Vaseline before the plaster was poured, the set plaster and core easily slid out and was transferered to the Robertson Geologging Portable Shear Box in the rock mechanics laboratory, civil engineering department. The plastic wrap was cut along the line of the shear so that the top was free to move relative to stationary bottom. The sample was then consolidated by applying the normal load chosen for the test, by a NIKE® hydraulic pump. Again low normal loads were chosen due to the relatively shallow nature of the proposed excavation. The preliminary displacement measurement was taken and the shear force was applied by another hydraulic pump at a constant rate so that shear displacement took place at 0.5mm per minute. A measurement of displacement (mm) and shear force (kN) was recorded every minute until shear force was no longer increasing. The sample was then returned to its original position and the test repeated at a different normal force.

Calculations

Area of oval shear surface [m^2] = (Pi x length [mm] x width [mm] / 4) / 1000000

From ISRM (Brown, 1981):

Normal Stress [MPa] = (Total normal force [kN] / Area of shear surface [m^2]) / 1000

Shear Stress [MPa] = (Total shear force [kN] / Area of shear surface [m^2]) / 1000

Raw Data

Sample	**37**
Unit	CM
Oval length (mm)	60
Oval width (mm)	70
X-sectional area (m^2)	0.0033

Normal Stress (MPa)	0.6063		1.5158		2.2736	
Shear Stress (MPa)	0.0606		0.3032		0.6063	
Normal Force (kN)	2		5		7.5	
Time min	Shear kN	Distance mm	Shear kN	Distance mm	Shear kN	Distance mm
0	0	6.21	0	4.92	0	5.22
1	0	6.31	0	4.93	0	5.26
2	0	7.31	0.2	4.94	0.3	5.28
3	0	8.92	0.6	5.67	1	5.41
4	0.2	10.25	0.9	7.31	1.1	5.82
5	0.2	11.52	1	8.04	1.1	5.92
6	0.2	12.81	1	9.08	1.1	6
7	0.2	14.69	1	9.68	1.2	6.03
8	0.2	15.42	1	10.54	1.2	6.1
9	0.2	16.14	1	12.5	1.2	6.18
10	0.2	17.68	1	14.04	1.3	6.42
11			1	15.55	1.4	6.56
12			1	16.31	1.4	6.61
13					1.4	6.67
14					1.4	6.73
15					1.5	6.88
16					1.7	7.03
17					1.8	7.11
18					1.8	7.17
19					1.8	7.22
20					1.8	7.3
21					1.8	7.31
22					1.8	7.45
23					1.8	7.59
24					1.9	7.66
25					1.9	7.86
26					1.9	7.94
27					1.9	8.13
28					2	8.28
29					2	8.36
30					2	8.38
31					2	8.57
32					2	8.69
33					2	8.84
34					2	9.05
35					2	9.29
36					2	9.49
37					2	9.68
38					2	9.8
39					2	9.93
40					2	10.2

41						
42						
43						
44						
45						

14
SS/CM
105
60
0.0049

11
CM
75
52.5
0.0031

0.4042		1.0105		1.5158		0.6467		1.6168	
0.2021		0.6467		1.2126		0.1617		0.5659	
2		5		7.5		2		5	
Shear kN	Distance mm	Shear kN	Distance mm	Shear kN	Distance mm	Shear kN	Distance mm	Shear kN	Distance mm
0	8.41	0	8.85	0	7.78	0	10.64	0	12.38
0.5	8.51	0	8.9	0	7.78	0.2	10.68	0.5	12.81
0.7	8.52	0.75	9.2	0.9	7.89	0.4	11.64	1	14.4
0.9	8.53	1	9.3	1	7.96	0.5	13.7	1.3	15.98
1	8.72	1	9.4	1.2	8	0.5	15.05	1.4	17.3
1	9.35	1.2	9.51	2	8.11	0.5	15.8	1.4	17.89
1	9.7	1.2	9.63	2.1	8.17	0.5	17.56	1.4	18.013
1	10.18	1.2	9.78	2.42	8.26	0.5	18.24	1.6	18.4
1	10.64	2	9.92	2.75	8.38	0.5	20.02	1.75	18.65
1	11.1	2	10.08	2.8	8.44			1.75	18.94
1	12.6	2	10.27	3	8.62			1.75	19.15
1	13.08	2	10.45	3.2	8.92			1.75	19.39
1	14.95	2	10.68	3.2	9.33			1.75	19.73
		2	10.85	3.3	9.72			1.75	20.12
		2	11.03	3.3	10.13			1.75	20.48
		2	11.17	3.4	10.62				
		2.1	11.3	3.6	10.8				
		2.1	11.53	4	11.22				
		2.3	11.7	4	11.46				
		2.3	11.83	4.1	11.78				
		2.3	11.97	4.5	12.2				
		2.3	12.14	4.5	12.47				
		2.3	12.31	4.9	12.85				
		2.3	12.35	4.95	13.18				
		2.3	12.58	5	13.58				
		2.3	12.9	5	14.13				
		2.4	13.07	5.3	14.6				
		2.5	13.61	5.6	15.18				
		2.75	14	5.75	15.44				
		3	14.49	5.75	15.66				
		3	14.97	6	16.33				
		3.1	15.47	6	16.69				
		3.1	15.85	6	17.49				
		3.1	16.26	6	18.01				
		3.2	16.7	6	18.94				
		3.2	16.96	6	19.88				
		3.2	17.21						
		3.2	17.8						

49
CM
63
62
0.0031

0.6519		1.6299		2.4448	
0.2934		0.3912		0.6193	
2		5		7.5	
Shear kN	Distance mm	Shear kN	Distance mm	Shear kN	Distance mm
0	6.42	0	5.95	0	5.26
0	6.6	0.5	6.43	0	5.28
0.2	6.9	0.9	7.6	0.5	5.43
0.3	7.28	1	8.9	0.75	5.6
0.4	7.48	1	9.51	1	5.98
0.5	7.6	1	10.54	1	6.44
0.6	7.7	1	11.53	1.1	7.16
0.7	7.84	1	12.44	1.1	7.57
0.8	8.03	1	13.25	1.2	7.8
0.9	8.26	1	13.92	1.2	7.9
0.9	8.51	1	14.25	1.3	7.95
0.9	8.7	1.1	15.5	1.3	8.06
0.9	9	1.1	15.7	1.3	8.16
0.9	9.42	1.2	15.83	1.3	8.23
0.9	10.98	1.2	15.98	1.3	8.4
0.9	11.63	1.2	16.12	1.5	8.63
0.9	12.25	1.2		1.5	8.75
0.9	12.9	1.2	16.42	1.5	8.85
0.9	13.51	1.2	16.55	1.6	8.98
0.9	14.39			1.6	9.06
0.9	14.7			1.6	9.11
0.9	15.5			1.7	9.32
0.9	16.92			1.7	9.62
				1.7	9.88
				1.8	10.25
				1.8	10.5
				1.8	10.72
				1.8	11.04
				1.9	11.3
				1.9	11.42
				1.9	11.71
				1.9	12.04
				1.9	12.5
				2	12.91
				2	13.32
				2	13.8
				2	14.19
				2	14.57
				2.1	15.05
				2.2	15.4
				2.5	16
				2.5	16.52
				2.6	17.01

				2.75	18
				2.8	18.51
				2.8	19.22

Appendix 1.10 Core Sample Information

Drill Hole	Box No.	Sample No.	From (m)	To (m)	Interval (m)	Unit
654	1	1	12.48	12.74	0.26	3 SS/CM
654	1	2	12.74	12.96	0.22	3 SS/CM
654	1	3	13.26	13.52	0.26	3 SS/CM
654	1	4	14.17	14.38	0.21	3 SS/CM
654	2	5	16.56	16.76	0.2	3 SS/CM
654	2	6	17.58	17.88	0.3	3 SS/CM
660	1	7	6.5	6.71	0.21	3 SS/CM
660	2	8	11.49	11.59	0.1	3 SS/CM
660	3	9	12.85	13.03	0.18	3 SS/CM
653	1	10	12.6	12.93	0.33	4 SS
653	2	11	16.93	17.12	0.19	2 CM
653	4	14	23.81	24	0.19	3 SS/CM
658	1	16	11.49	11.8	0.31	1 ZS
658	2	17	14.17	14.37	0.2	3 SS/CM
658	2	18	16.55	16.8	0.25	3 SS/CM
658	3	19	18.56	18.81	0.25	3 SS/CM
658	4	20	20.2	20.38	0.18	4 SS
658	5	21	23.2	23.4	0.2	3 SS/CM
658	5	22	24.86	24.97	0.11	2 CM
658	6	23	27.46	27.67	0.21	3 SS/CM
658	7	24	28.4	28.71	0.31	3 SS/CM
658	8	25	31.61	31.84	0.23	3 SS/CM
658	9	26	33.07	33.3	0.23	3 SS/CM
656	1	27	15.3	15.57	0.27	3 SS/CM
656	2	28	17.93	18.13	0.2	2 CM
656	3	29	22.1	22.45	0.35	2 CM
656	4	30	25.1	25.5	0.4	3 SS/CM
656	5	31	27.16	27.39	0.23	3 SS/CM
662	5	32	34.63	34.94	0.31	3 SS/CM
662	6	33	36.65	37.14	0.49	1 ZS
662	7	35	41.99	42.19	0.2	3 SS/CM
662	8	36	44.27	44.64	0.37	2 CM
662	9	37	45.72	45.9	0.18	2 CM
662	10	38	49.7	50.3	0.6	1 ZS
662	13	41	57.13	57.55	0.42	1 ZS
662	14	42	60.5	60.68	0.18	2 CM
662	15	43	63.44	63.85	0.41	2 CM
662	16	44	64.98	65.19	0.21	2 CM
662	17	58	67.81	67.94	0.13	3 SS/CM & 1ZS
663	8	47	42.99	43.19	0.2	2 CM
663	9	48	43.94	44.25	0.31	3 SS/CM
663	10	49	53.67	53.8	0.13	2 CM
663	12	50	56.99	57.22	0.23	2 CM
663	13	51	61.22	61.55	0.33	2 CM

663	14	52	62.8	63.34	0.54	3 SS/CM
663	16	56	70.51	70.76	0.25	2 CM
657	3	59	20.95	21.12	0.17	2 CM
657	4	60	23	23.29	0.29	2 CM
657	5	61	27.78	27.97	0.19	1 ZS
657	6	62	29.9	30.11	0.21	1 ZS
657	7	63	33.01	33.25	0.24	1 ZS
657	9	65	38.42	38.6	0.18	3 SS/CM
657	10	66	40.61	40.75	0.14	2 CM
657	12	67	46.42	46.62	0.2	2 CM
656	3	A	21.51	22.1	0.59	2 CM
657	7	B	31.59	32.11	0.52	1 ZS
658	8	D	32.5	32.78	0.28	3 SS/CM
662	16	E	64.53	64.83	0.3	2 CM
662	16	F	65.19	65.38	0.19	2 CM
662	10	G	50.3	50.68	0.38	1 ZS

Location of Drill Holes

HOLEID	Easting	Northing	Elevation
643	328021.29	725401.24	239.02
644	327999.77	725450.93	235.45
645	328192.17	725258.58	268.79
646	328093.39	725314.13	261.38
647	328119.68	725210.56	276.88
648	328138.32	725240.00	272.95
649	328131.00	725271.13	268.37
650	328162.00	725254.39	266.59
653	327464.12	725096.94	229.06
654	327552.13	725104.82	230.39
655	327503.73	725045.88	230.27
656	327565.78	725164.80	229.52
657	327549.15	725239.12	227.88
658	327509.44	725144.79	228.71
660	327518.65	725068.63	229.60
661	327616.84	725139.93	230.29
662	327466.82	725228.14	226.67
663	327512.29	725304.47	225.62
664	327478.68	725022.09	231.49
664A	327480.81	724992.92	231.99
664B	327481.73	724977.23	232.54

Appendix 2: Rock Mass Characterisation

Table of Contents

Appendix 2.1 Surveyed Scanline Locations

Eastings	Northings	Height	Name
327309.01	724693.24	282.94	1a
327336.71	724674.11	282.89	1b
327325.51	724696.10	267.26	2a
327343.65	724685.19	267.79	2b
327325.77	724701.60	270.91	3a
327332.42	724711.44	271.04	3b
327351.56	724688.33	262.04	4a
327340.49	724701.42	259.11	4b
327353.19	724719.57	257.59	4c
327301.08	724503.39	291.38	5a
327300.72	724535.11	287.09	5b
327301.66	724549.13	287.00	5c
327802.32	725176.79	263.14	6a
327813.13	725165.88	262.06	6b
327811.59	725159.94	259.35	7a
327818.54	725145.06	259.11	7b
327942.38	725062.97	279.67	8a
327973.87	725053.25	283.76	8b

The scanlines are numbered 1-8, and a and b indicates the start and finish, in the direction along which they were measured. The heights are relative to sea level and were measured from a peg at the bottom of the outcrop beneath the scanline

Appendix 2.2 Scanline Survey Sheet

Geological Society Engineering Group Working Party (Anon, 1977)

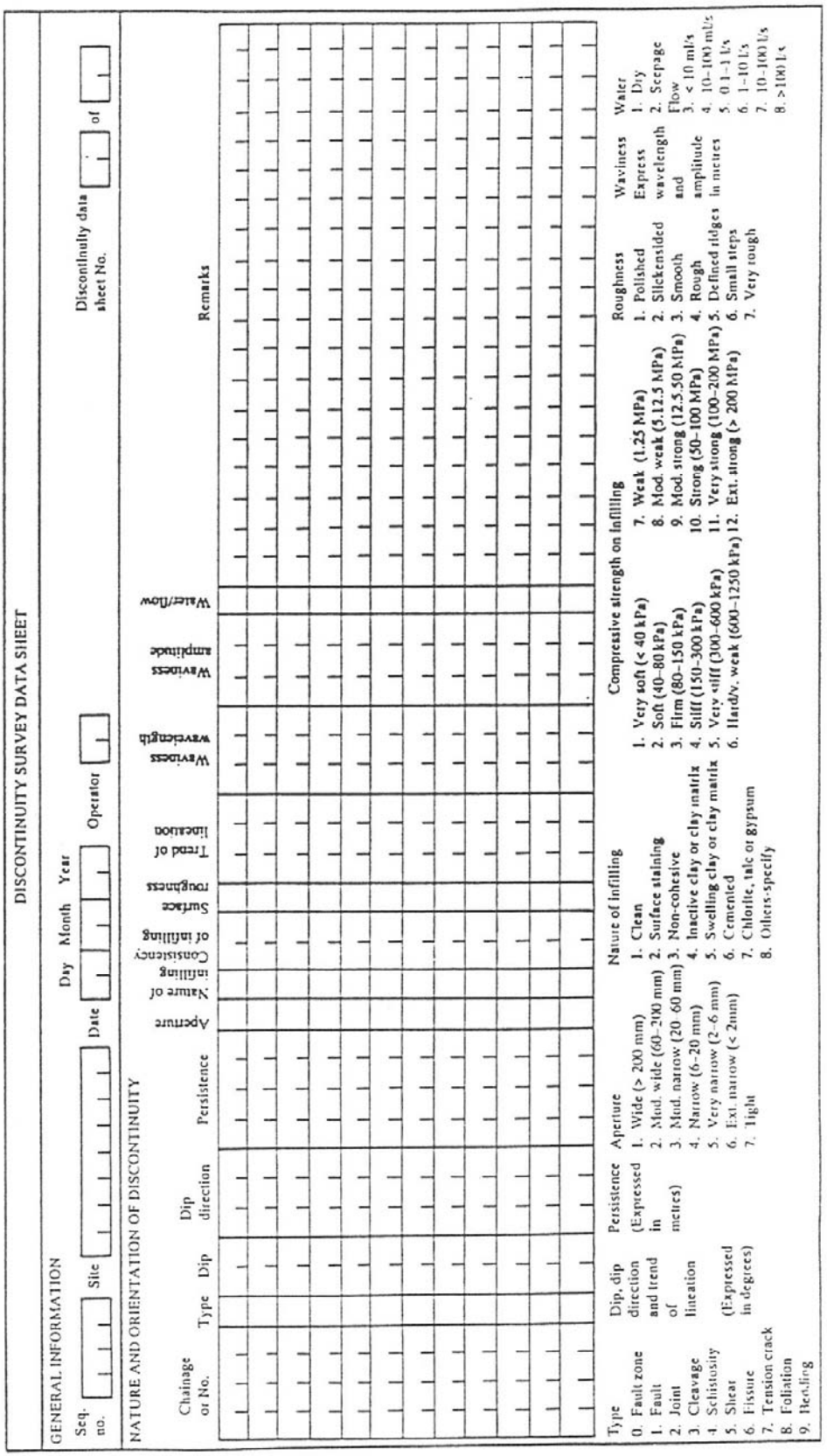

DISCONTINUITY SURVEY DATA SHEET

GENERAL INFORMATION

Seq. no. | | | | Site | | | | | | | | Date | | Day | Month | Year | Operator | | Discontinuity data sheet No. | | of | |

NATURE AND ORIENTATION OF DISCONTINUITY

Chainage or No.	Type	Dip	Dip direction	Persistence	Aperture	Nature of infilling	Consistency of infilling	Surface roughness	Trend of lineation	Wayiness wavelength	Waviness amplitude	Water/flow	Remarks

Type
0. Fault zone
1. Fault
2. Joint
3. Cleavage
4. Schistosity
5. Shear
6. Fissure
7. Tension crack
8. Foliation
9. Bedding

Dip, dip direction and trend of lineation (Expressed in degrees)

Persistence (Expressed in metres)

Aperture
1. Wide (> 200 mm)
2. Mod. wide (60–200 mm)
3. Mod. narrow (20–60 mm)
4. Narrow (6–20 mm)
5. Very narrow (2–6 mm)
6. Ext. narrow (< 2mm)
7. Tight

Nature of Infilling
1. Clean
2. Surface staining
3. Non-cohesive
4. Inactive clay or clay matrix
5. Swelling clay or clay matrix
6. Cemented
7. Chlorite, talc or gypsum
8. Others-specify

Compressive strength on infilling
1. Very soft (< 40 kPa)
2. Soft (40–80 kPa)
3. Firm (80–150 kPa)
4. Stiff (150–300 kPa)
5. Very stiff (300–600 kPa)
6. Hard/v. weak (600–1250 kPa)
7. Weak (1.25 MPa)
8. Mod. weak (5.12.5 MPa)
9. Mod. strong (12.5.50 MPa)
10. Strong (50–100 MPa)
11. Very strong (100–200 MPa)
12. Ext. strong (> 200 MPa)

Roughness
1. Polished
2. Slickensided
3. Smooth
4. Rough
5. Defined ridges
6. Small steps
7. Very rough

Waviness
Express wavelength and amplitude in metres

Water
1. Dry
2. Seepage Flow
3. < 10 ml/s
4. 10–100 ml/s
5. 0.1–1 l/s
6. 1–10 l/s
7. 10–100 l/s
8. >100 l/s

Appendix 2.3 Scanline Data

Definitions

Rock Type	ss = sandstone (f/m/c) lss =laminated sandstone ms = mudstone (carb-cm/high carb-HCM) zs = siltstone co = coal (So/D/Md/Mbri/Bri) HAC =high ash coal p = pyrite cg =conglomerate GGB = Greenland Group Basement		
Defect Type	fz = fracture fault f = fault j = joint c = cleavage b = bedding s = shear cz = crush zone	*Persistence* (Terminations)	x = extends outside exposure r = terminates in rock d = terminates against another

Infilling	**Nature**	**Strength**
	1 = clean	vs = very soft
	2 = air	s = soft
	3 = surface staining	f = firm
	4 = non-cohesive	st = stiff
	5 = sand	vst = very stiff
	6 = clay	w = weak
	7 = cemented	vw = very weak
	8 = gouge/breccia	str = strong
	9 = detritus	vstr = very strong
	10 = evaporites	

Roughness (small scale)	p = polished slick = slickensides sm = smooth rgh = rough dr = defined ridges ss = small steps vr = very rough	*Water*	d = dry s =seepage f = flow	dp = damp (low/med/high)
(intermediate scale)	st = stepped un = undulating pl = planar c =curved ir =irregular	*Strength*	Schmidt hammer (mean of highest 5/10) Weathering Manual index	

Scanline Survey Data Sheets

Traverse Number:	1	Length:	33.7m	Orientation:	124/06 SE	Date:	19/04/05	Location:	Sheet no. 1 of 2

No.	Distance (m)	Rock Type	Defct Type	Defct Set	Total Spcng	Spcng (m)	Dip	Dip Direction	Hardness vh	h	m	s	vs	Strength	Persistence (m)	Top	Btm	Aperture (mm)	Infilling Nature	Strength	Roughness Nature	JRC	Waviness λ(m)	Amp	i	Water	Notes
1	0.50	lss	j	A			58	74 NE			x			R2	1.10	d	d				pl/sm	6				d	Case hardening weaker than first scanline
2	1.50	lss	j	B	1.00		76	5 NE			x			R2	1.10	d	d				c/sm	4				d	Dripping clay covers face
3	1.60	lss	j	A	0.10	0.10	66	62 NE			x			R2	0.70	d	x				pl/sm	5				d	
4	1.70	lss	j	B	0.10	0.15	80	350 NW			x			R2	1.00	d	d				c/sm	4				d	
5	1.85	lss	j	A	0.15	0.25	66	87 NE			x			R2	1.00	d	d	3	6/mos	vs	pl/sm	6				d	
6	2.00	lss	b	C	0.15		14	317 NW			x			R2	25.00	x	x				pl/sm	3				d	Boundary between cm bove and lss below
7	3.00	lss	j	A	1.00	1.50	72	84 NE			x			R2	2.50	d	d				un/rgh	14				d	
8	3.70	lss	j	A	0.70	0.20	66	83 NE			x			R2	0.35	d	x				c/sm	8				d	
9	4.00	lss	j	E	0.30		85	264 SW		x	x			R3	0.20	r	x				pl/rgh	8				d	Thin case hardening
10	4.20	lss	j	A	0.20	0.60	69	78 NE		x	x			R3	0.50	r	d				pl/sm	5				d	
11	5.60	lss	j	D	1.40		90	34 N			x			R2	2.00	d	d				c/sm	7				d	
12	5.80	lss	j	D	0.20	0.15	64	14 N			x			R2	0.30	r	x	2	2		pl/sm	4				d	
13	5.90	lss	j	D	0.10	0.05	59	3 N		x	x			R3	0.50	r	x	1	6	5	c/sm	5				d	
14	6.40	lss	j	F	0.50		55	166 SE			x	x		R1	0.60	r	d				pl/sm	3				d	Thin clay layer on surface
15	9.00	lss/cm	b	G	2.60	1.00	11	310 NW			x	x		R1	25.00	x	x	1	2		pl/sm	4				d	
16	9.40	cm	b	C	0.40	0.50	18	318 NW			x			R1	5+	r	x				pl/sm	5				d	Bed in sandstone
17	9.50	lss	j	B	0.10		86	21 NE		x				R2	0.70	d	x				c/sm	2				d	May be undersampled
18	10.00	lss	j	B	0.50		82	355 NW		x				R2	0.60	d	x				c/sm	3				d	
19	10.90	lss	j		0.90		59	80 NE			x	x		R3	0.80	d	d	3	6		c/sm	4				d	
20	11.30	lss	j		0.40		90	27 N		x				R2	2.00	r	r				c/sm	7				d	Cuts both beds
21	11.50	lss	j	A	0.20		68	74 NE			x			R2	0.70	r	r		6		pl/sm	3				d	
22	12.50	lss	j		1.00		45	310 NW			x	x		R1	0.70	d	d				pl/slic	3				dp	
23	13.00	lss	j	B2	0.50		84	354 NW			x			R2	0.90	r	d	8	6		c/sm	6				d	20/04/2005
24	13.50	lss	b	C	0.50	1.00	14	326 NW				x		R1	?	x	r				pl/sm	2				d	
25	14.00	lss	j		0.50		76	356 NW		x				R2	0.50	d	x	4	9/3		pl/sm	2				d	
26	14.50	lss	j		0.50	0.60	76	326 NW		x				R2	0.40	d	r	0.05	2		c/sm	2				d	
27	15.50	cm	j		1.00			42 NE			x	x		R2	0.60	d	x		3		un/c	12				d	Dip 35-70 (curved)
28	16.50	cm	j		1.00	0.20	89	154 SE				x		R0	0.50	d	r	8	2		pl/rgh	8				d	
29	16.60	cm	j		0.10		71	44 NE			x			R2	0.50	r	d		3		st/rgh	18				d	
30	18.90	lss	j		2.30		59	82 NE	x					R3	0.60	d	r				c/sm	8				f	Case hardening from running water
31	19.00	cm/lss	b		0.10		13	310 NW		x				R2	5.00	x	r		3		pl/sm	2				d	
32	19.40	lss	j	A?	0.40		49	56 NE						R3	5.00	d	r				un/rgh	15				s	
33	22.00	ls	j	A	2.60		84	74 NE			x			R1	0.70	d	d	5	6		c/sm	3				d	
34	22.10	lss/cm	b		0.10		16	336 NW			x			R1	2.00	r	x				pl/rgh	8				d	
35	22.70	cm/lss	j		0.60		76	338 NW			x	x		R1	0.70	d	d	2	6		c/sm	8				d	Cuts both beds
36	23.40	lss	j		0.70		61	319 NW			x			R2	0.20	d	r		3		pl/sm	2				d	
37	23.50	lss	j		0.10		73	225 SW			x			R2	1.50	r	x	5	2		v rgh		0.8	0.2		d	A lot of carb beds
38	24.00	lss	j		0.50		78	170 SE			x	x		R2	0.80	d	x	1	6		pl/sm	7				d	**Orientation: 121/06SE**

Traverse Number:	1	Length:	33.7m	Orientation:	121/06 SE	Date:	20/04/05	Location:	Sheet no. 2 of 2

No.	Distance (m)	Rock Type	Defct Type	Defct Set	Total Spcng	Spcng (m)	Dip	Dip Direction		Hardness vh	h	m	s	vs	Strength	Persistence (m)	Top	Btm	Aperture (mm)	Infilling Nature	Strength	Roughness Nature	JRC	Waviness λ(m)	Amp	i	Water	Notes
39	24.35	lss	j		0.35		86	80	NE			x			R2	0.90	d	x	1	6	5	ir/sm	16				d	
40	24.60	lss	j		0.25		75	334	NW			x			R1	0.7	d	d				st/rgh	17				d	
41	24.70	lss	j		0.10		75	54	NE			x			R2	1	d	x				un/sm	9				d	High level of carb material + schm info
42	24.90	lss	j		0.20		50	62	NE			x			R2	0.5	d	x				un/sm	9				d	
43	25.00	lss	j		0.10		86	331	NW			x			R2	1	d	x	0.05	tight		pl/rgh	8				d	
44	25.25	lss	j		0.25		82	340	NW			x	x		R2	1.5	r	x	2-10	6		pl/rgh	8				d	
45	25.45	lss	j		0.20		64	62	NE		x				R1	0.5	d	d				c/wavy	14				d	
46	26.20	lss	j		0.75		78	326	NW			x			R2	0.5	d	d	4	6		pl/rgh	8				d	Schm hammer data
47	26.60	lss	j		0.40		66	58	NE			x			R2	1	d	d	2-5	2/3		c/rgh	10				d	
48	27.30	cm	b		0.70		9	324	NW				x		R1	8	x	x				pl/st	16				d	lss below
49	27.60	lss	j		0.30		64	59	NE		x				R2	0.5	x	d				pl/sm	6				d	case hardened yellow colour
50	28.70	lss	j		1.10		82	154	SE			x			R2	2	d	x				pl/sm	6	2	0.25		d	
51	29.10	lss	j		0.40		82	29	NE			x			R3	0.4	r	x				pl/sm	8				d	
52	31.30	cm	b		2.20		16	309	NW				x		R1	5	x	x				pl/sm	4				dp	Curves up dip
53	33.70	cm	f		2.40		86	285	NW				x		R1	2	x	x	20	8		un/vr					d	Beds above turned up (photo 6-7)
																												0m = 2417365/5899157±17m
																												33.7m = 2417374/5899150±12m

Scanline Survey Data Sheets

Traverse Number: 2	Length: 21m	Orientation: 114/06 NEE	Date: 19/04/05	Location: Hollarans	Sheet no. 1 of 1

No.	Distance (m)	Rock Type	Defct Type	Defec (from	Defct Set	Total spcng	Spcng (m)-set	Dip	Dip Direction		Hardness vh	h	m	s	vs	Strength	Persistence (m)	Top	Btm	Aperture (mm)	Infilling Nature	Strength	Roughness Nature	JRC	Waviness λ(m)	Amp	i	Water	Notes
1	5	cm	b	B	A			16	315	NW				x		R2	18.00	x	x		1		pl/sm	3				dp	Granule ss above fg ss
2	5.55	lss	j	A	B	0.55	0.5	76	71	NE		x				R3	0.66	d	r	1	3		pl/sm	7				f	Carb beds, case hardened (weathering)
3	5.6	lss	j	C2	C	0.05	0.5	82	164	SE			x	x		R2	0.58	r	r		1		pl/sm	9				f	Lots of moss
4	6.1	lss	j	A	B	0.5	0.5	77	81	NE		x				R2	0.77	d	r	5	2		pl/sm	8				f	Case hardened, fine grained
5	6.3	lss	j	C2	C	0.2	0.5	71	160	SE			x	x		R2	0.30	r	r		1		pl/sm	8				f	Googy clay covering face
6	6.45	cm	b	B	A	0.15	0.05	20	324	NW			x			R2	5.00	r	x		1		pl/sm	4				f	Thin carb bed on surface
7	6.6	lss	j	A	B	0.15	0.5	70	85	NE		x				R3	0.90	d	r	2	5	soft	c/sm	11				f	
8	7.35	lss	j	A	B	0.75	0.7	77	75	NE		x				R3	1.50	d	x		1		c/sm	8				f	
9	7.55	lss	j	A	B	0.2	0.1	78	67	NE		x				R3	1.90	d	x	2	1		c/sm	6				f	
10	7.85	lss	j	A	B	0.3	0.3	71	58	NE		x				R3	1.00	d	d		1		c/sm	6	1.5	0.25		dp	
11	8.15	lss	j	A	D	0.3		50	86	E		x				R3	1.20	d	r		1		pl/sm	6				d	
12	9	lss	j	A	B	0.85	1.3	79	82	NE		x				R3	2.00	d	r		3	Str	c/sm	7				dp	
13	9.2	lss	j	C	E	0.2	0.25	65	360	N		x				R3	0.70	x	d				ir/rgh	16	0.7	0.1		s	
14	9.5	lss	j	A	B	0.3	0.5	71	82	NE		x				R3	1.40	x	d	1	1		c/sm	6				dp	
15	9.55	lss	j	C	E	0.05	0.15	84	14	N		x				R3	0.70	r	d				c/rgh	14				dp	
16	9.65	lss	j	A	B	0.1	0.1	73	79	NE		x				R3	2.00	d	d				c/sm	6	3	0.3		d	Curves at bottom 46
17	10.25	lss	j	A	B	0.6	0.5	78	89	NE		x				R3	1.30	d	r				c/sm	6	2	0.2		d	Curves at bottom 52
18	11.5	cm	b	B	A	1.25	2	19	303	NW			x	x		R2	20.00	d	x				c/rgh	7	10	0.5		d	Hard layer in ss with fg ss interbedded with cm below
19	12.2	lss/cm	b	B	A	0.7	0.2	20	299	NW			x			R1	20.00	d	x				c/rgh	8	10	0.5		d	Changes from ss to cm **Orientation: 121/02 NEE**
20	13	cm	j	?	F	0.8	0.3	42	299	W		x				R1	1.50	d	x	1	3		pl/sm	3				d	
21	13.2	cm	j	B	F	0.2	0.2	24	291	W		x				R1	1.50	d	x				pl/sm	3				d	
22	13.9	ms	j	C	G	0.7	0.2	84	354	NW		x				R1	0.50	d	x	1	2		un/rgh	9				d	Possible water conduit but dry now (all G)
23	14.55	cm	j	C	G	0.65	0.4	74	344	NW				x		R0	0.90	d	x				ir/rgh	16				d	
24	14.7	cm	j	C	G	0.15	0.3	83	334	NW					x	R0	0.80	r	x	5	3/5	w/st	ir/rgh	17				d	Orange coloured infill (fg sand)
25	14.85	cm	j	C	G	0.15	0.15	90	331	NW					x	R0	0.60	r	x	5-10	3/5	w/st	ir/rgh	17				d	
26	15.2	cm	j	C	Ha	0.35		74	11	N			x			R1	0.60	r	r	5	2		pl/sm	2				d	
27	15.35	cm	j	C2	I	0.15		83	159	SE			x			R1	0.40	d	r	1	3		c/vsm	2				d	Infilling dark brown
28	15.5	cm	j	A	Hb	0.15		51	70	NE			x			R1	0.20	d	r				c/sm	4				d	
29	15.65	cm	j	C2	I	0.15	0.35	88	145	SE			x			R1	0.95	d	x	1	3		c/sm	4				d	
30	16.65	cm	cz	C2	I	1	0.4	77	184	SE			x			R1	3.00	d	x	2-30	2		c/rgh	16	1.5	0.4		d	
31	16.7	cm	c	A2		0.05		80	270	W							<1												
32	16.9	cm	c	C2		0.2		83	181	S							<1												Messy fractured mudstone with small
34	17.7	cm	c	A		0.8		77	56	NE							<1												joints that do not penetrate larger walls
33	18.5	cm	c	C		1.6		82	341	NW							<1												(this a few of more significant ones)
35	18.4	cm	c	A		0.7		76	67	NE							<1												
36	20.5	cm	c	C2		2		84	174	SE							<1												
																													0m = 2417416/5899173±40m
																													21m = 2417433/5899164±40m

Traverse Number:	3				Length:	11.5m	Orientation:	215/02SW			Date:	21/04/05	Location:	Lower bench east facing Hallorans											
No.	Distance	Rock	Defct	Defct	Total	Spcng	Dip	Dip		Hardness					Strength	Persistence			Aperture	Infilling		Roughness		Waviness			Water	Notes
	(m)	Type	Type	Set	Spcng	(m)		Direction		vh	h	m	s	vs		(m	Top	Btm	(mm)	Nature	Strength	Nature	JRC	λ(m)	Amp	i		Photos 10 and 11
1	0		j	A			77	68	NE							7	x	x									s	2417383/5899159±34m
2	1.9		j	C2	1.9		64	160	SE							7	x	x									d	
3	2.5		j	C2	0.6		72	156	SE							3	d	x									d	curved
4	3		j	A	0.5		46	74	NE							2	d	x									dp	curved
5	3.4		j	A	0.4		84	67	NE							2	d	x									d	
5	4.4		j	C2	1		61	162	SE							2	d	x									d	
7	7		j	C2	2.6		62	178	SE							8	x	x									s	
8	7.4		j	A	0.4		76	80	NE							3	d	x									d	
9	7.9		j	A	0.5		72	97	SE							1	d	x									d	
10	8		b	B	0.1		2	195	SW							2	r	r									d	
11	8.5		j	A	0.5		75	86	NE							2	d	d									d	
12	8.6		j?	C2	0.1		71	138	SE							2	d	d									d	
13	9		j	A	0.4		80	94	SE							2	x	d									d	
14	9.2		j	C2	0.2		76	170	SE							2	d	d									d	
15	9.8		j	A	0.6		85	82	NE							2	d	x									d	
16	10		j	C2	0.2		72	160	SE							1	d	x									d	
17	10.3		j	A	0.3		84	74	NE							2	d	x									d	
18	11.1		j	C2	0.8		74	150	SE							2	d	x									d	
19	11.5		j	C2	0.4		77	166	SE							6	x	x									F	2417391/5899165±34m

Traverse Number 4 Length: 43							Orientation:							140/13W	Date: 13/12/05			Location: Bottom of opencast						Sheet no. 1 of 1
No.	Distance (m)	Rock Type	Defct Type	Defct Set	Spcng (m)	Dip	Dip Direction	Hardness vh	h	m	s	vs	Strength	Persistence (m)	Top	Btm	Aperture (mm)	Infilling Nature	Strength	Roughness Nature	JRC	Waviness λ(m)	Amp	i	Water	Notes
1	0	lss	B	A		9	283	NW				x	x	R1	3	x	x				pl/sm	4				d	E2417422/N5899161±20m
2	0.7	lss	J	B	1	75	60	NE				x		R1	1.3	x	x				c/ir	11				d	
3	1.1	lss	J	C		75	159	SE				x		R1	1.7	x	x		3		c/ir	12				d	
4	4.4	cm	J	B		86	248	SW					x	R0	0.5	x	x				ir/rgh	16				d	
5	4.7	cm	B	A		9	354	NW				x		R1	3	x	x		3		pl/sm	7				d	
6	5.55	lss	J	C		86	168	SE			x			R3	1.5	r	x	1	1		pl/sm	5				d	
7	5.9	lss	J	C		86	175	SE		x	x			R3	4.5	x	x	10	6		pl/ir	5				d	
8	6.7	lss	J	B		72	246	SW				x		R2	0.8	d	x				ir/rgh	16				d	
9	7.4	lss	J	B		71	95	SE		x	x			R3	4.5	x	x				pl/ir	13				d	
10	7.6	lss	B	A		12	354	NW			x			R2	3.2	r	x				sm/pl	2				d	
11	7.75	lss	J	C		84	344	NW			x			R2	0.9	d	x	3	2		sm/pl	5				d	
12	8.6	lss	J	B		70	262	SW			x			R2	0.5	d	x				sm/pl	7				d	
13	8.6	lss	J	C		88	163	SE				x		R1	1.3	r	x	10	2		sm/pl	6				d	
14	9.1	cm	J	E		70	150	SE				x		R0	0.6	d	x				st/pl	8				d	
15	9.3	cm	J	D		60	258	SW				x		R1	0.5	d	x				c/pl	6				d	
16	10	lss	J	B		68	249	SW		x	x			R3	0.8	r	d				un	15				d	
17	10.53	lss	J			70	40	NE		x	x			R2	2.5	d	d		3		ir/rgh	4				d	**129/14SW**
18	11.25	lss	J			86	81	NE		x	x			R2	3	x	r	2	2		c/sm	3				d	
19	11.9	lss/c	J			82	308	NW							2.3	r	x				pl/ir	12				d	
20	12.8	lss	J			65	94	SE		x				R3	3.5	x	r	2-50	6		pl/st	4				d	
21	13	lss	J			73	43	NE		x				R3	3	x	d				ir/c					d	
22	13.96	lss	J			76	74	NE		x				R3	3	d	d	1-20	2		pl/ir					d	**165/7NW** E2417409/N5899178±16m
23	13.96	lss	J			86	14	NE		x				R3	2.7	d	d				ir/st					d	
24	15.3	lss	J			72	82	NE		x				R3	2.7	d	d				ir/st					d	
25	15.6	lss	J			76	109	SE		x				R3	1	r	r	1	2		sm/pl	2				d	
26	16	lss	J			64	35	NE		x				R3	2.5	d	x				un/ir	14				d	
27	16.5	lss	J			59	125	SE		x				R3	2.5	d	x	2	6		sm/c	3				d	
28	19.35	lss	J			84	83	NE		x				R3	2	d	x	10	2		pl/sm	2				d	
29	19.7	lss	J			79	112	E			x	x		R2	2.8	d	x				sm/pl	4				d	
30	19.8	lss	J			71	145	SE		x				R3	2.2	d	x				pl/sm	4				d	**035/05NE**
31	20.2	lss	J			65	165	SE		x				R3	1.3	d	x				st/sm	4				d	
32	21.1	lss	J			73	72	NE		x				R3	2.8	d	x	5-20	2		sm/pl	8				d	
33	21.3	lss	J			86	73	NE		x				R3	1.3	d	d				sm/c	4				d	
34	21.4	lss	J			82	82	NE		x				R3	0.5	d	x				cr/un	17				d	
35	21.5	lss	J			57	163	SE			x	x		R2	1.2	d	x				sm/pl	3				d	
36	21.8	lss	J			67	158	SE		x				R3	1.2	d	x				ss/pl	5				d	
37	22.1	lss	J			66	156	SE		x				R3	1.5	r	x				c/sm	4	1.5	0.2		d	
38	23.3	lss	J			76	163	SE		x	x			R2	2.3	d	x				c/ir	8				d	
39	23.4	lss	J			68	82	NE		x				R3	2.1	d	d				sm/pl	3				d	
40	23.5	lss	J			13	343	NW				x		R1	5	r	x				sm/pl	4					Mudstone bed
41	25	lss	J			82	153	SE		x				R1	4.5	x	x	1-20	6		sm/pl	6				d	**25.57m = 040/06N**
42	25-29.8	lss	J			64	125	SE																		d	
43	29.85	lss	J			72	91	E			x			R1	8	x	x	1-4	6		un/sm	4				d	To top of cliff (goes through cm too)
44	29.85-3	lss	J			74	128	SE													sm/pl	6				d	**34.57m = 037/05N**
45	39.2	lss	J			66	154	SE			x	x		R1	8	x	x	5	3		sm/pl	4				d	
46	39.2	lss	J			66	85	E		x				R3	1.8	d	x	10	2		sm/pl	2				d	
47	39.65	lss	J			82	205	S			x			R2	1.8	D	X				sm/pl	2				d	
48	40	lss	J			68	92	E		x				R3	1.6	r	x	1-20	2		pl/un	14				d	
49	40.2	lss	J			84	181	S		x				R3	1.6	r	x				pl/un	14				d	43.33m = E2417411/N5899179±15m

Traverse Number:	5	Length:	32m	Orientation:	005/03NE	Date:	21/04/05	Location:	Ridge line Hallorans	Sheet no. 1of 2

No.	Distance (m)	Rock Type	Defct Type	Defct Set	Total Spcng	Spcng (m)	Dip	Dip Direction	Hardness vh	h	m	s	vs	Strength	Persistence (m)	Top	Btm	Aperture (mm)	Infilling Nature	Strength	Roughness Nature	JRC	Waviness λ(m)	Amp	i	Water	Notes
																											Joints in lss and ss may be from flowingwater down face
1	1.2	lss	j	C			79	8 NE		x	x			R1	0.4	d	d	1	3		pl/sm	5				d	Occasional carb bed
2	1.3	cm	b	B	0.1		7	356 NW			x	x		R1	2	x	d				pl/sm					d	
3	1.6	lss	j	C	0.3		87	5 NE			x			R1	1.5	r	r				pl/rgh	13				d	
4	1.9	cm	j	?	0.3		45	106 SE			x			R2	0.5	x	x	1	2/3		c/sm	8				d	
5	2	cm	j	A	0.1		74	86 NE		x				R2	0.3	x	x		3		pl/sm					d	
6	2.6	lss/cm	j	?	0.6		86	206 SW		x				R2	1.5	d	r	3	2		c/sm					d	
7	2.65	lss	f	C	0.05		81	336 NW			x			R1	3	r	x	cz, 2-20	8	s/w	c/slick		1.00	0.15		d	Cuts cm/lss, dies out in ss
8	2.8	lss	j	?	0.15		60	30 NE			x			R2	0.5	d	d	5	2/3		pl/sm	5				d	Band of high freq carb beds
9	2.9	lss	j	C2	0.1		80	134 SE			x	x		R1	0.5	d	d				c/rgh	15				d	Band of high freq carb beds
10	3	lss	j	A2	0.1		50	37 NE			x			R2	0.5	d	d	2	2/3		pl/sm	6				d	Band of high freq carb beds
11	4.15	cm/lss	f	A	1.15		75	150 NE			x	x		R1	2	d	x	0.05	8		c/sm					d	Off set 11cm (branches at top)
12	4.75	cm/lss	f	C	0.6		72	24 NE			x			R2	2	r	x	5	8		un/sm					d	Off set 3cm
13	5.2	lss	j	A	0.45		60	65 NE		x	x			R2	1	x	d				vr	16				d	
14	6.15	lss	j	?	0.95		78	126 SE		x	x			R3	1	x	d				vr	16				d	
15	6.2	cm	f	C	0.05		84	337 NW				x		R0	1.5	r	r	10	8/6		c/sm					d	Off set 3cm, dies out in lss above
16	6.4	cm	f	C	0.2		82	340 NW							1	r	x	2	yellow 6		c/rgh					d	Off set 2cm, dies out in lss above
17	6.8	cm	j	A	0.4		88	95 E		x				R3	0.4	x	x		3		pl/rgh	8					
18	7.5	cm/lss	f	C2	0.7		61	155 SE							3	r	r	1	3/8		c/un					d	Off set 8cm
19	10.25	cm/lss	f	C	2.75		80	345 NW							3	r	r	3	8		pl/sm					d	
20	10.4	cm	j	A	0.15		65	76 NE		x	x			R3	1	d	x		3		pl/rgh	12				d	Off set 23cm
21	11	cm/lss	f	C2	0.6		40-(	160 SE							1	r	r	10	2		c/sm					d	conjugate fault **Orientation: 003/07 NE**
22	11.4	cm/lss	j	A	0.4		74	75 NE		x				R3	2	d	d		3		pl/sm	8				d	case hardeneing, orange colour, **sample 24/1/1**
23	12.7	cm/lss	j	C2	1.3		80	156 SE		x	x			R3	1	r	d	2	6		c/sm					d	schm hammer data
24	14.4	cm/lss	j	C2	1.7		64	145 SE			x	x		R1	2.5	d	x	2	3/2		c/sm		0.80	0.05		d	Splits at top and curves (39 dip)
25	15	lss	j	A	0.6		70	75 NE		x	x			R1	1.5	d	x	1	2		pl/sm	6				d	
26	15.2	lss	j	?	0.2		62	238 SW		x	x			R2	0.5	d	x				st	12				d	
27	15.8	lss	j	C2	0.6		83	148 SE				x		R1	0.5	d	r				c/sm	5				d	
28	15.9	lss	j	?	0.1		76	200 S			x	x		R1	1	d	x	3	2		c/ir	8				d	
29	16.1	lss	j	A	0.2		65	82 NE				x		R1	1	x	x				c/ir	8				d	Black substance on face
30	17.85	lss	j	C2	1.75		85	175 SE				x		R1	1.2	r	x				ir/c		1.00	0.20		d	
31	18.1	lss	j	A	0.25		66	93 SE				x		R1	0.8	x	x				sm/pl	4				d	Top of unit
32	20.8	lss	j	A2	2.7		76	265 W		x	x			R2	0.5	r	x				pl	12				d	
33	21.15	lss	j	C2	0.35		87	162 SE			x	x		R1	0.6	x	x				pl/sm					d	Covered in moss
34	21.7	lss	j	?	0.55		65	302 NW			x	x		R1	0.5	d	d				pl/sm	8				d	**Orientation at 21.8m: 008/08 NE**
35	23	lss	j	A	1.3		66	66 NE			x	x		R1	1	x	x				c/sm	6				d	
36	24.3	lss	j	?	1.3		62	307 NW				x		R1	0.4	d	r				ir	9				d	
37	24.7	lss	j	A2	0.4		65	267 W			x	x		R2	1	r	x	0.05	2		c/ir	10				d	
38	26.5	cm/lss	f	C	1.8		86	352 NW							1.4	r	x	0.05	8							d	Off set 3cm
39	27.3	cm/lss	f	C2	0.8		70	175 SE							1.2	d	x	1	6		c/ir					d	Off set 4cm
40	27.8	lss	j	A2	0.5		85	274 SW				x		R1	1.5	r	d	1	2		st					d	
41	27.9	cm/lss	f	C	0.1		86	345 NW							3	x	x	200	8/9							d	Off set 1m (sub vert carb beds messed around)
42	28.9	lss	j	A	1		69	72 NE			x			R2	1	x	r	2	fine grain 5		ir	8				d	
43	29.2	lss	j	C	0.3		81	5 NE				x		R1	0.8	d	r				c/st	10				d	
44	29.75	cm/lss	f	C2	0.55		87	165 SE							1.5	r	x	1	8							d	Off set 2cm, 2cm zone altered (**photo 13 & 14**)
45	29.9	lss	j	A	0.15		70	53 NE				x	x	R1	1	r	d				c/ir	7				d	
46	30.3	lss	j	?	0.4		58	115 SE				x	x	R1	1	r	d				c/ir	7				d	
47	30.5	cm	j	C	0.2		82	35 NE		x				R3	0.4	d	x				pl/sm	4				d	
48	30.6	cm/lss	f	?	0.1		54	350 NW							3	r	x	wedge	8							d	Off set 1.10m
49	31	lss	j	?	0.4		51	270 W					x	R1	1.5	x	x	2	3		c/sm					d	0m = 2417358/5898967±11m
50	31.85	lss	j	C2	0.85		86	168 SE					x	R1	1	x	r				ir					d	32m = 2417378/5898978±12m

Traverse Number:	5	Length:	14.45m	Orientation:	030/15NE	Date:	16/06/05	Location:	Extented Section	Sheet no. 2 of 2

No.	Distance (m)	Rock Type	Defct Type	Defct Set	Total Spcng	Spcng (m)	Dip	Dip Direction		Hardness vh	h	m	s	vs	Strength	Persistence (m)	Top	Btm	Aperture (mm)	Infilling Nature	Strength	Roughness Nature	JRC	Waviness λ(m)	Amp	i	Water	Notes
																												Photos 40-41
1	0.8	cs	j	C			63	324	NW					x	R0	1.4	x	x		6		ir					d	
2	1.8	cs	j	A	1		42	289	W					x	R0	0.3	x	r		6		sm/pl	2				d	
3	1.8	cs	j	?	0		84	350	N					x	R0	0.5+	r	x		6		cr/sm	2				d	
4	1.8	cs	j	?	0		40	77	NE				x		R0	0.4	r	x		3		sm/ir	6				d	
5	2.7	cs	j	A	0.9		74	74	NE					x	R0	1.3	x	x				cr/sm	2				d	**Trend 346/13 NW**
6	3.5	cs & cm	j	C	0.8		72	10	NE					x		3	x	r	3	6		pl/sm	5				d	Fault? Cuts both units
7	4.65	cs & cm	f	C	1.15		73	4	NE							2.6	x	r		1		ir/un					d	
8	5	cm	b	B?	0.35		38	260	SW			x			R1	0.6	x	x	3	2		ir/pl	8				d	
9	5.4	cm	j	C	0.4		61	14	NE			x			R1	0.4	d	r				ir/pl	7				d	
10	5.8	cm	j	A	0.4		70	87	NE			x			R1	0.4	d	r		3		ir/pl	7				d	
11	5.85	cs	j	C	0.05		85	350	NW				x		R0	1.7	r	d		3		sm/cr	2				d	
12	5.85	cs & cm	j	A	0		66	69	NE							1.2	r	r		3		ir/st					d	Cuts both units
13	6.5	cs & cm	j	?	0.65		74	113	SE							1.5	r	x		3		pl/sm					d	
14	8.4	cs & cm	f	C	1.9		79	341	NW							3.5	r	x	5	8		un/pl					d	**Trend 015/07 NE**
15	8.65	cs & cm	j	A	0.25		77	73	NE							2	x	x				ir/sm					d	
16	9.6	cm	j	C	0.95		76	360	N			x			R1	0.3	r	x	2	6		cr/sm	2				d	May extend further
17	9.65	cm	b	B?	0.05		20	241	SW			x			R1	0.5	x	x	0.5	2		st/sm	3				d	
18	10.25	cs & cm	f	C	0.6		84	342	NW							2.6	x	x	10-50	8		pl/sm					d	Only small offset
19	10.4	cs & cm	j	A	0.15		76	72	NE							2	x	x	2	2		pl/ir					d	
20	11.8	cs & cm	j	C	1.4		84	359	N							2.2	x	x				cr/ir					d	Fault?
21	11.9	cs	j	C	0.1		77	36	NE			x			R1	1.5	r	r	20	2		pl/cr					d	
22	12.3	cs & cm	j	C2	0.4		90	184	S							1	x	r				pl/un					d	
23	12.3	cs & cm	j	A	0		84	81	E							1	x	x				pl/sm					d	
24	12.9	cs & cm	j	C2	0.6		67	154	SE							1	x	x	5	2		pl/ir					d	
25	12.9	cm	j	A	0		82	67	NE			x			R1	0.5	x	r	1	6		pl/sm	2				d	
26	13.25	cm	j	C2	0.35		74	186	S			x			R1	0.8	x	r	5	2		sm/pl	4					
27	13.4	cm	j	A	0.15		81	75	NE			x			R1	1.6	x	x	1	6		ir/rgh						
28	14.45	cm	j	C	1.05		86	340	NW			x			R1	1.4	x	x	3	6		ir/rgh						
																												46.45m = 2417373/5899009±17m

Traverse Number:	6	Length:	15.65m	Orientation:	324/16	Date:	15/06/05	Location:	other side of valley	Sheet no.	1 of 1

No.	Distance (m)	Rock Type	Defct Type	Defct Set	Total Spcng	Spcng (m)	Dip	Dip Direction		Hardness					Strength	Persistence			Aperture	Infilling		Roughness		Waviness			Water	Notes
										vh	h	m	s	vs		(m)	Top	Btm	(mm)	Nature	Strength	Nature	JRC	λ(m)	Amp	i		
1	0	cm	j	A			67	172	SE		x	x			R0	1	x	d	3	2		sm/cr	2				d	
2	0	cm	b	B	0	1	4	333	NW			x			R0	20	x	x	1	6	w	st/pl	2				d	
3	0.8	cm	j	C	0.8		45	330	NW			x	x		R0	0.5	r	x	10-20	8	w	cr/slick	3				d	SHZ???
4	0.9	cm	j	A	0.1		66	222	SW				x		R0	0.7	d	x	2	3		pl/ir	5				d	
5	1.1	cm	j	A	0.2	0	80	200	S			x			R0	1	d	d	2	2, 3		pl/ir	14				d	
6	1.5	cm	j	D	0.4		63	305	W			x			R0	1	d	x				st/ir	20				d	
7	2.6	cm	j	D	1.1		54	292	NW			x			R0	0.5	d	r	0	1		cr/pl	2				d	
8	3.4	cm	j	E	0.8		88	305	NW		x	x			R1	0.9	d	x	0	1		cr/pl	6				d	
9	3.4	cm	j	A?	0		62	246	SW			x			R1	0.6	d	x	0			st/pl	18				s	
10	4.2	cm	j		0.8		75	350	NW				x		R0	3	d	x	150	9	w	st/cr	18	2	0.3		d	Cuts across bedding
11	4.2	cm	j	A	0		81	224	SW				x		R0	3	d	x				ir/rgh					d	
12	4.9	cm	j		0.7		76	317	NW				x		R0	1.4	d	x	3	2		sm/pl	2				d	
13	5.45	cm	j		0.55		80	173	SE			x			R1	4	r	r	5	2		pl/cr		2	0.5		d	
14	6	cm	j		0.55		65	250	SW				x		R0	0.6	d	d				ir/st	8				d	
15	8	cm	j		2		71	199	S		x				R3	1.3	x	d	2	3		sm/cr	2	1	0.2		d	Length = 8-9.5m along face/scanline
16	8.1	cm	j		0.1		81	154	SE				x		R0	2	d	d				ir/rgh					d	
17	9	cm	j		0.9		65	235	SW			x			R1	1	d	x				pl/st	14				d	
18	9.5	cm	j		0.5		86	179	SE			x			R1	3.5	d	x	5	3, 6	w	sm/cr	2				d	
19	11.3	cm	j		1.8		69	314	NW			x			R3	1.5	d	x				st/pl	10				d	
20	12.1	cm	j		0.8		83	209	S			x			R2	1.2	x	x		3		st/pl	5				d	
21	13.4	cm	j		1.3		70	216	S			x			R2	3.6	x	x	300	9		sm/pl	4				d	
22	15.65	cm	j		2.25		80	310	W			x			R2	2.5	x	x		3		cr/ir					d	

Traverse Number:	7	Length:			16.9		Orientation:			330/05		Date:	16/06/05			Location:	Next to 5								Sheet no.	1 of 1
No.	Distance	Rock	Defct	Defct	Total	Spcng	Dip	Dip		Hardness					Strength	Persistence				Aperture	Infilling		Roughness		Waviness			Water	Notes
	(m)	Type	Type	Set	Spcng	(m)		Direction		vh	h	m	s	vs		(m)	Top	Btm	(mm)	Nature	Strength	Nature	JRC	λ(m)	Amp	i		Photos 42-44
1	0	cs & cm	j				77	156	SE							5	x	x	500	2		pl/sm	5				d	Fault?????
2	0.2	cs & cm	j		0.2		83	40	NE							3	x	x	1500			ir/st					d	
3	4	cs	j		3.8		56	54	NE			x			R1	3.6	d	x	1500	2, 9		cr/sm	4				d	
4	5	cs	j		1		77	214	SW			x			R2	1.2	d	x		3		sm/pl	2				d	**At 5.6m =Trend 345/06**
5	5.9	cm	j		0.9		84	245	SW			x			R2	1.4	d	x				sm/pl	2				d	
6	7.35	cm	j		1.45		79	145	SE			x			R3	1.7	d	x	1	1		un/ir	12				d	
7	7.6	cm	j		0.25		74	79	NE			x			R3	1.4	d	x				sm/ir	5				d	
8	7.65	cm	j		0.05		76	186	S			x			R3	0.5	d	x		1		st/sm					d	
9	7.7	cm	j		0.05		79	160	SE			x			R3	1.7	d	x	20	6		pl/sm	3				d	Fault ?
10	8	cm	j		0.3		84	60	NE			x			R3	0.8	d	x		3		pl/sm	6				d	Same failure (nice square)
11	8	cs	j		0		5	58	NE			x			R3	0.3	x	d		3		pl/sm	6				d	Same failure (nice square)
12	8.35	cm	f		0.35	0.5	67	332	NW			x			R3	6	x	x	20	6		pl/sm	6				d	Fault ?
13	8.4	cs	j		0.05	0.2	88	174	SE			x			R3	0.8	d	x		3		pl/sm	6				d	Same failure (nice square)
14	8.9	cs	j		0.5		85	348	NW			x			R3	0.8	d	x				pl/ir	3				d	Same failure (nice square)
15	9	cs	j		0.1		87	58	NE			x			R2	2.1	x	x	30	2, 9		sm/pl	4				d	
16	10.15	cs	j		1.15		79	342	NW			x			R2	1.8	r	x	10	2, 3, 6		pl/cr	3				d	
17	10.6	cs	j		0.45		74	206	SW			x			R3	1.9	d	x	10	2, 6		cr/sm	3				d	
18	11.9	cs	j		1.3		85	178	SE				x		R0	2.1	d	r	20-30	2		pl/un	5				d	
19	12.4	cs	j		0.5		69	65	NE			x			R3	2.5	d	x		3		st/sm	4				d	
20	12.4	cs	j		0		80	221	SW				x		R1	2.3	d	x				sm/cr	2				s	
21	13.92	cs	j		1.52		80	310	NW		x	x			R2	2.4	d	d	5	6		sm/pl	3				d	**Trend 333/04**
22	13.92	cs	j		0		26	306	W			x			R1	0.4	d	x		3		st/sm	7				d	
23	13.92	cs	j		0		76	243	SW			x			R3	3.2	d	x		3		sm/pl	4				s	
24	15.6	cs	j		1.68		74	106	SE			x			R1	5	x	x	20	2,9		sm/pl	3				d	
25	15.75	cs	b		0.15		14	339	NW			x			R1	1	r	r				sm/pl	2				s	????
26	15.9	cs	j		0.15		65	228	SW			x			R1	1	d	d	5	6		st/cr	9				s	
27	16.9	cs	j		1		89	239	SW		x	x			R3	4.5	d	x	2	2, 3		s/pl	2				d	

Traverse Number:	8	Length:				33.4m		Orientation:						286/01 W	Date:	16/06/05			Location:	Along track					Sheet no. 1	of 1
No.	Distance	Rock	Defct	Defct	Total	Spcng	Dip	Dip		Hardness					Strength	Persistence			Aperture	Infilling		Roughness		Waviness			Water	Notes
	(m)	Type	Type	Set	Spcng	(m)		Direction		vh	h	m	s	vs		(m)	Top	Btm	(mm)	Nature	Strength	Nature	JRC	λ(m)	Amp	i		Photos 45-47
1	0	ss	j				77	152	SE				x		R0	2.1	d	d	20	2		cr/sm	4				d	
2	0.8	ss	j		0.8		84	170	SE			x			R3	1.3	d	r	10	2, 6, 3		sm/pl	1				d	
3	1.6	ss	j		0.8		84	177	SE				x		R1	1.1	d	x				ir/cr	12				d	
4	1.8	ss	j		0.2		86	282	W			x			R1	1	r	r				pl/cr	6				d	
5	2.3	ss	b		0.5		28	355	N				x		R0	0.3	x	r		6		pl/sm	2				d	
6	2.5	ss	j		0.2		85	234	SW				x		R0	0.5	r	x		3		ir/cr					d	
7	2.5	ss	j		0		75	180	S			x			R1	2.2	d	x		3		st/sm	7				d	
8	4.5	ss	j		2		85	287	W				x		R0	1.2	d	x	2	2		ir	16				d	
9	4.5	ss	j		0		86	186	S			x	x		R0	2.5	d	d		3		sm/pl	5				d	
10	5.5	ss	j		1		84	280	W			x	x		R0	1	d	x		3		cr/ir	9				d	
11	5.5	ss	j		0		85	182	S			x	x		R0	1	d	d		3		ir/rgh					d	
12	6.35	ss	b		0.85		7	25	N			x	x		R0	20	x	x				sm/pl	2				d	Mudstone bed. **Trend 291/04**
13	6.8	ss	j		0.45		78	168	SE					x	R0	2.7	d	x				ir/st	17				d	
14	8.4	ss	j		1.6		79	184	S		x				R0	0.3	d	r		6		sm/pl	3				d	
15	8.9	ss	j		0.5		86	230	SW				x		R0	1.7	d	d				ir/rgh					d	
16	9.05	ss	j		0.15		67	274	W				x		R0	0.3	r	r	2	6		sm/pl	3				d	
17	10.83	ss	j		1.78		77	204	S				x		R0	1.6	d	d		6		ir/rgh	17				d	
18	11	ss	j		0.17		76	170	SE			x			R1	1	d	x		3, 6		ir/cr	8				d	
19	14	ss	b		3		9	35	N			x			R1	2	r	r		3		sm/pl	2				d	
20	14	ss	j		0		76	229	SW				x		R0	1.5	d	x		6		ir/cr	18				d	
21	17.28	ss	j		3.28		85	174	SE				x		R0	2	d	x		6		ir/cr	18				d	Shallow rounded wedge
22	18.45	ss	j		1.17		72	230	SW				x		R0	2	d	x		6		ir/cr	18				d	Shallow rounded wedge
23	18.5	ss	j		0.05		81	198	SW					x	R0	2	d	x		6		sm/cr	2				d	Trend **291/08**
24	18.6	ss	j		0.1		56	181	S					x	R0	2	d	x		6		sm/cr	6				d	
25	20.55	ss	j		1.95		68	177	SE					x	R0	3	d	x		3		sm/pl	2				d	
26	23.6	ss	j		3.05		84	114	SE					x	R0	3	d	x		1		ir/pl					d	Loose sandstone
27	28.5	ss	j		4.9		75	225	SW					x	R0	3	d	x	20	2		ir/sm	5				d	
28	33.3	ss	j		4.8		83	281	W					x	R0	0.5	x	r		9		sm/pl	4				d	
																												0m= 2418008/5899534±10m
																												33.3m= 2418029/5899526±10m

Dips plots of Joint Sets

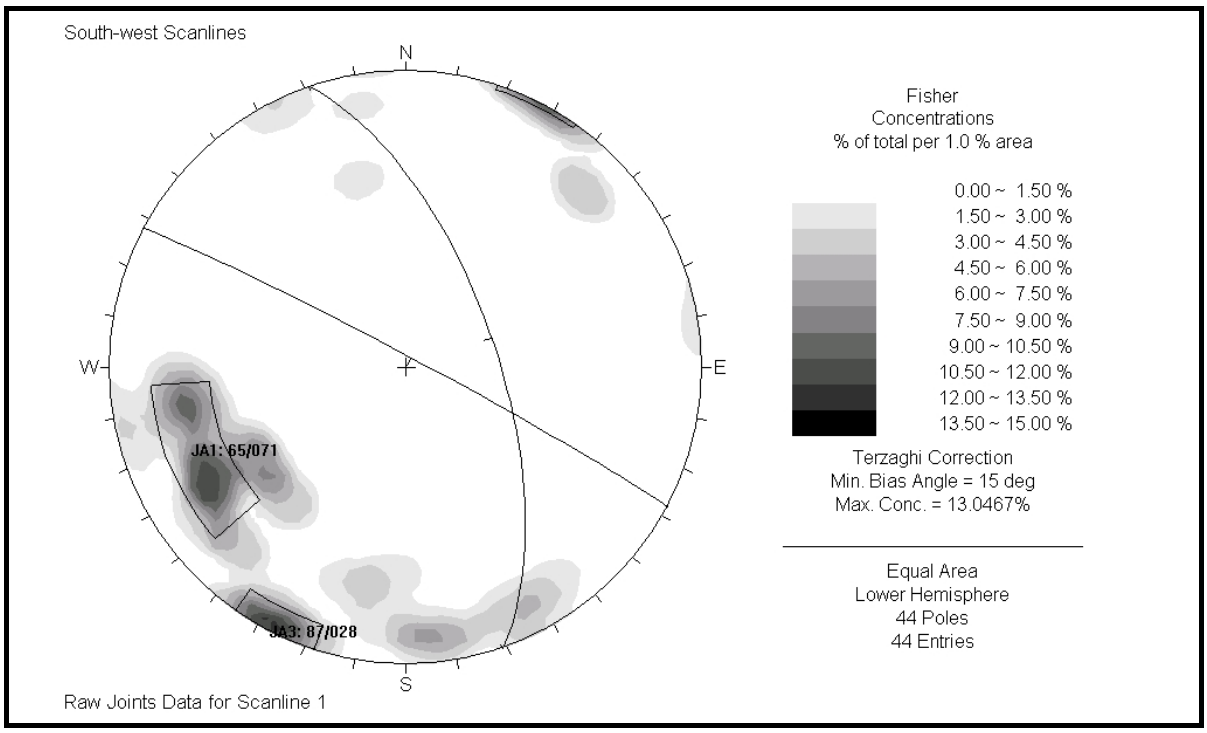

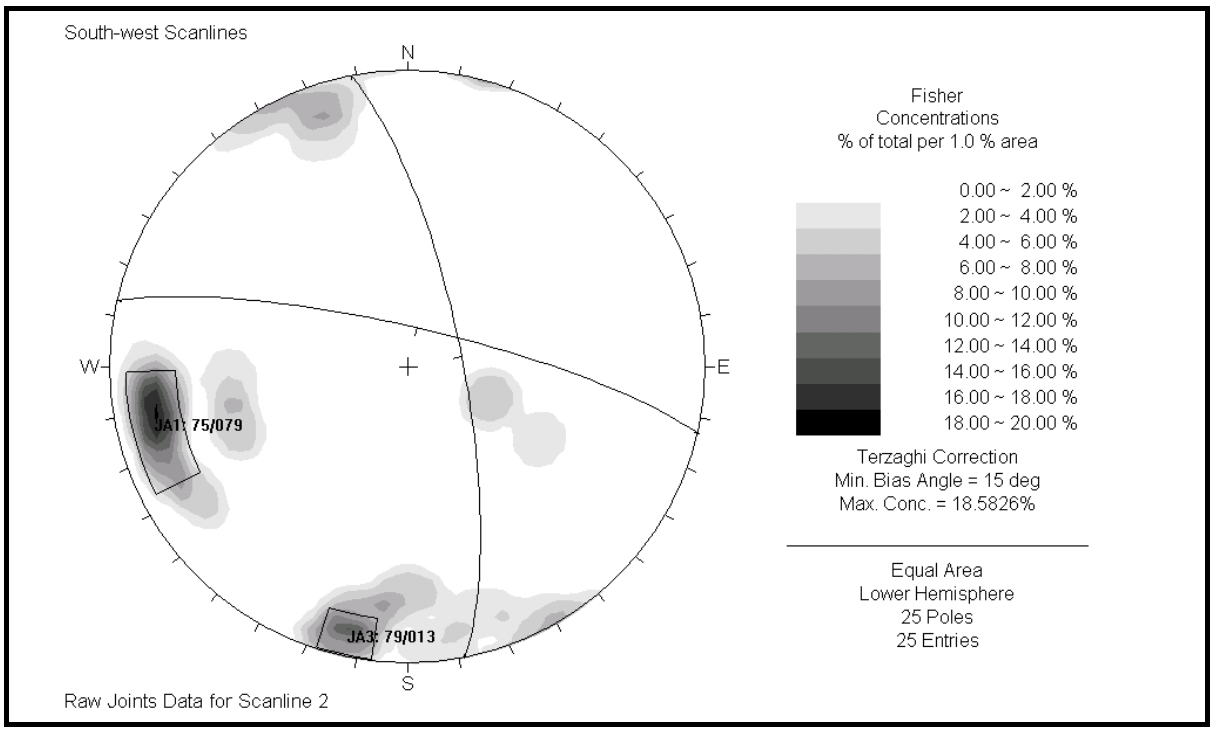

South-west Scanlines

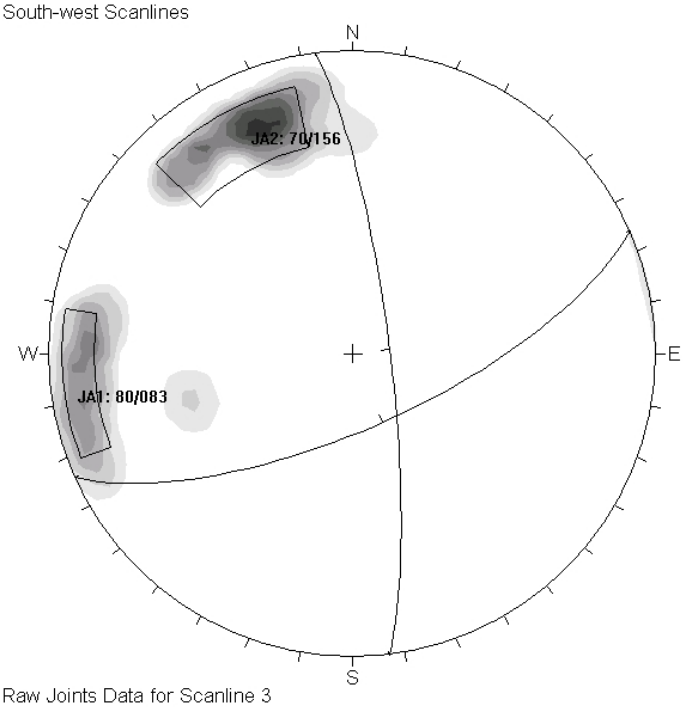

Fisher
Concentrations
% of total per 1.0 % area

0.00 ~ 2.50 %
2.50 ~ 5.00 %
5.00 ~ 7.50 %
7.50 ~ 10.00 %
10.00 ~ 12.50 %
12.50 ~ 15.00 %
15.00 ~ 17.50 %
17.50 ~ 20.00 %
20.00 ~ 22.50 %
22.50 ~ 25.00 %

Terzaghi Correction
Min. Bias Angle = 15 deg
Max. Conc. = 21.0888%

Equal Area
Lower Hemisphere
18 Poles
18 Entries

Raw Joints Data for Scanline 3

South-west Scanlines

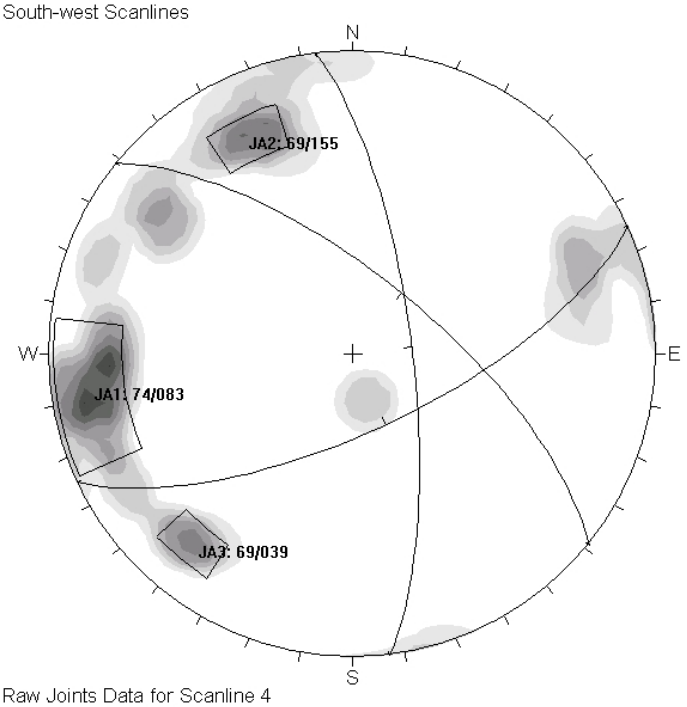

Fisher
Concentrations
% of total per 1.0 % area

0.00 ~ 1.50 %
1.50 ~ 3.00 %
3.00 ~ 4.50 %
4.50 ~ 6.00 %
6.00 ~ 7.50 %
7.50 ~ 9.00 %
9.00 ~ 10.50 %
10.50 ~ 12.00 %
12.00 ~ 13.50 %
13.50 ~ 15.00 %

Terzaghi Correction
Min. Bias Angle = 15 deg
Max. Conc. = 12.0435%

Equal Area
Lower Hemisphere
46 Poles
46 Entries

Raw Joints Data for Scanline 4

South-west Scanlines

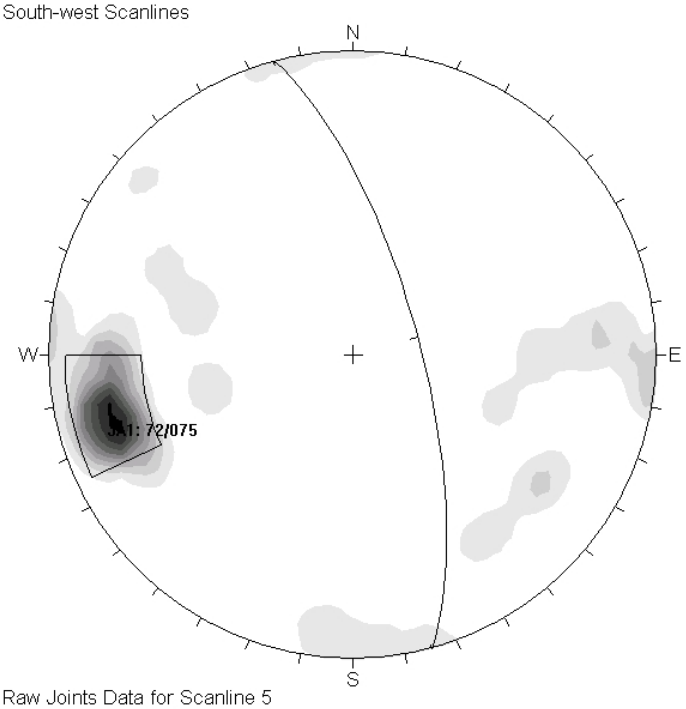

Fisher
Concentrations
% of total per 1.0 % area

0.00 ~ 2.00 %
2.00 ~ 4.00 %
4.00 ~ 6.00 %
6.00 ~ 8.00 %
8.00 ~ 10.00 %
10.00 ~ 12.00 %
12.00 ~ 14.00 %
14.00 ~ 16.00 %
16.00 ~ 18.00 %
18.00 ~ 20.00 %

Terzaghi Correction
Min. Bias Angle = 15 deg
Max. Conc. = 18.4525%

Equal Area
Lower Hemisphere
59 Poles
59 Entries

Raw Joints Data for Scanline 5

North-east Scanlines

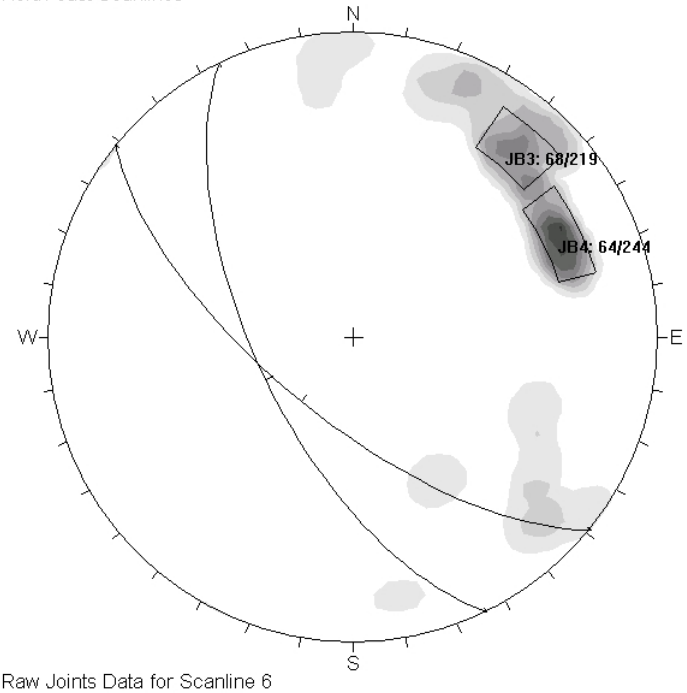

Fisher
Concentrations
% of total per 1.0 % area

0.00 ~ 2.50 %
2.50 ~ 5.00 %
5.00 ~ 7.50 %
7.50 ~ 10.00 %
10.00 ~ 12.50 %
12.50 ~ 15.00 %
15.00 ~ 17.50 %
17.50 ~ 20.00 %
20.00 ~ 22.50 %
22.50 ~ 25.00 %

Terzaghi Correction
Min. Bias Angle = 15 deg
Max. Conc. = 20.3622%

Equal Area
Lower Hemisphere
21 Poles
21 Entries

Raw Joints Data for Scanline 6

North-east Scanlines

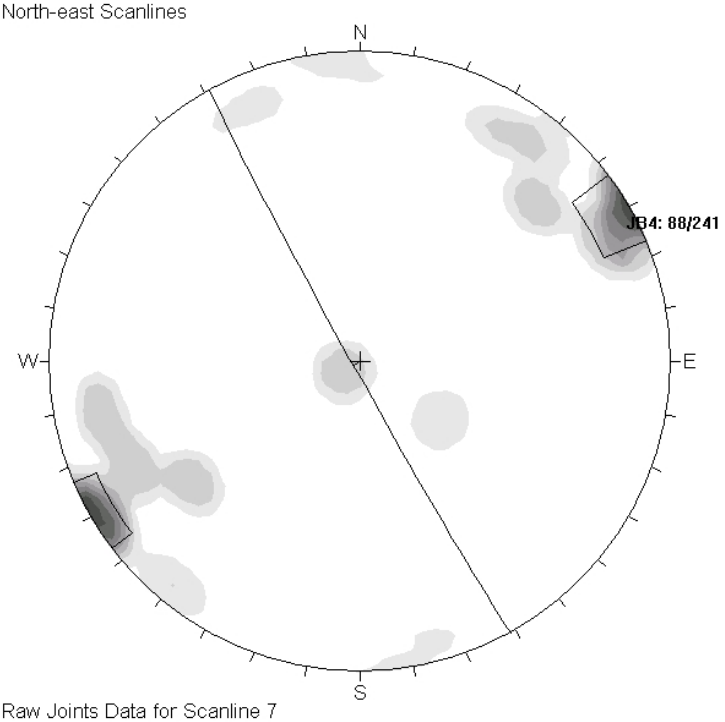

Fisher
Concentrations
% of total per 1.0 % area

0.00 ~ 2.50 %
2.50 ~ 5.00 %
5.00 ~ 7.50 %
7.50 ~ 10.00 %
10.00 ~ 12.50 %
12.50 ~ 15.00 %
15.00 ~ 17.50 %
17.50 ~ 20.00 %
20.00 ~ 22.50 %
22.50 ~ 25.00 %

Terzaghi Correction
Min. Bias Angle = 15 deg
Max. Conc. = 21.0335%

Equal Area
Lower Hemisphere
25 Poles
25 Entries

Raw Joints Data for Scanline 7

North-east Scanlines

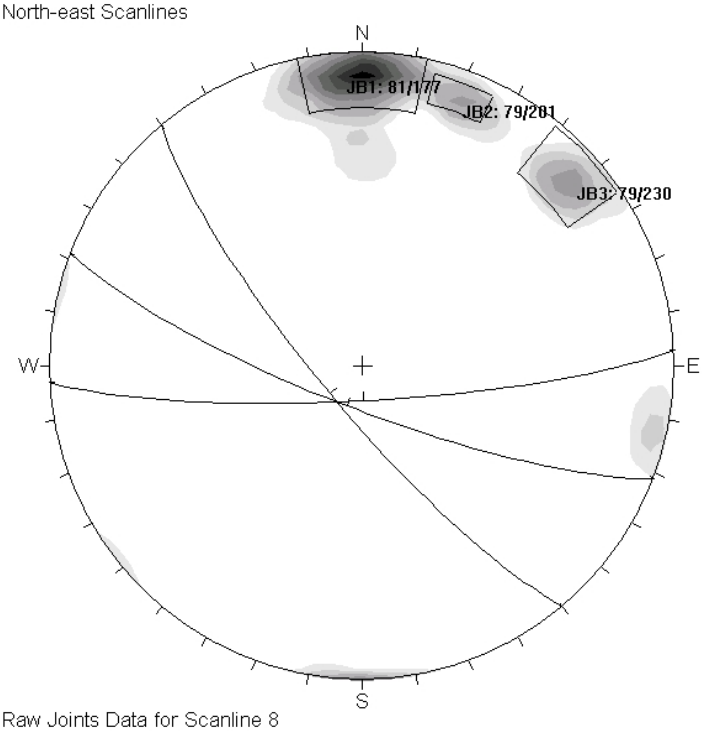

Fisher
Concentrations
% of total per 1.0 % area

0.00 ~ 3.00 %
3.00 ~ 6.00 %
6.00 ~ 9.00 %
9.00 ~ 12.00 %
12.00 ~ 15.00 %
15.00 ~ 18.00 %
18.00 ~ 21.00 %
21.00 ~ 24.00 %
24.00 ~ 27.00 %
27.00 ~ 30.00 %

Terzaghi Correction
Min. Bias Angle = 15 deg
Max. Conc. = 28.7102%

Equal Area
Lower Hemisphere
25 Poles
25 Entries

Raw Joints Data for Scanline 8

Appendix 2.4 Schimdt Hammer Data

Scanline	2	1	1	1	5	5
Reading						
1	22	13	27	13	18	20
2	22	17	27	13	18	21
3	25	17	30	15	19	22
4	25	18	30	25	20	23
5	27	18	31	25	21	23
6	28	20	31	26	21	24
7	28	22	31	27	22	24
8	28	28	31	27	22	25
9	29	28	32	29	24	25
10	29	28	33	29	25	26
11			34			

Appendix 2.5 RQD Data

653	654	656	657	658	660	662	663
0	0	0	0	77.5	0	0	0
0	19.48052	0	0	84.375	35	0	0
0	65.21739	19.48052	0	84.44444	54.66667	0	0
0	70.83333	78.57143	6.666667	91.46341	67.36842	0	0
10.32258	71.83099	84.61538	16.66667	95.48387	92.30769	0	0
10.34483	73.19588	91.42857	19.48052	95.625		0	0
11.81818		100	21.33333	99.29078		0	0
13.33333		100	31.33333	100		33.84615	0
19.48052		100	44	100		40	0
24.51613		100	44.28571	100		51.40187	0
29.37063		100	56	100		71.42857	0
40.64516		100	57.33333	100		75	14.19355
			61.42857	100		76.12903	20.86957
			66.66667	100		81.25	21.42857
			70.66667	100		81.81818	30
			76	100		83.63636	34.18803
			80	100		87.5	65
			81.33333			89.65517	66.66667
			82			90.625	68.75
			87.14286			90.90909	69.23077
			90.66667			93.75	69.28571
			91.33333			93.75	71.25
			92.46575			95	76.25
			96.66667			95	80
			98			100	80.64516
						100	85.29412
						100	90.16393
						100	91.66667
						100	92.85714
						100	93.75
						100	96.42857
						100	97.01493
						100	99.29078
							100
							100

							100
							100
							100
							100

Appendix 2.6 Raw Pump Test Data –provided by Adrian Field (Consultant Geologist to Solid Energy)

Pump Test No.1

Pumped Bore:		DH656	"r"		TOC, magl:	0.60		
Observation Bores:		pz656/2	2.88		0.50			
		pz656/7	7.25		0.76			
Pumping details			Recovery details					
Start:	7/02/2005	1530	Start:	7/02/2005	1710			
Finish:	7/02/2005	1710	Finish:	7/09/2001	1735			
Initial static water levels, mbTOC						Pump rate:	190.43	cmpd
							2.24	lps
DH656	pz656/2	pz656/7				Duration:	100	mins
2.45	2.25	2.56						

DH656(pumped bore)			BH 2			BH 3		
Time t, min	PWL, mbTOC	Drawdown, m	Time t, min	WL, mbTOC	Drawdown, m	Time t, min	WL, mbTOC	Drawdown, m
1	3.38	0.93	0.5	2.42	0.17	6	2.96	0.40
2	3.46	1.01	1	2.50	0.25	7	3.00	0.44
3	3.57	1.12	3	2.70	0.45	12	3.05	0.49
4	3.62	1.17	5	2.96	0.71	19	3.09	0.53
5	3.65	1.20	9	3.12	0.87	23.5	3.10	0.54
8	3.78	1.33	10	3.13	0.88	32	3.12	0.56
10.5	3.82	1.37	13.5	3.18	0.93	42	3.14	0.58
13	3.85	1.40	15	3.20	0.95	47	3.15	0.59
15	3.87	1.42	21	3.23	0.98	50	3.15	0.59
19	3.90	1.45	25	3.26	1.01	61.5	3.16	0.60
24.5	3.92	1.47	30	3.27	1.02	70	3.17	0.61
31	3.93	1.48	35.5	3.29	1.04	82	3.18	0.62
35	3.95	1.50	40	3.29	1.04	94	3.18	0.62
41	3.95	1.50	45	3.29	1.04	100	3.18	0.62
44.5	3.95	1.50	52	3.30	1.05	103.5	2.84	0.28
51	3.96	1.51	60	3.31	1.06	104.5	2.80	0.24
59.5	3.97	1.52	72	3.33	1.08	110	2.71	0.15
71	3.98	1.53	80	3.34	1.09	117	2.66	0.10
80	3.98	1.53	92	3.34	1.09	133	2.62	0.06
93	3.99	1.54	100	3.34	1.09	141	2.64	0.07
100	3.99	1.54	100.5	3.19	0.94			
101.5	3.09	0.64	101	3.04	0.79			
102	3.09	0.64	103	2.73	0.48			
105.5	2.75	0.30	106	2.52	0.27			
109	2.65	0.20	108	2.47	0.22			
114.5	2.57	0.12	115	2.37	0.12			
120	2.53	0.08	121	2.33	0.08			
125	2.51	0.06	126	2.31	0.06			
			135	2.29	0.04			

Drawdown and Recovery Data
SENZ Reefton Opencast Project - Burkes Creek

Pump Test No.2

Pumped Bore:		DH658	"r"	TOC, magl:	1.00		
Observation Bores:		pz658/2	2.44	0.00			
		pz658/10	10.06	0.00			
Pumping details			Recovery details				
Start:	14/02/2005	1548	Start:	14/02/2005	1638		
Finish:	14/02/2005	1638	Finish:	15/02/2005	1009		
Initial static water levels, mbTOC					Pump rate:	150.88	cmpd
DH658	pz658/2	pz658/10				1.75	lps
2.39	1.43	1.21			Duration:	50	mins

DH656 (pumped bore)			pz2			pz10		
Time t, min	PWL, mbTOC	Drawdown, m	Time t, min	WL, mbTOC	Drawdown, m	Time t, min	WL, mbTOC	Drawdown, m
0.5	3.28	0.89	1.5	1.82	0.39	2	1.91	0.70
1	3.42	1.03	4	2.17	0.74	6	2.12	0.91
3	3.81	1.42	11	2.39	0.96	11.5	2.21	1.00
5	3.95	1.56	15	2.41	0.98	16	2.21	1.00
10	4.07	1.68	22.5	2.42	0.99	31.5	2.24	1.03
14	4.09	1.70	30	2.42	0.99	37.5	2.24	1.03
22	4.10	1.71	39	2.42	0.99	50	2.24	1.03
30.5	4.10	1.71	50	2.42	0.99	53.5	1.44	0.23
38	4.10	1.71	53	1.80	0.37	57	1.32	0.11
50	4.10	1.71	56.5	1.56	0.13	61.5	1.27	0.06
50.5	3.29	0.90	60.5	1.51	0.08	67.5	1.25	0.04
51	3.10	0.71	66.5	1.48	0.05	81.5	1.24	0.03
52	2.82	0.43	71	1.47	0.04	86.5	1.23	0.02
55	2.55	0.16	75.5	1.47	0.04	93	1.23	0.02
56	2.52	0.13	82	1.46	0.03	1105	1.21	0.00
60	2.45	0.06	1103	1.44	0.01			
66	2.43	0.04						
70.5	2.41	0.02						
75	2.41	0.01						
81.5	2.40	0.01						
1101	2.39	0.00						

Appendix 2.7 Walton Graphical Method

Noneqilibrium radial flow in a leaky, confined aquifer with no storage in the aquitard

Hantush-Jacob Equations (from Fetter, 2001):

$T = (Q / 4\pi Z) \times W(u, r/B)$

$S = 4Tut / r^2$

$r/B = r /(Tb'/ K')^{1/2}$

$K' = [Tb'(r/B)^2] / r^2$

Where Q is the pumping rate,
T is transmissivity of the confined aquifer,
t is the time since pumping began, Z is the drawdown (h_0-h),
S is the storativity of the confined aquifer,
r is the distance from the pumping well to the observation well,
K' is the vertical hydraulic conductivity of the aquitard,
b' is the thickness of the aquifer,
B is the leakage factor $(Tb/ K)^{1/2}$.

Assumptions (Hantush and Jacob, 1955 cited in Walton, 1960):

- The aquifer is infinite in areal extent and is the same thickness throughout.
- It is homogeneous and anisotropic.
- It is confined between an impermeable bed and a bed through which leakage can occur.
- The coefficient of storage is constant.
- Water is released from storage instantaneously with a decline in head.
- The well has an infinitesimal diameter and penetrates the entire thickness of the formation.
- The leakage through the confining bed into the aquifer is vertical and proportional to the drawdown.
- The hydraulic head in the deposits supplying leakage remains more or less uniform.

Appendix 3: Kinematic Feasibility Assessment

Table of Contents

Appendix 3.1 Additional plots used to perform kinematic feasibility checks for planar failures on the southwest scanlines.

Southwest Scanlines with a pit slope of 60/130, showing planar failures not possible.

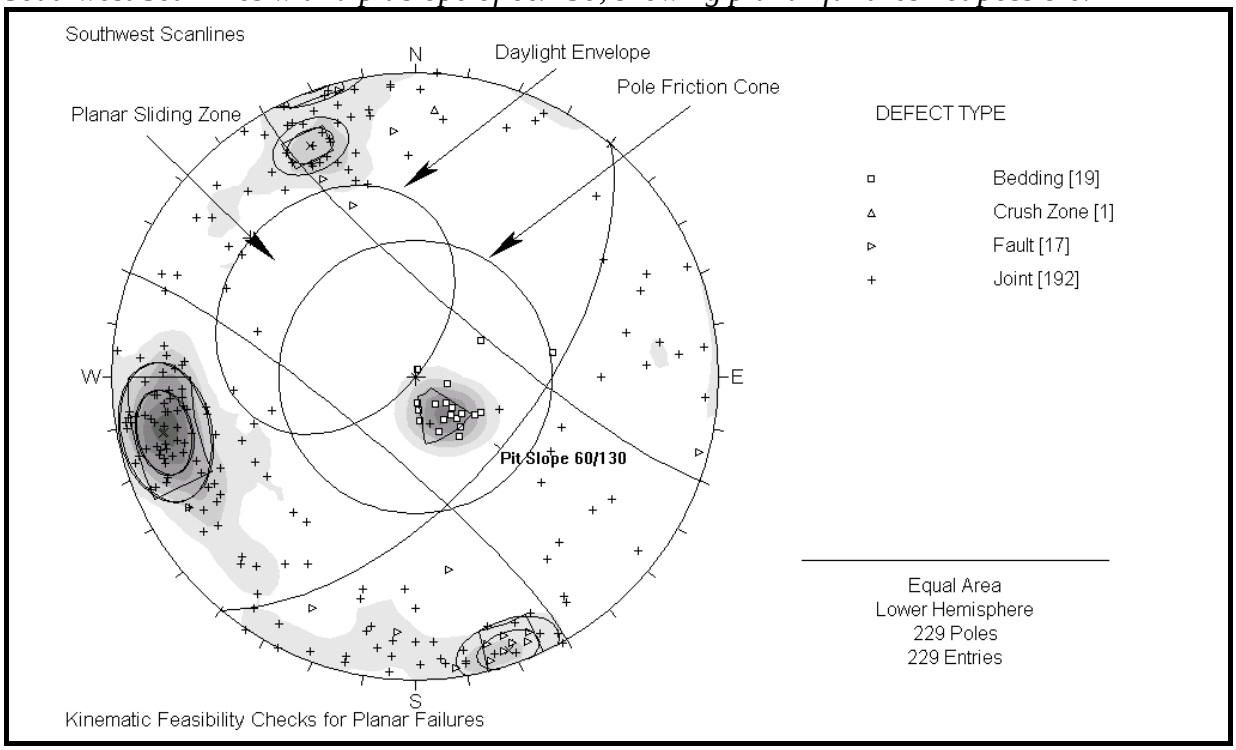

Southwest scanlines with a pit slope of 60/150, showing planar failures unlikely as only the edge of minor joint set (JA2) within sliding zone.

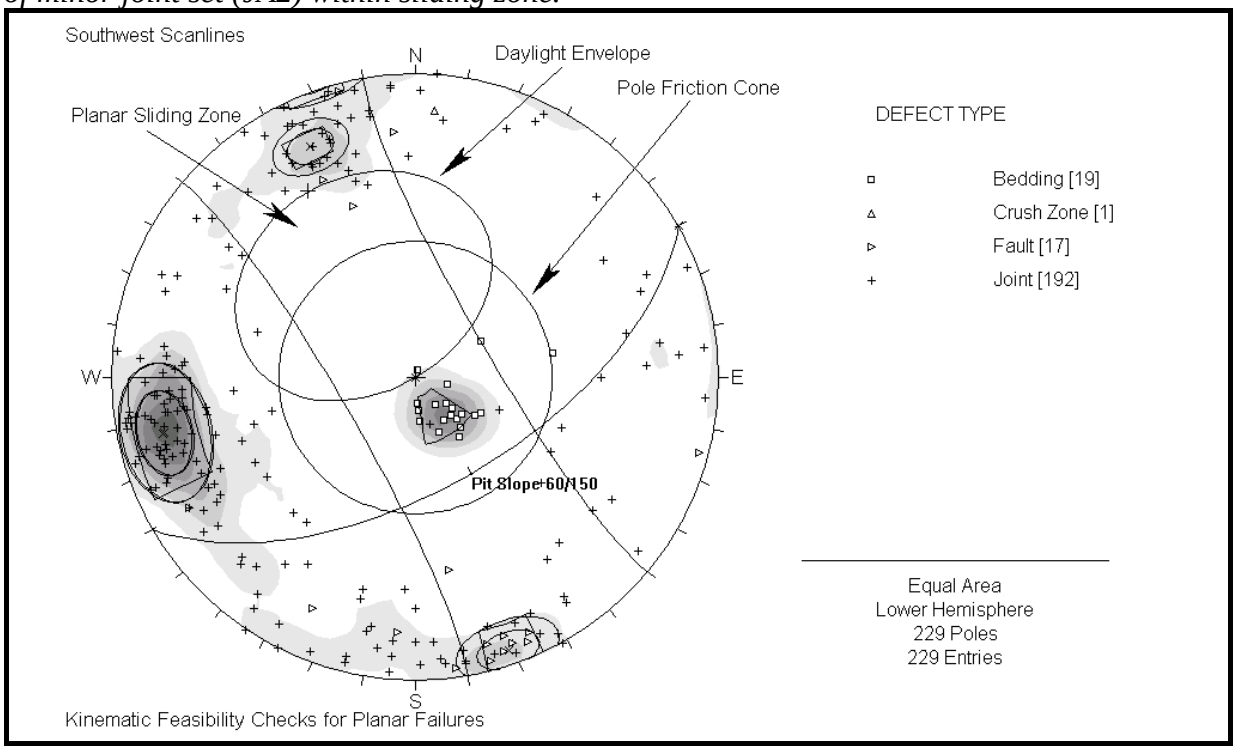

Southwest scanlines with a pit slope of 76/130, showing planar failures unlikely as only the corner of minor joint set (JA2) within sliding zone.

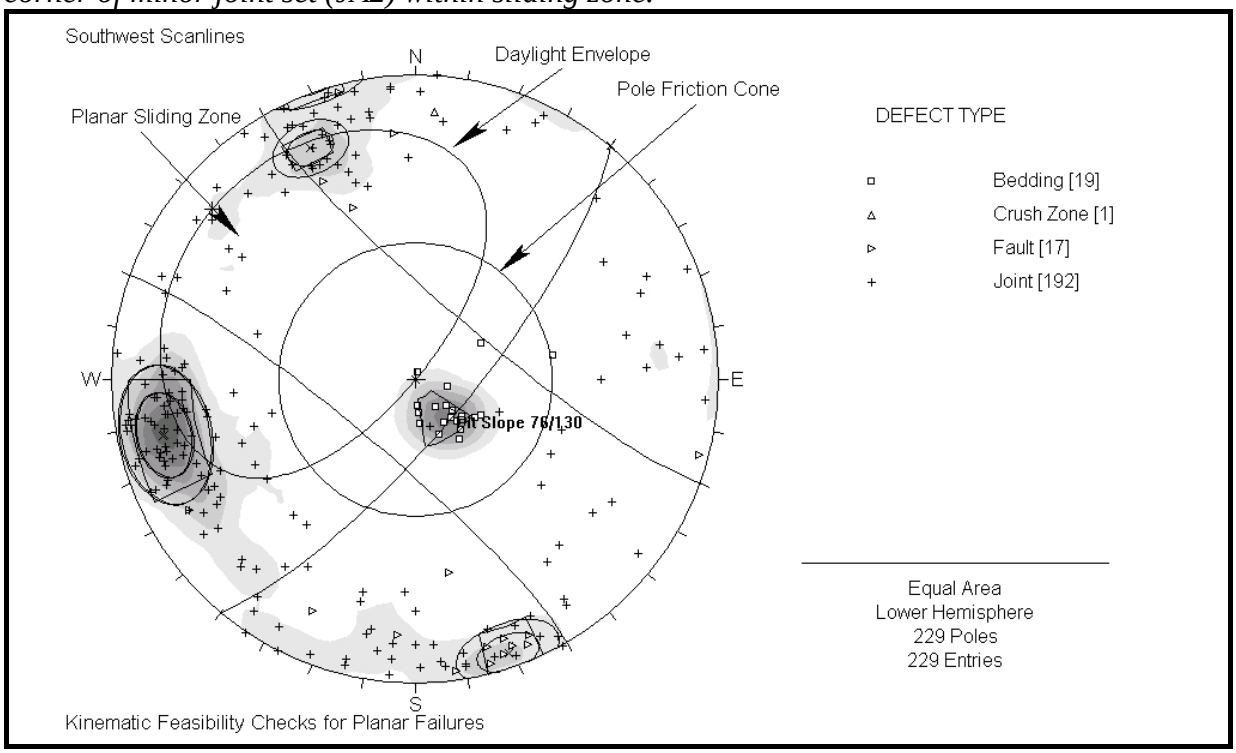

Southwest scanlines with a pit slope of 76/130, showing planar failures highly possible as most of the minor joint set (JA2) is within sliding zone.

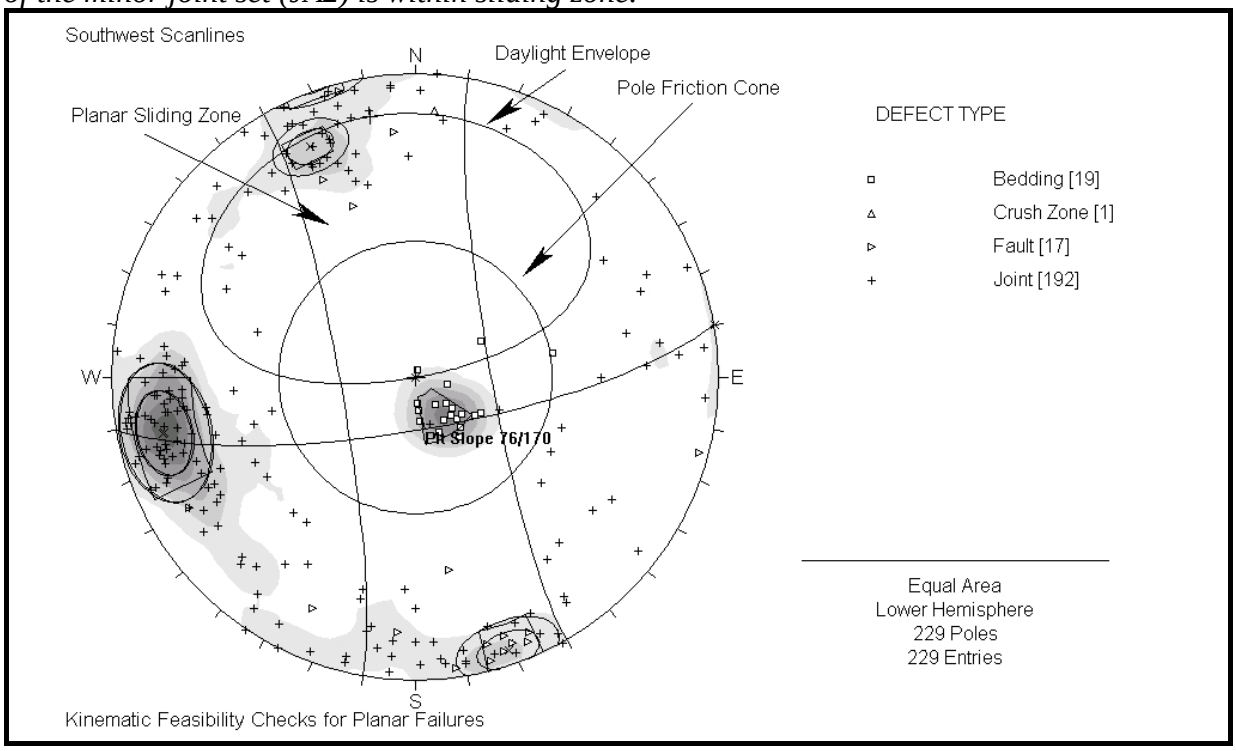

Appendix 3.2 Additional plots used to perform kinematic feasibility checks for wedge failures on the southwest scanlines.

Southwest scanlines with a pit slope of 60˚/130, showing no defect intersection within sliding zone.

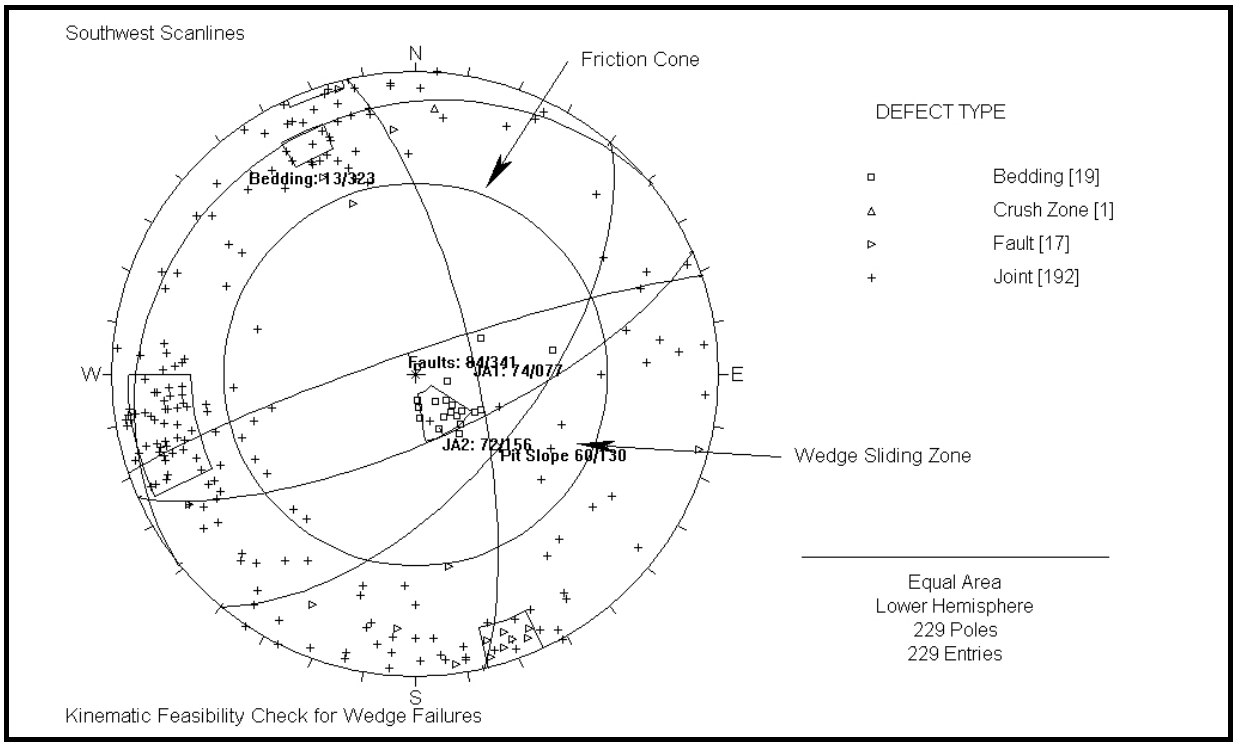

Southwest scanlines with a pit slope of 60˚/170, showing no defect intersection within sliding zone.

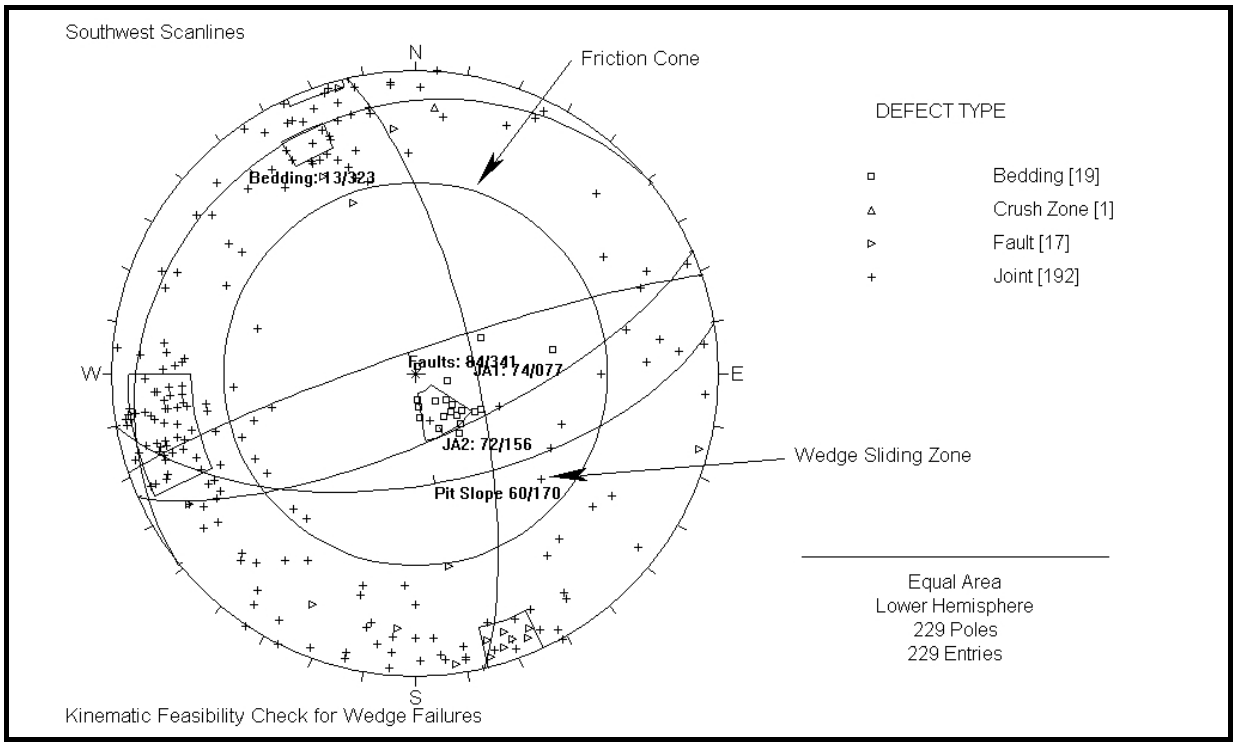

Southwest scanlines with a pit slope of 76˚/150, showing an intersection between JA1 and JA2 within the sliding zone.

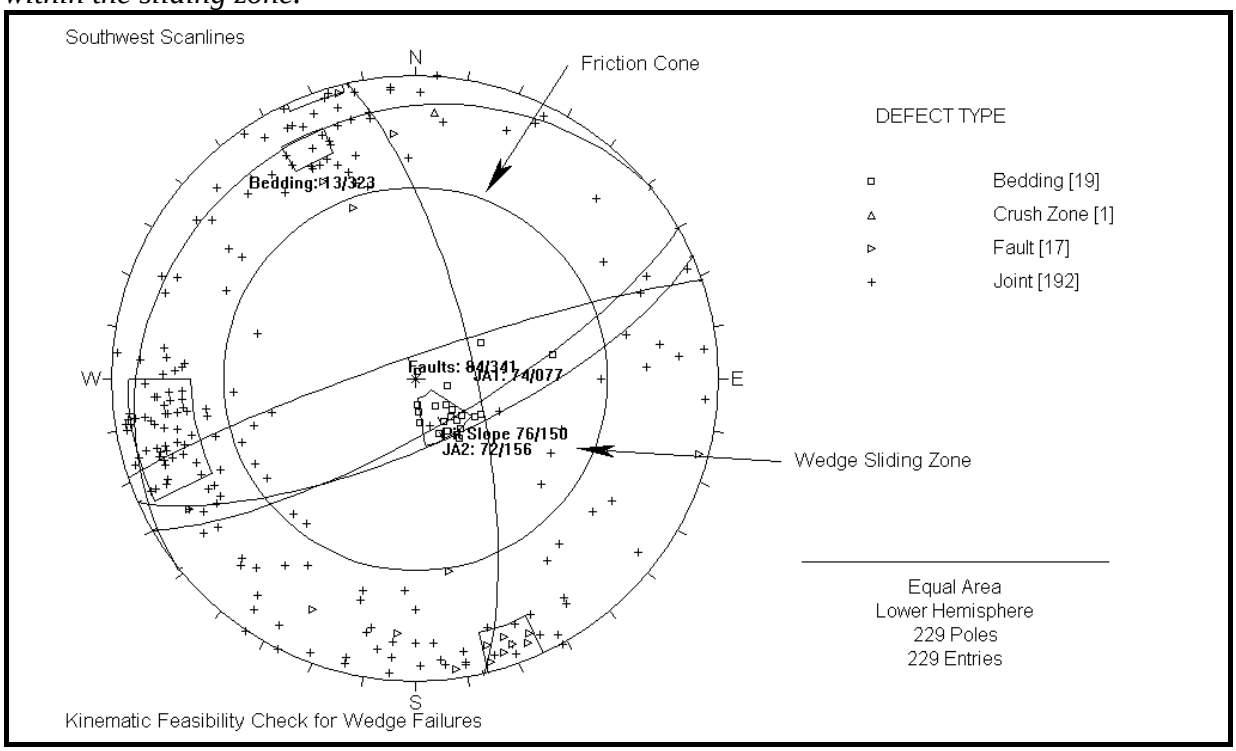

Southwest scanlines with a pit slope of 76˚/170, showing an intersection between JA1 and JA2 within the sliding zone.

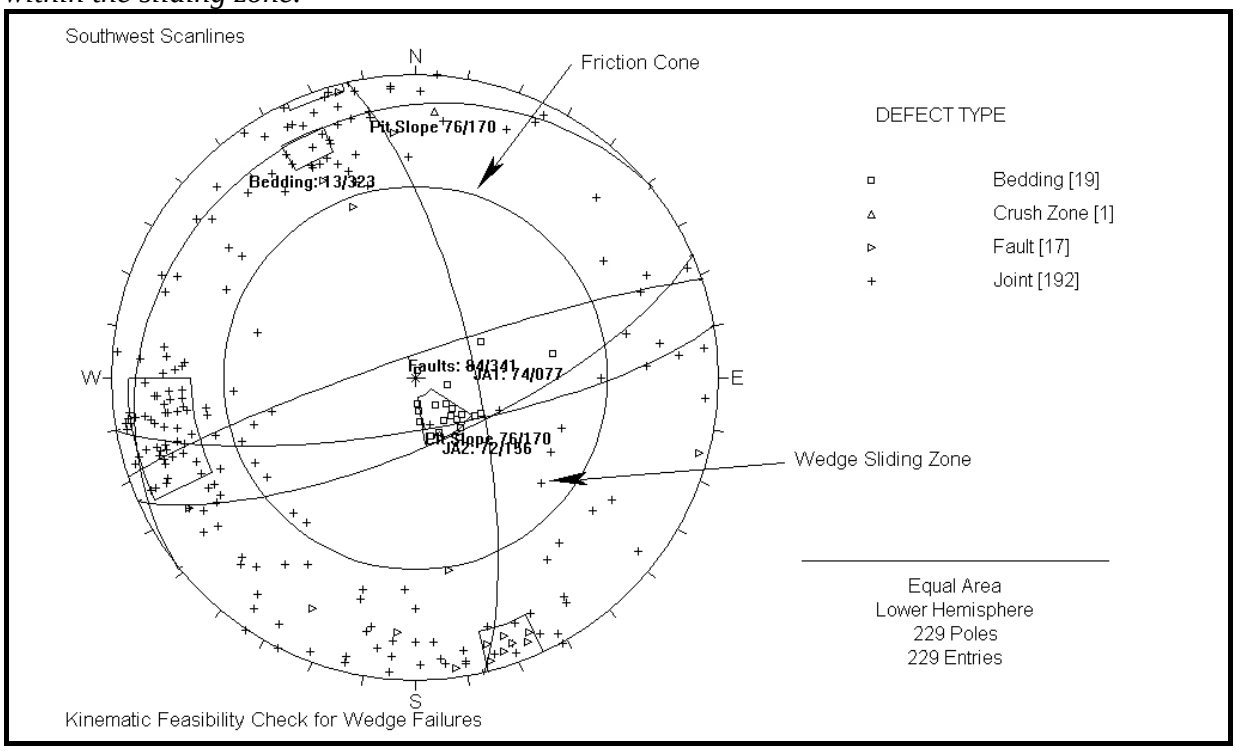

Appendix 3.3 Additional plots used to perform kinematic feasibility checks for toppling failure on the southwest scanlines.

Southwest scanlines with a pit slope of 60˚/130, showing the fault concentration partially within the toppling region.

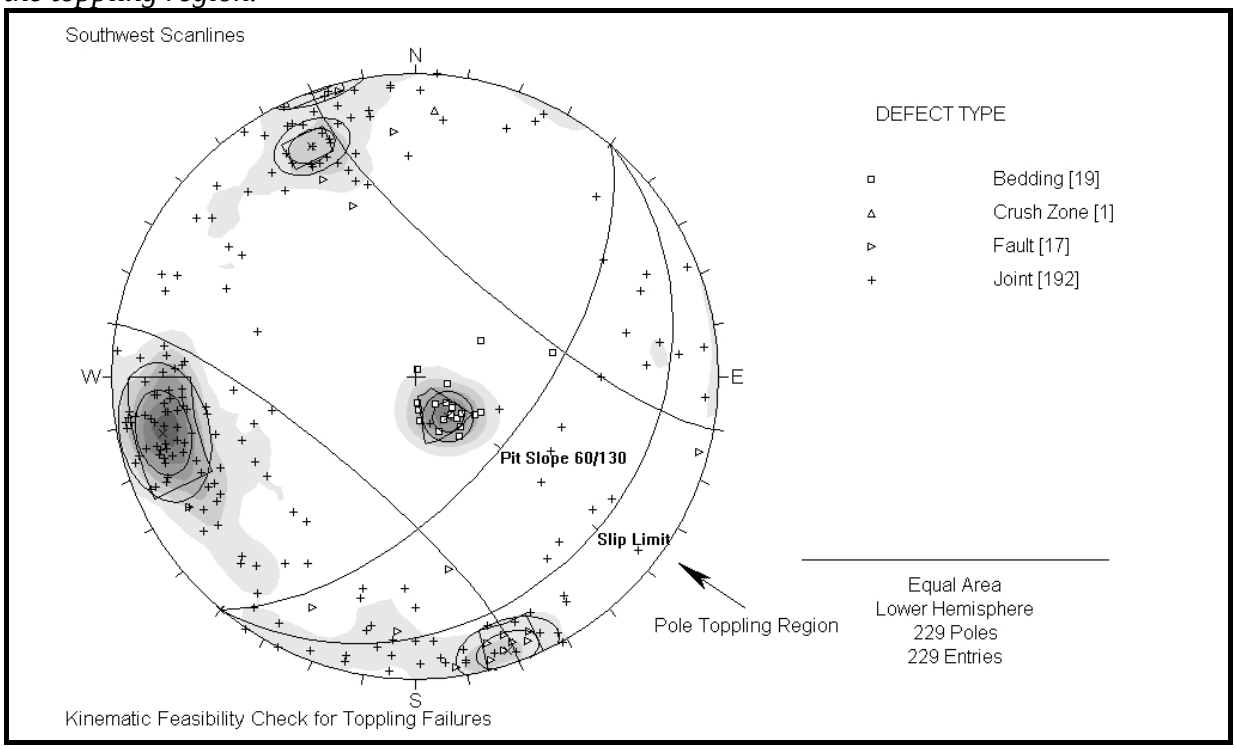

Southwest scanlines with a pit slope of 60˚/150, showing the fault concentration within the toppling region.

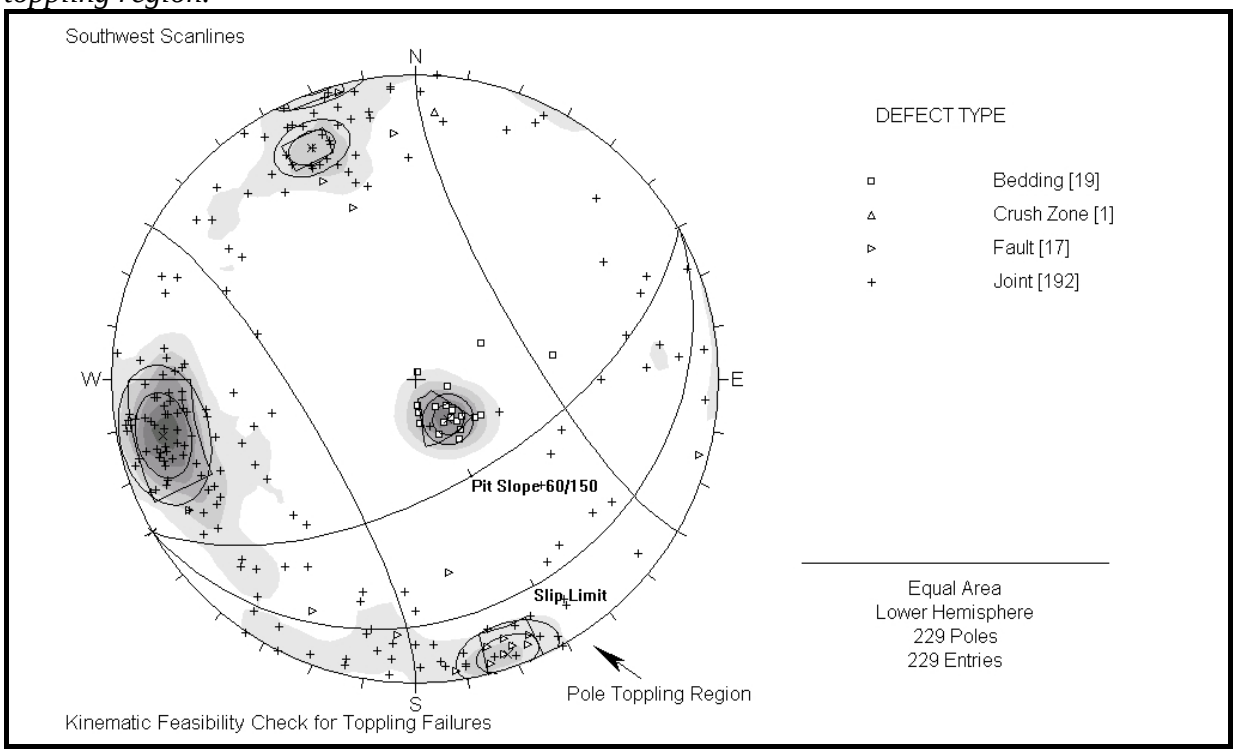

Southwest scanlines with a pit slope of 76˚/150, showing the fault concentration within the toppling region.

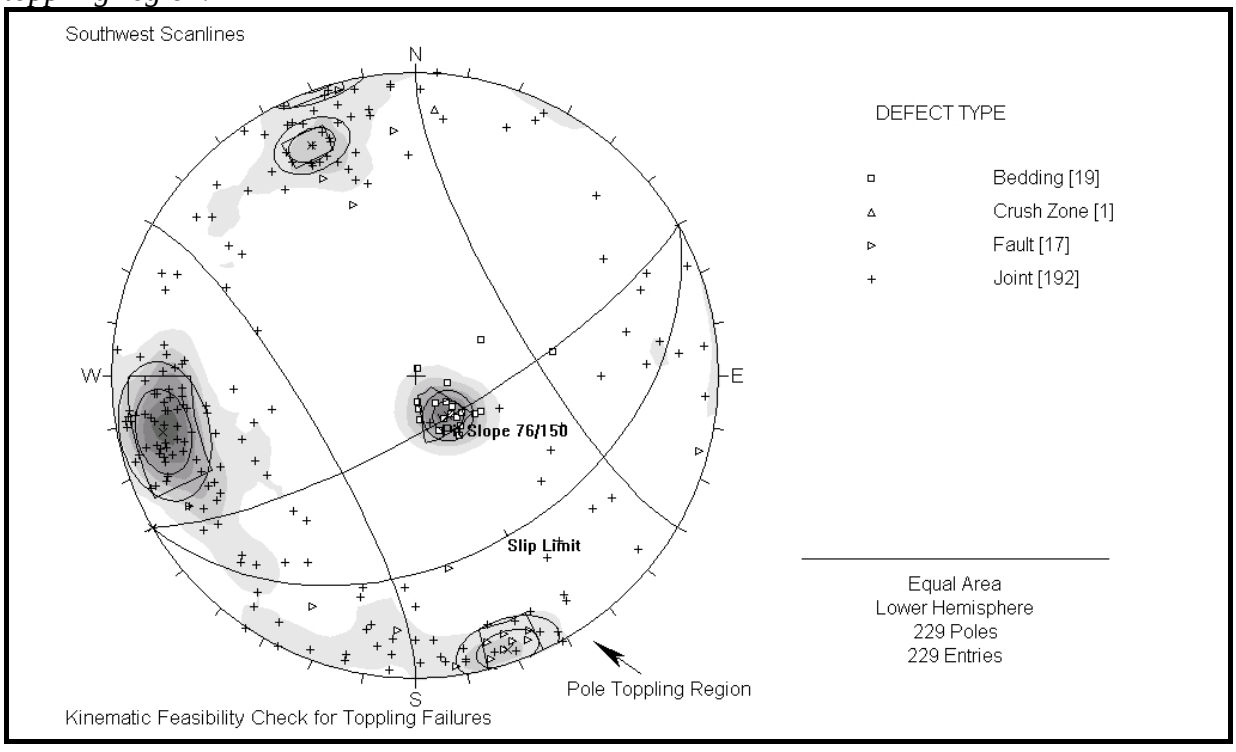

Southwest scanlines with a pit slope of 76˚/170, showing the fault concentration within the toppling region.

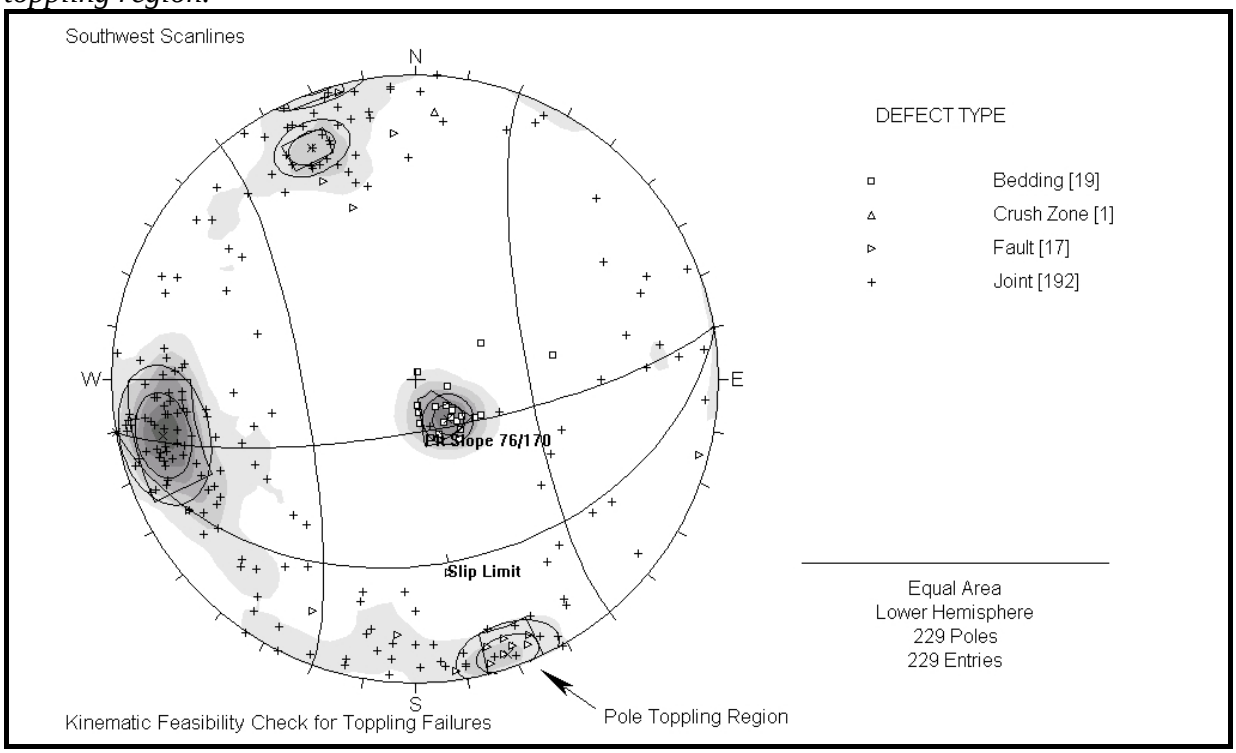

Appendix 3.4 Additional plots used to perform kinematic feasibility checks for planar failure in the northeast scanlines.

Northeast Scanlines with a pit slope of 60/150, showing planar failures not possible .

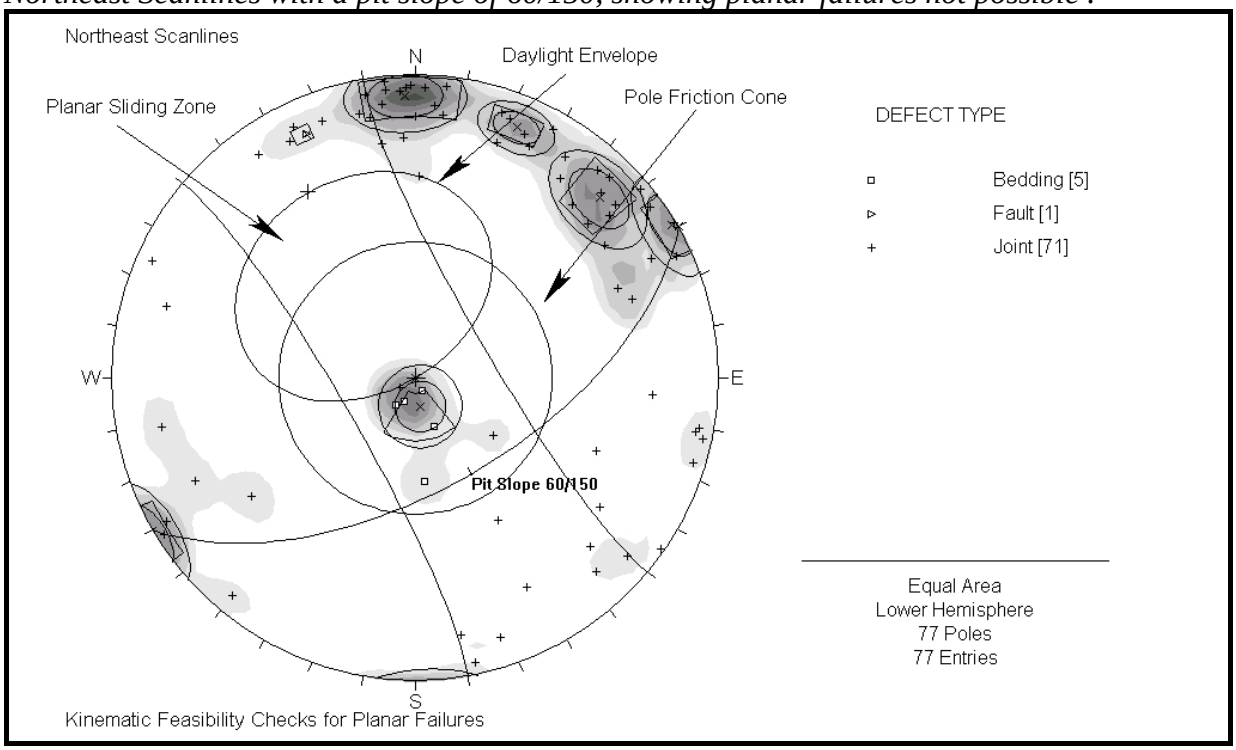

Northeast scanlines with a pit slope of 60/170, showing planar sliding very unlikely.

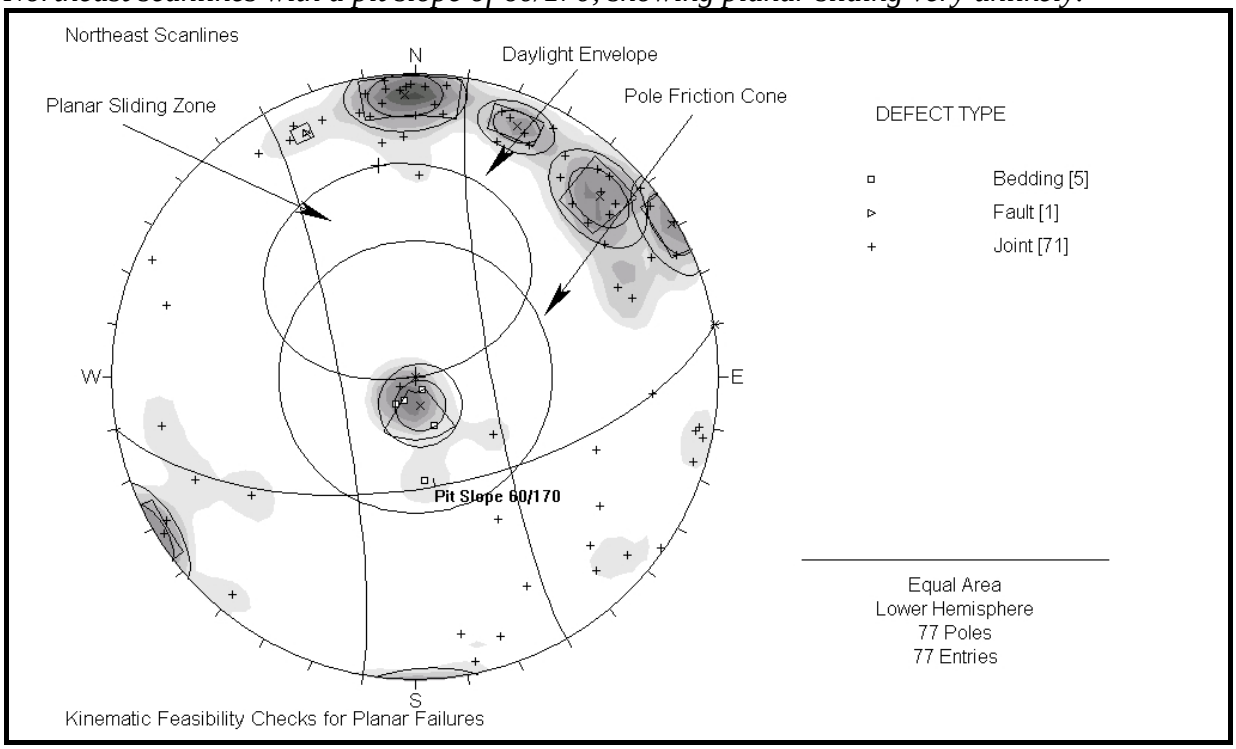

Northeast scanlines with a pit slope of 76/130, showing planar sliding not possible.

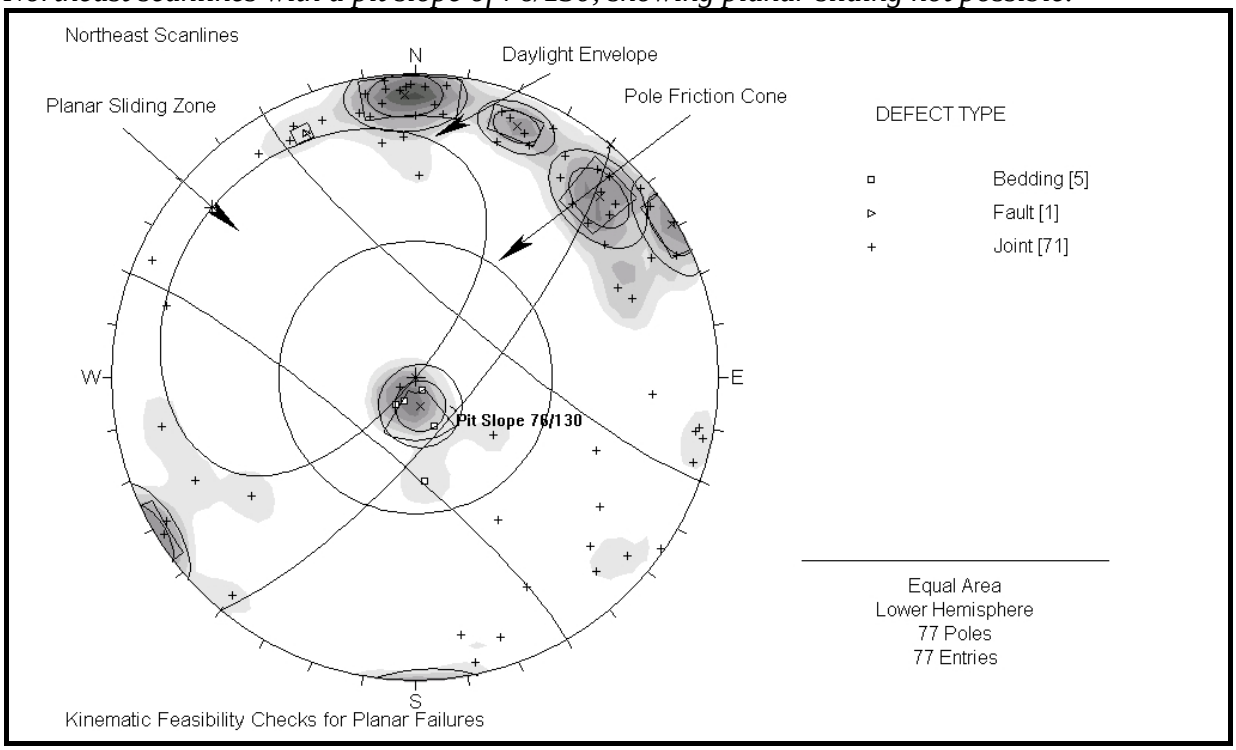

Appendix 3.5 Additional plots used to perform kinematic feasibility checks for wedge failure in the northeast scanlines.

Northeast scanlines with a pit slope of 60˚/130, showing an intersection between JB3 and JB4 within the sliding zone.

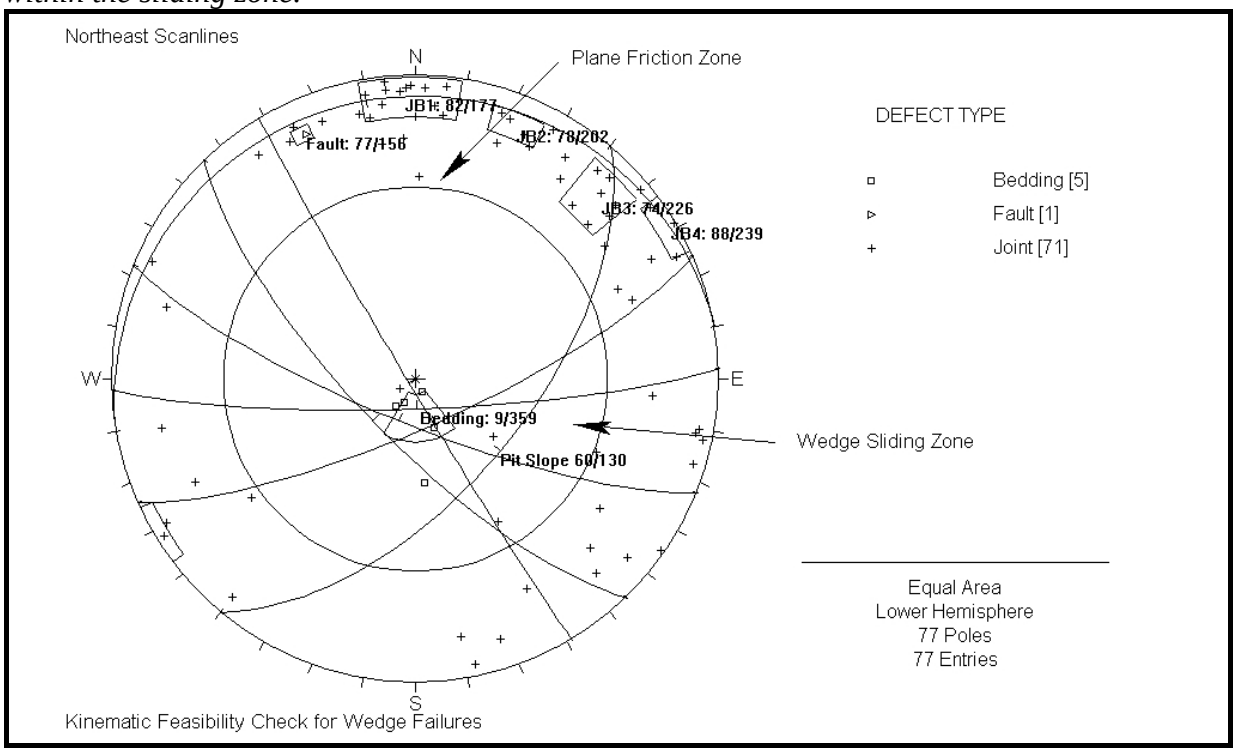

Northeast scanlines with a pit slope of 60˚/170, showing an intersection between JB3 and JB4 within the sliding zone.

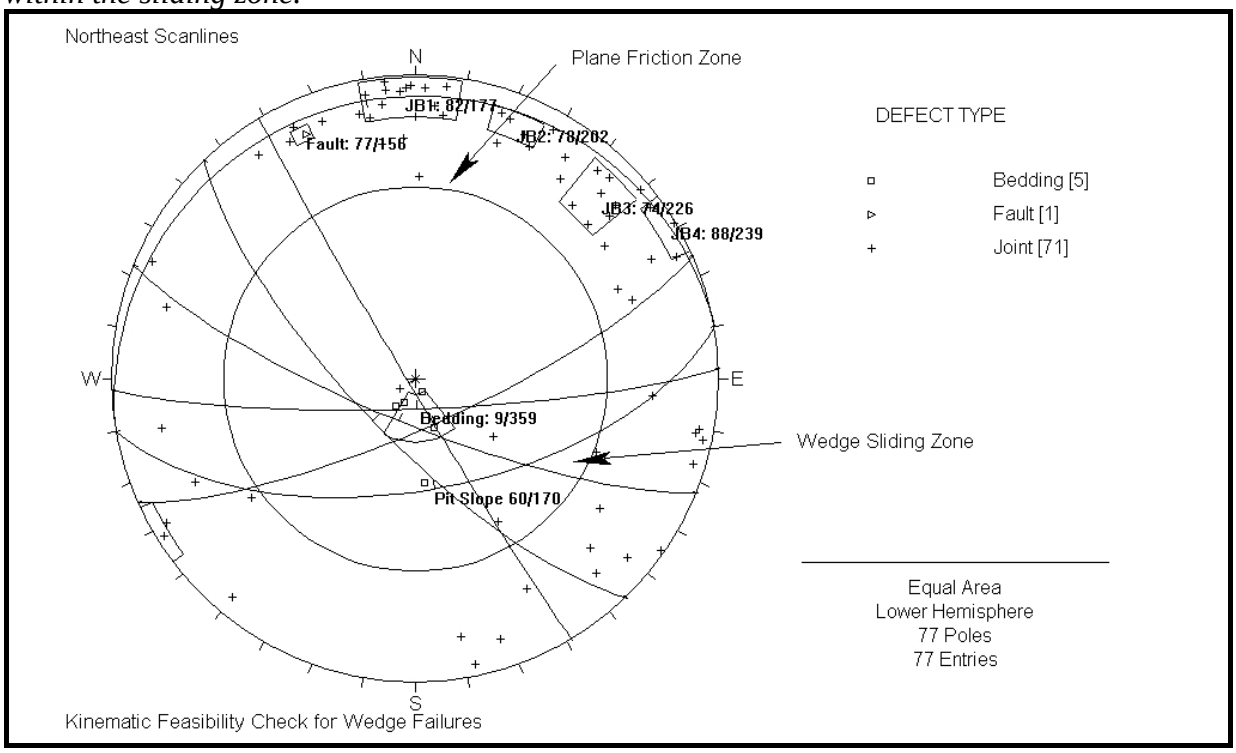

Northeast scanlines with a pit slope of 76˚/150, showing intersections between JB3 and JB4, JB2 and JB4, JB1and the fault within the sliding zone.

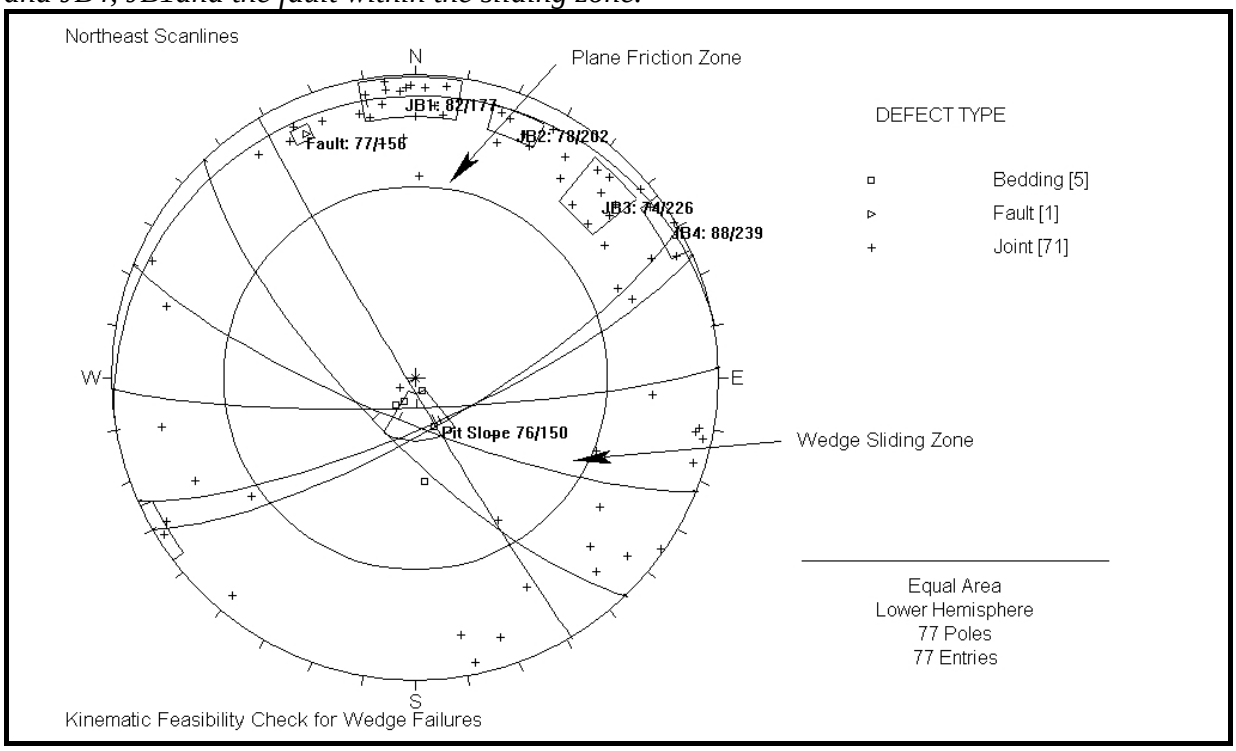

Appendix 3.6 Additional plots used to perform kinematic checks for toppling failure in the northeast scanlines.

Northeast scanlines with a pit slope of 60˚/150, showing the edge of JB1 within the toppling region.

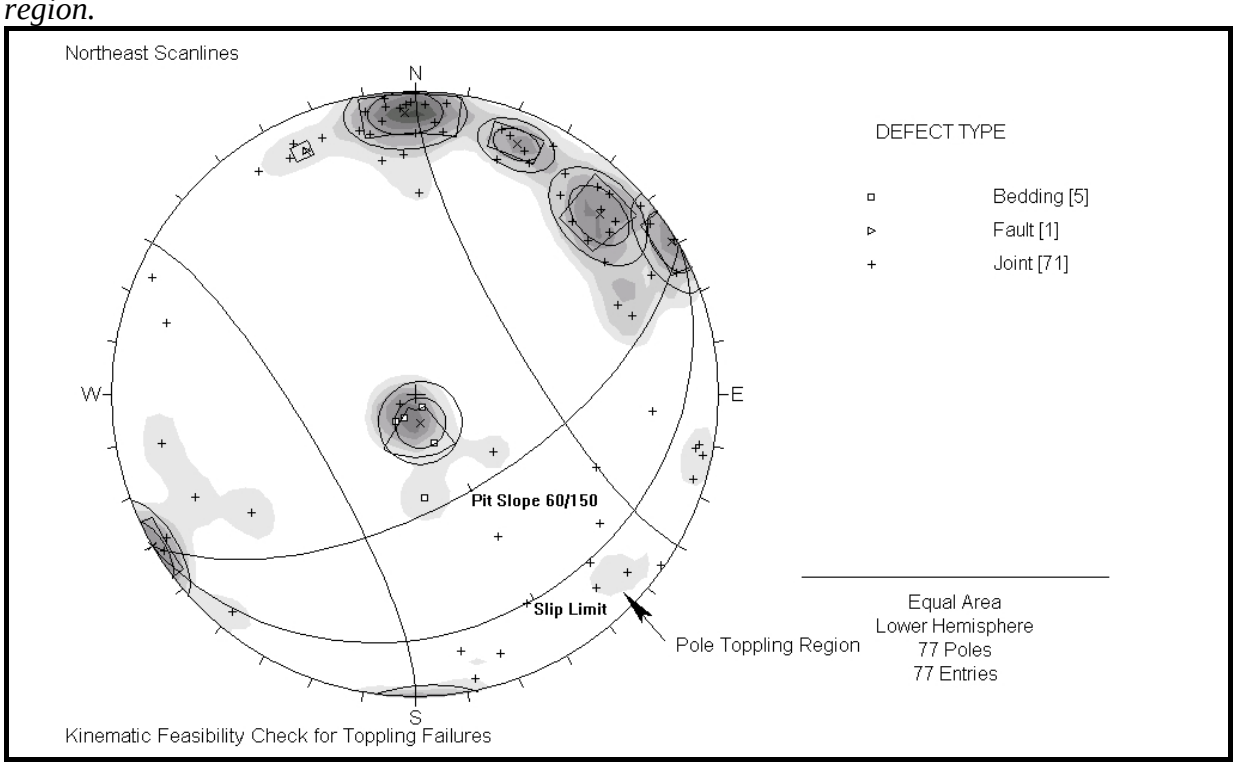

Northeast scanlines with a pit slope of 60˚/170, showing the edge of JB1 within the toppling region.

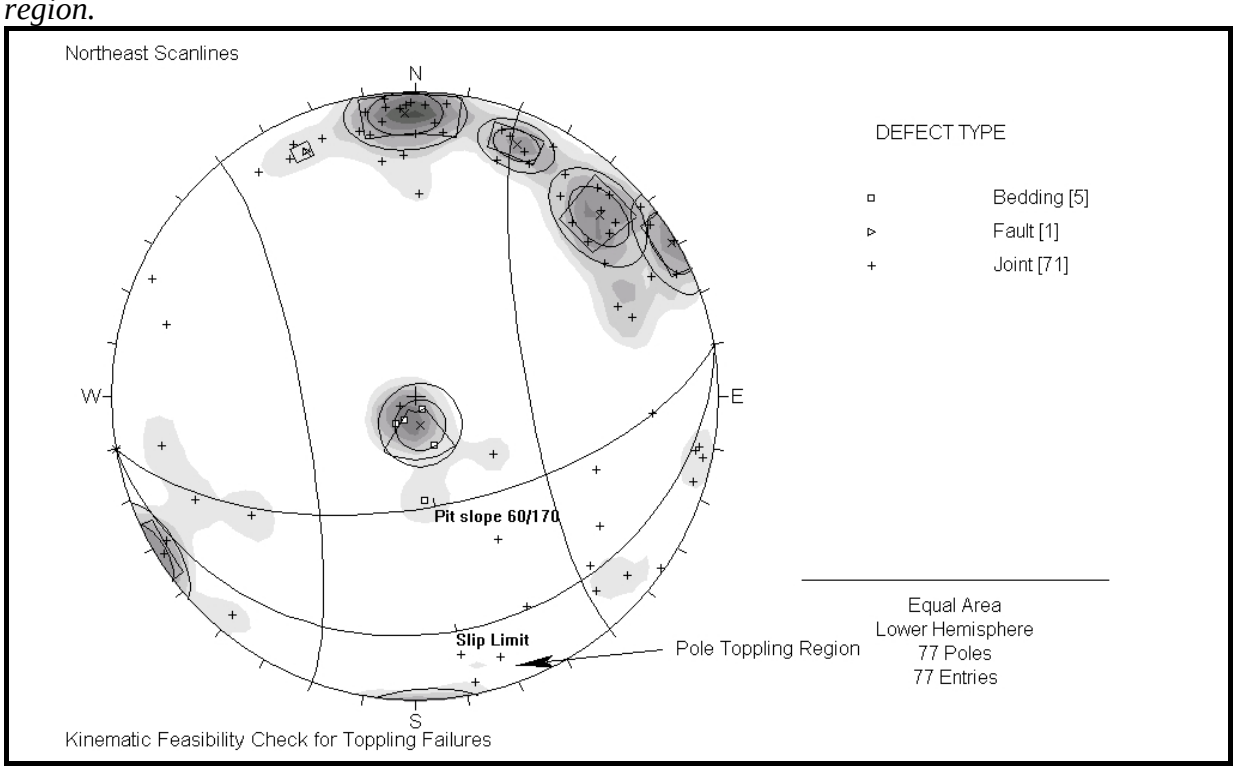

Northeast scanlines with a pit slope of 76˚/130, showing no possibility of toppling.

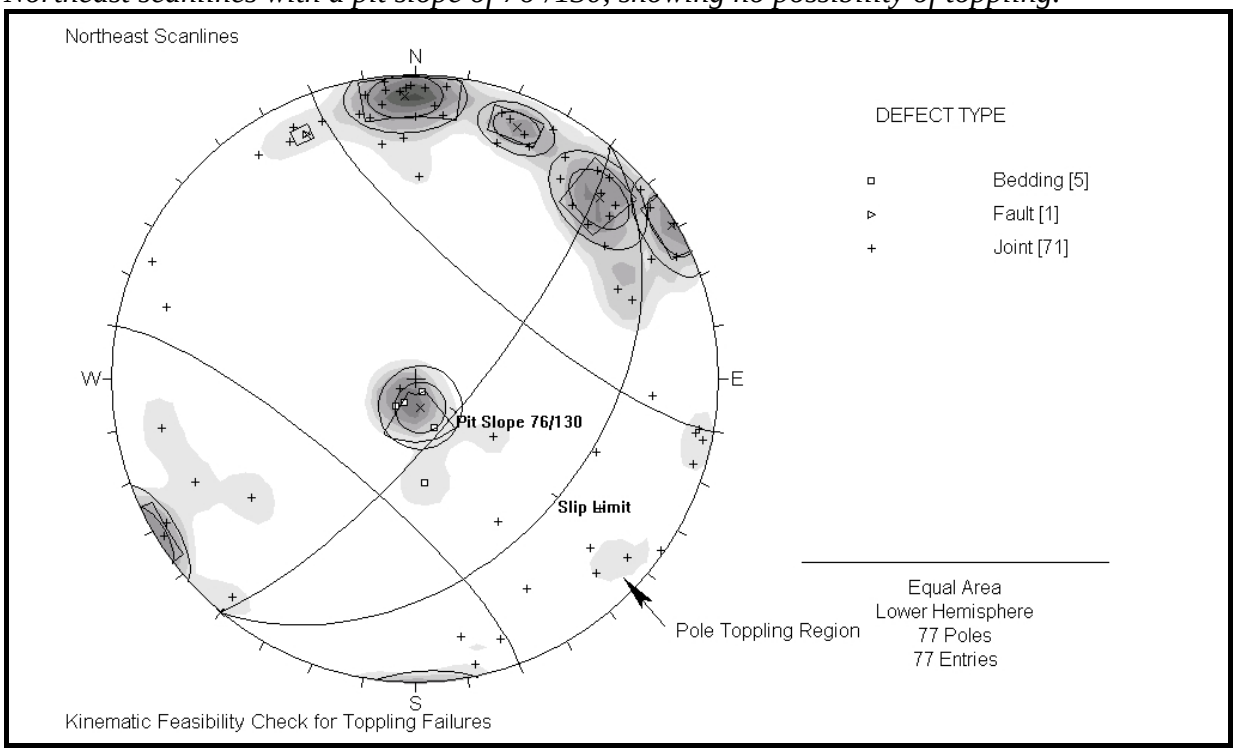

Northeast scanlines with a pit slope of 76˚/150, showing the edge of JB1 within the toppling region.

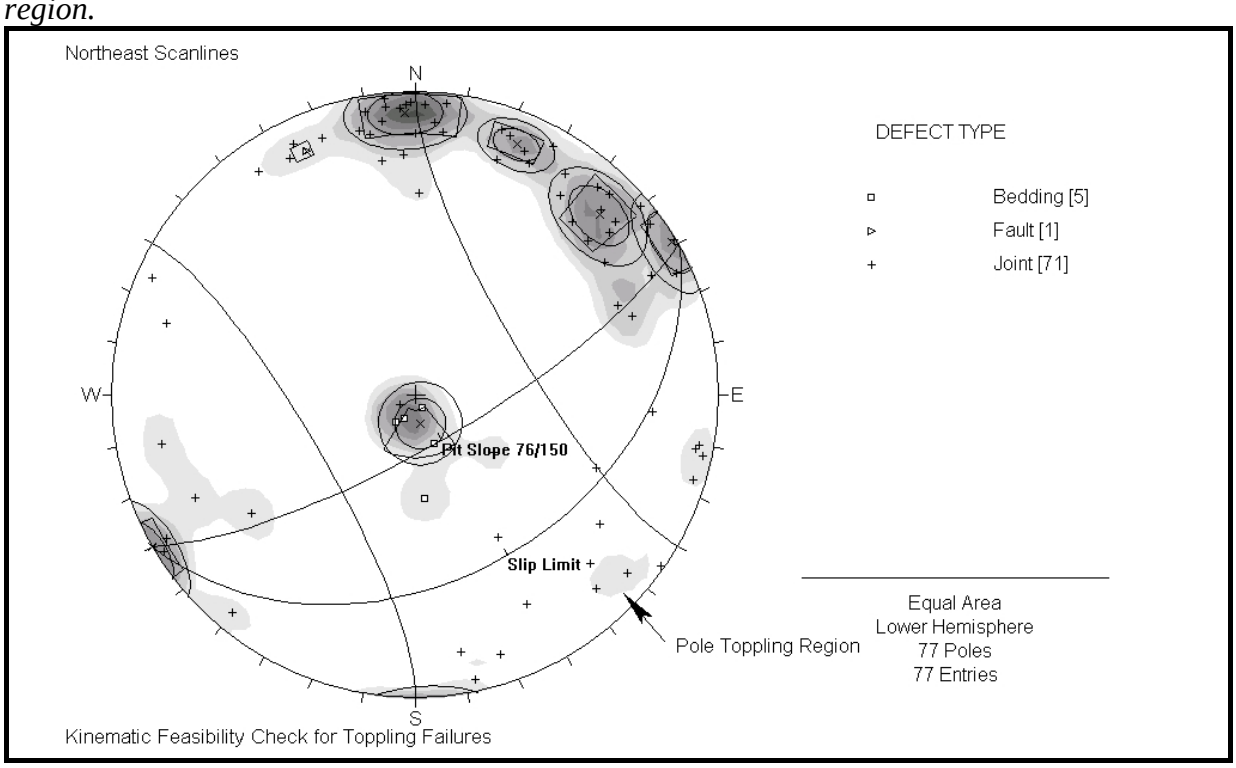

Appendix 3.7 Pole plots for scanlines 6-8 with defects sets overlain.

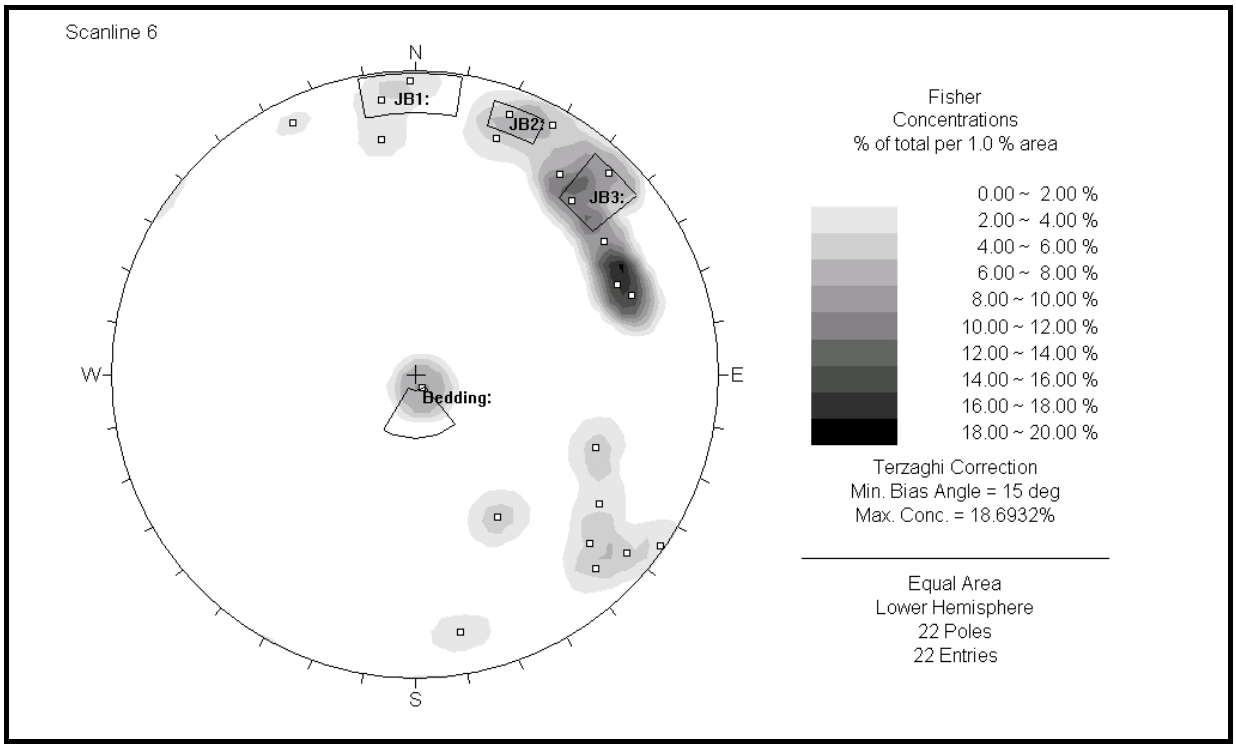

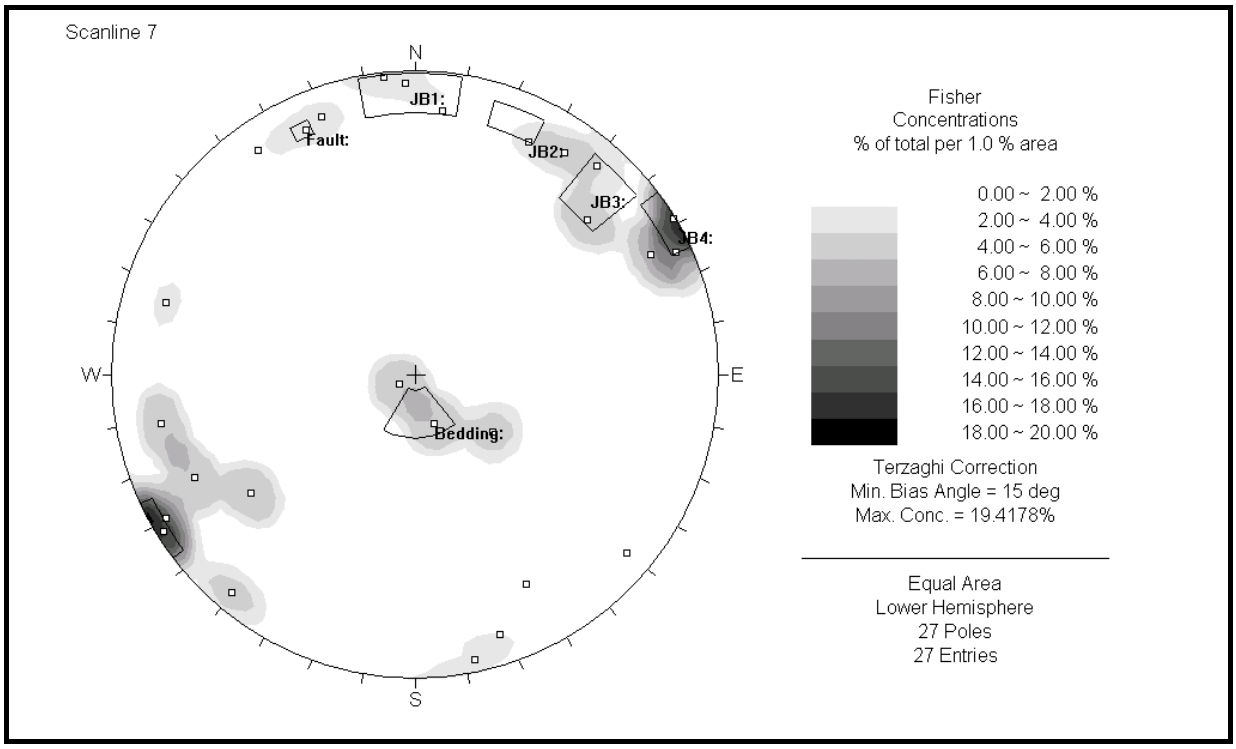
Scanline 7
N
W
E
S
JB1:
Fault:
JB2:
JB3:
JB4:
Bedding:
Fisher
Concentrations
% of total per 1.0 % area
0.00 ~ 2.00 %
2.00 ~ 4.00 %
4.00 ~ 6.00 %
6.00 ~ 8.00 %
8.00 ~ 10.00 %
10.00 ~ 12.00 %
12.00 ~ 14.00 %
14.00 ~ 16.00 %
16.00 ~ 18.00 %
18.00 ~ 20.00 %
Terzaghi Correction
Min. Bias Angle = 15 deg
Max. Conc. = 19.4178%
Equal Area
Lower Hemisphere
27 Poles
27 Entries

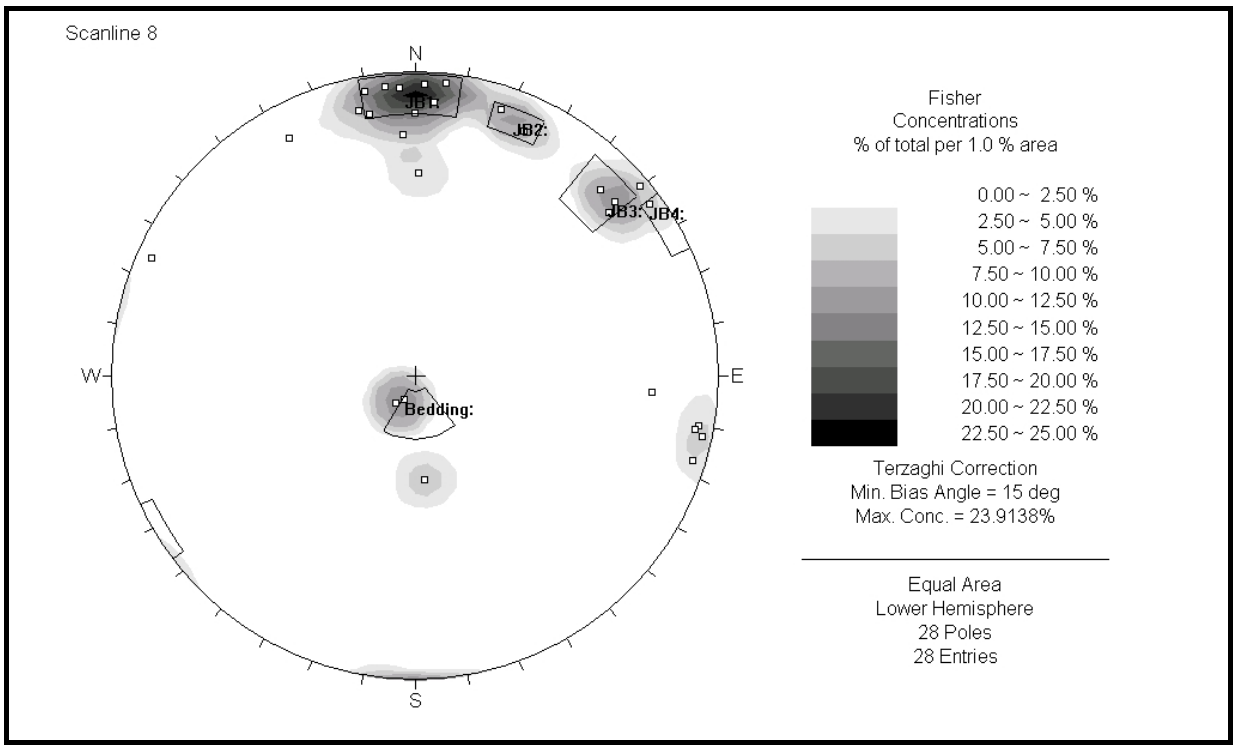
Scanline 8
N
W
E
S
JB1:
JB2:
JB3:
JB4:
Bedding:
Fisher
Concentrations
% of total per 1.0 % area
0.00 ~ 2.50 %
2.50 ~ 5.00 %
5.00 ~ 7.50 %
7.50 ~ 10.00 %
10.00 ~ 12.50 %
12.50 ~ 15.00 %
15.00 ~ 17.50 %
17.50 ~ 20.00 %
20.00 ~ 22.50 %
22.50 ~ 25.00 %
Terzaghi Correction
Min. Bias Angle = 15 deg
Max. Conc. = 23.9138%
Equal Area
Lower Hemisphere
28 Poles
28 Entries

Appendix 3.8 Swedge results.

Swedge Analysis Information

Document Name:
Test 1

Job Title:
SWEDGE - Surface Wedge Stability Analysis

Analysis Results:

Analysis type=Deterministic
Safety Factor=5.0237
Wedge height(on slope)=15 m
Wedge width(on upper face)=7.49021 m
Wedge volume=37.528 m3
Wedge weight=86.3144 tonnes
Wedge area (joint1)=60.7956 m2
Wedge area (joint2)=64.2689 m2
Wedge area (slope)=16.5847 m2
Wedge area (upper face)=7.5056 m2
Normal force (joint1)=198.132 tonnes
Normal force (joint2)=184.356 tonnes
Driving force=57.3731 tonnes
Resisting force=288.225 tonnes

Failure Mode:
Sliding on intersection line (joints 1&2)

Joint Sets 1&2 line of Intersection:
plunge=41.6592 deg, trend=150.78 deg
length=22.5666 m

Trace Lengths:
Joint1 on slope face=17.7741 m
Joint2 on slope face=17.1453 m
Joint1 on upper face=7.79207 m
Joint2 on upper face=8.56397 m

Maximum Persistence:
Joint1=22.5666 m
Joint2=22.5666 m

Intersection Angles:
J1&J2 on slope face = 6.2487 deg
J1&Crest on slope face = 68.6178 deg
J1&Crest on upper face = 106 deg
J2&Crest on slope face = 105.133 deg
J2&Crest on upper face = 61 deg
J1&2 on upper face = 13 deg

Joint Set 1 Data:

dip=74 deg, dip direction=226 deg
cohesion=0 tonnes/m2, friction angle=37 deg

Joint Set 2 Data:

dip=88 deg, dip direction=239 deg
cohesion=0 tonnes/m2, friction angle=37 deg

Slope Data:

dip=65 deg, dip direction=120 deg
slope height=15 meters
bench width=8.5 meters
rock unit weight=2.3 tonnes/m3
Water pressures in the slope=NO
Overhanging slope face=NO
Externally applied force=NO
Tension crack=NO

Upper Face Data:

dip=0 deg, dip direction=120 deg

Wedge Vertices:

Coordinates in Easting,Northing,Up Format
1=Joint1, 2=Joint2, 3=Upper Face, 4=Slope
Point 124: 0, 0, 0
Point 134: -2.82, 9.11, 15
Point 234: -3.82, 7.37, 15
Point 123: -8.23, 14.7, 15

Swedge Analysis Information

Document Name:
Test 2

Job Title:
SWEDGE - Surface Wedge Stability Analysis

Analysis Results:

Analysis type=Deterministic
Safety Factor=0.917118
Wedge height(on slope)=15 m
Wedge width(on upper face)=7.49021 m
Wedge volume=37.528 m3
Wedge weight=86.3144 tonnes
Wedge area (joint1)=60.7956 m2
Wedge area (joint2)=64.2689 m2
Wedge area (slope)=16.5847 m2
Wedge area (upper face)=7.5056 m2
Normal force (joint1)=46.1428 tonnes
Normal force (joint2)=23.6835 tonnes
Driving force=57.3731 tonnes
Resisting force=52.6179 tonnes

Water Pressures/Forces:
Average pressure on fissures=2.5 tonnes/m2
Water force on joint1=151.989 tonnes
Water force on joint2=160.672 tonnes

Failure Mode:
Sliding on intersection line (joints 1&2)

Joint Sets 1&2 line of Intersection:
plunge=41.6592 deg, trend=150.78 deg
length=22.5666 m

Trace Lengths:

Joint1 on slope face=17.7741 m
Joint2 on slope face=17.1453 m
Joint1 on upper face=7.79207 m
Joint2 on upper face=8.56397 m

Maximum Persistence:
Joint1=22.5666 m
Joint2=22.5666 m

Intersection Angles:
J1&J2 on slope face = 6.2487 deg
J1&Crest on slope face = 68.6178 deg
J1&Crest on upper face = 106 deg
J2&Crest on slope face = 105.133 deg
J2&Crest on upper face = 61 deg
J1&2 on upper face = 13 deg

Joint Set 1 Data:

dip=74 deg, dip direction=226 deg
cohesion=0 tonnes/m2, friction angle=37 deg

Joint Set 2 Data:

dip=88 deg, dip direction=239 deg
cohesion=0 tonnes/m2, friction angle=37 deg

Slope Data:

dip=65 deg, dip direction=120 deg
slope height=15 meters
bench width=8.5 meters
rock unit weight=2.3 tonnes/m3
Water pressures in the slope=YES
Overhanging slope face=NO
Externally applied force=NO
Tension crack=NO

Upper Face Data:

dip=0 deg, dip direction=120 deg

Water Pressure Data:

Water unit weight=1 tonnes/m3
Pressure definition method=Filled Fissures

Wedge Vertices:

Coordinates in Easting,Northing,Up Format
1=Joint1, 2=Joint2, 3=Upper Face, 4=Slope
Point 124: 0, 0, 0
Point 134: -2.82, 9.11, 15
Point 234: -3.82, 7.37, 15
Point 123: -8.23, 14.7, 15

Swedge Analysis Information

Document Name:
Test 3

Job Title:

SWEDGE - Surface Wedge Stability Analysis

Analysis Results:

Analysis type=Deterministic
Safety Factor=1.43604
Wedge height(on slope)=15 m
Wedge width(on upper face)=1.92252 m
Wedge volume=29.5576 m3
Wedge weight=67.9826 tonnes
Wedge area (joint1)=43.425 m2
Wedge area (joint2)=45.9059 m2
Wedge area (slope)=16.5847 m2
Wedge area (upper face)=3.35848 m2
Wedge area (tension crack)=4.29462 m2
Normal force (joint1)=57.5041 tonnes
Normal force (joint2)=38.7064 tonnes
Driving force=50.4858 tonnes
Resisting force=72.4998 tonnes

Water Pressures/Forces:
Average pressure on fissures=1.9219 tonnes/m2
Water force on joint1=83.4587 tonnes
Water force on joint2=88.2268 tonnes
Water force on tension crack=8.25386 tonnes

Failure Mode:
Sliding on intersection line (joints 1&2)

Joint Sets 1&2 line of Intersection:
plunge=41.6592 deg, trend=150.78 deg
length=13.8924 m

Trace Lengths:
Joint1 on slope face=17.7741 m
Joint2 on slope face=17.1453 m
Joint1 on upper face=2 m
Joint2 on upper face=2.19812 m
Tension crack on upper face=1.48971 m

Maximum Persistence:
Joint1=18.8137 m
Joint2=18.3092 m

Intersection Angles:
J1&J2 on slope face = 6.2487 deg
J1&Crest on slope face = 68.6178 deg
J1&Crest on upper face = 106 deg
J2&Crest on slope face = 105.133 deg
J2&Crest on upper face = 61 deg
J1&TC on upper face = 74 deg
J2&TC on upper face = 119 deg

Joint Set 1 Data:

dip=74 deg, dip direction=226 deg
cohesion=0 tonnes/m2, friction angle=37 deg

Joint Set 2 Data:

dip=88 deg, dip direction=239 deg
cohesion=0 tonnes/m2, friction angle=37 deg

Slope Data:

dip=65 deg, dip direction=120 deg
slope height=15 meters
bench width=8.5 meters
rock unit weight=2.3 tonnes/m3
Water pressures in the slope=YES
Overhanging slope face=NO
Externally applied force=NO
Tension crack=YES

Upper Face Data:

dip=0 deg, dip direction=120 deg

Tension Crack Data:

dip=90 deg, dip direction=120 deg
trace length=2 meters

Water Pressure Data:

Water unit weight=1 tonnes/m3
Pressure definition method=Filled Fissures

Wedge Vertices:

Coordinates in Easting,Northing,Up Format
1=Joint1, 2=Joint2, 3=Upper Face, 4=Slope, 5=Tension Crack
Point 124: 0, 0, 0
Point 134: -2.82, 9.11, 15
Point 234: -3.82, 7.37, 15
Point 135: -4.21, 10.5, 15
Point 125: -5.07, 9.06, 9.23
Point 235: -4.95, 9.26, 15

Appendix 4 Case Hardening Investigation

Table of Contents

Appendix 4.1 Investigation methods

Outcrop Description

Six sites were selected showing representative rock coatings, which appeared to be case-hardening the sandstone units. These were situated in the existing highwalls on the southwest side of the Reddale Valley and in the neighbouring Peerless Gully. Hand specimens that displayed well developed crust were taken from each site. Photographs of each site were taken at varying scales to assess location factors and continuity of the coating. A handheld GPS was used to record the co-ordinates of each site, which are displayed in appendix 4.1. The sites are also plotted on Map C (Aerial Photograph –map pocket).

A Proceq Type L Concrete Test Hammer (Schmidt Hammer) was used to assess any difference in strength between the weathered surface and fresh rock. The same method as outlined in chapter 3, where the average of the highest 5 out of 10 or more readings, was used to calculate a rebound number. The higher the rebound number, the stronger the rock. There is some debate concerning the effectiveness of the Schmidt hammer on producing meaningful readings from weathered surfaces. The hammer may have a ‘depth of influence’, within which the results are affected by discontinuities and weakened material (Hack and Huisman, 2002). However there

have been many studies conducted that validate the use of the hammer to show how weathering weakens if not hardens the outer crust (Aydin and Basu, 2005), and it has been used here as an indication of alteration. The strength of the rock coating was also assessed by scraping and amount of penetration with a knife blade.

Hand specimen examination

Hand specimens were collected at each site with some difficulty as the crust tended to disintegration during the process. A hammer and chisel proved the most effective in collecting reasonably sized samples of the rock coatings. The sample was wrapped in glad warp and surrounded in cotton wool to prevent breakage during transportation. A description of the samples from each site was completed with the use of a handlens, and photographs were captured using a Heerbrugg Wild reflected light microscope.

Thin section Study

Thin sections for petrographic analysis were prepared in the Department of Geological Sciences, University of Canterbury. The sandstones were impregnated with Epo-teck 301 resin so that they could be successfully cut. They were ground with silica carbide on a Logitech LP50 to standard thickness (approximately 30μm) and a cover slip applied. Digital photographs were taken on a Leica DMRXP polarising microscope. The gradation in natural colours was observed better in some samples under the reflected light microscope. The thin sections where found to be of limited use when analysing the extremely fine grained cement between grains. Mineral identification was conducted with assistance from Dr David Shelley, Department of Geological Sciences, University of Canterbury.

SEM (Scanning Electron Microscope) Investigation

The SEM in the School of Biological Sciences at the University of Canterbury was used to take photos of the rock coating at very high magnification. A SEM uses electrons instead of light to form a picture and the samples are made electrically conductive by the application of a thin coating of metal before use. Small ($1.5cm^2$) samples were trimmed to provide as smooth a surface as possible and mounted on stubs with Araldite glue. The samples were orientated to either view the top surface or a cross-section through the crust and underlying material. After drying the samples were coated in gold using a Polaron E5000, which was operated for four minutes at 1.2kV and 20mA. The SEM used was a Leica S440, and variable settings were used according to the sample dimensions. For each sample the lowest possible kV and spot size were

used to get the best quality photographs. A basic diagram illustrating how the SEM works is given below.

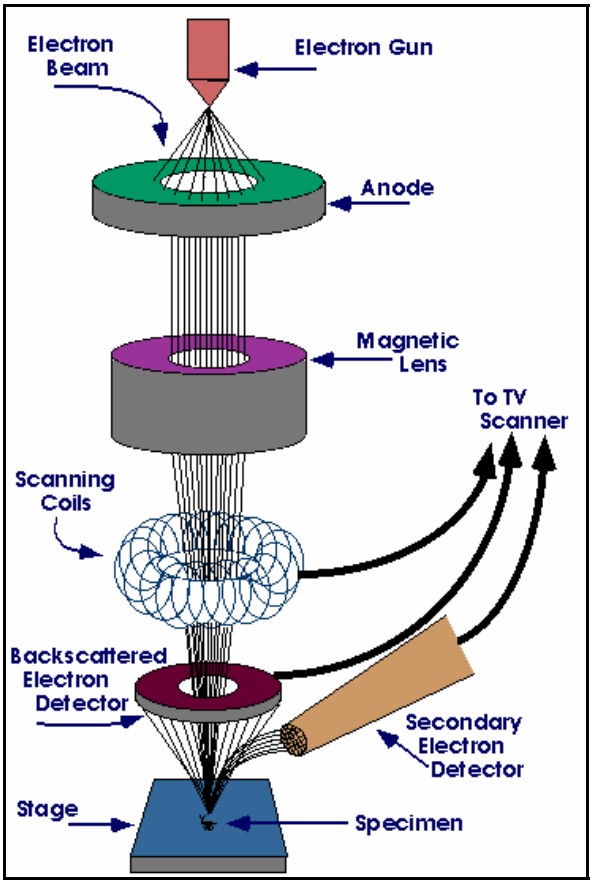

Source: http://mse.iastate.edu/microscopy/college.html

A Robinson backscatter detector produced the clearest photographs. The images were taken at a range of magnifications to gather information on the surface as a whole, as well as individual crystal/biological details. As biological elements were not originally expected the samples were stored at room temperature for up to week before preparation and very thin fungal hypae can be observed in many of the photos on the surface of the sample. These must be regarded as post sampling growths and not part of the in-situ rock coatings. General identification of biological matter was conducted with aid from Associate Professor, Dr Laurie Greenfield, School of Biological Sciences, University of Canterbury.

EDS (Energy Dispersive Spectra) Analysis

When an EDS analyser is used with the SEM it is able to identify the elements at any particular location on the sample. Polished thin sections were used to remove any distortion from uneven sample surfaces. The samples once impregnated with resin and mounted on a slide were firstly polished with 3µ diamond paste on a ceramic lap. They were then polished with 1µm followed by 0.25µm diamond paste on a Lamplan cloth lap. Ethan diol was used as lubricant and the thin sections were prepared in the Department of Geological Sciences, University of Canterbury. An

Edwards Carbon Coater in the School of Biological Sciences was used to apply a light carbon coating to the thin sections. An Oxford Pentafet link EDS was attached to the SEM used above. A Link ISIS computer system recorded the resulting spectra. Spot and bulk scans provided an idea of the elements present and their abundance relative to one another.

Interpretation was conducted with the help of Professor Steve Weaver of the Department of Geological Sciences. Line scans were also performed and show the relative concentration of elements along the length of the line. That is the horizontal axis provides the actual length of the scan while the relative concentration is shown on the vertical axis. These were conducted more than 3 times at different points along the thin sections to confirm that they were representative. This method produced limited results; some sites did not produce any pattern in terms of increasing or decreasing amounts of elements.

XRD (X-ray Diffraction) Analysis

When illuminated by an x-ray source, crystalline material will generate x-ray diffraction peaks, which can be analysed to understand the material and molecular structure of the substance. The surface of the rock coating was carefully scrapped off and ground with ethanol to form a slurry. This was applied to a glass slide and left to dry at room temperature. The slide was then trimmed and placed in the Phillips PW 1729 X-ray generator, which is housed in the Department of Geological Sciences at the University of Canterbury. A tube copper target was used and operated at 50kV and 40mA. The data was recorded as a digital file and compared against known crystal phases to identify the minerals present. The percentage of each mineral in that particular sample was also estimated.

pH and EC (Electrical Conductivity) Determination

To gain an idea of the acidity and the amount of total dissolved salts of the rock coating, the pH and EC was measured for each site. A 25g sample was pulverised using a mortar and pestle and made into a slurry by adding 50g of distilled water, while continuously stirring (Ian Wark Research Institute, Test procedure, 2002). This was left to stand overnight and then readings were taken using a CyberScan PC 300 by Eutech Instruments.

Appendix 4.2 Handheld GPS co-ordinates for investigation of case hardening.

Site	Easting	Northing	Accuracy (±m)
1	2417383	5899158	14
2	2417397	5899161	7
3	2417371	5898974	7
4	2417372	5898921	11
5	2418420	5899851	16
6	2418405	5899851	15

Appendix 4.3 Raw Schmidt Hammer data.

	Site 1		**Site 2**		**Site 3**	
No. of tests	Crust	Fresh	Crust	Fresh	Crust	Fresh
1	20	12	22	14	20	16
2	28	14	22	15	20	19
3	28	14	24	16	21	21
4	29	15	24	16	21	21
5	29	16	24	19	21	22
6	29	18	25	20	23	22
7	29	20	25	20	25	22
8	29	22	25	21	25	22
9	30	24	27	21	25	23
10	30	24	28	24	26	23
11						26
Rebound No. (Av. of highest 5)	**30**	**23**	**26**	**22**	**25**	**24**

	Site 4		**Site 5**		**Site 6**	
No. of tests	Crust	Fresh	Crust	Fresh	Crust	Fresh
1	10	10	15	15	10	10
2	10	10	15	15	10	10
3	10	11	15	20	10	10
4	10	11	15	20	11	11
5	11	12	16	20	11	11
6	12	12	16	21	12	13
7	12	13	16	22	12	13
8	12	14	20	25	12	14
9	13	14	21	25	12	15
10	14	15	22	26	12	15
11			23			
12			25			
Rebound No. (Av. of highest 5)	**13**	**14**	**23**	**25**	**12**	**14**

Appendix 4.4 XRD Results

Site 1

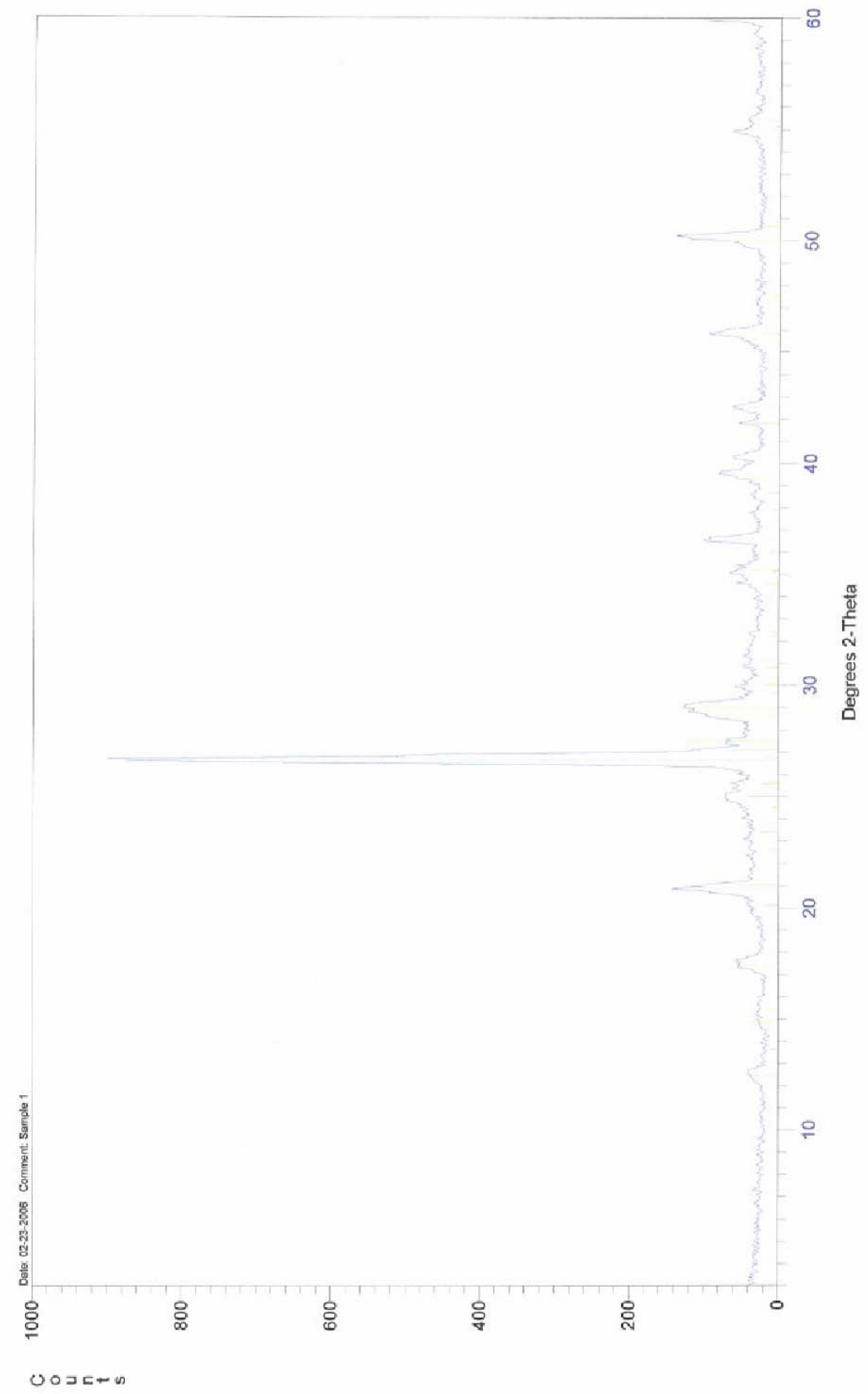

Site 2

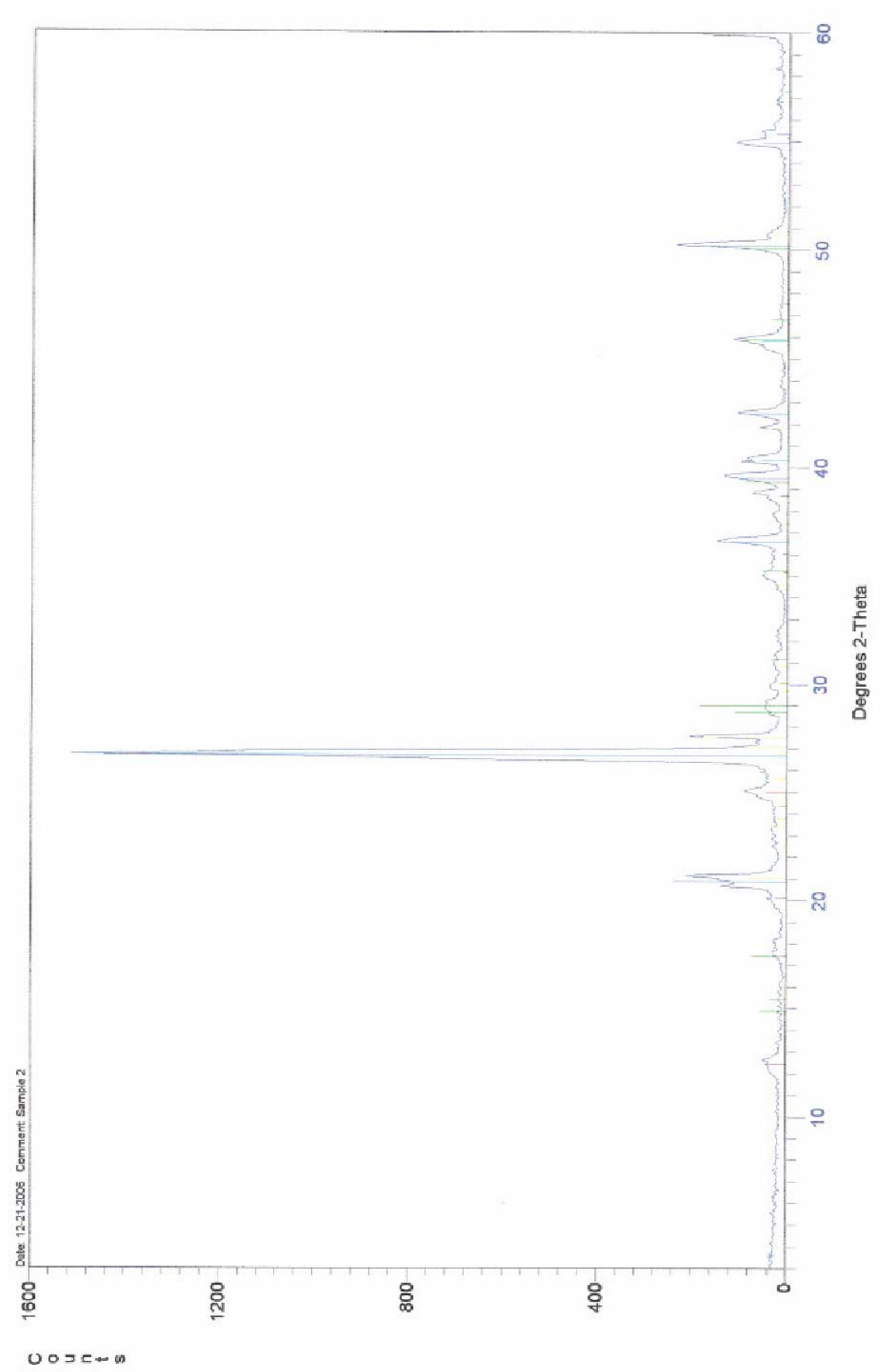
Date: 12-21-2006 Comment: Sample 2
Counts
1600
1200
800
400
0
10
20
30
40
50
60
Degrees 2-Theta

Site 3

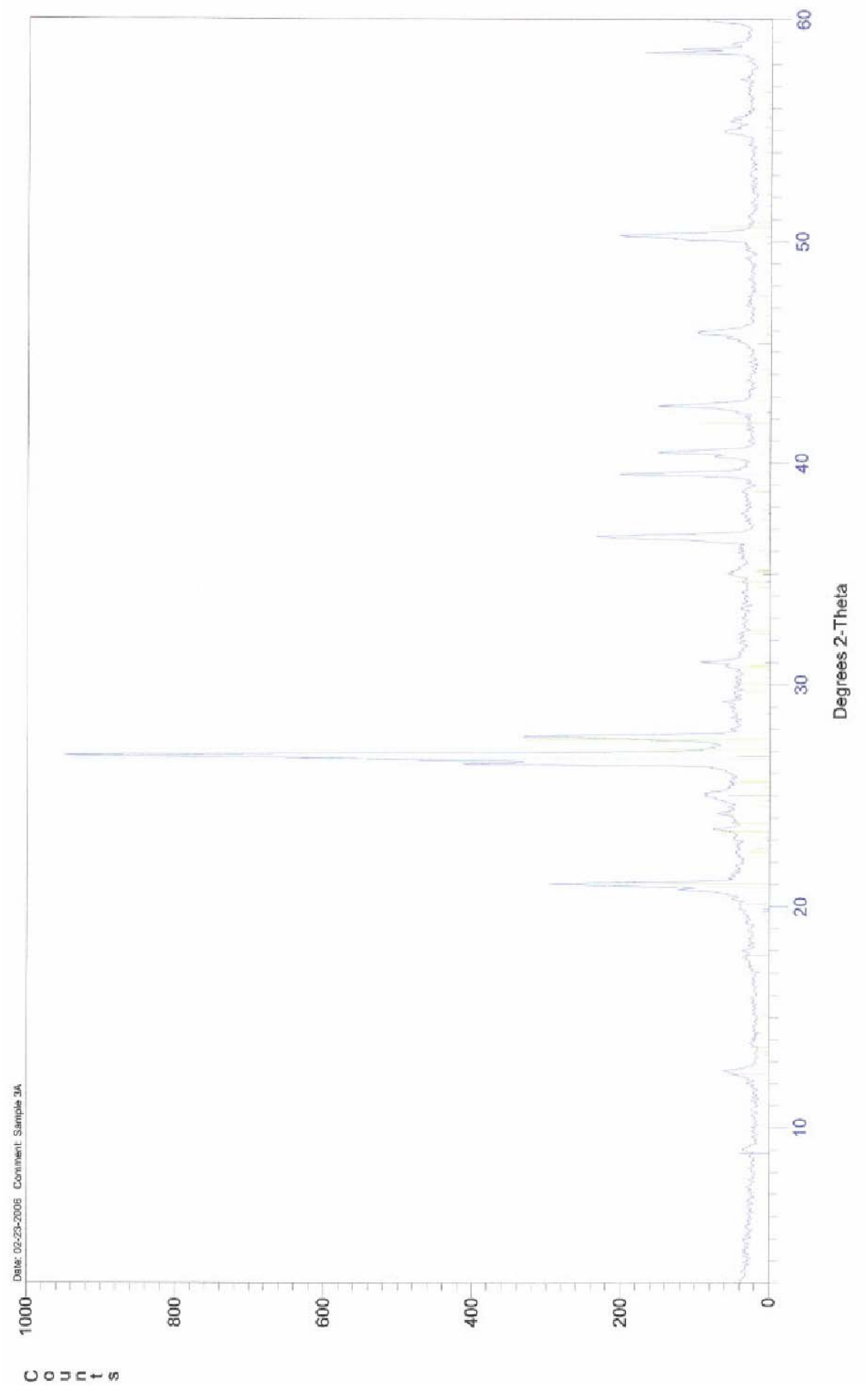
Date: 02-23-2006 Comment: Sample 3A
Counts
1000
800
600
400
200
0
10
20
30
40
50
60
Degrees 2-Theta

Site 4

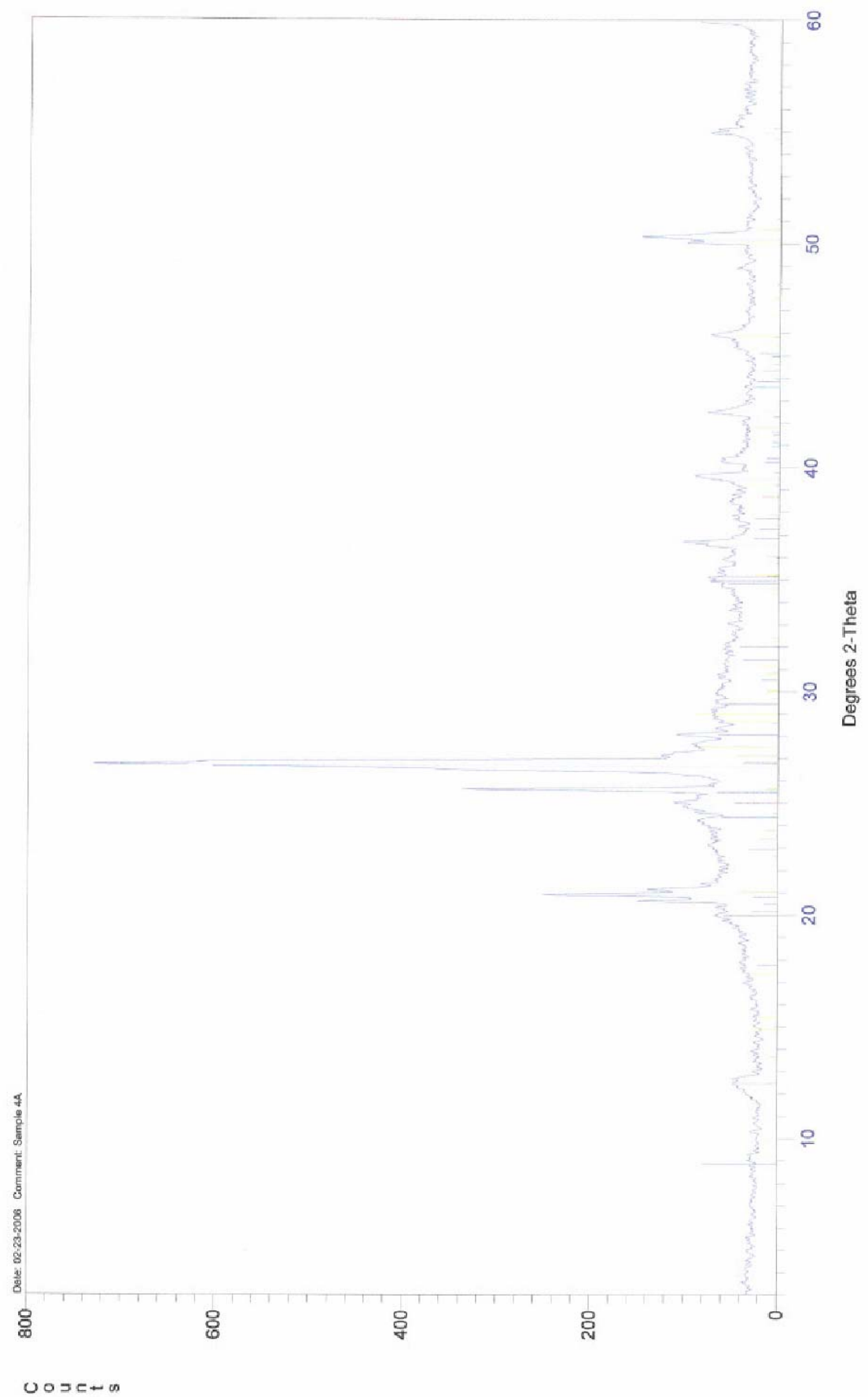
Date: 02-23-2006 Comment: Sample 4A
Counts
800
600
400
200
0
10
20
30
40
50
60
Degrees 2-Theta

Site 5

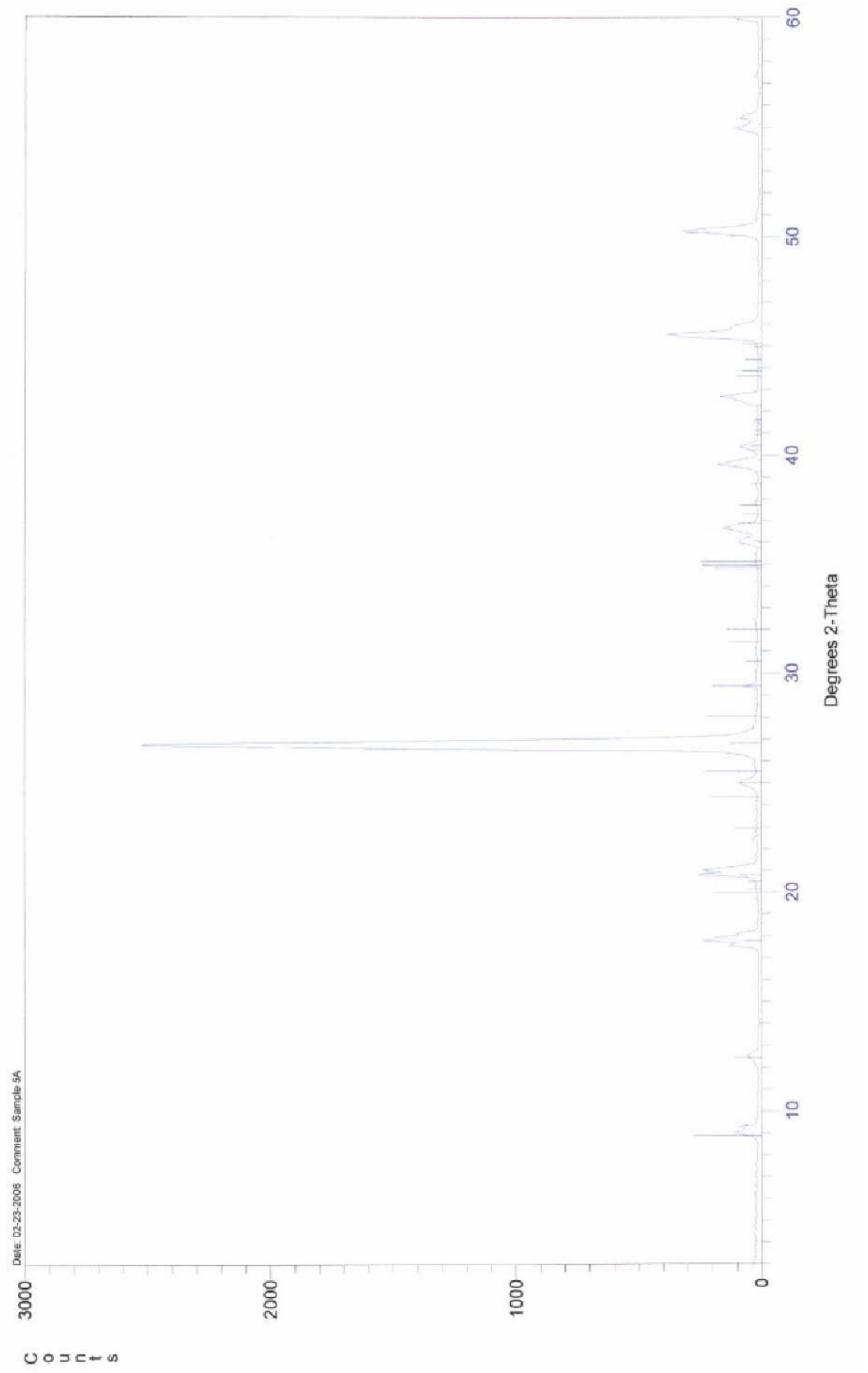
Date: 02-23-2006 Comment: Sample 5A
Counts
3000
2000
1000
0
10
20
30
40
50
60
Degrees 2-Theta

Site 6

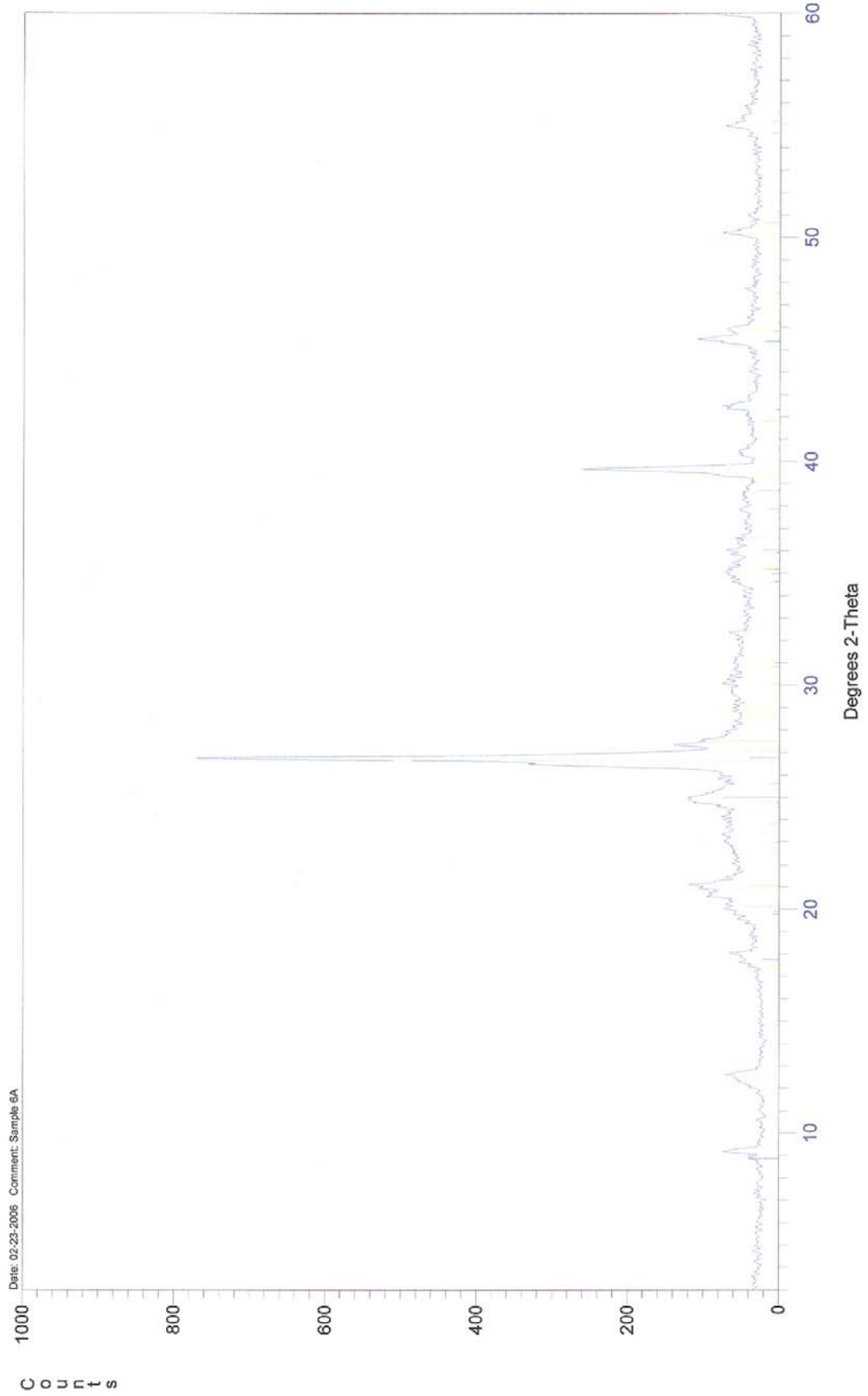
Date: 02-23-2006 Comment: Sample 6A
Counts
1000
800
600
400
200
0
10
20
30
40
50
60
Degrees 2-Theta

Appendix 4.5 Bulk EDS scans

Site 1

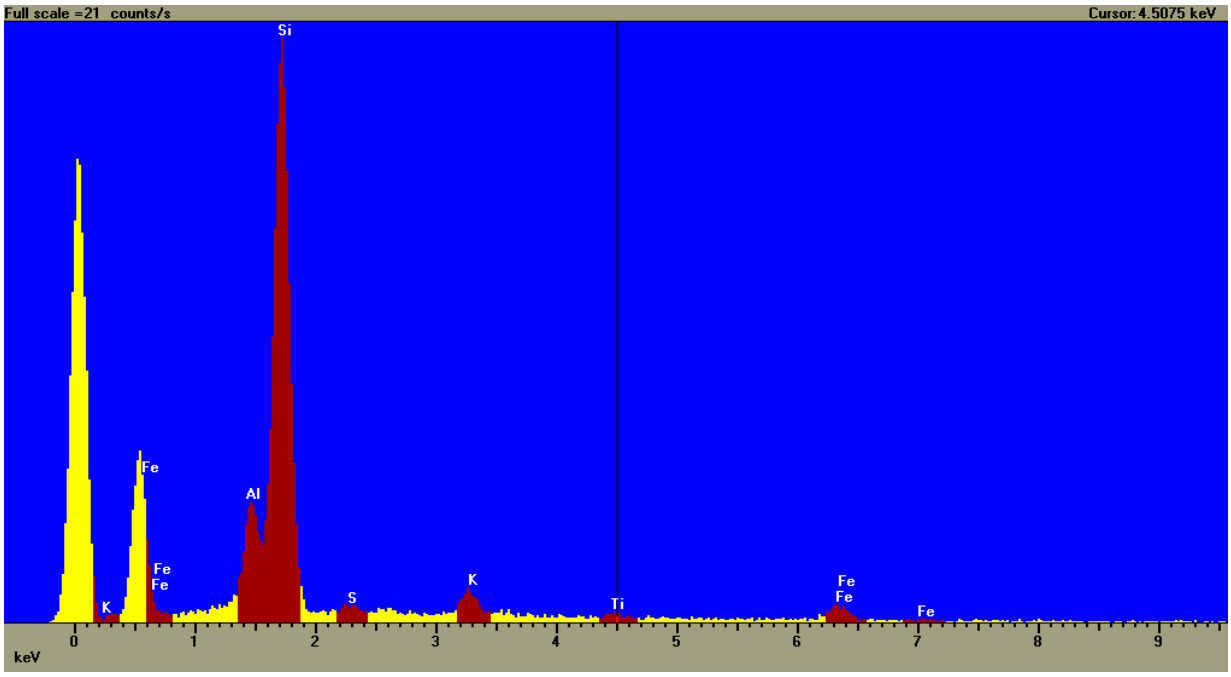

Site 2

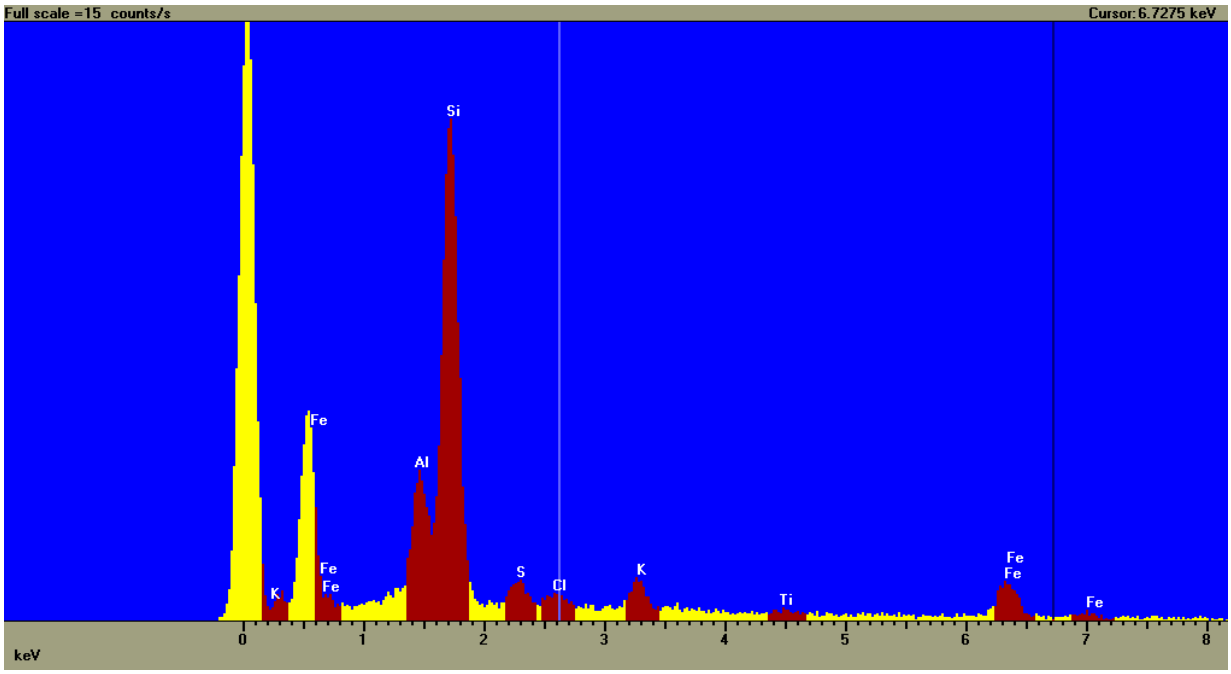

Site 3

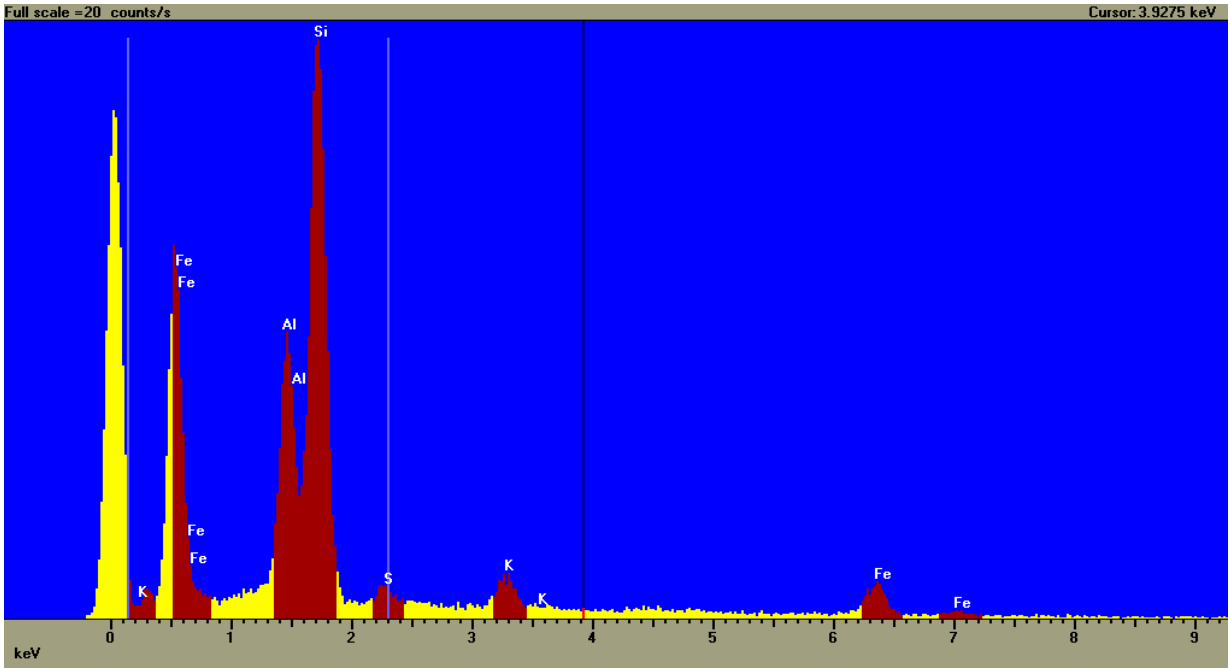
Full scale =20 counts/s
Cursor: 3.9275 keV
Si
Fe
Fe
Al
Al
Fe
Fe
K
S
K
K
Fe
Fe
0
1
2
3
4
5
6
7
8
9
keV

Site 4

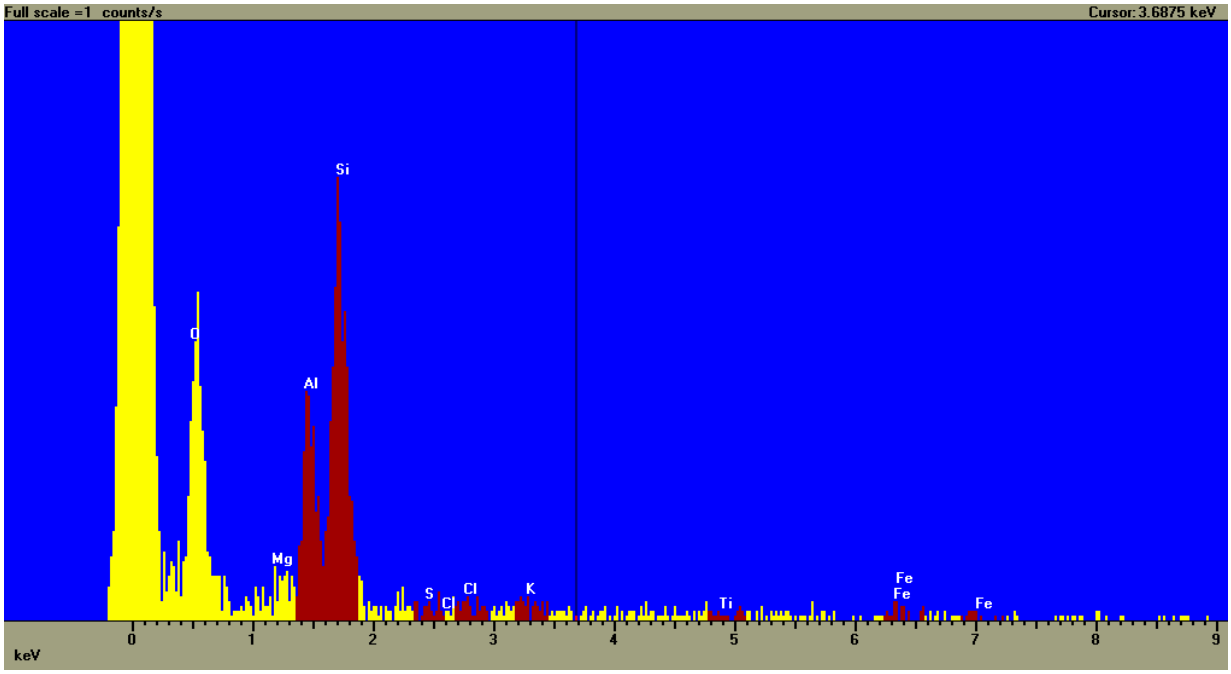
Full scale =1 counts/s
Cursor: 3.6875 keV
Si
O
Al
Mg
S
Cl
Cl
K
Ti
Fe
Fe
Fe
0
1
2
3
4
5
6
7
8
9
keV

Site 5

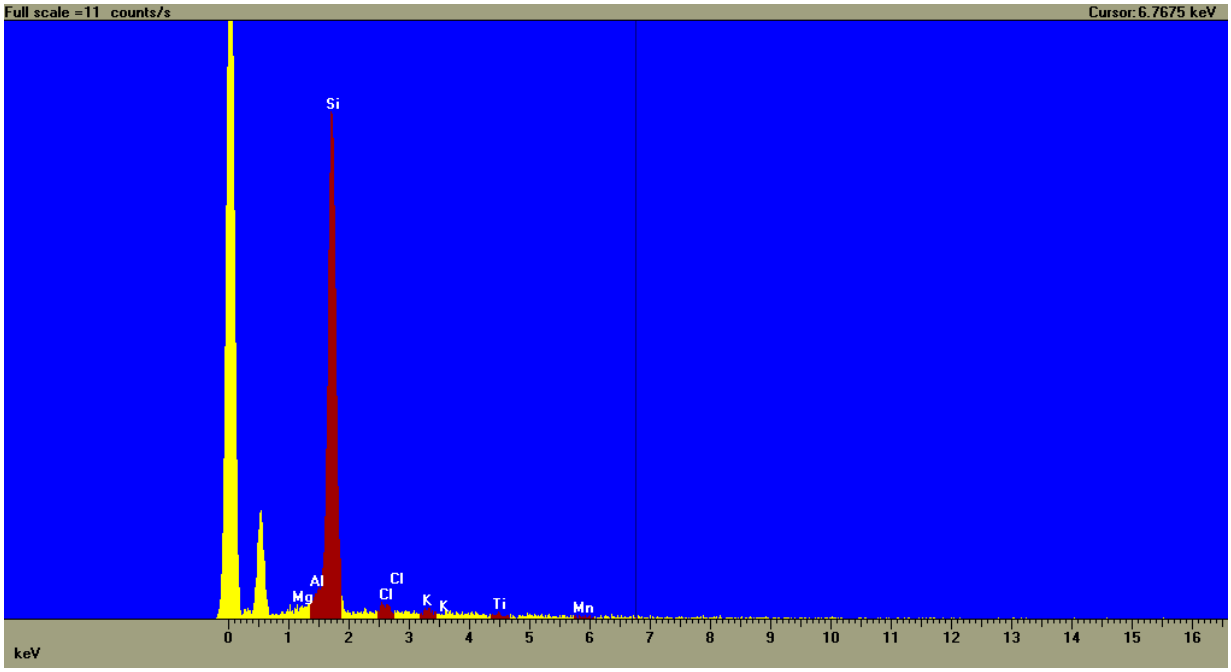
Full scale =11 counts/s
Cursor: 6.7675 keV
Si
Al
Mg
Cl
Cl
K
K
Ti
Mn
0 1 2 3 4 5 6 7 8 9 10 11 12 13 14 15 16
keV

Site 6

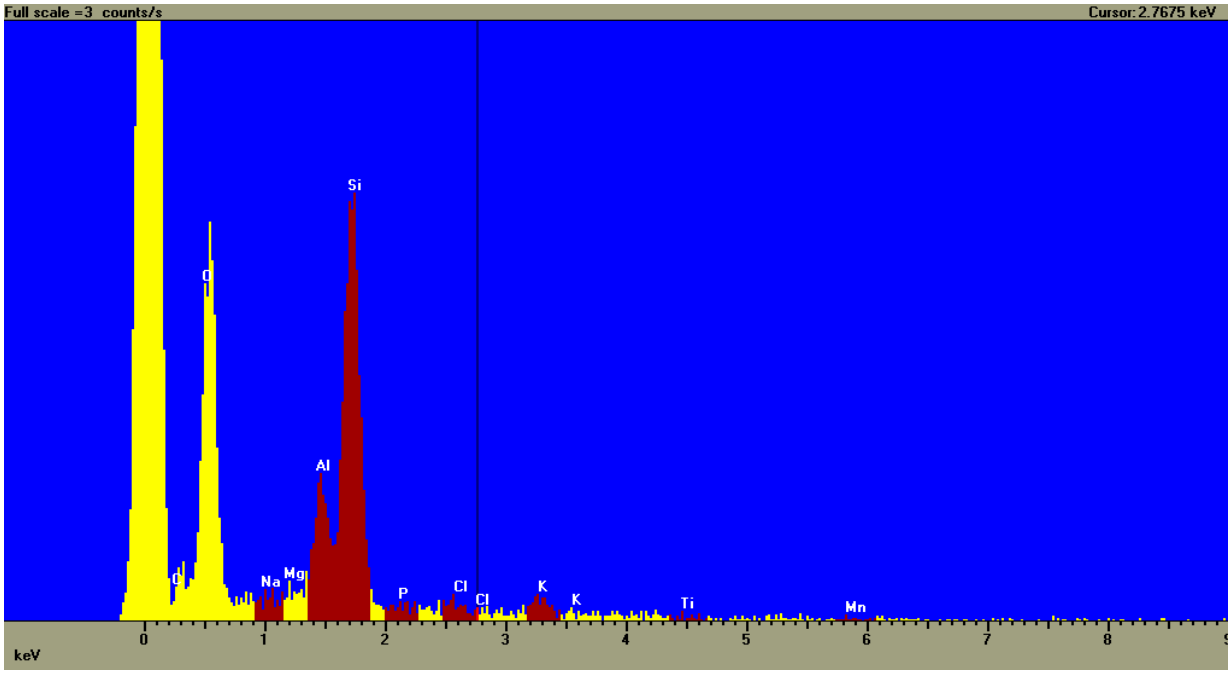
Full scale =3 counts/s
Cursor: 2.7675 keV
Si
O
Al
Na
Mg
P
Cl
Cl
K
K
Ti
Mn
0 1 2 3 4 5 6 7 8
keV

Appendix 4.6 Line EDS

Please note the lengths on the scans are incorrect for sites 1 to 3 due to a calibration error.

Site 1

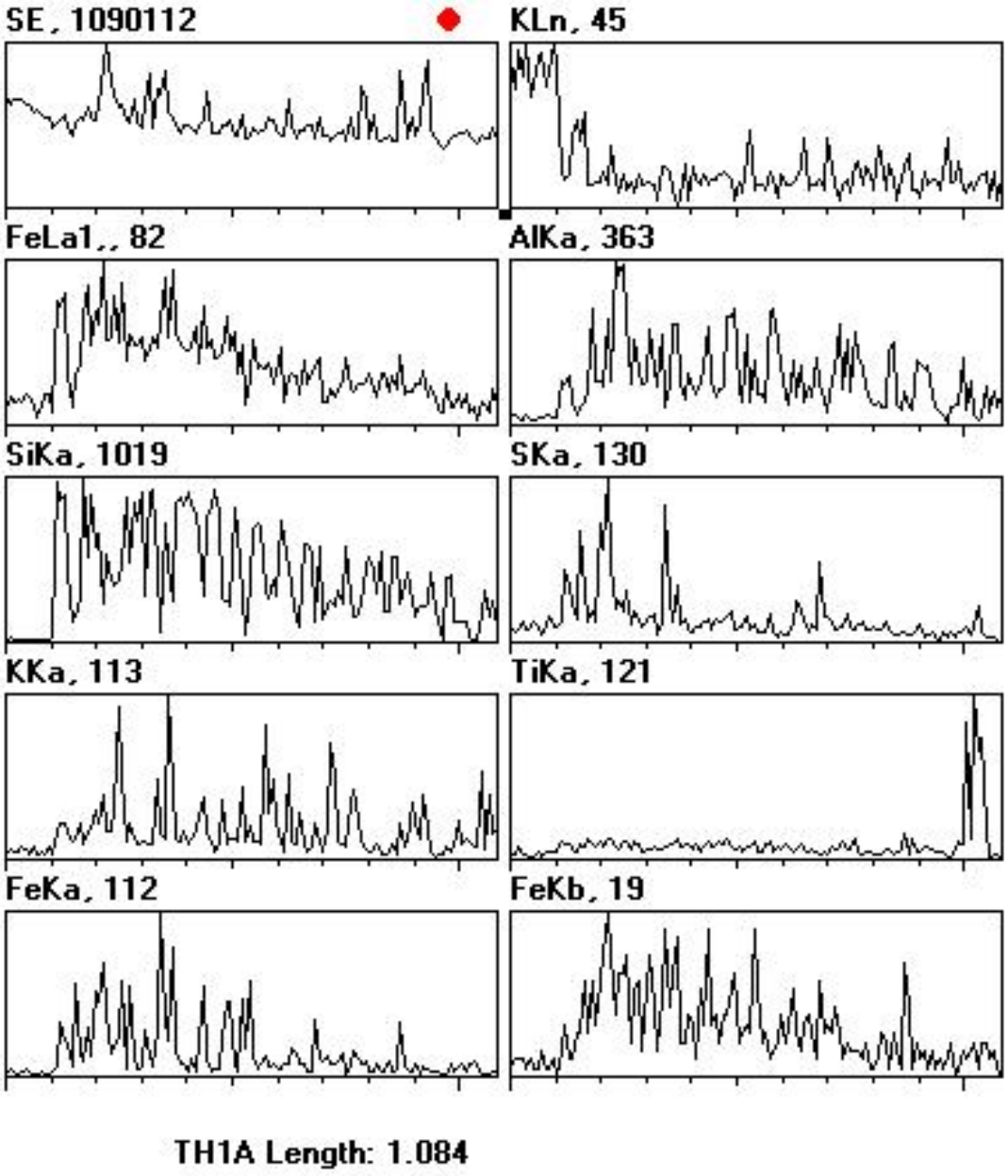

Site 2

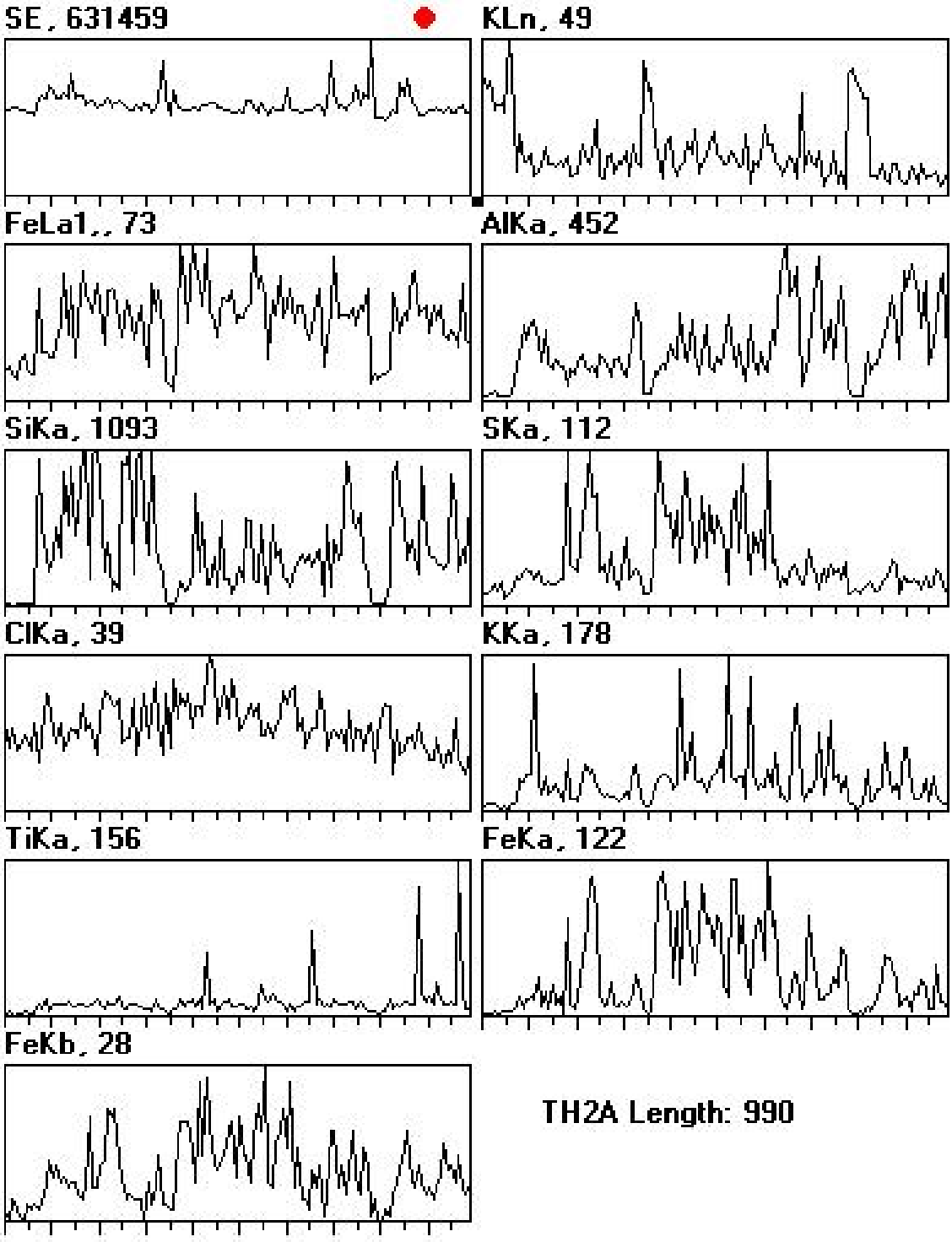
SE, 631459
KLn, 49
FeLa1,, 73
AlKa, 452
SiKa, 1093
SKa, 112
ClKa, 39
KKa, 178
TiKa, 156
FeKa, 122
FeKb, 28
TH2A Length: 990

Site 3

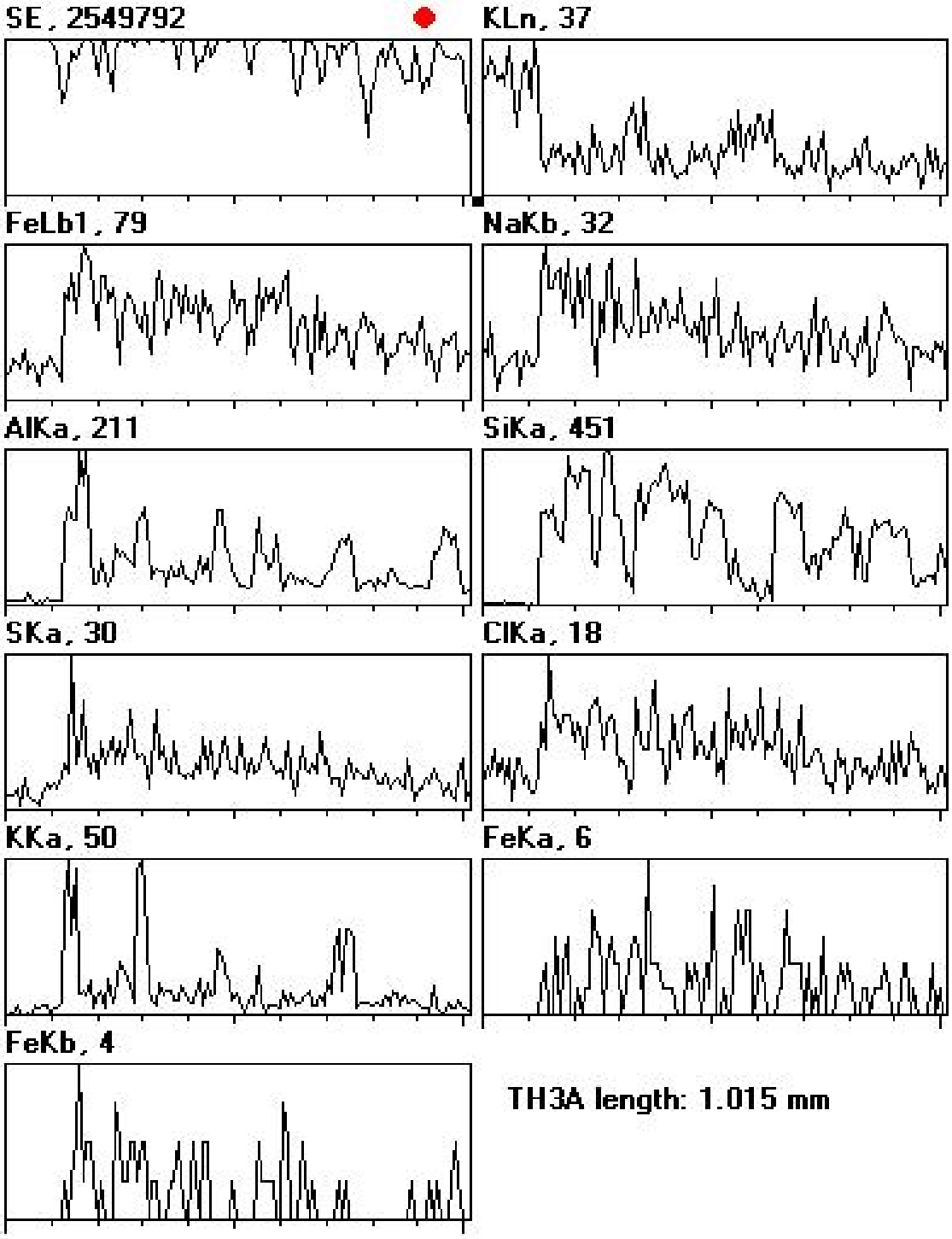
SE, 2549792
KLn, 37
FeLb1, 79
NaKb, 32
AlKa, 211
SiKa, 451
SKa, 30
ClKa, 18
KKa, 50
FeKa, 6
FeKb, 4
TH3A length: 1.015 mm

Site 4

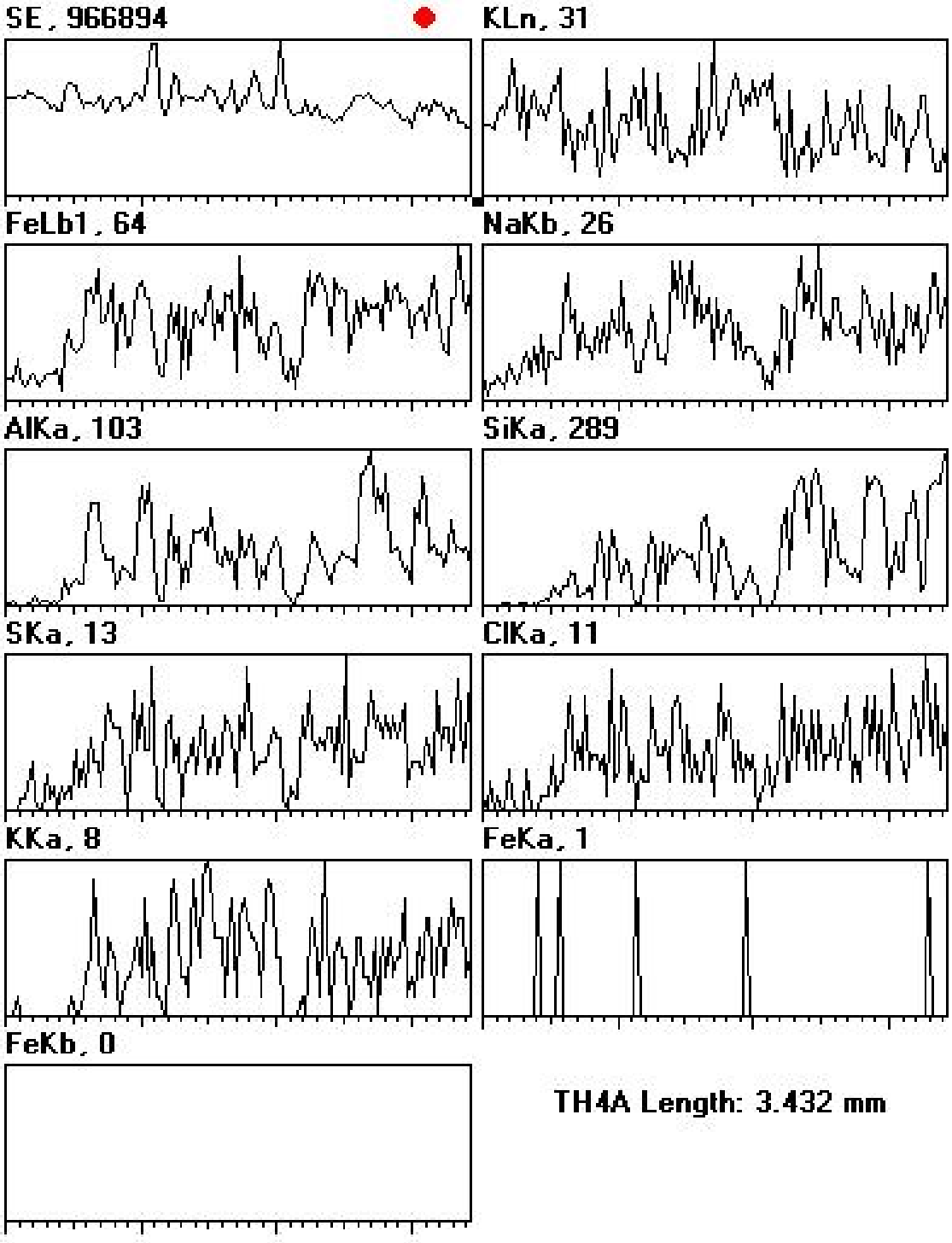
SE, 966894
KLn, 31
FeLb1, 64
NaKb, 26
AlKa, 103
SiKa, 289
SKa, 13
ClKa, 11
KKa, 8
FeKa, 1
FeKb, 0
TH4A Length: 3.432 mm

Site 5

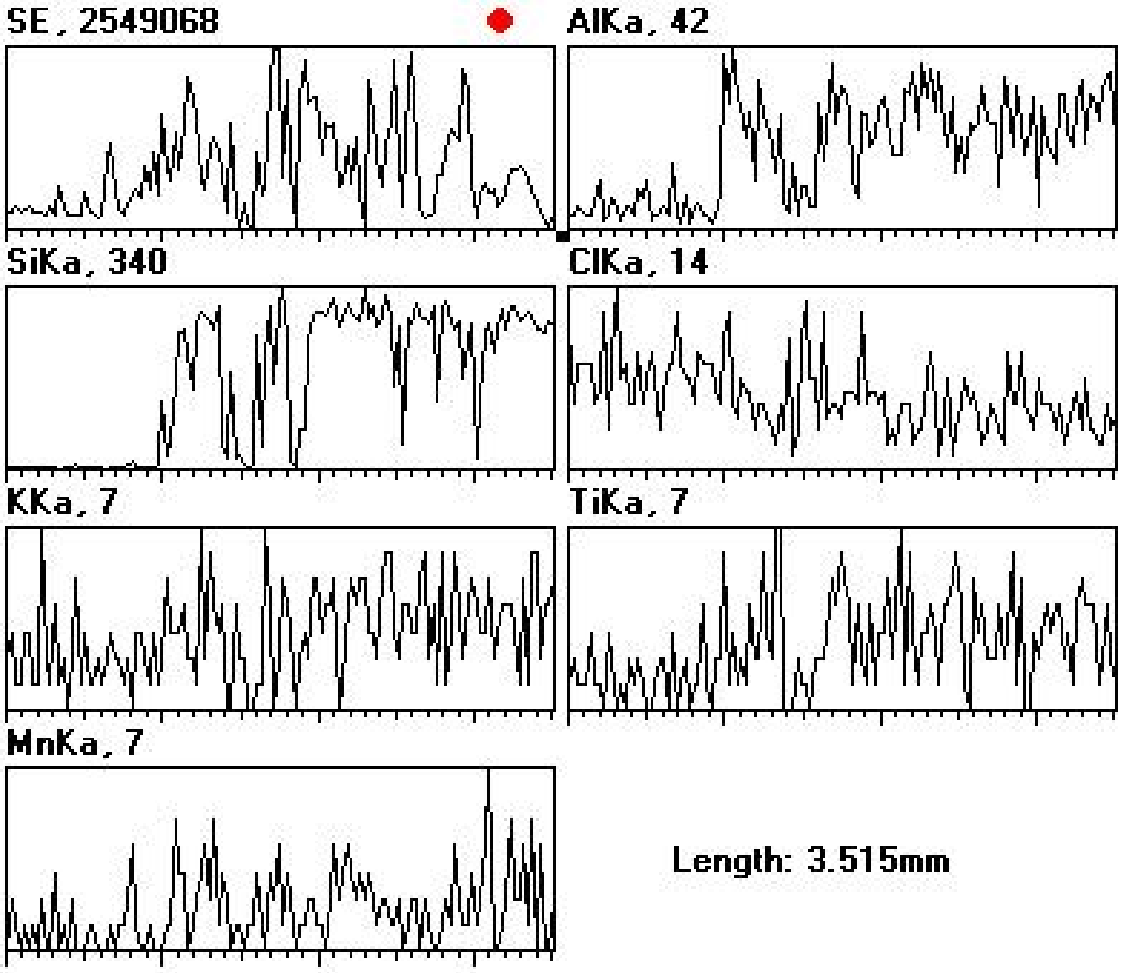
SE, 2549068
AlKa, 42
SiKa, 340
ClKa, 14
KKa, 7
TiKa, 7
MnKa, 7
Length: 3.515mm

Site 6

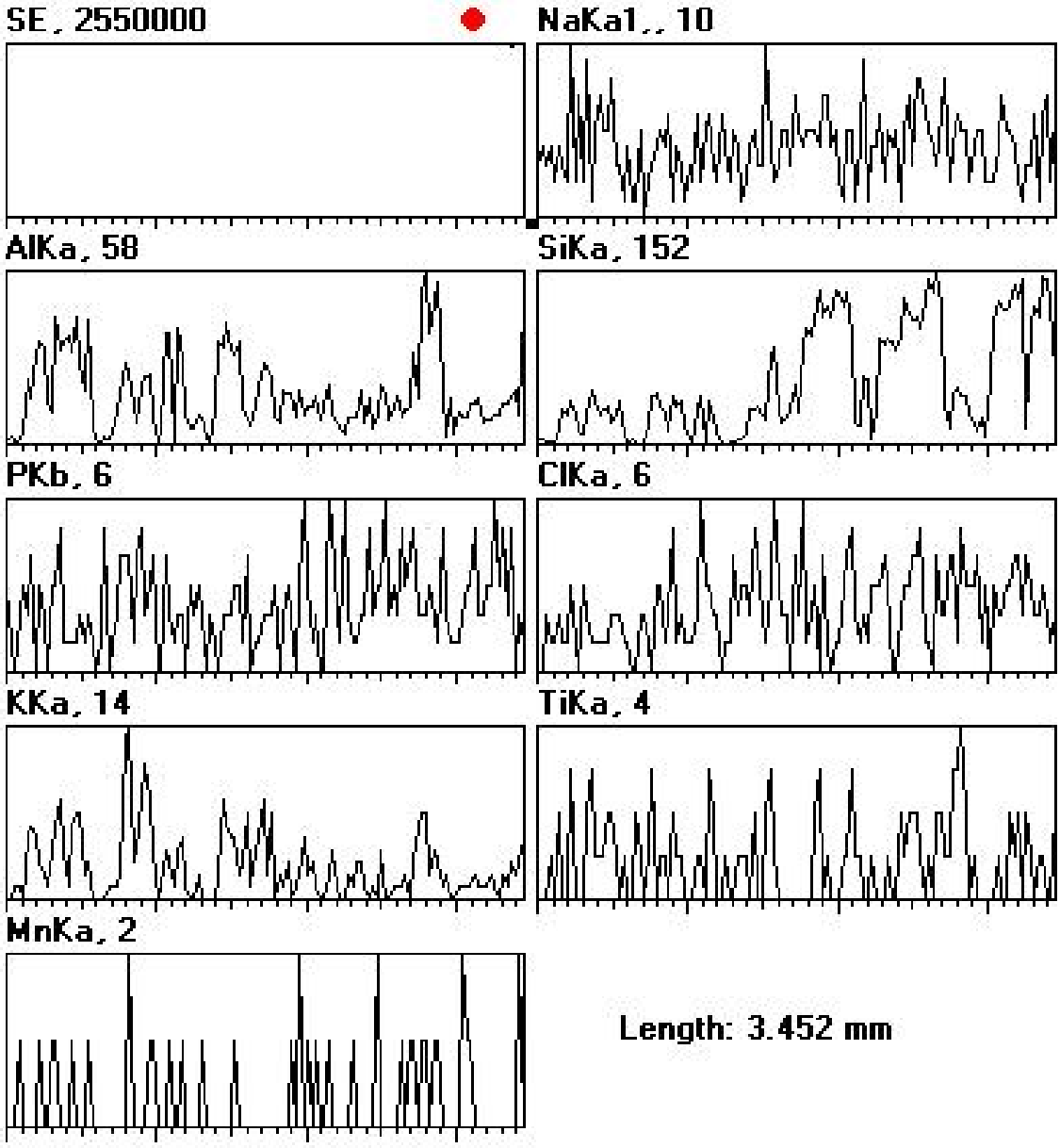
SE, 2550000
NaKa1,, 10
AlKa, 58
SiKa, 152
PKb, 6
ClKa, 6
KKa, 14
TiKa, 4
MnKa, 2
Length: 3.452 mm

Burkes Creek

Burkes Creek Underground Mine

M165
McKenzies

McKenzie Party
No. 2 Seam

Monsvale Fault

M156
Peerless

Peerless Workings
No. 2 Seam

M61
Turner
& Muirs

Prospect
Drive

M40
Lockingtons
No. 2 Seam

Stevenson's Old workings

QEII Trust Trees

A

M116
Ferndale
No. 1 Entrance

M60
Old Konini Dip
No. 2 Seam

B'

Turners
Old Workings

Old Peerless Workings
No. 2 Seam

Thin Dirty Coal

Burkes Creek Fault

Woodlands Mine
No. 1 Seam

Monsvale Fault

New Ferndale Opencast
(No. 2 Seam)

M172 New
Ferndale

6a
6b
7a
7b

New Ferndale Opencast
(No. 4 Seam)

No. 4 Seam Subcrop

Stock Yards

Buildings now removed

Abandoned mining shed

Ferndale Coal

8a
8b

Reddale Underground Mine
No. 2 Seam

Farm shed

Ferndale Opencast
(No. 4 Seam)

M113
Ferndale Opencast

B

Reddale Fault

Hallorans Dip Mine
No. 4 Seam

Burkes Creek Fault

A'

"Old" Terrace Opencast

Hallorans Fault

Limit of Terrace
Underground
Mine Workings

1a
1b
2
3a
3b
3c
4a

Terrace Opencast

5a
5b
5c

No. 4 Seam Subcrop

Halloran Bros. Mine

220
240
260
280
300
320
340
360
380

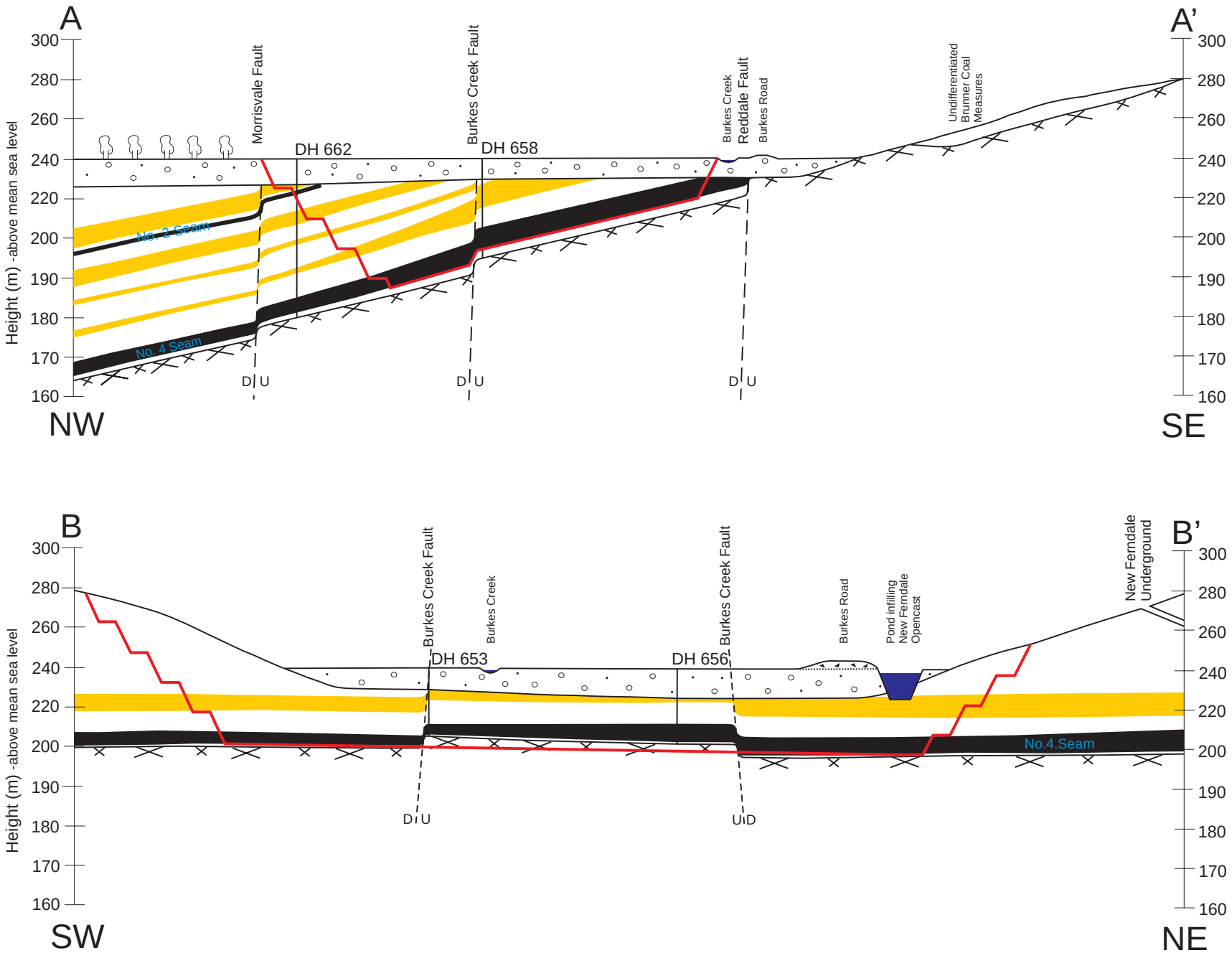

Legend:

- Outwash Gravels
- Sandstone
- Interbedded carbonaceous sandstone, mudstone and siltstone
- Coal

Brunner Coal Measures

- Overburden Dump
- Water
- Basement (Greenland Group)
- Proposed Pit Outline
- Drill Hole
- Normal Fault (approximately 6m downthrow to NW)
- Tress protected by QEII Trust Covenant

Map B: Cross Sections

Reddale Valley
Reefton Coalfield
New Zealand

Drawn by Joanna Lea
University of Canterbury

June 2006

Scale 1: 2000

100m

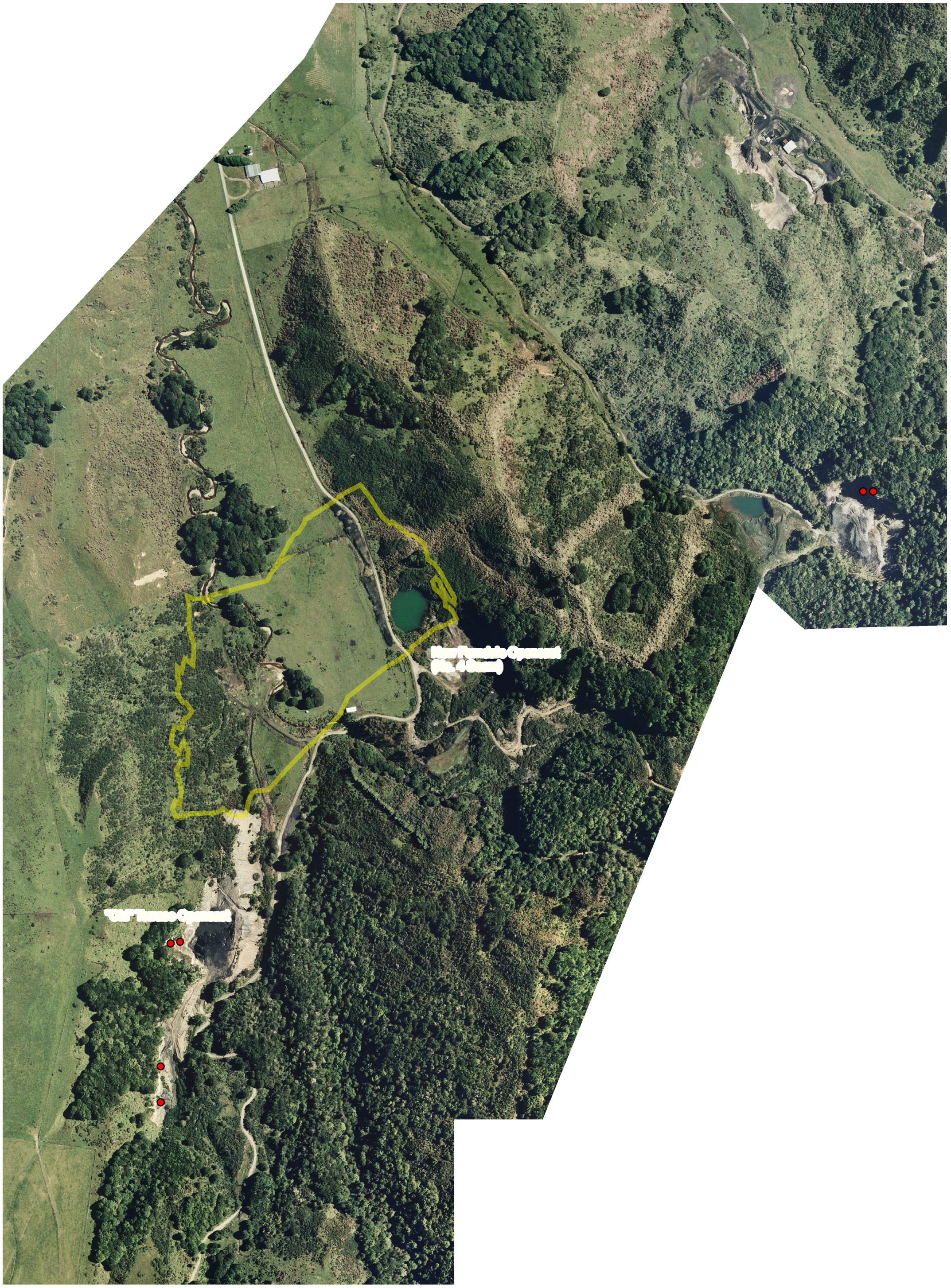
New Ferndale Opencast
(No. 4 Seam)
"Old" Terrace Opencast